BULLETIN OF RUSSIAN STATE MEDICAL UNIVERSITY

BIOMEDICAL JOURNAL OF PIROGOV RUSSIAN NATIONAL RESEARCH MEDICAL UNIVERSITY

EDITOR-IN-CHIEF Denis Rebrikov, DSc, professor

DEPUTY EDITOR-IN-CHIEF Alexander Oettinger, DSc, professor

EDITORS Valentina Geidebrekht, PhD; Nadezda Tikhomirova

TECHNICAL EDITOR Evgeny Lukyanov

TRANSLATORS Nadezda Tikhomirova, Vyacheslav Vityuk

DESIGN AND LAYOUT Marina Doronina

SUBMISSION

EDITORIAL BOARD

Averin VI, DSc, professor (Minsk, Belarus)
Azizoglu M, MD PhD (Istanbul, Turkey)
Alipov NN, DSc, professor (Moscow, Russia)
Belousov VV, DSc, professor (Moscow, Russia)
Bozhenko VK, DSc, CSc, professor (Moscow, Russia)
Bylova NA, CSc, docent (Moscow, Russia)
Gainetdinov RR, CSc (Saint-Petersburg, Russia)
Gendlin GYe, DSc, professor (Moscow, Russia)
Ginter EK, member of RAS, DSc (Moscow, Russia)
Gorbacheva LR, DSc, professor (Moscow, Russia)
Gordeev IG, DSc, professor (Moscow, Russia)
Gudkov AV, PhD, DSc (Buffalo, USA)
Gulyaeva NV, DSc, professor (Moscow, Russia)
Gusev EI, member of RAS, DSc, professor (Moscow, Russia)
Danilenko VN, DSc, professor (Moscow, Russia)
Zarubina TV, DSc, professor (Moscow, Russia)
Zatevakhin II, member of RAS, DSc, professor (Moscow, Russia)
Kagan VE, professor (Pittsburgh, USA)
Kzyshkowska YuG, DSc, professor (Heidelberg, Germany)
Kobrinskii BA, DSc, professor (Moscow, Russia)
Kozlov AV, MD PhD, (Vienna, Austria)
Kotelevtsev YuV, CSc (Moscow, Russia)
Lebedev MA, PhD (Darem, USA)
Manturova NE, DSc (Moscow, Russia)
Milushkina OYu, DSc, professor (Moscow, Russia)
Mitupov ZB, DSc, professor (Moscow, Russia)
Moshkovskii SA, DSc, professor (Moscow, Russia)
Munblit DB, MSc, PhD (London, Great Britain)
Negrebetsky VV, DSc, professor (Moscow, Russia)
Novikov AA, DSc (Moscow, Russia)
Pivovarov YuP, member of RAS, DSc, professor (Moscow, Russia)
Polunina NV, corr. member of RAS, DSc, professor (Moscow, Russia)
Poryadin GV, corr. member of RAS, DSc, professor (Moscow, Russia)
Razumovskii AYu, corr. member of RAS, DSc, professor (Moscow, Russia)
Rebrova OYu, DSc (Moscow, Russia)
Rudoy AS, DSc, professor (Minsk, Belarus)
Rylova AK, DSc, professor (Moscow, Russia)
Semiglazov VF, corr. member of RAS, DSc, professor (Saint-Petersburg, Russia)
Skoblina NA, DSc, professor (Moscow, Russia)
Slavyanskaya TA, DSc, professor (Moscow, Russia)
Smirnov VM, DSc, professor (Moscow, Russia)
Spallone A, DSc, professor (Rome, Italy)
Starodubov VI, member of RAS, DSc, professor (Moscow, Russia)
Stepanov VA, corr. member of RAS, DSc, professor (Tomsk, Russia)
Suchkov SV, DSc, professor (Moscow, Russia)
Takhchidi KhP, member of RAS, DSc, professor (Moscow, Russia)
Trufanov GE, DSc, professor (Saint-Petersburg, Russia)
Tumanova UN, MD (Moscow, Russia)
Favorova OO, DSc, professor (Moscow, Russia)
Filipenko ML, CSc, leading researcher (Novosibirsk, Russia)
Khazipov RN, DSc (Marsel, France)
Chundukova MA, DSc, professor (Moscow, Russia)
Schegolev AI, MD, professor (Moscow, Russia)
Shimanovskii NL, corr. member of RAS, Dsc, professor (Moscow, Russia)
Shishkina LN, DSc, senior researcher (Novosibirsk, Russia)
Yakubovskaya RI, DSc, professor (Moscow, Russia)

SUBMISSION http://vestnik.rsmu.press/login?lang=en
CORRESPONDENCE editor@rsmu.press
COLLABORATION manager@vestnikrgmu.ru
ADDRESS ul. Ostrovityanova, d. 1, Moscow, Russia, 117997

Indexed in Scopus. CiteScore 2023: 0,8

Indexed in WoS. JCR 2021: 0.5

Five-year h-index is 10

SCImago Journal & Country Rank 2020: 0.14

Listed in HAC 31.12.2023 (No. 44) by the order of the Ministry of Science and Higher Education of the Russian Federation from 31.05.2023 No. 534

Open access to archive

Issue DOI: 10.24075/brsmu.2025-06
Mass media registration certificate No. 012769, issued on July 29, 1994.
ISSN (Print): 2500-1094, ISSN (Online): 2542-1204.
Founder and publisher: Pirogov Russian National Research Medical University (Moscow, Russia).
The journal is indexed in the following scientific databases: Scopus, Web of Science, Google Scholar, SJR, DOAJ, Scilit, CyberLeninka, Embase, EZB, Lens.org, MIT Libraries, OpenAlex, Research4Life, Scholia, Wikidata, and ZDB.

The journal is distributed under the terms of the Creative Commons Attribution 4.0 International License (www.creativecommons.org).

Approved for print 31.12.2025
Circulation: 100 copies. Printed by Print.Formula
www.print-formula.ru

ВЕСТНИК РОССИЙСКОГО ГОСУДАРСТВЕННОГО МЕДИЦИНСКОГО УНИВЕРСИТЕТА

НАУЧНЫЙ МЕДИЦИНСКИЙ ЖУРНАЛ РНИМУ ИМ. Н. И. ПИРОГОВА

ГЛАВНЫЙ РЕДАКТОР Денис Ребриков, д. б. н., профессор

ЗАМЕСТИТЕЛЬ ГЛАВНОГО РЕДАКТОРА Александр Эттингер, д. м. н., профессор

РЕДАКТОРЫ Валентина Гейдебрехт, к. б. н.; Надежда Тихомирова

ТЕХНИЧЕСКИЙ РЕДАКТОР Евгений Лукьянов

ПЕРЕВОДЧИКИ Надежда Тихомирова, Вячеслав Витюк

ДИЗАЙН И ВЕРСТКА Марины Дорониной

ПОДАЧА РУКОПИСЕЙ

РЕДАКЦИОННАЯ КОЛЛЕГИЯ

В. И. Аверин, д. м. н., профессор (Минск, Белоруссия)
М. Азизоглу, MD PhD (Стамбул, Турция)
Н. Н. Алипов, д. м. н., профессор (Москва, Россия)
В. В. Белоусов, д. б. н., профессор (Москва, Россия)
В. К. Боженко, д. м. н., к. б. н., профессор (Москва, Россия)
Н. А. Былова, к. м. н., доцент (Москва, Россия)
Р. Р. Гайнетдинов, к. м. н. (Санкт-Петербург, Россия)
Г. Е. Гендлин, д. м. н., профессор (Москва, Россия)
Е. К. Гинтер, академик РАН, д. б. н. (Москва, Россия)
Л. Р. Горбачева, д. б. н., профессор (Москва, Россия)
И. Г. Гордеев, д. м. н., профессор (Москва, Россия)
А. В. Гудков, PhD, DSc (Буффало, США)
Н. В. Гуляева, д. б. н., профессор (Москва, Россия)
Е. И. Гусев, академик РАН, д. м. н., профессор (Москва, Россия)
В. Н. Даниленко, д. б. н., профессор (Москва, Россия)
Т. В. Зарубина, д. м. н., профессор (Москва, Россия)
И. И. Затевахин, академик РАН, д. м. н., профессор (Москва, Россия)
В. Е. Каган, профессор (Питтсбург, США)
Ю. Г. Кжышковска, д. б. н., профессор (Гейдельберг, Германия)
Б. А. Кобринский, д. м. н., профессор (Москва, Россия)
А. В. Козлов, MD PhD (Вена, Австрия)
Ю. В. Котелевцев, к. х. н. (Москва, Россия)
М. А. Лебедев, PhD (Дарем, США)
Н. Е. Мантурова, д. м. н. (Москва, Россия)
О. Ю. Милушкина, д. м. н., доцент (Москва, Россия)
З. Б. Митупов, д. м. н., профессор (Москва, Россия)
С. А. Мошковский, д. б. н., профессор (Москва, Россия)
Д. Б. Мунблит, MSc, PhD (Лондон, Великобритания)
В. В. Негребецкий, д. х. н., профессор (Москва, Россия)
А. А. Новиков, д. б. н. (Москва, Россия)
Ю. П. Пивоваров, д. м. н., академик РАН, профессор (Москва, Россия)
Н. В. Полунина, член-корр. РАН, д. м. н., профессор (Москва, Россия)
Г. В. Порядин, член-корр. РАН, д. м. н., профессор (Москва, Россия)
А. Ю. Разумовский, член-корр. РАН, д. м. н., профессор (Москва, Россия)
О. Ю. Реброва, д. м. н. (Москва, Россия)
А. С. Рудой, д. м. н., профессор (Минск, Белоруссия)
А. К. Рылова, д. м. н., профессор (Москва, Россия)
В. Ф. Семиглазов, член-корр. РАН, д. м. н., профессор (Санкт-Петербург, Россия)
Н. А. Скоблина, д. м. н., профессор (Москва, Россия)
Т. А. Славянская, д. м. н., профессор (Москва, Россия)
В. М. Смирнов, д. б. н., профессор (Москва, Россия)
А. Спаллоне, д. м. н., профессор (Рим, Италия)
В. И. Стародубов, академик РАН, д. м. н., профессор (Москва, Россия)
В. А. Степанов, член-корр. РАН, д. б. н., профессор (Томск, Россия)
С. В. Сучков, д. м. н., профессор (Москва, Россия)
Х. П. Тахчиди, академик РАН, д. м. н., профессор (Москва, Россия)
Г. Е. Труфанов, д. м. н., профессор (Санкт-Петербург, Россия)
У. Н. Туманова, д. м. н. (Москва, Россия)
О. О. Фаворова, д. б. н., профессор (Москва, Россия)
М. Л. Филипенко, к. б. н. (Новосибирск, Россия)
Р. Н. Хазипов, д. м. н. (Марсель, Франция)
М. А. Чундокова, д. м. н., профессор (Москва, Россия)
Н. Л. Шимановский, член-корр. РАН, д. м. н., профессор (Москва, Россия)
Л. Н. Шишкина, д. б. н. (Новосибирск, Россия)
А. И. Щеголев, д. м. н., профессор (Москва, Россия)
Р. И. Якубовская, д. б. н., профессор (Москва, Россия)

ПОДАЧА РУКОПИСЕЙ https://vestnik.rsmu.press/login?lang=ru
ПЕРЕПИСКА С РЕДАКЦИЕЙ editor@vestnikrgmu.ru
СОТРУДНИЧЕСТВО manager@vestnikrgmu.ru
АДРЕС РЕДАКЦИИ ул. Островитянова, д. 1, г. Москва, 117997

Журнал включен в Scopus. CiteScore 2023: 0,8

Журнал включен в WoS. JCR 2021: 0,5

Индекс Хирша (h^5) журнала по оценке Google Scholar: 10

SCImago Journal & Country Rank 2020: 0,14

Журнал включен в Перечень 31.12.2023 (№ 44) приказом Минобрнауки России от 31.05.2023 № 534

Здесь находится открытый архив журнала

DOI выпуска: 10.24075/vrgmu.2025-06
Свидетельство о регистрации средства массовой информации № 012769 от 29 июля 1994 г.
ISSN (Print): 2500-1094, ISSN (Online): 2542-1204.
Учредитель и издатель — Российский национальный исследовательский медицинский университет имени Н. И. Пирогова (Москва, Россия).
Журнал индексируется в научных базах Scopus, Web of Science, Google Scholar, SJR, DOAJ, Scilit, CyberLeninka, Embase, EZB, Lens.org, MITLibaries, OpenAlex, Research4Life, Scholia, Wikidata, ZDB.

Журнал распространяется по лицензии Creative Commons Attribution 4.0 International (www.creativecommons.org).

Подписано в печать 31.12.2025
Тираж 100 экз. Отпечатано в типографии Print.Formula
www.print-formula.ru

BULLETIN OF RSMU **6, 2025**
ВЕСТНИК РГМУ

Contents
Содержание

ORIGINAL RESEARCH 6

Assessment of blood catecholamine and serotonin levels in anxiety and depressive disorders
Solovyova NV, Chuprova NA, Kochergina KV, Mitrofanov AA, Chausova SV, Kichuk IV

Оценка уровня катехоламинов и серотонина в крови при тревожно-депрессивных расстройствах
Н. В. Соловьева, Н. А. Чупрова, К. В. Кочергина, А. А. Митрофанов, С. В. Чаусова, И. В. Кичук

ORIGINAL RESEARCH 13

Reconsolidation of early memories in reliving the traumatic combat experience
Petrash EA, Uynina-Pakulova NYu, Kuryishina SA, Karpenko AS, Kuznetsova AA

Реконсолидация ранних воспоминаний в переживаниях травматического опыта участия в боевых действиях
Е. А. Петраш, Н. Ю. Юнина-Пакулова, С. А. Курышина, А. С. Карпенко, А. А. Кузнецова

ORIGINAL RESEARCH 21

Features of the immune response to tumor alloantigens in the context of decreased clonal diversity of T cells
Korotkova MS, Persiyantseva NA, Kalinina AA, Khromykh LM, Kazansky DB

Особенности иммунного ответа на опухолевые аллоантигены в условиях сокращенного клонального разнообразия Т-клеток
М. С. Короткова, Н. А. Персиянцева, А. А. Калинина, Л. М. Хромых, Д. Б. Казанский

ORIGINAL RESEARCH 29

Perivascular mast cells and angiogenesis in the tumor microenvironment of synovial sarcoma
Bulanov DV, Makhachev DR, Suntsov MA, Gubich DS, Filippova YD, Krutilina AA, Svoyak AV, Ivannikova AA, Ghabibullaev RM

Периваскулярные мастоциты и ангиогенез в опухолевом микроокружении синовиальной саркомы
Д. В. Буланов, Д. Р. Махачев, М. А. Сунцов, Д. С. Губич, Ю. Д. Филиппова, А. А. Крутилина, А. В. Свояк, А. А. Иванникова, Р. М. Габибуллаев

ORIGINAL RESEARCH 36

Results of phase IIa clinical trial of the RAS-GTPase inhibitor («Ing-Ras») for treatment of gastrointestinal tumors
Kulinich TM, Kukoleva EA, Goncharov SV, Kudinova EA, Puchkov IA, Goncharova OI, Kaminsky VV, Bozhenko VK

Результаты клинического исследования IIa фазы ингибитора RAS-ГТФазы («Инг-Рас») для лечения опухолей желудочно-кишечного тракта
Т. М. Кулинич, Е. А. Куколева, С. В. Гончаров, Е. А. Кудинова, И. А. Пучков, О. И. Гончарова, В. В. Каминский, В. К. Боженко

ORIGINAL RESEARCH 44

Expression of chemokine receptors CXCR4 and CXCR7 in circulating tumor cells of breast cancer
Grigoryeva ES, Tashireva LA, Savelieva OE, Zavyalova MV, Cherdyntseva NV, Perelmuter VM

Экспрессия рецепторов хемокинов CXCR4 и CXCR7 в циркулирующих опухолевых клетках при раке молочной железы
Е. С. Григорьева, Л. А. Таширева, О. Е. Савельева, М. В. Завьялова, Н. В. Чердынцева, В. М. Перельмутер

ORIGINAL RESEARCH 56

Genetic portraits of Volga–Oka region in the context of the Central Russia's gene pool (Y-SNP polymorphism)
Ponomarev GYu, Shlykov AG, Gorin IO, Voronina MM, Potanina AYu, Petrov VA, Koshel SM, Adamov DS, Balanovska EV

Генетические портреты Волго-Окского региона в контексте генофонда Центральной России (Y-SNP полиморфизм)
Г. Ю. Пономарев, А. Г. Шлыков, И. О. Горин, М. М. Воронина, А. Ю. Потанина, В. А. Петров, С. М. Кошель, Д. С. Адамов, Е. В. Балановская

ORIGINAL RESEARCH 66

Transcriptional kinase CDK8, but not CDK19, promotes the development of atherosclerotic lesions in mice
Neznamov AN, Baykova YuP, Korshunov EN, Isaeva EM, Bruter AV, Kubekina MV

Транскрипционная киназа CDK8, но не CDK19 способствует развитию атеросклеротических поражений у мышей
А. Н. Незнамов, Ю. П. Байкова, Е. Н. Коршунов, Е. М. Исаева, А. В. Брутер, М. В. Кубекина

ORIGINAL RESEARCH 73

Single nucleotide variant r*s293795 OGG1* as a genetic risk factor for diabetic nephropathy
Semikina EV, Azarova IE, Panichev SA, Basareva OI, Dzhanchatova NV, Alferova EYu, AV Polonikov

Однонуклеотидный вариант *rs293795 OGG1* как генетический фактор риска диабетической нефропатии
Е. В. Семикина, Ю. Э. Азарова, С. А. Паничев, О. И. Басарева, Н. В. Джанчатова, Е. Ю. Алферова, А. В. Полоников

ORIGINAL RESEARCH 82

Expression of MTCO1 in cell cultures from patients with Leigh syndrome under the action of AAV9-SURF1
Adrianov MA, Gauthier MS, Degtyareva AV, Marey MV, Manukhova LA, Rastorguev SM, Simonov VS, Ushakova LV, Vysokikh MY

Экспрессия MTCO1 в культурах клеток пациентов с синдромом Ли при действии AAV9-SURF1
М. А. Адрианов, М. С. Готье, А. В. Дегтярева, М. В. Марей, Л. А. Манухова, С. М. Расторгуев, В. С. Симонов, Л. В. Ушакова, М. Ю. Высоких

ORIGINAL RESEARCH 89

Pipelle and Endobrush Catheters Do Not Prevent Contamination of Endometrial Samples by Cervical Microbiota
Zornikov DL, Bekhter AA, Kornilov DO, Simarzina VM, Nechaeva DM, Karyakina AE, Leshukova MA, Amineva PG, Voroshilina ES

Урогенитальные зонды типа Пайпель-С не предотвращают контаминацию эндометриальных образцов цервикальной микробиотой
Д. Л. Зорников, А. А. Бехтер, Д. О. Корнилов, В. М. Симарзина, Д. М. Нечаева, А. Е. Карякина, М. А. Лешукова, П. Г. Аминева, Е. С. Ворошилина

ORIGINAL RESEARCH 96

Characteristics of systemic inflammation in patients with endometritis-associated infertility
Savelieva OE, Krivolesova TA, Zhigalina AS, Sigareva LP, Saburov AV, Reznik VA

Особенности системного воспалительного статуса пациенток при эндометрит-ассоциированном бесплодии
О. Е. Савельева, Т. А. Криволесова, А. С. Жигалина, Л. П. Сигарева, А. В. Сабуров, В. А. Резник

ORIGINAL RESEARCH 102

Ribosomal gene copy number in peripheral leukocytes of women with normal and complicated pregnancy
Ershova ES, Veiko NN, Kostyuk EV, Poletkina AA, Rozhnova TM, Nizyaeva NV, Muzaffarov DU, Klimenko PA, Kostyuk SV

Количество копий рибосомных генов в лейкоцитах периферической крови у женщин с физиологической и осложненной беременностью
Е. С. Ершова, Н. Н. Вейко, Э. В. Костюк, А. А. Полеткина, Т. М. Рожнова, Н. В. Низяева, Д. У. Музаффаров, П. А. Клименко, С. В. Костюк

METHOD 110

Preparation and procedure for scanning electron microscopy examination of cells adhered to bioceramic surfaces
Danilko KV, Solntsev VA, Plotnitsky RV, Mikhailova AV, Bilyalov AR, Chugunov SS, Galautdinov MF, Akbashev VN, Akhatov ISh

Подготовка и алгоритм исследования адгезированных на поверхности биокерамики клеток методом сканирующей электронной микроскопии
К. В. Данилко, В. А. Солнцев, Р. В. Плотницкий, А. В. Михайлова, А. Р. Билялов, С. С. Чугунов, М. Ф. Галаутдинов, В. Н. Акбашев, И. Ш. Ахатов

ORIGINAL RESEARCH 119

Development of the vascular condition classifier using supervised machine learning methods
Besedovskaia ZV, Korobov AYu, Kudriashova NI

Разработка классификатора состояний сосудов с использованием методов контролируемого машинного обучения
З. В. Беседовская, А. Ю. Коробов, Н. И. Кудряшова

ORIGINAL RESEARCH 127

Detection of *Salmonella enterica* by loop-mediated isothermal amplification of DNA using a fluorescently labeled loop primer
Shamovskaya DV, Gordukova MA, Smertina MA, Galeeva EV, Oscorbin IP, Khrapov EA, Boyarskikh UA, Filipenko ML

Детекция *Salmonella enterica* петлевой изотермальной амплификацией ДНК с использованием флуоресцентно меченого петлевого праймера
Д. В. Шамовская, М. А. Гордукова, М. А. Смертина, Е. В. Галеева, И. П. Оскорбин, Е. А. Храпов, У. А. Боярских, М. Л. Филипенко

ORIGINAL RESEARCH 133

Anti-opisthorchiasis and hepatoprotective effects of *Populus tremula* bark extract: *in vitro* studies
Perina EA, Buyko EE, Kaidash OA, Efimova LV, Diksas EB, Krivoshchekov SV, Ivanov AA, Ivanov VV, Udut EV

Противоописторхозная и гепатопротекторная активность экстракта коры осины (*Populus tremula L.*) в экспериментах *in vitro*
Е. А. Перина, Е. Е. Буйко, О. А. Кайдаш, Л. В. Ефимова, Е. Б. Диксас, С. В. Кривощеков, А. А. Иванов, В. В. Иванов, Е. В. Удут

ORIGINAL RESEARCH 140

Blood expression of CD39 and CD73 ectonucleotidases in patients with various forms of metabolic-associated fatty liver disease
Zhulai GA, Kurbatova IV, Dudanova OP

Экспрессия эктонуклеотидаз CD39 и CD73 в крови больных разными формами метаболически ассоциированной жировой болезни печени
Г. А. Жулай И. В. Курбатова, О. П. Дуданова

ORIGINAL RESEARCH 148

Antiviral activity of mRNAs encoding intracellular scFv antibodies against conserved influenza virus epitopes
Plotnikova MA, Oleynik VA, Klotchenko SA

Противовирусная активность мРНК, кодирующих внутриклеточные scFv-фрагменты антител к консервативным эпитопам вируса гриппа
М. А. Плотникова, В. А. Олейник, С. А. Клотченко

ORIGINAL RESEARCH 158

HMGB1 and anti-HMGB1 antibodies in systemic lupus erythematosus and other rheumatic diseases
Melamud MM, Ermakov EA, Tolmacheva AS, Sizikov AE, Klyaus NA, Nevinsky GA, Buneva VN

HMGB1 и анти-HMGB1 антитела при системной красной волчанке и других ревматических заболеваниях
М. М. Меламуд, Е. А. Ермаков, А. С. Толмачева, А. Э. Сизиков, Н. А. Кляус, Г. А. Невинский, В. Н. Бунева

OPINION 166

Follicular T cells in peripheral blood: increasing complexity and key questions
Grigorova IL

Фолликулярные Т-клетки периферической крови: нарастающая сложность и первоочередные вопросы
И. Л. Григорова

ORIGINAL RESEARCH 171

Etiological structure of enterovirus infection in children in the Moscow region
Polyakova VA, Davydova EE, Luparev AR, Matsvay AD, Gnusareva NI, Gordukova MA, Galeeva EV, Tolokonceva AA, Shipulin GA

Этиологическая структура энтеровирусной инфекции у детей в Московском регионе
В. А. Полякова, Е. Е. Давыдова, А. Р. Лупарев, А. Д. Мацвай, Н. И. Гнусарева, М. А. Гордукова, Е. В. Галеева, А. А. Толоконцева, Г. А. Шипулин

ORIGINAL RESEARCH 180

Comparative imaging of the HAEE-Cy5 and EEAH-Cy5 tetrapeptide binding to the Aβ aggregates on the SH-SY5Y cells
Ivanova AV, Chmelyuk NS, Kuzmichev IA, Shilyaeva MI, Abakumov MA

Сравнительная визуализация связывания тетрапептидов HAEE-Cy5 и EEAH-Cy5 с агрегатами Aβ на клетках SH-SY5Y
А. В. Иванова, Н. С. Чмелюк, И. А. Кузьмичев, М. И. Шиляева, М. А. Абакумов

ORIGINAL RESEARCH 187

Determining targets for personalized multitarget noninvasive stimulation of the frontoparietal control network
Poydasheva AG, Sinitsyn DO, Bakulin IS, Zabirova AH, Lagoda DYu, Suponeva NA, Piradov MA

Определение мишеней для персонализированной мультитаргетной неинвазивной стимуляции лобно-теменной сети контроля
А. Г. Пойдашева, Д. О. Синицын, И. С. Бакулин, А. Х. Забирова, Д. Ю. Лагода, Н. А. Супонева, М. А. Пирадов

ORIGINAL RESEARCH 195

Differentiation of iPSCs into corneal epithelial precursors in three-dimensional *in vitro* culture
Zhigmitova EB, Kosykh AV, Gurskaya NG

Дифференцировка иПСК в предшественники эпителия роговицы в трехмерных условиях *in vitro*
Е. Б. Жигмитова, А. В. Косых, Н. Г. Гурская

ORIGINAL RESEARCH 201

Development and assessment of the bone allograft-based material for DLP 3D printing
Bilyalov AR, Chugunov SS, Akhatov ISh, Tikhonov AA, Shangina OR, Pavlov VN, Danilko KV, Galautdinov MF, Akbashev VN

Разработка и исследование материала на основе костного аллотрансплантата для DLP-3D-печати
А. Р. Билялов, С. С. Чугунов, И. Ш. Ахатов, А. А. Тихонов, О. Р. Шангина, В. Н. Павлов, К. В. Данилко, М. Ф. Галаутдинов, В. Н. Акбашев

ORIGINAL RESEARCH 209

Expression of microRNA miR146a in the blood plasma of rats with obesity and knee arthrosis after administration of dexamethasone
Ivanov AS, Tananakina TP, Kashchenko SA, Pogorelova IA

Экспрессия микроРНК miR146a в плазме крови крыс с ожирением и артрозом коленного сустава на фоне введения дексаметазона
А. С. Иванов, Т. П. Тананакина, С. А. Кащенко, И. А. Погорелова

CLINICAL CASE 216

Severe acute α-PVP poisoning complicated by systemic rhabdomyolysis syndrome: case report
Makarovskaya NP, Lodyagin AN, Batocyrenov ChB, Razamasova SYu, Antonova AM, Narzikulov RA, Sokolova ES

Клинический случай острого тяжелого отравления α-PVP, осложненный развитием синдрома системного рабдомиолиза
Н. П. Макаровская, А. Н. Лодягин, Ч. Б. Батоцыренов, С. Ю. Разамасова, А. М. Антонова, Р. А. Нарзикулов, Е. С. Соколова

OPINION 220

Earthworms as a source of new approaches in biomedical research
Khokhlova AN, Vavilov MV, Chepurnykh TV, Rodionova NS, Petushkov VN, Yampolsky IV, Dubinnyi MA

Почвенные черви как источник новых подходов в биомедицинских исследованиях
А. Н. Хохлова, М. В. Вавилов, Т. В. Чепурных, Н. С. Родионова, В. Н. Петушков, И. В. Ямпольский, М. А. Дубинный

ASSESSMENT OF BLOOD CATECHOLAMINE AND SEROTONIN LEVELS IN ANXIETY AND DEPRESSIVE DISORDERS

Solovyova NV[1], Chuprova NA[1], Kochergina KV[2], Mitrofanov AA[3], Chausova SV[4], Kichuk IV[4] ✉

[1] Scientific Centre of Personalized Medicine, Moscow, Russia
[2] Diagnostic and Treatment Center, Berezin Medical Institute, Moscow, Russia
[3] Mental Health Research Center, Moscow, Russia
[4] Pirogov Russian National Research Medical University, Moscow, Russia

In psychiatric practice, there is a need to develop simple, pathogenetically substantiated biomarkers for prediction of the patient's current affective status and his/her status short-term perspective. The study aimed to analyze the association of the affective status of patients with mood disorders with the peripheral blood catecholamine and serotonin levels. The Hospital Anxiety and Depression Scale (HADS) was used for affective status evaluation. Concentrations of catecholamines (adrenaline, norepinephrine, and dopamine) in blood plasma and serotonin in blood serum were assessed by high-performance liquid chromatography (HPLC). The study included 114 individuals with affective disorders, the average age was 34.57 (SD = 10.36) years, the share of females was 64%. We revealed no significant prognostic effects of peripheral blood neurotransmitter levels relative to the current affective status. The serotonin/norepinephrine ratio, the increase in which significantly decreases the risk of clinical depression according to HADS-D considering the patient's sex and age ($p = 0.059$), turned out to be the only marker at the level of trends. In patients diagnosed with recurrent depressive disorder or depressive episode, a slight decrease in serotonin levels ($p = 0.068$) compared to the patients diagnosed with the disorders beyond the category of mood disorders is reported. In the same group a negative correlation has been found between the HADS-A scores (anxiety) and norepinephrine levels (Rs = –0.410, $p < 0.05$). The findings suggest that it will be possible to confirm the preliminary results obtained and acquire new data in the expanded clinically homogenous samples.

Keywords: depression, anxiety, non-psychotic mental disorders, catecholamines, serotonin, biological markers

Author contribution: Solovyova NV, Kichuk IV — study concept and design; Solovyova NV, Kochergina KV, Mitrofanov AA, Kichuk IV — material collection and processing; Chuprova NA, Kochergina KV — statistical data processing; Mitrofanov AA, Kichuk IV, Solovyova NV, Kochergina KV — manuscript writing; Mitrofanov AA, Kichuk IV, Solovyova NV, Kochergina KV, Chausova SV — editing.

Compliance with ethical standards: the study was approved by the Ethics Committee of the Joint Stock Company "Scientific Centre of Personalized Medicine" (protocol No. 33 dated 1 December 2025). The subjects' personal data were hidden during the study. All the subjects submitted the informed consent for participation in the study.

✉ **Correspondence should be addressed:** Irina V. Kichuk
Ostrovityanova, 1, Moscow, 119021, Russia; mail2irina@mail.ru

Received: 30.10.2025 **Accepted:** 08.12.2025 **Published online:** 19.12.2025

DOI: 10.24075/brsmu.2025.080

ОЦЕНКА УРОВНЯ КАТЕХОЛАМИНОВ И СЕРОТОНИНА В КРОВИ ПРИ ТРЕВОЖНО-ДЕПРЕССИВНЫХ РАССТРОЙСТВАХ

Н. В. Соловьева[1], Н. А. Чупрова[1], К. В. Кочергина[2], А. А. Митрофанов[3], С. В. Чаусова[4], И. В. Кичук[4] ✉

[1] Научный центр персонализированной медицины, Москва, Россия
[2] Лечебно-диагностический центр Международного института биологических систем «Столица», Москва, Россия
[3] Научный центр психического здоровья, Москва, Россия
[4] Российский национальный исследовательский медицинский университет имени Н. И. Пирогова, Москва, Россия

В психиатрической практике существует необходимость разработки простых, патогенетически обоснованных и надежных биомаркеров для прогноза аффективного статуса пациентов в текущий момент и в ближайшей перспективе. Целью работы было провести анализ ассоциации аффективного статуса пациентов с непсихотическими расстройствами с уровнями катехоламинов и серотонина в периферической крови. Для оценки аффективного статуса использовали Госпитальную шкалу тревоги и депрессии (HADS). Концентрацию катехоламинов (адреналина, норадреналина и дофамина) в плазме и серотонина в сыворотке крови оценивали методом высокоэффективной жидкостной хроматографии (ВЭЖХ). В исследование вошли 114 человек с непсихотическими расстройствами, средний возраст составил 34,57 (SD = 10,36) лет, доля женщин — 64%. Мы не выявили достоверных прогностических эффектов уровней нейромедиаторов в периферической крови в отношении текущего аффективного статуса. Единственным маркером на уровне тенденции оказалось соотношение «серотонин / норадреналин», повышение значения которого снижает риск статуса клинической депрессии по HADS-D с учетом пола и возраста пациентов ($p = 0,059$). У пациентов с диагнозом рекуррентное депрессивное расстройство или депрессивный эпизод отмечено небольшое снижение уровня серотонина ($p = 0,068$) по сравнению с пациентами с диагнозами вне категории аффективных расстройств. В этой же группе обнаружена отрицательная корреляция между баллами по HADS-A (тревога) и уровнем норадреналина (Rs = –0,410, $p < 0,05$). Полученные результаты дают основания предполагать, что на расширенных клинически гомогенных выборках будет возможность подтверждения полученных предварительных результатов и получения новых данных.

Ключевые слова: депрессия, тревога, непсихотические психические расстройства, катехоламины, серотонин, биологические маркеры

Вклад авторов: Н. В. Соловьева, И. В. Кичук — концепция и дизайн исследования; Н. В. Соловьева, К. В. Кочергина, А. А. Митрофанов, И. В. Кичук — сбор и обработка материала; Н. А. Чупрова, К. В. Кочергина — статистическая обработка данных; А. А. Митрофанов, И. В. Кичук, Н. В. Соловьева, К. В. Кочергина — написание текста; А. А. Митрофанов, И. В. Кичук, Н. В. Соловьева, К. В. Кочергина, С. В. Чаусова — редактирование.

Соблюдение этических стандартов: исследование одобрено этическим комитетом Акционерного общества «Научный центр персонализированной медицины» (протокол № 33 от 01 декабря 2025 г.). Персональные данные участников были скрыты при проведении исследования. Все участники подписали добровольное информированное согласие на участие в исследовании.

✉ **Для корреспонденции:** Ирина Викторовна Кичук
ул. Островитянова, д. 1, г. Москва, 119021, Россия; mail2irina@mail.ru

Статья получена: 30.10.2025 **Статья принята к печати:** 08.12.2025 **Опубликована онлайн:** 19.12.2025

DOI: 10.24075/vrgmu.2025.080

According to the World Health Organization (WHO) data on mental health, more than a billion people in the world suffer from mental disorders. Moreover, a significant proportion of mental disorders are mood (affective) disorders, which include both depressive and anxiety disorders [1].

Depression is a chronic recurrent mental disorder manifesting most often in young and middle age that significantly affects the patients' quality of life and social functioning. Among mental disorders, depression plays the most important role in the structure of global burden of diseases. According to the WHO prognosis, it will become one of the leading causes of disability and mortality by the year 2030 [2]. These predictions are based on high prevalence of depression: the disorder is reported in 19% of the general population during life; in general, more than 350 million people all over the world are affected [2]. Furthermore, 30–50% of healthy people experience subclinical depression that does not meet the diagnostic criteria of mood disorders, but nevertheless is associated with the risk of developing the clinically significant disorder later in life [3].

In aggregate, life expectancy in patients with depression is reduced by more than 10 years [4].

Depression is associated with high risk of suicide, the second most common cause of death at the age of 15–29 years. About 800,000 people die from suicide worldwide annually [2]. The WHO data suggest that 2/3 of people, who had made suicide attempts, showed manifestations of depression. A total of 21% of patients suffering from depressive disorders make suicide attempts, a significant proportion of which are completed [5].

Symptoms of depression being an important element of many mental disorders constitute a significant part of clinical features, although these may not reach a clinically significant diagnostic level. Depression and anxiety tend to cluster in families and often overlap, which is also supported by the results of current genome-wide studies. From a clinical perspective, the combination of depression and anxiety is associated with a more severe course and a worse response to antidepressant therapy [6].

In real clinical practice, when treating patients with non-psychotic disorders, the patient's current affective status becomes a priority for the psychiatrist. There is a clear need to develop simple, pathogenetically substantiated and reliable biomarkers, the use of which could provide the physician with stable guidelines for predicting affective status in the near future [7].

Such markers may include levels of catecholamines and serotonin, assessed peripherally, for example, by analyzing the patient's blood.

It is believed that serotonin and catecholamines play an important role in the pathogenesis of depression and anxiety [8–10]; these are associated with the disease course severity [10]. Serotonin and catecholamines also modulate the response to therapy for mood disorders [11].

We have previously analyzed the relationship between serotonin levels and the clinical status of patients with depression [12, 13].

Considering the transdiagnostic nature of the depression and anxiety symptoms [14], as well as the important role of catecholamines and serotonin in the pathogenesis of most mental disorders, it seems appropriate to analyze the relationship between the current affective status and neurotransmitter levels. Most of the studies are focused on the analysis of neurotransmitter levels as the therapy efficacy markers [11, 15], as well as markers of the disease status within the framework of case-control studies [16, 17] and the development of the well-known kynurenine hypothesis of the etiology and pathogenesis of mental disorders [18].

In this study we assumed that peripheral blood neurotransmitter (catecholamine and serotonin) levels can be associated with the current affective status of patients with non-psychotic mental disorders, these can be used as biomarkers of the anxiety and depression symptom severity and for prediction of the patient's actual affective status.

The study aimed to analyze the association of the affective status of patients with mood disorders with the peripheral blood catecholamine and serotonin levels.

METHODS

Patients

The study involved patients with non-psychotic mental disorders aged 18–65 years, who contacted the Scientific Centre of Personalized Medicine (Moscow) seeking outpatient care. Inclusion criteria: the fact of having a disorder diagnosed within the last month in accordance with the ICD-10 criteria by a psychiatrist: bipolar affective disorder, current episode mild or moderate depression (F31.3), depressive episode (F32), recurrent depressive disorder (F33), dysthymia (F34.1), Other recurrent mood (affective) disorders (F38.1), other anxiety disorders (F41), obsessive-compulsive disorder (F42), somatoform disorders (F45). Exclusion criteria: schizophrenic spectrum disorders, psychotic level of bipolar affective disorder, psychoactive substance addiction, exacerbation of chronic disorder, history of seizures.

Psychometric assessment

The subjects' current affective status was assessed using the Hospital Anxiety and Depression Scale (HADS) [19]; the HADS Russian version was used [20]. The scale has two independent subscales: depression symptoms (HADS-D) and anxiety symptoms (HADS-A). The scale gradations are as follows: score 0–7 баллов — no anxiety or depression symptoms, score 8–10 баллов — subclinical anxiety or depression manifestations, score 10 or more — clinical anxiety or depression manifestations. Based on individual HADS scores the patient's status was recorded in accordance with the gradations, along with the anxiety/depression (A/D) score ratio as a ratio of the anxiety score (HADS-A) to the depression score (HADS-D).

Biochemical testing

Concentrations of catecholamines (adrenaline, norepinephrine, and dopamine) in blood plasma and serotonin concentrations in blood serum were assessed by high-performance liquid chromatography (HPLC). Blood sampling was performed in the fasting state on the day of the questionnaire survey; the samples were transferred to the Chromolab laboratory (Moscow, Russia) for analysis. Both neurotransmitter levels itself and the ratios of those (serotonin/dopamine, serotonin/norepinephrine, serotonin/adrenaline, norepinephrine/dopamine, norepinephrine/adrenaline, adrenaline/dopamine) were used for analysis, which could be informative indirect indicators of the neurotransmission state.

Study design

The study was cross-sectional and comparative. All patient information was obtained during a single visit. To assess the association of the current affective status with neurotransmitter levels, groups were allocated in accordance with the current affective status based on the HADS-D and HADS-A scores,

Table 1. Comparison of patients with clinical anxiety based on HADS-A with other patients

	Clinical anxiety HADS-A			Other (normal and subclinical anxiety) HADS-A			*U*	*p*
	n = 92			*n* = 22				
	Mean value	SD	Me (Q_1; Q_3)	Mean value	SD	Me (Q_1; Q_3)		
Age (years)	35.53	10.036	33.5 (28; 43)	32.24	11.09	30 (23; 35)	797.5	0.123
Serotonin (SER), ng/mL	117.72	78.33	95.2 (56; 184.25)	95.68	65.99	81 (44.21; 125.1)	899.5	0.419
Dopamine (DA), ng/mL	44.31	56.69	34.62 (16.9; 53)	43.4	47.19	30 (15; 44.5)	860.5	0.525
Adrenaline (A), ng/mL	52.34	50.9	37.2 (23; 68.5)	43.18	39.55	33.39 (26.5; 46.2)	832.5	0.397
Norepinephrine (HE), ng/mL	346.56	183.21	319.6 (223; 432)	323.73	213.02	279 (186; 389)	811.5	0.315
Serotonin/Dopamine (SER/DA)	5.5	5.71	3.69 (1.57; 7.13)	6.3	10.96	2.93 (1.21; 7.36)	898	0.723
Serotonin/Norepinephrine	0.626	1.5	0.329 (0.18; 0.58)	0.357	0.24	0.29 (0.16; 0.63)	870	0.572
Serotonin/Adrenaline	4.015	4.73	2.41 (1.43; 5.48)	3.959	5.524	1.93 (1.06; 4.09)	857	0.508
Norepinephrine/Dopamine	16.57	16.92	9.27 (5.68; 20.91)	21.66	38.56	9.42 (6.53; 16.09)	930	0.91
Norepinephrine/Adrenaline	11.82	10.93	7.9 (3.94; 15.92)	11.48	9.45	7.98 (4.69; 18.68)	907	0.775
Adrenaline/Dopamine	2.17	1.75	1.34 (0.77; 2.36)	2	2.08	1.4 (0.78; 2.56)	940	0.97

Note: *p* — asymptote (bilateral), *U* — Mann–Whitney *U*-test.

regardless of the clinical diagnosis. These groups were compared with each other based on biochemical indicator levels. The correlation analysis was performed for the relationship between biochemical indicators and the HADS-D and HADS-A scores, along with the regression analysis for the estimated HADS-D and HADS-A scores predicted based on biochemical indicators.

In the second phase, the diagnostic groups of patients (depression, anxiety, other) were compared with each other based on biochemical indicator values to assess a possible relationship between the diagnosis and neurotransmitter levels. Regression models adjusted for sex and age were constructed when finding significant intergroup differences.

Statistical processing

Statistical analysis was performed using SPSS 23.0. The distribution of most test variables was non-normal (Kolmogorov–Smirnov test), therefore, nonparametric methods were used. The nonparametric Mann–Whitney *U*-test was used to compare the groups based on quantitative variables. To assess the factors for prediction of clinical depression/anxiety based on the HADS scores, the logistic regression (stepwise) method using a dependent binary variable (present/absent) adjusted for sex and age was used. Linear regression was applied to assess the possibility of predicting the HADS-D and HADS-A scores based on neurotransmitter levels.

Spearman's rank correlation was used in the common cohort and diagnostic groups to assess the correlations between the HADS-D and HADS-A scores, as well as between the A/D ratio and the concentrations of catecholamines and serotonin.

RESULTS

A total of 114 individuals were enrolled, the average age was 34.57 (SD = 10.36) years, the share of females was 64% (73 individuals). The average HADS-D score of the sample was 14.83 (SD = 4.752); the HADS-A score was 19.29 (SD = 7.397).

Current affective status

For further analysis the sample was divided into groups based on the presence of depression and anxiety according to HADS. It was found that in the sample there were only five subjects with the HADS-A scores below 7 (0–7) ("normal") and six subjects with the HADS-D scores below 7 (0–7) ("normal"). In this regard, further analysis was conducted in two comparison groups: "Clinical Depression/Anxiety" and "Other" (normal and subclinical depression/anxiety). The analysis was conducted independently for anxiety and depression.

Patients with clinical anxiety (HADS-A) accounting for 80.7% of the sample (92 individuals) did not differ from other patients in age, neurotransmitter levels and their ratios (Table 1).

Patients with clinical depression (HADS-D) accounting for 75.4% of the cohort (86 individuals) showed a trend towards lower average serotonin/norepinephrine ratio values (0.39 (0.38)) compared to the "Other" group (1.19 (2.66), $p = 0.084$) (Table 2).

Then a regression model was constructed to predict the clinical depression status, including the serotonin/norepinephrine ratio and the relationship with sex, clinical diagnoses, as well as age and sex as covariates, explaining 20.8% of variance (Nagelkerke R Square = 0.208) and predicting 78.2% of possible outcome. It has been found that the presence of depression symptoms based on the HADS-A score ($p = 0.011$) and the increase in serotonin/norepinephrine ratio values ($p = 0.059$, trend) reduce the risk of clinical depression status according to HADS-D independently, considering the patients' sex and age (Table 3).

Comparison of diagnostic groups

For further analysis the cohort of patients was divided based on the clinical diagnosis (depression, anxiety, and other). The pairwise comparison of the diagnostic groups based on biochemical indicators was conducted. The "Depression" diagnostic group (RDD, depressive episode) accounted for 29.8% of the sample (34 subjects), "Anxiety" (anxiety disorders) — 41.2% (47 subjects), "Other" (other diagnoses) — 28.9% (33 subjects).

No differences in neurotransmitter levels and their ratios between the "Depression" and "Anxiety" (Table 4) and "Anxiety" and "Other" (Table 5) groups were revealed. In the "Depression" group, the average serotonin levels show a downward trend ($p = 0.068$) relative to the "Other" group (Table 6), but this result has not been confirmed by the regression analysis.

The analysis of the correlations between the HADS-D and HADS-A scores and neurotransmitter levels in the common cohort of patients revealed no significant correlations. The same analysis conducted separately in diagnostic subgroups

Table 2. Comparison of patients with clinical depression based on HADS-D with other patients

	Clinical depression HADS-D *n* = 86			Other (normal and subclinical depression) HADS-D *n* = 28			*U*	*p*
	Mean value	SD	Me (Q_1; Q_3)	Mean value	SD	Me (Q_1; Q_3)		
Age (years)	35.15	10.183	33 (27; 43)	34.12	10.727	31.5 (28.75; 40)	1097	0.481
Serotonin, ng/mL	111.16	75.15	88.11 (56; 178)	121.36	81.24	95.2 (48.57; 181.75)	1137.5	0.662
Dopamine, ng/mL	39.44	34.34	32.9 (17.1; 49.1)	59.5	94.56	30.65 (11.23; 58.73)	1074	0.829
Adrenaline, ng/mL	46.67	35.52	36.95 (24.4; 65)	63.49	77.9	36.5 (17.58; 79.75)	1071	0.813
Norepinephrine, ng/mL	354.96	177.54	315 (243.25; 470.57)	300.67	218.84	293.49 (140.6; 388.2)	885.5	0.126
Serotonin/Dopamine	4.9	5.28	3.35 (1.3; 6.1)	8.11	10.52	4.9 (1.73; 10.05)	922	0.203
Serotonin/Norepinephrine	0.39	0.38	0.3 (0.17; 0.52)	1.19	2.66	0.41 (0.22; 0.8)	857	0.084
Serotonin/Adrenaline	4.04	5.19	2.1 (1.47; 4.9)	3.89	3.65	3.14 (0.99; 5.98)	1082	0.873
Norepinephrine/Dopamine	16	16.13	9.93 (5.9; 17.7)	22.55	36.3	7.04 (4.4; 35.9)	1032	0.611
Norepinephrine/Adrenaline	12.39	11.07	8.77 (4.6; 16.1)	9.7	8.9	5.76 (3.4; 18.2)	889	0.133
Adrenaline/Dopamine	1.97	2.19	1.25 (0.7; 2.3)	2.71	3.59	1.59 (0.9; 2.6)	948	0.274

Note: *p* — asymptote (bilateral), *U* — Mann–Whitney *U*-test.

revealed only one correlation (HADS-A) — norepinephrine in the "Other" diagnostic group (Rs = –0.410, $p < 0.05$). According to the linear regression results adjusted for sex and age in the common cohort of patients, neurotransmitter levels and their ratios do not predict the HADS-A (F = 0.573, $p = 0.751$) and HADS-D (F = 0.434, $p = 0.854$) scores, as well as the A/D ratio (F = 0.814, $p = 0.561$).

DISCUSSION

The presence of platelet serotonin is the most reliable indicator of serotonin metabolism disorder in the central nervous system. Platelets are considered as an extracerebral model of serotonergic neurons. A highly significant correlation between serotonin levels in platelets and cerebrospinal fluid was found [22].

Serum serotonin is primarily platelet serotonin, and the changes in serum serotonin levels allow one to indirectly assess the activity of the brain serotonergic system. In this regard, we chose serum serotonin for the study.

In our study involving a small cohort of patients with non-psychotic mental disorders, we have revealed no significant prognostic effects of the peripheral blood neurotransmitter (catecholamine and serotonin) levels relative to the current affective status. At a trend level, the only marker was the serotonin/norepinephrine ratio, the increase in which reduced the risk of the clinical depression status according to HADS-D considering the patients' sex and age ($p = 0.059$). Furthermore, in the group of patients diagnosed with recurrent depressive disorder or depressive episode, there was a slight decrease in serotonin levels ($p = 0.068$) compared to patients

Table 3. Clinical depression prognosis (HADS-D) regression analysis results

	B	SE	Wald	Degree of freedom	*p*	Exp (B)	95% confidence interval for EXP(B)	
							Lower	Upper
Serotonin/Norepinephrine	–0.948	0.502	3.569	1	0.059	0.387	0.145	1.036
Clinical diagnosis of depression	–0.81	0.826	0.962	1	0.327	0.445	0.088	2.244
Clinical diagnosis of anxiety	–1.877	0.734	6.546	1	0.011	0.153	0.036	0.645
Constant	2.838	0.751	14.27	1	0	17.085		

Note: SE — standard error of the mean. Model characteristics: $X^2 = 16.398$, $p = 0.001$; –2 Log-likelihood=103.909.

Table 4. Comparison of patients with the clinical diagnoses of depression and anxiety based on biochemical indicators

	Depression *n* = 34			Anxiety *n* = 47			*U*	*p*
	Mean value	SD	Me (Q_1; Q_3)	Mean value	SD	Me (Q_1; Q_3)		
Age	34.5	11.67	32.5 (25.5; 39.5)	35.87	10.04	33.5 (28; 44.25)	705	0.368
Serotonin, ng/mL	100.81	70.31	76.84 (43.6; 171)	105.64	67.44	91.55 (50; 169.75)	748	0.625
Dopamine, ng/mL	44.32	49.82	30.5 (15.65; 46.84)	41.15	42.04	35 (18; 53)	685	0.604
Adrenaline, ng/mL	40.06	32.67	32.24 (25.25; 44.24)	61.76	66.14	47.1 (17.72; 76.5)	607.5	0.192
Norepinephrine, ng/mL	329.95	184.71	306.1 (207.1; 379.6)	341.05	196.75	310 (214.75; 422.5)	720	0.871
Serotonin/Dopamine	5.83	9.29	3.14 (1.12; 6.43)	4.75	4.53	3.45 (1.59; 7.13)	732	0.968
Serotonin/Norepinephrine	0.34	0.22	0.3 (0.16; 0.49)	0.64	1.84	0.28 (0.18; 0.52)	713	0.815
Serotonin/Adrenaline	4.11	4.94	1.95 (1.06; 6.08)	3.9	5.79	2.14 (1; 4.8)	723	0.895
Norepinephrine/Dopamine	20.37	32.8	10.03 (6.25; 16.4)	15.11	15.29	8.86 (5.65; 18.18)	697	0.692
Norepinephrine/Adrenaline	11.5	8.17	9.22 (4.58; 15.7)	11.6	11.6	6.78 (3.84; 17.87)	646	0.361
Adrenaline/Dopamine	1.84	1.96	1.16 (0.66; 2.27)	2.35	3.07	1.38 (0.79; 2.43)	666.5	0.48

Note: *p* — asymptote (bilateral), *U* — Mann–Whitney *U*-test.

Table 5. Comparison of patients with the clinical diagnoses of anxiety and "Other" based on biochemical indicators

	Anxiety $n = 47$			Other $n = 32$			U	p
	Mean value	SD	Me (Q_1; Q_3)	Mean value	SD	Me (Q_1; Q_3)		
Age	35.87	10.04	33.5 (28; 44.25)	34.19	9.38	33 (27.3; 42.8)	710	0.675
Serotonin, ng/mL	105.64	67.44	91.55 (50; 169.75)	134.99	90.43	103.79 (61.1; 194)	628.5	0.217
Dopamine, ng/mL	41.15	42.04	35 (18; 53)	49.33	74.4	36.87 (13.21; 56.5)	712	0.807
Adrenaline, ng/mL	61.76	66.14	47.1 (17.72; 76.5)	45.19	27.33	37.73 (25; 69.75)	695.5	0.681
Norepinephrine, ng/mL	341.05	196.75	310 (214.75; 422.5)	356.48	187.74	344 (208.48; 483)	685	0.604
Serotonin/Dopamine	4.75	4.53	3.45 (1.59; 7.13)	6.27	6.72	4.2 (1.59; 8.72)	654	0.405
Serotonin/Norepinephrine	0.64	1.84	0.28 (0.18; 0.52)	0.71	1.22	0.4 (0.19; 0.71)	641	0.335
Serotonin/Adrenaline	3.9	5.79	2.14 (1; 4.8)	4.04	3.26	2.55 (1.62; 6.17)	609	0.197
Norepinephrine/Dopamine	15.11	15.29	8.86 (5.65; 18.18)	17.59	18.72	8.36 (5.6; 30.8)	710	0.792
Norepinephrine/Adrenaline	11.6	11.6	6.78 (3.84; 17.87)	12.4	11.71	7.95 (4.02; 19.37)	692	0.655
Adrenaline/Dopamine	2.35	3.07	1.38 (0.79; 2.43)	2.04	2.38	1.43 (0.73; 2.5)	689.5	0.637

Note: p — asymptote (bilateral), U — Mann–Whitney U-test.

Table 6. Comparison of patients with the clinical diagnoses of depression and "Other" based on biochemical indicators

	Depression $n = 34$			Other $n = 32$			U	p
	Mean value	SD	Me (Q_1; Q_3)	Mean value	SD	Me (Q_1; Q_3)		
Age	34.5	11.67	32.5 (25.5; 39.5)	34.19	9.38	33 (27.3; 42.8)	503	0.599
Serotonin, ng/mL	100.81	70.31	76.84 (43.6; 171)	134.99	90.43	103.79 (61.1; 194)	402	0.068
Dopamine, ng/mL	44.32	49.82	30.5 (15.65; 46.84)	49.33	74.4	36.87 (13.21; 56.5)	471	0.582
Adrenaline, ng/mL	40.06	32.67	32.24 (25.25; 44.24)	45.19	27.33	37.73 (25; 69.75)	438.5	0.324
Norepinephrine, ng/mL	329.95	184.71	306.1 (207.1; 379.6)	356.48	187.74	344 (208.48; 483)	441.5	0.344
Serotonin/Dopamine	5.83	9.29	3.14 (1.12; 6.43)	6.27	6.72	4.2 (1.59; 8.72)	447.5	0.386
Serotonin/Norepinephrine	0.34	0.22	0.3 (0.16; 0.49)	0.71	1.22	0.4 (0.19; 0.71)	411	0.175
Serotonin/Adrenaline	4.11	4.94	1.95 (1.06; 6.08)	4.04	3.26	2.55 (1.62; 6.17)	426	0.248
Norepinephrine/Dopamine	20.37	32.8	10.03 (6.25; 16.4)	17.59	18.72	8.36 (5.6; 30.8)	493	0.799
Norepinephrine/Adrenaline	11.5	8.17	9.22 (4.58; 15.7)	12.4	11.71	7.95 (4.02; 19.37)	477	0.638
Adrenaline/Dopamine	1.84	1.96	1.16 (0.66; 2.27)	2.04	2.38	1.43 (0.73; 2.5)	488	0.747

Note: p — asymptote (bilateral), U — Mann–Whitney U-test.

with psychiatric diagnoses that were beyond the category of mood disorders. It is interesting that it is this group, where the only correlation between the HADS-A scores (anxiety) and norepinephrine levels (Rs = –0.410, $p < 0.05$) has been found: the higher the anxiety score, the lower the norepinephrine level.

The study conducted is the first with such design; there is no possibility to directly compare the results with that of previous studies. The relationship between the anxiety severity and the functioning of stress response systems, in particular autonomic regulation with active involvement of noradrenergic mechanisms, is well known [21], and our results confirm these views. The serotonin/norepinephrine ratio may indirectly reflect, with known limitations, the interaction of autonomic mechanisms (norepinephrine) and emotional regulation systems (serotonin). The fact that we have received confirmation of the influence of this marker on affective status regardless of the formal psychiatric diagnosis may be a serious reason to continue research in this area using larger samples.

Study limitations

The reported pilot study involved small samples of subjects, which considerably limited the possibilities of data interpretation. The objective of the study was to assess the relationship between neurotransmitter levels and affective status. The affective status was assessed using the simple HADS screening self-report questionnaire, without the use of any clinical psychometric instruments. The HADS scale is successfully used for screening of anxiety and depression symptoms all over the world and in our country. The HADS scale was recently tested in a large online population-based study of depression in the Russian population [23], and a correct validation of this scale was carried out in the Russian general population [24].

CONCLUSIONS

The preliminary pilot study involving a mixed cohort of patients has revealed no significant associations between the patient's current affective status and peripheral blood catecholamine and serotonin levels. However, the effect of norepinephrine and the serotonin/norepinephrine ratio on the affective status of patients with clinical depression has been revealed. This suggests that in the next phase of the study involving larger and more homogeneous samples it will be possible to confirm preliminary results and obtain new data.

References

1. WHO. World mental health report: Transforming mental health for all. 2022.
2. World Health Organization. The Global Burden of Disease. [cited 2024 Mar 24]. Available from: https://www.who.int/healthinfo/global_burden_disease/estimates/en/index1.html.
3. Lewinsohn PM, Shankman SA, Gau JM, Klein DN. The prevalence and co-morbidity of subthreshold psychiatric conditions. Psychol Med. 2004; 34 (4): 613–22. DOI: 10.1017/S0033291703001466.
4. Chang C-K, Hayes RD, Perera G, Broadbent MTM, Fernandes AC, Lee WE, et al. Life Expectancy at Birth for People with Serious Mental Illness and Other Major Disorders from a Secondary Mental Health Care Case Register in London. PLoS One. 2011; 6 (5): Available from: e19590. DOI: 10.1371/journal.pone.0019590.
5. Bachmann S. Epidemiology of Suicide and the Psychiatric Perspective. Int J Environ Res Public Health. 2018; 15(7): 1425. DOI: 10.3390/ijerph15071425.
6. Mazo GM, Kasyanov ED, Kibitov AO. Mercayushchaya gran' mezhdu depressiej i trevogoj: klinicheskie i geneticheskie aspekty. Social'naya i klinicheskaya psihiatriya. 2022; 32 (4): 50–8. Russian.
7. Neznanov NG, Martynihin IA, Mosolov SN. Diagnostika i terapiya trevozhnyh rasstrojstv v Rossijskoj Federacii: rezul'taty oprosa vrachej-psihiatrov. Sovremennaya terapiya psihicheskih rasstrojstv. 2017; 2: 2–13. Russian.
8. Mosolov SN. Sovremennye biologicheskie gipotezy rekurrentnoj depressii (obzor). ZHurnal nevrologii i psihiatrii im. S. S. Korsakova. 2012; 122 (11–22): 29–40. Russian.
9. Lee E-H, Han P-L. Reciprocal interactions across and within multiple levels of monoamine and cortico-limbic systems in stress-induced depression: A systematic review. Neurosci Biobehav Rev. 2019; 101: 13–31. DOI: 10.1016/j.neubiorev.2019.03.014.
10. Wang L, Yang P, Yang C, Yang D, Wu X, Cao T, et al. Disturbance of neurotransmitter metabolism in drug-naïve, first-episode major depressive disorder: a comparative study on adult and adolescent cohorts. Eur Arch Psychiatry Clin Neurosci. 2022; 272 (7): 1283–96. DOI: 10.1007/s00406-022-01406-8.
11. Jeuring HW, D'Angremont E, Tol JMH, Risselada AJ, Sommer IEC, Oude Voshaar RC. The effectiveness of off-label dopamine stimulating agents in depressive disorder: A systematic review and meta-analysis. Psychiatry Res. 2023; 319: 115010. DOI: 10.1016/j.psychres.2022.115010.
12. Kichuk IV, Petrova EA, Mitrofanov AA, Soloveva NV, Vilyanov VB. Izmeneniya pokazatelej elektroencefalogrammy i koncentracii serotonina pri depressivnyh i trevozhnyh rasstrojstvah. Nevrologiya, nejropsihiatriya, psihosomatika. 16AD; 8 (3): 34–8. Russian.
13. Soloveva NV, Zvezdin VA, Urnyaeva SI, Mosova UV, Sokolov RV, Vilyanov VB. Soderzhanie biogennyh monoaminov v syvorotke krovi bol'nyh s endogennymi i ekzogennymi psihicheskimi rasstrojstvami. Akademicheskij zhurnal zapadnoj sibiri. 2013; 9 1 (44): 42–3. Russian.
14. Solmi M, Cortese S, Vita G, De Prisco M, Radua J, Dragioti E, et al. An umbrella review of candidate predictors of response, remission, recovery, and relapse across mental disorders. Mol Psychiatry. 2023; 28 (9): 3671–87. DOI: 10.1038/s41380-023-02298-3.
15. Li X, Fan Y, Xiao S, Peng S, Dong X, Zheng X, et al. Decreased platelet 5-hydroxytryptamin (5-HT) levels: a response to antidepressants. J Affect Disord. 2015; 187: 84–90. DOI: 10.1016/j.jad.2015.08.025.
16. Pech J, Forman J, Kessing LV, Knorr U. Poor evidence for putative abnormalities in cerebrospinal fluid neurotransmitters in patients with depression versus healthy non-psychiatric individuals: A systematic review and meta-analyses of 23 studies. J Affect Disord. 2018; 240: 6–16. DOI: 10.1016/j.jad.2018.07.031.
17. Esler M, Alvarenga M, Barton D, Jennings G, Kaye D, Guo L, et al. Measurement of Noradrenaline and Serotonin Metabolites With Internal Jugular Vein Sampling: An Indicator of Brain Monoamine Turnover in Depressive Illness and Panic Disorder. Front Psychiatry. 2022; 13. DOI: 10.3389/fpsyt.2022.818012.
18. Pompili M, Lionetto L, Curto M, Forte A, Erbuto D, Montebovi F, et al. Tryptophan and Kynurenine Metabolites: Are They Related to Depression? Neuropsychobiology. 2019; 77(1): 23–8. DOI: 10.1159/000491604.
19. Zigmond AS, Snaith RP. The Hospital Anxiety and Depression Scale. Acta Psychiatr Scand. 1983; 67 (6): 361–70. DOI: 10.1111/j.1600-0447.1983.tb09716.x.
20. Andryushchenko A. V., Drobizhev M. YU., Dobrovol'skij A. V. Sravnitel'naya ocenka shkal CES-D, BDI i HADS v diagnostike depressij v obshchemedicinskoj praktike. ZHurnal nevrologii i psihiatrii im. S. S. Korsakova. 2003; (5): 11–8.
21. Kalisch R, Russo SJ, Müller MB. Neurobiology and systems biology of stress resilience. Physiol Rev. 2024. DOI: 10.1152/physrev.00042.2023.
22. Bezrukov MV, Shilov YuE, Shestakova NV, Klyushnik TP. Biologicheskaya ocenka vyrazhennosti depressii: novyj metod opredeleniya koncentracii trombocitarnogo serotonina. ZHurnal nevrologii i psihiatrii im. S. S. Korsakova. 2014; 114 (8): 51–57. Russian.
23. Kibitov AA, Rakitko AS, Kasyanov ED, Rukavishnikov GV, Kozlova KA, Ilinsky VV, et al. Screening of Depressive Symptoms in a Russian General Population Sample: A Web-based Cross-sectional Study. Clin Pract Epidemiol Ment Heal. 2021; 17 (1): 205–11. DOI: 10.2174/1745017902117010205.
24. Morozova MA, Potanin SS, Beniashvili AG, Burminskij DS, Lepilkina TA, Rupchev GE, i dr. Validaciya russkoyazychnoj versii gospital'noj shkaly trevogi i depresii v obshchej populyacii. Profilakticheskaya medicina. 2023; 26 (4): 7–14.

Литература

1. WHO. World mental health report: Transforming mental health for all. 2022.
2. World Health Organization. The Global Burden of Disease. [cited 2024 Mar 24]. Available from: https://www.who.int/healthinfo/global_burden_disease/estimates/en/index1.html.
3. Lewinsohn PM, Shankman SA, Gau JM, Klein DN. The prevalence and co-morbidity of subthreshold psychiatric conditions. Psychol Med. 2004; 34 (4): 613–22. DOI: 10.1017/S0033291703001466.
4. Chang C-K, Hayes RD, Perera G, Broadbent MTM, Fernandes AC, Lee WE, et al. Life Expectancy at Birth for People with Serious Mental Illness and Other Major Disorders from a Secondary Mental Health Care Case Register in London. PLoS One. 2011; 6 (5): Available from: e19590. DOI: 10.1371/journal.pone.0019590.
5. Bachmann S. Epidemiology of Suicide and the Psychiatric Perspective. Int J Environ Res Public Health. 2018; 15(7): 1425. DOI: 10.3390/ijerph15071425.
6. Мазо Г. М., Касьянов Е. Д., Кибитов А. О. Мерцающая грань между депрессией и тревогой: клинические и генетические аспекты. Социальная и клиническая психиатрия. 2022; 32 (4): 50–8.
7. Незнанов Н. Г., Мартынихин И. А., Мосолов С. Н. Диагностика и терапия тревожных расстройств в Российской Федерации: результаты опроса врачей-психиатров. Современная терапия психических расстройств. 2017; 2: 2–13.
8. Мосолов С. Н. Современные биологические гипотезы рекуррентной депрессии (обзор). Журнал неврологии и психиатрии им. С. С. Корсакова. 2012; 122 (11–22): 29–40.
9. Lee E-H, Han P-L. Reciprocal interactions across and within multiple levels of monoamine and cortico-limbic systems in stress-induced depression: A systematic review. Neurosci Biobehav Rev. 2019; 101: 13–31. DOI: 10.1016/j.neubiorev.2019.03.014.
10. Wang L, Yang P, Yang C, Yang D, Wu X, Cao T, et al. Disturbance of neurotransmitter metabolism in drug-naïve, first-episode major depressive disorder: a comparative study on adult and adolescent cohorts. Eur Arch Psychiatry Clin Neurosci. 2022; 272 (7): 1283–96. DOI: 10.1007/s00406-022-01406-8.
11. Jeuring HW, D'Angremont E, Tol JMH, Risselada AJ, Sommer IEC, Oude Voshaar RC. The effectiveness of off-label dopamine stimulating agents in depressive disorder: A systematic review

and meta-analysis. Psychiatry Res. 2023; 319: 115010. DOI: 10.1016/j.psychres.2022.115010.
12. Кичук И. В., Петрова Е. А., Митрофанов А. А., Соловьева Н. В., Вильянов В. Б. Изменения показателей электроэнцефалограммы и концентрации серотонина при депрессивных и тревожных расстройствах. Неврология, нейропсихиатрия, психосоматика. 16AD; 8 (3): 34–8.
13. Соловьева Н. В., Звездин В. А., Урняева С. И., Мосова У. В., Соколов Р. В., Вильянов В. Б. Содержание биогенных моноаминов в сыворотке крови больных с эндогенными и экзогенными психическими расстройствами. Академический журнал западной сибири. 2013; 9 1 (44): 42–3.
14. Solmi M, Cortese S, Vita G, De Prisco M, Radua J, Dragioti E, et al. An umbrella review of candidate predictors of response, remission, recovery, and relapse across mental disorders. Mol Psychiatry. 2023; 28 (9): 3671–87. DOI: 10.1038/s41380-023-02298-3.
15. Li X, Fan Y, Xiao S, Peng S, Dong X, Zheng X, et al. Decreased platelet 5-hydroxytryptamin (5-HT) levels: a response to antidepressants. J Affect Disord. 2015; 187: 84–90. DOI: 10.1016/j.jad.2015.08.025.
16. Pech J, Forman J, Kessing LV, Knorr U. Poor evidence for putative abnormalities in cerebrospinal fluid neurotransmitters in patients with depression versus healthy non-psychiatric individuals: A systematic review and meta-analyses of 23 studies. J Affect Disord. 2018; 240: 6–16. DOI: 10.1016/j.jad.2018.07.031.
17. Esler M, Alvarenga M, Barton D, Jennings G, Kaye D, Guo L, et al. Measurement of Noradrenaline and Serotonin Metabolites With Internal Jugular Vein Sampling: An Indicator of Brain Monoamine Turnover in Depressive Illness and Panic Disorder. Front Psychiatry. 2022; 13. DOI: 10.3389/fpsyt.2022.818012.
18. Pompili M, Lionetto L, Curto M, Forte A, Erbuto D, Montebovi F, et al. Tryptophan and Kynurenine Metabolites: Are They Related to Depression? Neuropsychobiology. 2019; 77(1): 23–8. DOI: 10.1159/000491604.
19. Zigmond AS, Snaith RP. The Hospital Anxiety and Depression Scale. Acta Psychiatr Scand 1983; 67 (6): 361–70. DOI: 10.1111/j.1600-0447.1983.tb09716.x.
20. Андрющенко А. В., Дробижев М. Ю., Добровольский А. В. Сравнительная оценка шкал CES-D, BDI и HADS в диагностике депрессий в общемедицинской практике. Журнал неврологии и психиатрии им. С. С. Корсакова. 2003; (5): 11–8.
21. Kalisch R, Russo SJ, Müller MB. Neurobiology and systems biology of stress resilience. Physiol Rev. 2024. DOI: 10.1152/physrev.00042.2023.
22. Безруков М. В., Шилов Ю. Е., Шестакова Н. В., Клюшник Т. П. Биологическая оценка выраженности депрессии: новый метод определения концентрации тромбоцитарного серотонина. Журнал неврологии и психиатрии им. С. С. Корсакова. 2014; 114 (8): 51–57.
23. Kibitov AA, Rakitko AS, Kasyanov ED, Rukavishnikov GV, Kozlova KA, Ilinsky VV, et al. Screening of Depressive Symptoms in a Russian General Population Sample: A Web-based Cross-sectional Study. Clin Pract Epidemiol Ment Heal. 2021; 17 (1): 205–11. DOI: 10.2174/1745017902117010205.
24. Морозова М. А., Потанин С. С., Бениашвили А. Г., Бурминский Д. С., Лепилкина Т. А., Рупчев Г. Е., и др. Валидация русскоязычной версии госпитальной шкалы тревоги и депресии в общей популяции. Профилактическая медицина. 2023; 26 (4): 7–14.

RECONSOLIDATION OF EARLY MEMORIES IN RELIVING THE TRAUMATIC COMBAT EXPERIENCE

Petrash EA[1] ✉, Uynina-Pakulova NYu[1], Kuryishina SA[1], Karpenko AS[2], Kuznetsova AA[3]

[1] Pirogov Russian National Research Medical University, Moscow, Russia

[2] Moscow State Institute of International Relations of the Ministry of Foreign Affairs of the Russian Federation, Moscow, Russia

[3] Kursk State Medical University of the Russian Ministry of Health, Kursk, Russia

Memory in all the variety of the types and processes ensuring its functioning has a psychotherapeutic resource that is realized when working with manifestations of post-traumatic stress disorder (PTSD). One of these is obsessive repetitive memories with traumatic content. The study aimed to look into reconsolidation of early memories in reliving the traumatic experience of participation in combat. The total sample size was 62 individuals (males aged 21–46 years). The experimental group included 31 respondents with combat experience having the status of war veterans (the average period of participation was 1 year and 5 months). The control group consisted of 31 respondents with no combat experience. The Mini-Mental State Examination (MMSE) scale, set of functional neuropsychological tests ("10 Words" by A.R. Luria, "Pictograms" method by A.R. Luria, "Difficult-to-Verbalize Figures" by T.V. Akhutina, "Rhythm Reproduction Test" by A.R. Luria), analysis of the transcripts of audio recordings of early memories were used. It has been reliably found that the early memory of a positive, negative or neutral modality resulting from the influence of combat experience is changed through the reconsolidation mechanism, which is reflected in the linguistic and semantic parameters. The linguistic and semantic structure of the combat veterans' early memories is characterized by the event-based model, with a predominance of verbs and adverbs. The semantic core of the combat veterans' early memories is more often negatively colored, despite the general ambivalent or positive modality.

Keywords: early memories, autobiographical memory, combat experience, reconsolidation

Author contribution: all authors contributed to study planning, literature review, data acquisition, analysis, and interpretation equally.

Compliance with ethical standards: the study was approved by the Ethics Committee of the Pirogov Russian National Research Medical University (protocol No. 13 dated 23 November 2023), and conducted in accordance with the requirements of Fundamentals of legislation "On Protection of Public Health"; all subjects submitted the informed consent to assessment.

✉ **Correspondence should be addressed:** Ekaterina A. Petrash
Ostrovityanova, 1, Moscow, 117997, Russia; petrash@mail.ru

Received: 25.10.2025 **Accepted:** 22.11.2025 **Published online:** 11.12.2025

DOI: 10.24075/brsmu.2025.069

Copyright: © 2025 by the authors. **Licensee:** Pirogov University. This article is an open access article distributed under the terms and conditions of the Creative Commons Attribution (CC BY) license (https://creativecommons.org/licenses/by/4.0/).

РЕКОНСОЛИДАЦИЯ РАННИХ ВОСПОМИНАНИЙ В ПЕРЕЖИВАНИЯХ ТРАВМАТИЧЕСКОГО ОПЫТА УЧАСТИЯ В БОЕВЫХ ДЕЙСТВИЯХ

Е. А. Петраш[1] ✉, Н. Ю. Юнина-Пакулова[1], С. А. Курышина[1], А. С. Карпенко[2], А. А. Кузнецова[3]

[1] Российский национальный исследовательский медицинский университет имени Н. И. Пирогова, Москва, Россия

[2] Московский государственный институт международных отношений МИД Российской Федерации, Москва, Россия

[3] Курский государственный медицинский университет Минздрава России, Курск, Россия

Память во всем многообразии видов и процессов, обеспечивающих ее функционирование, обладает психотерапевтическим ресурсом, который реализуется при работе с проявлениями посттравматического стрессового расстройства (ПТСР). Одним из них являются навязчивые повторяющиеся воспоминания с травматическим содержанием. Цель данного исследования — изучить реконсолидацию ранних воспоминаний в переживаниях травматического опыта участия в боевых действиях. Общий объем выборки составил 62 человека (мужчины в возрасте 21–46 лет). В экспериментальную группу вошли 31 респондент с опытом участия в боевых действиях в статусе ветерана боевых действий (средний срок участия составил 1 год 5 месяцев). Контрольная группа состояла из 31 респондента без опыта участия в боевых действиях. Использовали Краткую шкалу оценки психического статуса (MMSE), набор функциональных нейропсихологических проб («10 слов» А. Р. Лурия, методику «Пиктограммы» А. Р. Лурия, методику «Трудно-вербализуемые фигуры» Т. В. Ахутиной, «Тест на воспроизведение ритмов» А. Р. Лурия), анализ стенограмм аудиозаписей ранних воспоминаний. Достоверно установлено, что раннее воспоминание положительной, отрицательной или нейтральной модальности, обусловленное влиянием опыта участия в боевых действиях, изменяется через механизм реконсолидации, что проявляется в лингвистических и семантических параметрах. Лингво-семантическая структура ранних воспоминаний ветеранов боевых действий характеризуется событийно-действенной моделью, с преобладанием глаголов и наречий. Семантическое ядро ранних воспоминаний ветеранов боевых действий чаще окрашено негативно, несмотря на общую амбивалентную или положительную модальность.

Ключевые слова: ранние воспоминания, автобиографическая память, опыт участия в боевых действиях, реконсолидация

Вклад авторов: все авторы внесли равнозначный вклад в планирование исследования, анализ литературы, сбор, анализ, интерпретацию данных.

Соблюдение этических стандартов: исследование одобрено этическим комитетом ФГАОУ ВО РНИМУ имени Н. И. Пирогова Минздрава России (протокол № 13 от 23 ноября 2023 г.), проведено в соответствии с требованиями Основ законодательства «Об охране здоровья граждан»; все участники подписали информированное согласие на обследование.

✉ **Для корреспонденции:** Екатерина Анатольевна Петраш
ул. Островитянова, д. 1, г. Москва, 117997, Россия; petrash@mail.ru

Статья получена: 25.10.2025 **Статья принята к печати:** 22.11.2025 **Опубликована онлайн:** 11.12.2025

DOI: 10.24075/vrgmu.2025.069

Авторские права: © 2025 принадлежат авторам. **Лицензиат:** РНИМУ им. Н. И. Пирогова. Статья размещена в открытом доступе и распространяется на условиях лицензии Creative Commons Attribution (CC BY) (https://creativecommons.org/licenses/by/4.0/).

Memory is inherently socially contingent; it is involved in organization of the subject's individual experience; it contributes to the increase in his/her productivity considering social and cultural factors of the activity (specifically, due to better memorization of certain information that is personally meaningful for a certain individual) [1]. Memory, studied in all the variety of types and processes that ensure its functioning, has a psychotherapeutic resource that is also realized when working with manifestations of post-traumatic stress disorder (PTSD), which include obsessive repetitive memories with traumatic content.

Investigation of early memories as an essential component of autobiographical memory attracts considerable attention in the context of psychological studies. The researchers focus mainly on the phenomenological features. There are very few studies of the linguistic and semantic structure of the combat veterans' early memories in the research space, as suggested by the bibliometric analysis. It has been reported that in 2014–2024 there were almost no scientific papers focused directly on studying early memories of this specific category of participants, which emphasizes the potential value of the research in this area. The papers discovered concerning the general aspects of studying early memories (17 papers in eLibrary and 181 papers in Scopus) indicate the growing interest in the issue in the international research space, as well as the need to more thoroughly study the phenomenon of early memories in specific groups of participants. The apparent contradiction between great scientific interest to the phenomenon of early memories in general and the lack of the targeted research focused on combat veterans substantiates the relevance of the study reported.

Methodological grounds of the study were as follows: the autobiographical memory concept by V.V. Nurkova also considered in the context of the reported cultural and historical approach [2]; provisions of the theory of functional systems by P.K. Anokhin [3] considering memory as one of the leading components of afferent synthesis; neurophysiological mechanisms of mnestic processes described in the papers by K.V. Anokhin [4].

The conceptual model scheme is presented in Fig. 1.

The autobiographical memory being part of the mnestic system determines the semantic organization of personally correlated experience, the subjective affiliation of which is ensured by integrity of the system of autobiographical memories (representing the memory traces) [2]. Early memories and traumatic experience represent the consolidated content of the autobiographical memory ordered in a certain chronology: in terms of chronology, consolidation of early experience precedes consolidation of traumatic experience. In terms of neurophysiology, neural circuits are formed during consolidation through alteration of synaptic activity between the neurons that constitute the circuit. The access system is formed to retrieve the necessary information at a particular time, as well as for reconsolidation of memory traces after their retrieval [4]. When the memory traces are retrieved, active reconstruction of those occurs (accompanied by recategorization); i.e. an old memory trace is replaced by the new contents [5–7].

Each memory (memory trace) has a semantic component in its structure: the sensory-perceptive core that remains conditionally unchanged in terms of its content. The semantic core is surrounded by an emotional envelope that characterizes modality of a certain memory.

All the memory traces that have been preciously shaped and saved are through the affective contents of the traumatic memories (experience) to change their modality.

We interpreted the early memory as the memory trace represented by a verbal description of an event that happened to the respondent in childhood, indicating the age at which the described event occurred. Each early memory has some macro-characteristics (space and time of the memory, duration, size, other people's presence, and modality).

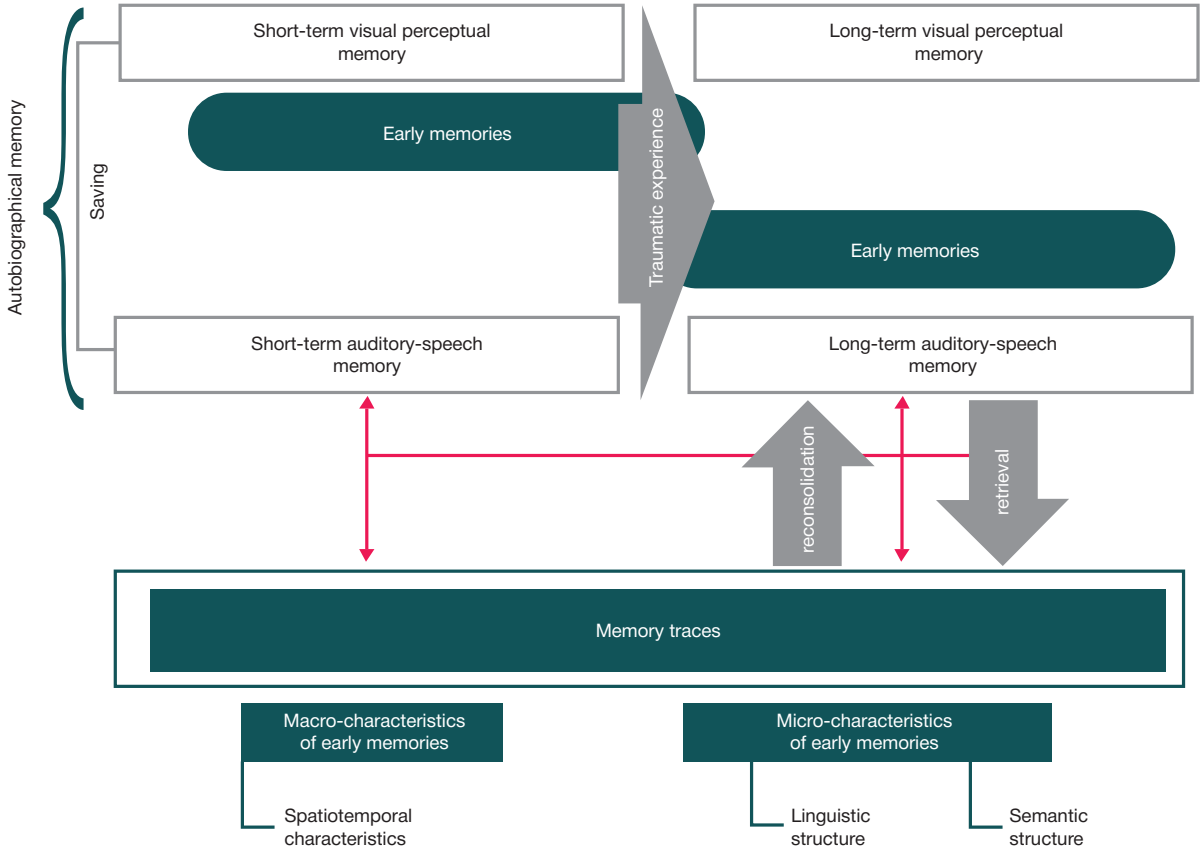


Fig. 1. Scheme of the conceptual model for studying reconsolidation of early memories in reliving the traumatic experience of participation in combat

The early memory modality is determined by the semantic core emotional coloring and its consistency with the overall emotionality of the memory (negative, positive, ambivalent, or neutral). Micro-characteristics have a linguistic and semantic structure (linguistic structure — parts of speech: verb, noun, pronoun, adjective, adverb, affective elements and other parts of speech; semantic structure — the memory's semantic core, modality; memory's secondary parameters).

It is mnestic processes, representing an essential part of the afferent synthesis in functioning of any functional system, that ensure analysis, synthesis, and comparison of afferent signals with the subsequent development of certain strategies of behavior in certain situations on the basis of those taking into account previous experience and restructurization of that under changing environmental conditions [3].

The experience of participating in combat, which is traumatic and characterized by the fact of having spontaneous repetitive traumatic memories, manifestations of psychomotor agitation, emotional and cognitive changes, as well as symptoms of avoidance (representing the PTSD manifestations), is embedded in the autobiographical memory systems, which results in transformation of early memories.

Foreign scientific literature reflects extensive studying of the traumatic memory reconsolidation, while transformation of the earliest childhood memories is a more ambiguous domain that is usually covered in theoretical papers by the researchers following the psychoanalytic paradigm [8; 9].

When describing the earliest childhood memories arbitrarily transformed by an individual, V.V. Nurkova points out that these provide the basis for the formation of personal identity and life scenario [10]. Therefore, deliberate change of the individual's maladaptive life scenario and coping with his/her traumatic experience through reconsolidation of the earliest childhood memories, which play a key role in the structure and contents of the individual's identity, preferred patterns of perception and social reality assessment, seem to be possible [11].

Under conditions of reliving the traumatic experience of participating in combat, the early memories are transformed (in terms of macro- and micro-characteristics) in both retrieval and further reconsolidation phases. The repetition compulsion symptoms (including repetition of the intrusive, suddenly emerging, recurrent traumatic memories), symptoms of avoidance, negative changes in the cognitive and emotional sphere, as well as symptoms of psychomotor agitation (described by N.V. Tarabrina as PTSD manifestations) lead to changes in the linguistic and semantic structure of early memories, affecting their modality, simplifying their structure and "embedding" elements of intrusive traumatic memories in them.

The use of deliberate linguistic and semantic reconstruction of the combat veterans' early memories during their reconsolidation will make it possible to ensure rearrangement of the subject's integral individual experience, including his/her traumatic memories.

The study aimed to look into reconsolidation of early memories in reliving the traumatic experience of participation in combat.

METHODS

The total research sample size was 62 individuals aged 21–46. All the subjects were males. Inclusion criteria: young adulthood and middle age (18–59 years according to the WHO classification); no severe decompensated somatic disorder; no mental disorder. The study groups were formed based on the criterion of combat experience. The experimental group (EG) included 31 participants with combat experience having the status of war veterans, who underwent inpatient treatment at the rehabilitation department for the consequences of mine-explosive and gunshot wounds (the average age was 32.2 ± 0.17 years). In the experimental group, the period of the participants' participation in combat was monitored; the period of participation varied between 4 days and 2 years 7 months, the average period was 1 year 5 months, and the range of values was 2 years 7 months. The control group (CG) included 31 participants without combat experience (the average age was 26.1 ± 0.43 years). In both groups of subjects, the age of early memories was monitored, the memory duration and size (number of sentences) criteria were specified. Primary results of assessing the features of the linguistic and semantic structure of the combat veterans' early memories were set out in the personal questionnaire applying the encryption procedure.

The study was organized into three sequential phases. In the first phase, the participants' cognitive status was assessed using the Mini–Mental State Examination (MMSE) scale [12]. Furthermore, severity of PTSD manifestations was assessed in order to determine the fact of having traumatic experience and its sequelae. For that the Mississippi Scale (MS) for Combat-Related Posttraumatic Stress Disorder by Keane et al. (adaptation by N.V. Tarabrina) was used: a military variant for the participants having combat experience and a civil variant for the participants having no combat experience. The experimental group included the participants with combat experience, who had high PTSD manifestation scores (95.4 ± 4.27). The control group included the participants having no combat experience and low PTSD manifestation scores (72.4 ± 4.27).

In the second phase, the problem of assessing the combat veterans' mnestic functions was solved. In this phase of the study the following set of functional neuropsychological tests was used as methods: "10 Words" to diagnose the direct short-term and long-term auditory-speech memory volume (A.R. Luria) [13]; "Pictograms" method to diagnose the indirect short-term and long-term auditory-speech memory (A.R. Luria) [13]; "Difficult-to-Verbalize Figures" method to assess accuracy, volume, durability of the visual-spatial memory traces (T.V. Akhutina) [14]; "Rhythm Reproduction Test" to assess the ability to perceive and reproduce rhythmic patterns, which is important for the diagnosis of the auditory gnosis and memory impairment (A.R. Luria) [14].

The objective of the third phase was to assess macro- and micro-characteristics of the combat veterans' early memories. In this phase, the clinical conversation (with audio recording), together with the linguistic and semantic analysis of the early memories presented, were used as assessment methods. The study participants were given the following instructions: "Now I'm going to ask you to recall the earliest memory; as soon as you recall, tell me about it in some detail, in at least three sentences; specify your age in this memory". The combat veterans' early memory macro- and micro-characteristics were assessed based on the audio recording transcript, in which macro-characteristics (space and time of the memory, duration, size, other people's presence, and modality) and micro-characteristics represented by the description of the early memory linguistic and semantic structure were determined.

Quantification of the results obtained was performed by the following methods: descriptive (mean, standard deviation, frequency analysis, mode, median, размах) and comparative (Mann–Whitney *U*-test, Fischer's angular transformation, $p < 0.05$) statistical methods.

RESULTS

Based on the cognitive status assessment results obtained using MMSE, 54.8% of the participants had a mental status

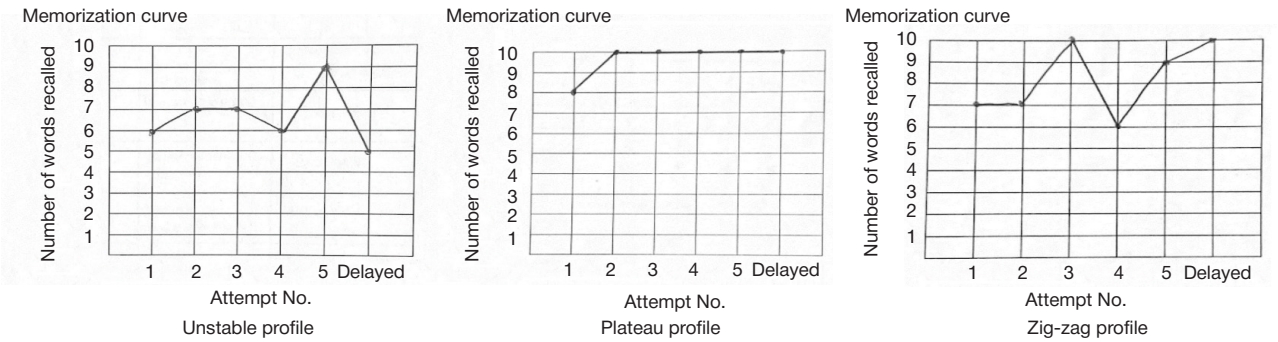


Fig. 2. Averaged profiles of the curves of memorizing 10 words by combat veterans

without cognitive impairment (score 28–30), while subjective cognitive impairment (score 24–27) was reported in 45.2%. No mild cognitive impairment (below 24 points) was reported. It should be noted that all the participants, in whom subjective cognitive impairment was detected, reported the history of contusion due to participation in combat. When assessing significance of differences in cognitive status indicators of the participants of the experimental and control groups, the lack of significant differences was reliably determined ($p = 0.172$).

The high level of the direct auditory-speech memorization was detected in combat veterans: a total of 9–10 words were recalled by the fifth attempt, 8–10 words upon delayed recall in 21 participants (67.7%). In 6 participants (19.3%), the medium level was reported (6–8 words by the fifth test and 5–7 words upon delayed recall); 4 individuals (12.9 %) showed an unstable profile of results. The averaged profiles of memorization curves characterizing the memorization pattern were plotted based on the data obtained (Fig. 2).

Thus, the combat veterans show a steady rise between the attempts, which is especially clear between tests 1 and 3 (an increase of more than 2.7 words); low variation on the fifth attempt (standard deviation 0.86) suggests stable results in the majority of subjects; variation increases with the delayed recall (standard deviation ≈ 1.5), which can indicate differences in the strategies of encryption in the long-term memory.

When assessing indirect memorization in the combat veterans using the "Pictograms" method, high levels were reported for 32.3% of the participants (they recalled 10–11 word combinations), medium levels were reported in 38.7% (they recalled 7–9 words), and the levels below average were reported in 25.8% of the combat veterans, who correctly recalled only 5–6 word combinations. Low levels were reported in 3.2%.

The data on the word combinations can be matched to the direct memorization results in the “10 Words” test. Normally, it is expected, that a pictogram (semantic mediation) must ensure better memorization compared to mechanical reproduction. However, the data obtained suggest impairment or insufficient realization of this strategy. In 54.8% of the subjects, the direct memory volume was larger, than that of the indirect memory. This is contrary to theoretical expectations and can indicate cognitive rigidity in turning to abstract thinking or higher motivation for reproduction of specific material in combat veterans that just reflects specificity of their occupation, i.e. acting on specific commands. In 32.3% of subjects, the direct and indirect memory levels coincided. The hypothesis about the predominant recall by means of indirect memorization was confirmed in 12.9% of the participants only.

Based on the results of the analysis of the tempo-rhythmic memorization test using an auditory image without visual support, high levels of test completion (5 correct series out of 5) were reported only in 5.2%, medium levels (3–4 series) — in 38.5%, low levels (0–1 series) — in 56.3% of the participants. The typical errors observed include extra taps suggesting functional insufficiency of the parieto-temporal brain regions; rhythm reduction, slowdown suggesting possible dysfunction of the posterior frontal structures. This allows us to speak about the poorly shaped auditory-motor coordination in combat veterans.

Based on the results of the "Difficult-to-Verbalize Figures" method (visual-spatial memory assessment), manifestations of high memorization levels were reported in 37.4% of the participants, moderate in 56.8% of the combat veterans; the levels below average were reported only in 5.8%. The visual-spatial memory involving the non-verbal material turned out to be rather productive.

No significant differences in the localization type parameter were revealed in the experimental and control groups based on the early memory macro-characteristic assessment (Table 1).

Spatial localization was differentiated between the following locations: “kindergarten / specific city / at the grandma’s / home / entrance / suburban area / field”. In turn, in the participants having no combat experience, spatial localization was differentiated based on the location: home / specific city / outpatient clinic / water basin / suburban train station (village) / yard / recreation facility / kindergarten / countryhouse. Furthermore, those, in whom spatial localization was not identified, were found in both groups.

The largest share in both EG (68%) and CG (49%) was constituted by the memories, in which the place of action was not clearly established. Moreover, the common specifically identified localizations were found, among which the CG participants more often specified the following: “specific city” (20% vs. 7% in the EG) and “home” (10% vs. 3%). In the EG, such locations, as “kindergarten” and “specific city” were more often mentioned in equal proportions (7%). Other locations were rare (3% each), which suggests their individually limited role in the structure of early autobiographical memories.

Table 1. Indicators of comparative analysis of the early memory localization type parameter in the experimental and control groups

Groups	Home	Specific city	Kindergarten	Rural area	Localization not identified	Sums
	Percentage of subjects in the groups					
EG	3.20%	6.50%	6.50%	3.20%	67.70%	100%
CG	9.70%	19.40%	3.20%	3.20%	48.4%	100%
φ*emp	1.075	1.559	0.614	0	1.551	<1.64

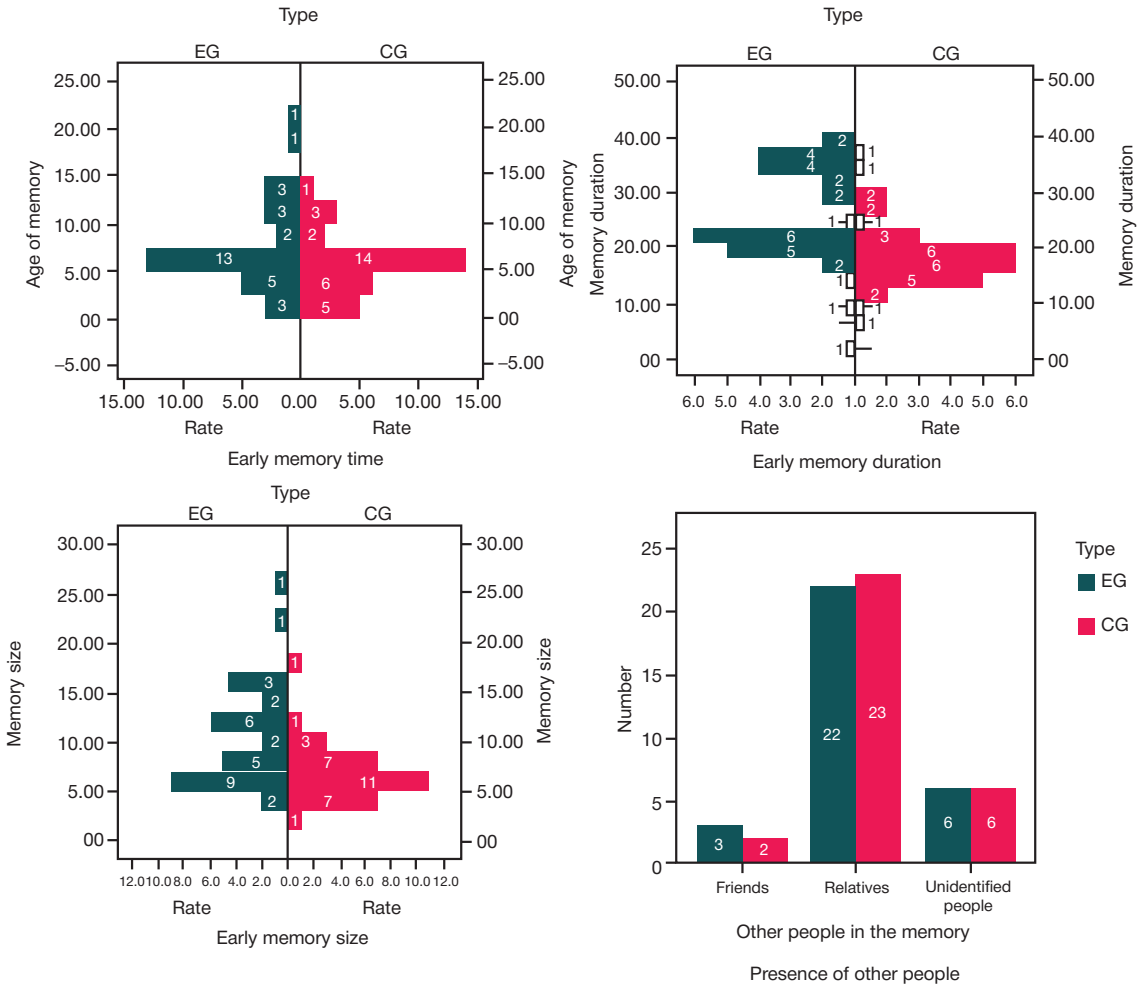


Fig. 3. Histogram of frequency distributions for the "time" and "duration" parameters of early memories in the experimental and control groups

When assessing the “time” parameter of early memories, i.e. the age in the early memory, in the participants with combat experience, variation between 2 and 22 years was revealed, and the average value was 7 ± 0.4. The participants having no combat experience showed variation between 1 and 13 years, the average value was 5 ± 0.4. The proportional age difference in early memories shows that in the participants having no combat experience most memories are concentrated at the age of 4–6 years: 23% of memories are related to the age of 6 years, 19% to the age of 5 years, 16% to the age of 4 years. In the participants with combat experience, the peak of memories is observed at almost the same age as reported for the CG: 5 (19%) and 6 (16%) years. The difference has been also revealed: the combat veterans show a broad age span in their memories, including adolescence and young adulthood (Fig. 3).

The less early memories are typical for combat veterans compared to the subjects having no combat experience. The peak of memories in both groups falls on the age of 4–6 years, which is consistent with the general autobiographical memory formation patterns. However, the higher age variability of memories (2–22 years) is typical for the EG (combat veterans), in contrast to the CG (1–13 years), and the average value is higher (7 years vs. 5 years). This trend suggests that veterans draw the later in terms of chronology, but important in terms of contents episodes, including adolescence and young adulthood, into the zone of “early” memories. It is likely that such memories have high affective intensity or role significance, which facilitates their integration into the autobiographical core of memory, despite going beyond the typical age range of early memories.

As for the early memory “duration” parameters, specifically the distance between the current age and the age in the early memory, the values of the participants having combat experience were as follows: variation between 2 and 40 years, average age 25 ± 0.7. In the participants having no combat experience, variation was between 8 and 38 years, and the average age was 19 ± 0.6. The analysis of proportional distribution of the early memories by the distance between the current age and the age in the early memory showed a well-defined peak within an interval of 17–21 years in both groups, which corresponds to the effect of the “peak of autobiographic memories” described by V.V. Nurkova. According to this effect, it is the events that occur in late adolescence and early adulthood that have an increased likelihood of being retained in the long-term memory due to their emotional richness, social significance, and association with the identity formation [18]. The combat veterans show the more sprawling distribution of memories, including those distant based on the age interval: from 30 to 40 years with even distribution across 3–6% (Fig. 3).

The following values were reported for the “memory size” parameter: in the combat veterans, variation was between 3 and 25 sentences, the average size was 9 ± 0.6. In the participants having no combat experience, variation was between 2 and 17 sentences, the average value was 6 ± 0.4. Memories sized 5–6 sentences (16–19% each) predominate in both experimental and control groups. However, in the CG the share decreases sharply as early as after 8 sentences, while in combat

Table 2. Results of comparative analysis of the early memory macro-charactertistics in the experimental and control groups

Parameters	Combat veterans		Control group		Mann–Whitney *U*-test	Significance level
	Mode	Median	Mode	Median		
Duration	21	22	17	19	405	0.284
Size	6	8	6	6	266.5	0.003**
Age in the memory	5	6	6	5	281.5	0.005**

Note: ** — significance at the level of 0.01

veterans (EG) a second wave of more detailed memories, about 11 (16%) and 15 (10%) sentences is observed, and cases of the most explicit memories (up to 25 sentences) are reported that are lacking in the CG (Fig. 3). The expanded form of early memories in the EG can be interpreted not only as the high degree of cognitive processing and meaning-making, but also as the attempt to process the potentially traumatic experience.

Based on the parameter "presence of other people" in early memories, the results of both groups are matched. Other people are present in the early memories of 100% of the participants, only the number varies: from 1 to 2 in the EG, from 1 to 3 in the CG. Relatives predominate in the combat veterans' memories — 70%, they are followed by unidentified people — 22%; only 8% are friends. In the participants having no combat experience, relatives also predominate — 73%, they are followed by unidentified people — 21%, and friends — 6% (Fig. 3). The central place in the early memories of both combat veterans and the participants having no combat experience is occupied by close relatives (70 and 73%, respectively). This emphasizes an important role of family in the individual's emotional development and the autobiographical memory formation. Friends are far less often reported in the memories; in every fifth case, people with the unspecified identity are mentioned. Such a distribution suggests that it is family relations that form the basis for storage and recall of big moments of childhood.

To assess significance of differences in macro-charactertistics of early memories between combat veterans and individuals having no such experience, we performed comparative analysis of the quantitative data obtained using the nonparametric Mann–Whitney *U*-test (Table 2).

Comparative analysis of the early memory quantitative macro-charactertistics revealed significant differences in the memory size and age in the memory ($p < 0.01$) in the experimental and control groups. In combat veterans, a second wave of prolonged memories is reported, which can be considered as the mechanism of posttraumatic processing and adaptation though storytelling. In the CG having no combat experience, the early memory size decreases sharply after 8 sentences.

When assessing the early memory modality, ambivalent and positive memories are more often reported in the EG, while the neutral and negative ones are less frequent. The early memories that are neutral in terms of modality predominate in the participants having no combat experience (Fig. 4).

The results obtained suggest that the combat experience transforms early memories during their reconsolidation in the direction of emotional ambiguity or the emphasis shift towards positive modality, while when there is no combat experience, the early memories that are emotionally neutral in terms of modality predominate.

Micro-characteristics describe the linguistic and semantic structure of early memories.

The analysis of the percentage of various parts of speech in the transcripts characterizing the linguistic structure of early memories in combat veterans and the participants having no combat experience makes it possible to identify a number of substantial and cognitive-linguistic differences correlated with the functional characteristics of speech units.

The combat veterans demonstrate a higher percentage of the verb forms (on average 21.35% vs. 18.03% in the CG), which suggests richness of their statements with event-related content, the desire to structure memory as a sequence of actions, not descriptions, which reflects the combat experience specifics with capturing current events and plays a protective cognitive role [16; 17]. The rates of using nouns are comparable in both groups (20.16 % — EG; 21.06 % — CG), which confirms the unique nominative function of this part of speech: representation of objects, persons, phenomena, and abstractions providing the basis for the cognitive categorization of experience [18]. Pronouns that ensure coherence and reference are more often found in the participants having no combat experience: 16.87% (15.77% in the group of combat veterans). This suggests a higher degree of subjective involvement in the memory among representatives of the CG, as well as the orientation towards the story's internal perspective [19]. The combat veterans, on the contrary, show a trend of distancing from the early experience manifested by the decrease in the rate of using the personally marked units. The decrease in the share of the attributive and evaluative characteristics in the combat veterans' statements (4.55% vs. 6.58% in the CG) suggests the reduced need for details, as well as the specific nature of the memories, in which actions and situations predominate instead of value judgements [20; 21]. The differences in the percentage of adverbs (higher in the group of combat veterans — 11.61% vs. 9.93% in the CG) suggest the importance of spatiotemporal parameters and subjective assessment of the intensity of what is happening by combat veterans [22]. Significance of differences in the linguistic structure parameters of early memories are provided in Table 3.

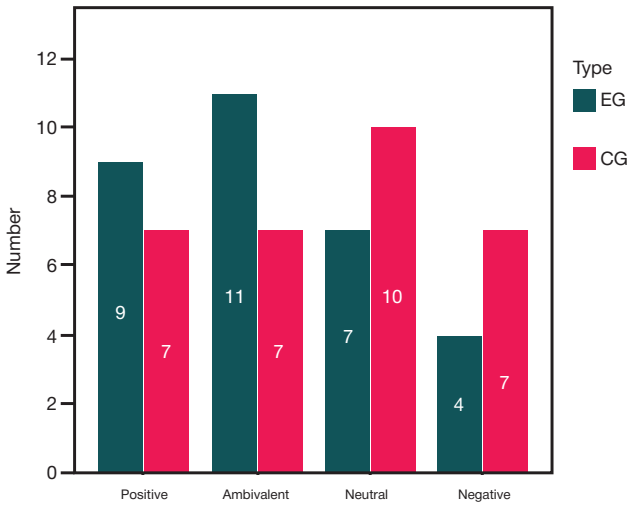


Fig. 4. Histogram of frequency distributions for the early memory modalities in the experimental and control groups

Table 3. Significance of differences in the linguistic structure parameters of early memories modalities in the experimental and control groups

	EG		CG		Mann–Whitney *U*-test	Significance level
	Mode	Median	Mode	Median		
Noun	9	16	19	18	563	0.244
Pronoun	13	13	8	15	575	0.182
Verb	12	20	10	15	307.5	0.015*
Adjective	2	3	2	5	647	0.018*
Adverb	7	9	6	8	366	0.105
Other parts of speech	12	21	18	24	531	0.475

Note: ** — significance at the level of 0.01.

Thus, the identified differences in the speech unit composition allow us to speak about the existence of two cognitive-discursive models of the early memory representation: an event-based model in the group of combat veterans (characterized by relying on the verb forms and adverbs reflecting the action dynamics and situation, with the minimum evaluative vocabulary) and a descriptive-reflexive model (that is based on the nouns, pronouns, and adjectives that create a subjectively colored and emotionally detailed picture of past experience) for the participants with no combat experience.

Assessment of the combat veterans' early memory semantic core suggests fixation of an event in memory with a predominance of the negative emotional envelope of the semantic core. Memories with the semantic core positive modality predominate in the participants with no traumatic experience. Such semantic structure features reflect the qualitative characteristics of the life context impact on the selection and consolidation of the key meanings. The semantic core emotional vector can be considered as a reflection of both individual perception and the conditions of the autobiographical memory formation.

DISCUSSION

The shift of the combat veterans' early memory emotional modality vector results from the desire to maintain internal stability and integrity of experience: under the influence of the negatively colored obsessively repeating traumatic memories, the direction of the vector of emotional modality in the structure of the autobiographical memory changes towards the positive coloring of early memories.

It has been shown that after the exposure to combat traumatic psychological stress, combat veterans have to essentially recreate the structure of their subjective life space under the conditions of peaceful life, including the structure of self-attitude, self-esteem and life-purpose orientations. This is why, in the context of reconsolidating early memories, such participants resort to a more detailed presentation, at the same time trying to reconstruct their own life [23]. The thesis specified has been also confirmed in our study: through the recording of a more expanded form of early memories in combat veterans, suggesting a high degree of cognitive processing and meaning-making, potentially enabling the processing of traumatic experiences. Interpersonal relationships are not addressed in the contents of early memories of the participants, who took part in the study, when recalled, which is typical for males [24]. It has been shown that high severity of PTSD manifestations results in violation of the chronological boundaries of one's own life, as well as in the reduced quantity of the memory trace details [25]. According to our results, it is the expanded form of the early memory verbal representation in combat veterans that ensures the traumatic memory processing psychotherapeutic resource and restoration of the chronological integrity and order of the autobiographical memory contents.

CONCLUSIONS

Based on the study it was reliably determined that the experience of participating in combat transforms early memories through the reconsolidation mechanism, which is manifested by macro- and micro-characteristics. The expanded form of the early memory verbal representation in combat veterans suggests processing of personal experience, including traumatic, in which the narrative detailing serves as the means of understanding and integrating life events into an autobiographical context. The linguistic and semantic structure of the combat veterans' early memories is characterized by an event-based model, with a predominance of verbs and adverbs. It has been found that the semantic core of the combat veterans' early memories is more often negatively colored, despite its general ambivalent or positive modality.

References

1. Leontev AN. Razvitie pamyati. Eksperimental'noe issledovanie vysshih psihologicheskih funkcij. Leningrad: Uchpedgiz, 1931; 280 s. Russian.
2. Nurkova VV. Avtobiograficheskaya pamyat' kak problema psihologicheskogo issledovaniya. Vestnik MGU. Seriya 14. Psihologiya. 1996; 1: 58–59. Russian.
3. Anohin PK. Uzlovye voprosy teorii funkcional'noj sistemy. M., 1980; 200 s. Russian.
4. Anohin KV. Mozg i pamyat': biologiya sledov proshedshego vremeni. Vestnik Rossijskoj akademii nauk. 2010; 80 (5–6): 455–61. Russian.
5. Suzuki A, Josselyn SA, Frankland PW, Masushige S, Silva J, Kida S. Memory reconsolidation and extinction have distinct temporal and biochemical signatures. Journal of Neuroscience. 2004; 24 (20): 4787– 95.
6. Anohin KV, Sudakov KV. Sistemnaya organizaciya povedeniya: novizna kak vedushchij faktor ekspressii rannih genov v mozge pri obuchenii. Uspekhi fiziologicheskih nauk. 1993; 24: 53–70. Russian.
7. Kindt M, A. van Emmerik. New avenues for treating emotional memory disorders: towards a reconsolidation intervention for posttraumatic stress disorder. Therapeutic Advances in Psychopharmacology. 2016; 6 (4): 283–95.
8. Nurkova VV, Masolova GYu. Harakteristiki vospominanij o detstve

i psihologicheskij oblik vzroslogo. Psihologicheskaya nauka i obrazovanie. 2009; 4: 1–16. Russian.
9. Gray RM, Budden-Potts D, Schwall RJ, Bourke FF. An open-label, randomized controlled trial of the reconsolidation of traumatic memories protocol (RTM) in military women. Psychological Trauma: Theory, Research Practice, and Policy. 2021; 13 (6): 641–58.
10. Nurkova VV, Vasilenko DA. Formirovanie variativnogo repertuara samoopredelyayushchih vospominanij kak sredstvo razvitiya samoidentichnosti. Vestnik Rossijskogo gosudarstvennogo gumanitarnogo universiteta. Seriya «Psihologicheskie nauki». 2013; 18 (119): 11–30. Russian.
11. Nurkova VV, Mihajlova OI, Nazloyan GM. Avtoportret kak sredstvo samoregulyacii lichnosti. ZHurnal prakticheskogo psihologa. 2005; 1: 100–19. Russian.
12. Folstein MF, Folstein SE, McHugh PR. Mini-mental state. A practical method for grading the cognitive state of patients for the clinician. Journal of psychiatric research. 1975; 12 (3): 189–98.
13. Rubinshtejn SYa. Eksperimental'nye metodiki patopsihologii. M.: EKSMO-Press, 1999; 448 s. Russian.
14. Cvetkova LS. Metodika nejropsihologicheskoj diagnostiki detej. M.: Pedagogicheskoe obshchestvo Rossii, 2002; 96 s. Russian.
15. Nurkova VV. Analiz fenomenologii avtobiograficheskoj pamyati s pozicij kul'turno-istoricheskogo podhoda. Kul'turno-istoricheskaya psihologiya. 2008; 4 (1): 17–26. Russian.
16. Mihajlina OA. Rol' glagolov v kommunikativnoj organizacii teksta. Voprosy filologii. 2014; 1 (47): 330–2. Russian.
17. Plotnikova AM. Kognitivnoe modelirovanie leksicheskogo znacheniya glagola (na materiale glagolov social'nyh dejstvij i otnoshenij). Izvestiya Rossijskogo gosudarstvennogo pedagogicheskogo universiteta imeni A. I. Gercena. 2008; 11 (71): 73–80. Russian.
18. Kruchinkina ND. Leksiko-semanticheskij i funkcional'no-semanticheskij potencial sushchestvitel'nogo. Nauchnyj rezul'tat. Voprosy teoreticheskoj i prikladnoj lingvistiki. 2017; 3 (3): 22–31.
19. Sin'ko LA. Mestoimenie v sintaksicheskoj sisteme: osnovnye funkcii. YAzykoznanie. 2008; 80–88. Russian.
20. Kopkova EV. K ontologii grammatiki imeni prilagatel'nogo: atributivnaya i predikativnaya funkcii. Filologiya. 2020; 196–9. Russian.
21. Malygina MV. Tekstovye funkcii prilagatel'nyh i narechij. Vestnik Pskovskogo gosudarstvennogo pedagogicheskogo universiteta. Seriya: Social'no-gumanitarnye i psihologo-pedagogicheskie nauki. 2011; 15: 96–100. Russian.
22. Agalieva A. Narechie: struktura, funkcii i rol' v russkom yazyke. Ceteris Paribus. 2024; 10: 87–89. Russian.
23. Shamardina MV, Ralnikova IA, Orlova OA. Metody i priemy psihologicheskoj pomoshchi uchastnikam boevyh dejstvij. Altajskij gosudarstvennyj universitet. Barnaul: AltGU, 2023. Russian.
24. Sitnyanskaya EA. Gendernaya specifika rannih vospominanij u lic molodogo vozrasta. Psihologicheskie issledovaniya. 2023; 16 (92). Russian.
25. Pitts BL, Eisenberg ML, Bailey HR, Zacks JM. PTSD is associated with impaired event processing and memory for everyday events. Cogn Res Princ Implic. 2022; 7 (1): 35.

Литература

1. Леонтьев А. Н. Развитие памяти. Экспериментальное исследование высших психологических функций. Ленинград: Учпедгиз, 1931; 280 с.
2. Нуркова В. В. Автобиографическая память как проблема психологического исследования. Вестник МГУ. Серия 14. Психология. 1996; 1: 58–59.
3. Анохин П. К. Узловые вопросы теории функциональной системы. М., 1980; 200 с.
4. Анохин К. В. Мозг и память: биология следов прошедшего времени. Вестник Российской академии наук. 2010; 80 (5–6): 455–61.
5. Suzuki A, Josselyn SA, Frankland PW, Masushige S, Silva J, Kida S. Memory reconsolidation and extinction have distinct temporal and biochemical signatures. Journal of Neuroscience. 2004; 24 (20): 4787– 95.
6. Анохин К. В., Судаков К. В. Системная организация поведения: новизна как ведущий фактор экспрессии ранних генов в мозге при обучении. Успехи физиологических наук. 1993; 24: 53–70.
7. Kindt M, A. van Emmerik. New avenues for treating emotional memory disorders: towards a reconsolidation intervention for posttraumatic stress disorder. Therapeutic Advances in Psychopharmacology. 2016; 6 (4): 283–95.
8. Нуркова В. В., Масолова Г. Ю. Характеристики воспоминаний о детстве и психологический облик взрослого. Психологическая наука и образование. 2009; 4: 1–16.
9. Gray RM, Budden-Potts D, Schwall RJ, Bourke FF. An open-label, randomized controlled trial of the reconsolidation of traumatic memories protocol (RTM) in military women. Psychological Trauma: Theory, Research Practice, and Policy. 2021; 13 (6): 641–58.
10. Нуркова В. В., Василенко Д. А. Формирование вариативного репертуара самоопределяющих воспоминаний как средство развития самоидентичности. Вестник Российского государственного гуманитарного университета. Серия «Психологические науки». 2013; 18 (119): 11–30.
11. Нуркова В. В., Михайлова О. И., Назлоян Г. М. Автопортрет как средство саморегуляции личности. Журнал практического психолога. 2005; 1: 100–19.
12. Folstein MF, Folstein SE, McHugh PR. Mini-mental state. A practical method for grading the cognitive state of patients for the clinician. Journal of psychiatric research. 1975; 12 (3): 189–98.
13. Рубинштейн С. Я. Экспериментальные методики патопсихологии. М.: ЭКСМО-Пресс, 1999; 448 с.
14. Цветкова Л. С. Методика нейропсихологической диагностики детей. М.: Педагогическое общество России, 2002; 96 с.
15. Нуркова В. В. Анализ феноменологии автобиографической памяти с позиций культурно-исторического подхода. Культурно-историческая психология. 2008; 4 (1): 17–26.
16. Михайлина О. А. Роль глаголов в коммуникативной организации текста. Вопросы филологии. 2014; 1 (47): 330–2.
17. Плотникова А. М. Когнитивное моделирование лексического значения глагола (на материале глаголов социальных действий и отношений). Известия Российского государственного педагогического университета имени А. И. Герцена. 2008; 11 (71): 73–80.
18. Кручинкина Н. Д. Лексико-семантический и функционально-семантический потенциал существительного. Научный результат. Вопросы теоретической и прикладной лингвистики. 2017; 3 (3): 22–31.
19. Синько Л. А. Местоимение в синтаксической системе: основные функции. Языкознание. 2008; 80–88.
20. Копкова Е. В. К онтологии грамматики имени прилагательного: атрибутивная и предикативная функции. Филология. 2020; 196–9.
21. Малыгина М. В. Текстовые функции прилагательных и наречий. Вестник Псковского государственного педагогического университета. Серия: Социально-гуманитарные и психолого-педагогические науки. 2011; 15: 96–100.
22. Агалиева А. Наречие: структура, функции и роль в русском языке. Ceteris Paribus. 2024; 10: 87–89.
23. Шамардина М. В., Ральникова И. А., Орлова О. А. Методы и приемы психологической помощи участникам боевых действий. Алтайский государственный университет. Барнаул: АлтГУ, 2023.
24. Ситнянская Э. А. Гендерная специфика ранних воспоминаний у лиц молодого возраста. Психологические исследования. 2023; 16 (92).
25. Pitts BL, Eisenberg ML, Bailey HR, Zacks JM. PTSD is associated with impaired event processing and memory for everyday events. Cogn Res Princ Implic. 2022; 7 (1): 35.

FEATURES OF THE IMMUNE RESPONSE TO TUMOR ALLOANTIGENS IN THE CONTEXT OF DECREASED CLONAL DIVERSITY OF T CELLS

Korotkova MS, Persiyantseva NA, Kalinina AA, Khromykh LM, Kazansky DB ✉

Blokhin National Medical Research Center of Oncology, Ministry of Health of the Russian Federation, Moscow, Russia

A T cell receptor (TCR), an αβ heterodimer, recognizes peptide antigens presented by self molecules of the major histocompatibility complex (MHC). A significant number of T cell clonotypes are alloreactive: they can interact with various allelic variants of MHC and the associated peptides. Currently, it is unclear whether the effectiveness of the allogeneic immune response depends on the diversity of the TCR repertoire. Seeking to experimentally narrow the diversity of T cell clonotypes, we used mice with transgenic expression of the β-chain TCR (TCRβ) in this work. We analyzed how the TCRß-transgenic mice on the CBA/Lac (H-2^k) background respond to EL-4 (H-$2K^b$) lymphoma cells *in vivo* with the aim to assess the effect of a narrower repertoire on the allogeneic immune response. The study has shown that transgenic mice develop a weak immune response to transplant antigens, and the formed pool of cytotoxic T cells is 1.5–1.7-fold smaller than that in wild-type animals. Consequently, the mice failed to reject the allogeneic tumor, leading to 100% mortality rate. The results of this work are consistent with the data from our earlier studies that employed another TCRß-transgenic model. They confirm that the decreased diversity of the TCR repertoire impairs the response to alloantigens, allowing the tumor to evade the immune response and progress in the allogeneic recipient.

Keywords: T-cell, T-cell receptor, allogeneic response, decreased clonal diversity

Funding: the study was financially supported by the Russian Science Foundation grant No. 22-15-00342-П (https://rscf.ru/project/22-15-00342/).

Author contribution: Korotkova MS — experimental work, analysis of the results; Persiyantseva NA — experimental work, analysis of the results, article editing; Kalinina AA — study planning, analysis and interpretation of the results, analysis of the available literature, article authoring and editing; Khromykh LM — article editing; Kazansky DB — study planning, analysis and interpretation of the results, analysis of the available literature, article editing.

Compliance with ethical standards: the study was approved by the Ethics Committee of the N.N. Blokhin National Research Medical Center of Oncology of the Ministry of Health of the Russian Federation (Minutes No. 3-П10.06.2022 of June 10, 2022) and conducted in strict accordance with the provisions of Directive 2010/63/EU of the European Parliament and of the Council of 22 September 2010 on the protection of animals used for scientific purposes.

✉ **Correspondence should be addressed:** Dmitry B. Kazansky
Kashirskoe shosse, 24, str. 15, Moscow, 115478, Russia; kazansky1@yandex.ru

Received: 06.10.2025 **Accepted:** 01.11.2025 **Published online:** 14.11.2025

DOI: 10.24075/brsmu.2025.057

Copyright: © 2025 by the authors. **Licensee:** Pirogov University. This article is an open access article distributed under the terms and conditions of the Creative Commons Attribution (CC BY) license (https://creativecommons.org/licenses/by/4.0/).

ОСОБЕННОСТИ ИММУННОГО ОТВЕТА НА ОПУХОЛЕВЫЕ АЛЛОАНТИГЕНЫ В УСЛОВИЯХ СОКРАЩЕННОГО КЛОНАЛЬНОГО РАЗНООБРАЗИЯ Т-КЛЕТОК

М. С. Короткова, Н. А. Персиянцева, А. А. Калинина, Л. М. Хромых, Д. Б. Казанский ✉

Национальный медицинский исследовательский центр онкологии имени Н. Н. Блохина Минздрава России, Москва, Россия

Т-клеточный рецептор (ТКР), представляющий собой αβ-гетеродимер, предназначен для распознавания пептидных антигенов в комплексе с собственными молекулами главного комплекса гистосовместимости (МНС). При этом значительная доля клонотипов Т-клеток обладает аллореактивностью, т. е. способностью взаимодействовать с различными аллельными вариантами МНС и ассоциированными с ними пептидами. В настоящее время нет четкой определенности, зависит ли эффективность аллогенного иммунного ответа от широты репертуара ТКР. В данной работе использовали мышей с трансгенной экспрессией β-цепи ТКР (ТКРβ), что позволило экспериментально сузить разнообразие клонотипов Т-клеток. Цель работы — проанализировать развитие ответа ТКРβ-трансгенных мышей на генетической основе CBA/Lac (H-2^k) на клетки лимфомы EL-4 (H-$2K^b$) *in vivo* для оценки влияния сужения репертуара на аллогенный иммунный ответ. Показано, что у трансгенных мышей развивается слабый иммунный ответ на трансплантационные антигены с формированием пула цитотоксических Т-клеток, в 1,5–1,7 раза сокращенного по сравнению с животными дикого типа. Вследствие этого отторжение аллогенной опухоли становится невозможным, и наступает гибель 100% животных. Полученные данные согласуются с результатами наших ранних исследований с использованием другой ТКРβ-трансгенной модели и подтверждают, что снижение разнообразия репертуара ТКР ухудшает эффективность ответа на аллоантигены и создает условия для избегания опухолью иммунного ответа и ее прогрессирования в аллогенном реципиенте.

Ключевые слова: Т-клетка, Т-клеточный рецептор, аллогенный ответ, сокращение клонального разнообразия

Финансирование: работа выполнена при финансовой поддержке гранта РНФ № 22-15-00342-П (https://rscf.ru/project/22-15-00342/).

Вклад авторов: М. С. Короткова — проведение экспериментов, анализ результатов; Н. А. Персиянцева — проведение экспериментов, анализ результатов, редактирование; А. А. Калинина — планирование исследования, анализ и интерпретация результатов, анализ литературы, написание статьи, редактирование; Л. М. Хромых — редактирование; Д. Б. Казанский — планирование исследования, анализ и интерпретация результатов, анализ литературы, редактирование.

Соблюдение этических стандартов: исследование одобрено этическим комитетом ФГБУ «НМИЦ онкологии им. Н. Н. Блохина» Минздрава России (протокол № 3П-10.06.2022 от 10 июня 2022 г.) и проведено в строгом соответствии с положениями Директивы 2010/63/EU Европейского парламента и Совета Европейского союза от 22 сентября 2010 г. по охране животных, используемых в научных целях.

✉ **Для корреспонденции:** Дмитрий Борисович Казанский
Каширское ш., д. 24, стр. 15, г. Москва, 115478, Россия; kazansky1@yandex.ru

Статья получена: 06.10.2025 **Статья принята к печати:** 01.11.2025 **Опубликована онлайн:** 14.11.2025

DOI: 10.24075/vrgmu.2025.057

Авторские права: © 2025 принадлежат авторам. **Лицензиат:** РНИМУ им. Н. И. Пирогова. Статья размещена в открытом доступе и распространяется на условиях лицензии Creative Commons Attribution (CC BY) (https://creativecommons.org/licenses/by/4.0/).

T cells, the component of the adaptive immune system, can recognize antigens via the highly specialized T-cell receptor (TCR), which is an αß heterodimer in the dominant type of T-cells with the unique structure in each individual clonotype. The peripheral TCR repertoire matures and undergoes selection within the thymus; it is capable of effective interaction with the molecules of the major histocompatibility complex (MHC) that present a foreign peptide or a peptide of an endogenous mutant protein [1]. At that, a significant portion, if not all, clones of peripheral T-cells are alloreactive [2]; that is, they can react to allogeneic MHC molecules and the associated peptides [3–5]. Up to 10% of T-cells of the recipient's T-cell repertoire can participate in the response to an individual allogeneic transplant [6].

Alloreactive T-cells are the key mediators of transplant immunity that mediate acute allograft rejection [7]. Current knowledge is inconsistent regarding whether the diversity of the TCR repertoire determines the intensity of the allogeneic response; the available data are conflicting [8]. Several studies have shown an association between baseline high diversity of the recipient's TCR repertoire and an increased risk of acute rejection of allogeneic transplants [9, 10]. At the same time, it has been established that only a narrow oligoclonal repertoire is involved in graft rejection [11–13].

Experimental models involving transplantation of a tumor different in one transplant antigen [14, 15] enable *in vivo* exploration of the dynamics and features of development of allogeneic immune response. Direct recognition of allogeneic MHC class I molecules induces an intense cytotoxic $CD8^+$ T-cell response, and the allogeneic tumor is rapidly rejected, with immunological memory formed in the process [14–16]. In this work, we sought to confirm our earlier findings about the dependence of the effectiveness of the allogeneic immune response on the diversity of the TCR repertoire [14]. For this purpose, we used mice with transgenic expression of the β-chain TCR (TCRß) of hybridoma 7, which was described earlier [17]. TCRß transgenesis allows reducing the diversity of T-lymphocyte receptors [14, 18]: under the allelic exclusion rule, the expression of transgenic TCRß blocks gene rearrangement and, consequently, the expression of endogenous β-chains in T-cells. As a result, the repertoire becomes mainly comprised of clonotypes with an invariant β-chain, and its diversity stems only from the endogenous α-chains in the receptor structure.

This study aimed to analyze the development of the immune response to tumor alloantigens in the TCRβ transgenic model *in vivo*, in which the T-cell clonal diversity is reduced.

METHODS

We used female mice of the inbred lines CBA/Lac ($H\text{-}2^k$) and C57BL/6 ($H\text{-}2^b$) and transgenic mice 7B (6–8 weeks old, 18–20 g) bred at N.N. Blokhin National Medical Research Center of Oncology. The process of breeding the 7B transgenic mice was described earlier [18]. Initially, the transgene was transferred to the genetic background of C57BL/6 mice. Since the lifetime of the generated mice was limited, which hindered their breeding, the transgene was transferred to the genetic background of the CBA/Lac line; it is currently a part of the collection of the Laboratory of Regulatory Mechanisms in Immunity, Institute of Carcinogenesis (N.N. Blokhin National Medical Research Center of Oncology). 7B transgenic mice express the β-chain TCR, specific to the mutant MHC class I molecule K^{bm3} and the MHC class II molecule $I\text{-}A^b$ [17]. The animals were kept at 20–24 °C and 40% relative humidity, with a 12-hour light cycle, and had unrestricted access to feed and water. Transgenic 7B mice and control animals (non-transgenic wild-type siblings) were injected intraperitoneally with EL-4 ($H\text{-}2K^b$) lymphoma cells at a dose of 1×10^6 cells per mouse in 500 µl of phosphate-buffered saline (PBS). After injection, we monitored the life span of mice with a follow-up period of more than 30 days. The Kaplan-Meier survival curves were plotted using SRplot [19]. Some of the animals were removed from the experiment by cervical dislocation on the 12th day after EL-4 cell transplantation, with subsequent extraction of peritoneal cells. The obtained lavage cell samples were analyzed by flow cytometry.

We used fluorescently labeled antibodies (BioLegend, USA; BD Bioscience, USA; BD Horizon, USA): CD3 — APC-Cy7, CD8 — Percp-Cy5.5, CD44 — Pacific blue, CD62L — APC, Vb8.3 — PE, Kb — FITC. Cell samples ($0.5 – 1 \times 10^6$) were incubated with Fc block antibodies (clone 2.4G2, BD Pharmingen, USA) for 10 minutes at 4 °C to prevent nonspecific binding of antibodies, then stained with labeled antibodies for 40 minutes at 4 °C. For the analysis, we used a BD FACS Canto II flow cytometer (BD Bioscience) and the FACSDiva 6.0 software (BD Bioscience). Leukocytes were gated using forward scatter (FSC-A) and side scatter (SSC-A) parameters, and single cells were identified by plotting forward scatter height (FSC-H) against forward scatter area (FSC-A). The LIVE/DEAD fixable yellow dead cell stain kit (Invitrogen, USA) was used to stain dead cells; dead cells were excluded based on this staining and scatter parameters. The expression of surface markers was evaluated in a population of live single leukocytes. The relative number of T-lymphocytes expressing the transgenic TCR β-chain was assessed by staining with anti-Vb8.3 antibodies (the Vß family, to which the 7B transgenic β-chain belongs). The relative number of EL-4 tumor cells in the peritoneal cavity of experimental animals was determined by the expression of the MHC class I molecule $H\text{-}2K^b$ (Kb). The populations of T-lymphocytes were analyzed after exclusion of Kb-positive cells. The data was processed in the FlowJo 7.6 software (TreeStar Inc., USA). Figure 1 presents the cytofluorimetric analysis strategy.

The data are presented as the mean ± standard error of the mean. For statistical analysis, we used the Student's unpaired *t*-test, ANOVA, and the post-hoc Tukey test. The data samples were pre-checked for normality of the distribution using the Kolmogorov–Smirnov test, which confirms the validity of the selection of these statistical methods. For statistical analysis, we used the SRplot online service [19]. The differences were considered significant at $p \leq 0.05$.

RESULTS

As noted above, the transgenesis of the TCR β-chain significantly reduces the diversity of the peripheral TCR repertoire. Seeking to investigate the features of functioning of the T-cell immune system when the diversity of clonotypes is reduced, we studied the immune response of 7B transgenic mice ($H\text{-}2^k$) to allogeneic EL-4 lymphoma cells ($H\text{-}2K^b$) *in vivo*. T-lymphocytes at the transplantation site (in the peritoneal cavity) were analyzed on the 12th day after EL-4 injection. Normally, by this day, the response of cytotoxic T-cells to EL-4 lymphoma alloantigens peaks [14, 16].

Immunized 7B mice (TG+EL-4) had the absolute number of cells in the peritoneal cavity increased by two orders of magnitude compared with intact (non-immunized) transgenic mice (TG) and 20-fold compared with immunized wild-type animals (WT+EL-4) (Fig. 2A). The lavage from the immunized 7B animals contained over 90% EL-4 (Kb^+) cells, whereas in control mice (WT+EL-4), the allogeneic tumor was almost completely eliminated by this time, and the proportion of Kb^+ cells was only 5% (Fig. 2B).

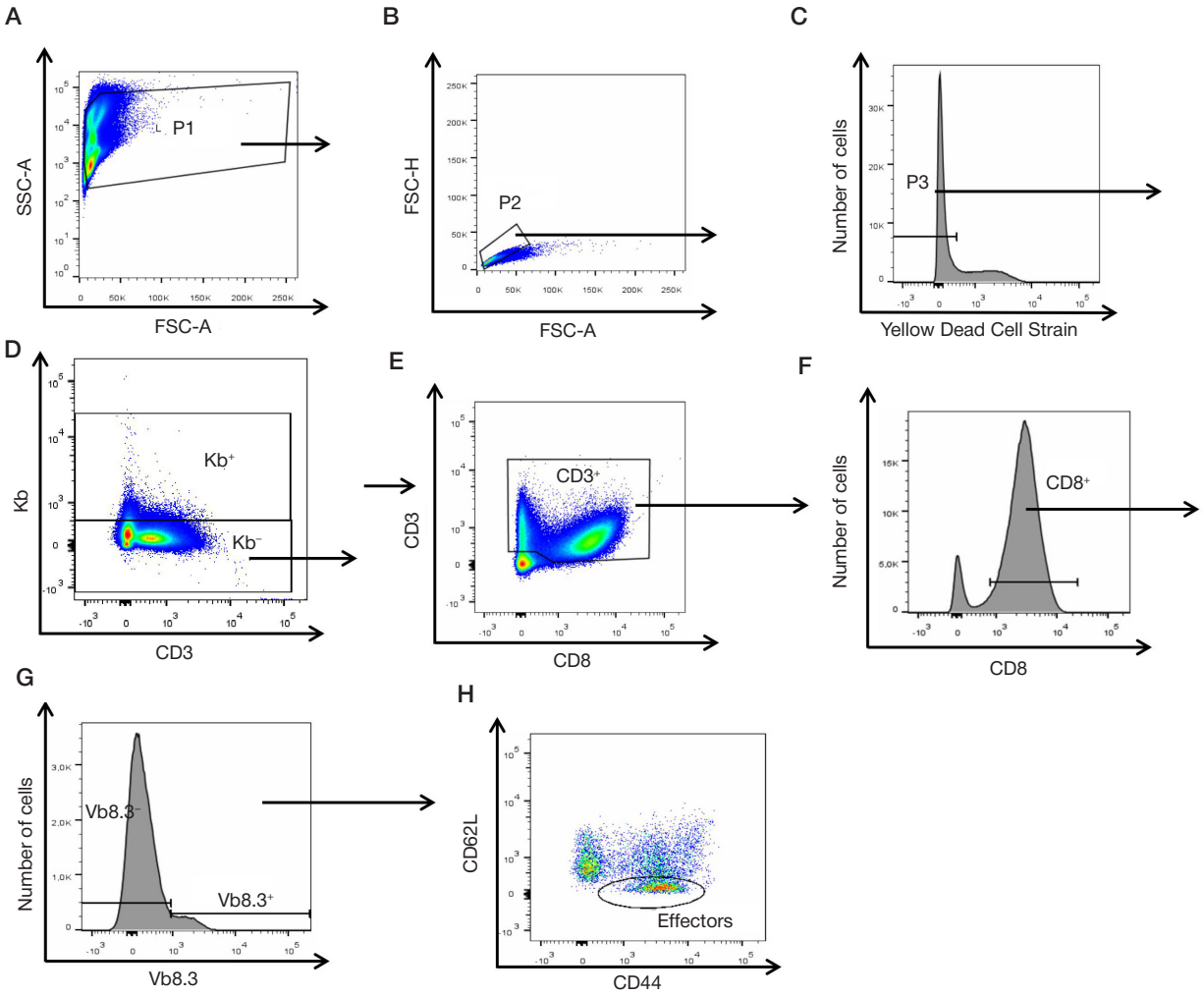


Fig. 1. Analysis of cells in the peritoneal cavity by flow cytometry (strategy). The analysis involved sequential gating of the following populations: leukocytes, gated by forward (FSC-A) and side (SSC-A) light scattering (P1) (**A**); single cells, gated by FSC-H vs. FSC-A (P2) (**B**); living cells negative as per yellow dead cell staining (P3) (**C**); EL-4 cells and recipient leukocytes, gated by co-expression of Kb and CD3 markers: Kb^+CD3^+ EL-4 cells (Kb^+), Kb-$CD3^+$ recipient cells (Kb^-) (**D**). **E**. In a population of Kb^-CD3^+ cells (Kb^-), T-cells ($CD3^+$) were gated by co-expression of CD3 and CD8 ($CD3^+CD8^+$ cells). **F**. Cytotoxic $CD8^+$ T-cells ($CD8^+$) were gated from the $CD3^+$- cell population. **G**. In the $CD8^+$ T-cell population, cells expressing endogenous β-chains of the T-cell receptor (TCRβ) ($Vb8.3^-$) and cells with the transgenic TCRβ ($Vb8.3^+$) were gated. **H**. For the $Vb8.3^-$ and $Vb8^+$ populations of $CD8^+$ T-cells, co-expression of CD44 and CD62L markers was analyzed, and the proportion (%) of effectors ($CD62L^-CD44^+$) was determined

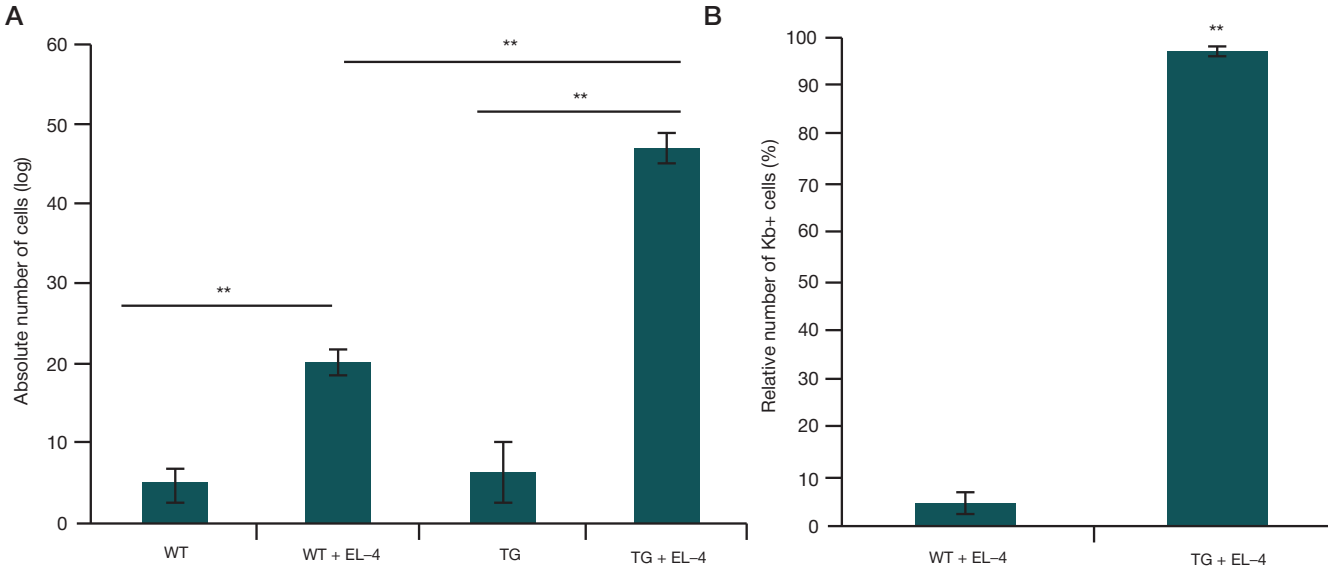


Fig. 2. Features of the development of EL-4 allogeneic lymphoma in 7B transgenic mice. Allogeneic lymphoma EL-4 ($H\text{-}2K^b$) cells were injected intraperitoneally to 7B ($H\text{-}2^k$) transgenic mice (TG+EL-4). Non-transgenic siblings (WT+EL-4) were used as controls. On day 12 after EL-4 injection, perinoteal cells were analyzed by flow cytometry. **A**. The absolute number (log) of cells. ** — $p \leq 0.01$ (ANOVA, post-hoc Tukey test). **B**. The relative number (%) of EL-4 (Kb^+) tumor cells. ** — $p \leq 0.01$ (Student's unpaired *t*-test). Data from two independent experiments ($n = 4–6$) are presented

7B mice were unable to reject allogeneic EL-4 lymphoma; as shown in Figure 3, all of them died after an average of 19 days. It should be noted that these animals endured longer than C57BL/6 mice, as for the latter, EL-4 is syngeneic and typically kills them within 10–12 days (Fig. 3). This finding indicates that in 7B transgenic mice, the response to allogeneic EL-4 lymphoma includes elimination and equilibrium phases — albeit insufficiently effective — before the tumor adapts to evade it.

The active immune response to EL-4 cells in wild-type mice (WT+EL-4) was characterized by an accumulation of T-cells, the number of which increased approximately fourfold (Fig. 4A, B), and a fivefold growth of the proportion of cytotoxic CD8⁺ cells compared with the intact control (WT) (Fig. 4C, D). Such developments were not registered in immunized transgenic mice (TG+EL-4): compared with the non-immunized control animals (TG), the relative number of T-lymphocytes (Fig. 4A, B) and CD8⁺ T-cells (Figure 4C, D) did not increase in them. However, the ratio of CD8⁺ T-cells expressing the transgenic β-chain TCR (Vb8.3⁺) or endogenous β-chains TCR (Vb8.3⁻) in the peritoneal cavity of immunized 7B mice (TG+EL-4) was approximately 1:1 compared with 2:1 in the control group (TG) (Fig. 4D, E), which indicates the involvement of both subpopulations of cytotoxic T-cells in response to EL-4 cells.

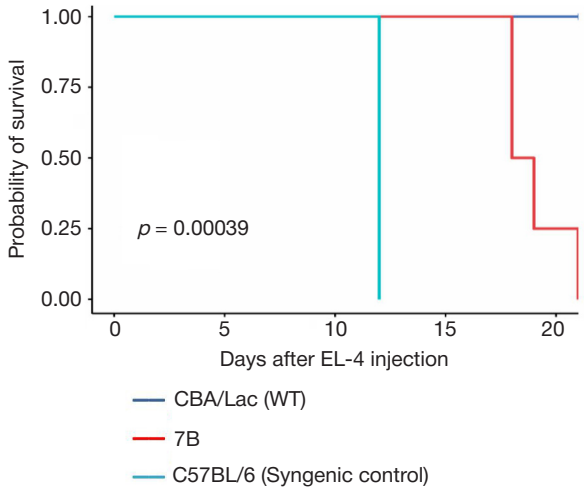


Fig. 3. Survival curves of 7B transgenic mice after EL-4 lymphoma transplantation. Parental CBA/Lac (WT) mice and C57BL/6 mice, for which EL-4 is a syngeneic tumor, were used as controls. The data from one representative experiment (n = 4) are presented

Accordingly, immunized 7B mice showed a 1.8-fold increase in the proportion of effector (CD44⁺CD62L⁻) CD8⁺ T-cells with transgenic TCRβ (Fig. 5A, B) and a 1.5-fold increase in effector CD8⁺ T-cells with endogenous TCRβ (Figure 5C, D), compared

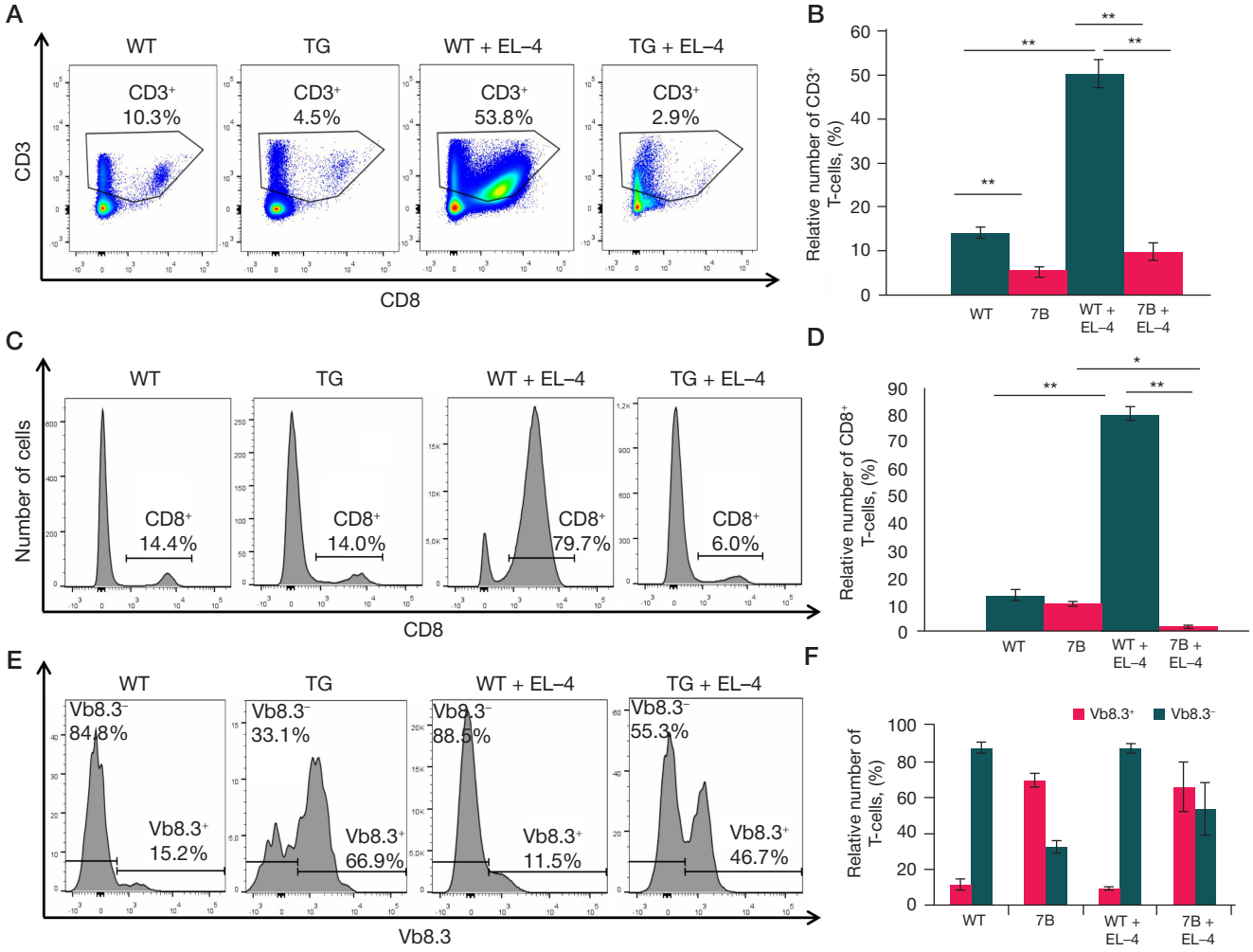


Fig. 4. Analysis of the immune response of 7B mice to an allogeneic tumor *in vivo*. Transgenic 7B mice (TG+EL-4) and non-transgenic siblings (WT+EL-4) were injected intraperitoneally with EL-4 allogeneic lymphoma cells. On day 12 after EL-4 injection, peritoneal cells were analyzed by flow cytometry. Intact (non-immunized) animals of the CBA/Lac (WT) parent line and the 7B (TG) transgenic line were used as controls. **A**, **B**. The relative number (%) of T-cells (CD3⁺). **C**, **D**. The relative number (%) of cytotoxic CD8⁺ T-cells. **E**, **F**. The relative number (%) of CD8⁺ T-cells with the transgenic β-chain of the T-cell receptor (TCRβ) (Vb8.3⁺) and CD8⁺ T-cells with endogenously rearranged TCRβ (Vb8.3⁻). **A**, **C**, **E**. Data from one representative staining are presented. **B**, **D**, **F**. Data from the two experiments are presented as the mean ± standard error of the mean (n = 4–6). * — $p \le 0.05$; ** — $p \le 0.01$, ANOVA, post-hoc Tukey test

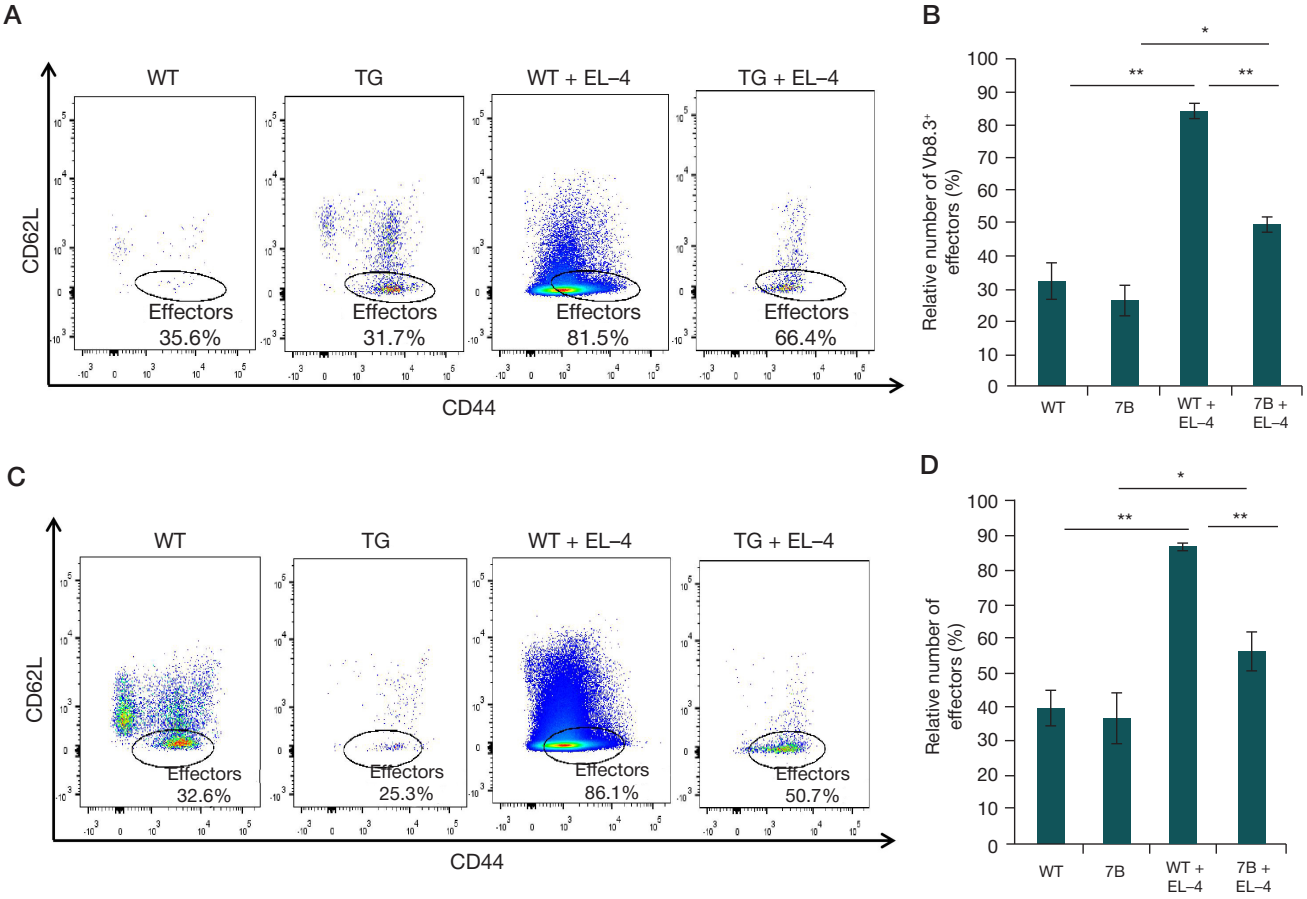


Fig. 5. Analysis of the pool of cytotoxic effector T-cells in 7B transgenic mice in response to EL-4 allogeneic lymphoma *in vivo*. Analysis of effector $CD44^+CD62L^-$ $CD8^+$ T-cells in the peritoneal cavity of 7B transgenic mice (TG+EL-4) and non-transgenic siblings (WT+EL-4) on day 12 after EL-4 injection. Intact (non-immunized) animals of the CBA/Lac (WT) parent line and the 7B (TG) transgenic line were used as controls. **A**, **B**. The relative number (%) of effector T-cells with transgenic TCRß ($Vb8.3^+$). **C**, **D**. The relative number (%) of effector T-cells with endogenously rearranged TCRß ($Vb8.3^-$). **A**, **C**. Data from one representative staining are presented. **B**, **D**. Data from the two experiments are presented as the mean ± standard error of the mean (n = 4–6). * — $p \le 0.05$; ** — $p \le 0.01$, ANOVA, post-hoc Tukey test

with the corresponding $CD44^+CD62L^-$ T-cell subpopulations in intact transgenic mice (TG). Meanwhile, the relative number of $Vb8.3^+$ and $Vb8.3^-$ $CD8^+$ effectors in the peritoneal cavity of immunized transgenic mice (TG+EL-4) was 1.5–1.7 times lower than in immunized wild-type animals (WT+EL-4) (50–56% vs. 84–86%) (Fig. 5).

DISCUSSION

The results of this study indicate the development of a weak immune response to alloantigens in 7B transgenic mice *in vivo* with the formation of a small pool of effector cytotoxic T-cells, which is consistent with the data of our early work that used a different TCRβ-transgenic model [14].

Several studies have shown that TCRß-transgenic animals retain the ability to respond to various antigens, including allogeneic MHC molecules [20, 21]. These findings point to the high plasticity of the TCR repertoire, which allows compensating for the significant reduction in the diversity of clonotypes caused by the expression of the transgenic β-chain [20, 21]. However, the intensity of the immune response in TCRß-transgenic mice is lower than in wild-type animals [14, 20, 21] because of the low frequency of responding T-cell clones [20, 22]; consequently, these mice show a slower development of T-cell responses *in vivo* [21]. An important factor in this context is that the cytotoxic $CD8^+$ immune response that TCRß-transgenic mice develop to the allogeneic MHC class I molecule ($H\text{-}2K^b$) is insufficient to reject the allogeneic tumor (Figure 4, Figure 5) [14]. Thus, the response even to a strong transplant antigen becomes ineffective due to the reduction of the diversity of the TCR repertoire.

In this regard, recognition of allogeneic tumor antigens follows the same patterns as recognition of tumor antigens in combination with self MHC molecules. The effectiveness of the antitumor response and, consequently, elimination of the transformed cells is largely determined by the mutation load of the tumor — its immunogenicity [23, 24] — and the clonal diversity of T-cells capable of recognizing tumor neoantigens or tumor-associated antigens [24, 25]. It has been shown that a high diversity of T-cell receptors (TCRs) circulating in peripheral blood is a favorable prognostic factor in several cancers, such as melanoma [26], non-small cell lung cancer [27, 28], and breast cancer [29]. In contrast, a low TCR diversity of tumor-infiltrating T-cells is associated with a poor prognosis in stomach cancer and some other malignancies [30–32].

The natural aging of the immune system, especially thymus involution and clonal expansion of memory cells in the periphery, causes a reduction in the diversity of the repertoire of T-lymphocytes [33-35], which leads to a greater predisposition of the elderly to infections and cancer [33, 36]. In addition, experimental studies involving mice have shown that at 12 months of age, the animals exhibit decreased responses to alloantigens, which are partly attributable to an age-associated narrowing of the T-cell clonotype repertoire [34, 37].

The results of this study confirm that the effectiveness of the immune response to tumor alloantigens directly depends on the breadth of the repertoire of mature T lymphocytes, as previously established [14].

CONCLUSIONS

This study shows that 7B transgenic mice develop an *in vivo* immune response that is not effective enough to eliminate allogeneic tumor cells. Due to the expression of the transgenic β-chain TCR, the number and frequency of cytotoxic T-cell clonotypes capable of recognizing allogeneic MHC molecules decrease. However, the neoplastic process in such animals progresses through all stages of immunoediting, from ineffective stages of elimination and equilibrium to the tumor escaping from immune surveillance. The results of this study are consistent with our earlier findings; they confirm that decreased diversity of the TCR repertoire is a factor preventing rejection of the allogeneic tumor, allowing it to progress. In this case, the weak immune response that develops in the allogeneic recipient contributes to the selection of the least immunogenic malignant clones, thereby driving tumor immunoediting.

References

1. Murphy K., Weaver C., Berg L. Janeway's Immunobiology. 10th ed. New York: W. W. Norton & Company, Inc, 2022.
2. DeWolf S, Grinshpun B, Savage T, Lau SP, Obradovic A, Shonts B, et al. Quantifying size and diversity of the human T cell alloresponse. JCI Insight. 9; 3 (15): e121256.
3. Tian G, Li M, Lv G. Analysis of T-Cell Receptor Repertoire in Transplantation: Fingerprint of T Cell-mediated Alloresponse. Front Immunol. 2022; 12: 778559.
4. Lin CM, Gill RG. Direct and indirect allograft recognition: pathways dictating graft rejection mechanisms. Curr Opin Organ Transplant. 2016; 21 (1): 40–44.
5. Kazansky DB. MHC restriction and allogeneic immune responses. J Immunotoxicol. 2008; 5 (4): 369–84.
6. D'Orsogna LJ, Roelen DL, Doxiadis II, Claas FH. TCR cross-reactivity and allorecognition: new insights into the immunogenetics of allorecognition. Immunogenetics. 2012; 64 (2): 77–85.
7. Duneton C, Winterberg PD, Ford ML. Activation and regulation of alloreactive T cell immunity in solid organ transplantation. Nat Rev Nephrol. 2022; 18 (10): 663–76.
8. Link-Rachner CS, Eugster A, Rücker-Braun E, Heidenreich F, Oelschlägel U, Dahl A, et al. T-cell receptor-α repertoire of CD8+ T cells following allogeneic stem cell transplantation using next-generation sequencing. Haematologica. 2019; 104 (3): 622–31.
9. Tian G, Song S, Zhi Y, Qiu W, Chen Y, Sun X, et al. Alloreactive T cells temporarily increased in the peripheral blood of patients before liver allograft rejection. Liver Transpl. 2024; 30 (12): 1250–63.
10. Mendoza Rojas A, Verhoeven JGHP, de Kuiper R, Clahsen-van Groningen MC, Boer K, Hesselink DA, et al. Alloreactive T cells to Assess Acute Rejection Risk in Kidney Transplant Recipients. Transplant Direct. 2023; 9 (5): e1478.
11. Kim JY, Lei Z, Maienschein-Cline M, Chlipala GE, Balamurugan A, McDiarmid SV, et al. Longitudinal Analysis of the T-cell Receptor Repertoire in Graft-infiltrating Lymphocytes Following Hand Transplantation. Transplantation. 2021; 105 (7): 1502–9.
12. Obata F, Yoshida K, Ikeda Y, Ohkubo M, Saito T, Takeuchi Y, et al. Clonality analysis of T cells mediating acute and chronic rejection in kidney allografts. Transpl Immunol. 2004; 13 (3): 233–7.
13. Zeng G, Huang Y, Huang Y, Lyu Z, Lesniak D, Randhawa P. Antigen-Specificity of T Cell Infiltrates in Biopsies With T Cell-Mediated Rejection and BK Polyomavirus Viremia: Analysis by Next Generation Sequencing. Am J Transplant. 2016; 16 (11): 3131–8.
14. Silaeva YY, Grinenko TS, Vagida MS, Kalinina AA, Khromykh LM, et al. Immune selection of tumor cells in TCR β-chain transgenic mice. J Immunotoxicol. 2014; 11 (4): 393–9.
15. Grinenko TS, Pobezinskaya EL, Pobezinskii LA, Baturina IA, Zvezdova ES, Kazanskii DB. Suppression of primary allogenic response by CD8+ memory cells. Bull Exp Biol Med 2005; 140 (5): 545–9.
16. Zamkova M, Kalinina A, Silaeva Y, Persiyantseva N, Bruter A, Deikin A, et al. Dominant role of the α-chain in rejection of tumor cells bearing a specific alloantigen in TCRα transgenic mice and in in vitro experiments. Oncotarget. 2019; 10: 4808–21.
17. Pobezinskij LA, Pobezinskaya EL, Grinenko TS, CHervonskij AV, Kazanskij DB. Perifericheskij pul T-kletok CD8+ soderzhit limfocity s antigenspecificheskimi receptorami, raspoznayushchimi singennnye molekuly MNS klassa II. Ontogenez. 2004; 35 (3): 183–9.
18. Silaeva Y, Kalinina A, Vagida M, Khromykh LM, Deikin AV, Ermolkevich TG, et al. Decrease in pool of T lymphocytes with surface phenotypes of effector and central memory cells under influence of TCR transgenic β-chain expression. Biochemistry (Moscow). 2013; 78: 549–59.
19. Tang D, Chen M, Huang X, Zhang G, Zeng L, Zhang G, et al. SRplot: A free online platform for data visualization and graphing. PLoS ONE. 2023: 18 (11): e0294236.
20. Listman JA, Rimm IJ, Wang Y, Geller MC, Tang JC, Ho S, et al. Plasticity of the T cell receptor repertoire in TCR beta-chain transgenic mice. Cell Immunol. 1996; 167 (1): 44–55.
21. Ewing C, Allan W, Daly K, Hou S, Cole GA, Doherty PC, et al. Virus-specific CD8+ T-cell responses in mice transgenic for a T-cell receptor beta chain selected at random. J Virol. 1994; 68 (5): 3065–70.
22. Jenkins MK, Moon JJ. The role of naive T cell precursor frequency and recruitment in dictating immune response magnitude. J Immunol. 2012; 88 (9): 4135–40.
23. Jardim DL, Goodman A, de Melo Gagliato D, Kurzrock R. The Challenges of Tumor Mutational Burden as an Immunotherapy Biomarker. Cancer Cell. 2021; 39 (2): 154–73.
24. Aran A, Garrigós L, Curigliano G, Cortés J, Martí M. Evaluation of the TCR Repertoire as a Predictive and Prognostic Biomarker in Cancer: Diversity or Clonality? Cancers (Basel). 2022; 14 (7): 1771.
25. Wilczyński JR, Nowak M. Cancer Immunoediting: Elimination, Equilibrium, and Immune Escape in Solid Tumors. In: Klink M., Szulc-Kielbik I, editors. Interaction of Immune and Cancer Cells. Experientia Supplementum, vol 113: Springer, 2022.
26. Charles J, Mouret S, Challende I, Leccia MT, De Fraipont F, Perez S, et al. T-cell receptor diversity as a prognostic biomarker in melanoma patients. Pigment Cell Melanoma Res. 2020; 33 (4): 612–24.
27. Qian L, Zhaohui Z, Yaping X, Zhentian L, Zhentao L, Qiqi W, et al. Blood T cell diversity associated with the prognosis of advanced non-small cell lung carcinoma treated with first-line pemetrexed based chemotherapy. Thorac Cancer. 2021; 12 (7): 997–1005.
28. Abed A, Beasley AB, Reid AL, Law N, Calapre L, Millward M, et al. Circulating pre-treatment T-cell receptor repertoire as a predictive biomarker in advanced or metastatic non-small-cell lung cancer patients treated with pembrolizumab alone or in combination with chemotherapy. ESMO Open. 2023; 8 (6): 102066.
29. Manuel M, Tredan O, Bachelot T, Clapisson G, Courtier A, Parmentier G, et al. Lymphopenia combined with low TCR diversity (divpenia) predicts poor overall survival in metastatic breast cancer patients. Oncoimmunology. 2012; 1 (4): 432–40.
30. Jia Q, Zhou J, Chen G, Shi Y, Yu H, Guan P, et al. Diversity index of mucosal resident T lymphocyte repertoire predicts clinical prognosis in gastric cancer. Oncoimmunology. 2015; 4 (4): e1001230.
31. Jin YB, Luo W, Zhang GY, Lin KR, Cui JH, Chen XP, et al. TCR repertoire profiling of tumors, adjacent normal tissues, and peripheral blood predicts survival in nasopharyngeal carcinoma. Cancer Immunol Immunother. 2018; 67 (11): 1719–30.
32. Cui JH, Lin KR, Yuan SH, Jin YB, Chen XP, Su XK, Jet al. TCR Repertoire as a Novel Indicator for Immune Monitoring and Prognosis Assessment of Patients With Cervical Cancer. Front Immunol. 2018; 9: 2729.

33. Fulop T, Larbi A, Pawelec G, Khalil A, Cohen AA, Hirokawa K, et al. Immunology of Aging: the Birth of Inflammaging. Clin Rev Allergy Immunol. 2023; 64 (2): 109–22.
34. Britanova OV, Putintseva EV, Shugay M, Merzlyak EM, Turchaninova MA, Staroverov DB, et al. Age-related decrease in TCR repertoire diversity measured with deep and normalized sequence profiling. J Immunol. 2014; 192 (6): 2689–98.
35. Shevyrev DV, Tereshchenko VP, Kozlov VA. Gomeostaticheskaya proliferaciya: ot normy k patologii. Rossijskij immunologicheskij zhurnal. 2018; 21 (2): 91–105. Russian.
36. Montégut L, López-Otín C, Kroemer G. Aging and cancer. Mol Cancer 2024; 23 (1): 106.
37. Kalinina AA, Ziganshin RK, Silaeva YY, Sharova NI, Nikonova MF, Persiyantseva NA, et al. Physiological and Functional Effects of Dominant Active TCRα Expression in Transgenic Mice. Int J Mol Sci. 2023; 24 (7): 6527.

Литература

1. Murphy K., Weaver C., Berg L. Janeway's Immunobiology. 10th ed. New York: W. W. Norton & Company, Inc, 2022.
2. DeWolf S, Grinshpun B, Savage T, Lau SP, Obradovic A, Shonts B, et al. Quantifying size and diversity of the human T cell alloresponse. JCI Insight. 9; 3 (15): e121256.
3. Tian G, Li M, Lv G. Analysis of T-Cell Receptor Repertoire in Transplantation: Fingerprint of T Cell-mediated Alloresponse. Front Immunol. 2022; 12: 778559.
4. Lin CM, Gill RG. Direct and indirect allograft recognition: pathways dictating graft rejection mechanisms. Curr Opin Organ Transplant. 2016; 21 (1): 40–44.
5. Kazansky DB. MHC restriction and allogeneic immune responses. J Immunotoxicol. 2008; 5 (4): 369–84.
6. D'Orsogna LJ, Roelen DL, Doxiadis II, Claas FH. TCR cross-reactivity and allorecognition: new insights into the immunogenetics of allorecognition. Immunogenetics. 2012; 64 (2): 77–85.
7. Duneton C, Winterberg PD, Ford ML. Activation and regulation of alloreactive T cell immunity in solid organ transplantation. Nat Rev Nephrol. 2022; 18 (10): 663–76.
8. Link-Rachner CS, Eugster A, Rücker-Braun E, Heidenreich F, Oelschlägel U, Dahl A, et al. T-cell receptor-α repertoire of CD8+ T cells following allogeneic stem cell transplantation using next-generation sequencing. Haematologica. 2019; 104 (3): 622–31.
9. Tian G, Song S, Zhi Y, Qiu W, Chen Y, Sun X, et al. Alloreactive T cells temporarily increased in the peripheral blood of patients before liver allograft rejection. Liver Transpl. 2024; 30 (12): 1250–63.
10. Mendoza Rojas A, Verhoeven JGHP, de Kuiper R, Clahsen-van Groningen MC, Boer K, Hesselink DA, et al. Alloreactive T cells to Assess Acute Rejection Risk in Kidney Transplant Recipients. Transplant Direct. 2023; 9 (5): e1478.
11. Kim JY, Lei Z, Maienschein-Cline M, Chlipala GE, Balamurugan A, McDiarmid SV, et al. Longitudinal Analysis of the T-cell Receptor Repertoire in Graft-infiltrating Lymphocytes Following Hand Transplantation. Transplantation. 2021; 105 (7): 1502–9.
12. Obata F, Yoshida K, Ikeda Y, Ohkubo M, Saito T, Takeuchi Y, et al. Clonality analysis of T cells mediating acute and chronic rejection in kidney allografts. Transpl Immunol. 2004; 13 (3): 233–7.
13. Zeng G, Huang Y, Huang Y, Lyu Z, Lesniak D, Randhawa P. Antigen-Specificity of T Cell Infiltrates in Biopsies With T Cell-Mediated Rejection and BK Polyomavirus Viremia: Analysis by Next Generation Sequencing. Am J Transplant. 2016; 16 (11): 3131–8.
14. Silaeva YY, Grinenko TS, Vagida MS, Kalinina AA, Khromykh LM, et al. Immune selection of tumor cells in TCR β-chain transgenic mice. J Immunotoxicol. 2014; 11 (4): 393–9.
15. Grinenko TS, Pobezinskaya EL, Pobezinskii LA, Baturina IA, Zvezdova ES, Kazanskii DB. Suppression of primary allogenic response by CD8+ memory cells. Bull Exp Biol Med 2005; 140 (5): 545–9.
16. Zamkova M, Kalinina A, Silaeva Y, Persiyantseva N, Bruter A, Deikin A, et al. Dominant role of the α-chain in rejection of tumor cells bearing a specific alloantigen in TCRα transgenic mice and in in vitro experiments. Oncotarget. 2019; 10: 4808–21.
17. Pobezinskij LA, Pobezinskaya EL, Grinenko TS, CHervonskij AV, Kazanskij DB. Perifericheskij pul T-kletok CD8+ soderzhit limfocity s antigenspecificheskimi receptorami, raspoznayushchimi singennye molekuly MNS klassa II. Ontogenez. 2004; 35 (3): 183–9.
18. Silaeva Y, Kalinina A, Vagida M, Khromykh LM, Deikin AV, Ermolkevich TG, et al. Decrease in pool of T lymphocytes with surface phenotypes of effector and central memory cells under influence of TCR transgenic β-chain expression. Biochemistry (Moscow). 2013; 78: 549–59.
19. Tang D, Chen M, Huang X, Zhang G, Zeng L, Zhang G, et al. SRplot: A free online platform for data visualization and graphing. PLoS ONE. 2023: 18 (11): e0294236.
20. Listman JA, Rimm IJ, Wang Y, Geller MC, Tang JC, Ho S, et al. Plasticity of the T cell receptor repertoire in TCR beta-chain transgenic mice. Cell Immunol. 1996; 167 (1): 44–55.
21. Ewing C, Allan W, Daly K, Hou S, Cole GA, Doherty PC, et al. Virus-specific CD8+ T-cell responses in mice transgenic for a T-cell receptor beta chain selected at random. J Virol. 1994; 68 (5): 3065–70.
22. Jenkins MK, Moon JJ. The role of naive T cell precursor frequency and recruitment in dictating immune response magnitude. J Immunol. 2012; 88 (9): 4135–40.
23. Jardim DL, Goodman A, de Melo Gagliato D, Kurzrock R. The Challenges of Tumor Mutational Burden as an Immunotherapy Biomarker. Cancer Cell. 2021; 39 (2): 154–73.
24. Aran A, Garrigós L, Curigliano G, Cortés J, Martí M. Evaluation of the TCR Repertoire as a Predictive and Prognostic Biomarker in Cancer: Diversity or Clonality? Cancers (Basel). 2022; 14 (7): 1771.
25. Wilczyński JR, Nowak M. Cancer Immunoediting: Elimination, Equilibrium, and Immune Escape in Solid Tumors. In: Klink M., Szulc-Kielbik I, editors. Interaction of Immune and Cancer Cells. Experientia Supplementum, vol 113: Springer, 2022.
26. Charles J, Mouret S, Challende I, Leccia MT, De Fraipont F, Perez S, et al. T-cell receptor diversity as a prognostic biomarker in melanoma patients. Pigment Cell Melanoma Res. 2020; 33 (4): 612–24.
27. Qian L, Zhaohui Z, Yaping X, Zhentian L, Zhentao L, Qiqi W, et al. Blood T cell diversity associated with the prognosis of advanced non-small cell lung carcinoma treated with first-line pemetrexed based chemotherapy. Thorac Cancer. 2021; 12 (7): 997–1005.
28. Abed A, Beasley AB, Reid AL, Law N, Calapre L, Millward M, et al. Circulating pre-treatment T-cell receptor repertoire as a predictive biomarker in advanced or metastatic non-small-cell lung cancer patients treated with pembrolizumab alone or in combination with chemotherapy. ESMO Open. 2023; 8 (6): 102066.
29. Manuel M, Tredan O, Bachelot T, Clapisson G, Courtier A, Parmentier G, et al. Lymphopenia combined with low TCR diversity (divpenia) predicts poor overall survival in metastatic breast cancer patients. Oncoimmunology. 2012; 1 (4): 432–40.
30. Jia Q, Zhou J, Chen G, Shi Y, Yu H, Guan P, et al. Diversity index of mucosal resident T lymphocyte repertoire predicts clinical prognosis in gastric cancer. Oncoimmunology. 2015; 4 (4): e1001230.
31. Jin YB, Luo W, Zhang GY, Lin KR, Cui JH, Chen XP, et al. TCR repertoire profiling of tumors, adjacent normal tissues, and peripheral blood predicts survival in nasopharyngeal carcinoma. Cancer Immunol Immunother. 2018; 67 (11): 1719–30.
32. Cui JH, Lin KR, Yuan SH, Jin YB, Chen XP, Su XK, Jet al. TCR Repertoire as a Novel Indicator for Immune Monitoring and Prognosis Assessment of Patients With Cervical Cancer. Front Immunol. 2018; 9: 2729.
33. Fulop T, Larbi A, Pawelec G, Khalil A, Cohen AA, Hirokawa K, et al. Immunology of Aging: the Birth of Inflammaging. Clin Rev Allergy Immunol. 2023; 64 (2): 109–22.
34. Britanova OV, Putintseva EV, Shugay M, Merzlyak EM, Turchaninova MA, Staroverov DB, et al. Age-related decrease in TCR repertoire diversity measured with deep and normalized

sequence profiling. J Immunol. 2014; 192 (6): 2689–98.
35. Shevyrev DV, Tereshchenko VP, Kozlov VA. Gomeostaticheskaya proliferaciya: ot normy k patologii. Rossijskij immunologicheskij zhurnal. 2018; 21 (2): 91–105. Russian.
36. Montégut L, López-Otín C, Kroemer G. Aging and cancer. Mol Cancer 2024; 23 (1): 106.
37. Kalinina AA, Ziganshin RK, Silaeva YY, Sharova NI, Nikonova MF, Persiyantseva NA, et al. Physiological and Functional Effects of Dominant Active TCRα Expression in Transgenic Mice. Int J Mol Sci. 2023; 24 (7): 6527.

PERIVASCULAR MAST CELLS AND ANGIOGENESIS IN THE TUMOR MICROENVIRONMENT OF SYNOVIAL SARCOMA

Bulanov DV[1,2], Makhachev DR[1]✉, Suntsov MA[1], Gubich DS[1], Filippova YD[1], Krutilina AA[1], Svoyak AV[1], Ivannikova AA[1], Ghabibullaev RM[3]

[1] Pirogov Russian National Research Medical University, Moscow, Russia

[2] Priorov National Medical Research Center of Traumatology and Orthopedics, Moscow, Russia

[3] Dedov Endocrinology Research Centre, Moscow, Russia

Synovial sarcoma is characterized by marked histological and molecular heterogeneity, and angiogenesis as well as innate immune cells are considered potential sources of prognostic markers and therapeutic targets. This study aimed to evaluate the relationship between the quantitative and spatial characteristics of mast cells and angiogenesis in the tumor microenvironment of synovial sarcoma, as well as their prognostic significance. Using immunohistochemistry (tryptase/CD117, CD31/CD34, VEGF-A, α-SMA, CD3/CD8, CD68/CD163) and digital morphometry normalized to 1 mm^2, we analyzed 140 cases of synovial sarcoma. The intrathumoral, peritumoral, and perivascular (≤50 μm from CD31$^+$/CD34$^+$ vessels) zones, as well as the mastocyte degranulation index, were evaluated separately. Mast cells were detected in all observations; their density and signs of degranulation were greatest in the perivascular zone. Perivascular mast cells were positively correlated with both microvascular density and VEGF-A expression, and inversely correlated with α-SMA pericyte coverage; these relationships remained significant even after accounting for CD163$^+$ macrophages. A high microvascular density and increased perivascular mast cell counts were associated with an unfavorable survival prognosis, while pronounced CD8$^+$ infiltration predicted better outcomes. The developed integral Mast-Angio Score, which combines perivascular density, mast cell degranulation, microvascular density, and VEGF-A expression, improves the accuracy of prognostic stratification and can serve as a morphological basis for justifying combined antiangiogenic and immune therapy.

Keywords: mast cells, tryptase, angiogenesis, microvessel density, tumor microenvironment, synovial sarcoma, digital morphometry

Author contribution: Bulanov DV — study supervision, design, and conceptualization, article editing; Makhachev DR, Suntsov MA, Gubich DS — data analysis and interpretation, article authoring, editing; Filippova YuD, Krutilina AA, Ghabibullaev RM, Svoyak AV, Ivannikova AI — collection of the clinical data, article editing.

✉ **Correspondence should be addressed:** Dalgat R. Makhachev
Akademika Volgina, 37, Moscow, 117437, Russia; dalgat2002@mail.ru

Received: 07.10.2025 **Accepted:** 05.11.2025 **Published online:** 21.11.2025

DOI: 10.24075/brsmu.2025.059

Copyright: © 2025 by the authors. **Licensee:** Pirogov University. This article is an open access article distributed under the terms and conditions of the Creative Commons Attribution (CC BY) license (https://creativecommons.org/licenses/by/4.0/).

ПЕРИВАСКУЛЯРНЫЕ МАСТОЦИТЫ И АНГИОГЕНЕЗ В ОПУХОЛЕВОМ МИКРООКРУЖЕНИИ СИНОВИАЛЬНОЙ САРКОМЫ

Д. В. Буланов[1,2], Д. Р. Махачев[1]✉, М. А. Сунцов[1], Д. С. Губич[1], Ю. Д. Филиппова[1], А. А. Крутилина[1], А. В. Свояк[1], А. А. Иванникова[1], Р. М. Габибуллаев[3]

[1] Российский национальный исследовательский медицинский университет имени Н. И. Пирогова (Пироговский Университет), Москва, Россия

[2] Национальный медицинский исследовательский центр травматологии и ортопедии имени Н. Н. Приорова, Москва, Россия

[3] Научный медицинский исследовательский центр эндокринологии имени И. И. Дедова, Москва, Россия

Синовиальная саркома характеризуется выраженной гистологической и молекулярной гетерогенностью, а ангиогенез и клетки врожденного иммунитета рассматривают как потенциальные источники прогностических маркеров и терапевтических мишеней. Целью исследования было оценить взаимосвязь количественных и пространственных характеристик мастоцитов с ангиогенезом в опухолевом микроокружении синовиальной саркомы и их прогностическую значимость. Проанализировано 140 случаев синовиальной саркомы с применением иммуногистохимии (триптаза/CD117, CD31/CD34, VEGF-A, α-SMA, CD3/CD8, CD68/CD163) и цифровой морфометрии с нормированием на 1 мм^2. Отдельно оценивали интратуморную, перитуморальную и периваскулярную (≤ 50 мкм от CD31$^+$/CD34$^+$ сосудов) зоны, а также индекс дегрануляции мастоцитов. Мастоциты выявлялись во всех наблюдениях, их плотность и признаки дегрануляции были максимальны в периваскулярной зоне. Периваскулярные мастоциты положительно коррелировали с микрососудистой плотностью и экспрессией VEGF-A и обратно — с перицитарным покрытием по α-SMA, эти связи сохранялись после учета CD163$^+$-макрофагов. Высокие значения микрососудистой плотности и периваскулярных мастоцитов ассоциировались с неблагоприятной выживаемостью, тогда как выраженный CD8$^+$-инфильтрат — с лучшими исходами. Разработанный интегральный Mast-Angio Score, объединяющий периваскулярную плотность и дегрануляцию мастоцитов, микрососудистую плотность и VEGF-A, повышает точность прогностической стратификации и может служить морфологической основой для обоснования комбинированной антиангиогенной и иммунной терапии.

Ключевые слова: тучные клетки, триптаза, ангиогенез, микрососудистая плотность, микроокружение, синовиальная саркома, цифровая морфометрия

Вклад авторов: Д. В. Буланов — руководство исследованием, разработка концепции и дизайна работы, редактирование текста статьи; Д. Р. Махачев, М. А. Сунцов, Д. С. Губич — анализ и интерпретация данных, написание текста статьи, редактирование; Ю. Д. Филиппова, А. А. Крутилина, Р. М. Габибуллаев, А. В. Свояк, А. А. Иванникова — сбор клинических данных, редактирование.

✉ **Для корреспонденции:** Далгат Рамазанович Махачев
ул. Академика Волгина, д. 37, г. Москва, 117437, Россия; dalgat2002@mail.ru

Статья получена: 07.10.2025 **Статья принята к печати:** 05.11.2025 **Опубликована онлайн:** 21.11.2025

DOI: 10.24075/vrgmu.2025.059

Авторские права: © 2025 принадлежат авторам. **Лицензиат:** РНИМУ им. Н. И. Пирогова. Статья размещена в открытом доступе и распространяется на условиях лицензии Creative Commons Attribution (CC BY) (https://creativecommons.org/licenses/by/4.0/).

Synovial sarcoma (SS) accounts for 5–10% of soft tissue sarcomas. Its characteristic features include an aggressive clinical course, a high frequency of metastases, and a limited response to standard chemotherapy and immunotherapy. These facts justify the interest in studying the tumor microenvironment (TME), especially cells of innate immunity and angiogenesis, as potential sources of prognostic markers and therapeutic targets [1–3].

Mast cells are resident cells of the innate immune system; they contain granules with tryptase, chymase, histamine, cytokines, and growth factors. In tumor tissue, they can have both a pro-tumor effect, enhance angiogenesis, matrix remodeling, and immunosuppression via VEGF, tryptase, IL-8, and TNFb, and an antitumor effect, releasing TNFa, granzyme B, heparin, and mediators capable of inducing apoptosis of tumor cells or suppressing angiogenesis. There are two main phenotypes of mast cells: MCT (tryptase only) and MCTC (tryptase/chymase): their distribution and functional role depend on the type of tumor and the microenvironment [4–6].

The increased number of tryptase+ mast cells has been reported in various solid tumors, and it is known in such situations, the microvascular density (MVD) is often high; however, the role of the said mast cells in SS remains insufficiently studied. The data in literature are contradictory: on the one hand, mast cells are regarded as a source of proangiogenic factors; on the other hand, there are reports of their potential antitumor function and their association with a favorable prognosis in certain diseases. Most studies, however, lack a spatial assessment that factors in the localization of mast cells relative to blood vessels, although it is the perivascular zone that is key for angiogenesis and the delivery of nutrients to the tumor [4–9].

Another problem is methodological heterogeneity: researchers use different panels of immunohistochemical markers (tryptase, CD117), normalization methods (in the visual field or at 1 mm^2), rarely distinguish intra- and peritumoral zones, and almost never assess the perivascular density of mast cells or the degree of their degranulation. For SS, there are no standard criteria of quantitative and spatial assessment of mast cells aligned with angiogenesis (CD31/CD34, VEGF, MVD) and clinical prognostic data [10].

Taking into account the revealed role of mast cells as active regulators of the vascular niche and modulators of angiogenesis, this study aimed to give a comprehensive morphological description of these cells in the tissue of synovial sarcoma. We paid special attention to their quantitative and topographic parameters, including perivascular density and degree of degranulation, as well as the relationship with angiogenic features of the tumor microenvironment.

The purpose of this study was to evaluate the relationship between the quantitative and spatial characteristics of mast cells and angiogenesis in the tumor microenvironment of synovial sarcoma, and to determine their prognostic significance.

METHODS

The goal of this single-center retrospective study was to comprehensively describe morphometric characteristics of mast cells and angiogenic parameters in synovial sarcoma. The work included a standardized immunohistochemical assessment of mast cells (tryptase$^+$/CD117$^+$; density, perivascular localization, and degranulation index) and evaluation of vascular parameters (CD31/CD34, microvascular density, VEGF-A, and α-SMA), supplemented by digital morphometry normalized to the cut area (mm^2). The data for intra- and peritumoral zones (clinical and morphological characteristics, patient survival) were analyzed separately and then compared.

The study included 140 patients who were observed at the Pirogov Russian National Research Medical University. All of them had a morphologically confirmed synovial sarcoma (SS), which was the inclusion criterion. The cohort consisted of 74 men and 66 women; their age ranged from 4 to 84 years (median — 18.5 years). The materials used for the study were archival histological slides and paraffin blocks (FFPE). The cases considered included both first-time diagnoses and diagnostic reviews, provided that there was a sufficient volume of tumor tissue and enough clinical history data (age, gender, localization, size, stage, and treatment). Exclusion criteria: questionable diagnosis after revision, critically insufficient volume of tissue; repeated biopsy samples from the same lesion.

The factors and parameters assessed included the tumor's histological subtype (monophasic or biphasic), presence of necrosis, mitotic activity/Ki-67 index, stage, and metastatic status. There were two approaches to age stratification: ≤ 24 and ≥ 25 years, and < 18 and ≥ 18 years, which reflected the clinical and epidemiological features of SS.

For immunohistochemical study, we used the Leica Bond-III automatic stainer, Novocastra RTU antibodies (Leica Biosystems, UK), and Bond Polymer Refine (DAB) detection; Mayer hematoxylin was the counterstaining agent. For antigenic reprivelication, we used ER1 (pH 6.0) and/or ER2 (pH 9.0), as per IFU. The panel included tryptase and CD117 (mast cells), CD31 and CD34 (microvascular density), α-SMA (pericyte coverage), VEGF-A (angiogenic activity), CD3/CD8 (T cells), CD68/CD163 (macrophages). Additionally, we evaluated VEGFR2 (in the endothelium) and PDGFRa (in the stroma/perivascularly); the threshold of positivity was ≥ 10% of positive cells. H-score (0-300) was applied semi-quantitatively.

Scanned specimen normalized to 1 mm^2 were used for digital morphometry. Intra- and peritumoral zones were considered separately. Tissue within 50 μm of CD31$^+$/CD34$^+$ microvessels was defined as perivascular. Vessels with a lumen diameter >50 μm were excluded from the MVD calculation. To determine MVD, we used the Weidner hotspot method in fields of approximately 0.95 mm^2 and global WSI; additionally, we factored in the pericyte coverage by α-SMA.

Statistical analysis was performed in R 4.3.2. We used the Shapiro–Wilk test to assess the normality of distribution, the Mann–Whitney U or Kruskal–Wallis test for group comparisons, and Spearman's rank correlation test to evaluate relationships between variables. Spearman's partial correlation with CD163$^+$ control and multiple linear regression for MVD were used to account for the macrophage component. Multiple comparisons were adjusted using the Benjamini–Hochberg false discovery rate (FDR) procedure. Survival outcomes (MFS and OS) were evaluated using the Kaplan–Meier and Cox regression methods. The threshold of statistical significance was $p < 0.05$.

RESULTS

Immunohistochemical and morphometric studies were performed for all 140 cases. The immune infiltrate of SS had the "restrained-cold" TME profile: a low density of CD3$^+$/CD8$^+$-T-lymphocytes and a pronounced predominance of CD68$^+$/CD163$^+$ macrophages, which is consistent with the literature data on sarcomas. There were no significant differences in microvascular density (MVD) between monophasic and biphasic variants [11, 12].

Morphological analysis of the CD31-positive vascular bed showed clear zonal differences. A dense network of thin-walled capillaries with branching and looping contours,

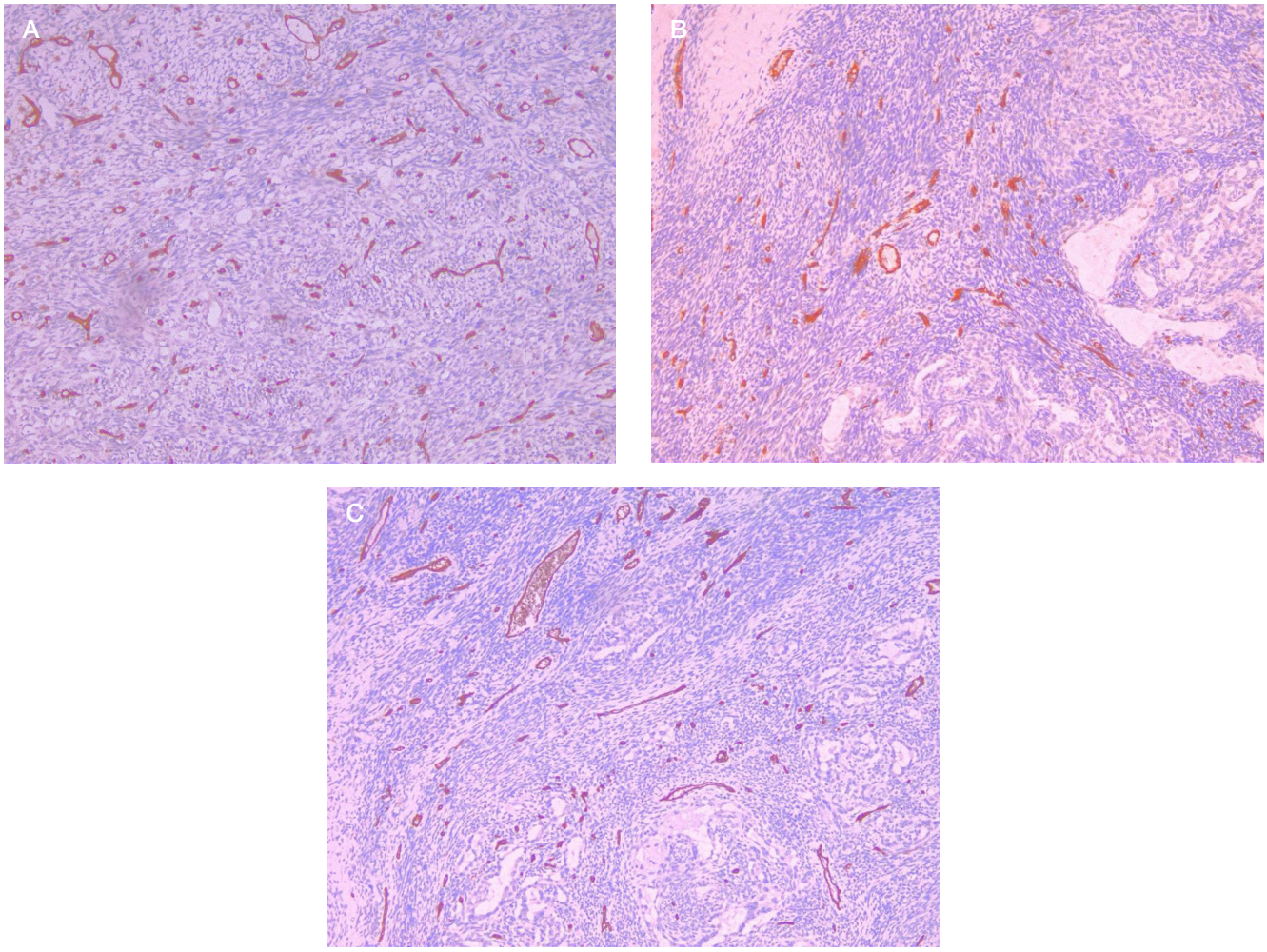


Fig. 1. A. Intratumoral zone (CD31, ×200). A dense network of thin-walled capillaries with branching and looping contours, peculiar to the hotspots of angiogenesis. **B**. Peritumoral zone (CD31, ×200). An ordered vascular network of lower density, vessels oriented along the collagen bundles. **C**. Peritumoral zone (CD31, ×200). Mosaic microvascular proliferation composed of small and medium vessels, reflecting the spatial heterogeneity of angiogenesis

corresponding to the "hot" spots of angiogenesis, was formed in the intratumoral areas. The endothelium was uniformly positive for CD31, with no signs of atypia, which reflects active sprouting angiogenesis. In the peritumoral stroma, the vascular network looked more orderly, with lower density and orientation along the collagen bundles. Near the invasive front, there was a mosaic microvascular proliferation composed of small and medium vessels, confirming the spatial heterogeneity of angiogenesis. These features are shown in Fig. 1 A, B, and Fig. 2 presents their quantitative differences; the median MVD in the intratumoral zone was ~110 vessels/mm^2, that in the peritumoral zone — about 80-90 vessels/mm^2.

CD34 staining revealed similar trends, but with expected higher values (intratumoral median ~127 vessels/mm^2, peritumoral median ~95 vessels/mm^2), which is associated with a wider marking of endothelial profiles. Thus, CD31 predominantly shows active angiogenic spots, whereas CD34 reveals the combination of mature and immature vessels.

Mast cells (MC) were visualized as CD117$^+$ elements, mostly oval in shape, with clear membrane and cytoplasmic positivity. Their distribution was governed by the topography: in the perivascular zone (≤ 50 μm from CD31$^+$/CD34$^+$ vessels), the density of MC was highest, reaching a median of ~154 cells/mm^2, while in the intratumoral areas it was about 93 cells/mm^2; the peritumoral zone had ~144 cells/mm^2, a value between the two above. From the viewpoint of spatial concentration of MC, there were detected signs of partial degranulation — extracellular granules along the cell periphery, indicating functional activity. In the intratumoral parenchyma, MCs were mainly single, not oriented along the vessels. Fig. 3 A, B present these observations, and Fig. 4 gives shows the quantitative comparison.

The analysis of angiogenic markers showed a moderately high expression of VEGF-A (H-score ~150 [100–220]) and partial vascular pericyte coverage by α-SMA (~25%), which indicates predominance of morphologically immature vessels. Expression of VEGFR2 and PDGFRa receptors was observed

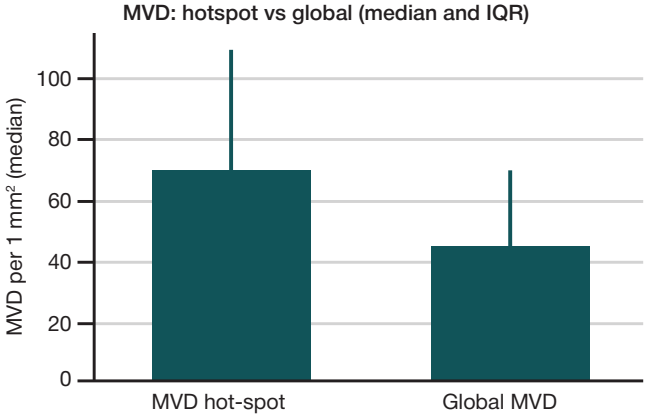


Fig. 2. Microvascular density (MVD, CD31): comparison of Weidner hotspots and whole-section assessment

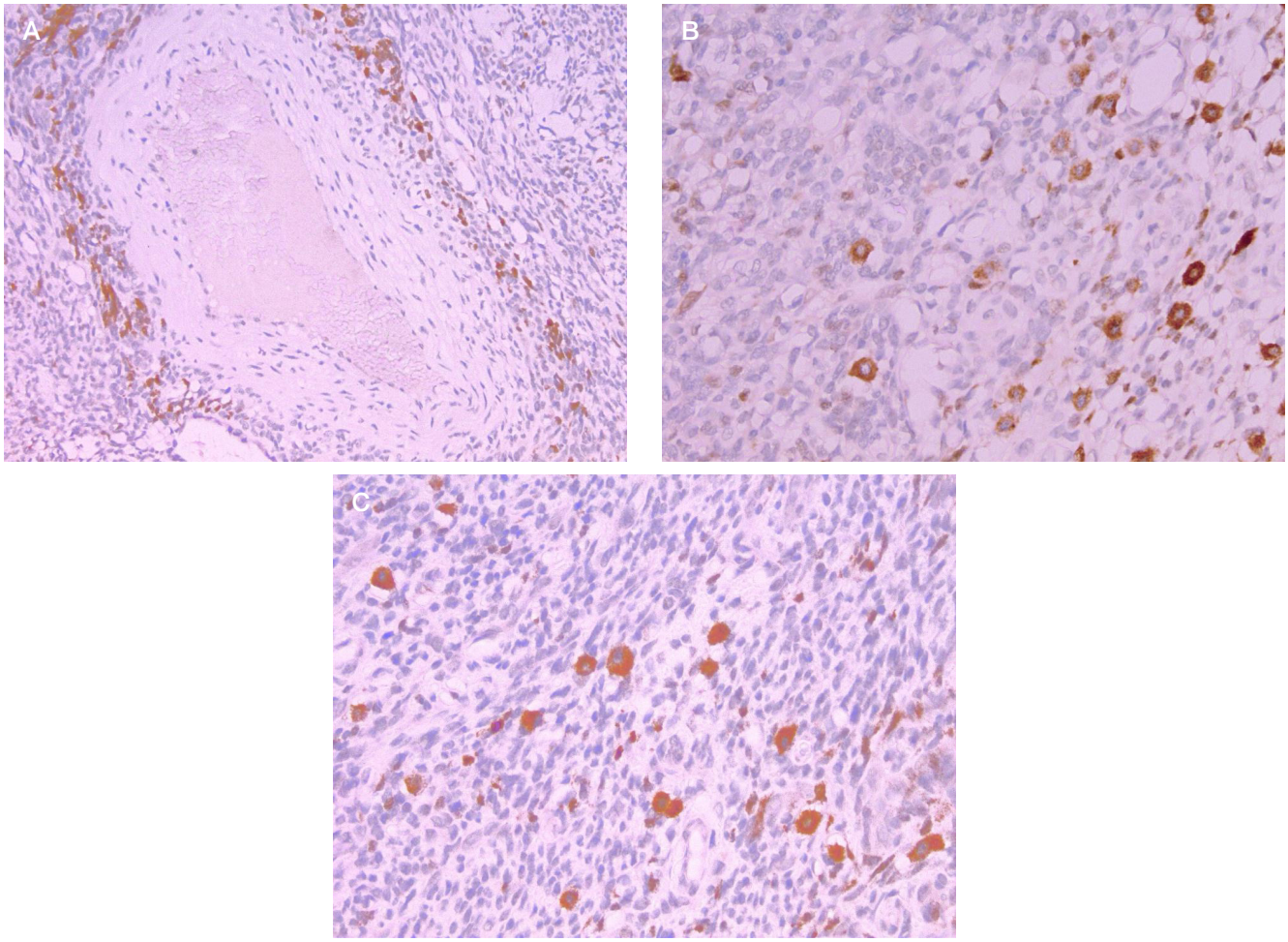


Fig. 3. A. Perivascular zone ≤ 50 μm (CD117, ×200). Clustering of mast cells along the vascular wall; individual cells with extracellular granules (an indirect sign of degranulation). **B**. Perivascular zone ≤ 50 μm (CD117, ×400). Clusters of mature granular mast cells forming vascular cuffing. **C**. Intratumoral zone (CD117, ×400). Solitary mast cells lacking pronounced perivascular orientation, with partial loss of granularity

in 20% and 46–70% of cases, respectively, which confirms the involvement of both signaling axes in the regulation of angiogenesis in synovial sarcoma (Fig. 5 A, B).

Correlation analysis (Fig. 6) confirmed a strong link between mast cell activity and angiogenesis: perivascular MC density positively correlated with MVD in hotspots (R_s = 0.70) and globally (r_s = 0.62), as well as with VEGF-A (r_s = 0.40), and degranulation index — with MVD (r_s = 0.55). These dependencies persisted after adjustment for CD163⁺ macrophages, which confirms independent contribution of mast cells to angiogenesis. The inverse correlation of MVD with α-SMA pericyte coverage (R_s = –0.35) points to the predominance of immature vessels in the zones of mastocytic activity.

Considering the sample though the lens of age (≤ 24 and ≥ 25 years old; < 18 and ≥ 18 years old), we failed to identify significant differences in MVD, VEGF-A, and MC density ($p > 0.05$), which means age is not a factor modifying angiogenic profile. In the subgroup for which we had the survival data, increased value of MVD and perivascular MC amount were associated with less favorable outcomes, while a high density of CD8⁺ T lymphocytes usually meant better MFS/OS.

An integral Mast–Angio Score was developed based on these parameters. It includes perivascular density of MC, MVD, VEGF-A, and degranulation index. Internal validation showed an improvement in the c-index and NRI/IDI indicators compared to traditional clinical and morphological models, which confirms the prognostic significance of mastocyte-angiogenic metrics in SS [13–15].

DISCUSSION

The obtained morphological and quantitative data confirm active angiogenesis and close vascular-immune interaction in the microenvironment of SS. The increased intratumoral CD31 and CD34 MVD reflects the predominance of sprouting angiogenesis in the tumor parenchyma, whereas the vascular network in the peritumoral stroma is less dense and more structured. The difference between the markers is explained by differences in their specificity: CD31 predominantly shows

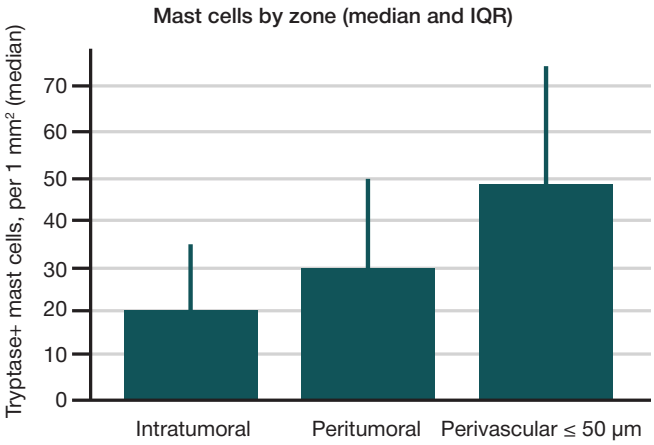


Fig. 4. The density of tryptase+ mast cells in the intratumoral, peritumoral, and perivascular (≤ 50 μm from CD31⁺/CD34⁺ vessels) zones

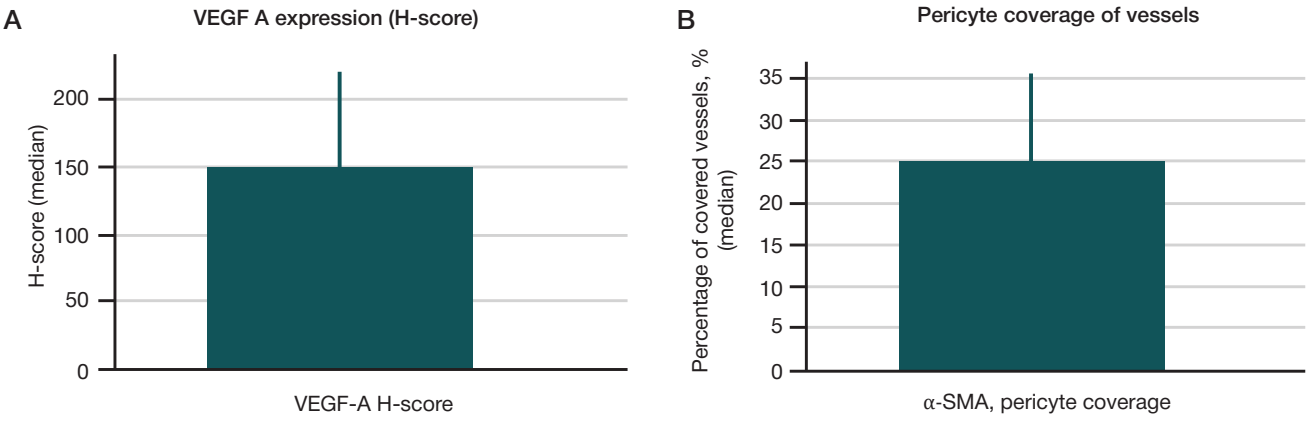


Fig. 5. A. VEGF-A expression (H-score) in synovial saracoma tissues. **B**. Pericyte coverage of vessels, α-SMA.

a functioning endothelium, while CD34 additionally reveals immature endothelial structures. Therefore, CD31 should be used as a basic marker for interzonal comparisons, and CD34 as a sensitive indicator of an expanded range of vascular structures.

A key observation is a pronounced perivascular accumulation of CD117⁺ mast cells in the zone ≤ 50 μm from microvessels with a relatively lower density in the intratumoral parenchyma. This pattern aligns with the known ability of mast cells to produce angiogenic mediators — tryptase, histamine, VEGF-A, FGF-2, proteases, and chemokines that mediate extracellular matrix remodeling and increase vascular permeability. This spatial convergence of MC with microvessels enables paracrine effects on the endothelium and pericytes, which enhance growth and stabilization of the newly formed vessels. Similar mechanisms have been described in Ewing's sarcoma and osteosarcoma, where mast cell density positively correlates with MVD and VEGF expression.

The observed correlations between the perivascular density of MC, MVD, and VEGF-A levels confirm the involvement of mast cells in the regulation of angiogenesis. The inverse correlation between MVD and α-SMA pericyte coverage points to the predominance of morphologically immature vessels in the areas of active angiogenesis. The independence of these associations from the density of CD163⁺ macrophages highlights the independence of contribution of mast cells to angiogenic processes.

The results of this study are consistent with the modern concepts of spatial organization of sarcoma cellular ecosystems, where angiogenic and immune niches form interconnected microenvironments that affect the prognosis [16]. Our data clarify one of the aspects of this model — the role of mast cells as active elements of the vascular niche. The described perivascular concentration of MCs and their degranulation confirm the tissue heterogeneity of mast cells and their involvement in the recruitment of other cells of innate immunity [17].

The revealed pattern is clinically significant because high MVD in combination with perivascular accumulation of MC forms the angiogenic phenotype of the tumor microenvironment that is associated with an unfavorable course. Such vascular-immune profiles are considered a potential target for complex treatment strategies combining antiangiogenic drugs with immunotherapy [18]. This is consistent with the concept of mast cells as mediators that modulate the antitumor immune response, and with data suggesting their potential therapeutic involvement when checkpoint inhibitors are used. [19, 20].

Thus, our results expand current understanding of vascular–immune interactions in synovial sarcoma and highlight the key role of perivascular mast cells in promoting the angiogenic phenotype of the tumor microenvironment, as well as their potential as therapeutic targets.

CONCLUSIONS

In synovial sarcoma, perivascular mast cells form a reproducible topographic pattern with the highest density in the zone ≤ 50 μm from CD31⁺/CD34⁺ microvessels and a higher degree of degranulation compared to parenchyma. Their accumulation is associated with the angiogenic TME phenotype: we revealed a positive correlation with MVD (both in hotspots and globally)

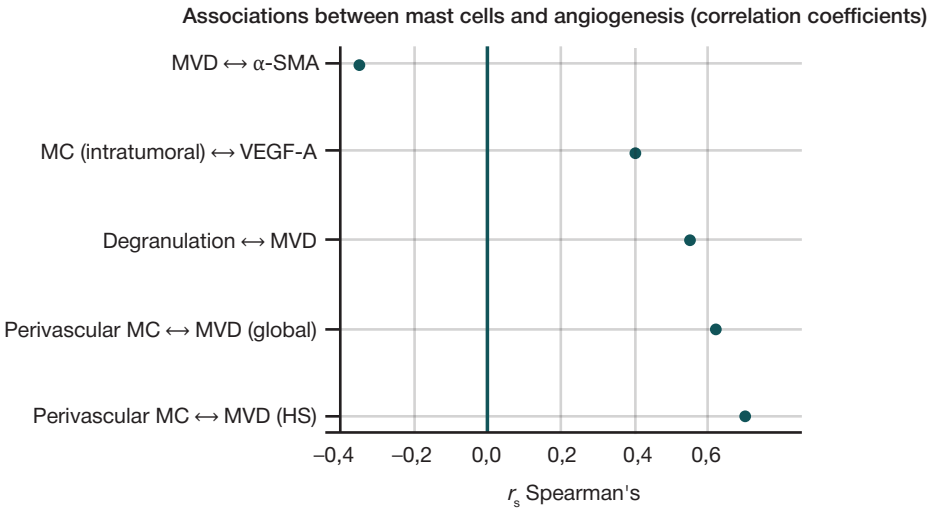


Fig. 6. Correlations between mast cell density, MVD, VEGF-A and α-SMA pericyte coverage (Spearman's coefficients)

and VEGF-A expression, and a simultaneous negative association with with α-SMA pericyte coverage, which points to the predominance of morphologically immature vessels. These dependencies persist after adjustment for $CD163^+$ macrophages, confirming the independent contribution of mast cells to the vascular niche. As for age, the respective analysis revealed that it does affect the mast cell angiogenic metrics significantly. In the subgroup with survival data, higher MVD and perivascular mast cell density were associated with worse outcomes, while pronounced $CD8^+$ infiltration meant better outcomes. The proposed integral Mast-Angio Score, which combines perivascular density and mast cell degranulation, MVD, and VEGF-A, increased the discriminative ability of the prognostic model (c-index growth, NRI/IDI improvement) in terms of the standard clinical and morphological features. Archived histological slides and FFPE blocks can be used in a standard IHC test aimed at learning the values of these parameters; it can be integrated into a synoptic report as an additional layer in risk stratification. The results of this study provide a rationale for clinical trials of complex approaches — antiangiogenic therapy combined with modulation of effector functions of mast cells and/or immunotherapy — in carefully selected subgroups of patients with an angiogenically active profile.

References

1. Fiore M, Sambri A, Spinnato P, et al. The biology of synovial sarcoma: state-of-the-art and future perspectives. Curr Treat Options Oncol. 2021; 22 (12): 109. DOI: 10.1007/s11864-021-00914-4.
2. Gazendam AM, Popovic S, Munir S, et al. Synovial sarcoma: a clinical review. Curr Oncol. 2021; 28 (3): 1909–20. DOI: 10.3390/curroncol28030177.
3. Ribatti D. Tryptase and tumor angiogenesis. Front Oncol. 2024; 14: 1500482. DOI: 10.3389/fonc.2024.1500482.
4. Ammendola M, Gadaleta CD, Patruno R, et al. Mast cells positive for c-Kit receptor and tryptase correlate with angiogenesis in cancerous and adjacent normal pancreatic tissue. Cells. 2021; 10 (2): 444. DOI: 10.3390/cells10020444.
5. Segura-Villalobos D, Bazany-Rosenzweig NR, Mayoral RJ, et al. Mast cell–tumor interactions: molecular mechanisms and clinical perspectives. Cells. 2022; 11 (3): 349. DOI: 10.3390/cells11030349.
6. Liu Z, Wang L, Wang J, et al. Angiogenic signaling pathways and anti-angiogenic therapy. Signal Transduct Target Ther. 2023; 8: 227. DOI: 10.1038/s41392-023-01460-1.
7. Panagi M, Lesuy Y, Tosti R, et al. Stabilizing tumor-resident mast cells restores T-cell infiltration in sarcomas and potentiates PD-L1 inhibition. Clin Cancer Res. 2024; 30 (11): 2582–97. DOI: 10.1158/1078-0432.CCR-24-0246.
8. Toulmonde M, Guégan J-P, Spalato-Ceruso M, et al. Reshaping the tumor microenvironment of cold soft-tissue sarcomas with anti-angiogenics: a phase 2 trial of regorafenib combined with avelumab. Signal Transduct Target Ther. 2025; 10: 202. DOI: 10.1038/s41392-025-02278-9.
9. Piccolo S, Panciera T, Contessotto P, Cordenonsi M. YAP/TAZ as master regulators in cancer: modulation, function and therapeutic approaches. Nat Cancer. 2023; 4 (1): 9–26. DOI: 10.1038/s43018-022-00473-z.
10. Chapeau EA, Sansregret L, Galli GG, Chène P, Wartmann M, Mourikis TP, et al. Direct and selective pharmacological disruption of the YAP–TEAD interface by IAG933 inhibits Hippo-dependent and RAS–MAPK-altered cancers. Nat Cancer. 2024; 5 (7): 1102–20. DOI: 10.1038/s43018-024-00754-9.
11. Luk S, Chokshi PR, Torres-Rodriguez I, et al. Immunological differences between monophasic and biphasic synovial sarcoma. Cancer Immunol Immunother. 2024; 74 (1): 31. DOI: 10.1007/s00262-024-03868-2.
12. Wisdom AJ, Mowery YM, Hong CS, et al. Single cell analysis reveals distinct immune landscapes in transplant and primary sarcomas that determine response or resistance to immunotherapy. Nat Commun. 2020; 11: 6410. DOI: 10.1038/s41467-020-19917-0.
13. Medina-Ceballos E, Liotta A, Ali S, et al. The prognostic impact of the tumor immune microenvironment in synovial sarcoma: an immunohistochemical analysis using digital pathology and conventional scoring. J Pers Med. 2025; 15 (5): 169. DOI: 10.3390/jpm15050169.
14. Giner F, Medina-Ceballos E, López-Reig R, et al. The combined immunohistochemical expression of GLI1 and BCOR in synovial sarcomas for the identification of three risk groups and their prognostic outcomes: a study of 52 patients. Int J Mol Sci. 2024; 25 (14): 7615. DOI: 10.3390/ijms25147615.
15. Recine F, Piciucchi S, De Vincenzo F, et al. Clinical and translational implications of immunotherapy in soft tissue and bone sarcomas. Front Immunol. 2024; 15: 1378398. DOI: 10.3389/fimmu.2024.1378398.
16. Subramanian A, Caswell DR, Wang H, et al. Sarcoma microenvironment cell states and ecosystems are associated with prognosis and predict response to immunotherapy. Nat Cancer. 2024; 5 (4): 642–58. DOI: 10.1038/s43018-024-00743-y.
17. West PW, Bulfone-Paus S. Mast cell tissue heterogeneity and specificity of immune cell recruitment. Front Immunol. 2022; 13: 932090. DOI: 10.3389/fimmu.2022.932090.
18. Spalato-Ceruso M, Valverde P, Italiano A. New strategies in soft tissue sarcoma treatment. J Hematol Oncol. 2024; 17 (1): 76. DOI: 10.1186/s13045-024-01580-3.
19. Lichterman JN, Reddy SM. Mast Cells: A New Frontier for Cancer Immunotherapy. Cells. 2021; 10 (6): 1270. DOI: 10.3390/cells10061270.
20. Ribatti D. New insights into the role of mast cells as a therapeutic target in cancer through the blockade of immune checkpoint inhibitors. Front Med (Lausanne). 2024; 11: 1373230. DOI: 10.3389/fmed.2024.1373230.

Литература

1. Fiore M, Sambri A, Spinnato P, et al. The biology of synovial sarcoma: state-of-the-art and future perspectives. Curr Treat Options Oncol. 2021; 22 (12): 109. DOI: 10.1007/s11864-021-00914-4.
2. Gazendam AM, Popovic S, Munir S, et al. Synovial sarcoma: a clinical review. Curr Oncol. 2021; 28 (3): 1909–20. DOI: 10.3390/curroncol28030177.
3. Ribatti D. Tryptase and tumor angiogenesis. Front Oncol. 2024; 14: 1500482. DOI: 10.3389/fonc.2024.1500482.
4. Ammendola M, Gadaleta CD, Patruno R, et al. Mast cells positive for c-Kit receptor and tryptase correlate with angiogenesis in cancerous and adjacent normal pancreatic tissue. Cells. 2021; 10 (2): 444. DOI: 10.3390/cells10020444.
5. Segura-Villalobos D, Bazany-Rosenzweig NR, Mayoral RJ, et al. Mast cell–tumor interactions: molecular mechanisms and clinical perspectives. Cells. 2022; 11 (3): 349. DOI: 10.3390/cells11030349.
6. Liu Z, Wang L, Wang J, et al. Angiogenic signaling pathways and anti-angiogenic therapy. Signal Transduct Target Ther. 2023; 8: 227. DOI: 10.1038/s41392-023-01460-1.
7. Panagi M, Lesuy Y, Tosti R, et al. Stabilizing tumor-resident mast cells restores T-cell infiltration in sarcomas and potentiates PD-L1 inhibition. Clin Cancer Res. 2024; 30 (11): 2582–97. DOI: 10.1158/1078-0432.CCR-24-0246.
8. Toulmonde M, Guégan J-P, Spalato-Ceruso M, et al. Reshaping the tumor microenvironment of cold soft-tissue sarcomas with

anti-angiogenics: a phase 2 trial of regorafenib combined with avelumab. Signal Transduct Target Ther. 2025; 10: 202. DOI: 10.1038/s41392-025-02278-9.
9. Piccolo S, Panciera T, Contessotto P, Cordenonsi M. YAP/TAZ as master regulators in cancer: modulation, function and therapeutic approaches. Nat Cancer. 2023; 4 (1): 9–26. DOI: 10.1038/s43018-022-00473-z.
10. Chapeau EA, Sansregret L, Galli GG, Chène P, Wartmann M, Mourikis TP, et al. Direct and selective pharmacological disruption of the YAP–TEAD interface by IAG933 inhibits Hippo-dependent and RAS–MAPK-altered cancers. Nat Cancer. 2024; 5 (7): 1102–20. DOI: 10.1038/s43018-024-00754-9.
11. Luk S, Chokshi PR, Torres-Rodriguez I, et al. Immunological differences between monophasic and biphasic synovial sarcoma. Cancer Immunol Immunother. 2024; 74 (1): 31. DOI: 10.1007/s00262-024-03868-2.
12. Wisdom AJ, Mowery YM, Hong CS, et al. Single cell analysis reveals distinct immune landscapes in transplant and primary sarcomas that determine response or resistance to immunotherapy. Nat Commun. 2020; 11: 6410. DOI: 10.1038/s41467-020-19917-0.
13. Medina-Ceballos E, Liotta A, Ali S, et al. The prognostic impact of the tumor immune microenvironment in synovial sarcoma: an immunohistochemical analysis using digital pathology and conventional scoring. J Pers Med. 2025; 15 (5): 169. DOI: 10.3390/jpm15050169.
14. Giner F, Medina-Ceballos E, López-Reig R, et al. The combined immunohistochemical expression of GLI1 and BCOR in synovial sarcomas for the identification of three risk groups and their prognostic outcomes: a study of 52 patients. Int J Mol Sci. 2024; 25 (14): 7615. DOI: 10.3390/ijms25147615.
15. Recine F, Piciucchi S, De Vincenzo F, et al. Clinical and translational implications of immunotherapy in soft tissue and bone sarcomas. Front Immunol. 2024; 15: 1378398. DOI: 10.3389/fimmu.2024.1378398.
16. Subramanian A, Caswell DR, Wang H, et al. Sarcoma microenvironment cell states and ecosystems are associated with prognosis and predict response to immunotherapy. Nat Cancer. 2024; 5 (4): 642–58. DOI: 10.1038/s43018-024-00743-y.
17. West PW, Bulfone-Paus S. Mast cell tissue heterogeneity and specificity of immune cell recruitment. Front Immunol. 2022; 13: 932090. DOI: 10.3389/fimmu.2022.932090.
18. Spalato-Ceruso M, Valverde P, Italiano A. New strategies in soft tissue sarcoma treatment. J Hematol Oncol. 2024; 17 (1): 76. DOI: 10.1186/s13045-024-01580-3.
19. Lichterman JN, Reddy SM. Mast Cells: A New Frontier for Cancer Immunotherapy. Cells. 2021; 10 (6): 1270. DOI: 10.3390/cells10061270.
20. Ribatti D. New insights into the role of mast cells as a therapeutic target in cancer through the blockade of immune checkpoint inhibitors. Front Med (Lausanne). 2024; 11: 1373230. DOI: 10.3389/fmed.2024.1373230.

RESULTS OF PHASE IIA CLINICAL TRIAL OF THE RAS-GTPASE INHIBITOR («ING-RAS») FOR TREATMENT OF GASTROINTESTINAL TUMORS

Kulinich TM, Kukoleva EA, Goncharov SV, Kudinova EA, Puchkov IA ✉, Goncharova OI, Kaminsky VV, Bozhenko VK

Russian Scientific Center of Roentgenoradiology, Moscow, Russia

Peritoneal carcinomatosis remains one of the most challenging forms of dissemination in gastric and colorectal cancer. It directly determines the disease prognosis and is highly resistant to treatment. The use of the existing therapeutic approaches is often limited by low benefit-risk ratio. It is necessary to develop innovative strategies aimed at overcoming the molecular mechanisms of tumor progression associated with RAS mutations, which play a crucial role in the carcinogenesis of both colorectal and gastric cancer. The study aimed to estimate safety and preliminary efficacy of the novel peptide RAS-GTPase inhibitor «Ing-Ras» when included in the treatment regimen of patients with stage III–IV gastric and colorectal cancer, including patients with peritoneal carcinomatosis. A total of 35 patients with the confirmed diagnosis of stage III–IV gastric and colorectal cancer were included in the study. The «Ing-Ras» drug was administered at a dose of 1.8 mg/kg twice with a 7-day interval using the Pressurized Intraperitoneal Aerosol Chemotherapy (PIPAC) technique. Primary efficacy was assessed by comparing the overall survival (OS) and progression-free survival (PFS) rates of the clinical trial patients with historical control groups. The OS and PFS rates for patients in the clinical trials were 92.1% and 84.22%, respectively, which significantly ($p < 0.05$) exceeded the values of these rates for the historical control group (50.8% and 65.25%). Thus, the use of «Ing-Ras» can significantly improve the treatment results for patients with advanced forms of colorectal and gastric cancer.

Keywords: peritoneal carcinomatosis, RAS-GTPase inhibitor, PIPAC therapy, progression-free survival, safety, KRAS G12C mutation, KRAS, HRAS, NRAS

Funding: the study was conducted with financial support from the Ministry of Health of the Russian Federation, the State Task project EGISU No. 1023021500033-4-3.2.21;3.1.5.

Author contribution: Kulinich TM — research concept and design, material collection and processing, data analysis, manuscript writing; Kukoleva EA — formation of patient groups, a set of clinical material, analysis of results, manuscript writing; Goncharov SV — design of the experimental part of the study, formation of patient groups, a set of clinical material, analysis of results; Kudinova EA, Goncharova OI — analysis of the clinical and experimental research results, manuscript writing and editing; Puchkov IA, Kaminsky VV — formation of patient groups, analysis of results, manuscript writing and editing; Bozhenko VK — research concept and design, manuscript editing and approval.

Compliance with ethical standards: the study was approved by the Ethics Committee of the Russian Scientific Center of Roentgenoradiology (protocol No. 4 dated 28 April 2023). The 2022-1-"Инг-Рас" trial was approved by the Ministry of Health of the Russian Federation (approval No. 177 for the clinical trial dated 30.03.2023). It was conducted in accordance with the ethical principles set out in the World Medical Association Declaration of Helsinki.

✉ **Correspondence should be addressed:** Ilya A. Puchkov
Profsoyuznaya, 86, 117997, Moscow, Russia; poutchkov@mail.ru

Received: 23.10.2025 **Accepted:** 21.11.2025 **Published online:** 09.12.2025

DOI: 10.24075/brsmu.2025.065

Copyright: © 2025 by the authors. **Licensee:** Pirogov University. This article is an open access article distributed under the terms and conditions of the Creative Commons Attribution (CC BY) license (https://creativecommons.org/licenses/by/4.0/).

РЕЗУЛЬТАТЫ КЛИНИЧЕСКОГО ИССЛЕДОВАНИЯ IIA ФАЗЫ ИНГИБИТОРА RAS-ГТФАЗЫ («ИНГ-РАС») ДЛЯ ЛЕЧЕНИЯ ОПУХОЛЕЙ ЖЕЛУДОЧНО-КИШЕЧНОГО ТРАКТА

Т. М. Кулинич, Е. А. Куколева, С. В. Гончаров, Е. А. Кудинова, И. А. Пучков ✉, О. И. Гончарова, В. В. Каминский, В. К. Боженко

Российский научный центр рентгенорадиологии, Москва, Россия

Перитонеальный канцероматоз остается одним из самых сложных вариантов диссеминации при раке желудка и толстой кишки. Он напрямую определяет прогноз заболевания и весьма резистентен к лечению. Использование существующих терапевтических подходов часто ограничено низким соотношением «польза–риск». Необходима разработка инновационных стратегий, направленных на преодоление молекулярных механизмов прогрессирования опухолей, ассоциированных с мутациями RAS, играющими важную роль в канцерогенезе как колоректального рака, так и рака желудка. Целью работы было оценить безопасность и эффективность нового пептидного ингибитора RAS-ГТФазы «Инг-Рас» при его включении в схему лечения пациентов с диагнозом рак желудка и толстой кишки III–IV стадий, включая пациентов с перитонеальным канцероматозом. В исследование было включено 35 пациентов с подтвержденными диагнозами рак желудка и толстой кишки III–IV стадий. Препарат «Инг-Рас» вводили в дозе 1,8 мг/кг двукратно с интервалом семь дней с помощью технологии внутрибрюшинной аэрозольной химиотерапии под давлением (PIPAC). Оценку первичной эффективности проводили на основании сравнения показателей общей (OS) и безрецидивной (PFS) одногодичной выживаемости пациентов КИ с группами исторического контроля. Показатели OS и PFS для пациентов клинического исследования составили 92,1 и 84,22% соответственно, что достоверно ($p < 0,05$) превышает значения данных показателей для группы исторического контроля — 50,8 и 65,25%. Таким образом, применение препарата «Инг-Рас» позволяет существенно повысить результаты лечения пациентов с распространенными формами колоректального рака и рака желудка.

Ключевые слова: перитонеальный канцероматоз, ингибитор RAS-ГТФазы, PIPAC-терапия, выживаемость без прогрессирования, безопасность, мутация KRAS G12C, KRAS, HRAS, NRAS

Финансирование: исследование выполнено при финансовой поддержке Министерства здравоохранения Российской Федерации, рег. № ЕГИСУ 1023021500033-4-3.2.21;3.1.5.

Вклад авторов: Т. М. Кулинич — концепция и дизайн исследования, сбор и обработка материала, анализ полученных данных, написание текста; Е. А. Куколева — формирование групп пациентов, набор клинического материала, анализ результатов, написание текста; С. В. Гончаров — дизайн экспериментальной части, формирование групп пациентов, набор клинического материала, анализ результатов; Е. А. Кудинова, О. И. Гончарова — анализ клинико-экспериментальных результатов, написание и редактирование текста; И. А. Пучков, В. В. Каминский — формирование групп пациентов, анализ результатов, написание и редактирование текста; В. К. Боженко — концепция и дизайн исследования, редактирование, утверждение рукописи.

Соблюдение этических стандартов: исследование одобрено этическим комитетом при ФГБУ «РНЦРР» Минздрава России (протокол заседания № 4 от 28 апреля 2023 г.). Исследование 2022-1-«Инг-Рас» одобрено Минздравом России разрешением № 177 на проведение клинических исследований от 30.03.2023. Проведено в соответствии с этическими принципами, изложенными в Хельсинкской декларации Всемирной медицинской ассоциации.

✉ **Для корреспонденции:** Илья Александрович Пучков
ул. Профсоюзная, 86, 117997, г. Москва, Россия; poutchkov@mail.ru

Статья получена: 23.10.2025 **Статья принята к печати:** 21.11.2025 **Опубликована онлайн:** 09.12.2025

DOI: 10.24075/vrgmu.2025.065

Авторские права: © 2025 принадлежат авторам. **Лицензиат:** РНИМУ им. Н. И. Пирогова. Статья размещена в открытом доступе и распространяется на условиях лицензии Creative Commons Attribution (CC BY) (https://creativecommons.org/licenses/by/4.0/).

Peritoneal carcinomatosis is one of the most prognostically unfavorable sequelae of malignant neoplasms. It's aggressive course and resistance to standard systemic chemotherapy determined by the peritoneum structural and physiological features, including its limited vascularization and formation of biological barriers, which leads to the rapid progression and adverse prognosis, as well as prevention of the penetration of cytostatics [1]. Systemic chemotherapy usually demonstrates limited efficacy. By now local drug therapy methods, such as PIPAC (Pressurized Intraperitoneal Aerosol Chemotherapy) and HIPEC (hyperthermic intraperitoneal chemotherapy) are being developed and implemented to improve treatment outcomes.

The PIPAC technique involving spraying a cytostatic agent aerosol under increased pressure of carbon dioxide ensures its uniform distribution in the abdominal cavity, even in the presence of adhesions after surgical interventions, and promotes its further penetration into tumor tissues to a depth up to 500 μm, which 3–5-times exceeds the values reported for the traditional intraperitoneal chemotherapy [2]. The use of this approach is particularly relevant for the treatment of tumors with RAS-mutations, which are highly prone to dissemination.

Mutations of RAS genes (KRAS, HRAS, NRAS) are found in 30–90% of cases of gastrointestinal adenocarcinomas, including cases of colorectal cancer (40–50%), pancreatic cancer (90%) and gastric cancer (> 8%) [3, 4]. Carcinogenic factors stabilize Ras-proteins in the GTP-bound state, blocking the GTP hydrolysis to GDP. This results in hyperstimulation of the MAPK/ERK and PI3K/AKT signaling pathways, enhancing proliferation, angiogenesis and the adenocarcinoma metastatic potential [5].

To overcome resistance of tumors with mutations in RAS genes, it is necessary to develop highly selective inhibitors capable of specifically suppressing the activity of overexpressed Ras-proteins. The peptide RAS-GTPase inhibitor «Ing-Ras» drug developed at the Russian Scientific Center of Roentgenoradiology of the Ministry of Health of the Russian Federation disrupts the formation of the Ras-Raf-GTP complex by suppressing signaling via the MAPK/ERK cascade pathway [6]. Pre-clinical trials have shown that «Ing-Ras» actively penetrates cell membranes, selectively binding carcinogenic Ras-isoforms, and induces apoptosis in colorectal cancer (HT-29) and ovarian cancer (OVCAR-3) cell lines [7].

A combined strategy for the inclusion of «Ing-Ras» in the standard treatment regimen with its intraperitoneal administration of the drug by PIPAC ensuring high intraperitoneal concentration of the drug has been proposed for patients with peritoneal carcinomatosis. Such a strategy will make it possible to overcome the limitations associated with the use of systemic chemotherapy and complement it to increase the treatment efficacy.

Combining PIPAC therapy with the targeted RAS inhibitors, such as «Ing-Ras», represents a promising approach to treatment of peritoneal carcinomatosis. This approach combines specific signaling pathway inhibition with the optimized drug delivery, ensuring high efficacy in tumors with RAS-mutations [8].

During the previously conducted phase I of clinical trials of the «Ing-Ras» under Protocol No. 2022-1-*Инг-Рас*, which was the first clinical trial of RAS-GTPase inhibitor in the Russian Federation, the tasks related to assessment of the drug safety and tolerability were successfully completed [6].

The study aimed to perform preliminary assessment of the efficacy of the «Ing-Ras» drug for treatment of patients diagnosed with gastrointestinal tumors, including patients with peritoneal carcinomatosis in the phase IIa clinical trial (second phase of the clinical trial protocol No. 2022-1-*Инг-Рас*).

METHODS

Patients and study design

The study was conducted as a phase I–IIa of prospective open-label non-randomized multicenter trial with adaptive design to assess safety and primary efficacy, as well as to determine the maximum tolerated dose of the drug based on the RAS-GTPase inhibitor («Ing-Ras»).

Safety of the 1.8 mg/kg «Ing-Ras» drug dose determined on the phase I results was assessed in phase II; the dose was approved at the session (05.12.2023) of the Independent Data Monitoring Committee (IDMC) founded at the Russian Scientific Center of Roentgenoradiology of the Ministry of Health of the Russian Federation [6]. A preliminary efficacy assessment of the optimal drug dose was also conducted in comparison with the historical control group. The phase II trial consisted of the following periods: screening — preliminary patient examination (up to 14 days); on day 1 of the trial the patients in hospital settings were administered the study drug intraperitoneally (using PIPAC) at a dose of 1.8 mg/kg. On day 8 of the trial the drug dose of 1.8 mg/kg was administered for the second time by the same method. Later the patients had eight outpatient visits to the research center between days 21 and 360 of participation in the trial. Parameters, safety and efficacy were assessed during each visit.

The trial was conducted from June 19, 2023 to December 25, 2024. The phase I trial results had been published earlier [6]. The phase IIa clinical trial was conducted at the clinic of the Russian Scientific Center of Roentgenoradiology of the Ministry of Health of the Russian Federation. The study included 35 patients with the morphologically confirmed peritoneal carcinomatosis in gastric and colorectal cancer, who received combination therapy with «Ing-Ras» and PIPAC (ITT population). Among them 23 patients were compliant with the trial protocol (PP population). Efficacy was assessed based on the RECIST 1.1 criteria, dynamic changes in the Peritoneal Cancer Index (PCI). Safety assessment was performed in accordance with the generally accepted Common Terminology Criteria for Adverse Events (CTCAE) version 5.0. The association of adverse events (AEs) and severe adverse events (SAEs) with the test drug was determined based on the researcher's clinical assessment. The median follow-up period was 388 days. The number of patients for assessment of safety and primary efficacy of the drug was determined in accordance with the guidelines on sample sizes for early phases of drug development [9]. Efficacy was analyzed for the entire populations of the patients enrolled (ITT, intention–to-treat) (n = 35).

Inclusion criteria: surgery due to one of the following conditions.

– Resectable gastric cancer showing signs of invading the serous membrane (T3) with the presence of cancer cells assessing with peritoneal lavage based on the cytological/immunocytochemistry analysis and/or showing signs of invading adjacent organs (T4) based on the preoperative assessment and/or intaoperative revision data or after radical surgery with the histologically confirmed regional metastasis (N+).

– Resectable colon cancer showing signs of invading the serous membrane (T3) and/or invading adjacent organs (T4) based on the preoperative assessment and/or intaoperative revision data.

– Resectable colon cancer after radical surgery with the histologically confirmed regional metastasis (N+).

– Resectable rectal cancer showing signs of invading the mesorectal fascia and/or the presence of metastatic

lymph nodes in the mesorectum based on the preoperative assessment data.

– Patients after the rectal cancer surgical treatment with the quality criteria P. Quirke of the performed total mesorectal excision (TME) that are both satisfactory (grade 2) and unsatisfactory (grade 1) based on the morphological examination of the removed specimen.

– Patients showing progression of the earlier radically treated gastric cancer or colorectal cancer in the form of isolated peritoneal carcinomatosis.

Exclusion criteria: the presence of systemic extraperitoneal metastasis, including metastasis in the central nervous system and/or carcinomatous meningitis, as well as the fact of having any other malignant tumor, except for the radically treated basal cell carcinoma, cervical cancer in situ at the time of enrollment or within 5 years before enrollment.

Based on open access publications, a historical control group was formed which included patients with diagnosed gastrointestinal tumors having a high risk of carcinomatosis after surgery and patients with metastatic forms, including peritoneal carcinomatosis. An additional retrospective group was formed based on the database of follow-up results of the patients diagnosed with gastric and colorectal cancer of the Russian Scientific Center of Roentgenoradiology of the Ministry of Health of the Russian Federation [10]. The database contains data on the disease course of 1423 patients, 449 patients diagnosed with gastric cancer, the median follow-up period for these patients is 27.7 months, progression is reported for 42.24% of cases, and the average time to relapse is 18.7 months from the date of surgery. A total of 974 patients diagnosed with colorectal cancer are included in the database, the median follow-up period is 41.15 months, relapse is reported in 29.72% of cases and the median time to relapse is 20.04 months.

Safety assessment

Safety assessment included the analysis of vital parameters, physical examination data, laboratory and instrumental testing results. The patient's overall health was evaluated using the ECOG (Eastern Cooperative Oncology Group) score [11].

Disease progression assessment

Progression was assessed based on the target foci measured and selected for control and the non-target foci using the radiological and RECIST 1.1 criteria [12].

The Peritoneal Cancer Index (PCI) was also assessed by the method reported in the literature [13].

The length of the trial based on the phase IIa protocol was 388 days (including 14 days of screening).

Progression-free survival (PFS) was determined as the time from the date of surgery to the date of progression, death or last contact with the patient. The disease progression was determined in accordance with the RECIST 1.1 criteria based on the comprehensive response assessment performed during the current visit.

Efficacy assessment

The «Ing-Ras» drug efficacy was analyzed concerning the following indicators:

– Overall survival (OS) (share of patients, who survived within a year). Overall survival was determined as the time from the date of surgery to the date of death or the last documented visit to the research center.

– Progression-free survival (PFS) (share of patients, who had no disease progression within a year). Progression-free survival was determined as the time from the date of surgery to the date of the documented fact of disease progression (in accordance with the RECIST 1.1 criteria) or death (of any cause).

– Median progression-free survival (mPFS) (time, in which disease progression occurs in 50% of patients).

– Dynamics of the Peritoneal Cancer Index (PCI). Comparative assessment of the method efficacy and the historical control data was performed. The data from several publications showing the results of treatment and monitoring the disease course in patients with advanced forms of gastric and colorectal cancer were used as a historical control population [14–22].

Statistical methods

Data analysis was performed in the R-Studio version 2023.06.1 software package using language-R version 4.2.2. The statistical analysis was based on the data from all patients included in the study within the framework of pre-defined analytical cohorts.

Continuous (quantitative) data are provided as the number of observations, the mean, 95% confidence interval (CI) for the mean (unless otherwise specified), standard deviation, median, interquartile range, minimum and maximum. Ordinal, categorical, and qualitative ones are presented as absolute rates of incidence (number of observations), relative rates (percentage), and 95% CI (unless otherwise specified). Survival was estimated using the Kaplan–Meier estimator [23].

RESULTS

Safety assessment

Safety assessment was performed in the ITT population based on the rate, type, association with the test drug administration, and severity of adverse events (AEs) and severe adverse events (SAEs) (including clinically significant deviation of laboratory parameters and instrumental assessment results). Safety was also estimated based on the rate of AEs associated with the PIPAC procedure (for which the association with the procedure was classified as "determined" or "probable"). The number of patients involved in safety assessment in phase IIa was 35 subjects. In the phase IIa trial, a total of 276 AEs were recorded in all 35 patients of the safety population. Among all the recorded 276 adverse events, 265 AEs (96.01%) were mild and 11 AEs (3.99%) were moderate. The following AEs and SAEs were recorded during the study. In the PP group (n = 23), five cases of AE were recorded, among these two cases (8.7%) of the grade 3 AE (elevated ALT/AST) associated with the drug were recorded in patients with gastric cancer. In the ITT group (n = 35), 12 AE cases were recorded, among these there were three cases (8.5%) of the grade 3 AE (elevated ALT/AST) and one case (2.8%) of the grade 4 AE (pancreatitis) also associated with the drug. The most common AEs included nausea (15% in ITT, 10% in PP), fatigue (12% in ITT, 8% in PP), and abdominal pain (10% in ITT, 5% in PP). No severe adverse events resulting in discontinuation of therapy were reported. All AEs were jugulated using symptomatic therapy.

When proceeding through phase II of the study, a total of three SAEs were recorded. Thus, the rate of SAE recording was 1.09% (3/276) of all AEs. The association of all SAEs with the use of the test drug and the applied PIPAC procedure was considered to be "dubious". The analysis of all the AEs in phase

IIa showed that none of these had any significant association with the tested drug or the procedure (the association was considered to be “dubious” based on the WHO classification). Furthermore, no association of the recorded changes in laboratory and vital parameters with the use of the test drug was determined.

Thus, therapy with the studied «Ing-Ras» preparation in patients diagnosed with gastrointestinal tumors, including patients with peritoneal carcinomatosis, was well tolerated by the patients, had a favorable safety profile and a high benefit-risk ratio.

Efficacy assessment

Overall survival (OS)

The one-year OS of the population of clinical trial patients was 92.1%. According to the data of official statistical reports in the RF mortality within 12 months after the diagnosis among patients diagnosed with colorectal cancer is 19.6% by this moment, while that among patients diagnosed with gastric cancer is 40.0% [14]. In 2023 in Russia, the average overall survival of patients diagnosed with gastric and colorectal cancer was 70.2%. According to the published data [15–16], the one-year survival of the historical control group is 50.8% [95% CI: 33.77–67.83%].

In the reported phase IIa clinical trial, the patient`s one-year OS was 92.1%, which almost twice exceeded the one-year survival of the historical control group and exceeded the official statistical data for the RF by 42.45%.

One-year progression-free survival (PFS) and median one-year PFS

Two patients (5.7%) had no data on the overall response estimate based on RECIST 1.1 due to withdrawal from the trial before visit 3.

During the study a total of nine cases of the underlying disease progression were reported. The one-year progression-free survival after surgery nevertheless was 84.22% [72.42–97.95%].

Considering the conditions of the clinical trial protocol, the specific characteristics of the «Ing-Ras» drug and the patient population included in the study a selection of publications was conducted to form the historical control group. This selection included data on the recurrence rate in patients with advanced gastric and colorectal cancer diagnoses who had a high risk of carcinomatosis and follow-up period of at least 12 months [17–22]. The analysis of open access publications made it possible to determine a number of indicators for certain disease entities. Thus, according to the papers focused on the studies of stage III–IV gastric cancer, the one-year PFS was less than 65% [17, 18], mPFS was within the range of 0.9–7.0 months [21]. The analysis of the data from open sources providing the treatment outcomes of patients diagnosed with metastatic colorectal cancer showed that mPFS was 5.5–12.3 months, depending on the treatment option [22].

However, the available open access data on the treatment outcomes and follow-up of patients of appropriate groups did not allow us to conduct the necessary statistical analysis to yield the reliable results. In this regard, to further assess the results for primary efficacy of the «Ing-Ras» preparation and to obtain the statistically significant information, we used the database of follow-up results of the patients diagnosed with gastric and colorectal cancer of the Russian Scientific Center of Roentgenoradiology of the Ministry of Health of the Russian Federation [10].

To compare the patients included in the 2022-1-*Инг*-Рас clinical trial and the patients from the database of the Russian Scientific Center of Roentgenoradiology of the Ministry of Health of the Russian Federation, the database censoring procedure was applied, and the patients were selected, who were most closely matched according on such criteria as sex, age, disease stage, and follow-up period to the clinical trial patients. Personal data of control patients were completely blinded for the research team members, who formed the group and conducted the data analysis.

Preliminary PFS was determined from the date of surgery (data of patient enrollment or date of the beginning of follow-up — for the control group) to the date of patient’s death or the date of the documented fact of relapse or disease progression (in accordance with the RECIST 1.1 criteria). The mPFS analysis conducted using the Kaplan–Meier estimator allowing one to estimate the probability of the event (relapse) within the specified 12-year follow-up is provided in Fig.

Significance of intergroup differences in PFS was proven using several statistical methods/tests: Cox's F-test: (T1 = 65.99039; T2 = 12.00962; F(6.148) = 4.489096; p = 0.00033); Gehan–Wilcoxon test (WW = –1519; sum = 3881E3; variance = 4602E2; statistical test = –2.23850; p = 0.02519); Cox–Mantel test (I = 7.348708; U = –5.37040; statistical test = –1.98108; p = 0.04758).

The results of conducted analysis suggest an upward trend of progression-free survival (PFS) in the study group compared to the historical control group; inclusion of the «Ing-Ras» drug in the treatment regimen makes it possible to improve treatment outcomes in patients diagnosed with stage III–IV gastric and colorectal cancer.

Dynamics in Peritoneal Cancer Index

Comparative analysis of the Peritoneal Cancer Index (PCI) in the dynamics of treatment for the ITT population is provided in Table.

The differences in PCI estimates between visits were assessed using the Friedman’s test. The resulting p-value of 0.2484 did not allow us to draw a conclusion about the PCI differences between each pair of visits. Comparison of PCI with the historical control PCI values turned out to be inapplicable due to the lack of data or insufficient data on the comparison group.

DISCUSSION

In the phase IIa clinical trial, primary assessment of the efficacy of the «Ing-Ras» preparation (peptide RAS-GTPase inhibitor), intraperitoneally administered twice at a dose of 1.8 mg/kg with a 7-day interval to patients diagnosed with gastrointestinal tumors, including peritoneal carcinomatosis, was performed.

It was shown that the one-year OS was 100%, which almost twice exceeded the one-year survival rate of the historical control group [15, 16] and exceeded the official statistical data for the RF by 42.45% [14].

The one-year progression-free survival of the PP and ITT populations was 100% and 84.22%, respectively. The median PFS for both populations was 4.45 years.

The analysis of the recorded adverse events detected in phase IIa of the trial showed that none of these were significantly associated with the studied drug or research procedure (the association was considered to be “dubious”).

The use of the drug «Ing-Ras» in patients with gastrointestinal tumors, including cases of peritoneal carcinomatosis, was not associated with the development of severe adverse reactions,

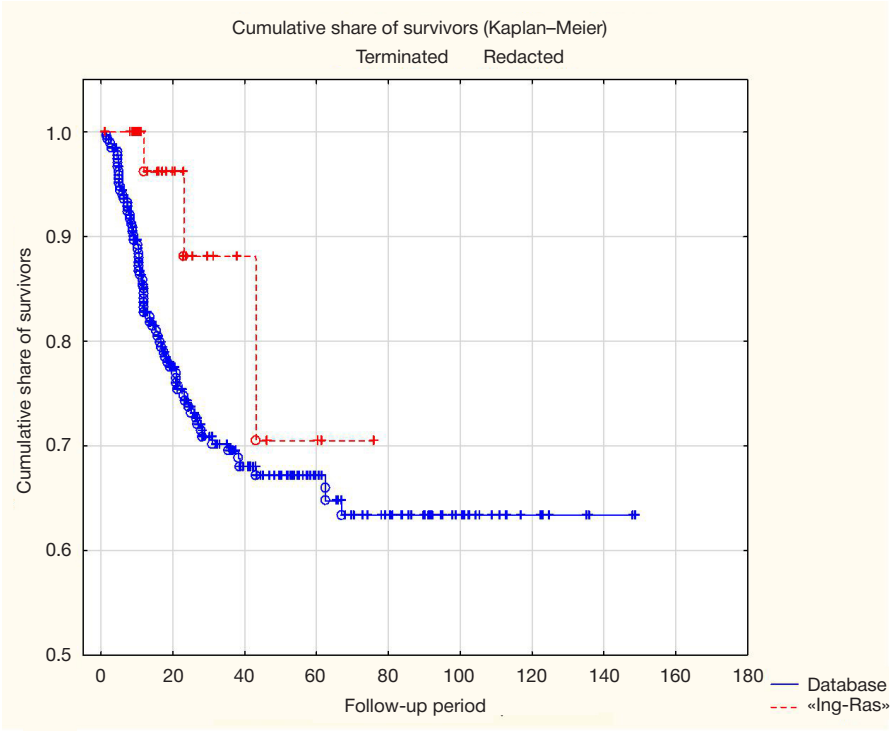


Fig. Comparison of progression-free survival (PFS) in the groups of the 2022-1-*Инг*-Рас clinical trial protocol and the group of patients from the database of the Russian Scientific Center of Roentgenoradiology of the Ministry of Health of the Russian Federation within the 12-year follow-up period.

was characterized by a low frequency of undesirable effects, and demonstrated an optimal benefit-risk ratio. The data confirm that it is promising in terms of further assessment in phase IIb–III of clinical trials.

To date, only two RAS-GTPase inhibitors have been approved for clinical use: Sotorasib and Adagrasib. Both drugs selectively inhibit the KRAS G12C mutation, which represents an important, but highly specific achievement in the field of precision oncology. Sotorasib (AMG-510), the first covalent inhibitor targeting KRAS(G12C)-positive non-small-cell lung cancer (NSCLC) [22], obtained the FDA's accelerated approval in May 2021 based on the CodeBreak 100 trial results [24]. And already in June 2023 the drug was registered in Russia under the brand name Lumykras®. In clinical trials oral Sotorasib at a dose of 960 mg taken once daily showed its efficacy in 37.1% of patients with the average PFS of 6.8 months [25].

Adagrasib (MRTX849/Krazati) became the second inhibitor [24, 26] that was first approved by FDA (in 2022) for the therapy of locally-advanced or metastatic non-small-cell lung cancer (NSCLC) with the KRAS-G12C mutation [27]. In 2024, after receiving the clinical trial results demonstrating a significant anti-tumor response, the Adagrasib+Cetuximab combination was assigned the status of "breakthrough therapy" and received the FDA's accelerated approval for the use for patients with the locally-advanced or metastatic colorectal cancer (CRC) associated with the KRAS-G12C mutation [27].

However, despite high clinical efficacy, marked side effects are observed when using both drugs. In particular, Sotorasib can cause hepatotoxicity, including elevated liver enzymes (ALT/AST), with severe cases in 3% of patients and critical abnormalities (degree 3/4) in 6%, leading to subsequent treatment discontinuation. As for severe complications (in 50% of patients), pneumonia (8%), hepatotoxicity (3%), diarrhea (2%), as well as fatal outcomes (3%) and sporadic cases of interstitial lung damage (0.8%) were reported during the post-marketing follow-up period [28].

Adagrasib can cause hepatotoxicity and provoke gastrointestinal disorders, so the dose adjustment is often required [29, 30]. Specific risks associated with the use of Adagrasib include prolongation of the QT interval increasing the likelihood of arrhythmia when combined with other QT prolonging drugs, as well as high rate of dosage adjustment (52% of patients) and temporal therapy discontinuation (61%) [30, 31].

In general, both inhibitors demonstrate serious toxic effects, but the use of Adagrasib is associated with the more frequent dosage adjustment and cardiovascular risk [31].

The «Ing-Ras» antitumor drug developed at the Russian Scientific Center of Roentgenoradiology of the Ministry of Health of the Russian Federation showed high therapeutic efficacy in the phase I–IIa of clinical trials (2023–2024) when administered intraperitoneally to patients with gastrointestinal tumors diagnoses, including patients with the peritoneal

Table. Dynamics of the Peritoneal Cancer Index in the ITT population

Parameter	Visit	*n*	Med	Mean	95% CI	SD	min	max	Q1	Q3	IQR
PCI, overall score	Screening	35	0	2.09	[0.23–3.95]	5.41	0	22	0	0	0
	Visit 3, day 28 (±1)	33	0	2.24	[0.09–4.39]	6.06	0	24	0	0	0
	Visit 6, day 180 (±14)	27	0	1.63	[–0.63–3.89]	5.71	0	25	0	0	0
	Visit 7, day 270 (±14)	27	0	0.93	[–0.48–2.33]	3.56	0	17	0	0	0
	Visit 8, day 360 (±14)	12	0	1.42	[–1.7–4.53]	4.91	0	17	0	0	0
	End of the trial	26	0	0.65	[–0.69–2]	3.33	0	17	0	0	0

carcinomatosis. The following results of the trial conducted were reported: 100% overall survival (OS) within 12 months in both PP and ITT populations. The median progression-free survival (PFS) was 4.45 years (53.4 months), and 84.22% of patients in the ITT group showed no signs of disease progression [32]. These values significantly exceed the historical data on Sotorasib and Adagrasib, which in CodeBreak100 and KRYSTAL-1 studies involving patients with metastatic colorectal cancer, demonstrated a median progression-free survival of 5.6 and 6.5 months, respectively, with an annual overall survival (OS) of approximately 45% trials [33–35].

The «Ing-Ras» mechanism of action is fundamentally different from that one of the KRAS-G12C covalent inhibitors (Sotorasib, Adagrasib). The drug directly inhibits the RAS-protein GTP-active form, suppressing the MAPK/ERK signaling pathway, regardless of the tumor mutational status [32]. The key of «Ing-Ras» advantage is high therapeutic efficacy in patients with peritoneal carcinomatosis, which is traditionally characterized by resistance to systemic therapy. The use of the PIPAC technique for local drug administration provides its maximum concentration in the abdominal cavity with the minimum systemic effect, thereby reducing the rate of AEs [32, 35].

The use of Adagrasib is associated with serious side effects. The potential of the «Ing-Ras» use is related to its capability to overcome tumor cell resistance to the drug, a characteristic not typical of first-generation RAS-GTPase inhibitors. While disease progression develops within 6–12 months in 60% of patients undergoing therapy with first-generation drugs due to the activation of alternative signaling pathways (PI3K/AKT, STAT3), 84.22% of patients receiving 'Ing-Ras' treatment showed no signs of progression over 4.45 years. This can be due to the drugs simultaneous effect on the tumor microenvironment in addition to the direct RAS-GTPase inhibition [32].

CONCLUSIONS

In the I–IIa phase of clinical trials the «Ing-Ras» drug administered intraperitoneally by PIPAC to patients with gastrointestinal tumors (including peritoneal carcinomatosis) showed high efficacy, beneficial safety profile and optimal benefit-risk ratio. The data demonstrate that more than 80% of patients had no disease progression, and progression-free survival increased approximately by 30%. These findings need to be confirmed in the randomized IIb–III phase trials. It is planned to conduct a IIb phase to expand the analysis of the long-term safety and efficacy in the larger cohort of patients, as well as to validate the results using independent groups. The studied «Ing-Ras» preparation demonstrated higher efficacy and safety compared to foreign analogues of RAS-GTPase inhibitors, which poses it as a promising targeted antitumor drug.

References

1. Coccolini F, Gheza F, Lotti M, Virzì S, Iusco D, Ghermandi C, Melotti R, Baiocchi G, Giulini SM, Ansaloni L, Catena F. Peritoneal carcinomatosis. World J Gastroenterol. 2013; 19 (41): 6979–94. DOI: 10.3748/wjg.v19.i41.6979.
2. Solass W, Kerb R, Mürdter T, Giger-Pabst U, Strumberg D, Tempfer C, et al. Intraperitoneal chemotherapy of peritoneal carcinomatosis using pressurized aerosol as an alternative to liquid solution: first evidence for efficacy. Ann Surg Oncol. 2014; 21 (2): 553–9. DOI: 10.1245/s10434-013-3213-1.
3. Wu X, Song W, Cheng C, Liu Z, Li X, Cui Y, et al. Small molecular inhibitors for KRAS-mutant cancers. Front Immunol. 2023; 14: 1223433. DOI: 10.3389/fimmu.2023.1223433. Available from: https://www.frontiersin.org/journals/immunology/articles/10.3389/fimmu.2023.1223433/full. English.
4. Wu L, Rao W, Guo L, Zhang F, Li W, Ying J. Pan-cancer analysis to character the clinicopathological and genomic features of KRAS-mutated patients in China. J Cancer Res Clin Oncol. 2025; 151 (2): 94. DOI: 10.1007/s00432-025-06118-9.
5. Wiechmann S, Maisonneuve P, Grebbin BM, Hoffmeister M, Kaulich M, Clevers H, et al. Conformation-specific inhibitors of activated Ras GTPases reveal limited Ras dependency of patient-derived cancer organoids. J Biol Chem. 2020; 295 (14): 4526–40. DOI: 10.1074/jbc.RA119.011025.
6. Bozhenko VK, Goncharov SV, Kudinova EA, Kulinich TM, Kukoleva EA, Filippov MS, i dr. Ocenka bezopasnosti s ustanovleniem maksimal'no perenosimoj dozy ingibitora RAS-GTFazy («Ing-Ras») dlya lecheniya opuholej zheludochno-kishchechnogo trakta: predvaritel'nye rezul'taty issledovaniya I fazy. Al'manah klinicheskoj mediciny. 2023; 51 (7): 376–96. DOI: 10.18786/2072-0505-2023-51-045. Russian.
7. Kulinich TM, SHishkin AM, Ivanov AV, Kaminskij VV, Bozhenko VK. Izuchenie protivoopuholevyh svojstv peptidnoj konstrukcii, vklyuchayushchej internalizuemuyu posledovatel'nost' i ingibitor RAS-GTfazy, v otnoshenii kletok linij raka tolstoj kishki (NT29) i raka yaichnika (OAW-42, OVCAR-3). Vestnik Rossijskogo nauchnogo centra rentgenoradiologii Minzdrava Rossii. 2021; 4 (21). Dostupno po ssylke: https://vestnik.rncrr.ru/vestnik/v21/docs/kulinich_t4.pdf. Russian.
8. Yaeger R, Weiss J, Pelster MS, Spira AI, Barve M, Ou SHI, et al. Adagrasib with or without Cetuximab in Colorectal Cancer with Mutated KRAS G12C. N Engl J Med. 2023; 388 (1): 44–54. DOI: 10.1056/NEJMoa2212419.
9. Mironov AN, redaktor. Rukovodstvo po provedeniyu klinicheskih issledovanij lekarstvennyh sredstv. M.: Grif i K; 2012. 944 s. Russian.
10. Goncharov SV, Bozhenko VK, Zaharenko MV, Kiseleva YaYu, Chaptykov AA, Kulinich TM, i dr. Analiz molekulyarnyh fenotipov embrional'no-anatomicheskih otdelov tolstoj kishki v normal'noj slizistoj obolochke i pri kolorektal'nom rake. Al'manah klinicheskoj mediciny. 2023; 51 (8): 441–55. DOI: 10.18786/2072-0505-2023-51-046. Russian.
11. Farias ST, Weakley A, Harvey D, Chandler J, Huss O, Mungas D. The Measurement of Everyday Cognition (ECog): Revisions and Updates. Alzheimer Dis Assoc Disord. 2021; 35 (3): 258–64. DOI: 10.1097/WAD.0000000000000450.
12. Eisenhauer EA, Therasse P, Bogaerts J, Schwartz LH, Sargent D, Ford R, et al. New response evaluation criteria in solid tumours: revised RECIST guideline (version 1.1). Eur J Cancer. 2009; 45 (2): 228–47. DOI: 10.1016/j.ejca.2008.10.026.
13. Rubcova NA, Levshakova AV, Peshkov AO, Homyakov VM, Utkina AB, Sidorov DV, i dr. Komp'yuternaya i magnitno-rezonansnaya tomografiya v diagnostike peritoneal'nogo karcinomatoza». Luchevaya diagnostika i terapiya. 2019; 2 (10): 32–41. DOI: 10.22328/2079-5343-2019-10-2-32-41. Russian.
14. Kaprin AD, Starinskij VV, SHahzadova AO, redaktory. Sostoyanie onkologicheskoj pomoshchi naseleniyu v 2023 godu. M.: MNIOI im. P.A. Gercena, 2024; 262 s. Russian.
15. O'Neil BH, Wallmark JM, Lorente D, Elez E, Raimbourg J, Gomez-Roca C, et al. Safety and antitumor activity of the anti-PD-1 antibody pembrolizumab in patients with advanced colorectal carcinoma. PLoS One. 2017; 12 (12): e0189848. DOI: 10.1371/journal.pone.0189848. Available from: https://journals.plos.org/plosone/article?id=10.1371/journal.pone.0189848. English.
16. Janjigian YY, Shitara K, Moehler M, Garrido M, Salman P, Shen L, et al. First-line nivolumab plus chemotherapy versus chemotherapy alone for advanced gastric, gastro-oesophageal junction, and oesophageal adenocarcinoma (CheckMate 649): a randomised, open-label, phase 3 trial. Lancet. 2021; 398 (10294):

27–40. DOI: 10.1016/S0140-6736(21)00797-2.
17. Sánchez-Hidalgo JM, Rodríguez-Ortiz L, Arjona-Sánchez Á, Rufián-Peña S, Casado-Adam Á, Cosano-Álvarez A, et al. Colorectal peritoneal metastases: Optimal management review. World J Gastroenterol. 2019; 25 (27): 3484–502. DOI: 10.3748/wjg.v25.i27.3484.
18. Nors J, Iversen LH, Erichsen R, Gotschalck KA, Andersen CL. Incidence of Recurrence and Time to Recurrence in Stage I to III Colorectal Cancer: A Nationwide Danish Cohort Study. JAMA Oncol. 2024; 10 (1): 54–62. DOI: 10.1001/jamaoncol.2023.5098.
19. Balboa-Barreiro V, Pértega-Díaz S, García-Rodríguez T, González-Martín C, Pardeiro-Pértega R, Yáñez-González-Dopeso L, Seoane-Pillado T. Colorectal cancer recurrence and its impact on survival after curative surgery: An analysis based on multistate models. Dig Liver Dis. 2024; 56 (7): 1229–36. DOI: 10.1016/j.dld.2023.11.041.
20. Zhang ZT, Xiao WW, Li LR, Wu XJ, Wang QX, Chang H, et al. Neoadjuvant chemoradiotherapy versus neoadjuvant chemotherapy for initially unresectable locally advanced colon cancer: short-term outcomes of an open-label, single-centre, randomised, controlled, phase 3 trial. EClinicalMedicine. 2024; 76: 102836. DOI: 10.1016/j.eclinm.2024.102836. Available from: https://www.clinicaloncologyonline.net/article/S0936-6555(24)00488-6/fulltext.
21. Joshi SS, Maron SB, Catenacci DV. Pembrolizumab for treatment of advanced gastric and gastroesophageal junction adenocarcinoma. Future Oncol. 2018; 14 (5): 417–30. DOI: 10.2217/fon-2017-0436.
22. Fedyanin MYu, Polyanskaya EM, Elsnukaeva HM, Tryakin AA, Pokataev IA, Bulanov AA, i dr. Metaanaliz issledovanij po sravneniyu effektivnosti rezhimov FOLFOXIRI i FOLFOX ili FOLFIRI s targetnoj terapiej pri metastaticheskom rake tolstoj kishki s mutaciej v gene BRAF. Medicinskij Sovet. 2020; (20): 125–32. DOI: 10.21518/2079-701X-2020-20-125-132. Russian.
23. Ogorodnikova SYu, Konstantinova ED. Metody vizualizacii dannyh v mediko-biologicheskih issledovaniyah. Traektoriya issledovanij — chelovek, priroda, tekhnologii. 2022; 3 (3): 4–18. Dostupno po ssylke: https://restrajectory.ru/3-2.pdf. Russian.
24. Mahran R, Kapp JN, Valtonen S, Champagne A, Ning J, Gillette W, et al. Beyond KRAS(G12C): Biochemical and Computational Characterization of Sotorasib and Adagrasib Binding Specificity and the Critical Role of H95 and Y96. ACS Chem Biol. 2024; 19 (10): 2152–64. DOI: 10.1021/acschembio.4c00315.
25. Miyashita H, Kato S, Hong DS. KRAS G12C inhibitor combination therapies: current evidence and challenge. Front Oncol. 2024: 14: 1380584. DOI: 10.3389/fonc.2024.1380584. Available from: https://www.frontiersin.org/journals/oncology/articles/10.3389/fonc.2024.1380584/full.
26. Prajapati V, Singh AK, Kumar A, Singh H, Pathak P, Grishina M, et al. Structural insights, regulation, and recent advances of RAS inhibitors in the MAPK signaling cascade: a medicinal chemistry perspective. RSC Med Chem. 2025; 5 (16): 1923–40. DOI: 10.1039/d4md00923a. Available from: https://pubs.rsc.org/en/content/articlelanding/2025/md/d4md00923a.
27. Haddad SF, Bouferraa Y, Nair KG. Adagrasib in the treatment of colorectal cancer. Future Oncol. 2025; 21 (18): 2275–85. DOI: 10.1080/14796694.2025.2524311. Epub 2025 Jul 6. PMID: 40619745; PMCID: PMC12323406.
28. Ding Y, Su H, Shu Y, Chen J. Post-marketing safety concerns of sotorasib: A disproportionality analysis based on FDA adverse event reporting system. Heliyon. 2024; 10 (9): e30437. DOI: 10.1016/j.heliyon.2024.e30437.Availablefrom:https://www.sciencedirect.com/science/article/pii/S2405844024064685?via%3Dihub.
29. Luo J, Florez N, Donnelly A, Lou Y, Lu K, Ma PC, et al. Adagrasib Treatment After Sotorasib-Related Hepatotoxicity in Patients With KRAS-G12C-Mutated Non-Small Cell Lung Cancer: A Case Series and Literature Review. JCO Precis Oncol. 2024; 8: e2300644. DOI: 10.1200/PO.23.00644. Available from: https://ascopubs.org/doi/pdf/10.1200/PO.23.00644.
30. Zhang J, Johnson M, Barve M, Bazhenova L, McCarthy M, Schwartz R, et al. Practical Guidance for the Management of Adverse Events in Patients with KRASG12C-Mutated Non-Small Cell Lung Cancer Receiving Adagrasib. Oncologist. 2023; 28 (4): 287–96. DOI: 10.1093/oncolo/oyad051.
31. Jänne PA, Riely GJ, Gadgeel SM, Heist RS, Ou SHI, Pacheco JM, et al. Adagrasib in Non-Small-Cell Lung Cancer Harboring a KRASG12C Mutation. N Engl J Med. 2022; 387 (2): 120–31. DOI: 10.1056/NEJMoa2204619.
32. Kulinich TM, Shishkin AM, Ivanov AV, Kaminskij VV, Puchkov IA, Bozhenko VK. Razrabotka innovacionnyh protivoopuholevyh preparatov na osnove targetnyh peptidnyh konstrukcij. Vestnik Rossijskogo nauchnogo centra rentgenoradiologii Minzdrava Rossii 2024; (2): 59–68. Dostupno po ssylke: https://vestnik.rncrr.ru/vypusk/vypusk-ub100/?ELEMENT_ID=172. Russian.
33. Skoulidis F, Li BT, Dy GK, Price TJ, Falchook GS, Wolf J, et al. Sotorasib for Lung Cancers with KRAS p.G12C Mutation. N Engl J Med. 2021; 384 (25): 2371–81. DOI: 10.1056/NEJMoa2103695.
34. Parums DV. Editorial: Recent Approval of Sotorasib as the First Targeted Therapy for KRAS G12C-Mutated Advanced Non-Small Cell Lung Cancer (NSCLC). Med Sci Monit. 2022; 28: e938746. DOI: 10.12659/MSM.938746. Available from: https://medscimonit.com/abstract/full/idArt/938746.
35. Xia W, Geng Y, Hu W. Peritoneal Metastasis: A Dilemma and Challenge in the Treatment of Metastatic Colorectal Cancer. Cancers (Basel). 2023; 15 (23): 5641. DOI: 10.3390/cancers15235641.

Литература

1. Coccolini F, Gheza F, Lotti M, Virzì S, Iusco D, Ghermandi C, Melotti R, Baiocchi G, Giulini SM, Ansaloni L, Catena F. Peritoneal carcinomatosis. World J Gastroenterol. 2013; 19 (41): 6979–94. DOI: 10.3748/wjg.v19.i41.6979.
2. Solass W, Kerb R, Mürdter T, Giger-Pabst U, Strumberg D, Tempfer C, et al. Intraperitoneal chemotherapy of peritoneal carcinomatosis using pressurized aerosol as an alternative to liquid solution: first evidence for efficacy. Ann Surg Oncol. 2014; 21 (2): 553–9. DOI: 10.1245/s10434-013-3213-1.
3. Wu X, Song W, Cheng C, Liu Z, Li X, Cui Y, et al. Small molecular inhibitors for KRAS-mutant cancers. Front Immunol. 2023; 14: 1223433. DOI: 10.3389/fimmu.2023.1223433. Available from: https://www.frontiersin.org/journals/immunology/articles/10.3389/fimmu.2023.1223433/full. English.
4. Wu L, Rao W, Guo L, Zhang F, Li W, Ying J. Pan-cancer analysis to character the clinicopathological and genomic features of KRAS-mutated patients in China. J Cancer Res Clin Oncol. 2025; 151 (2): 94. DOI: 10.1007/s00432-025-06118-9.
5. Wiechmann S, Maisonneuve P, Grebbin BM, Hoffmeister M, Kaulich M, Clevers H, et al. Conformation-specific inhibitors of activated Ras GTPases reveal limited Ras dependency of patient-derived cancer organoids. J Biol Chem. 2020; 295 (14): 4526–40. DOI: 10.1074/jbc.RA119.011025.
6. Боженко В. К., Гончаров С. В., Кудинова Е. А., Кулинич Т. М., Куколева Е. А., Филиппов М. С., и др. Оценка безопасности с установлением максимально переносимой дозы ингибитора RAS-ГТФазы («Инг-Рас») для лечения опухолей желудочно-кищечного тракта: предварительные результаты исследования I фазы. Альманах клинической медицины. 2023; 51 (7): 376–96. DOI: 10.18786/2072-0505-2023-51-045.
7. Кулинич Т. М., Шишкин А. М., Иванов А. В., Каминский В. В., Боженко В. К. Изучение противоопухолевых свойств пептидной конструкции, включающей интернализуемую последовательность и ингибитор RAS-ГТфазы, в отношении клеток линий рака толстой кишки (HT29) и рака яичника (OAW-42, OVCAR-3). Вестник Российского научного центра рентгенорадиологии Минздрава России. 2021; 4 (21). Доступно по ссылке: https://vestnik.rncrr.ru/vestnik/v21/docs/kulinich_t4.pdf.
8. Yaeger R, Weiss J, Pelster MS, Spira AI, Barve M, Ou SHI, et al. Adagrasib with or without Cetuximab in Colorectal Cancer with Mutated KRAS G12C. N Engl J Med. 2023; 388 (1): 44–54. DOI: 10.1056/NEJMoa2212419.
9. Миронов А. Н., редактор. Руководство по проведению клинических исследований лекарственных средств. М.: Гриф

и К; 2012. 944 с.
10. Гончаров С. В., Боженко В. К., Захаренко М. В., Киселева Я. Ю., Чаптыков А. А., Кулинич Т. М., и др. Анализ молекулярных фенотипов эмбрионально-анатомических отделов толстой кишки в нормальной слизистой оболочке и при колоректальном раке. Альманах клинической медицины. 2023; 51 (8): 441–55. DOI: 10.18786/2072-0505-2023-51-046.
11. Farias ST, Weakley A, Harvey D, Chandler J, Huss O, Mungas D. The Measurement of Everyday Cognition (ECog): Revisions and Updates. Alzheimer Dis Assoc Disord. 2021; 35 (3): 258–64. DOI: 10.1097/WAD.0000000000000450.
12. Eisenhauer EA, Therasse P, Bogaerts J, Schwartz LH, Sargent D, Ford R, et al. New response evaluation criteria in solid tumours: revised RECIST guideline (version 1.1). Eur J Cancer. 2009; 45 (2): 228–47. DOI: 10.1016/j.ejca.2008.10.026.
13. Рубцова Н. А., Левшакова А. В., Пешков А. О., Хомяков В. М., Уткина А. Б., Сидоров Д. В., и др. Компьютерная и магнитно-резонансная томография в диагностике перитонеального карциноматоза». Лучевая диагностика и терапия. 2019; 2 (10): 32–41. DOI: 10.22328/2079-5343-2019-10-2-32-41.
14. Каприн А. Д., Старинский В. В., Шахзадова А. О., редакторы. Состояние онкологической помощи населению в 2023 году. М.: МНИОИ им. П.А. Герцена, 2024; 262 с.
15. O'Neil BH, Wallmark JM, Lorente D, Elez E, Raimbourg J, Gomez-Roca C, et al. Safety and antitumor activity of the anti-PD-1 antibody pembrolizumab in patients with advanced colorectal carcinoma. PLoS One. 2017; 12 (12): e0189848. DOI: 10.1371/journal.pone.0189848. Available from: https://journals.plos.org/plosone/article?id=10.1371/journal.pone.0189848. English.
16. Janjigian YY, Shitara K, Moehler M, Garrido M, Salman P, Shen L, et al. First-line nivolumab plus chemotherapy versus chemotherapy alone for advanced gastric, gastro-oesophageal junction, and oesophageal adenocarcinoma (CheckMate 649): a randomised, open-label, phase 3 trial. Lancet. 2021; 398 (10294): 27–40. DOI: 10.1016/S0140-6736(21)00797-2.
17. Sánchez-Hidalgo JM, Rodríguez-Ortiz L, Arjona-Sánchez Á, Rufián-Peña S, Casado-Adam Á, Cosano-Álvarez A, et al. Colorectal peritoneal metastases: Optimal management review. World J Gastroenterol. 2019; 25 (27): 3484–502. DOI: 10.3748/wjg.v25.i27.3484.
18. Nors J, Iversen LH, Erichsen R, Gotschalck KA, Andersen CL. Incidence of Recurrence and Time to Recurrence in Stage I to III Colorectal Cancer: A Nationwide Danish Cohort Study. JAMA Oncol. 2024; 10 (1): 54–62. DOI: 10.1001/jamaoncol.2023.5098.
19. Balboa-Barreiro V, Pértega-Díaz S, García-Rodríguez T, González-Martín C, Pardeiro-Pértega R, Yáñez-González-Dopeso L, Seoane-Pillado T. Colorectal cancer recurrence and its impact on survival after curative surgery: An analysis based on multistate models. Dig Liver Dis. 2024; 56 (7): 1229–36. DOI: 10.1016/j.dld.2023.11.041.
20. Zhang ZT, Xiao WW, Li LR, Wu XJ, Wang QX, Chang H, et al. Neoadjuvant chemoradiotherapy versus neoadjuvant chemotherapy for initially unresectable locally advanced colon cancer: short-term outcomes of an open-label, single-centre, randomised, controlled, phase 3 trial. EClinicalMedicine. 2024; 76: 102836. DOI: 10.1016/j.eclinm.2024.102836. Available from: https://www.clinicaloncologyonline.net/article/S0936-6555(24)00488-6/fulltext.
21. Joshi SS, Maron SB, Catenacci DV. Pembrolizumab for treatment of advanced gastric and gastroesophageal junction adenocarcinoma. Future Oncol. 2018; 14 (5): 417–30. DOI: 10.2217/fon-2017-0436.
22. Федянин М. Ю., Полянская Е. М., Эльснукаева Х. М., Трякин А. А., Покатаев И. А., Буланов А. А., и др. Метаанализ исследований по сравнению эффективности режимов FOLFOXIRI и FOLFOX или FOLFIRI с таргетной терапией при метастатическом раке толстой кишки с мутацией в гене BRAF. Медицинский Совет. 2020; (20): 125–32. DOI: 10.21518/2079-701X-2020-20-125-132.
23. Огородникова С. Ю., Константинова Е. Д. Методы визуализации данных в медико-биологических исследованиях. Траектория исследований — человек, природа, технологии. 2022; 3 (3): 4–18. Доступно по ссылке: https://restrajectory.ru/3-2.pdf.
24. Mahran R, Kapp JN, Valtonen S, Champagne A, Ning J, Gillette W, et al. Beyond KRAS(G12C): Biochemical and Computational Characterization of Sotorasib and Adagrasib Binding Specificity and the Critical Role of H95 and Y96. ACS Chem Biol. 2024; 19 (10): 2152–64. DOI: 10.1021/acschembio.4c00315.
25. Miyashita H, Kato S, Hong DS. KRAS G12C inhibitor combination therapies: current evidence and challenge. Front Oncol. 2024: 14: 1380584. DOI: 10.3389/fonc.2024.1380584. Available from: https://www.frontiersin.org/journals/oncology/articles/10.3389/fonc.2024.1380584/full.
26. Prajapati V, Singh AK, Kumar A, Singh H, Pathak P, Grishina M, et al. Structural insights, regulation, and recent advances of RAS inhibitors in the MAPK signaling cascade: a medicinal chemistry perspective. RSC Med Chem. 2025; 5 (16): 1923–40. DOI: 10.1039/d4md00923a. Available from: https://pubs.rsc.org/en/content/articlelanding/2025/md/d4md00923a.
27. Haddad SF, Bouferraa Y, Nair KG. Adagrasib in the treatment of colorectal cancer. Future Oncol. 2025; 21 (18): 2275–85. DOI: 10.1080/14796694.2025.2524311. Epub 2025 Jul 6. PMID: 40619745; PMCID: PMC12323406.
28. Ding Y, Su H, Shu Y, Chen J. Post-marketing safety concerns of sotorasib: A disproportionality analysis based on FDA adverse event reporting system. Heliyon. 2024; 10 (9): e30437. DOI: 10.1016/j.heliyon.2024.e30437.Availablefrom:https://www.sciencedirect.com/science/article/pii/S2405844024064685?via%3Dihub.
29. Luo J, Florez N, Donnelly A, Lou Y, Lu K, Ma PC, et al. Adagrasib Treatment After Sotorasib-Related Hepatotoxicity in Patients With KRAS-G12C-Mutated Non-Small Cell Lung Cancer: A Case Series and Literature Review. JCO Precis Oncol. 2024; 8: e2300644. DOI: 10.1200/PO.23.00644. Available from: https://ascopubs.org/doi/pdf/10.1200/PO.23.00644.
30. Zhang J, Johnson M, Barve M, Bazhenova L, McCarthy M, Schwartz R, et al. Practical Guidance for the Management of Adverse Events in Patients with KRASG12C-Mutated Non-Small Cell Lung Cancer Receiving Adagrasib. Oncologist. 2023; 28 (4): 287–96. DOI: 10.1093/oncolo/oyad051.
31. Jänne PA, Riely GJ, Gadgeel SM, Heist RS, Ou SHI, Pacheco JM, et al. Adagrasib in Non-Small-Cell Lung Cancer Harboring a KRASG12C Mutation. N Engl J Med. 2022; 387 (2): 120–31. DOI: 10.1056/NEJMoa2204619.
32. Кулинич Т. М., Шишкин А. М., Иванов А. В., Каминский В. В., Пучков И. А., Боженко В. К. Разработка инновационных противоопухолевых препаратов на основе таргетных пептидных конструкций. Вестник Российского научного центра рентгенорадиологии Минздрава России 2024; (2): 59–68. Доступно по ссылке: https://vestnik.rncrr.ru/vypusk/vypusk-ub100/?ELEMENT_ID=172.
33. Skoulidis F, Li BT, Dy GK, Price TJ, Falchook GS, Wolf J, et al. Sotorasib for Lung Cancers with KRAS p.G12C Mutation. N Engl J Med. 2021; 384 (25): 2371–81. DOI: 10.1056/NEJMoa2103695.
34. Parums DV. Editorial: Recent Approval of Sotorasib as the First Targeted Therapy for KRAS G12C-Mutated Advanced Non-Small Cell Lung Cancer (NSCLC). Med Sci Monit. 2022; 28: e938746. DOI: 10.12659/MSM.938746. Available from: https://medscimonit.com/abstract/full/idArt/938746.
35. Xia W, Geng Y, Hu W. Peritoneal Metastasis: A Dilemma and Challenge in the Treatment of Metastatic Colorectal Cancer. Cancers (Basel). 2023; 15 (23): 5641. DOI: 10.3390/cancers15235641.

EXPRESSION OF CHEMOKINE RECEPTORS CXCR4 AND CXCR7 IN CIRCULATING TUMOR CELLS OF BREAST CANCER

Grigoryeva ES[1]✉, Tashireva LA[1], Savelieva OE[2], Zavyalova MV[1], Cherdyntseva NV[1], Perelmuter VM[1]

[1] Cancer Research Institute, Tomsk National Research Medical Center of the Russian Academy of Sciences, Tomsk, Russia

[2] Saint Petersburg State Pediatric Medical University, Saint Petersburg, Russia

It is known that chemokine receptors CXCR4 and CXCR7 in primary tumor cells are associated with tumor growth progression; however, the significance of their expression in circulating tumor cells (CTCs) remains insufficiently studied. The objective of this study was to investigate the expression of chemokine receptors CXCR4 and CXCR7 in subpopulations of CTCs with positive (EpCAM$^+$) and negative (EpCAM$^-$) EpCAM expression in breast cancer patients, as well as assessed their correlation with clinicopathological parameters and prognostic relevance.The study methods included protein expression analysis and transcriptome profiling of CTCs obtained from peripheral blood. This study comprehensively characterized CXCR4 and CXCR7 expression across EpCAM$^+$ and EpCAM$^-$ CTC subsets and assessed their clinical relevance through protein-level detection, transcriptomic profiling, and long-term patient follow-up. CXCR4 and CXCR7 receptors were predominantly expressed in EpCAM$^+$ CTCs, whereas EpCAM$^-$ cells were largely negative. Importantly, an increased number of EpCAM$^-$ CTCs, irrespective of CXCR4/7 status, was associated with disease progression over a six-year period (p = 0,0007). Prognostic significance was specifically attributed to EpCAM$^-$ CXCR4/7$^-$ CTCs, with counts exceeding 1.25 cells/ml predicting progression with high sensitivity and specificity. Distinct CTC subpopulations were further characterized by stemness and epithelial-mesenchymal transition (EMT) markers, underscoring the aggressive phenotype of EpCAM$^-$ cells exhibiting EMT traits. Transcriptomic analysis of *EpCAM$^-$CXCR4/7$^-$* CTCs revealed upregulation of genes involved in ferroptosis (p = 3.315 × 10^{-7}) and androgen receptor signaling pathways (p = 8.0 v 10^{-5}), alongside identification of progression-associated genes (*HBB*, *IGLC2*, and *IGHM*). Conversely, *MALAT1* was overexpressed in patients without progression, indicating a potential metastasis-suppressive function (p = 1.52 × 10^{-2}). These findings highlight the pathogenetic importance of EpCAM$^-$ CTCs in breast cancer progression and support a paradigm shift in CTC research towards this subpopulation. Further investigations are warranted to elucidate the functional roles of these cells and their utility as prognostic biomarkers.

Keywords: circulating tumor cells, chemokine receptors, epithelial-mesenchymal transition, stemness, transcriptomics, breast cancer progression

Funding: the study was supported by the Russian Science Foundation (grant No. 23-15-00135).

Author contribution: Grigorieva ES, Savelieva OE, Zavyalova MV — data collection and analysis; Grigorieva ES, Tashireva LA — writing and editing; Perelmuter VM — research supervision; Cherdyntseva NV — project funding.

Compliance with ethical standards: the study was approved by the Local Ethics Committee of Tomsk National Research Medical Center (17 June 2016, the approval No. 8) and complied with the Declaration of Helsinki. All participants gave written informed consent.

✉ **Correspondence should be addressed:** Evgeniya S. Grigoryeva
per. Kooperativny, 5, Tomsk, 634009, Russia; grigoryeva.es@gmail.com

Received: 24.10.2025 **Accepted:** 29.11.2025 **Published online:** 08.12.2025

DOI: 10.24075/brsmu.2025.064

Copyright: © 2025 by the authors. **Licensee:** Pirogov University. This article is an open access article distributed under the terms and conditions of the Creative Commons Attribution (CC BY) license (https://creativecommons.org/licenses/by/4.0/).

ЭКСПРЕССИЯ РЕЦЕПТОРОВ ХЕМОКИНОВ CXCR4 И CXCR7 В ЦИРКУЛИРУЮЩИХ ОПУХОЛЕВЫХ КЛЕТКАХ ПРИ РАКЕ МОЛОЧНОЙ ЖЕЛЕЗЫ

Е. С. Григорьева[1]✉, Л. А. Таширева[1], О. Е. Савельева[2], М. В. Завьялова[1], Н. В. Чердынцева[1], В. М. Перельмутер[1]

[1] Научно-исследовательский институт онкологии, Томский национальный исследовательский медицинский центр Российской академии наук, Томск, Россия

[2] Санкт-Петербургский государственный педиатрический медицинский университет, Санкт-Петербург, Россия

Хемокиновые рецепторы CXCR4 и CXCR7 в клетках первичной опухоли связаны с прогрессией опухолевого роста. Цель исследования — изучить экспрессию CXCR4 и CXCR7 в субпопуляциях ЦОК с положительной (EpCAM$^+$) и отрицательной (EpCAM$^-$) экспрессией EpCAM у пациентов с раком молочной железы (РМЖ), а также оценить их связь с клинико-патологическими параметрами и прогностической значимостью. Анализ белковой экспрессии и транскриптомное профилирование ЦОК, полученных из периферической крови, показали, что CXCR4 и CXCR7 преимущественно экспрессировались в EpCAM$^+$ ЦОК, тогда как EpCAM$^-$ клетки в основном не имели экспрессии CXCR4 и CXCR7 (p < 0,001). Важно, что увеличение количества EpCAM$^-$ ЦОК, независимо от экспрессии CXCR4/7, было связано с прогрессированием заболевания в течение шестилетнего периода (p = 0,0007). Прогностическое значение показано для EpCAM$^-$CXCR4/7$^-$ ЦОК, при этом количество, превышающее 1,25 кл./мл периферической крови, предсказывало прогрессирование заболевания с чувствительностью 100% и специфичностью 95,1%. Отдельные субпопуляции ЦОК были дополнительно охарактеризованы по маркерам стволовости и эпителиально-мезенхимального перехода (ЭМП), что подчеркивает агрессивный фенотип EpCAM$^-$ клеток, проявляющих признаки ЭМП. Транскриптомный анализ *EpCAM$^-$CXCR4/7$^-$* ЦОК выявил повышенную экспрессию генов, участвующих в ферроптозе (p = 3,315 × 10^{-7}) и сигнальных путях андрогенового рецептора (p = 8,0 × 10^{-5}), а также генов, ассоциированных с прогрессированием (*HBB*, *IGLC2* и *IGHM*). Напротив, *MALAT1* был сверхэкспрессирован у пациентов без прогрессирования, что указывает на потенциальную подавляющую метастазирование функцию (p = 1,52 × 10^{-2}). Результаты подчеркивают патогенетическую значимость EpCAM$^-$ ЦОК в прогрессировании РМЖ и поддерживают смену парадигмы в исследованиях ЦОК в сторону этой субпопуляции.

Ключевые слова: циркулирующие опухолевые клетки, хемокиновые рецепторы, эпителиально-мезенхимальный переход, стволовые клетки, транскриптомика, прогрессирование рака молочной железы

Финансирование: исследование проведено при поддержке Российского научного фонда (грант № 23-15-00135).

Вклад авторов: Е. С. Григорьева, О. Е. Савельева, М. В. Завьялова — сбор и анализ данных, Е. С. Григорьева, Л. А. Таширева — написание и редактирование, В. М. Перельмутер — курирование исследования, Н. В. Чердынцева — финансирование проекта.

Соблюдение этических стандартов: исследование одобрено этическим комитетом Томского национального исследовательского медицинского центра (протокол № 8 от 17 июня 2016 г.,), проведено согласно требованиям Хельсинкской декларации. Все участники дали письменное информированное согласие.

✉ **Для корреспонденции:** Евгения Сергеевна Григорьева
пер. Кооперативный, д. 5, г. Томск, 634009, Россия; grigoryeva.es@gmail.com

Статья получена: 24.10.2025 **Статья принята к печати:** 29.11.2025 **Опубликована онлайн:** 08.12.2025

DOI: 10.24075/vrgmu.2025.064

Авторские права: © 2025 принадлежат авторам. **Лицензиат:** РНИМУ им. Н. И. Пирогова. Статья размещена в открытом доступе и распространяется на условиях лицензии Creative Commons Attribution (CC BY) (https://creativecommons.org/licenses/by/4.0/).

Breast cancer (BC) remains one of the most significant challenges in modern oncology due to its high prevalence, substantial mortality rate, and frequent metastasis. The recent advances in liquid biopsy techniques have opened new avenues for developing approaches to better predict the clinical course of the disease. Among the most promising targets for investigation are circulating tumor cells (CTCs), which are tumor cells that have detached from the primary tumor and circulate in the bloodstream. Elevated levels of CTCs in the peripheral blood often correlate with poor prognosis, making them a valuable tool for patient stratification and optimizing treatment strategies [1]. However, the clinical application of CTCs faces several challenges, including their low concentration in blood and technical difficulties in their detection [2]. Most studies on CTCs rely on EpCAM (epithelial cell adhesion molecule)-based methods [3]. This preference is largely due to the availability of commercially certified systems designed to detect EpCAM-positive CTCs [4]. Although EpCAM-expressing tumor cells have traditionally been considered the primary drivers of metastasis, increasing evidence highlights the important role of subpopulations lacking EpCAM expression [5]. The loss of membrane EpCAM expression is often associated with epithelial-mesenchymal transition (EMT), a process in which epithelial cells lose polarity and cell-cell adhesion, acquiring mesenchymal traits such as enhanced motility and resistance to apoptosis [6]. In tumor progression, EMT facilitates tumor cell motility, invasion, intravasation, survival in circulation, and the formation of metastases following extravasation into distant organs [7]. Consequently, CTCs constitute a heterogeneous population comprising cells with varying epithelial and mesenchymal phenotypes, as well as stem cell-like properties, which may underlie their metastatic potential.

In the context of investigating CTC heterogeneity, the chemokine receptors CXCR4 and CXCR7, which are activated by their common ligand SDF-1 (CXCL12), are of considerable interest. The most well-characterized function of the CXCR4–SDF-1 axis is to mediate the directed migration of bone marrow progenitor cells and immune cells to sites of inflammation. It is well established that CXCR4 and CXCR7 are frequently overexpressed in tumor cells, and their interaction with SDF-1 plays a critical role in cancer progression and metastasis [8]. Tumor cells with elevated CXCR4 expression exhibit increased proliferation, driven by activation of the MAPK and PI3K/Akt signaling pathways, while enhanced levels of anti-apoptotic proteins and reduced expression of death receptors promote cell survival [9]. Initially, CXCR7 was considered a decoy receptor that sequesters CXCL12, thereby attenuating CXCR4 activity [10]. However, recent evidence reveals that CXCR7 can signal via the noncanonical β-arrestin pathway, leading to activation of intracellular cascades including protein kinase B (AKT) and JAK/STAT pathways, which further stimulate tumor cell proliferation and migration [11]. According to the literature, high CXCR4 expression correlates with an increased risk of breast cancer metastasis to lymph nodes and distant organs, as well as with reduced relapse-free and overall survival [12]. In summary, while the expression patterns of CXCR4 and CXCR7 in primary breast tumors have been extensively characterized, studies examining their expression in circulating tumor cells remain very limited.

Thus, the aim of this study is to investigate the expression of chemokine receptors CXCR4 and CXCR7 in CTC subpopulations with positive ($EpCAM^+$) and negative ($EpCAM^-$) EpCAM expression in breast cancer patients, and to evaluate their association with clinicopathological parameters and prognostic significance.

METHODS

Patients

The study included 65 female patients with invasive breast carcinoma of no special type, who were treated at the Oncology Research Institute Clinic of the Tomsk National Research Medical Center (Tables 1, 2). CTC analysis was performed prior to any treatment. Patients received full treatment according to the clinical guidelines of the Ministry of Health of the Russian Federation. The follow-up period was 6 years.

Flow cytometry

Venous blood samples collected from breast cancer patients was used for CTC detection. Cell concentrates were prepared by sedimentation, followed by collection of the white cell layer at the interface between the erythrocyte sediment and the separated plasma, as well as the entire supernatant, according to the method described by R. A. Pospelova [13].

Table 1. Clinicopathological characteristics of patients included in the study of CTC subpopulation composition

Parameter		Frequency, % (*n*)
Age	≤ 50	26.67% (12/45)
	> 50	73.33% (33/45)
Tumor size (cT)	1	35.56% (16/45)
	2	60.00% (27/45)
	4	4.44% (2/45)
Stage	IA	28.89% (13/45)
	IIA	33.33% (15/45)
	IIB	33.33% (15/45)
	IIIB	4.44% (2/45)
Lymph node status (cN)	0	53.33% (24/45)
	1	46.67% (21/45)
Molecular subtype	Luminal A	26.67% (12/45)
	Luminal B ($HER2^-$)	37.78% (17/45)
	Luminal B ($HER2^+$)	20.00% (9/45)
	Triple negative	6.67% (3/45)

Table 2. Clinicopathological characteristics of patients included in the study of the transcriptional profile of circulating tumor cells

Parameter		Frequency, % (*n*)
Age	≤ 50	30.0% (6/20)
	> 50	70.0% (14/20)
Tumor size (cT)	1	5.0% (1/40)
	2	80.0% (15/40)
	3 4	5.0% (1/20) 5.0% (3/20)
Stage	I	5.0% (1/20)
	IIA	20.0% (5/20)
	IIB IIIA	40.0% (8/20) 15.0% (3/20)
	IIIB	10.0% (2/20)
	IIIC	5.0% (1/20)
Lymph node status (cN)	0	30.0% (6/20)
	1	70.0% (14/20)
Molecular subtype	Luminal A	10.0% (2/20)
	Luminal B ($HER2^-$) Luminal B ($HER2^+$)	65.0% (13/20) 10.0% (2/20)
	Triple negative	5.0% (5/20)
	$HER2^+$	10.0% (1/20)

Samples for flow cytometry were prepared as follows. The cell concentrate was washed by adding 1 ml of CellWASH solution (BD Biosciences, USA) and centrifuged at 300 × g for 10 minutes. To lyse erythrocytes, 500 µl of OptiLyse C buffer (Beckman Coulter, France) was added, and the samples were washed with 2 ml of CellWASH solution for 10 minutes at 300 × g, followed by removal of the supernatant. After blocking nonspecific Fc receptor binding with Human TruStain FcX™ Fc Receptor Blocking Solution (BioLegend, USA), 5 µl of the following monoclonal antibodies were added to the cell concentrate: BV570 anti-human CD45 (clone HI30; Sony Biotechnology, USA), BV650 anti-human CD326 (EpCAM) (clone 9C4; Sony Biotechnology, USA), BV510 anti-human CD44 (clone G44-26; BD Horizon, USA), PerCP/Cy5.5 anti-human CD24 (clone ML5; Sony Biotechnology, USA), BV421 anti-human CXCR4 (clone 12G5; Sony Biotechnology, USA), BV421 anti-human CXCR7 (clone 10D1; BD Biosciences; USA) and PE/Cy7 anti-human N-Cadherin (clone 8C11; Sony Biotechnology, USA). The samples were then incubated in the dark at room temperature for 20 minutes.

Following incubation, probes were washed with 2 ml of CellWASH solution for 10 minutes at 300 × g and removing the supernatant. For intracellular staining, 250 µl of BD Cytofix/Cytoperm solution (BD Biosciences, USA) was added to each unstained and stained sample, followed by incubation in the dark at 4 °C for 20 minutes. Samples were then washed twice in 1 ml of BD Perm/Wash buffer (BD Biosciences, USA) by centrifugation at 300 × g for 6 minutes. Subsequently, 50 µl of BD Perm/Wash buffer was added to each sample, along with 5 µl of the following antibodies: AF647-anti-human CK7/8 (clone CAM5.2; BD Pharmingen, USA), AF488-anti-human Snail1 (clone 20C8; eBioscience, USA), and AF750-anti-human Vimentin (R&D Systems, USA). The samples were incubated at 4 °C for 20 minutes.

Each sample was then washed in 1 ml of CellWASH buffer (BD Biosciences; USA) by centrifugation at 300 g for 6 min. At the final stage, 100 µl of Cell Staining Buffer (Sony Biotechnology; USA) were added to the sediment and the sample was resuspended.

Samples were analyzed on a Novocyte 3000 flow cytometer (ACEA Biosciences; USA) using NovoExpress 1.3.0 (ACEA Biosciences; USA). The concentration of circulating cells was calculated per 1 ml of blood.

Statistical analysis was performed using the Prism 10.4.1 package (GraphPad Software; USA). The Kruskal–Wallis test was used to analyze independent groups, and the Mann–Whitney test was used to analyze two independent groups. ROC analysis was used to assess the prognostic value of the prediction accuracy. Differences were considered significant at $p < 0.05$.

scRNA-seq analysis of CTCs

Public scRNA-seq data set from 20 BC patients (T1-4N0-3M0, all molecular subtypes) generated in our previous study [14] and available via BioProject under the accession number PRJNA776403 was used for investigation of transcriptional profile of EPCAM-negative and EPCAM-positive CTCs.

The Seurat software package, version 4.0.4 [15], was employed for quality control and analysis of single-cell RNA sequencing data. Cell doublets were identified using DoubletFinder [16] and subsequently removed from each dataset. Integration of the 20 datasets with default parameters was performed. The aggregated data underwent preprocessing, involving the exclusion of cells with unique feature counts less than 200 and mitochondrial percent exceeding 25. Raw RNA UMI counts of the aggregated data were normalized, followed by principal component analysis (PCA). The dataset was visualized and explored using the uniform manifold approximation and projection (UMAP) method, a nonlinear dimensional reduction technique.

Spatial transcriptomics data analysis of breast tumor tissue

Spatial transcriptomics dataset generated in our previous study [17] and available via GEO Database under the accession number GSE242311 was used to investigate gene expression of EPCAM-negative and EPCAM-positive tumor cells in primary tumor of five BC patients (invasive carcinoma of nonspecific type, luminal A and B, stage I–IIA, grade 2–3). Samples

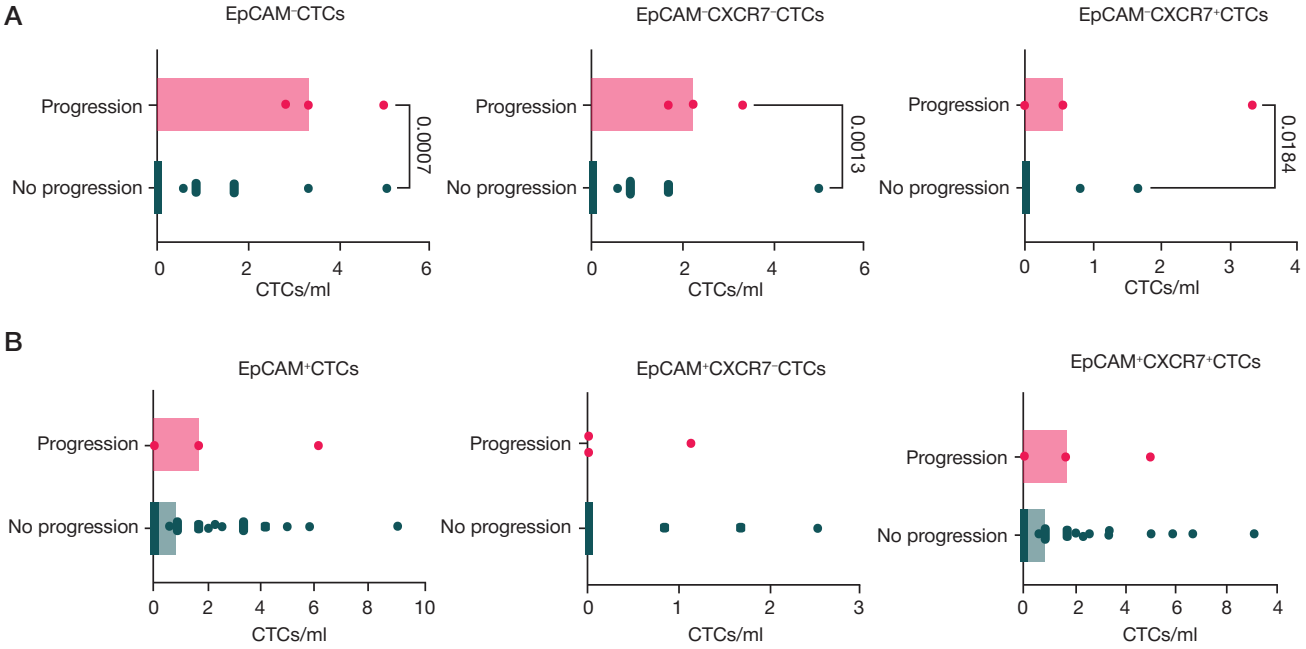


Fig. 1. Number of EpCAM⁻ (**A**) and EpCAM⁺ (**B**) CTCs according to CXCR4/7 expression in breast cancer patients with tumor progression during the 6-year follow-up period

were filtered, excluding genes with nonzero expression in fewer than 10 tissue spots and tissue spots with fewer than 200 filtered genes. The raw counts were normalized using the SCTransform [18] function with default parameters. The uniform manifold approximation and projection (UMAP) technique were then applied to the SCTransform-normalized counts, utilizing the first 30 principal components determined through principal component analysis (PCA). The results were visualized using the Seurat package.

RESULTS

Association between the Number of EpCAM⁺ and EpCAM⁻ CTCs Expressing CXCR4 and CXCR7 and Clinical Parameters in BC Patients

The number of EpCAM⁺ and EpCAM⁻ CTCs was evaluated in the peripheral blood of breast cancer patients. EpCAM⁺ CTCs were defined as cells expressing EpCAM but lacking the leukocyte common antigen CD45, irrespective of cytokeratin 7/8 expression. In contrast, EpCAM⁻ CTCs were defined as CD45-negative cells without EpCAM expression but positive for cytokeratins 7/8. The analysis revealed that the number of EpCAM⁺ CTCs was significantly higher than that of EpCAM⁻ CTCs (p = 0.0237). The median counts of EpCAM⁺ and EpCAM⁻ CTCs were 0.00 (0.00–1.25) and 0.83 (0.00–3.32) cells/ml, respectively.

EpCAM⁺ CTCs exhibited significantly higher expression of the chemokine receptors CXCR4 and CXCR7 compared to EpCAM⁻ CTCs (25/45 vs. 6/45, $p < 0.001$). Specifically, CXCR4/7-positive cells predominated among EpCAM⁺ CTCs, whereas CXCR4/7-negative cells were more common among EpCAM⁻ CTCs. The median number of CXCR4/7-positive cells was 0.83 (0.00–2.12) cells/ml for EpCAM⁺ CTCs and 0.00 (0.00–0.00) cells/ml for EpCAM⁻ CTCs. Conversely, the median number of CXCR4/7-negative cells was 0.00 (0.00–0.00) cells/ml in EpCAM⁺ CTCs and 0.00 (0.00–0.83) cells/ml in EpCAM⁻ CTCs.

Moreover, the number of CXCR4/7-expressing CTCs was significantly higher among EpCAM⁺ CTCs compared to EpCAM⁻ CTCs ($p < 0.001$), with median values of 0.83 (0.00–2.12) cells/ml and 0.00 (0.00–0.00) cells/ml, respectively.

Analysis of the number of EpCAM⁺ and EpCAM⁻ CTCs expressing CXCR4/7, in relation to clinicopathological parameters, revealed no significant associations with clinical variables (Supplementary, Fig. 1A–D).

During the 6-year follow-up period, disease progression was observed in 3 patients: one experienced tumor recurrence, while two developed distant metastases. These patients were grouped as having tumor progression, whereas the remaining patients were classified as without progression. Comparative analysis of the number of EpCAM⁺ and EpCAM⁻ CTCs expressing CXCR4 and CXCR7 demonstrated a significant increase in the total population of EpCAM⁻ CTCs, as well as in both EpCAM⁻CXCR4/7⁺ and EpCAM⁻CXCR4/7⁻ CTC subsets in patients with progression (p = 0.0007, p = 0.0184, and p = 0.0013, respectively) (Fig. 1A). No significant differences were detected in the number of EpCAM⁺ CTCs, regardless of CXCR4/7 expression, between patients with and without signs of progression during the follow-up period ($p > 0.05$) (Fig. 1B).

ROC analysis of EpCAM⁻ CTC counts considering CXCR4/7 expression in patients with progression over a 6-year follow-up demonstrated the prognostic value of both EpCAM⁻ and EpCAM⁻CXCR4/7⁻ parameters (Fig. 2). An EpCAM⁻ CTC count > 2.23 cells/ml of peripheral blood predicted progression with 100.0% sensitivity and 95.1% specificity (AUC=0.96, 95% CI: 0.91–1.00; p = 0.008). Similarly, an EpCAM⁻CXCR4/7⁻CTC count >1.25 cells/ml predicted progression with 100.0% sensitivity and 85.7% specificity (AUC = 0.96, 95% CI: 0.89–1.00; p = 0.009). These results indicate that the EpCAM⁻CXCR4/7⁻ CTC population has prognostic significance, whereas the EpCAM⁻CXCR4/7⁺ cells do not (AUC = 0.80, 95% CI: 0.47–1.00; p = 0.089).

Analysis of stemness and EMT markers in EpCAM⁻CXCR4/7⁻ CTCs associated with tumor progression revealed the presence of stemness features based on the expression of CD44/CD24, CD133, and ALDH1A1. The number of EpCAM⁻CXCR4/7⁻ CD44⁺CD24⁻CD133⁺ALDH1A1⁺ CTCs was significantly higher in patients with progression during the observation period compared to those without progression (p = 0.003). The median count of CTCs exhibiting the CD44⁺CD24⁻CD133⁺ALDH1A1⁺ phenotype was 0.00 (0.00–0.00) cells/ml in patients without

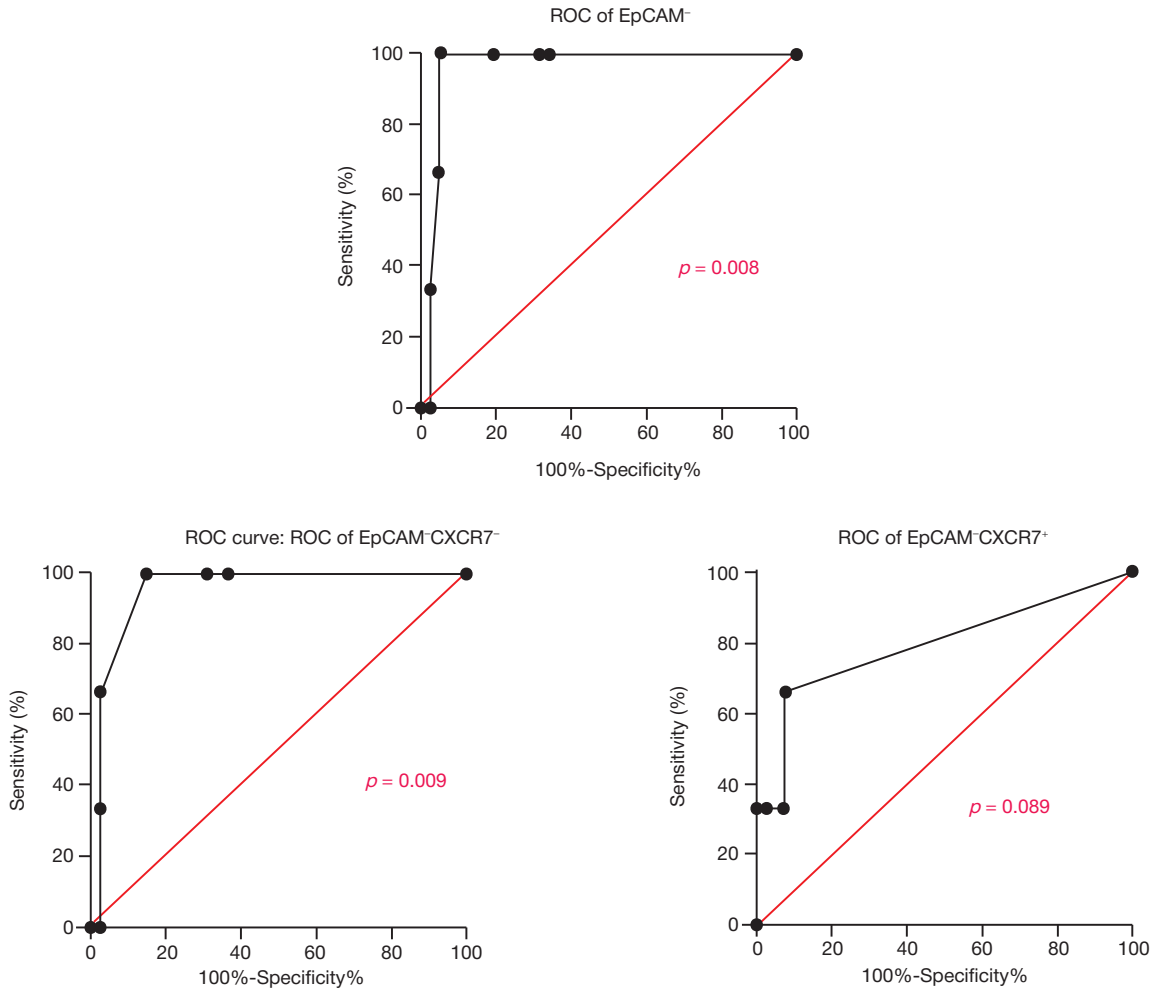


Fig. 2. ROC analysis of EpCAM⁺ CTCs according to CXCR4/7 expression in breast cancer patients with tumor progression during the 6-year follow-up period

progression and 1.66 (0.00–1.68) cells/ml in patients with progression.

The assessment features of EMT revealed the expression of N-cadherin and Snail (p = 0.003). The median number of CTCs with the N-cadherin+Snail+Vimentin– phenotype in patients without and with the presence of signs of progression was 0.00 (0.00–0.00) cells/ml and 2.24 (0.00–4.98) cells/ml, respectively.

Association of chemokine receptor CXCR4 and CXCR7 expression with stemness traits among EpCAM⁺ and EpCAM⁻ CTCs

To evaluate the association between stemness features and the expression of chemokine receptors CXCR4 and CXCR7, the frequency and number of CTCs expressing stemness markers CD44/CD24, CD133, and ALDH1 were analyzed among EpCAM⁺ and EpCAM⁻ CTCs, considering CXCR4/7 expression. Among EpCAM⁺ CTCs, the highest frequency was observed in cells with the CD44⁺CD24⁻CD133⁺ALDH1⁺ phenotype. Specifically, the frequency of these cells was 51.1% (23/45) when CXCR4/7 was expressed, compared to 11.1% (5/45) in its absence. Thus, the occurrence of CD44⁺CD24⁻CD133⁺ALDH1⁺ cells was significantly higher in EpCAM⁺ CTCs expressing CXCR4/7 chemokine receptors ($p < 0.0001$).

The greatest number of cells were also characterized by the CD44⁺CD24⁻CD133⁺ALDH⁺ phenotype, regardless of CXCR4/7 expression (Fig. 3A). The number of cells with this stem phenotype was higher among EpCAM⁺CXCR4/7⁺ CTCs ($p < 0.0001$). The median CD44⁺CD24⁻CD133⁺ALDH⁺ among EpCAM⁺CXCR4/7⁺ CTCs was 0.56 (0.00–1.67) cells/ml and 0.00 (0.00–0.00) cells/ml among EpCAM⁺CXCR4/7⁻ CTCs. Among EpCAM⁻CXCR4/7⁺ CTCs, the frequency of occurrence and the number of cells with stemness variants did not differ ($p > 0.05$) (Fig. 3B).

The frequency of EpCAM⁻CXCR4/7⁻ CTCs was extremely low. The most common phenotype among these cells was CD44⁻CD24⁻CD133⁻ALDH⁻, observed in 12 out of 45 cases, while the frequency of all other phenotypes did not exceed 2 out of 45 (p = 0.02). Additionally, the number of CD44⁻CD24⁻CD133⁻ALDH⁻ cells was significantly higher compared to other phenotypes, with significance levels indicated in the figure above. The median number of cells with this phenotype was 0.00 (0.00–0.70) cells/ml (Fig. 4B).

Evaluation of chemokine receptors CXCR4 and CXCR7 expression in EpCAM⁺ CTCs with distinct stemness phenotypes revealed that a significantly higher proportion of CD44⁺CD24⁻CD133⁺ALDH1⁺ cells expressed CXCR4/7 ($p < 0.0001$) (Fig. 4A). In contrast, the number of CTCs with or without CXCR4/7 expression did not differ significantly among cells exhibiting other stemness phenotypes ($p > 0.05$).

Analysis of chemokine receptors CXCR4 and CXCR7 expression in EpCAM⁻ CTCs, considering stemness characteristics, showed no significant differences in CXCR4/7 expression among stem-like CTCs (Fig. 4B). However, a significantly greater number of cells lacking stemness features, characterized by the CD44⁻CD24⁻CD133⁻ALDH⁻ phenotype, were negative for CXCR4/7 expression (p = 0.0011).

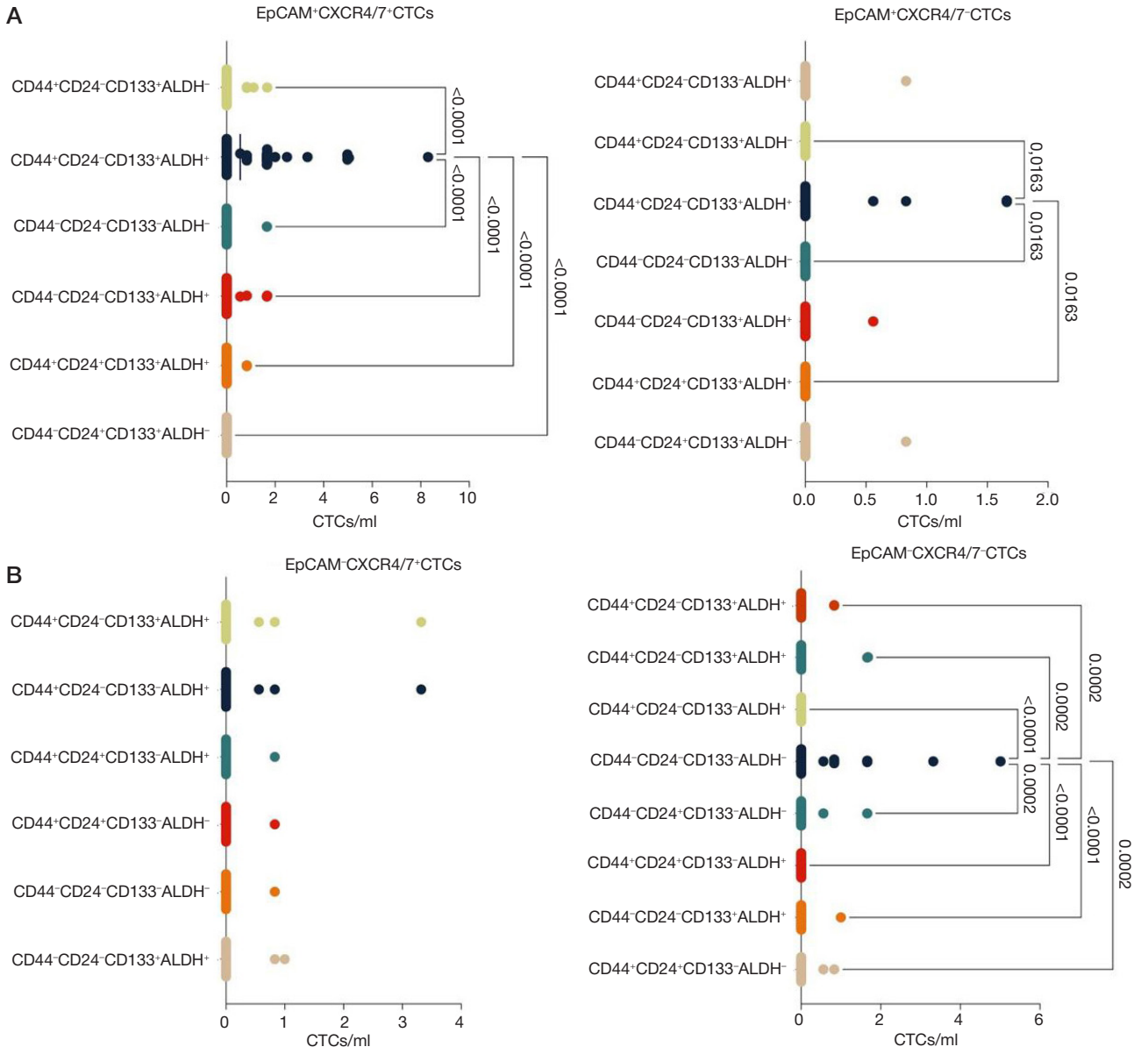


Fig. 3. Number of EpCAM⁺ (**A**) and EpCAM⁻ (**B**) CTCs considering CXCR4/7 expression with stem features in breast cancer patients

Association of chemokine receptor CXCR4 and CXCR7 expression with EMT features among EpCAM⁺ and EpCAM⁻ CTCs

In EpCAM⁺ and EpCAM⁻ CTCs, the expression of the early EMT marker Snail, which represses epithelial markers and promotes mesenchymal marker expression, was evaluated alongside late EMT markers N-cadherin and vimentin. Among EpCAM⁺CXCR4/7⁺ CTCs, the highest frequency was observed in cells expressing the late EMT markers N-cadherin and vimentin, accounting for 35.6% (16/45). Furthermore, the number of N-cadherin⁺Snail⁻vimentin⁺ cells was significantly higher compared to both N-cadherin⁺Snail⁻ vimentin⁻ and N-cadherin⁻Snail⁻vimentin⁻ CTCs (p = 0.0003 and p = 0.0009, respectively) (Fig. 5A). In contrast, among EpCAM⁺ CTCs lacking CXCR4/7 expression, the distribution of cells with different EMT phenotypes did not differ significantly ($p > 0.05$). In this case, N-cadherin⁺Snail⁻Vimentin⁺ cells were practically not found among CXCR4/7⁻ CTCs; their number was higher among CXCR4/7⁺ CTCs ($p < 0.0001$) (Fig. 5B).

Analysis of early and late EMT marker expression in EpCAM⁻ CTCs, considering CXCR4/7 expression, revealed no significant differences ($p > 0.05$) (Fig. 6A). Notably, among EpCAM⁻ CTCs expressing CXCR4/7, no cells were found to co-express all three EMT markers analyzed.

Among EpCAM⁻ CTCs lacking N-cadherin and expressing Snail, regardless of vimentin status, a significantly greater number of cells were negative for CXCR4/7 expression (p = 0.0061 and p = 0.0189, respectively) (Fig. 6B).

Expression of CXCR4 and CXCR7 genes in *EPCAM*⁺ and *EPCAM*⁻ CTCs

In 20 BC patient samples analyzed, a total of 239 CTCs were identified. *EPCAM*⁻ CTCs were defined as cells lacking *PTPRC* (CD45) and EPCAM gene expression but exhibiting positive expression of cytokeratin genes (*KRT7*, *KRT8*, or *KRT18*). Conversely, *EPCAM*⁺ CTCs were characterized as cells without *PTPRC* (CD45) expression and with *EPCAM* gene expression levels greater than zero, regardless of cytokeratins expression. Consequently, the *EPCAM*⁺ and *EPCAM*⁻ CTC groups comprised 11 and 228 cells, respectively. The frequency of SDF-1 chemokine receptor gene expression — *CXCR4* or *CXCR7* — did not differ significantly between *EPCAM*⁺ and *EPCAM*⁻ CTCs, being 54.5% (6/11) and 53.5% (122/228), respectively.

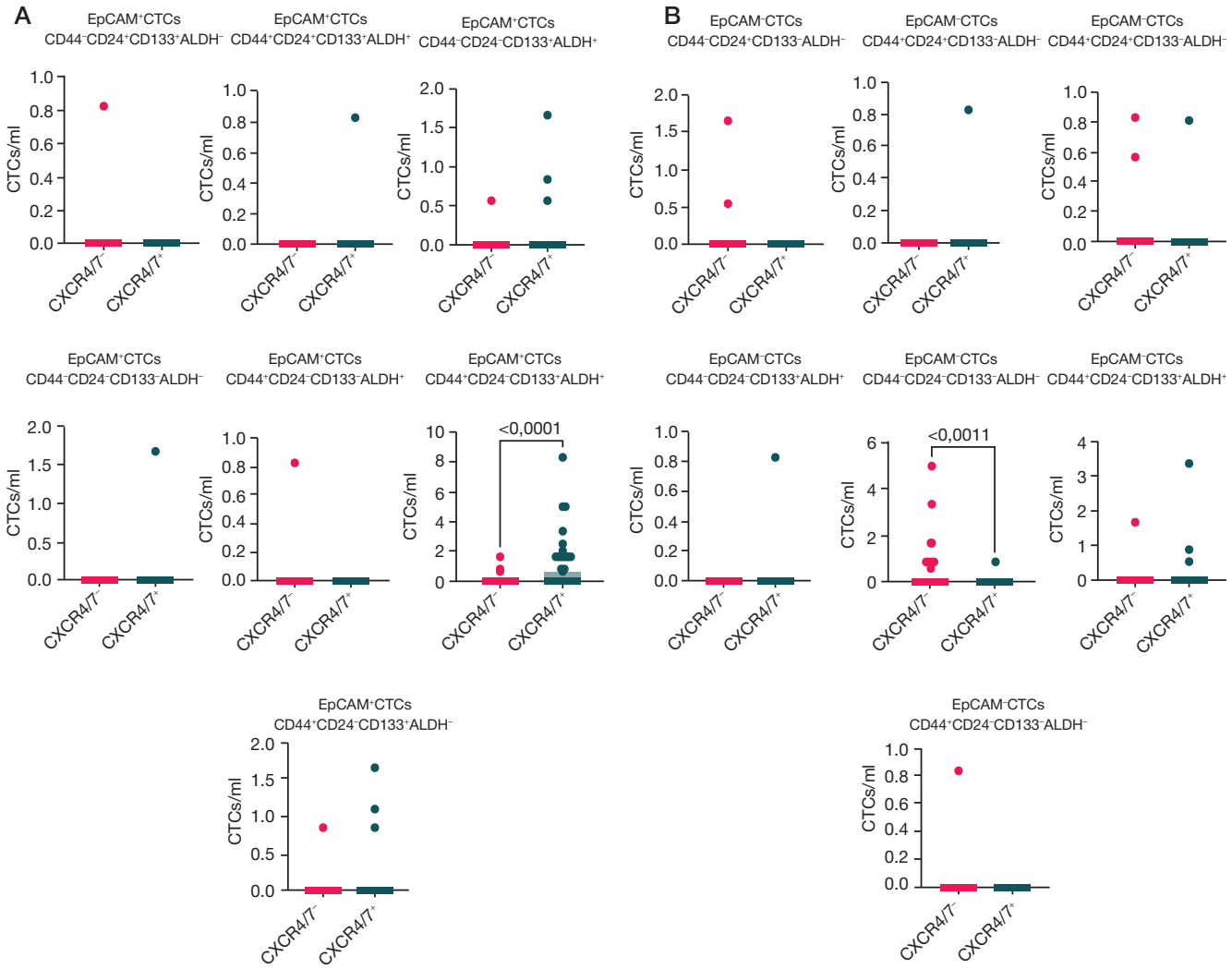


Fig. 4. Comparison of the number of EpCAM⁻ (**A**) and EpCAM⁺ (**B**) CTCs with stemness properties according to CXCR4/7 expression in breast cancer

Differential gene expression analysis among *EPCAM*⁺ cells with and without *CXCR4/7* expression revealed no significant differences ($p > 0.05$). In contrast, comparison within *EPCAM*⁻ CTCs showed significant differences. The most overexpressed genes in *EPCAM*⁻ *CXCR4/7*⁺ CTCs included *POSTN* ($p = 6.63 \times 10^{-13}$), *FN1* ($p = 5.24 \times 10^{-14}$), *COL3A1* ($p = 1.08 \times 10^{-11}$), *VIM* ($p = 2.33 \times 10^{-19}$), *S100A6* ($p = 4.60 \times 10^{-9}$), and *CD74* ($p = 1.11 \times 10^{-7}$). According to the KEGG 2021 Human database, the ribosome metabolism pathway showed the highest enrichment of overexpressed genes ($p = 2.365 \times 10^{-143}$), while the MSigDB Hallmark 2020 database identified the Myc Targets V1 pathway as the most upregulated in *EPCAM*⁻ *CXCR4/7*⁺ cells ($p = 7.59 \times 10^{-11}$) (Supplementary, Fig. 2A).

In the *EPCAM*⁻*CXCR4/7*⁻ CTC population, increased expression of numerous genes was observed, with the most significantly overexpressed being *PF4* ($p = 1.33 \times 10^{-24}$), *PPBP* ($p = 5.40 \times 10^{-23}$), and *TUBB1* ($p = 1.62 \times 10^{-20}$). According to the KEGG 2021 Human database, the largest group of upregulated genes was associated with the ferroptosis pathway ($p = 3.315 \times 10^{-7}$), while the MSigDB Hallmark 2020 database highlighted the androgen receptor signaling pathway as significantly enriched ($p = 8.0 \times 10^{-5}$) (Supplementary, Fig. 2B).

Comparison of the transcriptional profiles between *EPCAM*⁺ and *EPCAM*⁻ CTCs expressing *CXCR4/7* revealed no significant differences ($p > 0.05$).

During the observation period starting in 2020, disease progression was observed in 4 out of 20 patients. Among these, 3 patients developed metastases to distant organs, while one patient exhibited metastasis to regional lymph nodes. The distribution of CTC subpopulations in individual patient samples is summarized in the Supplementary, Table 1.

No significant differences were observed in the frequency and number of *EPCAM*⁺ and *EPCAM*⁻ CTCs expressing *CXCR4/7* chemokine receptor genes between patients with different treatment outcomes over the 6-year follow-up period ($p > 0.05$). Additionally, differential gene expression analysis was performed on *EpCAM*⁻ *CXCR4/7*⁻ cells from patients with and without disease progression during the follow-up. In the group of patients with tumor progression, three genes showed significantly increased expression: *HBB* ($p = 1.34 \times 10^{-5}$), *IGLC2* ($p = 7.49 \times 10^{-6}$), and *IGHM* ($p = 1.05 \times 10^{-5}$). In contrast, among patients without progression, only one gene, *MALAT1*, was significantly overexpressed ($p = 1.52 \times 10^{-2}$).

Spatial transcriptomic analysis of *EPCAM*⁺ and *EPCAM*⁻ tumor cells in relation to *CXCR4* and *CXCR7* gene expression

Manual annotation of spots in five BC samples was conducted to identify those containing tumor cells. Spots exclusively featuring stromal cells or spots where the number of stromal cells surpassed that of tumor cells were excluded from the analysis. Subsequently, employing the Gene Filter tool, all spots were categorized into two groups based on *EPCAM* gene

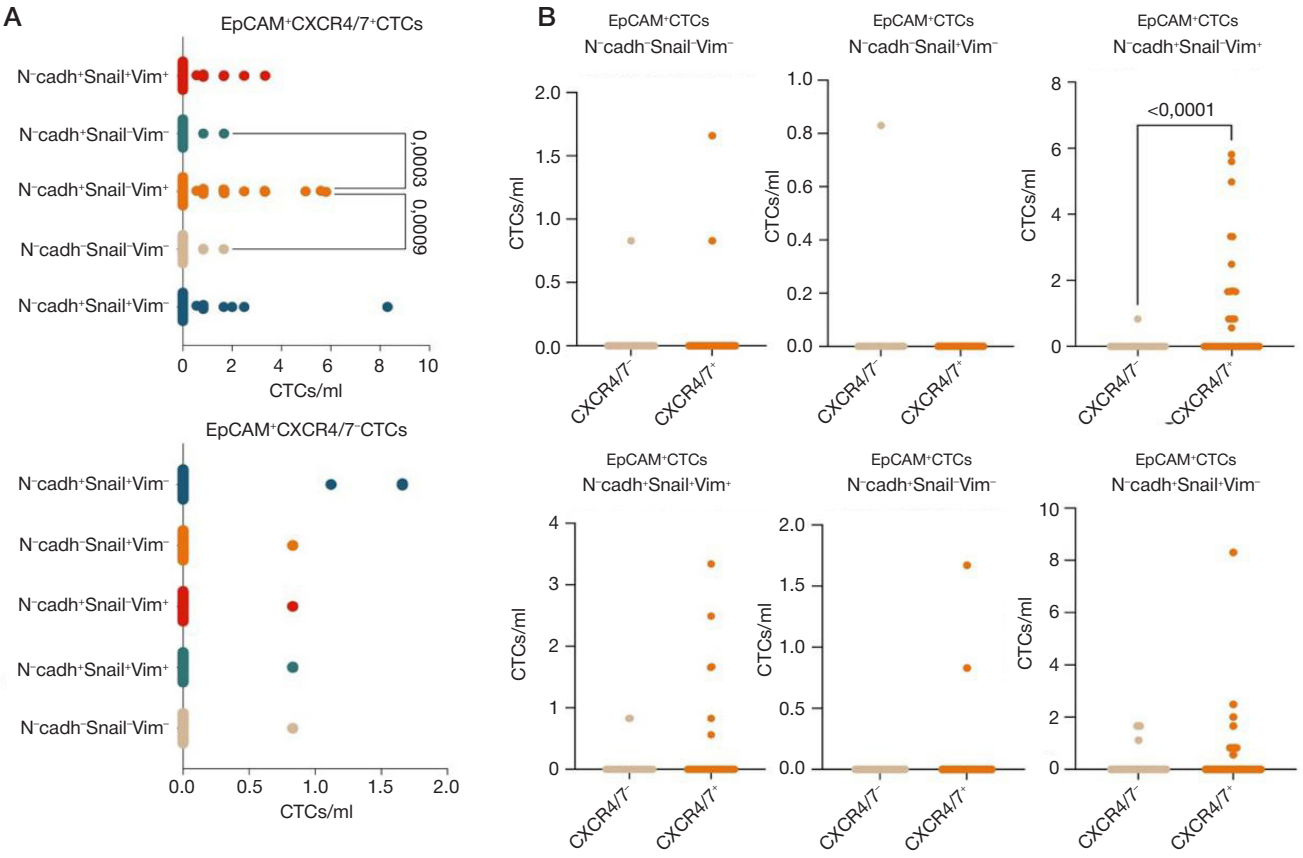


Fig. 5. Number of EpCAM+ CTCs considering CXCR4/7 expression with EMT features in breast cancer patients

expression levels. Spots with *EPCAM* expression ≤ 2 units were designated as *EPCAM*$^-$, spots with *EPCAM* expression ≥ 3 units were classified as *EPCAM*$^+$. Within each group of *EPCAM*$^+$ and *EPCAM*$^-$ spots, the expression of the chemokine receptor genes *CXCR4* and *CXCR7* was assessed, leading to the identification of clusters comprising spots negative for both genes (*CXCR4/7*$^-$) and clusters containing spots expressing at least one of the two genes (*CXCR4/7*$^+$). The transcriptional profiles of *EPCAM*$^+$ spots expressing *CXCR4* and/or *CXCR7* were compared to those lacking *CXCR4/7* expression. *EPCAM*$^+$*CXCR4/7*$^+$ spots exhibited a substantial number of differentially expressed genes, with the top 100 listed in Supplementary, Table 3. Most upregulated genes were associated with estrogen signaling pathways (p = 0.0039) and cell-cell or cell-matrix adhesion processes (p = 0.0039) (Supplementary, Fig. 3A). While, *EPCAM*$^+$*CXCR4/7*$^-$ spots showed activation of endocytosis (p = 0.0359) and an early response to estrogen ($p = 1.435 \times 10^{-7}$) (Supplementary, Fig. 3B). Comparison of *EPCAM*$^-$ spots based on *CXCR4/7* chemokine receptor gene expression revealed significant activation of EMT ($p = 1.6223 \times 10^{-58}$) and protein digestion and absorption pathway ($p = 5.723 \times 10^{-13}$) in *EPCAM*$^-$*CXCR4/7*$^+$ tumor cells (Supplementary, Fig. 4A). (Supplementary, Table 5). Additionally, in *EPCAM*$^-$*CXCR4/7*$^+$ tumor cells, the largest number of overexpressed genes were associated with the early response to estrogen signature ($p = 1.442 \times 10^{-13}$) (Supplementary, Fig. 4B).

We also compared the transcriptional profiles of *EPCAM*$^+$ and *EPCAM*$^-$ tumor cells expressing *CXCR4* and/or *CXCR7*. The analysis revealed activation of the G2-M checkpoint signature in *EPCAM*$^+$ *CXCR4/7*$^+$ tumor cells ($p = 1.086 \times 10^{-8}$) (Supplementary, Fig. 5A).

In contrast, *EPCAM*$^-$*CXCR4/7*$^+$ tumor cells were characterized by activation of the protein digestion and absorption signature ($p = 4.231 \times 10^{-16}$) and EMT ($p = 3.952 \times 10^{-30}$) (Supplementary, Fig. 5B).

DISCUSSION

The findings of this study reveal a profound heterogeneity in CTCs of BC patients, with distinct phenotypic and transcriptional signatures that correlate with clinical outcomes. By integrating flow cytometry and transcriptomic data, we provided a comprehensive view of CTC subpopulations according chemokine receptors CXCR4 and CXCR7 expression and their functional implications.

There are relatively few studies in the literature focusing on chemokine receptor expression in CTCs. Notably, Mego et al. (2016) isolated CTCs from peripheral blood using CD45-negative selection, followed by RT-PCR to evaluate the expression of target genes [19]. The authors identified CTCs expressing epithelial markers (*KRT19*) as well as mesenchymal markers (*TWIST1*, *SNAIL1*, *SLUG*, and *ZEB1*) and further characterized the gene expression of various chemokine receptors within these populations. Their findings demonstrated that epithelial *KRT19*$^+$ CTCs exhibited higher expression levels of the *CXCR4* receptor, and its ligand SDF-1 compared to mesenchymal CTCs. In our study, flow cytometry analysis demonstrated a clear dichotomy in CXCR4/7 expression between different subpopulations of epithelial CTCs. While CXCR4/7-positive cells were predominant among EpCAM$^+$ CTCs, the EpCAM$^-$ population was enriched for CXCR4/7-negative cells. This segregation suggests that these markers define distinct subpopulations of epithelial CTCs with different biological behaviors.

It is important to note that tumor cells expressing CXCR4 are frequently associated with cancer stem cells in the literature [20]. Indeed, CXCR4$^+$ tumor cells exhibit key stem cell characteristics, including a high proliferation rate, resistance to conventional therapies, and enhanced metastatic potential [21]. However, our study did not find a correlation between

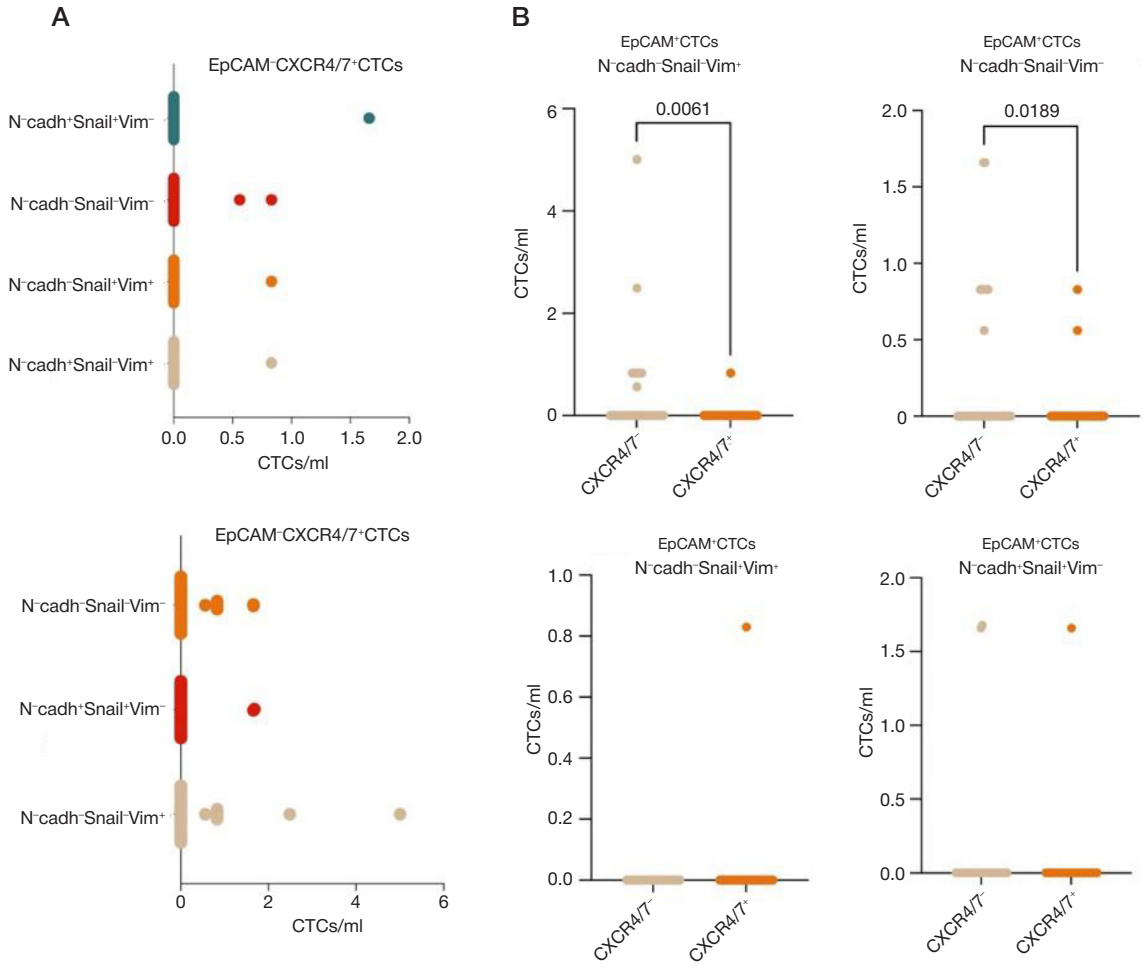


Fig. 6. Number of EpCAM⁺ CTCs considering CXCR4/7 expression with EMT features in breast cancer patients

stemness features and the expression of CXCR4/7 chemokine receptors in either the EpCAM⁺ or EpCAM⁻ CTC populations. However, stem cell features characteristic of the EpCAM⁺ and EpCAM⁻ CTC subpopulations were identified. EpCAM⁺ CTCs were predominantly characterized by a stem cell phenotype defined as CD44⁺CD24⁻CD133⁺ALDH⁺, whereas EpCAM⁻ CTCs largely consisted of cells lacking stemness markers (CD44⁻CD24⁻CD133⁻ALDH⁻).

Analysis of the expression of early (Snail) and late (N-cadherin and vimentin) EMT markers revealed a correlation between N-cadherin and vimentin expression and CXCR4/7 chemokine receptor presence in EpCAM⁻ CTCs. The N-cadherin⁺Snail⁻ vimentin⁺ phenotype was predominantly observed in the EpCAM⁻ CXCR4/7⁺ CTC subpopulation. This finding aligns with existing evidence indicating that activation of the CXCL12/CXCR4 signaling axis can induce EMT in breast cancer cells via stimulation of the Wnt/⁻-catenin and mTOR signaling pathways [22].

Our findings highlight the necessity to move beyond EpCAM-based CTC detection. Thus, the analysis of CXCR4/7 protein expression in CTCs enabled the identification of an association between EpCAM⁻CXCR4/7⁻ CTCs and tumor progression, suggesting the potential prognostic value of this subpopulation. While EpCAM-expressing cells have traditionally been regarded as the primary drivers of metastasis, accumulating evidence highlights the importance of EpCAM⁻ subpopulations [5]. Loss of EpCAM expression is frequently linked to EMT, with the hybrid EMT phenotype — characterized by the concurrent expression of epithelial and mesenchymal markers — being considered the most aggressive and metastatic [23]. Consistent with this, the EpCAM⁻CXCR4/7⁻ CTC population identified in our study exhibited expression of EMT markers such as N-cadherin and Snail. Surprisingly, the EpCAM⁻CXCR4/7⁻ subset — rather than the expected CXCR4/7⁺ population — emerged as the most prognostically significant, indicating that metastatic potential may not solely depend on chemokine receptor-driven dissemination pathways.

The lack of prognostic value in EpCAM⁻CXCR4/7⁺ CTCs (despite statistical significance in Mann–Whitney tests) raises important questions. These cells may represent a transient or dormant state, where CXCR4/7 signaling facilitates survival in circulation but does not directly drive metastatic outgrowth. In contrast, the EpCAM⁻CXCR4/7⁻ subset may harbor more aggressive, immune-evasive clones that bypass conventional detection methods yet drive progression. Clarification of the stem and EMT traits in the detected population of CTCs showed that progression was associated with cells characterized by stemness based on the expression of CD44/CD24, CD133 and ALDH1A1 markers, as well as those with the EMT phenotype — N-cadherin⁺Snail⁺vimentin⁻. The obtained results are consistent with the data of the world literature indicating a high metastatic potential of tumor cells with signs of stemness and EMT [24].

Transcriptomic analysis of CTCs uncovered striking differences between subpopulations. EPCAM⁻CXCR4/7⁺ CTCs exhibited marked overexpression of genes associated with extracellular matrix (ECM) remodeling and stromal activation (POSTN, FN1, COL3A1, VIM, S100A6, CD74), suggesting a role in premetastatic niche formation. In contrast, EPCAM⁻ CXCR4/7⁻ CTCs displayed upregulation of PF4, PPBP, and TUBB1, genes linked to platelet and microtubule dynamics,

potentially indicating alternative mechanisms of dissemination. Notably, in patients with tumor progression, HBB, IGLC2, and IGHM were significantly overexpressed, possibly reflecting immune evasion or clonal selection, whereas MALAT1 was the sole gene elevated in non-progressors, consistent with its known role in tumor suppression. The HBB gene, which encodes beta-globin — a key component of hemoglobin — exhibits a complex and context-dependent role in breast cancer. Although HBB expression is traditionally associated with erythrocytes, it has also been detected in breast cancer cells, where its function appears to be dualistic. Some studies report that elevated HBB expression correlates with increased tumor aggressiveness, enhanced metastatic potential, and poorer patient prognosis [25]. Conversely, other research suggests that HBB may exert tumor-suppressive effects under specific conditions in certain cancer types [26]. Two others differentially expressed genes identified are associated with immunoglobulin synthesis. The IGLC2 gene encodes the constant region of the immunoglobulin lambda light chain (Immunoglobulin lambda constant 2), which is involved in antigen binding. To date, the only available study linking IGLC2 expression to breast cancer indicates its role as a predictor of a favorable clinical outcome in the triple-negative breast cancer subtype [27]. In contrast, no data currently exist regarding the association of IGHM expression, which encodes the constant region of the immunoglobulin M heavy chain, with tumor growth or progression. In the group of patients without signs of progression, only one gene, MALAT1, was found to be overexpressed. MALAT1 is a long non-coding RNA associated with metastasis in lung adenocarcinoma. Its function is linked to the regulation of cell motility and invasive potential [28]. Notably, MALAT1 has also been reported to suppress breast cancer metastasis [29]. Specifically, the study demonstrated that MALAT1 can bind to the pro-metastatic transcription factor TEAD, inactivating it and thereby inhibiting tumor cell migration and invasion. Furthermore, the authors observed that MALAT1 expression is frequently reduced in more aggressive and metastatic breast cancer forms, supporting its role as a metastasis suppressor.

Spatial transcriptomics (Visium 10X) of primary breast tumors further corroborated these findings, revealing that EPCAM$^-$CXCR4/7$^+$ regions were enriched for ECM-related genes (COL1A1, COL3A1, FN1, POSTN, SPARC, BGN), indicative of a fibrotic, immune-modulated microenvironment. Conversely, EPCAM$^-$CXCR4/7$^-$ regions overexpressed a wide range of genes, among which STC2, TFF3, NPNT, and CD24 were the most functionally significant in our opinion, suggesting features associated with an aggressive phenotype. Despite the controversial association with the prognosis, recent data show, that secreted STC2 functions as a ligand in an autocrine/paracrine manner to promote cell survival by alleviating oxidative stress [30]. Cancer tissue expression of Trefoil factor 3 (TFF3) are identified as prognostic indicators of dormant ER$^+$ BC with TFF3 functioning as an epigenetically regulated driver of dormancy-associated behaviors [31]. The experiment demonstrated that knockdown of NPNT reduced the adhesion of cancer cells to osteoblasts, confirming its role in bone metastasis in breast cancer [32]. Several genes in the EpCAM$^-$CXCR4/7$^-$ regions (CDH1, CRABP2, THSD4, SERPINA1, SERPINA3, HSPB1, KRT8, CD9, NUPR1, AZGP1) have been associated with suppression of migration and invasion. However, considering the existence of intravasation mechanisms that do not require invasion, and in light of the data above, this may indicate a functional metastatic phenotype characteristic of this population. Probably, this phenotype is capable of withstanding the effects of an aggressive environment while remaining dormant, with the ability to adapt within a premetastatic niche.

These results challenge the conventional view of CTC biology, as the EpCAM$^-$ subset emerged as a key predictor of progression. Notably, EpCAM$^-$CXCR4/7$^+$ CTCs exhibit mesenchymal and extracellular matrix remodeling characteristics, whereas the CXCR4/7$^-$ subset may harbor more aggressive clones. Further functional studies are required to elucidate the mechanistic roles of these CTC subsets in metastasis and therapy resistance.

Despite the significant findings, this study has several important limitations. The primary objective was to characterize CTCs based on chemokine receptor CXCR4 and CXCR7 expression and their role in receptor-driven dissemination pathways. However, the prospective study design limited patient recruitment, resulting in only three cases with disease progression. While this small sample size precludes definitive conclusions, the results provide a valuable foundation for future research aimed at identifying pathogenetically relevant CTC subpopulations. Notably, our reanalysis of single-cell transcriptomic data confirmed the functional profiles of CTCs associated with progression. Further support comes from spatial transcriptomics data, which revealed CXCR4/7-associated heterogeneity within the primary tumor, consistent with our CTC findings and underscoring their biological relevance. It is important to emphasize that this observational study identifies associations between CTC phenotypes and clinical outcomes that require mechanistic validation *in vitro* and *in vivo*. Additionally, spatial transcriptomics, while informative about the tumor microenvironment, has limited resolution (~55 μm), potentially resulting in signal averaging across different cell types.

However, these limitations do not diminish the significance of the findings and instead highlight the need for further studies with larger cohorts, employing single-cell analysis and functional experiments to validate the identified patterns. The current data provide a solid foundation for expanded investigations into the role of CXCR4/7-expressing CTCs in disease progression.

CONCLUSIONS

Taking into account the limitations of this study, particularly the small sample size including patients with tumor progression in follow-up period, several conclusions can be drawn. Tumor progression, characterized by tumor cell dissemination to distant organs, may not be directly associated with the presence of CXCR4 and CXCR7 receptors on CTCs. At the same time, the EpCAM$^-$ CTC population appears to be pathogenetically significant for tumor progression. The number of EpCAM$^-$ CTCs, irrespective of CXCR4 and CXCR7 expression, was higher in patients exhibiting progression during the follow-up period. This finding underscores the need to shift the focus of CTC research from EpCAM$^+$ CTCs — which have shown limited prognostic value in early breast cancer over more than two decades — to the EpCAM$^-$ subpopulation. Transcriptomic analysis of EPCAM$^-$CXCR4/7$^-$ CTCs revealed distinct gene expression profiles; however, their precise role in breast cancer progression remains inadequately understood. Considering both quantitative and qualitative alterations in these cells, it is plausible that patients with poor prognosis are characterized not only by an increased number of EPCAM$^-$CXCR4/7$^-$CTCs but also by changes in their functional properties.

Data availability

The datasets analyzed in this study are available in the Gene Expression Omnibus (GEO) Database under the accession number GSE242311 and in the BioProject under the accession number PRJNA776403.

References

1. Thomas-Bonafos T, Pierga JY, Bidard FC, Cabel L, Kiavue N, et al. Circulating tumor cells in breast cancer: clinical validity and utility. NPJ Breast Cancer. 2024; 10: 103.
2. Ju S, Chen C, Zhang J, Xu L, Zhang X, Li Z, Chen Y, Zhou J, Ji F, Wang L, et al. Detection of circulating tumor cells: opportunities and challenges. Biomark Res. 2022; 10: 58.
3. Eslami-S Z, Cortés-Hernández LE, Alix-Panabières C. Epithelial Cell Adhesion Molecule: An Anchor to Isolate Clinically Relevant Circulating Tumor Cells. Cells. 2020; 9: 1836.
4. Riethdorf S, Fritsche H, Müller V, Rau T, Schindlbeck C, Rack B, Janni W, Coith C, Beck K, Jänicke F, et al. Detection of circulating tumor cells in peripheral blood of patients with metastatic breast cancer: A validation study of the CellSearch system. Clin Cancer Res. 2007; 13: 920–28.
5. Ye F, Zhong X, Qiu Y, Yang L, Wei B, Zhang Z, Bu H. The presence of EpCAM^{-}/CD49f^{+} cells in breast cancer is associated with a poor clinical outcome. J Breast Cancer. 2015; 18: 242–8.
6. Nieto MA, Huang RY, Jackson RA, Thiery JP. Cell. 2016; 166: 21–45.
7. Aiello NM, Kang Y. Context-dependent EMT programs in cancer metastasis. J Exp Med. 2019; 216: 1016–26.
8. Rueda A, Serna N, Mangues R, Vázquez E, Villaverde A. Targeting the chemokine receptor CXCR4 for cancer therapies. Biomark Res. 2025; 13: 68.
9. Chatterjee S, Behnam Azad B, Nimmagadda S. The intricate role of CXCR4 in cancer. Adv Cancer Res. 2014; 124: 31–82.
10. Boldajipour B, Mahabaleshwar H, Kardash E, Reichman-Fried M, Blaser H, Minina S, et al. Control of chemokine-guided cell migration by ligand sequestration. Cell. 2008; 132: 463–73.
11. Yang Y, Li J, Lei W. CXCL12-CXCR4/CXCR7 Axis in Cancer: from Mechanisms to Clinical Applications. Int J Biol Sci. 2023; 19: 3341–59.
12. Wu C, Zhao H, Chen H, Yao Q. CXCR4 in breast cancer: oncogenic role and therapeutic targeting. Drug Des Devel Ther. 2015; 9: 4953–64.
13. Pospelova RA. Leukocyte concentration in clinical practice: diagnostic value. M.: Meditsina, 1973.
14. Menyailo M, Zainullina V, Khozyainova A, Tashireva L, Zolotareva S, Gerashchenko T, et al. Heterogeneity of Circulating Epithelial Cells in Breast Cancer at Single-Cell Resolution: Identifying Tumor and Hybrid Cells. Adv Biol (Weinh). 2023; 7: e2200206.
15. Satija Lab. Seurat: Tools for Single Cell Genomics. GitHub. 2023. Available from: https://github.com/satijalab/seurat.
16. McGinnis CS. DoubletFinder: Doublet Detection in Single-Cell RNA Sequencing Data. GitHub. 2023. Available from: https://github.com/chris-mcginnis-ucsf/DoubletFinder.
17. Tashireva L, Grigoryeva E, Alifanov V, et al. Spatial Heterogeneity of Integrins and Their Ligands in Primary Breast Tumors. Discov Med. 2023; 35: 910–20.
18. Hafemeister C, Satija R. Normalization and variance stabilization of single-cell RNA-seq data using regularized negative binomial regression. Genome Biol. 2019; 20: 296.
19. Mego M, Cholujova D, Minarik G, Sedlackova T, Gronesova P, Karaba M, et al. CXCR4-SDF-1 interaction potentially mediates trafficking of circulating tumor cells in primary breast cancer. BMC Cancer. 2016; 16: 127T.
20. Shi Q, Yang W, Ouyang Y, Zhou S, Xu L, Liu J, et al. CXCR4 promotes tumor stemness maintenance and CDK4/6 inhibitors resistance in ER-positive breast cancer. Breast Cancer Res. 2025; 27: 15.
21. Nengroo MA, Maheshwari S, Singh A, Verma A, Arya RK, Chaturvedi P, et al. CXCR4 intracellular protein promotes drug resistance and tumorigenic potential by inversely regulating the expression of Death Receptor 5. Cell Death Dis. 2021; 12: 464.
22. Garg P, Jallepalli VR, Verma S. Unravelling the CXCL12/CXCR4 Axis in breast cancer: Insights into metastasis, microenvironment interactions, and therapeutic opportunities. Hum Gene. 2024; 40: 201272.
23. Jolly MK, Mani SA, Levine H. Hybrid epithelial/mesenchymal phenotype(s): The 'fittest' for metastasis? Biochim Biophys Acta Rev Cancer. 2018; 1870: 151–7.
24. Fabregat I, Malfettone A, Soukupova J. New Insights into the Crossroads between EMT and Stemness in the Context of Cancer. J Clin Med. 2016; 5: 37.
25. Ponzetti M, Capulli M, Angelucci A, Delle Monache S, Sica AR, Festuccia C, et al. Non-conventional role of haemoglobin beta in breast malignancy. Br J Cancer. 2017; 117: 994–1006.
26. Zhang X, Yang H, Zhang L, Li Y, Ma H. A Pan-Cancer Analysis of the Hemoglobin Subunit Beta (HBB) in Human Tumors. Front Genet. 2022; 13: 880647.
27. Chang YT, Tsai WC, Lin WZ, Chen YS, Hou MF, Wu YC, et al. A Novel IGLC2 Gene Linked With Prognosis of Triple-Negative Breast Cancer. Front Oncol. 2022; 11: 759952.
28. Tsyganov MM, Ibragimova MK. MALAT1 Long Non-coding RNA and Its Role in Breast Carcinogenesis. Acta Naturae. 2023; 15: 32–41.
29. Kim J, Piao HL, Kim BJ, Yao F, Han Z, Wang Y, et al. Long noncoding RNA MALAT1 suppresses breast cancer metastasis. Nat Genet. 2018; 50: 1705–15.
30. Qie S, Xiong H, Liu Y, et al. Stanniocalcin 2 governs cancer cell adaptation to nutrient insufficiency through alleviation of oxidative stress. Cell Death Dis. 2024; 15: 567. https://doi.org/10.1038/s41419-024-06961-7.
31. Chen S, Zhang X, Basappa B, et al. TFF3 facilitates dormancy of anti-estrogen treated ER+ mammary carcinoma. Commun Med. 2025; 5: 45. https://doi.org/10.1038/s43856-024-00710-9.
32. Wang D, Zhao C, Gao L, Wang Y, Gao X, Tang L, et al. NPNT promotes early-stage bone metastases in breast cancer by regulation of the osteogenic niche. J Bone Oncol. 2018; 13: 91–96. DOI: 10.1016/j.jbo.2018.09.006.

Литература

1. Thomas-Bonafos T, Pierga JY, Bidard FC, Cabel L, Kiavue N, et al. Circulating tumor cells in breast cancer: clinical validity and utility. NPJ Breast Cancer. 2024; 10: 103.
2. Ju S, Chen C, Zhang J, Xu L, Zhang X, Li Z, Chen Y, Zhou J, Ji F, Wang L, et al. Detection of circulating tumor cells: opportunities and challenges. Biomark Res. 2022; 10: 58.
3. Eslami-S Z, Cortés-Hernández LE, Alix-Panabières C. Epithelial Cell Adhesion Molecule: An Anchor to Isolate Clinically Relevant Circulating Tumor Cells. Cells. 2020; 9: 1836.
4. Riethdorf S, Fritsche H, Müller V, Rau T, Schindlbeck C, Rack B, Janni W, Coith C, Beck K, Jänicke F, et al. Detection of circulating tumor cells in peripheral blood of patients with metastatic breast cancer: A validation study of the CellSearch system. Clin Cancer Res. 2007; 13: 920–28.
5. Ye F, Zhong X, Qiu Y, Yang L, Wei B, Zhang Z, Bu H. The presence of EpCAM^{-}/CD49f^{+} cells in breast cancer is associated with a poor clinical outcome. J Breast Cancer. 2015; 18: 242–8.
6. Nieto MA, Huang RY, Jackson RA, Thiery JP. Cell. 2016; 166: 21–45.
7. Aiello NM, Kang Y. Context-dependent EMT programs in cancer metastasis. J Exp Med. 2019; 216: 1016–26.
8. Rueda A, Serna N, Mangues R, Vázquez E, Villaverde A. Targeting the chemokine receptor CXCR4 for cancer therapies. Biomark Res. 2025; 13: 68.
9. Chatterjee S, Behnam Azad B, Nimmagadda S. The intricate role of CXCR4 in cancer. Adv Cancer Res. 2014; 124: 31–82.
10. Boldajipour B, Mahabaleshwar H, Kardash E, Reichman-Fried M, Blaser H, Minina S, et al. Control of chemokine-guided cell migration by ligand sequestration. Cell. 2008; 132: 463–73.
11. Yang Y, Li J, Lei W. CXCL12-CXCR4/CXCR7 Axis in Cancer: from Mechanisms to Clinical Applications. Int J Biol Sci. 2023; 19: 3341–59.
12. Wu C, Zhao H, Chen H, Yao Q. CXCR4 in breast cancer: oncogenic role and therapeutic targeting. Drug Des Devel Ther. 2015; 9: 4953–64.

13. Pospelova RA. Leukocyte concentration in clinical practice: diagnostic value. M.: Meditsina, 1973.
14. Menyailo M, Zainullina V, Khozyainova A, Tashireva L, Zolotareva S, Gerashchenko T, et al. Heterogeneity of Circulating Epithelial Cells in Breast Cancer at Single-Cell Resolution: Identifying Tumor and Hybrid Cells. Adv Biol (Weinh). 2023; 7: e2200206.
15. Satija Lab. Seurat: Tools for Single Cell Genomics. GitHub. 2023. Available from: https://github.com/satijalab/seurat.
16. McGinnis CS. DoubletFinder: Doublet Detection in Single-Cell RNA Sequencing Data. GitHub. 2023. Available from: https://github.com/chris-mcginnis-ucsf/DoubletFinder.
17. Tashireva L, Grigoryeva E, Alifanov V, et al. Spatial Heterogeneity of Integrins and Their Ligands in Primary Breast Tumors. Discov Med. 2023; 35: 910–20.
18. Hafemeister C, Satija R. Normalization and variance stabilization of single-cell RNA-seq data using regularized negative binomial regression. Genome Biol. 2019; 20: 296.
19. Mego M, Cholujova D, Minarik G, Sedlackova T, Gronesova P, Karaba M, et al. CXCR4-SDF-1 interaction potentially mediates trafficking of circulating tumor cells in primary breast cancer. BMC Cancer. 2016; 16: 127T.
20. Shi Q, Yang W, Ouyang Y, Zhou S, Xu L, Liu J, et al. CXCR4 promotes tumor stemness maintenance and CDK4/6 inhibitors resistance in ER-positive breast cancer. Breast Cancer Res. 2025; 27: 15.
21. Nengroo MA, Maheshwari S, Singh A, Verma A, Arya RK, Chaturvedi P, et al. CXCR4 intracellular protein promotes drug resistance and tumorigenic potential by inversely regulating the expression of Death Receptor 5. Cell Death Dis. 2021; 12: 464.
22. Garg P, Jallepalli VR, Verma S. Unravelling the CXCL12/CXCR4 Axis in breast cancer: Insights into metastasis, microenvironment interactions, and therapeutic opportunities. Hum Gene. 2024; 40: 201272.
23. Jolly MK, Mani SA, Levine H. Hybrid epithelial/mesenchymal phenotype(s): The 'fittest' for metastasis? Biochim Biophys Acta Rev Cancer. 2018; 1870: 151–7.
24. Fabregat I, Malfettone A, Soukupova J. New Insights into the Crossroads between EMT and Stemness in the Context of Cancer. J Clin Med. 2016; 5: 37.
25. Ponzetti M, Capulli M, Angelucci A, Delle Monache S, Sica AR, Festuccia C, et al. Non-conventional role of haemoglobin beta in breast malignancy. Br J Cancer. 2017; 117: 994–1006.
26. Zhang X, Yang H, Zhang L, Li Y, Ma H. A Pan-Cancer Analysis of the Hemoglobin Subunit Beta (HBB) in Human Tumors. Front Genet. 2022; 13: 880647.
27. Chang YT, Tsai WC, Lin WZ, Chen YS, Hou MF, Wu YC, et al. A Novel IGLC2 Gene Linked With Prognosis of Triple-Negative Breast Cancer. Front Oncol. 2022; 11: 759952.
28. Tsyganov MM, Ibragimova MK. MALAT1 Long Non-coding RNA and Its Role in Breast Carcinogenesis. Acta Naturae. 2023; 15: 32–41.
29. Kim J, Piao HL, Kim BJ, Yao F, Han Z, Wang Y, et al. Long noncoding RNA MALAT1 suppresses breast cancer metastasis. Nat Genet. 2018; 50: 1705–15.
30. Qie S, Xiong H, Liu Y, et al. Stanniocalcin 2 governs cancer cell adaptation to nutrient insufficiency through alleviation of oxidative stress. Cell Death Dis. 2024; 15: 567. https://doi.org/10.1038/s41419-024-06961-7.
31. Chen S, Zhang X, Basappa B, et al. TFF3 facilitates dormancy of anti-estrogen treated ER+ mammary carcinoma. Commun Med. 2025; 5: 45. https://doi.org/10.1038/s43856-024-00710-9.
32. Wang D, Zhao C, Gao L, Wang Y, Gao X, Tang L, et al. NPNT promotes early-stage bone metastases in breast cancer by regulation of the osteogenic niche. J Bone Oncol. 2018; 13: 91–96. DOI: 10.1016/j.jbo.2018.09.006.

GENETIC PORTRAITS OF VOLGA–OKA REGION IN THE CONTEXT OF THE CENTRAL RUSSIA'S GENE POOL (Y-SNP POLYMORPHISM)

Ponomarev GYu[1]✉, Shlykov AG[1], Gorin IO[1], Voronina MM[1], Potanina AYu[1], Petrov VA[1], Koshel SM[2], Adamov DS[1], Balanovska EV[1]

[1] Research Centre for Medical Genetics, Moscow, Russia
[2] Lomonosov Moscow State University, Moscow, Russia

An urgent problem of the role of Slavic expansion in shaping gene pools of the population of Europe is being analyzed actively using various methods to study ancient and current populations. However, it is difficult to solve due to the lack of consolidated data on the Y-haplogroups in Slavic-, Finnish-, and Turkic-speaking populations of European Russia. The study aimed to look into genetic portraits of Mordovian populations and Russians of the Ryazan Region relative to the surrounding populations of indigenous peoples of Central Russia. For the first time the Y-gene pool of the Volga–Oka region (10 populations, *n* = 1136 individuals) was assessed in a broad context of our own data on the gene pools of European Russia (based on a single panel of 35 Y-haplogroups, 80 populations, *n* = 9712). The analysis was performed by multidimensional scaling (MDS) and computed cartography (GeneGeo). The produced series of 35 maps of the Y-gene pool of Central Russia and maps of genetic distances from peoples of the Volga–Oka region describe the gene-geographic landscape of the region in detail. It has been shown that all the assessed Russian populations belong to the common "Slavic" cluster that also includes representatives of Western Slavs. The cluster of populations of the Ural–Volga region including three Finnish-speaking populations of Mordovia (Erzya, Moksha, Shoksha) and 7 Turkic-speaking populations of the Chuvash and Mishar turned out to be the most genetically close to the Russian populations of Central Russia. It has been hypothesized that this group of populations can be traced back to the gene pool of the ancient indigenous Finnish-speaking population of the Volga–Oka region.

Keywords: gene pool, gene geography, Y-chromosome, haplogroups, Slavic expansion, Central Russia, Volga–Oka region

Funding: the study was supported by the RSF grant No. 25-28-01594.

Acknowledgements: the authors would like to thank all participants of the expedition survey, who provided their biological samples for the study, to Administration and employees of the Ministry of Healthcare of the Ryazan Region and Republic of Mordovia for institutional support and assistance in conducting expeditions, as well as to Biobank of North Eurasia for access to DNA collections.

Author contribution: Ponomarev GYu — genotyping and Y-SNP marker analysis, study design; Shlykov AG — manager of the expedition survey of the gene pool of the Ryazan Region and Mordovia; Ponomarev GYu, Voronina MM, Petrov VA — expedition members, questionnaire survey data analysis; Adamov DS, Potanina AYu, Gorin IO — statistical analysis; Koshel SM — cartographic analysis; Adamov DS, Balanovska EV — study design and manuscript writing.

Compliance with ethical standards: the study was approved by the Ethics Committee of the Research Centre for Medical Genetics (protocol No. 1 dated 29 June 2020). The data were acquired after obtaining the written informed consent from the assessed individuals and anonymised.

✉ **Correspondence should be addressed:** Georgy Yu. Ponomarev
Moskvorechye, 1, 115522, Moscow, Russia; st26i900@gmail.com

Received: 16.10.2025 **Accepted:** 22.11.2025 **Published online:** 01.12.2025

DOI: 10.24075/brsmu.2025.062

Copyright: © 2025 by the authors. **Licensee:** Pirogov University. This article is an open access article distributed under the terms and conditions of the Creative Commons Attribution (CC BY) license (https://creativecommons.org/licenses/by/4.0/).

ГЕНЕТИЧЕСКИЕ ПОРТРЕТЫ ВОЛГО-ОКСКОГО РЕГИОНА В КОНТЕКСТЕ ГЕНОФОНДА ЦЕНТРАЛЬНОЙ РОССИИ (Y-SNP ПОЛИМОРФИЗМ)

Г. Ю. Пономарев[1]✉, А. Г. Шлыков[1], И. О. Горин[1], М. М. Воронина[1], А. Ю. Потанина[1], В. А. Петров[1], С. М. Кошель[2], Д. С. Адамов[1], Е. В. Балановская[1]

[1] Медико-генетический научный центр, Москва, Россия
[2] Московский государственный университет имени М. В. Ломоносова, Москва, Россия

Актуальную проблему роли славянской экспансии в формировании генофондов народонаселения Европы активно анализируют с применением разных методов изучения древних и современных популяций. Но ее решение затрудняет отсутствие сводных данных о гаплогруппах Y-хромосомы в славяно-, финно- и тюркоязычных популяциях европейской части России. Цель работы — рассмотреть генетические портреты популяций Мордовии и русских Рязанской области в сравнении с окружающими популяциями коренного народонаселения Центральной России. Y-генофонд Волго-Окского региона (10 популяций, *n* = 1136 индивидов) изучен в широком контексте собственных данных о генофондах европейской части России (по единой панели 35 Y-гаплогрупп, 80 популяций, *n* = 9712). Анализ проведен методами многомерного шкалирования (MDS) и компьютерной картографии (GeneGeo). Созданная серия 35 карт Y-генофонда Центральной России и карт генетических расстояний от народов Волго-Окского региона детально описывает геногеографический ландшафт региона. Показано, что все изученные русские популяции входят в единый «славянский» кластер, включающий также представителей западных славян. К русским популяциям Центральной России наиболее генетически близким оказался кластер популяций Волго-Уральского региона, включающий три финноязычные популяции Мордовии (эрзя, мокша, шокша) и семь тюркоязычных популяций чувашей и мишарей. Выдвинута гипотеза, что этот массив популяций восходит к генофонду древнего автохтонного финноязычного населения Волго-Окского региона.

Ключевые слова: генофонд, геногеография, Y-хромосома, гаплогруппы, славянская экспансия, Центральная Россия, Волго-Окский регион

Финансирование: исследование выполнено при поддержке гранта РНФ № 25-28-01594.

Благодарности: авторы благодарны всем участникам экспедиционного обследования, предоставившим свои биологические образцы для исследования, администрации и сотрудникам Министерства здравоохранения Рязанской области и Республики Мордовия за организационную поддержку и содействие в проведении экспедиций, а также Биобанку Северной Евразии за предоставление коллекций ДНК.

Вклад авторов: Г. Ю. Пономарев — генотипирование и анализ Y-SNP маркеров, дизайн исследования; А. Г. Шлыков — организатор экспедиционного обследования генофонда Рязанской области и Мордовии; Г. Ю. Пономарев, М. М. Воронина, В. А. Петров — участники экспедиций, анализ анкетных данных; Д. С. Адамов, А. Ю. Потанина, И. О. Горин — статистический анализ; С. М. Кошель — картографический анализ; Д. С. Адамов, Е. В. Балановская — дизайн исследования и подготовка рукописи.

Соблюдение этических стандартов: исследование одобрено этическим комитетом Медико-генетического научного центра имени Н. П. Бочкова (протокол № 1 от 29 июня 2020 г.). Данные получены при добровольном письменном информированном согласии участников обследования и деперсонифицированы.

✉ **Для корреспонденции:** Георгий Юрьевич Пономарев
ул. Москворечье, д. 1, 115522, г. Москва, Россия; st26i900@gmail.com

Статья получена: 16.10.2025 **Статья принята к печати:** 22.11.2025 **Опубликована онлайн:** 01.12.2025

DOI: 10.24075/vrgmu.2025.062

Авторские права: © 2025 принадлежат авторам. **Лицензиат:** РНИМУ им. Н. И. Пирогова. Статья размещена в открытом доступе и распространяется на условиях лицензии Creative Commons Attribution (CC BY) (https://creativecommons.org/licenses/by/4.0/).

In the recent decade, the research focused on the origin of modern Slavic-speaking peoples has risen to a new level due to the studies of modern and ancient DNA. The genetic data on the autosomal DNA, Y-chromosome, mitochondrial DNA provide an opportunity to see various aspects of communication between pre-Slavic and Slavic populations during massive expansion of Slavic tribes in the large territories of Europe in the 6th–12th century A.D. One of the main issues of this communication is the relationship between two processes: population change (complete substitution of the indigenous people's gene pool with the newcomer Slavic tribes) and assimilation of the pre-Slavic population ("slavicisation" — interpenetration of gene pools of Slavic and pre-Slavic populations with the adoption of Slavic culture). With the historical, archaeological, linguistic, and genetic data accumulated to date, a clear answer to the question cannot be given.

Synthesis of data on the autosomal genome, Y-chromosome, and mtDNA of the modern Slavic population has shown that most of the Baltic-Slavic genetic variation is related mainly to assimilation of pre-Slavic gene pools that were different in Western, Eastern and Southern Slavs [1].

In 2025, two important reports were published, the authors of which analyzed communication between the pre-Slavic population and Slavic tribes based on various systems of genetic data of modern populations and ancient DNA. Autosomal genomes of ancient samples (*n* = 555) from burials in the eastern Germany, northwestern Balkans, Poland (and northwestern Ukraine) dating to the period before (6–7th century) and after the Slavic expansion were assessed [2]. In addition to these three major territorial clusters, the data for the Volga–Oka region are also provided. To calculate the extent, to which the indigenous population was substituted, samples from the earliest Slavic inhumations that replaced the cremation ceremony (Powiat Hrubieszowski, Poland, 600–900 A.D.) were used. DNA of these samples was used to calculate ancestral genetic components (qpAdm) as a reference. Based on the calculation results, the authors came to a conclusion about the dominance of the process of intense population substitution in the territories of Slavic expansion: the Slavs substituted 82 ± 1% of the local gene pools in the northwestern Balkans, 83 ± 6% in the eastern Germany, 93 ± 3% in Poland and Ukraine. The values reported for the Volga–Oka region are much lower: 65 ± 4% of the indigenous population was substituted by the newcomer Slavic migrants [2].

The second study performed by our team based on the Y-chromosome data was limited to the Slavic expansion northeastern periphery: the Volga–Oka region [3]. Haplogroup R1a predominates in modern Y gene pools of the population of the Volga–Oka interfluve (*n* = 935): 56% in Russians of the Ryazan Region and 44% in the indigenous population of Mordovia. That is why the authors focused mainly on the comprehensive analysis of the detailed data on the Y-SNP and Y-STR polymorphisms of haplogroups R1a-CTS1211 and R1a-Z92, along with five ancient samples dating to the 6th–12th century A.D. Calculation of the time to the most recent common ancestor (TMRCA) by two independent methods revealed 10 informative clusters in phylogenetic networks of the 37-marker Y-STR haplotypes aged 1600–2900 years, i.e. before the beginning of Slavic expansion. About a half of Russians of the Ryazan Region (carriers of the studied R1a branches) can be male descendants of the pre-Slavic population of the region, presumably the ancient indigenous Finnish-speaking tribes. In contrast to the findings of the previous paper [2], we concluded that the Russian population of the Volga–Oka interfluve was shaped largely through cultural assimilation, not complete substitution of the pre-Slavic population by the Slavs. This important conclusion is supported by the earlier studies conducted by our team that were focused on the Y-chromosome [1, 4–9] and the autosomal gene pool [1, 10].

The conclusions about substitution of about 65% of the gene pool of the pre-Slavic population of the Volga–Oka region [2] are based on the data on the ancient DNA of the Suzdal Opolye (*n* = 31) acquired by another team, which recorded the gene pool changes associated with the spread of the Slavs and was more careful when drawing conclusions about the scope of substitution [11]. These authors report that the medieval Suzdal principality was populated by various ethnic groups that eventually yielded a hybrid, but totally Russian-speaking population inhabiting this region by today.

It is clear that further research is necessary to clarify an important question: what is the relationship between the process of intense substitution of the indigenous population with the Slavs and the process of interpenetration of their gene pools. The question is difficult to answer due to the lack of consolidated data on Y-haplogroups in various Slavic-, Finnish-, and Turkic-speaking populations of European Russia. Such a gap in our knowledge prevents further solution to the problem of the nature of communication between Slavic and pre-Slavic populations in Russia. The study aimed to perform comparative analysis of the major Y-haplogroups in the context of the gene pool of central part of European Russia, which would help fill the gap.

METHODS

The data on the present-day indigenous population of the Volga–Oka region were collected during expedition surveys in 2005–2023 (*n* = 1136 in total): in the Ryazan Region (*n* = 497; Kadomsky, Kasimovsky, Mikhaylovsky, Sapozhkovsky, Sarayevsky, Spassky, Shilovsky districts) and the Republic of Mordovia (*n* = 639; Ardatovsky, Insarsky, Ichalkovsky, Krasnoslobodsky, Lukyanovsky, Ruzayevsky, Tengushevsky, Torbeyevsky, Chamzinsky districts). Inclusion criteria: samples exclusively from unrelated males, whose ethnicity was confirmed at least three generations deep.

DNA was isolated by nucleic acid purification on magnetic particles in the QIAsymphony system (Qiagen; Germany). The Y-SNP marker genotyping was performed by the TaqMan Open Array method in the QuantStudio 12K Flex thermocycler (Thermo Fisher Scientific; USA) using custom plates.

The data on the gene pool of 80 indigenous populations of Central Russia (*n* = 9712) provided by the Biobank of North Eurasia [12] were assessed based on the single panel of 35 haplogroups: C-M217, D-M174, E-M96, G1-M285, G2-P15, G-M201(xM285,P15), H-M69, I-M170(xM253,M223,P37), I-M223, I-M253, I-P37, J1-M267, J2-M172, L-M20, N2-P43, N3a1-B211, N3a2-M2118, N3a3-CTS10760, N3a4-Z1936, N3a5a-F4205, N-M231(xP43,M178), O-M175, Q-M242, R1a-M198(xM458,CTS1211,Z92,Z93), R1a-CTS1211, R1a-M458, R1a-Z92, R1a-Z93, R1b-M343(xM269,M73), R1b-M269 (xL51,Z2105), R1b-L51, R1b-M73, R1b-Z2105, R2-M124, T-M70. These were complemented with the published data on 10 populations of Latvia, Lithuania, Poland, Finland, Sweden, and Estonia [13–15]. Frequencies of 35 Y-haplogroups were used to calculate a pairwise matrix of Nei's genetic distances between 90 populations (DJgenetics [4]); the multidimensional scaling (MDS) plots were created in Statistica version 7.1 (TIBCO Software, USA).

Maps of the Y-haplogroup spread and maps of genetic distances were created in the GeneGeo 2.8 software package

Table. Frequencies of Y-chromosome haplogroups (%) in the indigenous population of the Ryazan Region and Mordovia

Population	Consolidated data on the populations			Russians from 7 districts of the Ryazan Region				Populations of Mordovia		
Y-haplogroups	Volga–Oka region	Russians of the Ryazan Region	Mordovia	Kadomsky	Kasimovsky	Shilovsky	Total for 4 other districts	Erzya	Moksha	Shoksha*
Number of samples	1136	497	639	79	110	91	217	322	252	65
R1a (total)	**50.7**	**57.3**	**45.5**	**58.2**	**63.6**	**58.2**	**53.5**	**55.3**	**33.3**	**44.6**
R1a-CTS1211	31.9	28.4	34.6	20.3	44.5	35.2	20.4	41.6	24.2	40,0
R1a-Z92	9.8	17.3	3.9	17.7	6.4	13.2	24.5	4,0	4.4	1.5
R1a-PF6202 (eq.M458)	4,0	7.2	1.4	5.1	9.1	8.8	6.5	2.5	0.4	–
R1a-Z93	2.9	1.9	3.8	3.8	1.8	–	2,0	6.5	1.2	–
R1a-M198*	2.1	2.5	1.8	11.3	1.8	1,0	0.1	0.7	3.1	3.1
N3 (total)	**14.1**	**11.3**	**16.3**	**11.4**	**16.4**	**5.5**	**11.1**	**13,0**	**13.5**	**43.1**
N3a1-B211	5.7	0.2	10,0	–	–	1.1	–	8.7	8.3	23.1
N3a3-CTS10760 (eq.VL29)	4.7	6.6	3.1	6.3	8.2	4.4	6.9	0.6	4.8	9.2
N3a4-Z1936	3.7	4.4	3.1	5.1	8.2	–	4.1	3.7	0.4	10.8
Haplogroups (xR1a, N3)	**35.2**	**31.4**	**38.2**	**30.4**	**20,0**	**36.3**	**35.5**	**31.7**	**53.2**	**12.3**
E-M78	6.7	4.6	8.3	1.3	0.9	5.5	7.4	2.8	16.7	3.1
J2-M172	6.1	2,0	9.2	–	2.7	1.1	2.8	5.6	15.9	1.5
I1-M253	4.4	4,0	4.7	7.6	0.9	3.3	4.6	8.7	0.8	–
I2-P37.2	4,0	8.5	0.6	8.9	8.2	11,0	7.4	0.9	0.4	–
G2-P15	3.8	1.4	5.6	–	0.9	4.4	0.9	4,0	9.1	–
R1b-L51	3.7	1.8	5.2	2.5	2.7	1.1	1.4	3.4	7.1	6.2
R1b-Z2105	2.2	1.6	2.7	5.1	1.8	2.2	–	5.0	0.4	–
Other	**4.3**	**7.4**	**1.9**	**5.1**	**1.8**	**7.7**	**11.1**	**1.2**	**2.8**	**1.5**

Note: The red background marks the values corresponding to the 5% polymorphism criterion. Haplogroups are presented in the descending order of their frequencies in the gene pool of the Volga–Oka region. * Shoksha — is not a generally accepted term for the population of Erzya of the Tengushevsky district in northwestern Mordovia

[16] by the weighted average interpolation method with an influence radius of 500 km and the weight function decrement 3.

RESULTS

Volga–Oka region gene pool diversity

Among 28 Y-haplogroups found in the gene pool of the studied populations of the Volga–Oka region, the macro-haplogroup R1a predominates, accounting for on average 51% (Table). However, populations of the region show considerable differences in its frequency: minimum 33% in Moksha, maximum 64% in Russians of the Kasimovsky district, Ryazan Region. The majority of other haplogroups vary much more (Fig. 1). Thus, the haplogroup N3 frequency varies between 5.5% in Russians of the Shilovsky district and 43% in Shoksha. The "Other" category (Table) includes haplogroups with the frequencies 5% in all studied populations (C-M217, G1-M285, I2-M223, J1-M267, L-M20, N2-P43, N-M231*, Q-M242, R1a-M198*, R1b-M269*, R1b-M73, R2a-M124, T1a-M70).

In the gene pool of Russians of the Ryazan Region, haplogroups are distributed by descending order of frequency as follows: R1a-CTS1211 (28%), R1a-Z92 (17%), I2a-P37.2 (9%), R1a-M458 (7%). This set of conditionally "Slavic" haplogroups is typical for the Russian populations of central and southern Russia in general [4]. Among the conditionally "Uralic" haplogroups the most common are N3a3 (7%) and N3a4 (4%).

The Erzya gene pool is close to the Russian populations of the Ryazan Region: R1a shows high frequency (55%), and the branch R1a-CTS1211 (44%) is much more common in Erzya, than R1a-Z92 (4%). In the Erzya gene pool, haplogroups R1a-Z93 (6,5%), N3a1 (9%), and I1-M253 (9%) are more frequent, than in Russian populations.

In Shoksha (Tengushevsky Erzya), the macrohaplogroup N3 (43%) predominates, which makes Shoksha dramatically different from Erzya (13%). All three N3 branches in the Shoksha gene pool reach their maximum in the Volga–Oka region: N3a1 (23%), N3a4 (11%), N3a3 (9%). Based on the frequency of R1a-CTS1211 (40%) Shoksha are close to Erzya (44%).

The Moksha gene pool uniqueness is represented not only by the reduced frequency of R1a (33%), but also by the increased frequencies of haplogroups E-M78 (17%), J2-M172 (16%), G2-P15 (9%), R1b-L51 (7%).

Frequencies of Y-haplogroups revealed significant genetic differences between populations of Mordovia, which suggests the need to consider these as separate populations, not allowing us to combine these into a single Mordva group.

Volga–Oka region gene pool position among populations of Central Russia

The fact that the detailed information about gene pools of the indigenous population of European Russia is available for the team allows us to consider the major patterns of the gene pool variation and assess the position of the Volga–Oka region gene pool in it.

Frequencies of 35 Y-haplogroups were used to calculate a pairwise matrix of Nei's genetic distances between 90 populations of Russia and the Baltics, as well as to create a multidimensional scaling (MDS) plot. Populations of Central Russia formed three major clusters in its genetic space (Fig. 2): Slavic, Western Finnish, Ural–Volga.

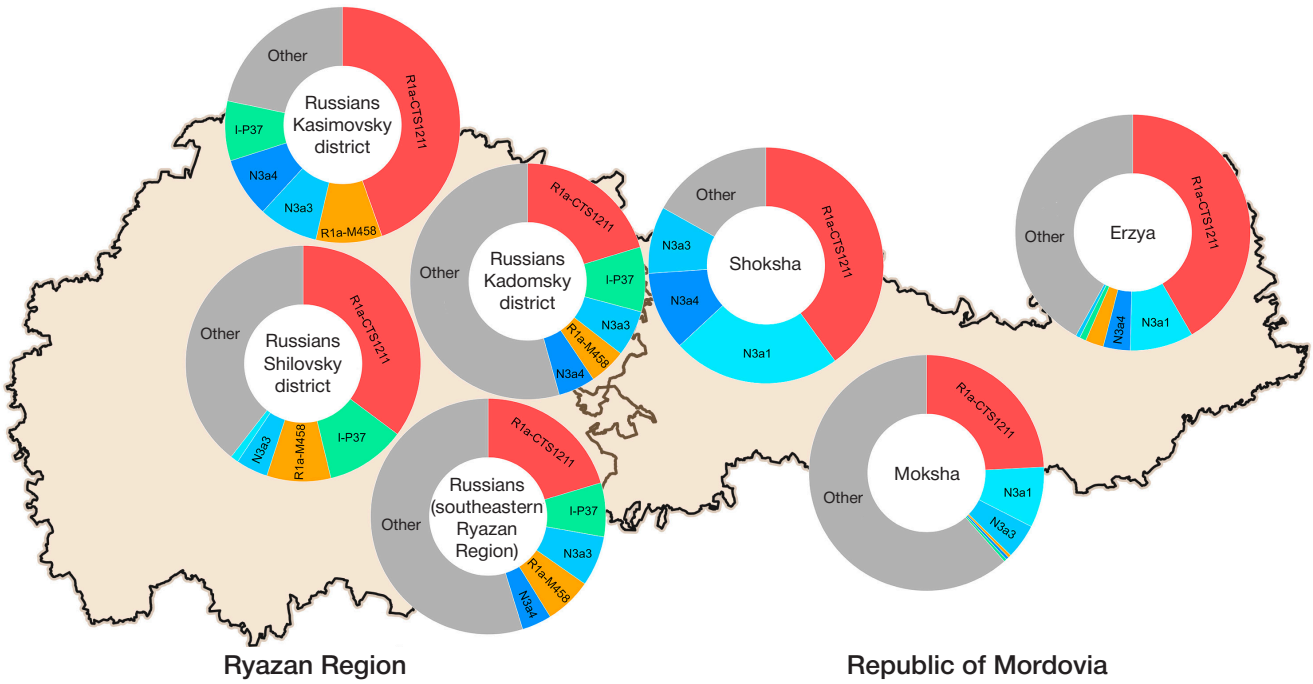


Fig. 1. Genetic portraits of populations of the Volga–Oka region (within the borders of the Ryazan Region and Mordovia). The data on the conditionally "Slavic" haplogroups R1a-CTS1211, R1a-M458, I2a-P37.2 and the conditionally "Uralic haplogroups N3a1, N3a3, N3a4 are provided for all populations; the set of other haplogroups is referred to as "Other"

The Slavic cluster is divided into two subclusters: the first one includes the northernmost population of Central Russia, the second one includes the main bulk of the Central Russia's populations.

The subcluster of Slavs including 17 Russian populations of central and southern Russia turned out to be the most dense and compact in the genetic space. It is significant that Poles, representatives of Western Slavs, are very close to it (n = 598) [14]. This suggests a large geographic range of the populations included in the central Slavic subcluster, as well as considerable similarity of their gene pools. High frequencies of haplogroups R1a-CTS1211,

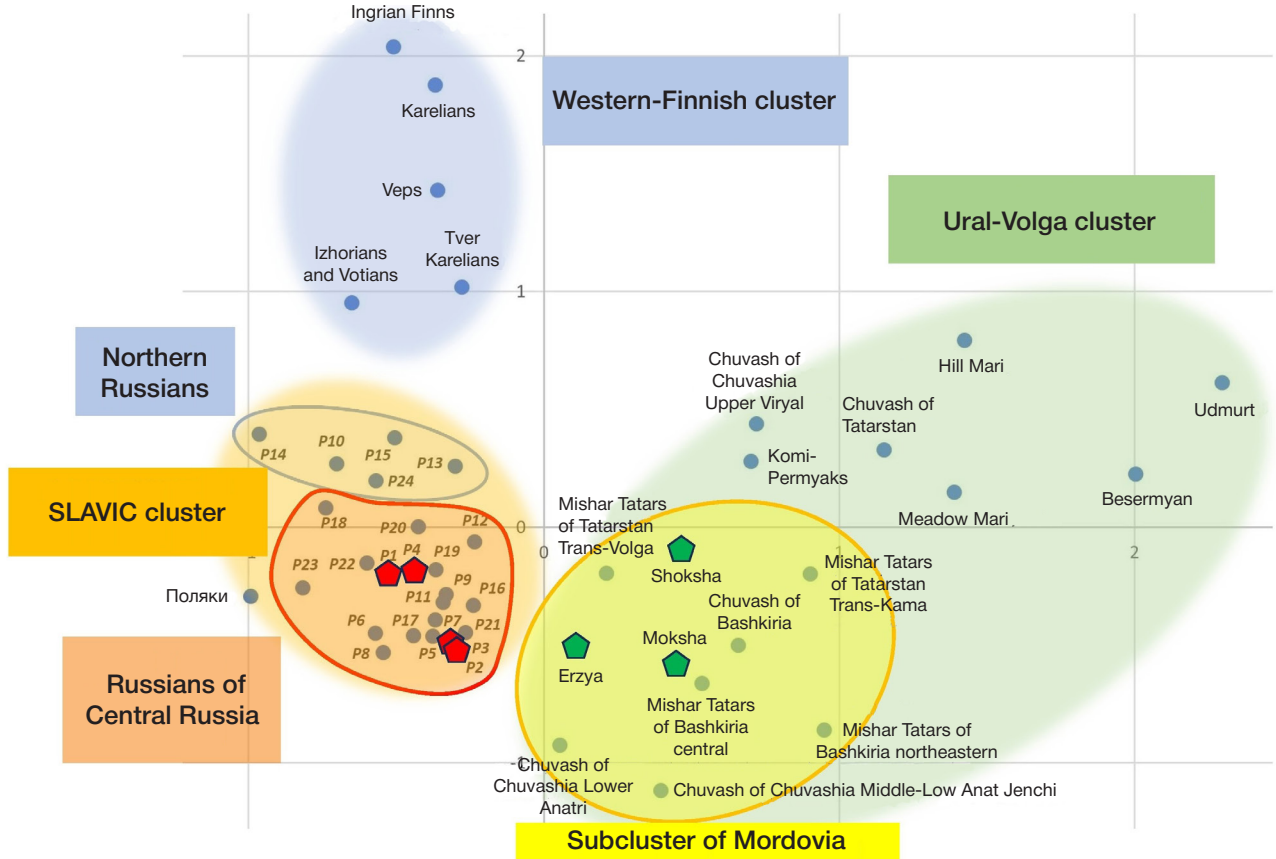


Fig. 2. Position of populations of European Russia in the genetic space based on the pairwise analysis of genetic distances (stress coefficient = 0.16; alienation coefficient = 0.17)

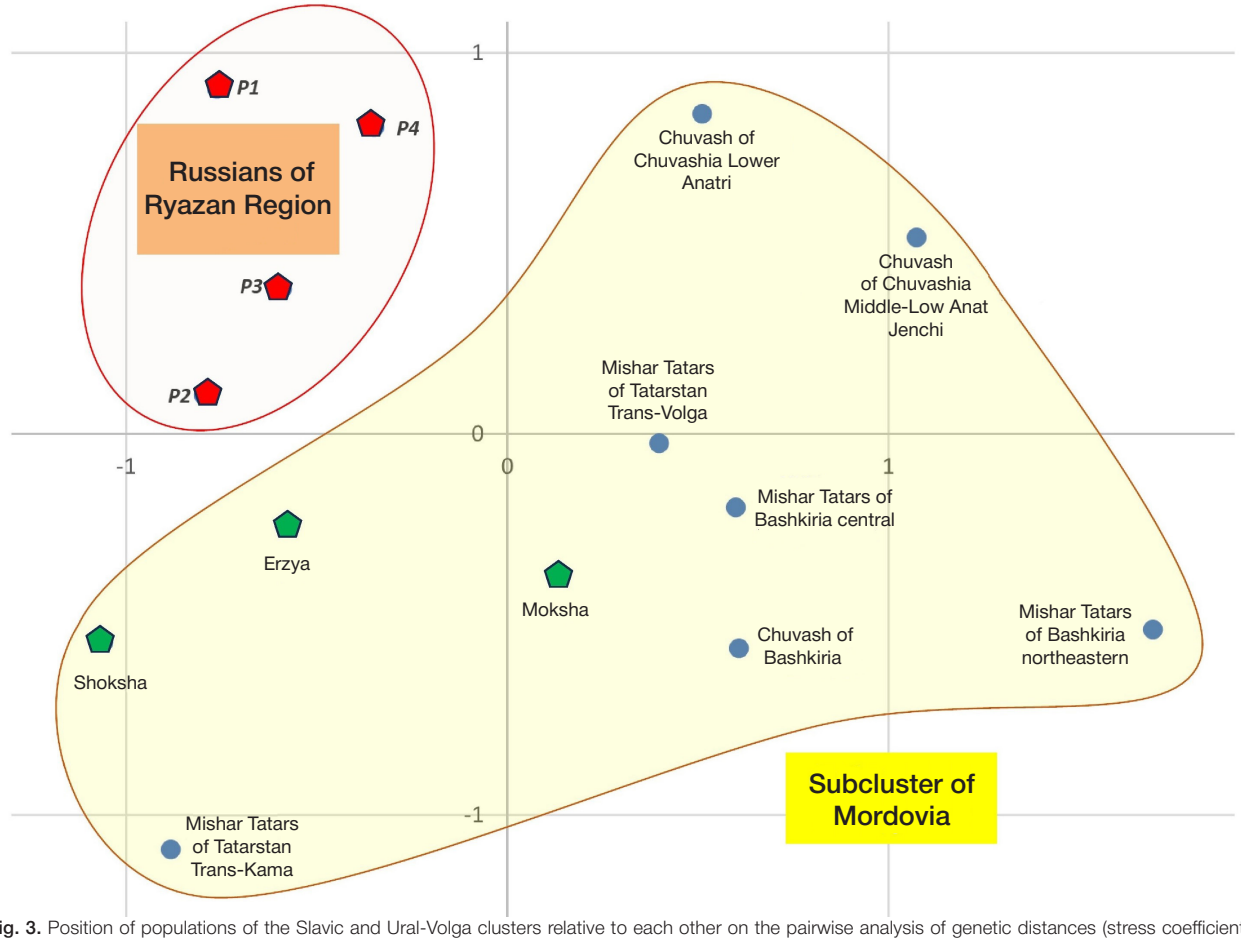


Fig. 3. Position of populations of the Slavic and Ural-Volga clusters relative to each other on the pairwise analysis of genetic distances (stress coefficient = 0.09; alienation coefficient = 0.13)

R1a-Z92, R1a-M458, I2a-P37.2, and N3a3 are the subcluster characteristic features.

The northern cluster of Central Russia's Slavs combined five populations of the Kostroma, Novgorod, and Yaroslavl regions [4, 8, 9]. Uniqueness of its gene pool is manifested by higher frequencies of haplogroups E and R1a-M458 and proximity to the gene pool of Finnish-speaking populations of northwestern Russia due to haplogroups I1-M253, I2a-P37.2, N3a4-Z1936, N2-P43, R1a-CTS1211, R1b-L51.

The Western Finnish cluster included all the studied populations of Finnish-speaking residents of northwestern Russia: Veps, Votians, Izhorians, Karelia`s Karelians, Tver Karelians, Ingrian Finns (the relationship between those and the gene pool of the Russian North was reported in [8, 17]). The cluster gene pool combines increased frequencies of haplogroups of the western (I1-M253, R1b-L51) and Uralic (N3a4, N2) origin.

The Ural–Volga cluster combined Finnish-speaking and Turkic-speaking peoples of the region. Its range in the genetic space is the largest, which suggests considerable differences between gene pools. Positions of populations on the plot do not depend on the linguistic identity, but reflect their location in the geographic space. The gene pools of those combine the "Uralic" haplogroups N3a1, N2 and the conditionally "steppe" ones E, G2-P15, J, R1a-Z93, R1b-M73, R1b-Z2105 in different proportions. It is important to highlight two features of the Volga–Oka populations. First, populations of Mordovia (Erzya, Moksha, Shoksha) are genetically most close to the cluster of Russian populations, which confirms the conclusions of our previous study considering significant pre-Slavic substrate in the gene pool of the central and southern parts of European Russia [3]. Second, the Mishar Tatars and Chuvash are close to the Volga–Oka populations (Fig. 3), which requires special discussion.

Gene-geographic landscape of Y-haplogroups in the indigenous population of Central Russia

The most important objective of the study is the analysis of the gene-geographic landscape of the indigenous peoples of European population providing valuable information about the nature and intensity of communication between the indigenous population and the newcomer Slavic tribes.

Being unable to provide all 35 maps of spatial variation of Y-haplogroup frequencies, we selected six most typical maps (Fig. 4): maps of "Slavic" (R1a-CTS1211, R1a-M458, and I2a-P37.2) and "Uralic" (N3a1, N3a3, N3a4) haplogroups. Both terms are very relative, since the maps themselves demonstrate how big the ranges are. However, the term "Uralic" also suggests both linguistic affiliation to the Uralic-speaking peoples and the geographic range, including the populations of Turkic-speaking peoples of the Ural–Volga region. Borders of the Ryazan Region and Mordovia allowing one to see the position of the Volga–Oka region in the gene-geographic landscape of Central Russia are provided in the maps.

Haplogroup R1a-CTS1211 (Fig. 4A) reaches its maximum frequencies (shades of red) not only in Russians of Central and Southern Russia, but also in Erzya and Moksha of Mordovia [3]. Its average frequencies (shades of yellow) cover all the periphery of the maps, except for minima (shades of green) in Kazakhstan, Udmurtia and Northwestern Finns.

Haplogroup R1a-M458 (Fig. 4B) is typical for the more western portion of the range compared to R1a-CTS1211.

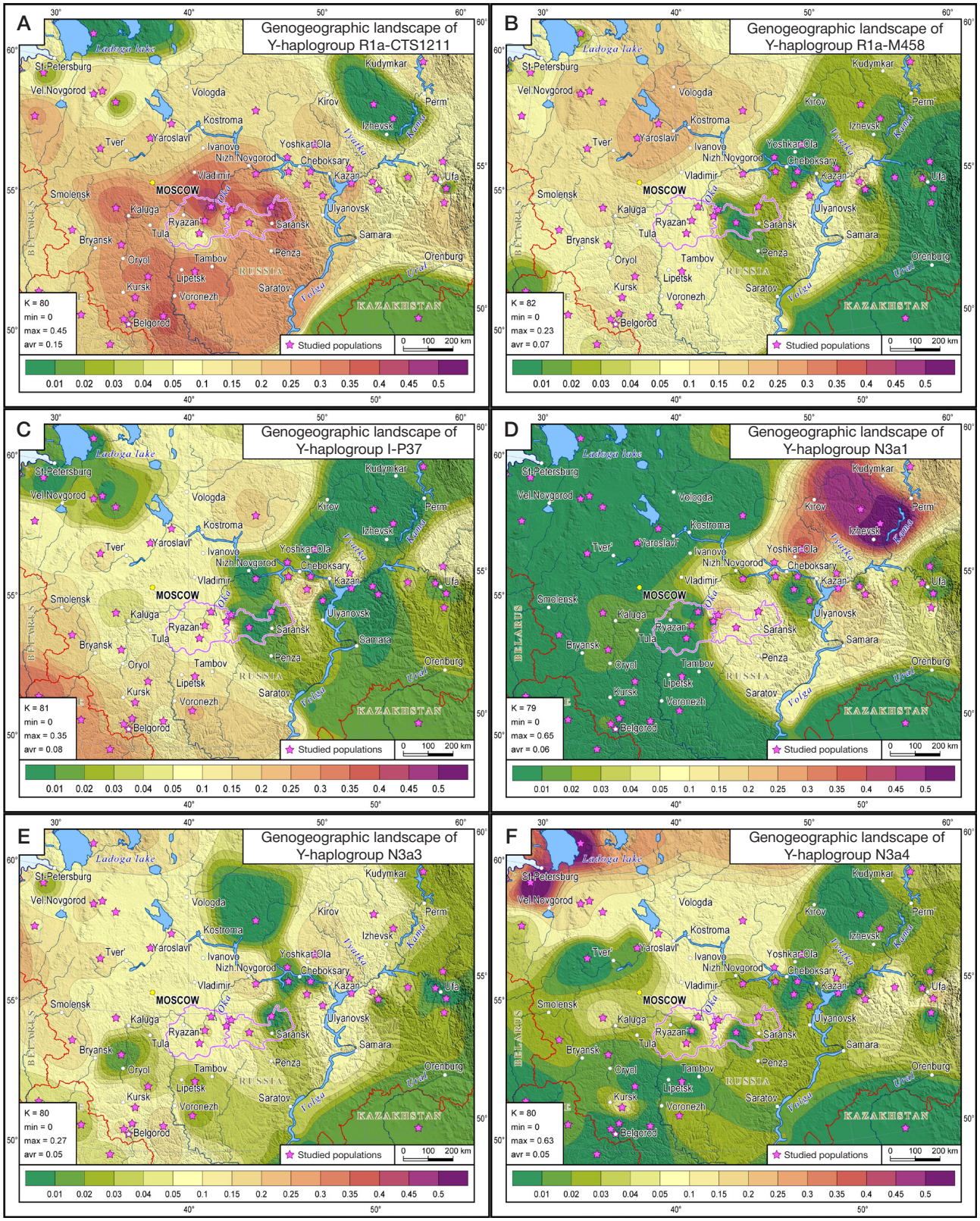


Fig. 4. Geographic distribution and frequencies of the major haplogroups of the indigenous population of European Russia: haplogroup R1a-CTS1211 (**A**); haplogroup R1a-M458 (**B**); haplogroup I-P37 (**C**); haplogroup N3a1 (**D**); haplogroup N3a3 (**E**); haplogroup N3a4 (**F**). Shades of *green* reflect the minimum haplogroup frequency; shades of *yellow* — medium frequencies; *orange* and *red* — maximum frequencies

The maximum frequencies are found in the populations of the northern subcluster of the MDS plot. The low-frequency zone (shades of green) stretches to Mordovia and Mari El.

Haplogroup I2a-P37.2 (Fig. 4C) having the same average gene-geographic landscape frequency ($0.07 \leq q \leq 0.08$), as R1a-M458, is characterized by the larger scale of frequencies, clearer transition boundaries, and the position of maximum frequencies in the southwest of European Russia.

Haplogroup N3a1 (Fig. 4D), as a truly "Uralic" one, is almost an alternative to the previous map of the "Slavic" I2a-P37.2. An absolute maximum (65%) is located in the north-east of Udmurtia, the boundary of average frequencies embraces

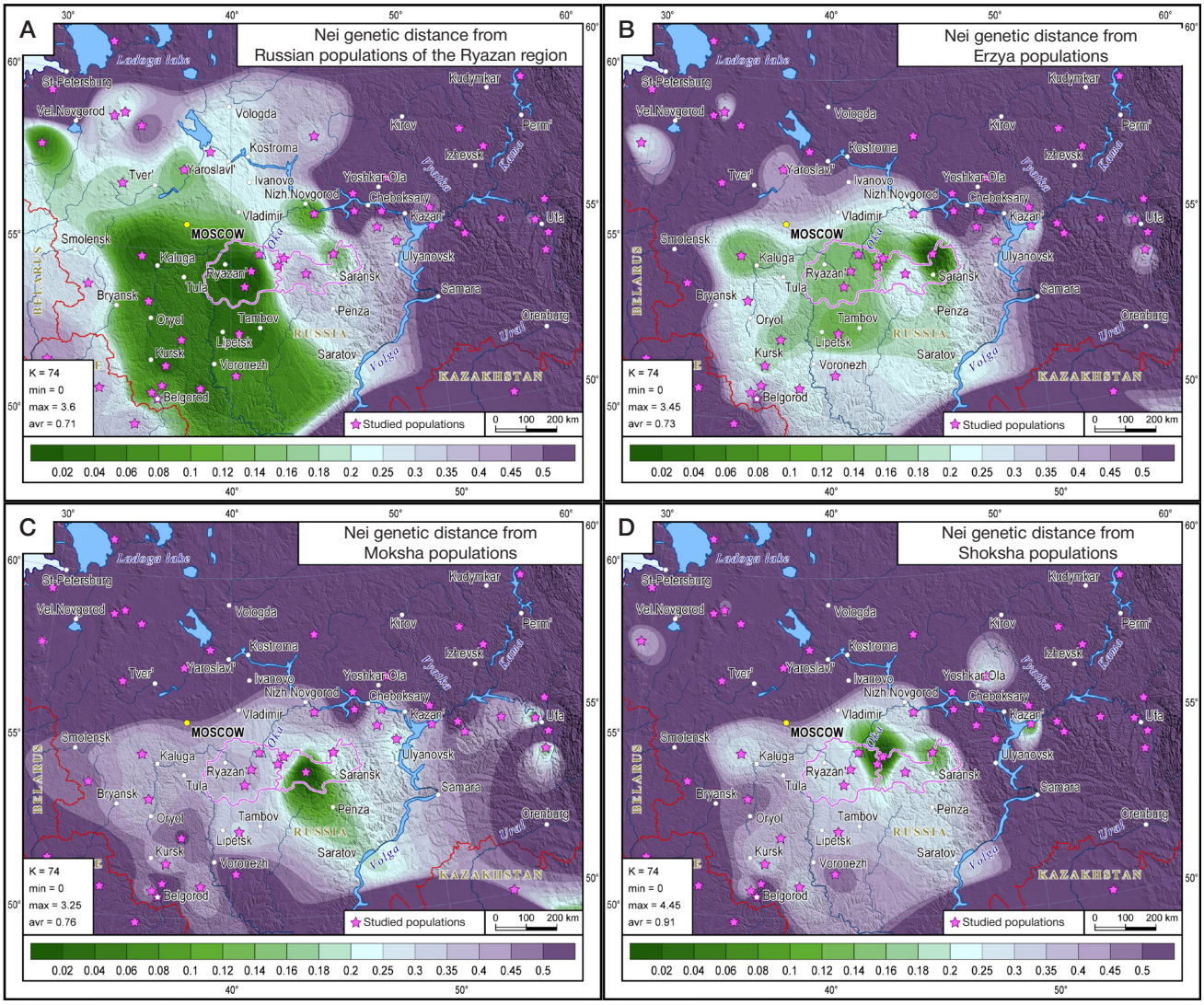


Fig. 5. Maps of Nei's genetic distances from the studied populations of the Volga–Oka region: from the total sample of Russian populations of the Ryazan Region (**A**); from populations of Erzya (**B**); from populations of Moksha (**C**); from populations of Shoksha (**D**). Shades of *green* reflect the minimum genetic distances (maximum similarity of gene pools); shades of *purple* and *blue* — medium genetic distances; shades of *violet* — maximum genetic distances (considerable differences between gene pools)

Mordovia (with the local maximum in Shoksha), but Russian populations are located in the low-frequency zone (shades of green).

Haplogroup N3a3 (Fig. 4E) is traditionally affiliated as "Uralic", since it is typical for the Uralic-speaking northwestern peoples. The frequency maximum is located in the Baltics (28–58%), Fennoscandia, and adjacent regions of the Russian North [18], but the local maximum is also found in the Volga Region in Mari (15%). N3a3 with the medium frequencies is spread across almost all European Russia, which reflects ancient "Baltic" influences.

Haplogroup N3a4 (Fig. 4F) is distinguished by a clear gradient of the frequency decrease from north to south. Its maxima are located in Fennoscandia [15], but very high frequencies (up to 60%) are found in the northwestern Finnish-speaking peoples of Russia and in the Russian North. Furthermore, the medium frequency zone (shades of yellow) extends to the south to Ryazan and to the east to the foothills of the Urals (17% N3a4 in Bashkir).

Volga–Oka region gene pool position in the gene-geographic landscape of Central Russia

Visual assessment of the Volga–Oka region genetic similarity to various populations of European Russia is provided by maps of Nei's genetic distances (dNei) (Fig. 5).

Genetic distances from Russians of the Ryazan Region (average values for seven districts; Fig. 5A) confirm the detected (MDS; Fig. 2) similarity of those to the gene pools of almost all Russian populations of Central Russia (shades of green). A green spot of maximum similarity is also found in Mordovia, in Erzya. The zone of medium genetic distances (shades of purple and blue) covers the northern Russian populations, eastern Slavs, and the entire Volga right bank.

However, the pattern of genetic distances from Erzya is surprising (Fig. 5B): the "green" zone of high similarity covers only Russian populations, stretching to the Kaluga and Kursk regions. The "violet" zone of medium values is even broader: this stretches to the Belgorod, Bryansk, Nizhny Novgorod regions, but of Uralic populations includes only Mishar Tatars of the Trans-Kama region (Alexeyevsky, Alkeyevsky, Spassky, Chistopolsky districts of Tatarstan).

The unique nature of the Moksha Y gene pool manifested by the lack of populations being on the small genetic distance from Moksha was mentioned above (Fig. 5C). However, the zone of medium values is rather large: along with Erzya and Shoksha, this includes the Mishar Tatars of Bashkiria and the Trans-Volga region (Drozhzhanovsky, Apastovsky districts of Tatarstan), Chuvash of Bashkiria, Anatri Chuvash of Chuvashia.

All these populations are located in the Mordovia subcluster on the plot (MDS, Fig. 3). The Shoksha gene pool (Fig. 5D) turned out to be the most close to that of the Mishar Tatars of the Trans-Kama region and Meadow Mari.

DISCUSSION

The analysis of all Slavic populations [1] showed a strong correlation of the data on the autosomal genome and Y chromosome. Such a correlation was confirmed in the earlier report: the autosomal gene pool substitution during the Slavic expansion was accompanied by the no less dramatic change of Y-haplogroups that resulted in predominance of haplogroups R1a-CTS1211, R1a-M458, and I2a-P37.2 [2].

Therefore, in this study special attention is paid to the geographic landscape of the conditionally "Slavic" haplogroups. The total frequency of haplogroups R1a-CTS1211, R1a-Z92, R1a-M458, R1a-M198*, and I2a-P37.2 calculated based on the set of 19 populations of Russians and 15 populations of Belarusians and Ukrainians constituted 67% of the gene pool of Eastern Slavs. This value is fully consistent with the total frequency of these "Slavic" haplogroups in Russians of Central Russia (66%) and is 3 times higher, than in Finnish-speaking and Turkic-speaking peoples of the Ural–Volga region (21%). However, this parameter is 2 times higher in populations of Mordovia (42%), than in the region (21%).

The in-depth phylogenetic study of modern and ancient carriers of haplogroups R1a-CTS1211 and R1a-Z92 in the Volga–Oka region has shown that about a half of the R1a-CTS1211 and R1a-Z92 haplogroup lineages on the Slavic expansion eastern periphery (Ryazan Region) are of pre-Slavic origin [3]. Frequency of these two haplogroups in Russians of the Ryazan Region eastern districts (46%) corresponds to their frequency in all Russian populations of central Russia (46%). This allows us to extend the lower estimate of the contribution of pre-Slavic population to the Y gene pool of Russians of central and southern Russia to all populations of Russians in this large region: this is about 43%. This estimate suggests the lower bound of the indigenous population contribution to the Slavic gene pool, since it was obtained specifically for the haplogroups most typical for the Slavs. Further in-depth phylogenetic study of modern and ancient carriers of "Uralic" haplogroups in the Volga–Oka region will show, how much higher could be the estimated contribution of pre-Slavic population to the Russian gene pool.

Among the conditionally "Uralic" haplogroups, haplogroups N3a1, N3a3, and N3a4 turned out to be the most common in the Volga–Oka region. However, we would like to emphasize again that the term "Uralic" is in this case both geographic and linguistic, it suggests the spread of these haplogroups across both studied peoples speaking Uralic languages (both northwestern — Veps, Votians, Izhorians, Karelians, Ingrian Finns; and eastern — Besermyan, Mari, Moksha, Udmurt, Shoksha, Erzya) and the considered Turkic-speaking populations of the Ural–Volga region (Bashkir, Kazan Tatars, Kryashens, Mishar Tatars, Chuvash). The total frequencies of the N3a1, N3a3, and N3a4 "Uralic" haplogroups in these three groups of populations are distributed in the following descending order: northwestern Finnish-speaking peoples (48%), eastern Finnish-speaking peoples (37%), Turks of the Ural–Volga region (12%). Based on the set of "Uralic" haplogroups, populations of Mordovia (23%) occupy an intermediate position in the Ural–Volga region, getting closer to Russians of the Ryazan Region (11%) and Russian populations of Central Russia in general (11%) in this parameter.

The first discovered "kinship" of the Mordovia's population Y gene pools, all four studied populations of the Mishar Tatars of Tatarstan and Bashkiria, and the majority of Chuvash populations (Anatri, Anat Jenchi, and Chuvash of Bashkiria) was an important finding of the analysis of the gene-geographic landscape of Central Russia. All these gene pools of the set of Finnish-speaking and Turkic-speaking populations form a common subcluster, which suggests their close genetic kinship. In the genetic space, this subcluster turned out to be close not only to the Ryazan Russians, but also to the entire set of Russian populations of Central and Southern Russia, based on the ratio of "Slavic" (35%) and "Uralic" haplogroups (14%) as well.

The fact, that all populations of Mordovia together with the Mishar Tatars and Chuvash form a common genetic set, allows us to hypothesize that all the populations of this cluster can be traced back to the common ancient Finnish-speaking population of the region. The sources of such unity can be different. It can be traced back to the early medieval Imenkovo archaeological culture or be related to migration of ancient Balts [19–21]. However, the Meschera hypothesis of the Mishar Tatar origin should be tested once again. According to anthropology data, [22] the Mishar Tatars are closer to Erzya, than to Meschera, but the new data on the Y gene pool suggest that not only Erzya and Mishar Tatars, but also all populations of Mordovia together with the Mishar Tatars and Chuvash form the common genetic set, which can result from the common nature of the tribes that included Meschera and the related tribes before Slavic expansion. These hypotheses can be tested based on the more thorough assessment of appropriate gene pools using the broad panels of Y-STR markers [3] and the ADMIXTURE analysis of the autosomal gene pool ancestral components.

CONCLUSIONS

1. The findings of the gene-geographic analysis of variation of 35 Y-haplogroups in 80 populations of indigenous peoples of Central Russia (our own data) and 10 populations of the North European countries [13–15] are presented as multidimensional scaling plots and a series of the gene-geographic landscape maps. 2. It has been shown that the gene pool of Russian populations of the Volga–Oka region (seven districts of the Ryazan Region) is completely inside the compact cluster of populations of Central Russia, it belongs to the common gene pool of the Eastern and Western Slavs. The map of genetic distances from Russians of the Ryazan Region and all the studied populations of indigenous peoples of Central Russia has fully confirmed this conclusion. 3. The gene pool of Finnish-speaking peoples of the Volga–Oka region (Moksha, Erzya, Shoksha) belongs to the large cluster of the Ural–Volga populations, but it shows maximum genetic proximity to the Russian populations of Central Russia. 4. It has been found that the subcluster that is close to the Russian gene pool includes the majority of Chuvash populations and all the studied populations of the Mishar Tatars of Tatarstan and Bashkiria, along with the Mordovia's populations. It has been hypothesized that this set of Finnish-speaking and Turkic-speaking populations can be traced back to the gene pool of the ancient indigenous Finnish-speaking population of the Volga–Oka region.

References

1. Kushniarevich A, Utevska O, Chuhryaeva M, Agdzhoyan A, Dibirova K, Uktveryte I, et al. Genetic heritage of the Balto-Slavic speaking populations: a synthesis of autosomal, mitochondrial and Y-chromosomal data. PLoS ONE. 2015; 10 (9): e0135820.
2. Gretzinger J, Biermann F, Mager H, King B, Zlámalová D, Traverso L, et al. Ancient DNA connects large-scale migration with the spread of Slavs. Nature. 2025. Available from: https://doi.org/10.1038/s41586-025-09437-6.
3. Adamov D, Shlykov A, Potanina A, Voronina M, Gorin I, Ponomarev G., et al. Pre-Slavic and Slavic Interaction at Eastern Periphery of Slavic Expansion in Northeastern Europe (Y-Gene Pools of Volga-Oka Region). Genes. 2025; 16 (10): 1149.
4. Balanovsky O, Rootsi S, Pshenichnov A, Kivisild T, Churnosov M, Evseeva I, et al. Two sources of the Russian patrilineal heritage in their Eurasian context. American Journal of Human Genetics. 2008; 82 (1): 236–50.
5. Balanovska EV, Balanovsky OP. Russkij genofond na Russkoj ravnine. M.: Luch, 2007; 416 s. Russian.
6. Okovancev VS, Ponomarev GYu, Agdzhoyan AT, Agdzhoyan AT, Pylyov VYu, Balanovska EV. Svoeobrazie pomorov Onezhskogo poluostrova i Zimnego berega v geneticheskom kontekste severa Evropy. Vestnik Moskovskogo universiteta. Seriya 23: Antropologiya. 2022; 5: 5–14. Russian.
7. Balanovska EV, Pezhemskij DV, Romanov AG, Baranova EE, Romashkina MV, Agdzhoyan AT i dr. Genofond Russkogo Severa: slavyane? finny? paleoevropejcy? Vestnik Moskovskogo universiteta. Seriya 23: Antropologiya. 2011; 3: 27–58. Russian.
8. Balanovska EV, Agdzhoyan AT, Skhalyaho RA, Balaganska OA, Frejdin GS, Chernevskij KG i dr. Genofond novgorodcev: mezhdu severom i yugom. Genetika. 2017; 53: 1259–71. Russian.
9. Chuhryaeva MI, Pavlova ES, Napolskih VV, Garin EV, Klopov AS, Temnyatkin SN i dr. Sohranilis' li sledy finno-ugorskogo vliyaniya v genofonde russkogo naseleniya YAroslavskoj oblasti? Svidetel'stva Y-hromosomy. Genetika. 2017; 53: 388–99. Russian.
10. Balanovska EV, Gorin IO, Ponomarev GYu, Pylyov VYu, Petrushenko VS, Markina NV i dr. Sledy vzaimodejstviya finnoyazychnogo, slavyanskogo i tyurkoyazychnogo naseleniya v sovremennom genofonde i ih otrazhenie v farmakogenetike. Vestnik RGMU. 2022; №2: 18–27. Russian.
11. Peltola S, Majander K, Makarov N, Dobrovolskaya M, Nordqvist K, Salmela E, et al. Genetic admixture and language shift in the medieval Volga-Oka interfluve. Current Biology. 2023; 33 (1): 174–82.
12. Balanovska EV, Zhabagin MK, Agdzhoyan AT, Chuhryaeva MI, Markina NV, Balaganskaya OA i dr. Populyacionnye biobanki: principy organizacii i perspektivy primeneniya v genogeografii i personalizirovannoj medicine. Genetika. 2016; 52 (12): 1371–87. Russian.
13. Ilumäe AM, Post H, Flores R, Karmin M, Sahakyan H, Mondal M, et al. Phylogenetic history of patrilineages rare in northern and eastern Europe from large-scale re-sequencing of human Y-chromosomes. Eur J Hum Genet. 2021; 29: 1510–19. Available from: https://doi.org/10.1038/s41431-021-00897-8.
14. Milewski M, Dawidziuk M. Most males in modern Poland carry Y-chromosomal lineages from clades that have recently expanded over Central, Eastern and SouthEastern Europe. Human Genetics. 2025; Available from: https://doi.org/10.1007/s00439-025-02781-7.
15. Preussner A, Leinonen J, Riikonen J, Pirinen M, Tukiainen T. Y chromosome sequencing data suggest dual paths of haplogroup N1a1 into Finland. Eur J Hum Genet. 2025; 33: 89–97. Available from: https://doi.org/10.1038/s41431-024-01707-7.
16. Koshel SM. Geoinformacionnye tekhnologii v genogeografii. V knige: I. K. Lur'e, V. I. Kravcova, redaktory. Sovremennaya geograficheskaya kartografiya. M.: Data+, 2012; s. 158–66. Russian.
17. Agdzhoyan A, Ponomarev G, Pylev V, (Kagazezheva) Zh, Gorin I, Evsyukov I, et al. The Finnic Peoples of Russia: Genetic Structure Inferred from Genome-Wide and Y-Chromosome Data. Genes. 2024; 15: 1610. Available from: https://doi.org/10.3390/genes15121610.
18. Ilumäe A M, Reidla M, Chukhryaeva M, Järve M, Post H, Karmin M, et al. Human Y Chromosome Haplogroup N: A Non-trivial TimeResolved Phylogeography that Cuts across Language Families. The American Journal of Human Genetics. 2016; 99 (1): 163–73.
19. Matveeva GI. O proiskhozhdenii imen'kovskoj kul'tury. Drevnie i srednevekovye kul'tury Povolzh'ya. Kujbyshev, 1981. Russian.
20. Sedov VV. Ocherki po arheologii slavyan. Moskva. 1994. 128 s. Russian.
21. Napolskih VV. Balto-slavyanskij yazykovoj komponent v Nizhnem Prikam'e v ser. I tys. n. e. Slavyanovedenie. 2006; 2: 3–19. Russian.
22. Alekseeva TI, Vasilev BA. K voprosu o geneticheskom rodstve russkoj meshchery i tatar-misharej. Kratkie soobshcheniya Instituta etnografii. 1959; 31: 3–13. Russian.

Литература

1. Kushniarevich A, Utevska O, Chuhryaeva M, Agdzhoyan A, Dibirova K, Uktveryte I, et al. Genetic heritage of the Balto-Slavic speaking populations: a synthesis of autosomal, mitochondrial and Y-chromosomal data. PLoS ONE. 2015; 10 (9): e0135820.
2. Gretzinger J, Biermann F, Mager H, King B, Zlámalová D, Traverso L, et al. Ancient DNA connects large-scale migration with the spread of Slavs. Nature. 2025. Available from: https://doi.org/10.1038/s41586-025-09437-6.
3. Adamov D, Shlykov A, Potanina A, Voronina M, Gorin I, Ponomarev G., et al. Pre-Slavic and Slavic Interaction at Eastern Periphery of Slavic Expansion in Northeastern Europe (Y-Gene Pools of Volga-Oka Region). Genes. 2025; 16 (10): 1149.
4. Balanovsky O, Rootsi S, Pshenichnov A, Kivisild T, Churnosov M, Evseeva I, et al. Two sources of the Russian patrilineal heritage in their Eurasian context. American Journal of Human Genetics. 2008; 82 (1): 236–50.
5. Балановская Е. В., Балановский О. П. Русский генофонд на Русской равнине. М.: Луч, 2007; 416 с.
6. Окованцев В. С., Пономарев Г. Ю., Агджоян А. Т., Агджоян А. Т., Пылёв В. Ю., Балановская Е. В. Своеобразие поморов Онежского полуострова и Зимнего берега в генетическом контексте севера Европы. Вестник Московского университета. Серия 23: Антропология. 2022; 5: 5–14.
7. Балановская Е. В., Пежемский Д. В., Романов А. Г., Баранова Е. Е., Ромашкина М. В., Агджоян А. Т. и др. Генофонд Русского Севера: славяне? финны? палеоевропейцы? Вестник Московского университета. Серия 23: Антропология. 2011; 3: 27–58.
8. Балановская Е. В., Агджоян А. Т., Схаляхо Р. А., Балаганская О. А., Фрейдин Г. С., Черневский К. Г. и др. Генофонд новгородцев: между севером и югом. Генетика. 2017; 53: 1259–71.
9. Чухряева М. И., Павлова Е. С., Напольских В. В., Гарин Э. В., Клопов А. С., Темняткин С. Н. и др. Сохранились ли следы финно-угорского влияния в генофонде русского населения Ярославской области? Свидетельства Y-хромосомы. Генетика. 2017; 53: 388–99.
10. Балановская Е. В., Горин И. О., Пономарев Г. Ю., Пылёв В. Ю., Петрушенко В. С., Маркина Н. В. и др. Следы взаимодействия финноязычного, славянского и тюркоязычного населения в современном генофонде и их отражение в фармакогенетике. Вестник РГМУ. 2022; №2: 18–27.
11. Peltola S, Majander K, Makarov N, Dobrovolskaya M, Nordqvist K, Salmela E, et al. Genetic admixture and language shift in the medieval Volga-Oka interfluve. Current Biology. 2023; 33 (1): 174–82.
12. Балановская Е. В., Жабагин М. К., Агджоян А. Т., Чухряева М. И., Маркина Н. В., Балаганская О. А. и др. Популяционные биобанки: принципы организации и перспективы применения в геногеографии и персонализированной медицине. Генетика. 2016; 52 (12): 1371–87.
13. Ilumäe AM, Post H, Flores R, Karmin M, Sahakyan H, Mondal M, et al. Phylogenetic history of patrilineages rare in northern and eastern Europe from large-scale re-sequencing of human

Y-chromosomes. Eur J Hum Genet. 2021; 29: 1510–19. Available from: https://doi.org/10.1038/s41431-021-00897-8.
14. Milewski M, Dawidziuk M. Most males in modern Poland carry Y-chromosomal lineages from clades that have recently expanded over Central, Eastern and SouthEastern Europe. Human Genetics. 2025; Available from: https://doi.org/10.1007/s00439-025-02781-7.
15. Preussner A, Leinonen J, Riikonen J, Pirinen M, Tukiainen T. Y chromosome sequencing data suggest dual paths of haplogroup N1a1 into Finland. Eur J Hum Genet. 2025; 33: 89–97. Available from: https://doi.org/10.1038/s41431-024-01707-7.
16. Кошель С. М. Геоинформационные технологии в геногеографии. В книге: И. К. Лурье, В. И. Кравцова, редакторы. Современная географическая картография. М.: Дата+, 2012; с. 158–66.
17. Agdzhoyan A, Ponomarev G, Pylev V, (Kagazezheva) Zh, Gorin I, Evsyukov I, et al. The Finnic Peoples of Russia: Genetic Structure Inferred from Genome-Wide and Y-Chromosome Data. Genes. 2024; 15: 1610. Available from: https://doi.org/10.3390/genes15121610.
18. Ilumäe A M, Reidla M, Chukhryaeva M, Järve M, Post H, Karmin M, et al. Human Y Chromosome Haplogroup N: A Non-trivial TimeResolved Phylogeography that Cuts across Language Families. The American Journal of Human Genetics. 2016; 99 (1): 163–73.
19. Матвеева Г. И. О происхождении именьковской культуры. Древние и средневековые культуры Поволжья. Куйбышев, 1981.
20. Седов В. В. Очерки по археологии славян. Москва. 128 с, 1994.
21. Напольских В. В. Балто-славянский языковой компонент в Нижнем Прикамье в сер. I тыс. н. э. Славяноведение. 2006; 2: 3–19.
22. Алексеева Т. И., Васильев Б. А. К вопросу о генетическом родстве русской мещеры и татар-мишарей. Краткие сообщения Института этнографии. 1959; 31: 3–13.

TRANSCRIPTIONAL KINASE CDK8, BUT NOT CDK19, PROMOTES THE DEVELOPMENT OF ATHEROSCLEROTIC LESIONS IN MICE

Neznamov AN[1,2], Baykova YuP[1], Korshunov EN[1], Isaeva EM[1], Bruter AV[1], Kubekina MV[1]✉

[1] Institute of Gene Biology Russian Academy of Sciences, Moscow, Russia
[2] Pirogov Russian National Research Medical University, Moscow, Russia

Atherosclerosis, being the main cause of myocardial infarction and stroke, remains a global medical and social problem. Despite the fact that it is recognized as a chronic inflammatory disorder, the intracellular molecular mechanisms that drive the disease progression are poorly understood. The CDK8 and CDK19 cyclin-dependent kinases being the key regulators of transcription and inflammation can potentially play an important role in the atherosclerosis pathogenesis. The study aimed to assess the impact of the *Cdk8* and *Cdk19* gene knockout on the development of atherosclerotic lesions in apolipoprotein E-deficient mice (ApoE$^{-/-}$). It has been shown that both endothelium-specific and systemic *Cdk8* knockout significantly reduce the area of atherosclerotic aortic lesions, and the total knockout has a more prominent anti-atherogenic effect. This suggests a pleiotropic role of CDK8 in the atherosclerosis pathogenesis mediated by its function not only in endothelial cells, but probably also in macrophages. In contrast to *Cdk8*, the systemic *Cdk19* knockout had no significant effect on the development of atherosclerosis. Thus, CDK8, but not CDK19, has been identified as a pro-atherogenic regulator, which makes it a promising target for the development of novel therapeutic strategies.

Keywords: atherosclerosis, genetically modified animals, transcriptional kinases CDK8 and CDK19, atherosclerotic lesions, apolipoprotein E

Funding: the study was supported by the Russian Science Foundation grant No. (24-25-00384), https://rscf.ru/project/24-25-00384/.

Author contribution: Neznamov AN — genotyping of animals, aortic image processing, manuscript writing; Baykova YuP — aorta separation and staining, preparation of specimens; Korshunov EN, Isaeva EM — animal handling, preparation of experimental groups; Bruter AV — providing antibodies for the Western blot assay, literature review, analysis of the results; Kubekina MV — literature review, study planning, Western blot assay, analysis of the results, manuscript writing.

Compliance with ethical standards: the study was approved by the Ethics Committee of the Institute of Gene Biology RAS (protocol No. 25 dated 15 may 2024), it was strictly compliant with the provisions of the Directive 2010/63/EU of the European Parliament and of the Council of 22 September 2010 on the protection of animals used for scientific purposes.

✉ **Correspondence should be addressed:** Marina V. Kubekina
Vavilova, 34/5, Moscow, 119334, Russia; marykumy@gmail.com

Received: 31.10.2025 **Accepted:** 01.12.2025 **Published online:** 16.12.2025

DOI: 10.24075/brsmu.2025.078

Copyright: © 2025 by the authors. **Licensee:** Pirogov University. This article is an open access article distributed under the terms and conditions of the Creative Commons Attribution (CC BY) license (https://creativecommons.org/licenses/by/4.0/).

ТРАНСКРИПЦИОННАЯ КИНАЗА CDK8, НО НЕ CDK19 СПОСОБСТВУЕТ РАЗВИТИЮ АТЕРОСКЛЕРОТИЧЕСКИХ ПОРАЖЕНИЙ У МЫШЕЙ

А. Н. Незнамов[1,2], Ю. П. Байкова[1], Е. Н. Коршунов[1], Е. М. Исаева[1], А. В. Брутер[1], М. В. Кубекина[1]✉

[1] Институт биологии гена Российской академии наук, Москва, Россия
[2] Российский национальный исследовательский медицинский университет имени Н. И. Пирогова, Москва, Россия

Атеросклероз, являющийся основной причиной инфаркта миокарда и инсульта, остается глобальной медико-социальной проблемой. Несмотря на его признание в качестве хронического воспалительного заболевания, внутриклеточные молекулярные механизмы, управляющие прогрессированием болезни, изучены недостаточно. Циклин-зависимые киназы CDK8 и CDK19, являющиеся ключевыми регуляторами транскрипции и воспаления, потенциально могут играть значительную роль в патогенезе атеросклероза. Целью исследования было изучить влияние нокаута генов *Cdk8* и *Cdk19* на развитие атеросклеротических поражений у мышей с дефицитом аполипопротеина Е (ApoE$^{-/-}$). Показано, что как эндотелиоспецифичный, так и системный нокаут *Cdk8* достоверно снижает площадь атеросклеротических поражений аорты, причем тотальный нокаут оказывает более выраженный антиатерогенный эффект. Это свидетельствует о плейотропной роли CDK8 в патогенезе атеросклероза, опосредованной его функцией не только в эндотелиальных клетках, но и, вероятно, в макрофагах. В отличие от *Cdk8*, системный нокаут *Cdk19* не оказал значимого влияния на развитие атеросклероза. Таким образом, CDK8, но не CDK19, идентифицирован в качестве проатерогенного регулятора, что делает его перспективной мишенью для разработки новых терапевтических стратегий.

Ключевые слова: атеросклероз, генетически модифицированные животные, транскрипционные киназы CDK8 и CDK19, атеросклеротические поражения, аполипопротеин Е

Финансирование: работа выполнена при финансовой поддержке гранта Российского научного фонда № (24-25-00384), https://rscf.ru/project/24-25-00384/.

Вклад авторов: А. Н. Незнамов — генотипирование животных, обработка изображений аорт, написание рукописи; Ю. П. Байкова — сепарация и окрашивание аорт, подготовка препаратов; Е. Н. Коршунов, Е. М. Исаева — работа с животными, подготовка экспериментальных групп; А. В. Брутер — предоставление антител для вестерн-блота, анализ литературы, анализ результатов; М. В. Кубекина — анализ литературы, планирование исследования, проведение вестерн-блота, анализ результатов, написание рукописи.

Соблюдение этических стандартов: исследование одобрено этическим комитетом ИБГ РАН (протокол № 25 от 15 мая 2024 г.) и проведено в строгом соответствии с положениями Директивы 2010/63/EU Европейского Парламента и Совета Европейского союза от 22 сентября 2010 г. по охране животных, используемых в научных целях.

✉ **Для корреспонденции:** Марина Владиславовна Кубекина
ул. Вавилова, д. 34/5, г. Москва, 119334, Россия; marykumy@gmail.com

Статья получена: 31.10.2025 **Статья принята к печати:** 01.12.2025 **Опубликована онлайн:** 16.12.2025

DOI: 10.24075/vrgmu.2025.078

Авторские права: © 2025 принадлежат авторам. **Лицензиат:** РНИМУ им. Н. И. Пирогова. Статья размещена в открытом доступе и распространяется на условиях лицензии Creative Commons Attribution (CC BY) (https://creativecommons.org/licenses/by/4.0/).

According to the World Health Organization, myocardial infarction and stroke, being the main complications of atherosclerosis, remain the leading causes of death worldwide. In 2019 in Russia, circulatory system diseases accounted for 46.8% of all fatal cases. The high mortality rate results largely from the long asymptomatic course of atherosclerosis, which at the later (diagnosed) stages often requires surgery and responds weakly to conservative therapy [1]. Despite the existing treatment methods aimed at decreasing low-density lipoprotein (LDL) cholesterol levels and restoring blood flow, atherosclerosis remains a global medical and social problem. It is generally accepted that atherosclerosis is a chronic inflammatory disease of the arteries [2], but intracellular molecular mechanisms that control such inflammation and disease progression are poorly understood [3]. The atherosclerotic plaque formation is the key event in its pathogenesis characterized by chronic inflammation, endothelial dysfunction, lipid accumulation, and proliferation of smooth muscle cells in the wall [4, 5].

The CDK8 and CDK19 cyclin-dependent kinases, being part of the mediator complex, represent the key regulators of the RNA polymerase II-mediated transcription. Despite the fact that their exact mechanisms of action are still poorly understood, it is well known that CDK8/19 play a central role in transcriptional reprogramming, which underlies cell differentiation and pathogenesis of various diseases [6]. CDK8/19 are modulators of the signaling pathways of transcription factors STAT1 and NF-kB which play a critical role in inflammatory processes [7, 8].

Recently, the data linking CDK8 to cardiovascular disorders has been accumulating. In particular, CDK8 is a co-regulator of the HIF-1α (hypoxia-inducible factor 1-alpha) transcription factor, the key mediator of the cellular response to hypoxia contributing greatly to the atherosclerosis development [9]. HIF-1α triggers expression of a broad range of genes contributing directly to the development of atherosclerosis, such as TNF, CD36, VEGF, ICAM-1, VCAM-1 [10–12]. Thus, HIF-1α mediates pro-atherogenic processes, such as lipid metabolism disturbances in macrophages, endothelial dysfunction, and enhanced inflammation [13]. Furthermore, CDK8 is a negative lipid biosynthesis regulator. CDK8 induces increased ubiquitination and degradation of SREBP through phosphorylation of this protein. The SREBP family includes the key transcription factors that regulate lipid metabolism, including transcription of the genes responsible for cholesterol synthesis and lipogenesis [14]. Since CDK8 regulates the expression of many genes associated with atherogenesis, it has been hypothesized than the CDK8 and/or CDK19 deletion may result in the slower progression of atherosclerosis due to the decrease in lipoprotein infiltration of the aortic intima.

Despite the well known CDK8/19 involvement in carcinogenesis and immune response [15, 16], their role in atherogenesis is poorly understood. In this regard, it seems promising to study the role of the CDK8/19 transcription kinases, being the well- known regulators of inflammation and contributors to cardiovascular disorders, in the development of atherosclerosis. Thus, the study aimed to assess the impact of the systemic and endothelium-specific *Cdk8* knockout, as well as systemic *Cdk19* knockout on the formation of atherosclerotic lesions in the mouse aorta against the background of the *ApoE* knockout, the well-known mouse model of atherosclerosis [17].

METHODS

Keeping mice

The study involved the use of mice of the Rosa26/Cre-ERT2 (B6.129-Gt(ROSA)26Sortm1(cre/ERT2)Tyj/J, Jackson Laboratory) and Tie2-Cre (B6.Cg-Tg(Tek-cre)1Ywa/J, Jackson Laboratory) activator lineages. Mice of these lineages were crossed with Cdk8fl/fl (Jax:008463, Jackson Laboratory) with exon 2 in the *Cdk8* gene flanked by loxP sites to obtain Rosa26/Cre-ERT2/Cdk8fl/fl (systemic knockout) and Tie2-Cre/Cdk8fl/fl (endothelium-specific knockout). Furthermore, the C57BL/6N-Cdk19 mice (RRID:MMRRC 047035-UCD, MMRRC) with the constitutive *Cdk19* knockout were used. Genotyping of the Cdk8fl/fl, C57BL/6N-Cdk19, Rosa26/Cre-ERT2 offspring was conducted as reported earlier [18]. The experiments involved mice of the above lineages against the background of the ApoE-/- status (apolipoprotein E knockout). The mice were a gift from Yury Kotelevtsev [19]. For genotyping of the ApoE-/- and Tie2-Cre mice, the P1, P2, P3 and P4, P5, P6 oligonucleotide primers, respectively, were used (Table). All primers were synthesized by Evrogen (Russia).

The mice were kept in the vivarium of the Institute of Gene Biology RAS with permanent access to water and food. The light/dark cycle was 12/12 h, air temperature — 23 ± 1 °C, humidity — 42 ± 5%.

Cdk8 knockout induction

To induce *Cdk8* knockout in the Rosa26/Cre-ERT2/Cdk8fl/fl mice, intraperitoneal injections of tamoxifen (Sigma-Aldrich, USA) dissolved in corn oil (Sigma-Aldrich, USA) were used as previously reported [20]: males aged 2 months were administered 0.15 mL of tamoxifen at a concentration of 20 mg/mL daily throughout 7 days. These mice were put on the atherogenic diet (Western type diet, WTD) a month after the knockout induction.

Experimental groups

The following experimental groups were formed of male mice of the specified lineages aged 3 months (Fig. 1), a total of 46 animals:

1. ApoE — apolipoprotein E-deficient mice fed with standard feed (negative control), $n = 4$;
2. ApoE WTD — ApoE-/- mice on the WTD (positive control of atherosclerosis model for the Cdk19-/-/ApoE-/- и Tie2-Cre/Cdk8fl/fl/ApoE-/- mice), $n = 8$;
3. ApoE + Oil WTD — ApoE-/- mice treated with corn oil throughout 7 days (150 μL a day), which were on the WTD (positive control of atherosclerosis model for the tamoxifen-treated mice Rosa26/Cre-ERT2/Cdk8fl/fl), $n = 5$;
4. Rosa WTD — Rosa26/Cre-ERT2 mice on the WTD (negative control of atherosclerosis model for the Rosa26/Cre-ERT2/Cdk8fl/fl mice), $n = 4$;
5. Tie WTD — Tie2-Cre mice on the WTD (negative control of atherosclerosis model for the Tie2-Cre/Cdk8fl/fl/ApoE-/- mice), $n = 4$;
6. Cdk19/ApoE WTD — mice with the *Cdk19* knockout against the background of the *ApoE* knockout, which were on the WTD, $n = 8$;
7. Cdk8/Rosa/ApoE WTD — Rosa26/Cre-ERT2/Cdk8fl/fl mice with the inducible *Cdk8* knockout against the background of the *ApoE* knockout, which were on the WTD, $n = 6$;
8. Cdk8/Tie/ApoE WTD — mice with the constitutive endothelium-specific *Cdk8* knockout against the background of the *ApoE* knockout, which were on the WTD, $n = 7$.

Exclusion criteria

The experiment involved males only. Animals were excluded from the experiment due to clinical status deterioration

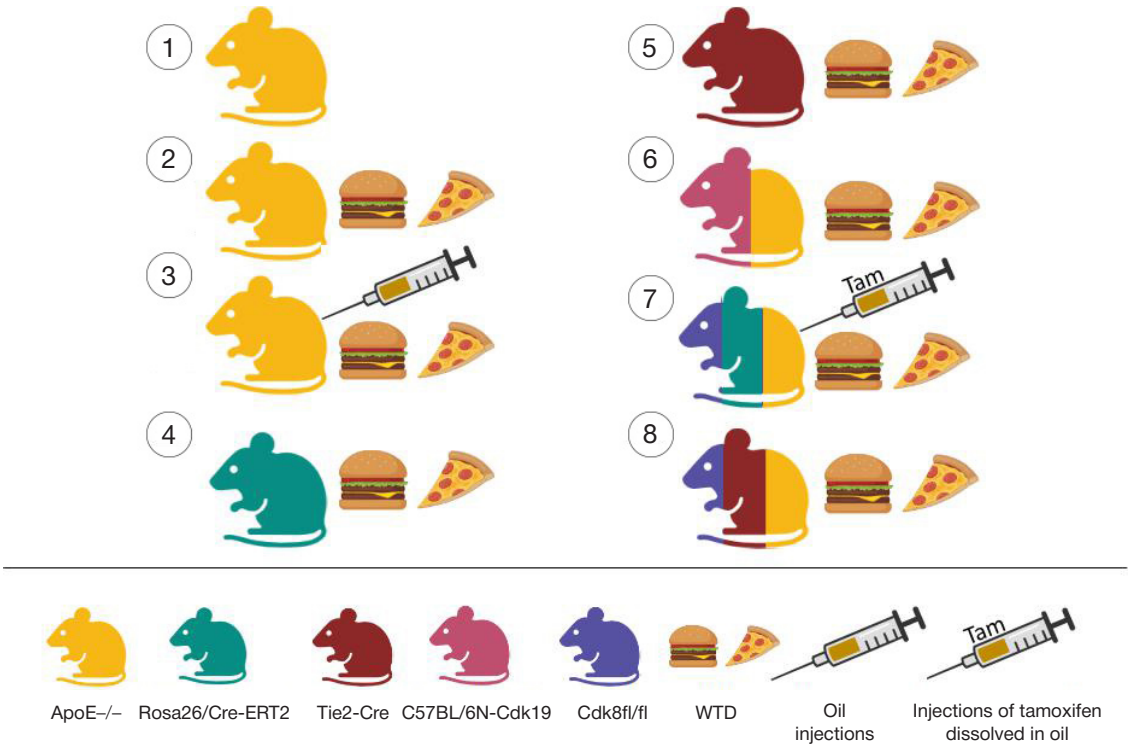


Fig. 1. Schematic representation of the experimental groups of mice used in the experiment

manifested by fatigue, apathy, refusal to eat, as well as in cases of the animal's spontaneous death before scheduled euthanasia. A total of five animals were excluded based on the latter criterion: two from group 1, one from groups 4, 5, and 7.

Atherogenic diet

Adult mice in different experimental groups aged 3 months were kept on the atherogenic diet. The diet composition was as follows: 21.2% dairy fat (Parmalat, Russia), 34% sucrose (Solarbio, China), and 0.2% cholesterol (Macklin, China) [21]. To induce the development of atherogenic lesions, mice were kept on the diet for 2 months.

Aortic examination

The mouse aorta separation and staining, as well as image processing were conducted as previously reported [22]. The mice were intraperitoneally anesthetized with the solution of 0.6 mL Zoletil (Virbac, France) + 0.3 mL Xylazine (Interchemie Werken "de Adelaar" BV, Netherlands) + 9 mL saline (PanEco, Russia) at the dose of 100 μL per 10 g of the animal's body weight, then the cardiovascular system was perfused through a puncture of the apex of the left ventricle with 10 mL of PBS (BioinnLabs, Russia) to flush out blood. The Zeiss Stemi DV4 stereo microscope (Carl Zeiss, Germany) was used to accurately separate the entire aorta, from the arch to the iliac arteries; perivascular adipose and connective tissues around the aorta were removed, avoiding damage to these. To immobilize tissues, perfusion with 10 mL of 4% paraformaldehyde solution (Medix, Russia) was performed. Then the aorta was put in 1 mL of the freshly prepared 0% Oil Red O solution (Sigma-Aldrich, USA) and incubated for 60 min at room temperature. After staining, the specimen was washed with the 60% isopropanol (Panreac AppliChem, Germany) for 20 min, then triple washed with the distilled water for 5 min. The microscope was used to completely clear the aorta of the remaining stained perivascular adipose tissue, put it onto the slide, and acquire high-resolution digital micrographs. The images obtained were processed using the ImageJ software tool. The percentage of atherosclerotic lesions was calculated as the ratio of the area of lesions to the total area of the ascending aorta and aortic arch.

Western blot

The CDK8 and CDK19 levels were assessed in the aortas of mice in all of the studied groups. To detect CDK8 and CDK19, the CDK8 (D6M3J) Rabbit 17395 antibody (Cell Signaling, USA) and CDK19 antibody from the paper [18], respectively, diluted 1 : 1000 were used. The β-actin protein levels were determined as a load control. For that the mouse monoclonal

Table. Oligonucleotides used in the study

	Sequence 5' → 3'
P1	GCC TAG CCG AGG GAG AGC CG
P2	TGT GAC TTG GGA GCT CTG CAG C
P3	GCC GCC CCG ACT GCA TCT
P4	CTG TGA CCT GAG TGC CCA GT
P5	GCG TTT AAG TAA TGG GAT GGT C
P6	CCA CAC ACG TGC ACA TAT AGA

anti-β-actin antibody (A2228, Sigma-Aldrich, USA) diluted 1 : 1000 was used. Detection involved the use of the secondary antibodies conjugated with horseradish peroxidase (HRP): anti-rabbit IgG (catalogue number 7074, Cell Signaling, USA) and anti-mouse IgG (catalogue number 7076, Cell Signaling, USA) diluted 1 : 2000. Visualization of the Western blot assay results was accomplished using the iBright FL1500 system (Invitrogen, USA).

Statistical data processing

Significance of differences was assessed using one-way ANOVA in GraphPad Prism 8.0.1 (GraphPad Software, USA). The data are presented as the mean ± standard error of the mean.

RESULTS

In this study, the genetically modified mice with the systemic and endothelium-specific knockout of the *Cdk8* gene, as well as with the systemic knockout of the *Cdk19* gene were the research objects. In the first phase of the study, the CDK8 and CDK19 protein levels in the aortas of mice of different experimental groups were validated (Fig. 2).

It has been found out, that in the aortas of the ApoE, Tie, and Rosa control mice, the CDK8 and CDK19 proteins are detected, while in mice with the systemic *Cdk8* knockout (group Cdk8/Rosa/ApoE) there is no CDK8, and in mice with the systemic *Cdk19* knockout (group Cdk19/ApoE) there is no CDK19. However, the CDK8 protein is detected in mice with the endothelium-specific *Cdk8* knockout (group Cdk8/Tie/ApoE). The reported presence of protein is consistent with the histological structure of the aorta consisting of three layers: tunica adventitia, media, and intima, which is constituted mainly by the endothelium [23]. Thus, in this group the *Cdk8* knockout affects mainly endothelial cells of the intima, which explains detection of the CDK8 protein in the homogenate of the entire aorta.

Then aortas were assessed in mice of all experimental groups after being kept on the atherogenic diet throughout 2 months. The values reported for the mice of the experimental groups Cdk19/ApoE WTD and Cdk8/Tie/ApoE WTD were compared to the values of the group ApoE WTD representing a positive control in the experiment and to the values of groups Tie WTD and ApoE kept on the standard diet representing a negative control (Fig. 3).

It has been found out that in the group of mice with the endothelium-specific *Cdk8* knockout there is a significant (p = 0.0295) reduction of the aortic lesion compared to the ApoE positive control. Furthermore, in the group with the systemic *Cdk19* knockout the lesion area does not differ from that in control groups.

When inducing the *Cdk8* knockout in the Cdk8/Rosa/ApoE group, the mice received injections of tamoxifen dissolved in corn oil daily. To create positive controls for this group, the ApoE mice treated with corn oil in accordance with the same scheme were used. After keeping on the atherogenic diet, atherosclerotic lesions of the aorta were assessed in the Cdk8/Rosa/ApoE WTD, ApoE + Oil WTD mice as a positive control; Rosa WTD, as well as ApoE on the standard diet as a negative control (Fig. 4).

It has been found out, that the values obtained in mice with the systemic *Cdk8* knockout are significantly (p = 0.0024) lower compared to the positive control values and do not differ from the negative control values.

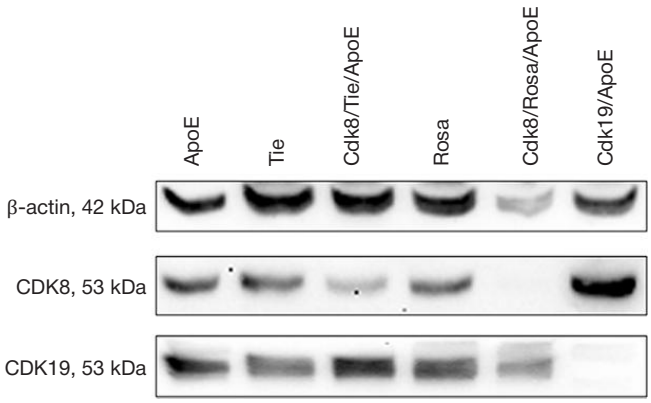


Fig. 2. Representative Western blot image showing the content of CDK8 and CDK19 in the aortas of mice of different experimental groups

DISCUSSION

Genetically modified animals represent a common tool for modeling and further investigation of pathogenesis of human disorders, as well as for the development of therapy methods [24]. This determines their important role in the study of such socially significant disorders, as atherosclerosis. Atherosclerosis, as a chronic progressive disorder, underlies most cases of cardiovascular disorders, which determines high mortality and disability rates in the population [25].

It is well known that the CDK8 transcription kinase and its paralogue CDK19 modulate signaling pathways of the STAT1 and NF-kB transcription factors, thereby regulating the inflammatory response. In a number of studies, it has been shown that the low molecular weight CDK8/19 inhibitors, such as SenexinA/B, Cmpd3/4, Cpd32, Cortistatin A, effectively suppress activation of the key pro-inflammatory transcription factors STAT1 and NF-kB *in vitro* and *in vivo* [7, 8, 26, 27]. Furthermore, the role of CDK8 in the pathogenesis of cardiovascular disorders has been shown, since this kinase is a co-regulator of HIF-1α involved in pro-atherogenic processes [9, 10, 28].

This research was focused on studying the role of the CDK8 and CDK19 transcription kinases in the atherosclerotic lesion formation using the genetically modified mice with the systemic and endothelium-specific *Cdk8* knockout, as well as with the systemic *Cdk19* knockout. To model accumulation of lipoproteins in the aortic wall, these mice were put against the *ApoE* knockout background. The *ApoE* gene encodes the apolipoprotein E protein playing a central role in lipoprotein metabolism. One of its main functions is to serve as a ligand for the hepatic receptors that remove chylomicron and LDL remnants from the bloodstream. The ApoE-/- mice have no key mechanism for blood plasma purification from cholesterol-rich lipoproteins, which results in the dramatic increase in plasma cholesterol levels, LDL accumulation in blood, and subsequent development of atherosclerotic lesions [17].

The *Cdk8* and *Cdk19* knockout in the aortas of the mice assessed was confirmed by Western blot assay (Fig. 2). It was shown that there were no CDK19 in the group of the CDK19/ApoE mice with the systemic *Cdk19* knockout, no CDK8 in the group of the CDK8/Rosa/ApoE mice with the systemic *Cdk8* knockout, and incomplete CDK8 removal in the CDK8/Tie/ApoE group with the endothelium-specific *Cdk8* knockout. Thus, we have shown that these models are relevant.

The study of the lipid inclusion accumulation in the aortas of experimental mice has shown that both endothelium-specific (Fig. 3) and systemic (Fig. 4) *Cdk8* knockout results in significant

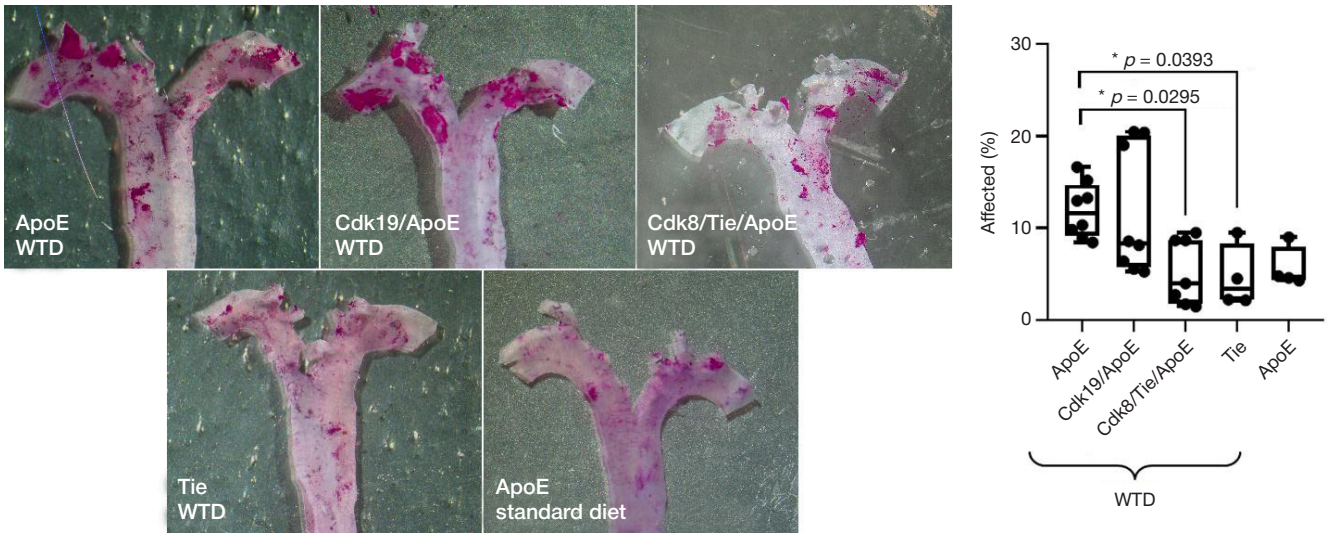


Fig. 3. Aorta assessment in mice of experimental groups ApoE WTD, Cdk19/ApoE WTD, Cdk8/Tie/ApoE WTD, Tie WTD, as well as ApoE fed with standard feed. Representative image of the studied aortas (on the left), diagram of the affected area calculation (on the right). The aortic lesions are marked with white dotted lines (*— $p < 0.05$)

reduction of the vascular lesion area. Furthermore, the total *Cdk8* knockout has a stronger anti-atherogenic effect compared to the endothelium-specific one. The data obtained suggest that the CDK8 contribution to the atherosclerosis pathogenesis is not limited to endothelial cells; it is also mediated by its function in the key cell types for this disorder, such as macrophages and possibly vascular smooth muscle cells. These findings are consistent with the literature data showing the decrease in the anti-inflammatory response upon CDK8/19 inhibition in monocytes/macrophages [29]. According to the results obtained, CDK8 is involved in the atherosclerotic phenotype enhancement, possibly through regulation of the transcription programs associated with the inflammatory response and lipid metabolism.

In contrast to *Cdk8*, the systemic *Cdk19* inactivation had no significant effect on the area of the aortic atherosclerotic lesions, which demonstrates the values comparable to that of both negative and positive control groups (Fig. 3). It should be noted, that in the Cdk19/ApoE group, a significant inter-individual variability was observed, including specimens with both large and minimal lesion areas. Such a distribution, along with the lack of the general effect, suggests that CDK19, in contrast to its paralogue CDK8, does not determine the atherosclerosis progression.

Chronic inflammation is a cornerstone of the atherosclerosis pathogenesis [2], and our results clearly indicate the CDK8 pro-atherogenic role. Considering the fact that CDK8 is an inflammatory response regulator [6–8], it can be assumed that pharmacological inhibition of this kinase will reproduce the reported anti-atherogenic effect by suppressing pro-inflammatory signaling pathways. Thus, the use of the well-known CDK8 inhibitors in experimental atherosclerosis models seems to be a promising area for the development of novel therapeutic approaches.

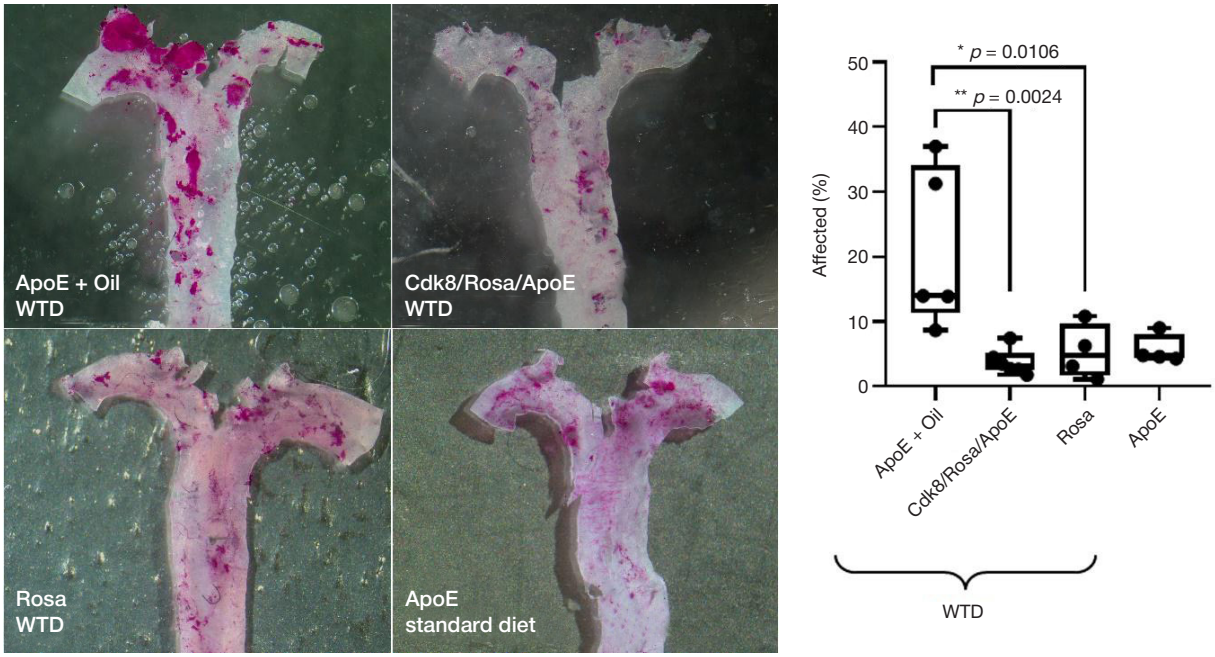


Fig. 4. Aorta assessment in mice of experimental groups ApoE + Oil WTD, Cdk8/Rosa/ApoE WTD, Rosa WTD, as well as ApoE fed with standard feed. Representative image of the studied aortas (on the left), diagram of the affected area calculation (on the right). The aortic lesion is marked with the white dotted line (*— $p < 0.05$, ** — $p < 0.01$)

CONCLUSIONS

The study conducted discloses the fundamental atherogenesis regulation aspects related to the function of the CDK8 and CDK19 transcription kinases. The use of genetic models in the ApoE$^{-/-}$ mice with the knockout of the above genes has shown that CDK8 functions as a pro-atherogenic regulator, which is confirmed by significant reduction of the atherosclerotic lesion area in knockout mice. The stronger anti-atherogenic effect of the systemic knockout compared to the endothelium-specific one suggests the pleiotropic nature of the CDK8 impact on the disease pathogenesis, including its role in not only endothelial cells, but also other cell populations, specifically in macrophages. The CDK8 pro-atherogenic effect molecular mechanisms are likely to be related to its capability of regulating the key transcription programs, including the HIF-1α, STAT1, and NF-κB pathways, which modulate the inflammatory response and lipid metabolism in the vascular wall. CDK19 has no significant effect on the development of atherosclerotic lesions, which emphasizes functional divergence between the structurally homologous kinases CDK8 and CDK19 in the context of atherosclerosis pathogenesis. The findings not only expand the knowledge about the atherosclerosis molecular basis, but also open up new opportunities for target therapy development. The CDK8 inhibition is a promising strategy for suppression of the atherosclerotic lesion progression. Further research should be focused on clarifying the cell-specific CDK8 mechanisms of actions in various populations of vascular wall cells and assessment of the CDK8 selective inhibitor efficacy in pre-clinical trials.

References

1. Kosolapov VP, YArmonova MV. Analiz vysokoj serdechno-sosudistoj zabolevaemosti i smertnosti vzroslogo naseleniya kak mediko-social'noj problemy i poisk putej ee resheniya. Ural'skij medicinskij zhurnal. 2021; 20 (1): 58–64. Russian.
2. Moriya J. Critical roles of inflammation in atherosclerosis. Journal of cardiology. 2019; 73 (1): 22–7.
3. Zhong J, Shi G. Regulation of inflammation in chronic disease. Frontiers in Immunology. 2019; 10: 737.
4. Hetherington I, Totary-Jain H. Anti-atherosclerotic therapies: milestones, challenges, and emerging innovations. Molecular Therapy. 2022; 30 (10): 3106–17.
5. Madaudo C, Coppola G, Parlati AL, Corrado E. Discovering inflammation in atherosclerosis: insights from pathogenic pathways to clinical practice. International journal of molecular sciences. 2024; 25 (11): 6016.
6. Yamamoto S, Hagihara T, Horiuchi Y, Okui A, Wani S, Yoshida T, et al. Mediator cyclin-dependent kinases upregulate transcription of inflammatory genes in cooperation with NF-κB and C/EBP β on stimulation of Toll-like receptor 9. Genes to Cells. 2017; 22 (3): 265–76.
7. Kokinos EK, Tsymbal SA, Galochkina AV, Bezlepkina SA, Nikolaeva JV, Vershinina SO, et al. Inhibition of cyclin-dependent kinases 8/19 restricts bacterial and virus-induced inflammatory responses in monocytes. Viruses. 2023; 15 (6): 1292.
8. Dannappel MV, Sooraj D, Loh JJ, Firestein R. Molecular and in vivo functions of the CDK8 and CDK19 kinase modules. Frontiers in cell and developmental biology. 2019; 6: 171.
9. Galbraith MD, Allen MA, Bensard CL, Wang X, Schwinn MK, Qin B et al. HIF1A employs CDK8-mediator to stimulate RNAPII elongation in response to hypoxia. Cell. 2013; 153 (6): 1327–39.
10. Knutson AK, Williams AL, Boisvert WA, Shohet RV. HIF in the heart: development, metabolism, ischemia, and atherosclerosis. The Journal of Clinical Investigation. 2021; 131 (17).
11. Liang X, Arullampalam P, Yang Z, Ming XF. Hypoxia enhances endothelial intercellular adhesion molecule 1 protein level through upregulation of arginase type II and mitochondrial oxidative stress. Frontiers in physiology. 2019; 10: 1003.
12. Ortiz-Masia D, Díez I, Calatayud S, Hernandez C, Cosín-Roger J, Hinojosa J et al. Induction of CD36 and thrombospondin-1 in macrophages by hypoxia-inducible factor 1 and its relevance in the inflammatory process. PLoS One. 2012; 7 (10): e48535.
13. Thomas C, Leleu D, Masson D. Cholesterol and HIF-1α: dangerous liaisons in atherosclerosis. Frontiers in immunology. 2022; 13: 868958.
14. Yin X, He Z, Chen K, Ouyang K, Yang C, Li J, et al. Unveiling the impact of CDK8 on tumor progression: mechanisms and therapeutic strategies. Frontiers in Pharmacology. 2024; 15: 1386929.
15. Roninson I, Győrffy B, Mack ZT, Shtil AA, Shtutman MS, Chen M, et al. Identifying Cancers for CDK8/19 Inhibitor Therapy. Cells. 2019; 8 (8).
16. Arnett A, Moo KG, Flynn KJ, Sundberg TB, Johannessen L, Shamji AF, et al. The cyclin-dependent kinase 8 (CDK8) inhibitor DCA promotes a tolerogenic chemical immunophenotype in CD4+ T cells via a novel CDK8-GATA3-FOXP3 pathway. Molecular and cellular biology. 2021; 41 (9): e00085–21.
17. Lo Sasso G, Schlage WK, Boué S, Veljkovic E, Peitsch MC, Hoeng J. The Apoe−/− mouse model: a suitable model to study cardiovascular and respiratory diseases in the context of cigarette smoke exposure and harm reduction. Journal of translational medicine. 2016; 14 (1): 146.
18. Bruter AV, Varlamova EA, Stavskaya NI, Antysheva ZG, Manskikh VN, Tvorogova AV, et al. Knockout of cyclin-dependent kinases 8 and 19 leads to depletion of cyclin C and suppresses spermatogenesis and male fertility in mice. Elife. 2025; 13: RP96465.
19. Deuchar GA, McLean D, Hadoke PW, Brownstein DG, Webb DJ, Mullins JJ, et al. 11β-hydroxysteroid dehydrogenase type 2 deficiency accelerates atherogenesis and causes proinflammatory changes in the endothelium in apoe−/− mice. Endocrinology. 2011; 152 (1): 236–46.
20. Ilchuk LA, Stavskaya NI, Varlamova EA, Khamidullina AI, Tatarskiy VV, Mogila VA, et al. Limitations of tamoxifen application for in vivo genome editing using Cre/ERT2 system. International journal of molecular sciences. 2022; 23 (22): 14077.
21. Hasegawa Y, Chen SY, Sheng L, Jena PK, Kalanetra KM, Mills DA, et al. Long-term effects of western diet consumption in male and female mice. Scientific reports. 2020; 10 (1): 14686.
22. Chen PY, Qin L, Simons M. Imaging and analysis of oil red o-stained whole aorta lesions in an aneurysm hyperlipidemia mouse model. Journal of visualized experiments: JoVE. 2022; (183): 10–3791.
23. Milutinović A, Šuput D, Zorc-Pleskovič R. Pathogenesis of atherosclerosis in the tunica intima, media, and adventitia of coronary arteries: An updated review. Bosnian journal of basic medical sciences. 2020; 20 (1): 21.
24. Bontzos G, Detorakis ET. Animal models of uveal melanoma for localized interventions. Critical Reviews™ in Oncogenesis. 2017; 22 (3–4).
25. Chen W, Li Z, Zhao Y, Chen Y, Huang R. Global and national burden of atherosclerosis from 1990 to 2019: trend analysis based on the Global Burden of Disease Study 2019. Chinese Medical Journal. 2023; 136 (20): 2442–50.
26. Guo Z, Wang G, Lv Y, Wan YY, Zheng J. Inhibition of Cdk8/Cdk19 Activity Promotes Treg Cell Differentiation and Suppresses Autoimmune Diseases. Front Immunol. 2018; 10: 1988.
27. Chen M, Li J, Liang J, et al. Systemic Toxicity Reported for CDK8/19 Inhibitors CCT251921 and MSC2530818 Is Not Due to Target Inhibition. Cells. 2019; 8 (11): 1413.
28. Hall DD, Ponce JM, Chen B, Spitler KM, Alexia A, Oudit GY, et al. Ectopic expression of Cdk8 induces eccentric hypertrophy and heart failure. JCI insight. 2017; 2 (15): e92476.
29. Neznamov AN, Baykova YP, Kubekina MV. The Role of CDKs in the Regulation of the Monocyte/Macrophage Immune Response. Curr Med Chem. Published online May 29, 2025.

Литература

1. Косолапов В. П., Ярмонова М. В.. Анализ высокой сердечно-сосудистой заболеваемости и смертности взрослого населения как медико-социальной проблемы и поиск путей ее решения. Уральский медицинский журнал. 2021; 20 (1): 58–64.
2. Moriya J. Critical roles of inflammation in atherosclerosis. Journal of cardiology. 2019; 73 (1): 22–7.
3. Zhong J, Shi G. Regulation of inflammation in chronic disease. Frontiers in Immunology. 2019; 10: 737.
4. Hetherington I, Totary-Jain H. Anti-atherosclerotic therapies: milestones, challenges, and emerging innovations. Molecular Therapy. 2022; 30 (10): 3106–17.
5. Madaudo C, Coppola G, Parlati AL, Corrado E. Discovering inflammation in atherosclerosis: insights from pathogenic pathways to clinical practice. International journal of molecular sciences. 2024; 25 (11): 6016.
6. Yamamoto S, Hagihara T, Horiuchi Y, Okui A, Wani S, Yoshida T, et al. Mediator cyclin-dependent kinases upregulate transcription of inflammatory genes in cooperation with NF-κB and C/EBP β on stimulation of Toll-like receptor 9. Genes to Cells. 2017; 22 (3): 265–76.
7. Kokinos EK, Tsymbal SA, Galochkina AV, Bezlepkina SA, Nikolaeva JV, Vershinina SO, et al. Inhibition of cyclin-dependent kinases 8/19 restricts bacterial and virus-induced inflammatory responses in monocytes. Viruses. 2023; 15 (6): 1292.
8. Dannappel MV, Sooraj D, Loh JJ, Firestein R. Molecular and in vivo functions of the CDK8 and CDK19 kinase modules. Frontiers in cell and developmental biology. 2019; 6: 171.
9. Galbraith MD, Allen MA, Bensard CL, Wang X, Schwinn MK, Qin B et al. HIF1A employs CDK8-mediator to stimulate RNAPII elongation in response to hypoxia. Cell. 2013; 153 (6): 1327–39.
10. Knutson AK, Williams AL, Boisvert WA, Shohet RV. HIF in the heart: development, metabolism, ischemia, and atherosclerosis. The Journal of Clinical Investigation. 2021; 131 (17).
11. Liang X, Arullampalam P, Yang Z, Ming XF. Hypoxia enhances endothelial intercellular adhesion molecule 1 protein level through upregulation of arginase type II and mitochondrial oxidative stress. Frontiers in physiology. 2019; 10: 1003.
12. Ortiz-Masia D, Díez I, Calatayud S, Hernandez C, Cosín-Roger J, Hinojosa J et al. Induction of CD36 and thrombospondin-1 in macrophages by hypoxia-inducible factor 1 and its relevance in the inflammatory process. PLoS One. 2012; 7 (10): e48535.
13. Thomas C, Leleu D, Masson D. Cholesterol and HIF-1α: dangerous liaisons in atherosclerosis. Frontiers in immunology. 2022; 13: 868958.
14. Yin X, He Z, Chen K, Ouyang K, Yang C, Li J, et al. Unveiling the impact of CDK8 on tumor progression: mechanisms and therapeutic strategies. Frontiers in Pharmacology. 2024; 15: 1386929.
15. Roninson I, Győrffy B, Mack ZT, Shtil AA, Shtutman MS, Chen M, et al. Identifying Cancers for CDK8/19 Inhibitor Therapy. Cells. 2019; 8 (8).
16. Arnett A, Moo KG, Flynn KJ, Sundberg TB, Johannessen L, Shamji AF, et al. The cyclin-dependent kinase 8 (CDK8) inhibitor DCA promotes a tolerogenic chemical immunophenotype in CD4+ T cells via a novel CDK8-GATA3-FOXP3 pathway. Molecular and cellular biology. 2021; 41 (9): e00085–21.
17. Lo Sasso G, Schlage WK, Boué S, Veljkovic E, Peitsch MC, Hoeng J. The Apoe−/− mouse model: a suitable model to study cardiovascular and respiratory diseases in the context of cigarette smoke exposure and harm reduction. Journal of translational medicine. 2016; 14 (1): 146.
18. Bruter AV, Varlamova EA, Stavskaya NI, Antysheva ZG, Manskikh VN, Tvorogova AV, et al. Knockout of cyclin-dependent kinases 8 and 19 leads to depletion of cyclin C and suppresses spermatogenesis and male fertility in mice. Elife. 2025; 13: RP96465.
19. Deuchar GA, McLean D, Hadoke PW, Brownstein DG, Webb DJ, Mullins JJ, et al. 11β-hydroxysteroid dehydrogenase type 2 deficiency accelerates atherogenesis and causes proinflammatory changes in the endothelium in apoe−/− mice. Endocrinology. 2011; 152 (1): 236–46.
20. Ilchuk LA, Stavskaya NI, Varlamova EA, Khamidullina AI, Tatarskiy VV, Mogila VA, et al. Limitations of tamoxifen application for in vivo genome editing using Cre/ERT2 system. International journal of molecular sciences. 2022; 23 (22): 14077.
21. Hasegawa Y, Chen SY, Sheng L, Jena PK, Kalanetra KM, Mills DA, et al. Long-term effects of western diet consumption in male and female mice. Scientific reports. 2020; 10 (1): 14686.
22. Chen PY, Qin L, Simons M. Imaging and analysis of oil red o-stained whole aorta lesions in an aneurysm hyperlipidemia mouse model. Journal of visualized experiments: JoVE. 2022; (183): 10–3791.
23. Milutinović A, Šuput D, Zorc-Pleskovič R. Pathogenesis of atherosclerosis in the tunica intima, media, and adventitia of coronary arteries: An updated review. Bosnian journal of basic medical sciences. 2020; 20 (1): 21.
24. Bontzos G, Detorakis ET. Animal models of uveal melanoma for localized interventions. Critical Reviews™ in Oncogenesis. 2017; 22 (3–4).
25. Chen W, Li Z, Zhao Y, Chen Y, Huang R. Global and national burden of atherosclerosis from 1990 to 2019: trend analysis based on the Global Burden of Disease Study 2019. Chinese Medical Journal. 2023; 136 (20): 2442–50.
26. Guo Z, Wang G, Lv Y, Wan YY, Zheng J. Inhibition of Cdk8/Cdk19 Activity Promotes Treg Cell Differentiation and Suppresses Autoimmune Diseases. Front Immunol. 2018; 10: 1988.
27. Chen M, Li J, Liang J, et al. Systemic Toxicity Reported for CDK8/19 Inhibitors CCT251921 and MSC2530818 Is Not Due to Target Inhibition. Cells. 2019; 8 (11): 1413.
28. Hall DD, Ponce JM, Chen B, Spitler KM, Alexia A, Oudit GY, et al. Ectopic expression of Cdk8 induces eccentric hypertrophy and heart failure. JCI insight. 2017; 2 (15): e92476.
29. Neznamov AN, Baykova YP, Kubekina MV. The Role of CDKs in the Regulation of the Monocyte/Macrophage Immune Response. Curr Med Chem. Published online May 29, 2025.

SINGLE NUCLEOTIDE VARIANT *rs293795 OGG1* AS A GENETIC RISK FACTOR FOR DIABETIC NEPHROPATHY

Semikina EV, Azarova IE ✉, Panichev SA, Basareva OI, Dzhanchatova NV, Alferova EYu, AV Polonikov

Kursk State Medical University, Kursk, Russia

Diabetic nephropathy (DNP) is a serious complication of type 2 diabetes mellitus (T2DM), leading to early disability and mortality from end-stage renal failure. Experimental and clinical studies have shown the leading role of oxidative stress-induced damage to macromolecules, including DNA, in the development and progression of DNP against the background of hyperglycemia. On the contrary, repair of this damage serves as a signal to stop ongoing oxidative stress. The key enzyme in DNA repair is 8-oxoguanine DNA glycosylase, encoded by the *OGG1* gene. The aim of this study was to analyze the associations of five polymorphic variants rs2072668, rs1052133, rs293795, rs2304277, rs6443265 of the *OGG1* gene with the risk of developing DNP in patients with T2DM. The study included 1461 patients with type 2 diabetes, 577 of whom were diagnosed with DNP. DNA genotyping was performed using real-time polymerase chain reaction (RT-PCR) with allele-specific fluorescent probes. Associations were established between the rs293795-G/G genotype (OR = 1.97, 95% CI = 1.23–3.16, p = 0.007) and the rs2072668C-rs1052133C-rs293795G-rs2304277G-rs6443265C haplotype (OR = 1.30, 95% CI = 1.06–1.60, p = 0.012) of the *OGG1* gene with a predisposition to DNP in patients with T2DM. In addition, 6 *OGG1* diplotypes associated with an increased risk of DNP and one diplotype associated with a reduced risk of DNP in patients with T2DM were identified. Thus, the study presents for the first time data on the association of the *OGG1* gene polymorphism with DNP, which creates a scientific foundation for further research on the contribution of disturbances in the DNA oxidative damage repair system to the development of microvascular complications of T2DM.

Keywords: DNA glycosylases, DNA repair, *OGG1*, genetic predisposition, genotyping methods, real-time PCR, type 2 diabetes mellitus, diabetic nephropathy

Funding: the study was supported by a grant from the Russian Science Foundation (project No. 25-25-20072) and the Ministry of Education and Science of the Kursk Region (agreement No. 241 dated May 19, 2025).

Author contribution: Semikina EV — genotyping of DNA samples, analysis of obtained data, writing of the text; Azarova YuE — concept and design of the study, fundraising, collection and processing of materials, writing of the text; Panichev SA — genotyping of DNA samples, entering genotyping results into the database; Basareva OI — selection of functionally significant polymorphic variants of the OGG1 gene, selection of primers and probes for SNP genotyping; Dzhanchatova NV — genotyping of DNA samples; Alferova EYu — sample preparation: DNA extraction from blood, measurement of concentration and purity of DNA samples; Polonikov AV — analyzed the data, reviewed the literature, and made final edits. The authors approved the version for publication and agreed to be accountable for all aspects of the work, ensuring that any questions related to the accuracy and integrity of any part of it are properly reviewed and resolved.

Compliance with ethical standards: the study was approved by the Regional Ethics Committee at Kursk State Medical University (meeting minutes No. 1 dated January 20, 2025).

✉ **Correspondence should be addressed:** Iuliia E. Azarova
Yamskaya, 18, Kursk, 305041, Russia;Email: azzzzar@yandex.ru

Received: 21.11.2025 **Accepted:** 19.12.2025 **Published online:** 24.12.2025

DOI: 10.24075/brsmu.2025.084

Copyright: © 2025 by the authors. **Licensee:** Pirogov University. This article is an open access article distributed under the terms and conditions of the Creative Commons Attribution (CC BY) license (https://creativecommons.org/licenses/by/4.0/).

ОДНОНУКЛЕОТИДНЫЙ ВАРИАНТ *rs293795 OGG1* КАК ГЕНЕТИЧЕСКИЙ ФАКТОР РИСКА ДИАБЕТИЧЕСКОЙ НЕФРОПАТИИ

Е. В. Семикина, Ю. Э. Азарова ✉, С. А. Паничев, О. И. Басарева, Н. В. Джанчатова, Е. Ю. Алферова, А. В. Полоников

Курский государственный медицинский университет, Курск, Россия

Диабетическая нефропатия (ДНФ) — грозное осложнение сахарного диабета 2-го типа (СД2), приводящее к ранней инвалидности и смертности от терминальной почечной недостаточности. В экспериментальных и клинических исследованиях показана ведущая роль индуцированных окислительным стрессом повреждений макромолекул, в том числе ДНК, в развитии и прогрессировании ДНФ на фоне гипергликемии. Восстановление этих повреждений служит сигналом для прекращения продолжающегося окислительного стресса. Ключевым ферментом репарации ДНК является 8-оксогуанин-ДНК-гликозилаза, кодируемая геном *OGG1*. Целью работы было провести анализ ассоциаций пяти полиморфных вариантов rs2072668, rs1052133, rs293795, rs2304277, rs6443265 гена *OGG1* с риском развития ДНФ у пациентов с СД2. В исследование включен 1461 пациент с СД2, у 577 из которых диагностирована ДНФ. Генотипирование ДНК выполнено методом полимеразно-цепной реакции в реальном времени с использованием аллель-специфичных флуоресцентно-меченых зондов. Установлены ассоциации генотипа rs293795-G/G (OR = 1,97, 95% CI = 1,23-3,16; p = 0,007) и гаплотипа rs2072668C-rs1052133C- rs293795G-rs2304277G-rs6443265C (OR = 1,30, 95% CI = 1,06–1,60; p = 0,012) гена *OGG1* с предрасположенностью к ДНФ на фоне СД2. Кроме того, установлено шесть диплотипов *OGG1*, ассоциированных с повышенным риском ДНФ, и один диплотип, ассоциированный с пониженным риском ДНФ у пациентов с СД2. Таким образом, в проведенном исследовании представлены данные об ассоциации полиморфизма гена *OGG1* с ДНФ, что создает научный потенциал для дальнейших работ по изучению вклада нарушений системы репарации окислительных повреждений ДНК в развитие микрососудистых осложнений СД2.

Ключевые слова: ДНК-гликозилазы, репарация ДНК, *OGG1*, генетическая предрасположенность, методы генотипирования, ПЦР в реальном времени, сахарный диабет 2-го типа, диабетическая нефропатия

Финансирование: исследование выполнено за счет гранта Российского научного фонда (проект № 25-25-20072) и Министерства образования и науки Курской области (соглашение №241 от 19.05.2025).

Вклад авторов: Е. В. Семикина — генотипирование образцов ДНК, анализ полученных данных, написание текста; Ю. Э. Азарова — концепция и дизайн исследования, привлечение финансирования, сбор и обработка материалов, написание текста; С. А. Паничев — генотипирование образцов ДНК, внесение результатов генотипирования в базу данных; О. И. Басарева — отбор функционально значимых полиморфных вариантов гена OGG1, подбор праймеров и зондов для генотипирования SNP; Н. В. Джанчатова — генотипирование образцов ДНК; Е. Ю. Алферова — пробоподготовка: экстракция ДНК из крови, измерение концентрации и чистоты образцов ДНК; А. В. Полоников — анализ полученных данных, обзор литературы, редактирование.

Соблюдение этических стандартов: исследование одобрено этическим комитетом Курского государственного медицинского университета (протокол № 1 от 20 января 2025 г.). Все участники подписали добровольное информированное согласие на участие в исследовании.

✉ **Для корреспонденции:** Юлия Эдуардовна Азарова
ул. Ямская, д. 18, г. Курск, 305041, Россия; azzzzar@yandex.ru

Статья получена: 21.11.2025 **Статья принята к печати:** 19.12.2025 **Опубликована онлайн:** 24.12.2025

DOI: 10.24075/vrgmu.2025.084

Авторские права: © 2025 принадлежат авторам. **Лицензиат:** РНИМУ им. Н. И. Пирогова. Статья размещена в открытом доступе и распространяется на условиях лицензии Creative Commons Attribution (CC BY) (https://creativecommons.org/licenses/by/4.0/).

Type 2 diabetes mellitus (T2DM) is the most common endocrine metabolic disorder worldwide [1]. Over the past 20 years, the number of people with T2DM worldwide has increased almost fourfold, from 151 million in 2000 to 589 million in 2025. More than 8.2 million people with T2DM live in the Russian Federation [2].

It is known that type 2 diabetes is one of the leading risk factors for the development of stroke and myocardial infarction, and is also the main cause of vision loss, non-traumatic amputations and the development of end-stage renal failure [3]. Diabetic nephropathy (DNP) is a clinical syndrome characterized by persistent albuminuria and progressive decline in renal function [4]. The mechanisms of DNP development are very complex, and despite decades of intensive research, the pathogenesis of this complication is still not fully understood [5–7]. It is known that numerous pathways and processes, such as oxidative stress, activation of the renin-angiotensin-aldosterone system, mitogen-activated protein kinases, formation of advanced glycation end products, excessive production of connective tissue growth factors and proinflammatory cytokines contribute to the development and progression of kidney damage in type 2 diabetes [8].

Recent genetic and biochemical studies in humans and animal models have confirmed the necessity of coordinated work of repair enzymes for cell survival under conditions of oxidative stress [9–12]. Excessive production of reactive oxygen species in the context of nutrient overload in overweight and obese patients can cause significant damage to any cellular macromolecules, especially DNA: It has been estimated that on average, 10,000 DNA damages occur per cell in the human body in 24 hours, with oxidative DNA damage being the most prevalent [13]. The structures of all four DNA nitrogenous bases are susceptible to oxidative damage when exposed to reactive oxygen species, and more than one hundred different types of oxidative base damage have been identified, including products with cleavage of heterocycles and the formation of oxidized aromatic derivatives [14–15]. Changes in the structure of nitrogenous bases as a result of oxidative damage alter their ability to form hydrogen bonds with a partner base during the synthesis of a complementary chain, which serves as a major source of mutations and the cause of disruption of gene expression [16].

In most cases, DNA repair mechanisms, including base excision repair, nucleotide excision repair, direct reversible repair, mismatch repair, and homologous recombination, correct the damage that has occurred and maintain cellular homeostasis [17]. Base excision repair is most effective in repairing endogenous oxidative damage to purines or pyrimidines of DNA and occurs with the use of DNA glycosylases such as mutY DNA glycosylase *MUTYH*, nth-like DNA glycosylase 1 *NTHL1*, 8-oxoguanine DNA glycosylase *OGG1* or nei-like DNA glycosylase 1 *NEIL1*, which recognize the aberrant nitrogenous base and excise it [18].

Of the four nitrogenous bases in DNA, guanine is the most frequently subject to oxidation [19]. The enzyme 8-oxoguanine DNA glycosylase *OGG1* has the ability to remove 8-oxoguanine and 2,6-diamino-4-hydroxy-5-N-methylformamidopyrimidine, being part of a complex system for repairing oxidative damage to guanine in DNA [20–21]. In an experimental study by Kumar V., a decrease in the efficiency of reparation processes in type 2 diabetes was demonstrated, which leads to cell aging, activation of inflammation, and ultimately, to fibrosis of the kidneys and lungs [22]. A genetically determined defect in the elimination of aberrant guanine in carriers of the 8-oxoguanine DNA glycosylase gene rs1052133 is associated with T2DM in Mexican Americans [23] and Japanese [24], however, in general, studies of the role of genes for the repair of oxidative DNA damage in the development of T2DM and its complications are few in number, contradictory, lack systemic coverage, were performed on small samples, and are poorly reproducible in replicative studies.

The aim of this study is to analyze the associations of five polymorphic variants rs2072668, rs1052133, rs293795, rs2304277, rs6443265 of the *OGG1* gene with the risk of developing DNP in patients with T2DM.

METHODS

Characteristics of the Study Subjects

The study was conducted in accordance with the international STREGA (STrengthening the REporting of Genetic Association Studies) guidelines on an ethnically homogeneous sample (1,461 individuals) of unrelated residents of Central Russia (primarily natives of the Kursk region) of Slavic origin. The study was carried out in accordance with the international STREGA (STrengthening the REporting of Genetic Association Studies) recommendations on an ethnically homogeneous sample (1461 people) of unrelated residents of Central Russia (mainly natives of the Kursk region) of Slavic origin. Based on written informed consent, 1,461 patients with type 2 diabetes (486 men and 975 women) were included in the study, receiving inpatient treatment in the endocrinology department of the Kursk City Clinical Emergency Hospital. The diagnosis of type 2 diabetes was established based on WHO criteria [25]. The inclusion criteria for the patient group were: a physician-verified diagnosis of the disease, confirmed by clinical and laboratory-instrumental methods, age over 35 years, and written informed consent to participate in the study. The criteria for exclusion of patients from the main sample were: severe decompensation of type 2 diabetes or coma, the presence of immune-mediated or idiopathic type 1 diabetes, the presence of gestational diabetes, the presence of specific types of diabetes, such as MODY, diseases of the exocrine pancreas — pancreatitis, trauma or pancreatectomy, pancreatic tumors, cystic fibrosis, hemochromatosis, fibrocalculous pancreatopathy, endocrinopathies (acromegaly, Cushing's syndrome, glucagonoma, pheochromocytoma, hyperthyroidism, somatostatinoma, aldosteronoma), hereditary diseases combined with diabetes (Down syndrome, Friedreich's ataxia, Huntington's chorea, Klinefelter syndrome, Lawrence–Moon–Biedl syndrome, myotonic dystrophy, porphyria, Prader–Willi syndrome, Turner syndrome), the onset of the disease before the age of 35, as well as the absence of written informed consent to participate in the project, were excluded. 577 patients with type 2 diabetes (110 men and 467 women) were diagnosed with DNP. Clinical and laboratory characteristics of the study participants are presented in Table 1.

Patients with DNP had higher body mass index, fasting blood glucose, and a longer duration of T2DM. The glomerular filtration rate (GFR), calculated using the CKD-EPI formula, was significantly lower in this group of patients than in patients with T2DM without DNP ($p < 0.0001$). DNA extraction and genotyping. A 5 ml sample of fasting venous blood was collected from all study participants into Vacuette tubes containing EDTA as an anticoagulant. Genomic DNA of 1461 blood samples of patients with type 2 diabetes from the biobank of the Research Institute of Genetic and Molecular Epidemiology of KSMU was isolated by the column method using Biolabmix reagent kits (Russia). The quality of the isolated DNA was assessed by the degree of purity and concentration of the solution using a

Table 1. Demographic, clinical and biochemical characteristics of patients with type 2 diabetes

Basic characteristics	Patients with type 2 diabetes without DNP, *n* = 884	Patients with type 2 diabetes with DNP, *n* = 577	*p*
Age, average ± SD	58.88 ± 10.31	66.21 ± 8.54	< 0.0001
Men, *n* (%)	376 (42.5)	110 (19.1)	< 0.0001
Women, *n* (%)	508 (57.5)	467 (80.9)	
ИBody mass index (kg/m^2), average value ± SD	31.65 ± 6.87	33.18 ± 6.30	< 0.0001
Duration of diabetes, Me (Q_1; Q_3)	7.0 (2.0; 12.0)	11.0 (6.0; 17.0)	< 0.0001
HbA_{1c} (%), Me (Q_1; Q_3)	9.0 (7.7; 10.5)	9.2 (7.8; 11.0)	0.09
Fasting blood glucose (mmol/L), Me (Q_1; Q_3)	12.0 (9.5; 15.0)	12.6 (10.0; 15.9)	0.026
Total cholesterol (mmol/L), Me (Q_1; Q_3)	5.02 (4.18; 5.90)	5.24 (4.33; 6.31)	0.0047
LDL (mmol/L),Me (Q_1; Q_3)	3.17 (2.50; 4.11)	3.10 (2.40; 4.07)	0.51
HDL (mmol/L), Me (Q_1; Q_3)	0.84 (0.72; 1.03)	0.85 (0.74; 1.03)	0.18
Triacylglycerols (mmol/l),Me (Q_1; Q_3)	2.12 (1.54; 2.82)	2.25 (1.55; 3.10)	0.14
SCF, ml/min /1,72м^2, Me (Q_1; Q_3)	73.7 (65.0; 83.6)	48.47 (43.0; 54.1)	< 0.0001

Note: Me (Q_1;Q_3) — median, first and third quartiles; GFR — glomerular filtration rate (CKD-EPI); LDL — low-density lipoproteins; HDL — high-density lipoproteins.

NanoDrop spectrophotometer (Thermo Fisher Scientific, USA). All analyzed DNA samples were diluted with deionized water to a concentration of 10 ng/µl at A260/280 = 1.5–2.0.

The selection of single nucleotide polymorphisms (SNPs) in the *OGG1* DNA glycosylase gene was performed using the Ensembl genome browser (https://www.ensembl.org/index.html) and the bioinformatics tools of the SNPinfo web server (https://snpinfo.niehs.nih.gov/), including GenePipe, FuncPred and TagSNP, the atSNP resource (http://atsnp.biostat.wisc.edu/) and was based on the assessment of the haplotype structure of the gene (selection of tagSNPs, r2 ≥ 0.8), the minor allele frequency (MAF > 5%) in the European populations of the HapMap project, parameters necessary for the most complete coverage of gene variability and the inclusion of functionally significant polymorphic loci that have regulatory potential and are capable of influencing the binding of transcription factors and microRNAs, splicing and/or the activity of the protein product of the *OGG1* gene. All five selected variants rs2072668, rs1052133, rs293795, rs2304277, rs6443265 affected the affinity of transcription factors in the corresponding DNA regions, rs1052133 and rs293795 are located in the microRNA binding sites. SNP rs2072668 (C>G) is a splicing variant of the polypyrimidine tract, rs1052133 (C>G) is a missense variant resulting in the substitution of serine for cysteine at position 326 of the protein, rs293795 (A>G) and rs6443265 (T>C) are located in the introns of the *OGG1* gene, rs2304277 (G>A) is in the non-coding transcript exon of *OGG1*.

Primer3web version 4.1.0 (https://primer3.ut.ee/) was used to design primers. Sequences of allele-specific fluorescently labeled probes were selected based on the nucleotide sequence of the *OGG1* gene (https://www.ensembl.org/Homo_sapiens/Gene/Sequence?db=core;g=ENSG00000114026; *r* = 3:9749944-9788219). The primers and probes presented in Table 2 were synthesized by Syntol (Moscow).

The total volume of the reaction mixture was 14.25 µl. 13.25 µl of the PCR mixture containing 9.4 µl of ddH2O, 1.3 µl of $MgCl_2$ solution (Eurogen, mass concentration 2.5%), 1.3 µl of PCR buffer (Biolabmix), 0.2 µl of dNTP mixture (Eurogen, concentration 2 mmol/l) were added to 1 µl of DNA solution with a concentration of 10 ng/µl., 0.05 µl of forward and reverse primer solution (concentration 100 pmol/µl), 0.025 µl of each TaqMan probe solution (concentration 100 pmol/µl) and 0.11 µl of Taq DNA polymerase (Biolabmix) with hot start (concentration 5 U/µl). PCR was performed using a CFX96 Real-Time System (Bio-Rad) using the following mode: 10 min at 95 °C, amplification of 38 cycles, including 15 sec at 95 °C, 30 s at *t* = 53 °C and 60 s at an experimentally selected annealing temperature, individual for each SNP (Table 2).

Identification of the reference and minor alleles of the studied SNPs was carried out based on a comparison of the fluorescence intensity of FAM and ROX dyes, respectively. The analysis of genotyping results was performed using the software for the CFX96 Real-Time System (Bio-Rad) amplifier, version Bio-Rad CFX Manager 2.1, which presents the genotyping results as an allele distribution. Figure 1 shows an example of genotype detection for the rs2304277 locus of the *OGG1* gene: rs2304277-G/G genotypes are shown in orange, rs2304277-G/A genotypes are shown in green, rs2304277-A/A genotypes are shown in blue, and the negative control is shown in black diamond.

Concentrations of glucose, glycated hemoglobin, creatinine, triglycerides, total cholesterol and its subfractions were determined using Diakon-DS kits on a Clima MC-15 semi-automatic biochemical analyzer (RAL, Spain). For functional annotation of DNA variants, the following online resources were used: GTEx Portal (https://www.gtexportal.org/home/), atSNP (http://atsnp.biostat.wisc.edu/), Gene Ontology Resource (https://geneontology.org/), mQTLdb [https://www.mqtldb.org/] and VannoPortal (http://www.mulinlab.org/vportal/index.html).

Statistical data processing. The analysis of associations of the studied SNPs and haplotypes with the risk of DNP was performed using the logistic regression method with adjustment for gender, age, and BMI using the SNPStats program [26]. The analysis of associations of *OGG1* diplotypes with DNP, as well as the calculation of quantitative indicators, was carried out using the STATISTICA v10.0 program. An association was considered significant at $p < 0.05$. The Kolmogorov–Smirnov test was used to test the normal distribution of biochemical parameters. Normally distributed variables were described using the mean and standard deviation. The Student's *t*-test was used to test statistical significance. Non-normally distributed variables were described using the median (Median), first (Q_1), and third (Q_3) quartiles, as follows: Median [Q_1; Q_3]. The Mann–Whitney test was used to test statistical significance in such cases. Differences between groups were considered statistically significant at $p < 0.05$.

RESULTS

The studied SNPs were in accordance with the Hardy–Weinberg equilibrium ($p > 0.05$). The results of the association analysis of

Table 2. Sequences of primers and allele-specific fluorescent probes for genotyping by real-time PCR

Gene	SNP	Oligo-nucleotide	Primer/probe sequence	*t* annealing in PCR
OGG1	rs2072668 C>G	F	5'-ACAGTAACCCCAGAGTGAAGG-3'	55 °C
		R	5'-CCTGGGGCTTGTCTAGGG-3'	
		FAM	5'-FAM-CCACAAGGGCTCATTC-RTQ1-3'	
		ROX	5'-ROX-CCACAAGGGCTCATTG-BHQ-3'	
	rs1052133 C>G	F	5'-CTAGTCTCACCAGCCCTGAC-3'	56 °C
		R	5'-GTGCCCCATCTAGCCTTCC-3'	
		FAM	5'-FAM-CCGACCTGCGCCAATC-RTQ1-3'	
		ROX	5'-ROX-CCGACCTGCGCCAATG-BHQ-3'	
	rs293795 A>G	F	5'-AGACAGCGCTAAGGATGGTT-3'	56 °C
		R	5'-CTCCCCTTCCCTCCCTGAA-3'	
		FAM	5'-FAM-TGAGGAGTGGTAGGGAA-RTQ1-3'	
		ROX	5'-ROX-TGAGGAGTGGTAGGGAG-BHQ-3'	
	rs2304277 G>A	F	5'-TCTGGAATAGAGAAGGTGTTGGG-3'	56 °C
		R	5'-GGACTCCTCCCCATCCCTA-3'	
		FAM	5'-FAM-AGTTACTGTGTGCCCAG-RTQ1-3'	
		ROX	5'-ROX-AGTTACTGTGTGCCCAA-BHQ-3'	
	rs6443265 T>C	F	5'-AGAGACTTGTTCGGGTTGCT-3'	54 °C
		R	5'-GGGAATCCATCACAGTGCCT-3'	
		FAM	5'-FAM-ATGTCACCTATACCCTT-RTQ1-3'	
		ROX	5'-ROX-ATGTCACCTATACCCTC-BHQ-3'	

Note: F — forward primer, R — reverse primer, FAM — reference allele-specific fluorescently labeled probe, ROX — minor allele-specific fluorescently labeled probe.

polymorphic variants of the *OGG1* gene with DNP are presented in Table 3. As can be seen from Table 3, the rs293795-G/G genotype (OR = 1.97, 95% CI = 1.23–3.16, $p = 0.007$) of OGG1 was associated with an increased risk of DNP in the background of T2DM, regardless of the gender, age, and body mass index of patients.

At the next stage, an analysis of associations of paired combinations of *OGG1* genotypes (diplotypes) with predisposition to DNP was performed, the statistically significant results of which are presented in Table 4.

It was found that carriage of the G/G genotype of rs293795 was associated with an increased risk of DNP in combination with the genotypes rs2072668-C/C (OR = 1.68, 95% CI = 1.10–2.56, $p = 0.015$), rs1052133-C/C (OR = 1.64, 95% CI = 1.07–2.51, $p = 0.021$), rs2304277-G/G (OR = 1.68, 95% CI = 1.10–2.56, $p = 0.015$) and rs6443265-C/C (OR = 1.64, 95% CI = 1.06–2.54, $p = 0.025$). The heterozygous genotype rs293795-A/G also determined the risk of DNP in combination with the genotypes rs2072668-C/G (OR = 1.48, 95% CI = 1.06–2.08, $p = 0.022$) and rs1052133-C/G (OR = 1.42, 95% CI = 1.01–1.99, $p = 0.043$), whereas the combination of the homozygous reference allele genotype rs293795-A/A with the genotype rs6443265–T/C had a protective effect against DNP: OR = 0.67, 95% CI = 0.49–0.92, $p = 0.013$ (Table 4).

Linkage disequilibrium (LD) analysis of the studied *OGG1* gene loci (Table 5) showed that rs293795 was in positive linkage disequilibrium with rs6443265 (D = 0.1561, D` = 0.9541, $p < 2 \times 10^{-16}$). At the same time, rs293795 was in negative

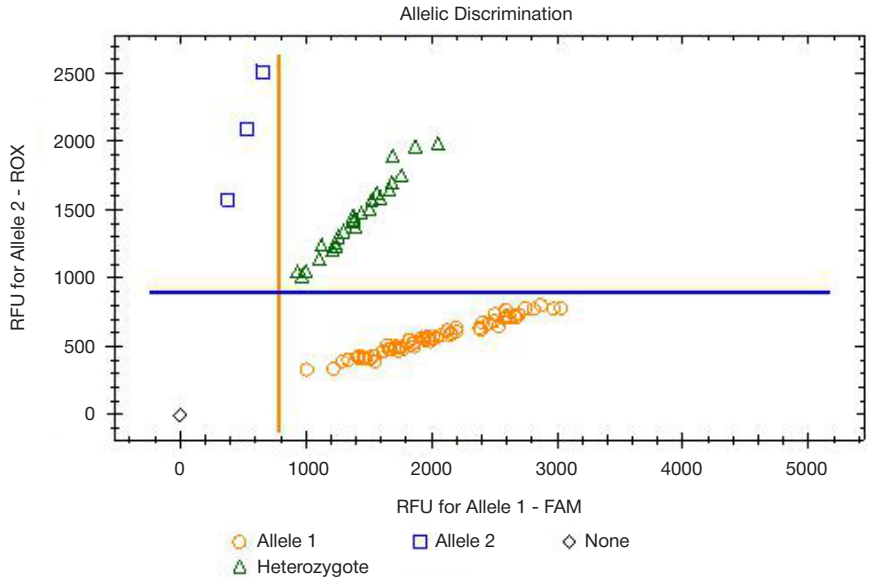


Fig. 1. Distribution of genotypes by locus rs2304277 of the *OGG1* gene

Table 3. Associations of *OGG1* gene polymorphic variants with the risk of developing DNP in patients with type 2 diabetes

SNP ID of the *OGG1* gene	Genotype	Genotype frequencies in patients with type 2 diabetes		OR[2] (95% CI)	*P*[3]
		without DNP *n* (%)[1]	with DNP *n* (%)[1]		
rs2072668 C>G	C/C	561 (63.7%)	350 (63%)	1.00	0.69
	C/G	274 (31.1%)	184 (33.1%)	1.05 (0.82–1.34)	
	G/G	46 (5.2%)	22 (4%)	0.81 (0.45–1.44)	
rs1052133 C>G	C/C	557 (63.4%)	350 (63.1%)	1.00	0.83
	C/G	278 (31.7%)	185 (33.3%)	1.01 (0.78–1.29)	
	G/G	43 (4.9%)	20 (3.6%)	0.83 (0.46–1.53)	
rs293795 A>G	A/A	517 (59%)	288 (51.8%)	1.00	0.007
	A/G	314 (35.8%)	220 (39.6%)	1.28 (1.00–1.63)	
	G/G	45 (5.1%)	48 (8.6%)	1.97 (1.23–3.16)	
rs2304277 G>A	G/G	619 (70.3%)	399 (71.8%)	1.00	0.68
	G/A	228 (25.9%)	140 (25.2%)	0.90 (0.69–1.18)	
	A/A	33 (3.8%)	17 (3.1%)	0.83 (0.43–1.62)	
rs6443265 T>C	T/T	374 (42.5%)	227 (40.8%)	1.00	0.31
	T/C	415 (47.2%)	258 (46.4%)	1.04 (0.81–1.33)	
	C/C	90 (10.2%)	71 (12.8%)	1.35 (0.92–1.99)	

Note: [1] — Absolute number and percentage of individuals with a particular genotype; [2] — Odds ratio and 95% confidence interval of the SNP association with the phenotype, adjusted for sex, age, and BMI; [3] — Significance level of association according to the codominant model, adjusted for sex, age, and BMI.

linkage disequilibrium with rs2072668 (D = –0.0514, D` = 0.9990, $p < 2 \times 10^{-16}$), rs1052133 (D = –0.0512, D` = 0.9989, $p < 2 \times 10^{-16}$) and with rs2304277 (D = –0.0406, D` = 0.9982, $p < 2 \times 10^{-16}$).

Haplotype analysis of the *OGG1* gene revealed five common haplotypes (Table 6). The H2 haplotype rs2072668C-rs1052133C-rs293795G-rs2304277G-rs6443265C, which contains the minor allele rs293795-G, was associated with an increased risk of DNP: OR = 1.30, 95% CI = 1.06–1.60, $p = 0.012$.

In addition, 12 rare *OGG1* haplotypes with a frequency of less than 1% were identified: H6 CCGGT, H7 GGAGC, H8 GGAAC, H9 GCAAT, H10 CGAGC, H11 CCGAT, H12 GCAGT, H13 CGAAT, H14 GGGGT, H15 CCGAC, H16 CCAAC and H17 CGGAC, which (the "rare" column in Table 6) did not affect the risk of DNP in type 2 diabetes ($p < 0.05$).

DISCUSSION

Recovery of oxidized DNA nitrogenous bases is primarily accomplished through the base excision repair pathway [18]. Due to the diversity of sizes and shapes of DNA lesions caused by oxidative stress, a diverse array of DNA glycosylases has evolved to maintain genomic stability and combat various base modifications. Based on their structural characteristics, DNA glycosylases are divided into four superfamilies: 1) uracil DNA glycosylases (UDG, SMUG1, TDG), 2) helix-hairpin-helix (HhH) glycosylases — NTHL1, OGG1 and MUTYH, 3) 3-methylpurine glycosylases (MPG) and 4) endonuclease VIII-like (NEIL) glycosylases — NEIL1, NEIL2 and NEIL3 [27].

The *OGG1* enzyme belongs to the second family and is a β-eliminating bifunctional DNA glycosylase, since it has both glycosylase and lyase activity and is responsible for the removal of the oxidized form of guanine 8-oxo-7,8-dihydro-2′-deoxyguanosine (8-oxoG) [28]. The resulting apurinic (AP) site is recognized by the AP endonuclease APEX1, which initiates repair by cleaving the sugar-phosphate backbone. DNA polymerase beta POLB fills the gap and, forming a complex with the XRCC1 protein and DNA ligase 3 LIG3, inserts the desired complementary base into the AP site [9].

Disruptions in the described reparation process aggravate metabolic disorders that develop during oxidative stress under conditions of chronic hyperglycemia and contribute to cell death. Thus, an immunohistochemical study of autopsy material from the pancreas of patients with type 2 diabetes revealed that a decrease in the volumetric density of beta cells significantly correlated with markers of oxidative DNA damage — 8-oxodG and histone γH2AX phosphorylated at the 139th serine residue, whereas associations with endoplasmic reticulum stress markers C/EBP-β and autophagy impairment

Table 4. Statistically significant associations of *OGG1* gene diplotypes with the risk of developing DNP in patients with type 2 diabetes

Genotype combinations	Patients with type 2 diabetes and DNP[1]		Patients with type 2 diabetes without DNP[1]		*p*[2]	OR (95% CI)[3]
	n	%	*n*	%		
rs293795-G/G × rs2072668-C/C	48	8.35	45	5.14	0.015	1.68 (1.10–2.56)
rs293795-G/G × rs1052133-C/C	47	8.19	45	5.15	0.021	1.64 (1.07–2.51)
rs293795-G/G × rs2304277-G/G	48	8.35	45	5.14	0.015	1.68 (1.10–2.56)
rs293795-G/G × rs6443265-C/C	44	7.65	42	4.81	0.025	1.64 (1.06–2.54)
rs293795-A/G × rs2072668-C/G	72	12.52	77	8.8	0.022	1.48 (1.06–2.08)
rs293795-A/G × rs1052133-C/G	71	12.37	79	9.05	0.043	1.42 (1.01–1.99)
rs293795-A/A × rs6443265-T/C	67	11.65	143	16.36	0.013	0.67 (0.49–0.92)

Note: [1] — Absolute number and percentage of individuals with a particular genotype; [2] — Significance level; [3] — Odds ratio and 95% confidence interval. Minor alleles are underlined.

Table 5. Linkage disequilibrium analysis of the studied loci of the *OGG1* gene

SNP	rs2072668	rs1052133	rs293795	rs2304277	rs6443265
rs2072668	–	0.1613	–0.0514	0.1275	–0.0665
	–	0.9898	0.9990	0.9854	0.9373
rs1052133	–	–	-0.0512	0.1263	–0.065
	–	–	0.9989	0.9758	0.9206
rs293795	–	–	–	–0.0406	0.1561
	–	–	–	0.9982	0.9541
rs2304277	–	–	–	–	–0.0527
	–	–	–	–	0.9402

Note: The gray cells show the D values, the white ones show the D` values. $p < 2 \times 10^{-16}$.

P62 were absent [29–30]. The danger of 8-oxoG accumulation is that it can pair with cytosine similarly to guanine, while rotation around its N-glycosidic bond allows pairing with adenine [31]. The stability of the 8-oxoG syn conformation in duplex DNA leads to an increase in G:C → T:A transversion mutations during subsequent rounds of replication. Another oxidative lesion of guanine, 2,6-diamino-4-hydroxy-5-formamidopyrimidine (FapyG), results from fragmentation of the imidazole ring of the purine and is more likely than 8-oxoG to result in a G:C → T:A transversion [32–33]. The influence of the prooxidative status of the cell on the expression of DNA glycosylases is noteworthy: hydrogen peroxide reduces the expression of *OGG1*, while N-acetylcysteine reduces the amount of the oxidation product 8-oxodG and increases the expression of the *OGG1* enzyme [34–36].

According to clinical and experimental studies, loss-of-function single nucleotide variants of the *OGG1* gene are associated with reduced genetic stability and a high risk of carcinogenesis [21]. In particular, rs1052133 is associated with a predisposition to chronic myeloid leukemia [37], rs1052133 and rs2072668 — to breast cancer [38–39], rs2304277 — to ovarian cancer [40]. The rs1052133 polymorphism of the *OGG1* gene is associated with T2DM in Mexican Americans [23] and Japanese [24]. *OGG1* deficiency in mice results in obesity, fatty liver, impaired glucose tolerance and metabolic dysfunction [41].

There are no data in the literature on the involvement of rs2072668, rs293795, rs2304277, rs6443265 *OGG1* in the development of diabetes mellitus and its complications. Our study was the first to establish associations between the rs293795-G/G genotype, seven diplotypes rs293795-G/G × rs2072668-C/C, rs293795-G/G × rs1052133-C/C, rs293795-G/G × rs2304277-G/G, rs293795-G/G × rs6443265-C/C, rs293795-A/G × rs2072668-C/G, rs293795-A/G × rs1052133-C/G, rs293795-A/A × rs6443265-T/C and the haplotype rs2072668C-rs1052133C-rs293795G-rs2304277G-rs6443265C of the *OGG1* gene with a predisposition to DNP against the background of T2DM. Moreover, an increased risk of DNP was associated with carriage of the minor allele rs293795-G, which, according to the GTEx Portal transcriptome analysis, is associated with a decrease in the expression of the *OGG1* gene (https://www.gtexportal.org/home/). Analysis of transcription factor affinity at SNP sites (http://atsnp.biostat.wisc.edu/) showed that the G allele of rs293795 forms binding sites for 25 proteins — BCL ($p = 0.0021$), BHLHE40 ($p = 0.0045$), CACBP ($p = 0.0014$), CHD2 ($p < 0.0001$), E2F1 ($p = 0.0046$), EGR ($p = 0.0018$), EGR1 ($p = 0.0088$), ELF1 ($p = 0.0012$), MAZ ($p = 0.0081$), MEIS1 ($p = 0.0055$), MYC ($p = 0.0000029$), NFE2 ($p < 0.0001$), PLAG1 ($p = 0.0006$), RAD21 ($p = 0.0068$), REST ($p < 0.0001$), SREBF ($p = 0.002$), TATA ($p = 0.0077$), TBX20 ($p = 0.0069$), TFAP2 ($p = 0.0091$), TLX1:NFIC ($p = 0.0061$), WT1 ($p = 0.0021$), YY1 ($p = 0.0032$), ZNF219 ($p = 0.00043$), ZNF740 ($p = 0.0056$), ZNF784 ($p = 0.0026$). The general terms of the gene ontologies of the listed transcription factors (The Gene Ontology Resource https://geneontology.org/) are regulation of proliferation of mesangial cells of the metanephric glomeruli ($p = 8.97 \times 10^{-7}$), positive regulation of cell proliferation, involved in kidney development ($p = 3.22 \times 10^{-5}$) and negative regulation of gene expression through methylation of CpG islands ($p = 1.07 \times 10^{-4}$). The association of the rs293795-G allele with hypermethylation of CpG islands of the *OGG1* gene (i.e., with low transcriptional activity of the gene) in adults was also established in a methylome analysis, the results of which were deposited in the mQTLdb online database [42].

According to the VannoPortal project (http://www.mulinlab.org/vportal/index.html), in kidney tissue rs293795 serves as a marker of the histone modification H3K36me3, which is involved in the response to DNA damage and maintains the

Table 6. Analysis of associations of *OGG1* haplotypes with the risk of DNP in patients with T2DM

SNPs *H1*	rs2072668	rs1052133	rs293795	rs2304277	rs6443265	Haplotype frequencies in patients with type 2 diabetes		OR[2] (95% CI)	p^3
						without DNP	with DNP		
H1	C	C	A	G	T	0.4522	0.4378	1	–
H2	C	C	G	G	C	0.2231	0.2676	1.30 (1.06– 1.60)	0.012
H3	G	G	A	A	T	0.1609	0.1497	0.99 (0.78–1.26)	0.93
H4	C	C	A	G	C	0.1079	0.08	0.80 (0.58–1.10)	0.17
H5	G	G	A	G	T	0.0384	0.0443	1.29 (0.85–1.96)	0.24
rare	*	*	*	*	*	0.0063	0.0073	1.04 (0.52–2.08)	0.91
General $p = 0.028$									

Note: [1] — Haplotype; [2] — Odds ratio and 95% confidence interval of the haplotype–phenotype association adjusted for sex, age, and BMI; [3] — Significance level of the association adjusted for sex, age, and BMI. Minor alleles are underlined.

repressive status of chromatin regardless of histone acetylation [43]. Another important role of H3K36me3 in gene expression is the regulation of RNA splicing [44], for which H3K36me3 forms an adapter system with the *MRG15* gene, thus recruiting the polypyrimidine tract-binding protein of the splicing regulator PTB [45].

CONCLUSIONS

Thus, the results obtained in the present study indicate the involvement of the polymorphism of the 8-oxoguanine DNA glycosylase gene for the repair of oxidative DNA damage in the development of diabetic nephropathy in patients with type 2 diabetes.

The data from the functional annotation of the polymorphic variant rs293795, associated with an increased risk of DNP, collectively indicate a kidney tissue-specific decrease in the function of the *OGG1* enzyme in carriers of the minor allele rs293795-G, which, under conditions of increased load on the reparation system during hyperglycemia and oxidative stress may contribute to the classic structural and functional damage to vessels and glomeruli characteristic of DNP. Further studies, including those in animal models of T2DM, will allow for a systematic assessment of the role of DNA glycosylase genes in the initiation and progression of diabetic kidney disease, thereby providing a deeper understanding of the pathogenesis of this microvascular complication of diabetes.

References

1. Reed J, Bain S, Kanamarlapudi V. A Review of Current Trends with Type 2 Diabetes Epidemiology, Aetiology, Pathogenesis, Treatments and Future Perspectives. Diabetes Metab Syndr Obes. 2021; 14: 3567–602. PMID: 34413662. DOI: 10.2147/DMSO.S319895.
2. Duncan BB, Magliano DJ, Boyko EJ. IDF diabetes atlas 11th edition 2025: global prevalence and projections for 2050. Nephrol Dial Transplant. 2025. DOI: 10.1093/ndt/gfaf177.
3. Gregg EW, Sattar N, Ali MK. The changing face of diabetes complications. Lancet Diabetes Endocrinol. 2016; 4 (6): 537–47. PMID: 27156051. DOI: 10.1016/S2213-8587(16)30010-9.
4. Selby NM, Taal MW. An updated overview of diabetic nephropathy: Diagnosis, prognosis, treatment goals and latest guidelines. Diabetes Obes Metab. 2020; Suppl 1: 3–15. PMID: 32267079. DOI: 10.1111/dom.14007.
5. Kopel J, Pena-Hernandez C, Nugent K. Evolving spectrum of diabetic nephropathy. World J Diabetes. 2019; 10: 269–79. DOI: 10.4239/wjd.v10.i5.269.
6. Samsu N. Diabetic Nephropathy: Challenges in Pathogenesis, Diagnosis, and Treatment. BioMed Res Int. 2021; 2021: 16740. DOI: 10.1155/2021/1497449.
7. Azarova I, Klyosova E, Polonikov A. Single Nucleotide Polymorphisms of the RAC1 Gene as Novel Susceptibility Markers for Neuropathy and Microvascular Complications in Type 2 Diabetes. Biomedicines. 2023; 11 (3): 981. PMID: 36979960. DOI: 10.3390/biomedicines11030981.
8. Gallagher H, Suckling RJ. Diabetic nephropathy: where are we on the journey from pathophysiology to treatment? Diabetes Obes Metab. 2016; 18 (7): 641–7. PMID: 26743887. DOI: 10.1111/dom.12630.
9. Grindel A, Guggenberger B, Eichberger L, Pöppelmeyer C, Gschaider M, Tosevska A et al. Oxidative Stress, DNA Damage and DNA Repair in Female Patients with Diabetes Mellitus Type 2. PLoS One. 2016; 11 (9): e0162082. PMID: 27598300. DOI: 10.1371/journal.pone.0162082.
10. Barnes RP, Fouquerel E, Opresko PL. The impact of oxidative DNA damage and stress on telomere homeostasis. Mech Ageing Dev. 2019; 177: 37–45. PMID: 29604323. DOI: 10.1016/j.mad.2018.03.013.
11. González-Quiroz M, Blondel A, Sagredo A, Hetz C, Chevet E, Pedeux R. When Endoplasmic Reticulum Proteostasis Meets the DNA Damage Response. Trends Cell Biol. 2020; 30 (11): 881–91. PMID: 33036871. DOI: 10.1016/j.tcb.2020.09.002.
12. Eguchi N, Vaziri ND, Dafoe DC, Ichii H. The Role of Oxidative Stress in Pancreatic — Cell Dysfunction in Diabetes. Int J Mol Sci. 2021; 22 (4): 1509. PMID: 33546200. DOI: 10.3390/ijms22041509.
13. Uphoff S, Lord ND, Okumus B, Potvin-Trottier L, Sherratt DJ, Paulsson J. Stochastic activation of a DNA damage response causes cell-to-cell mutation rate variation. Science. 2016; 351 (6277): 1094–7. DOI: 10.1126/science.aac9786.
14. Gu S, Li J, Li S, Cao J, Bu J, Ren Y, et al. Efficient replacement of long DNA fragments via non-homologous end joining at non-coding regions. J Mol Cell Biol. 2021; 13 (1): 75–77. DOI: 10.1093/jmcb/mjaa051.
15. Demin AA, Hirota K, Tsuda M, Adamowicz M, Hailstone R, Brazina J, et al. XRCC1 prevents toxic PARP1 trapping during DNA base excision repair. Mol Cell. 2021; 81 (14): 3018–30.e5. DOI: 10.1016/j.molcel.2021.05.009.
16. Paz-Elizur T, Sevilya Z, Leitner-Dagan Y, Elinger D, Roisman LC, Livneh Z. DNA repair of oxidative DNA damage in human carcinogenesis: potential application for cancer risk assessment and prevention. Cancer Lett. 2008; 266 (1): 60–72. DOI: 10.1016/j.canlet.2008.02.032.
17. Gartner A, Engebrecht J. DNA repair, recombination, and damage signaling. Genetics. 2022; 220 (2): iyab178. PMID: 35137093. DOI: 10.1093/genetics/iyab178.
18. David SS, O'Shea VL, Kundu S. Base-excision repair of oxidative DNA damage. Nature. 2007; 447 (7147): 941–50. PMID: 17581577. DOI: 10.1038/nature05978.
19. Ba X, Boldogh I. 8-Oxoguanine DNA glycosylase 1: Beyond repair of the oxidatively modified base lesions. Redox Biol. 2018; 14: 669–78. PMID: 29175754. DOI: 10.1016/j.redox.2017.11.008.
20. Fleming AM, Ding Y, Burrows CJ. Oxidative DNA damage is epigenetic by regulating gene transcription via base excision repair. Proc Natl Acad Sci USA. 2017; 114 (10): 2604–9. DOI: 10.1073/pnas.1619809114.
21. Boiteux S, Coste F, Castaing B. Repair of 8-oxo-7,8-dihydroguanine in prokaryotic and eukaryotic cells: Properties and biological roles of the Fpg and OGG1 DNA N-glycosylases. Free Radic Biol Med. 2017; 107: 179–201. DOI: 10.1016/j.freeradbiomed.2016.11.042.
22. Kumar V, Agrawal R, Pandey A, Kopf S, Hoeffgen M, Kaymak S, et al. Compromised DNA repair is responsible for diabetes-associated fibrosis. EMBO J. 2020; 39 (11): e103477. PMID: 32338774. DOI: 10.15252/embj.2019103477.
23. Thameem F, Puppala S, Lehman DM, Stern MP, Blangero J, Abboud HE, et al. The Ser(326)Cys polymorphism of 8-oxoguanine glycosylase 1 (OGG1) is associated with type 2 diabetes in Mexican Americans. Hum Hered. 2010; 70 (2): 97–101. PMID: 20606456. DOI: 10.1159/000291964.
24. Daimon M, Oizumi T, Toriyama S, Karasawa S, Jimbu Y, Wada K, et al. Association of the Ser326Cys polymorphism in the OGG1 gene with type 2 DM. Biochem Biophys Res Commun. 2009; 386 (1): 26–29. PMID: 19486888. DOI: 10.1016/j.bbrc.2009.05.119.
25. World Health Organization. Use of Glycated Haemoglobin (HbA1c) in the Diagnosis of Diabetes Mellitus. Abbreviated Report of a WHO Consultation (WHO/NMH/CHP/CPM/11.1). World Health Organization; 2011.
26. Solé X, Guinó E, Valls J, Iniesta R, Moreno V. SNPStats: a web tool for the analysis of association studies. Bioinformatics. 2006; 22 (15): 1928–9. PMID: 16720584. DOI: 10.1093/bioinformatics/btl268.
27. Mullins EA, Rodriguez AA, Bradley NP, Eichman BF. Emerging Roles of DNA Glycosylases and the Base Excision Repair Pathway. Trends Biochem Sci. 2019; 44 (9): 765–81. PMID: 31078398. DOI: 10.1016/j.tibs.2019.04.006.
28. Cai H, Wang W, Li M, Jin J, Ge Z. Expression of nucleic acid oxidation metabolites 8-Oxo-GSn and β-amyloid protein in the urine and cerebral tissues of diabetic rats. Journal of King Saud University — Science. 2022; 34 (3): 101776. DOI.org/10.1016/j.jksus.2021.101776.

29. Sakuraba H, Mizukami H, Yagihashi N, Wada R, Hanyu C, Yagihashi S. Reduced beta-cell mass and expression of oxidative stress-related DNA damage in the islet of Japanese Type II diabetic patients. Diabetologia. 2002; 45 (1): 85–96. PMID: 11845227. DOI: 10.1007/s125-002-8248-z.
30. Mizukami H, Takahashi K, Inaba W, Tsuboi K, Osonoi S, Yoshida T et al. Involvement of oxidative stress-induced DNA damage, endoplasmic reticulum stress, and autophagy deficits in the decline of β-cell mass in Japanese type 2 diabetic patients. Diabetes Care. 2014; 37 (7): 1966–74. PMID: 24705612. DOI: 10.2337/dc13-2018.
31. Ovcherenko SS, Shernyukov AV, Nasonov DM, Endutkin AV, Zharkov DO, Bagryanskaya EG. Dynamics of 8-Oxoguanine in DNA: Decisive Effects of Base Pairing and Nucleotide Context. J Am Chem Soc. 2023; 145 (10): 5613–7. PMID: 36867834. DOI: 10.1021/jacs.2c11230.
32. Whitaker AM, Schaich MA, Smith MR, Flynn TS, Freudenthal BD. Base excision repair of oxidative DNA damage: from mechanism to disease. Front Biosci (Landmark Ed). 2017; 22 (9): 1493–522. PMID: 28199214. DOI: 10.2741/4555.
33. Shikazono N, Akamatsu K. Mutagenic potential of 8-oxo-7,8-dihydroguanine (8-oxoG) is influenced by nearby clustered lesions. Mutat Res. 2018; 810: 6–12. PMID: 29870902. DOI: 10.1016/j.mrfmmm.2018.05.001.
34. Simone S, Gorin Y, Velagapudi C, Abboud HE, Habib SL. Mechanism of oxidative DNA damage in diabetes: tuberin inactivation and downregulation of DNA repair enzyme 8-oxo-7,8-dihydro-2'-deoxyguanosine-DNA glycosylase. Diabetes. 2008; 57 (10): 2626–36. PMID: 18599524. DOI: 10.2337/db07-1579.
35. Manoel-Caetano FS, Xavier DJ, Evangelista AF, Takahashi P, Collares CV, Puthier D, et al. Gene expression profiles displayed by peripheral blood mononuclear cells from patients with type 2 diabetes mellitus focusing on biological processes implicated on the pathogenesis of the disease. Gene. 2012; 511 (2): 151–60. PMID: 23036710. DOI: 10.1016/j.gene.2012.09.090.
36. Merecz A, Markiewicz L, Sliwinska A, Kosmalski M, Kasznicki J, Drzewoski J, et al. Analysis of oxidative DNA damage and its repair in Polish patients with diabetes mellitus type 2: Role in pathogenesis of diabetic neuropathy. Adv Med Sci. 2015; 60 (2): 220–30. PMID: 25932787. DOI: 10.1016/j.advms.2015.04.001.
37. Hassan FM. OGG1 rs1052133 Polymorphism and Genetic Susceptibility to Chronic Myelogenous Leukaemia. Asian Pac J Cancer Prev. 2019; 20 (3): 925–8. DOI: 10.31557/APJCP.2019.20.3.925.
38. Alanazi M, Pathan AAK, Shaik JP, Alhadheq A, Khan Z, Khan W, et al. The hOGG1 Ser326Cys gene polymorphism and breast cancer risk in Saudi population. Pathology and Oncology Research. 2017; 23 (3): 525–35.
39. Kim KY, Han W, Noh DY, Kang D, Kwack K. Impact of genetic polymorphisms in base excision repair genes on the risk of breast cancer in a Korean population. Gene. 2013; 532 (2): 192–6. PMID: 24076439. DOI: 10.1016/j.gene.2013.09.069.
40. Osorio A, Milne RL, Kuchenbaecker K, Vaclova T, Pita G, Alonso R, et al. DNA glycosylases involved in base excision repair may be associated with cancer risk in BRCA1 and BRCA2 mutation carriers. PLoS Genet. 2014; 10: e1004256. DOI: 10.1371/journal.pgen.1004256.
41. Sampath H, Vartanian V, Rollins MR, Sakumi K, Nakabeppu Y, Lloyd RS. 8-Oxoguanine DNA glycosylase (OGG1) deficiency increases susceptibility to obesity and metabolic dysfunction. PLoS One. 2012; 7 (12): e51697. PMID: 23284747. DOI: 10.1371/journal.pone.0051697.
42. Gaunt TR, Shihab HA, Hemani G, Min JL, Woodward G, Lyttleton O, et al. Systematic identification of genetic influences on methylation across the human life course. Genome Biology. 2016; 17: 61. DOI: 10.1186/s13059-016-0926-z.
43. Sun Z, Zhang Y, Jia J, Fang Y, Tang Y, Wu H, et al. H3K36me3, message from chromatin to DNA damage repair. Cell Biosci. 2020; 10: 9. PMID: 32021684. DOI: 10.1186/s13578-020-0374-z.
44. Barash Y, Calarco JA, Gao W, Pan Q, Wang X, Shai O, et al. Deciphering the splicing code. Nature. 2010; 465 (7294): 53–59. PMID: 20445623. DOI: 10.1038/nature09000.
45. Luco RF, Pan Q, Tominaga K, Blencowe BJ, Pereira-Smith OM, Misteli T. Regulation of alternative splicing by histone modifications. Science. 2010; 327 (5968): 996–1000. PMID: 20133523. DOI: 10.1126/science.1184208.

Литература

1. Reed J, Bain S, Kanamarlapudi V. A Review of Current Trends with Type 2 Diabetes Epidemiology, Aetiology, Pathogenesis, Treatments and Future Perspectives. Diabetes Metab Syndr Obes. 2021; 14: 3567–602. PMID: 34413662. DOI: 10.2147/DMSO.S319895.
2. Duncan BB, Magliano DJ, Boyko EJ. IDF diabetes atlas 11th edition 2025: global prevalence and projections for 2050. Nephrol Dial Transplant. 2025. DOI: 10.1093/ndt/gfaf177.
3. Gregg EW, Sattar N, Ali MK. The changing face of diabetes complications. Lancet Diabetes Endocrinol. 2016; 4 (6): 537–47. PMID: 27156051. DOI: 10.1016/S2213-8587(16)30010-9.
4. Selby NM, Taal MW. An updated overview of diabetic nephropathy: Diagnosis, prognosis, treatment goals and latest guidelines. Diabetes Obes Metab. 2020; Suppl 1: 3–15. PMID: 32267079. DOI: 10.1111/dom.14007.
5. Kopel J, Pena-Hernandez C, Nugent K. Evolving spectrum of diabetic nephropathy. World J Diabetes. 2019; 10: 269–79. DOI: 10.4239/wjd.v10.i5.269.
6. Samsu N. Diabetic Nephropathy: Challenges in Pathogenesis, Diagnosis, and Treatment. BioMed Res Int. 2021; 2021: 16740. DOI: 10.1155/2021/1497449.
7. Azarova I, Klyosova E, Polonikov A. Single Nucleotide Polymorphisms of the RAC1 Gene as Novel Susceptibility Markers for Neuropathy and Microvascular Complications in Type 2 Diabetes. Biomedicines. 2023; 11 (3): 981. PMID: 36979960. DOI: 10.3390/biomedicines11030981.
8. Gallagher H, Suckling RJ. Diabetic nephropathy: where are we on the journey from pathophysiology to treatment? Diabetes Obes Metab. 2016; 18 (7): 641–7. PMID: 26743887. DOI: 10.1111/dom.12630.
9. Grindel A, Guggenberger B, Eichberger L, Pöppelmeyer C, Gschaider M, Tosevska A et al. Oxidative Stress, DNA Damage and DNA Repair in Female Patients with Diabetes Mellitus Type 2. PLoS One. 2016; 11 (9): e0162082. PMID: 27598300. DOI: 10.1371/journal.pone.0162082.
10. Barnes RP, Fouquerel E, Opresko PL. The impact of oxidative DNA damage and stress on telomere homeostasis. Mech Ageing Dev. 2019; 177: 37–45. PMID: 29604323. DOI: 10.1016/j.mad.2018.03.013.
11. González-Quiroz M, Blondel A, Sagredo A, Hetz C, Chevet E, Pedeux R. When Endoplasmic Reticulum Proteostasis Meets the DNA Damage Response. Trends Cell Biol. 2020; 30 (11): 881–91. PMID: 33036871. DOI: 10.1016/j.tcb.2020.09.002.
12. Eguchi N, Vaziri ND, Dafoe DC, Ichii H. The Role of Oxidative Stress in Pancreatic — Cell Dysfunction in Diabetes. Int J Mol Sci. 2021; 22 (4): 1509. PMID: 33546200. DOI: 10.3390/ijms22041509.
13. Uphoff S, Lord ND, Okumus B, Potvin-Trottier L, Sherratt DJ, Paulsson J. Stochastic activation of a DNA damage response causes cell-to-cell mutation rate variation. Science. 2016; 351 (6277): 1094–7. DOI: 10.1126/science.aac9786.
14. Gu S, Li J, Li S, Cao J, Bu J, Ren Y, et al. Efficient replacement of long DNA fragments via non-homologous end joining at non-coding regions. J Mol Cell Biol. 2021; 13 (1): 75–77. DOI: 10.1093/jmcb/mjaa051.
15. Demin AA, Hirota K, Tsuda M, Adamowicz M, Hailstone R, Brazina J, et al. XRCC1 prevents toxic PARP1 trapping during DNA base excision repair. Mol Cell. 2021; 81 (14): 3018–30.e5. DOI: 10.1016/j.molcel.2021.05.009.
16. Paz-Elizur T, Sevilya Z, Leitner-Dagan Y, Elinger D, Roisman LC, Livneh Z. DNA repair of oxidative DNA damage in human carcinogenesis: potential application for cancer risk assessment and prevention. Cancer Lett. 2008; 266 (1): 60–72. DOI: 10.1016/j.canlet.2008.02.032.
17. Gartner A, Engebrecht J. DNA repair, recombination, and damage signaling. Genetics. 2022; 220 (2): iyab178. PMID: 35137093. DOI: 10.1093/genetics/iyab178.

18. David SS, O'Shea VL, Kundu S. Base-excision repair of oxidative DNA damage. Nature. 2007; 447 (7147): 941–50. PMID: 17581577. DOI: 10.1038/nature05978.
19. Ba X, Boldogh I. 8-Oxoguanine DNA glycosylase 1: Beyond repair of the oxidatively modified base lesions. Redox Biol. 2018; 14: 669–78. PMID: 29175754. DOI: 10.1016/j.redox.2017.11.008.
20. Fleming AM, Ding Y, Burrows CJ. Oxidative DNA damage is epigenetic by regulating gene transcription via base excision repair. Proc Natl Acad Sci USA. 2017; 114 (10): 2604–9. DOI: 10.1073/pnas.1619809114.
21. Boiteux S, Coste F, Castaing B. Repair of 8-oxo-7,8-dihydroguanine in prokaryotic and eukaryotic cells: Properties and biological roles of the Fpg and OGG1 DNA N-glycosylases. Free Radic Biol Med. 2017; 107: 179–201. DOI: 10.1016/j.freeradbiomed.2016.11.042.
22. Kumar V, Agrawal R, Pandey A, Kopf S, Hoeffgen M, Kaymak S, et al. Compromised DNA repair is responsible for diabetes-associated fibrosis. EMBO J. 2020; 39 (11): e103477. PMID: 32338774. DOI: 10.15252/embj.2019103477.
23. Thameem F, Puppala S, Lehman DM, Stern MP, Blangero J, Abboud HE, et al. The Ser(326)Cys polymorphism of 8-oxoguanine glycosylase 1 (OGG1) is associated with type 2 diabetes in Mexican Americans. Hum Hered. 2010; 70 (2): 97–101. PMID: 20606456. DOI: 10.1159/000291964.
24. Daimon M, Oizumi T, Toriyama S, Karasawa S, Jimbu Y, Wada K, et al. Association of the Ser326Cys polymorphism in the OGG1 gene with type 2 DM. Biochem Biophys Res Commun. 2009; 386 (1): 26–29. PMID: 19486888. DOI: 10.1016/j.bbrc.2009.05.119.
25. World Health Organization. Use of Glycated Haemoglobin (HbA1c) in the Diagnosis of Diabetes Mellitus. Abbreviated Report of a WHO Consultation (WHO/NMH/CHP/CPM/11.1). World Health Organization; 2011.
26. Solé X, Guinó E, Valls J, Iniesta R, Moreno V. SNPStats: a web tool for the analysis of association studies. Bioinformatics. 2006; 22 (15): 1928–9. PMID: 16720584. DOI: 10.1093/bioinformatics/btl268.
27. Mullins EA, Rodriguez AA, Bradley NP, Eichman BF. Emerging Roles of DNA Glycosylases and the Base Excision Repair Pathway. Trends Biochem Sci. 2019; 44 (9): 765–81. PMID: 31078398. DOI: 10.1016/j.tibs.2019.04.006.
28. Cai H, Wang W, Li M, Jin J, Ge Z. Expression of nucleic acid oxidation metabolites 8-Oxo-GSn and β-amyloid protein in the urine and cerebral tissues of diabetic rats. Journal of King Saud University — Science. 2022; 34 (3): 101776. DOI.org/10.1016/j.jksus.2021.101776.
29. Sakuraba H, Mizukami H, Yagihashi N, Wada R, Hanyu C, Yagihashi S. Reduced beta-cell mass and expression of oxidative stress-related DNA damage in the islet of Japanese Type II diabetic patients. Diabetologia. 2002; 45 (1): 85–96. PMID: 11845227. DOI: 10.1007/s125-002-8248-z.
30. Mizukami H, Takahashi K, Inaba W, Tsuboi K, Osonoi S, Yoshida T et al. Involvement of oxidative stress-induced DNA damage, endoplasmic reticulum stress, and autophagy deficits in the decline of β-cell mass in Japanese type 2 diabetic patients. Diabetes Care. 2014; 37 (7): 1966–74. PMID: 24705612. DOI: 10.2337/dc13-2018.
31. Ovcherenko SS, Shernyukov AV, Nasonov DM, Endutkin AV, Zharkov DO, Bagryanskaya EG. Dynamics of 8-Oxoguanine in DNA: Decisive Effects of Base Pairing and Nucleotide Context. J Am Chem Soc. 2023; 145 (10): 5613–7. PMID: 36867834. DOI: 10.1021/jacs.2c11230.
32. Whitaker AM, Schaich MA, Smith MR, Flynn TS, Freudenthal BD. Base excision repair of oxidative DNA damage: from mechanism to disease. Front Biosci (Landmark Ed). 2017; 22 (9): 1493–522. PMID: 28199214. DOI: 10.2741/4555.
33. Shikazono N, Akamatsu K. Mutagenic potential of 8-oxo-7,8-dihydroguanine (8-oxoG) is influenced by nearby clustered lesions. Mutat Res. 2018; 810: 6–12. PMID: 29870902. DOI: 10.1016/j.mrfmmm.2018.05.001.
34. Simone S, Gorin Y, Velagapudi C, Abboud HE, Habib SL. Mechanism of oxidative DNA damage in diabetes: tuberin inactivation and downregulation of DNA repair enzyme 8-oxo-7,8-dihydro-2'-deoxyguanosine-DNA glycosylase. Diabetes. 2008; 57 (10): 2626–36. PMID: 18599524. DOI: 10.2337/db07-1579.
35. Manoel-Caetano FS, Xavier DJ, Evangelista AF, Takahashi P, Collares CV, Puthier D, et al. Gene expression profiles displayed by peripheral blood mononuclear cells from patients with type 2 diabetes mellitus focusing on biological processes implicated on the pathogenesis of the disease. Gene. 2012; 511 (2): 151–60. PMID: 23036710. DOI: 10.1016/j.gene.2012.09.090.
36. Merecz A, Markiewicz L, Sliwinska A, Kosmalski M, Kasznicki J, Drzewoski J, et al. Analysis of oxidative DNA damage and its repair in Polish patients with diabetes mellitus type 2: Role in pathogenesis of diabetic neuropathy. Adv Med Sci. 2015; 60 (2): 220–30. PMID: 25932787. DOI: 10.1016/j.advms.2015.04.001.
37. Hassan FM. OGG1 rs1052133 Polymorphism and Genetic Susceptibility to Chronic Myelogenous Leukaemia. Asian Pac J Cancer Prev. 2019; 20 (3): 925–8. DOI: 10.31557/APJCP.2019.20.3.925.
38. Alanazi M, Pathan AAK, Shaik JP, Alhadheq A, Khan Z, Khan W, et al. The hOGG1 Ser326Cys gene polymorphism and breast cancer risk in Saudi population. Pathology and Oncology Research. 2017; 23 (3): 525–35.
39. Kim KY, Han W, Noh DY, Kang D, Kwack K. Impact of genetic polymorphisms in base excision repair genes on the risk of breast cancer in a Korean population. Gene. 2013; 532 (2): 192–6. PMID: 24076439. DOI: 10.1016/j.gene.2013.09.069.
40. Osorio A, Milne RL, Kuchenbaecker K, Vaclova T, Pita G, Alonso R, et al. DNA glycosylases involved in base excision repair may be associated with cancer risk in BRCA1 and BRCA2 mutation carriers. PLoS Genet. 2014; 10: e1004256. DOI: 10.1371/journal.pgen.1004256.
41. Sampath H, Vartanian V, Rollins MR, Sakumi K, Nakabeppu Y, Lloyd RS. 8-Oxoguanine DNA glycosylase (OGG1) deficiency increases susceptibility to obesity and metabolic dysfunction. PLoS One. 2012; 7 (12): e51697. PMID: 23284747. DOI: 10.1371/journal.pone.0051697.
42. Gaunt TR, Shihab HA, Hemani G, Min JL, Woodward G, Lyttleton O, et al. Systematic identification of genetic influences on methylation across the human life course. Genome Biology. 2016; 17: 61. DOI: 10.1186/s13059-016-0926-z.
43. Sun Z, Zhang Y, Jia J, Fang Y, Tang Y, Wu H, et al. H3K36me3, message from chromatin to DNA damage repair. Cell Biosci. 2020; 10: 9. PMID: 32021684. DOI: 10.1186/s13578-020-0374-z.
44. Barash Y, Calarco JA, Gao W, Pan Q, Wang X, Shai O, et al. Deciphering the splicing code. Nature. 2010; 465 (7294): 53–59. PMID: 20445623. DOI: 10.1038/nature09000.
45. Luco RF, Pan Q, Tominaga K, Blencowe BJ, Pereira-Smith OM, Misteli T. Regulation of alternative splicing by histone modifications. Science. 2010; 327 (5968): 996–1000. PMID: 20133523. DOI: 10.1126/science.1184208.

EXPRESSION OF MTCO1 IN CELL CULTURES FROM PATIENTS WITH LEIGH SYNDROME UNDER THE ACTION OF AAV9-SURF1

Adrianov MA[1,2] ✉, Gauthier MS[1], Degtyareva AV[1,3], Marey MV[1], Manukhova LA[1], Rastorguev SM[4], Simonov VS[4], Ushakova LV[1], Vysokikh MY[1,2]

[1] Kulakov National Medical Research Center for Obstetrics, Gynecology and Perinatology, Moscow, Russia
[2] Belozersky Research Institute of Physico-Chemical Biology at Lomonosov Moscow State University, Moscow, Russia
[3] Filatov Clinical Institute of Child Health, Sechenov First Moscow State Medical University, Moscow, Russia
[4] Pirogov Russian National Research Medical University, Moscow, Russia

The most common biochemical defect in Leigh syndrome is aberrations in proteins involved in the assembly of the electron transport chain (ETC) complex IV subunits — cytochrome C oxidase (COX). Among these, mutations in the *SURF1* gene are the most common. The SURF1 protein is embedded in the inner mitochondrial membrane and plays a crucial role in the COX complex assembly. All mutations in the *SURF1* gene result in the truncated protein biosynthesis and damage to the COX complex. Adeno-associated viral vectors (AAV9), which carry the not mutated *SURF1* gene (AAV9-SURF1), are being investigated for the treatment of this disease. The aim of this study was to evaluate the expression levels of SURF1 and MTCO1 proteins in whole blood from patients with Leigh syndrome compared to reference values obtained for a pool of patients without mutations, as well as to evaluate the expression of the MTCO1 cytochrome c oxidase subunit in skin fibroblast cultures from patients with Leigh syndrome treated with AAV9. To investigate the gene therapy efficacy, AAV9-SURF1 was added to fibroblasts derived from the skin of a patient with a mutation in the Surf1 gene and to control skin fibroblasts at an optimal dose that did not impair cell viability in the MTT assay. We used Western blot analysis and quantitative PCR to evaluate changes in the relative amounts of the studied proteins after the addition of AAV9-SURF1 to control cells and cells obtained from the patient and identified significant compensatory changes in skin fibroblasts from a patient with a SURF1 mutation.

Keywords: Leigh syndrome, SURF1, adeno-associated viral vector, gene replacement therapy, cytochrome oxidase, COX, MTCO1

Funding: The study was conducted under state assignment number EGISU 125022002694-7, "Development of gene therapy drugs based on viral delivery for the treatment of hemophilia, Leigh syndrome, and glycogen storage disease type Ia." The project was conducted at the FSBI «National Medical Research Center for Obstetrics, Gynecology and Perinatology named after Academician V.I.Kulakov», Ministry of Health of the Russian Federation.

Acknowledgements: The authors thank A. M. Gamisoniya and N. M. Marycheva for the help in the research.

Author contribution: Adrianov MA — gene expression assessment, manuscript preparation; Gautier MS, Degtyareva AV, Ushakova LV — clinical work with patients; Rastorguev SM, Simonov VS — construction and preparation the AAV vector; Marey MV — protein expression assessment, fibroblasts cultivation, transfection, and the viral construct toxicity assessment, microscopy; Manukhova LA — sample processing, protein expression assessment, data processing and statistical analysis; Vysokikh MY — overall supervision, the research coordination, writing the manuscript.

Compliance with ethical standards: all procedures with patients were carried out in accordance with the rules of Ethics Committee of the Kulakov National Medical Research Center for Obstetrics, Gynecology and Perinatology (Protocol No. 10, dated November 28, 2024). Voluntary informed consent was obtained from all study participants regarding their inclusion in the study and the use of their biological materials.

✉ **Correspondence should be addressed:** Mikhail A. Adrianov
Academica Oparina, 4, Moscow, 117997, Russia, ya.litsch@gmail.com

Received: 12.12.2025 **Accepted:** 23.12.2025 **Published online:** 29.12.2025

DOI: 10.24075/brsmu.2025.083

Copyright: © 2025 by the authors. **Licensee:** Pirogov University. This article is an open access article distributed under the terms and conditions of the Creative Commons Attribution (CC BY) license (https://creativecommons.org/licenses/by/4.0/).

ЭКСПРЕССИЯ MTCO1 В КУЛЬТУРАХ КЛЕТОК ПАЦИЕНТОВ С СИНДРОМОМ ЛИ ПРИ ДЕЙСТВИИ AAV9-SURF1

М. А. Адрианов[1,2] ✉, М. С. Готье[1], А. В. Дегтярева[1,3], М. В. Марей[1], Л. А. Манухова[1], С. М. Расторгуев[4], В. С. Симонов[4], Л. В. Ушакова[1], М. Ю. Высоких[1,2]

[1] Национальный медицинский исследовательский центр акушерства, гинекологии и перинатологии имени В. И. Кулакова, Москва, Россия
[2] Научно-исследовательский институт физико-химической биологии имени А. Н. Белозерского, Московский государственный университет имени М. В. Ломоносова, Москва, Россия
[3] Клинический институт детского здоровья имени Н. Ф. Филатова, Первый московский государственный медицинский университет имени И. М. Сеченова, Москва, Россия
[4] Российский национальный исследовательский медицинский университет имени Н. И. Пирогова, Москва, Россия

Самым частым биохимическим дефектом при синдроме Ли является нарушение белков, которые участвуют в сборке субъединиц IV комплекса электрон-транспортной цепи — цитохром-с-оксидазы (COX). Среди них наиболее часто встречаются мутации гена *SURF1*. Белок SURF1 встроен во внутреннюю мембрану митохондрии и играет решающую роль в сборке COX-комплекса. Все мутации в гене *SURF1* приводят к биосинтезу укороченного белка и повреждениям COX-комплекса. Для терапии данного заболевания исследуют возможность использования аденоассоциированных вирусных векторов (AAV9), в геном которых внесен немутированный *SURF1* (AAV9-SURF1). Целью исследования было дать оценку уровня экспрессии белков SURF1, MTCO1 в цельной крови пациентов с синдромом Ли на фоне полученных референсных значений для пула пациентов без мутаций, а также оценку экспрессии субъединицы цитохром-с-оксидазы MTCO1 в культурах фибробластов кожи пациентов с синдромом Ли при действии AAV9-SURF1. Для моделирования генотерапевтического воздействия к фибробластам, полученным из кожи пациента, и к контрольным фибробластам кожи был добавлен AAV9-SURF1 в подобранной оптимальной дозе, не приводящей к ухудшению жизнеспособности клеток в MTT-тесте. Методами вестерн-блота и количественной ПЦР мы оценили изменения в относительном количестве исследуемых белков после добавления AAV9-SURF1 на контрольные клетки и клетки, полученные от пациента. Нами были выявлены существенные компенсаторные изменения для фибробластов кожи пациента с мутацией SURF1.

Ключевые слова: синдром Ли, SURF1, аденоассоциированный вирусный вектор, генозаместительная терапия, цитохромоксидаза, COX, MTCO1

Финансирование: исследование выполнено в рамках государственного задания номер ЕГИСУ 125022002694-7 «Разработка генотерапевтических препаратов на основе вирусной доставки для лечения гемофилии, синдрома Ли, гликогеновой болезни Ia типа» на базе ФГБУ «НМИЦ АГП им. академика В. И. Кулакова».

Благодарности: авторы выражают глубокую благодарность А. М. Гамисонии и Н. М. Марычевой за помощь в проведении исследования.

Вклад авторов: М. А. Адрианов — изучение экспрессии генов, подготовка рукописи; М. С. Готье, А. В. Дегтярева, Л. В. Ушакова — клиническая работа с пациентами; С. М. Расторгуев, В. С. Симонов — конструирование и наращивание AAB-вектора; М. В. Марей — изучение экспрессии белков, культивация фибробластов, трансфекция, исследование токсичности вирусной конструкции, микроскопия; Л. А. Манухова — пробоподготовка, изучение экспрессии белков, процессинг, статистическая обработка данных; М. Ю. Высоких — общее руководство, координация исследований, написание статьи

Соблюдение этических стандартов: исследование одобрено этическим комитетом НМИЦ АГП им. В. И. Кулакова (протокол № 10 от 28 ноября 2024 г.); все участники подписали добровольное информированное согласие на включение в исследование и использование биологических материалов.

✉ **Для корреспонденции:** Михаил Андреевич Адрианов
ул. Академика Опарина, д. 4, г. Москва, 117997, Россия; ya.litsch@gmail.com

Статья получена: 12.12.2025 **Статья принята к печати:** 23.12.2025 **Опубликована онлайн:** 29.12.2025

DOI: 10.24075/vrgmu.2025.083

Авторские права: © 2025 принадлежат авторам. **Лицензиат:** РНИМУ им. Н. И. Пирогова. Статья размещена в открытом доступе и распространяется на условиях лицензии Creative Commons Attribution (CC BY) (https://creativecommons.org/licenses/by/4.0/).

Mitochondrial encephalomyopathies that manifest in early infancy with severe, progressive neurological impairment include subacute necrotizing encephalomyelopathy, or Leigh syndrome, described by Professor Denis Archibald Leigh in 1951 following a postmortem examination of a 7-month-old boy with progressive neurological symptoms [1].

Leigh syndrome is a rare hereditary disorder, with an incidence of approximately 1 in 34,000-36,000 newborns, it affects both boys and girls equally. It is an extremely heterogeneous disease, caused by defects in multiple genes located on autosomes, the X chromosome, and mitochondrial DNA. It is known that the most common biochemical defect in this syndrome is a disruption of the amino acid sequence of proteins involved in the assembly of the subunits of complex IV of the electron transport chain (ETC) of the inner mitochondrial membrane — cytochrome c oxidase (COX), which catalyzes the transfer of electrons in the ETC from cytochrome c to molecular oxygen and formation of water, thus, plays a key role in mitochondrial oxidative phosphorylation.

The most common mutations are in the gene encoding the *SURF1* (Sea Urchin Retroposon Family 1) protein, which is embedded in the inner mitochondrial membrane and plays a crucial role in the assembly of the COX complex [2]. Normally, the 35 kDa precursor of SURF1 is imported into the mitochondria, where its mature form (30 kDa) is formed after processing. However virtually all mutations (more than 60) in the *SURF1* gene result in protein biosynthesis that is already shortened at the precursor stage and damage to the COX complex, destabilized by defective SURF1. About 50% of mutations in the *SURF1* gene are missense, nonsense, and small deletions, with the most common being a 10-nucleotide deletion with a 2-nucleotide insertion (311-321del10insAT) in exon 4 and a 2-nucleotide deletion (845delCT) in exon 9 of the gene [3, 4].

Although it has been established that SURF1-associated Leigh syndrome has a typical course, leading to early mortality before the age of 10 in most cases, approximately 10% of cases exhibit milder symptoms with a longer lifespan [5]. In all cases, the onset of the disease occurs in infancy and is characterized by impaired feeding associated with the onset of damage to the central nervous system, hypotonic and poor coordination of sucking and swallowing, followed by further regression of already established psychomotor development [6]. According to a number of researchers, gastroparesis and delayed gastric emptying, as well as gastroesophageal reflux, in case of Leigh syndrome caused by mutations in the *SURF1* gene and most likely due to neuromuscular and mitochondrial dysfunction caused by disturbances in the ETC with cytochrome oxidase deficiency [7]. Typical manifestations of the developing disease also include such disorders as neuropathy, ataxia, ophthalmoplegia and hypertrichosis [8]. To investigate the molecular mechanisms and potential therapies for Leigh syndrome, mouse models deficient in the *SURF1*(–/–) gene were created. These mice exhibit significant reduction in birth weight, which recovers by the age of one month, with manifestation of moderate motor developmental delay against the background of defective assembly and deficiency of a number of critical COX subunits, including mitochondria-encoded MT-CO1 [9]. Despite the described impairments, these mice have a lifespan similar to the wild type, and it has been suggested that the loss of a COX assembly factor such as Surf1 in mice leads to compensatory responses, including activation of mitochondrial biogenesis and the Nrf2-dependent signaling cascade, which contribute to the alleviation of the manifestations of the pathological phenotype [10]. Furthermore, in this model, AAV serotype 9 (AAV9) adenoviral vector therapy for SURF1-associated Leigh syndrome, in which mice were injected with a codon-optimized human *SURF1* gene (hSURF1opt) (AAV9/hSURF1v1), was shown to restore not only SURF1 function but also complex IV activity and correct exercise-induced lactic acidosis without any toxicity to wild-type mice [11, 12].

Here, we used a similar approach with aim to explore the potential of gene therapy for Leigh syndrome in a model of subcutaneous fibroblasts from patients with a *SURF1* gene mutation transfected with an adenoviral construct containing a codon-optimized human *SURF1* gene.

METHODS

The study included three patients with a genetically confirmed diagnosis of Leigh syndrome and typical clinical manifestations. The inclusion criteria for the study were: 1) a genetically confirmed diagnosis of Leigh syndrome with frequently occurring mutations in the *SURF1* gene (Table 1); 2) age of disease manifestation up to 3 years; 3) informed consent from the patient's legal representative; exclusion criteria were the presence of another genetically determined disease, including a syndromic form of the pathology. Two patients were born full-term, in satisfactory condition at birth (Apgar score 8/9 points), with normal weight and length for gestational age; one patient was born at 30 weeks. All patients exhibited psychomotor developmental delays from the first months of life. Over time, their condition progressively worsened, with loss of motor and speech skills. The first two patients experienced metabolic crises — acetonemic states characterized by vomiting, food refusal, weakness, and lethargy. Severe bulbar dysfunction necessitated gastrostomy placement in the first and second patients, a tracheostomy in the third patient, and the first patient required respiratory support (NIVL). All patients were diagnosed after 1.5 years of age. MRI data revealed changes in brain tissue characteristic of the disease: the first patient, aged 2 years, showed MRI signs of bilateral symmetrical structural changes in the substantia nigra, red nuclei, along the conduction pathways in the medulla oblongata and in the middle cerebellar peduncles. The second patient (aged 14 months) showed bilateral symmetrical increases in signal intensity in the basal ganglia, corticospinal tracts and brainstem structures. The third patient (aged 12 months) showed increased signal intensity in the lower parts of the brainstem (pons, medulla oblongata) without involvement of the basal ganglia. The diagnosis was confirmed by molecular genetic research methods (Table 1).

At the time of the study, all patients' neurological status included impaired eye coordination and fixation, rotatory nystagmus with a vertical component, floating eye movements, bulbar-pseudobulbar syndrome, diffuse generalized trunk and limb hypotonic/atonic associated with mixed tetraparesis, decreased tendon-periosteal reflexes, polyneuropathy syndrome with distal muscle wasting of the limbs, and myogenic contractures in large joints.

The control group consisted of healthy children (3–13 years old) with undetected mutations in the *SURF1* gene and no symptoms who presented to the children's outpatient department of the Kulakov National Research Center for Obstetrics, Gynecology and Perinatology as part of a routine pediatric examination.

Collection of blood samples

Whole blood obtained in vacuette with EDTA was treated with ammonium chloride and potassium lysing buffer (AbiLyse

Table 1. Clinical and anamnestic data of patients included in the study

Gender		Patient 1	Patient 2	Patient 3
		Female	Female	Male
Variant in gene *SURF1*		Deletions in the heterozygous state: c.845 84delCT; p.(Ser282Cysfs*9) c.901 902delTC; p.(Ter301Thrext27)	Variants in compound heterozygous state:c.845_846delCT c.752-2A>G	Variants in compound heterozygous state:c.240G>C(p.Q8OH) c.870dupT(p.K29I)
Age of onset of disease		1 month psychomotor developmental delay	1 year metabolic crisis	2 years old hand tremors, gait disturbance, motor clumsiness
Age at the time of disease diagnosis		2.5 years	1.5 years	2.5 years
Age at the time of study		6 years	5.5 years	12 years
Clinical manifestations at the time of the study	Psychomotor retardation	+	+	+
	Bulbar disorders	+ gastrostomy	+ gastrostomy	+ tracheostomy
	Polyneuropathic syndrome	+	+	+
	Metabolic crysis	+	+	+
	Respiratory therapy	NIVL 10 hours/day	–	–
	Palliative status	+	+	+

ACK Lysing Buffer, USA) for 15–60 minutes after intravenous collection from patients, following the manufacturer's protocol for subsequent sample collection for Western blot analysis.

Fibroblast Cultivation

Primary subcutaneous fibroblast cell cultures were kindly provided by the Pirogov Russian National Research Medical University. Starting from passage 3, the cells were cultured in a complete nutrient medium consisting of DMEM (PanEco, Russia): F12 (PanEco, Russia) at a 1 : 1 ratio, supplemented with 100 U/ml penicillin, 100 µg/ml streptomycin (PenStrep, GIBCO, USA), and 10% fetal bovine serum (FBS, GIBCO, USA). The culture medium was maintained at 37 °C in a 5% CO_2 atmosphere. Upon reaching 60% confluence, the cells were subcultured at a 1:3 ratio using 0.05% trypsin/EDTA (PanEco, Russia) in culture flasks. Trypsin activity was suppressed by adding an appropriate amount of fresh nutrient medium. Cell counts were determined at each passage using a Goryaev chamber (MINIMED, Russia). Cell morphology was assessed using a NIKON ECLIPSE TS100 inverted light microscope (JAPAN).

Construction of the AAV vector carrying the *hSURF1* gene

Total RNA was isolated using the commercial RNA-solo kit (Eurogen) according to the manufacturer's protocol. Tissue samples were homogenized and lysed with ExtractRNA reagent (Eurogen, Russia), followed by RNA extraction and purification. The concentration and purity of the obtained RNA were assessed spectrophotometrically at 260/280nm on “Nanodrop spectrophotometer” (USA). RNA integrity and the absence of degradation were verified by electrophoresis in a 2% agarose gel on horizontal system (Helicon, Russia) according standard protocol (http://molbiol.ru/protocol/07_01.html). The results were visualized using the GenoSens 2250 Touch gel documentation system (Clinx). First-strand cDNA synthesis was performed on the isolated RNA template using the Magnus reverse transcriptase reagent kit (Eurogen). To amplify the complete coding sequence of the *SURF1* gene, specific primers containing additional nucleotide sequences at the 5'-ends complementary to the terminal regions of the linearized pAAV-CAG plasmid were designed for subsequent assembly by the TLTC method. The primers had the following structure: forward primer SURF1-dir:5'-tgtccaggcggccgccATGGCGGCG GTGGCT-3' reverse primer SURF1-rev: 5'-aggcacagtcgagg cagatctTCACACACCAGGTGTCCCAC-3' (lowercase letters denote sequences homologous to the vector, and uppercase letters denote regions complementary to the beginning and end of the *SURF1* gene open reading frame). Primer annealing temperatures and specificities were calculated using Primer3. The *SURF1* gene was amplified using polymerase chain reaction (PCR). The amplification protocol included an initial denaturation at 95 °C for 5 minutes, 30 cycles (denaturation at 95 °C for 30 seconds, annealing at 62 °C for 30 seconds, elongation at 72 °C for 1 minute), and a final elongation at 72 °C for 5 minutes. PCR products were analyzed by electrophoresis in a 1% agarose gel.

The pAAV-CAG plasmid vector was prepared for cloning using PCR amplification with the Vec-dir (AGATCTGCCTCGACTGTGCCT) and Vec-rev (GGCGGCCGCCTGGACA) primers and Kapa polymerase (Rosche). This ensured the production of a linear molecule with terminal sequences homologous to the amplified *SURF1* gene. Recombinant plasmid assembly was performed using the T5 exonuclease-dependent assembly method. The purified *SURF1* gene PCR product was mixed with the linearized vector supplemented with T5 exonuclease and the mixture was incubated on ice for 5 minutes. Two microliters of the reaction mixture were used to transform chemically competent E. coli strain XL-Blue (Eurogen) cells according to the standard method [13].

Plasmid DNA was isolated from the cultures using the miniprep method and Plasmid Miniprep 2.0 kit (Eurogen). Primary screening of positive clones was performed using PCR with SURF1-specific primers. The accuracy of the resulting recombinant construct was further confirmed by restriction analysis with PstI endonuclease in buffer Orange (SibEnzyme), followed by restriction profile analysis by agarose gel electrophoresis.

Assessing the cytotoxic effect of the AAV vector carrying the *hSURF1* gene

The cytotoxic effect of the virus was assessed using the MTT assay on the viability of subcutaneous fibroblasts from patients

Table 2. Primer characteristics

Gene	Primer direction	Primer sequence 5'->3'	Primer length, n.p.	Product length, n.p	Annealing T, C
GAPDH	Direct	GGATTTGGTCGTATTGGG	18	205	55.5
	Reverse	GGAAGATGGTGATGGGATT	19		
SURF1	Direct	GCGGCCTCATCTCCT	15	281	58.6
	Reverse	CTCTGCGCCTGTGATTC	17		
MTCO1	Direct	CCTACTCCTGCTCGCATCTG	20	363	59.4
	Reverse	AGAATGGGGTCTCCTCCTCC	20		

without the Surf1 mutation. Cell cultures from passage 4 were seeded in 96-well transparent flat-bottomed plates (Greiner Bio-One, Austria) at a concentration of 1 × 10^5 cells/well. After 24 hours of cultivation at 37 °C and 5% CO_2, the cells were treated with various concentrations of the vector: 10^{13}, 10^{12}, 10^{10}, and 10^8 viral particles per ml of culture medium. Control wells were supplemented with culture medium in appropriate quantities instead of viral particles. After adding viral particles, the cells were incubated for 24 hours under the conditions described above. At the end of the incubation, 20 µl of a solution containing 4,5-dimethylthiazol-2-yl-2,5-diphenyltetrazolium bromide (MTT, Santa Cruz) at a concentration of 5 mg/ml were added to each well of the microplate. After 4 hours, the medium with the MTT reagent was removed, and 100 µl of dimethyl sulfoxide (DMSO) were added to the wells to solubilize formazan crystals. Optical density was measured using an ELISA microplate reader at 570 nm. The assay was performed in triplicate to calculate the mean half-maximal inhibitory concentration (IC_{50}) of viral particles and standard deviation.

Electrophoresis and Western blot analysis of target proteins in whole blood and fibroblasts lysates

To analyze the relative content of the studied proteins in whole blood and subcutaneous fibroblasts lysates with and without viral infection, samples were separated by SDS-polyacrylamide gel electrophoresis followed by electro transfer to a nitrocellulose membrane (Bio-Rad) [15]. The membranes were incubated with specific primary antibodies (anti-Surf1 (Abcam; ab110256, 1 : 1000), anti-MTCO1 (Abcam; ab14705, 1 : 1000) followed by incubation with secondary anti-species HRP-linked antibodies. The signals were analyzed by enhanced chemiluminescence assay using the Novex™ ECL Chemiluminescent Substrate Reagent Kit (INVITROGEN, USA) according to the manufacturer's instructions. The signal from the proteins of interest was normalized to the total protein content determined by the staining intensity using Ponceau's dye (0.5% in 1% acetic acid).

Target Genes Expression Assessment in Fibroblasts Lysates after Transfection

Gene expression was assessed by real-time reverse transcription using polymerase chain reaction (PCR) with transcript-specific primers (Table 1). RNA isolation and purity analysis were performed as described above. For reverse transcription (RT), 2 µl of 20 µM random hexaprimer were added to 0.5 µg of total RNA and incubated for 2 min at 70 °C. The tube was then transferred to ice, and 4 µl of 5x RT buffer, 2 µl of 10 mM dNTP mixture, 2 µl of 20 mM DTT, and 1 µl of MMLV reverse transcriptase (50 U/µl) (Eurogen, Russia) were added. The mixture was incubated for 40 min at 40 °C and the reaction was stopped by heating for 10 min at 70 °C. Subsequent real-time PCR was carried out according to the following scheme: 50 ng of template cDNA, 0.4 µl of each forward and reverse primer (100 pmol), 2 µl of 5xqPCRmixHS SYBR. Amplification was monitored by electrophoresis in 3% agarose gel. Statistical data processing was performed using the QGENE software (2-ΔCt method). The expression of each target gene was normalized to the glyceraldehyde-3-phosphate dehydrogenase (*GAPDH*) gene. In the course of the study, primers specific to the transcripts of the corresponding genes were selected (Table 2).

RESULTS

The relative content of SURF1 and MTCO1 proteins in venous blood cells of 20 pediatric patients (3–11 years old) without mitochondrial pathologies (control group) was determined using Western blot analysis. Data for reference values are presented in Fig. 1. It was shown that the relative content of the studied proteins is reduced in patients with mutations in the *SURF1* gene compared to the control group.

To determine the safety of viral construction, a dose of 104 per cell was found to be optimal based on the results of a study examining the relationship between cell viability and the number of viral particles used for transfection (Fig. 2). Next,

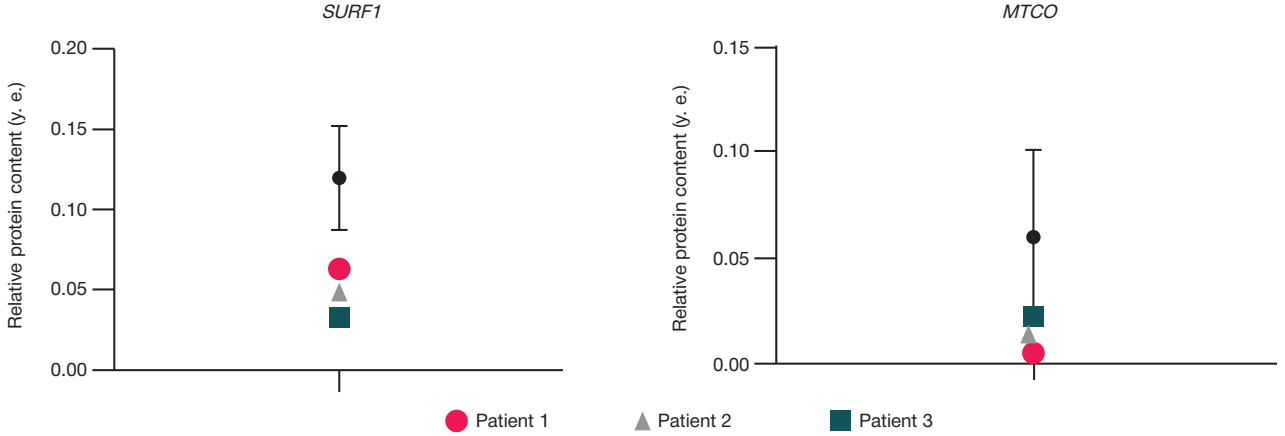


Fig. 1. Relative protein content in whole blood cells obtained for a samples (*n* = 20, *black circles*) of healthy patients (3–11 years) and patients with Leigh syndrome (*colored symbols*) are presented as mean with 95% percentiles in deviations

an adenoviral construct with a normal *SURF1* gene analogue was added to fibroblasts from patients with a mutation in the *SURF1* gene and to control fibroblasts at a dose optimized to ensure no reduction in cell viability in the MTT assay.

Expression of the *SURF1* and *MTCO1* genes in fibroblast lysates after infection with AAV9-SURF1

We used quantitative PCR to evaluate the expression levels of target genes in fibroblasts treated with the gene therapy construct (Fig. 3). First, we found that fibroblasts from patients without SURF1 mutations had significantly higher expression levels than fibroblasts from patients with Leigh syndrome and *SURF1* mutations (Fig.3, left panel). Furthermore, MTCO1 expression levels were not significantly different between fibroblasts from patients and controls (Fig.3, right panel). Second, SURF1 expression levels significantly increased in fibroblasts from patients with mutations and did not significantly differ from the expression levels of this gene in control fibroblasts treated with the gene therapy construct.

We observed a similar pattern for the *MTCO1* gene — a significant increase following transfection in diseased fibroblasts compared to pre-transfection levels. Interestingly, the *MTCO1* gene expression level after transfection was several times higher than baseline for both diseased and healthy cells (Fig. 3).

Western blot analysis of SURF1 and MTCO1 content in fibroblasts

When analyzing the levels of target proteins after exposure to the gene therapy construct, we identified significant differences between control cells and subcutaneous fibroblasts from a patient with the *SURF1* mutation. Using Western blot analysis, we assessed changes in the relative amounts of the studied proteins and showed that 24 hours after virus introduction into the culture medium, both wild-type cells and SURF1 mutants showed a significant increase in protein levels ($p < 0.05$), but this increase was more pronounced for fibroblasts from patients with the mutation (Fig. 4, left panel). We also demonstrated that the baseline SURF1 protein level in wild-type cells was significantly higher than in mutant cells. As for the MTCO1 protein, which is initially significantly more abundant in wild-type cells, no increase in its expression under the influence

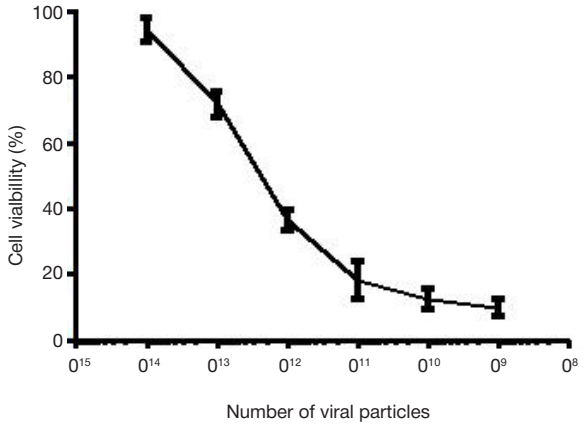


Fig. 2. Cytotoxic effect of the virus on control fibroblasts. The assay was performed three times to calculate the mean half-maximal inhibitory concentration (IC_{50}) and standard deviation

of the virus is observed in control fibroblasts, while for cells from patients with the SURF1 mutation, the MTCO1 level is significantly increased 24 hours after adding the virus to the cells (Fig.4, right panel) and even exceeds the protein level in wild-type cells ($p < 0.05$).

DISCUSSION

In frame of the generally accepted concept that SURF1 protein plays a critical role in the assembly of the cytochrome oxidase holoenzyme, from a mechanistic point of view it can be proposed that the loss of SURF1 protein affects COX activity by stabilizing the structure of the multiprotein complex in the mitochondrial membrane [15]. When Leigh syndrome manifests in patients with mutations in the *SURF1* gene, usually no more than 20% of COX activity is retained, while in model animals with a knockout of this gene, at least 50% of the enzyme activity remains, which leads to such a significant difference between the phenotypes of patients with Leigh syndrome and mice deficient in the SURF1 protein [12]. On the other hand, although the use of such models does not seem promising due to the observed phenotypic differences, gene therapy using an AAV9-SURF1-based vector resulted in a significant (up to 30%) [12] improvement in COX activity in the brain, muscle, and liver of SURF1-deficient mice.

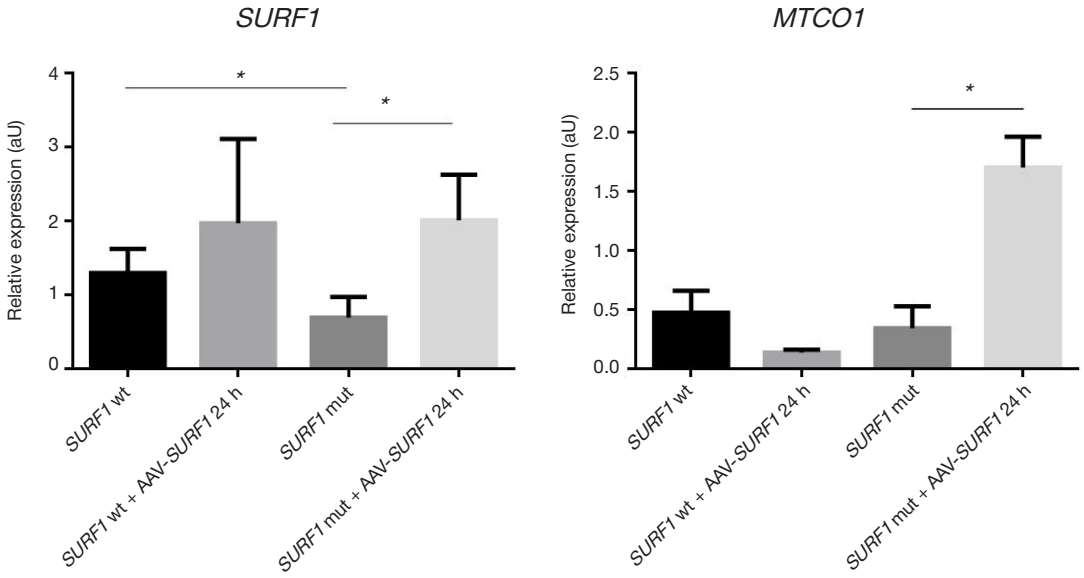


Fig. 3. Expression of the *SURF1* and *MTCO1* genes in lysates of subcutaneous fibroblasts from patients without the mutation (wt — wild type in the graphs) and with a mutation in the *SURF1* gene (SURF1 mut.) 24 hours after infection with AAV9-SURF1; * — $p < 0.05$ (Mann–Whitney)

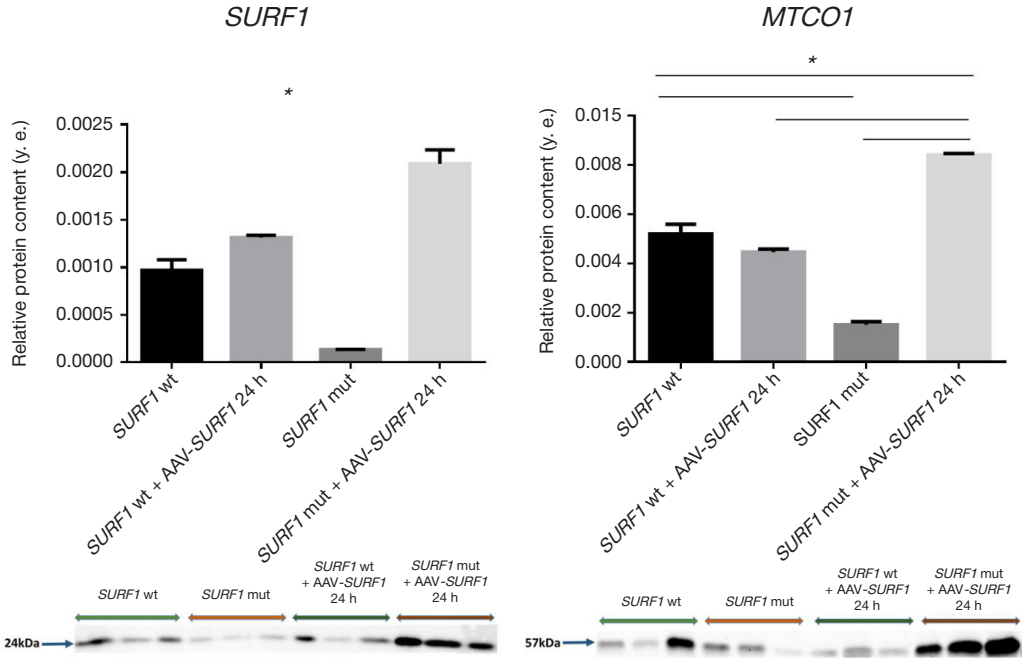


Fig. 4. Relative amount of SURF1 and MTCO1 proteins in lysates of subcutaneous fibroblast from patients without the *SURF1* mutation (wt — wild type in the graphs) and with the mutation in the *SURF1* gene (SURF1 mut.) 24 hours after infection with AAV9-SURF1 (upper panel); * — $p < 0.05$ (Mann–Whitney). The lower panel shows representative electrophoregrams illustrating changes in the levels of target proteins under the influence of the viral construct

In our model, in which we compared the effect of AAV9-SURF1 transfection of fibroblasts from patients with clinically diagnosed Leigh syndrome and fibroblasts from healthy children, we aimed to determine not only the expression level of SURF1 protein but also MTCO1, which is commonly used as a marker for the level and native structure of the entire cytochrome oxidase. The observed synchronous increase in the expression levels of both the *SURF1* and *MTCO1* genes and proteins in fibroblasts from patients, along with the previously observed improvements in the condition of model animals with similar changes in response to gene therapy, suggest the possibility of increased cytochrome oxidase activity. Measuring this activity is our goal for next study on cells from patients with Leigh syndrome to further substantiate the need to continue preclinical trials of the proposed adenoviral-based drug.

The proposed approach to studying the effectiveness of gene therapy in patient cells avoids the shortcomings of the mouse model, where, according to the researchers, a more severe phenotype must be created to detect an effect due to the absence of behavioral defects and neuromotor impairments. It has previously been shown that in existing model animals, the manifestation of the disease in a mild form is due to the activation of compensatory mechanisms in surviving individuals during natural selection, in contrast to humans, where medical care leads to survival even when a severe form of the disease manifests. [10].

CONCLUSIONS

The resulting AAV9-hSURF1 construct allows for safe transfection at a dose that, after just 24 hours, leads to the possibility of recording a reliable multiple increase in the expression of both genes and proteins *SURF1* and *MTCO1* in cells from patients with Leigh syndrome with an initially low content of these proteins compared to cells from healthy individuals.

References

1. Leigh D. Subacute necrotizing encephalomyelopathy in an infant. J Neurol Neurosurg Psychiatry. 1951; 14 (3): 216–21. DOI: 10.1136/jnnp.14.3.216
2. Freya A Bundschuh 1, Achim Hannappel, Oliver Anderka, Bernd Ludwig. Surf1, associated with Leigh syndrome in humans, is a heme-binding protein in bacterial oxidase biogenesis. J Biol Chem. 2009; 284 (38): 25735–41. DOI: 10.1074/jbc.M109.040295.
3. Valeria Tiranti, Konstanze Hoertnagel, Rosalba Carrozzo, Claudia Galimberti, Monica Munaro, Matteo Granatiero et al. Mutations of SURF-1 in Leigh Disease Associated with Cytochrome c Oxidase Deficiency.1998; 63: 1609–21.
4. Zhiqing Zhu, Jianbo Yao, Timothy Johns, Katherine Fu, Isabelle De Bie, Carol Macmillan, et al. SURF1, encoding a factor involved in the biogenesis of cytochrome c oxidase, is mutated in Leigh syndrome. Nature Genetics. 1998; 20: 337–43.
5. Inn-Chi Lee, Kuo-Liang Chiang. Clinical Diagnosis and Treatment of Leigh Syndrome Based on SURF1: Genotype and Phenotype Antioxidants. 2021; 10 (12): 1950. Available from: https://doi.org/10.3390/antiox10121950.
6. Shamima Rahman. Gastrointestinal and hepatic manifestations of mitochondrial disorders. SSIEM Symposium. 2012; Available from: https://doi.org/10.1007/s10545-013-9614-2
7. Albert Z Lim, Yi Shiau Ng, Alasdair Blain, Cecilia Jiminez-Moreno, Charlotte L Alston, Victoria Nesbitt, et al. Natural History of Leigh Syndrome: A Study of Disease Burden and Progression. Ann Neurol. 2022; 91 (1): 117–30. DOI: 10.1002/ana.26260. Epub 2021 Nov 12.
8. Yehani Wedatilake, Ruth M Brown, Robert McFarland, Joy Yaplito-Lee, Andrew A M Morris, Mike Champion, et al. SURF1 deficiency: a multi-centre natural history study. Orphanet Journal of Rare Diseases. 2013; 8 (96).
9. Andrzej Bartke. New findings in gene knockout, mutant and transgenic mice. Exp Gerontol. 2008; 43 (1): 11–4. DOI: 10.1016/j.exger.2007.10.009.

10. Daniel A Pulliam, Sathyaseelan S Deepa, Yuhong Liu, Shauna Hill, Ai-Ling Lin, Arunabh Bhattacharya, et al. Complex IV-deficient Surf1(–/–) mice initiate mitochondrial stress responses. Biochem J. 2014; 462 (2): 359–71. DOI: 10.1042/BJ20140291.
11. Qinglan Ling, Matthew Rioux, Harrison Higgs, Yuhui Hu, Scarlett E. Dwyer, Steven J. Gray Improved AAV9-based gene therapy design for SURF1-related Leigh syndrome with minimal toxicity. Molecular therapy. 2025; 33 (3): 101554.
12. Qinglan Ling, Matthew Rioux, Yuhui Hu, MinJae Lee, Steven J Gray. Adeno-associated viral vector serotype 9-based gene replacement therapy for SURF1-related Leigh syndrome. Mol Ther Methods Clin Dev. 2021; 23: 158–68. DOI: 10.1016/j.omtm.2021.09.001.
13. Hanahan D, Jessee J, Bloom FR. Plasmid transformation of Escherichia coli and other bacteria. Methods Enzymol. 1991; 204 (C): 63–113.
14. Khashchenko EP, Vysokikh MYu, Marey MV, Sidorova KO, Manukhova LA, Shkavro NN, et al. Altered Glycolysis, Mitochondrial Biogenesis, Autophagy and Apoptosis in Peritoneal Endometriosis in Adolescents. Int J Mol Sci. 2024; 25: 4238. Available from: https://doi.org/10.3390/ijms25084238.
15. Giuseppe Magro, Vincenzo Laterza, Federico Tosto. Leigh Syndrome: A Comprehensive Review of the Disease and Present and Future Treatments Biomedicines. 2025, 13 (3): 733. Available from: https://doi.org/10.3390/biomedicines13030733.

Литература

1. Leigh D. Subacute necrotizing encephalomyelopathy in an infant. J Neurol Neurosurg Psychiatry. 1951; 14 (3): 216–21. DOI: 10.1136/jnnp.14.3.216
2. Freya A Bundschuh 1, Achim Hannappel, Oliver Anderka, Bernd Ludwig. Surf1, associated with Leigh syndrome in humans, is a heme-binding protein in bacterial oxidase biogenesis. J Biol Chem. 2009; 284 (38): 25735–41. DOI: 10.1074/jbc.M109.040295.
3. Valeria Tiranti, Konstanze Hoertnagel, Rosalba Carrozzo, Claudia Galimberti, Monica Munaro, Matteo Granatiero et al. Mutations of SURF-1 in Leigh Disease Associated with Cytochrome c Oxidase Deficiency.1998; 63: 1609–21.
4. Zhiqing Zhu, Jianbo Yao, Timothy Johns, Katherine Fu, Isabelle De Bie, Carol Macmillan, et al. SURF1, encoding a factor involved in the biogenesis of cytochrome c oxidase, is mutated in Leigh syndrome. Nature Genetics. 1998; 20: 337–43.
5. Inn-Chi Lee, Kuo-Liang Chiang. Clinical Diagnosis and Treatment of Leigh Syndrome Based on SURF1: Genotype and Phenotype Antioxidants. 2021; 10 (12): 1950. Available from: https://doi.org/10.3390/antiox10121950.
6. Shamima Rahman. Gastrointestinal and hepatic manifestations of mitochondrial disorders. SSIEM Symposium. 2012; Available from: https://doi.org/10.1007/s10545-013-9614-2
7. Albert Z Lim, Yi Shiau Ng, Alasdair Blain, Cecilia Jiminez-Moreno, Charlotte L Alston, Victoria Nesbitt, et al. Natural History of Leigh Syndrome: A Study of Disease Burden and Progression. Ann Neurol. 2022; 91 (1): 117–30. DOI: 10.1002/ana.26260. Epub 2021 Nov 12.
8. Yehani Wedatilake, Ruth M Brown, Robert McFarland, Joy Yaplito-Lee, Andrew A M Morris, Mike Champion, et al. SURF1 deficiency: a multi-centre natural history study. Orphanet Journal of Rare Diseases. 2013; 8 (96).
9. Andrzej Bartke. New findings in gene knockout, mutant and transgenic mice. Exp Gerontol. 2008; 43 (1): 11–4. DOI: 10.1016/j.exger.2007.10.009.
10. Daniel A Pulliam, Sathyaseelan S Deepa, Yuhong Liu, Shauna Hill, Ai-Ling Lin, Arunabh Bhattacharya, et al. Complex IV-deficient Surf1(–/–) mice initiate mitochondrial stress responses. Biochem J. 2014; 462 (2): 359–71. DOI: 10.1042/BJ20140291.
11. Qinglan Ling, Matthew Rioux, Harrison Higgs, Yuhui Hu, Scarlett E. Dwyer, Steven J. Gray Improved AAV9-based gene therapy design for SURF1-related Leigh syndrome with minimal toxicity. Molecular therapy. 2025; 33 (3): 101554.
12. Qinglan Ling, Matthew Rioux, Yuhui Hu, MinJae Lee, Steven J Gray. Adeno-associated viral vector serotype 9-based gene replacement therapy for SURF1-related Leigh syndrome. Mol Ther Methods Clin Dev. 2021; 23: 158–68. DOI: 10.1016/j.omtm.2021.09.001.
13. Hanahan D, Jessee J, Bloom FR. Plasmid transformation of Escherichia coli and other bacteria. Methods Enzymol. 1991; 204 (C): 63–113.
14. Khashchenko EP, Vysokikh MYu, Marey MV, Sidorova KO, Manukhova LA, Shkavro NN, et al. Altered Glycolysis, Mitochondrial Biogenesis, Autophagy and Apoptosis in Peritoneal Endometriosis in Adolescents. Int J Mol Sci. 2024; 25: 4238. Available from: https://doi.org/10.3390/ijms25084238.
15. Giuseppe Magro, Vincenzo Laterza, Federico Tosto. Leigh Syndrome: A Comprehensive Review of the Disease and Present and Future Treatments Biomedicines. 2025, 13 (3): 733. Available from: https://doi.org/10.3390/biomedicines13030733.

PIPELLE AND ENDOBRUSH CATHETERS DO NOT PREVENT CONTAMINATION OF ENDOMETRIAL SAMPLES BY CERVICAL MICROBIOTA

Zornikov DL[1]✉, Bekhter AA[1], Kornilov DO[1], Simarzina VM[1], Nechaeva DM[1], Karyakina AE[1], Leshukova MA[1], Amineva PG[1,3], Voroshilina ES[1,2]

[1] Ural State Medical University, Yekaterinburg, Russia
[2] Medical Center “Garmonia”, Yekaterinburg, Russia
[3] LLC “Quality Med”, Yekaterinburg, Russia

The risk of contamination by cervical microbiota during transcervical sampling represents a fundamental methodological challenge in endometrial microbiome research. This study aimed to experimentally evaluate the efficacy of Pipelle and Endobrush endometrial sampling catheters in preventing this contamination. An *in vitro* cervix model with two anatomically distinct canal types (cylindrical and slit-like) was developed and filled with a synthetic cervical mucus containing a defined quantity of bacterial DNA. After catheter passage through the model cervical canal, a simulated ‘endometrial’ sample (sterile air) was collected and subjected to quantitative PCR analysis. Both catheter types facilitated substantial transfer of bacterial DNA from the cervical mucus into the endometrial sample. The median transfer of total bacterial DNA was 81.6% [54.4–107] for the Pipelle catheter and 29.8% [14.8–56.3] for the Endobrush catheter (p = 0.009), indicating that neither device provided sufficient protection for reliable characterization of the endometrial microbiota. Catheter efficacy was further dependent on cervical canal morphology and the specific microbial group analyzed. These findings demonstrate that transcervical sampling with either catheter type introduces a significant and variable degree of cervical contamination, thereby confounding the interpretation of endometrial microbiota data and underscoring the need to conceptualize and study a combined cervico-endometrial microbiota.

Keywords: endometrial microbiota, cervical canal, contamination, Pipelle catheter, Endobrush catheter, real-time PCR, molecular diagnostics

Author contribution: Zornikov DL — study organization, data analysis, statistical analysis, writing and editing of the article; Bekhter AA — development and creation of *in vitro* cervical models; Kornilov DO — development and creation of *in vitro* cervical models, preparation of illustrations; Simarzina VM — execution of experimental work (sampling from models), manuscript preparation; Nechaeva DM — execution of experimental work (sampling from models), performance of molecular genetic studies (PCR), manuscript preparation; Karyakina AE — performance of molecular genetic studies (PCR), preparation of the manuscript and illustrations; Leshukova MA — manuscript preparation; Amineva PG — preparation and provision of bacterial cultures for analysis; Voroshilina ES — scientific supervision and coordination, analysis and interpretation of data, writing and editing of the article.

Compliance with ethical standards: the study was approved by the Ethics Committee of Ural State Medical University (Protocol № 3 dated June 20, 2025).

✉ **Correspondence should be addressed:** Danila L. Zornikov
Kluchevskaya, 17, Yekaterinburg, Russia, 620109; zornikovdl@gmail.com

Received: 18.11.2025 **Accepted:** 05.12.2025 **Published online:** 13.12.2025

DOI: 10.24075/brsmu.2025.073

УРОГЕНИТАЛЬНЫЕ ЗОНДЫ ТИПА ПАЙПЕЛЬ-С НЕ ПРЕДОТВРАЩАЮТ КОНТАМИНАЦИЮ ЭНДОМЕТРИАЛЬНЫХ ОБРАЗЦОВ ЦЕРВИКАЛЬНОЙ МИКРОБИОТОЙ

Д. Л. Зорников[1]✉, А. А. Бехтер[1], Д. О. Корнилов[1], В. М. Симарзина[1], Д. М. Нечаева[1], А. Е. Карякина[1], М. А. Лешукова[1], П. Г. Аминева[1,3], Е. С. Ворошилина[1,2]

[1] Уральский государственный медицинский университет Минздрава России, Екатеринбург, Россия
[2] Медицинский центр «Гармония», Екатеринбург, Россия
[3] ООО «Кволити Мед», Екатеринбург, Россия

Существенным методологическим ограничением в изучении микробиома эндометрия выступает риск контаминации проб цервикальной микробиотой в ходе трансцервикального взятия материала. Целью работы было экспериментально оценить эффективность урогенитальных зондов типов Пайпель-С1 (Пайпель-биопсия) и Пайпель-С2 (Эндобраш) в предотвращении данного вида контаминации. Для этого была разработана *in vitro* модель шейки матки двух типов (с цилиндрическим и щелевидным каналом), заполненная модельной цервикальной слизью с известным количеством бактериальной ДНК. После прохождения зондами через модельный цервикальный канал выполняли забор «эндометриальной» пробы (стерильный воздух) с последующим количественным ПЦР-анализом. Оба типа зондов продемонстрировали значительный перенос бактериальной ДНК из цервикальной слизи в эндометриальную пробу. Медианный перенос общей бактериальной ДНК составил 81,6% [54,4–107] для Пайпель-С1 и 29,8% [14,8–56,3] для Пайпель-С2 (p = 0,009). Ни один из зондов не обеспечивал защиты от контаминации на уровне, позволяющем достоверно интерпретировать состав микробиоты эндометрия. Эффективность зондов в предотвращении контаминации зависела от анатомической формы канала и конкретной группы микроорганизмов. Полученные результаты свидетельствуют, что ни один из исследованных зондов не обеспечивает надежной защиты от контаминации, что затрудняет интерпретацию данных о составе микробиоты эндометрия в трансцервикально полученных образцах и указывает на целесообразность изучения совокупной цервико-эндометриальной микробиоты.

Ключевые слова: микробиота эндометрия, цервикальный канал, контаминация, зонд Пайпель, ПЦР в реальном времени, молекулярная диагностика

Вклад авторов: Д. Л. Зорников — организация исследования, анализ данных, статистический анализ, написание и редактирование статьи; А. А. Бехтер — разработка и изготовление *in vitro* моделей шейки матки; Д. О. Корнилов — разработка и изготовление *in vitro* моделей шейки матки, подготовка иллюстраций; В. М. Симарзина — проведение экспериментальных работ (взятие проб на моделях), подготовка рукописи; Д. М. Нечаева — проведение экспериментальных работ (взятие проб на моделях), проведение молекулярно-генетических исследований (ПЦР), подготовка рукописи; А. Е. Карякина — проведение молекулярно-генетических исследований (ПЦР), подготовка рукописи и иллюстраций; М. А. Лешукова — подготовка рукописи; П. Г. Аминева — подготовка и предоставление бактериальных культур для анализа; Е. С. Ворошилина — научное руководство и координация, анализ и интерпретация данных, написание и редактирование статьи.

Соблюдение этических стандартов: исследование одобрено этическим комитетом ФГБОУ ВО Уральский государственный медицинский университет Минздрава России (Протокол № 3 от 20 июня 2025 г.).

✉ **Для корреспонденции:** Данила Леонидович Зорников
ул. Ключевская, д. 17, г. Екатеринбург, 620109, Россия; zornikovdl@yandex.ru

Статья получена: 18.11.2025 **Статья принята к печати:** 05.12.2025 **Опубликована онлайн:** 13.12.2025

DOI: 10.24075/vrgmu.2025.073

Since the discovery of resident microbiota in the uterine cavity by molecular genetic methods [1], the study of endometrial microbiota has become a priority area in human microbiome research [2, 3]. That foundational study by Mitchell et al. [1] was performed on hysterectomy specimens, which guarantees the absence of vaginal and cervical microbiota contamination and confirms the presence of resident microorganisms specifically in the endometrium. Subsequent similar studies on excised uteri have shown that the total amount of bacterial DNA in the endometrium is approximately 10 times lower than [4], or comparable to, that in cervical mucus [5].

In clinical practice, transcervical sample collection from the uterine cavity is almost universally used for endometrial microbiome research: using intrauterine insemination catheters or embryo transfer catheters [6, 7], hysteroscopically [8–10], or with Pipelle and Endobrush catheters [11–20], or similar devices with outer and inner sheaths analogous to the Endobrush catheter [21, 22]. In most studies, additional measures are taken to reduce contamination risk, including preliminary washing of the vagina/cervix with saline or antiseptics and comparative analysis of microbiota from different reproductive tract compartments [6, 7, 9–22]. However, the reliability of these approaches, particularly in the context of molecular genetic diagnostics, remains debatable. Studies using transcervically collected endometrial samples reported associations between endometrial microbiota and pregnancy loss [23], chronic endometritis [24], endometrial polyps [10, 18], endometrial hyperplasia [20], endometriosis [25], and polycystic ovary syndrome [26].

Any transcervical sampling method risks contaminating the uterine sample with vaginal, and particularly cervical, microbiota, given the anatomy of the female reproductive tract. This is particularly relevant given that endometrial samples inherently contain fewer microorganisms than cervical samples [4].

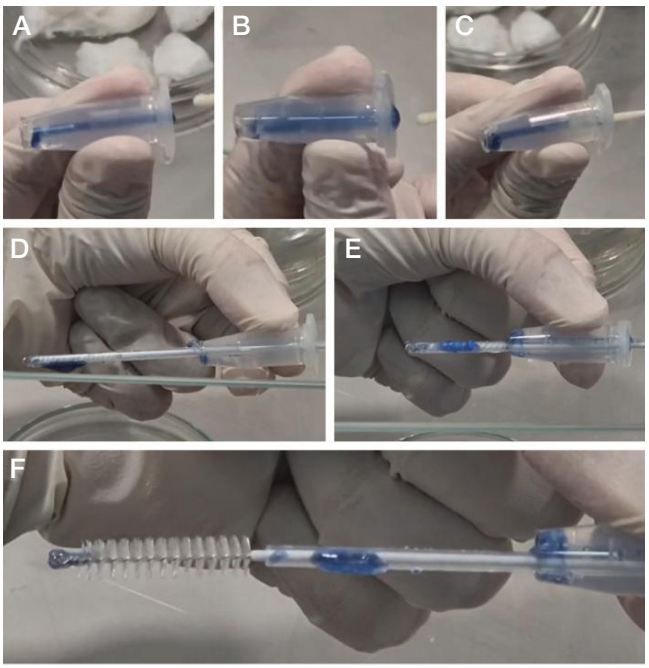


Fig. 1. Anatomical cervical models with canals filled with synthetic gelatin-alginate mucus. For better visualization, the mucus is stained with an aqueous methylene blue solution. **A**. Model with a cylindrical canal. **B**. Model with a slit-like canal. **C**. Sample collection from the cervical canal using a universal A2 catheter. **D**. 'Successful' exit of the Endobrush catheter beyond the cervical canal; the catheter is in the closed position, with minimal mucus on the protective sheath. **E**. 'Unsuccessful' exit of the Endobrush catheter beyond the cervical canal; the catheter is in the closed position, with abundant mucus on the protective sheath. **F**. Transfer of cervical mucus onto the brush of the catheter from the previous panel after the brush was extended

Most of the published studies do not adequately address the potential impact of this contamination on their results, raising questions about the true origin of the reported microbiota. This methodological gap calls into question whether the 'endometrial microbiome' reported in such studies is a true endometrial signal or either a mixture of cervical and endometrial microbiota or an artifact of cervical contamination. Furthermore, transcervical sampling is invasive and risks iatrogenically introducing pathogens from the lower tract into the uterine cavity.

Considering these risks, it is essential to thoroughly evaluate the capabilities and limitations of studying endometrial microbiota in transcervically collected samples, including the use of Pipelle and Endobrush catheters as the most popular tools for this purpose [11–20]. To assess these capabilities and limitations, we need to understand the true efficacy of the catheters in preventing contamination of endometrial samples by cervical microbiota.

The aim of the study was to experimentally evaluate the efficacy of Pipelle and Endobrush intrauterine catheters in preventing cervical microbiota contamination of endometrial samples intended for microbiota analysis.

METHODS

Development of an Experimental Cervical Model

For the experimental evaluation of the catheters efficacy, an *in vitro* model was developed to simulate passage through a cervical canal containing bacterially contaminated mucus.

Fabrication of Anatomical Cervical Models

Two types of cervical models were created using 2% agarose: a model with a cylindrical canal (n = 18), simulating the cervix of a nulliparous woman; and a model with a slit-like canal (n = 18), simulating the cervix of a parous woman.

Sterile Eppendorf tubes were modified by removing the bottom and creating a 5 mm diameter opening in the lid. Forming elements were placed inside: for the cylindrical canal — a 1.5 mm diameter rod (the inner part of the Endobrush catheter), for the slit-like canal — a plastic prism strip measuring 3 × 0.5 mm. The tubes were filled with agarose, and after polymerization, the forming elements were removed. Both openings of the tube (bottom and lid) were sealed with layers of sterile paraffin tape. Immediately before the experiment, the cervical canals of the models were filled with prepared synthetic mucus and incubated at 37°C. Photographs of the completed models are presented in Fig 1.

Preparation of Model (Synthetic) Cervical Mucus

Immediately before the experiment, model cervical mucus was prepared using a base of non-sterile gelatin (instant food-grade gelatin granules 220 bloom, Gold Gello, Tajikistan) and sodium alginate (food-grade sodium alginate powder viscosity 300–400, Qingdao Nanshan Yuanquan Seaweed Co., Ltd., China). Two separate solutions were prepared first: a 4% gelatin solution (40 mg in 1 ml of sterile water with 20 µl of 10% $CaCl_2$) and a 3% sodium alginate solution (30 mg in 1 ml of sterile water). Both initial solutions were incubated at 60°C for 30 minutes in a 'Gnome' thermostat (DNA-Technology LLC, Russia) and thoroughly mixed on a vortex mixer.

Equal volumes (2 ml each) of the prepared solutions were transferred to separate syringes, connected with a Luer Lock adapter, and carefully mixed manually for 2 minutes. The resulting final gel contained 2% gelatin and 1.5% sodium alginate and

demonstrated spinnbarkeit of 1–2 cm. For intentional mucus contamination, 200 µl of a mixture of bacterial cultures containing equal volumes of clinical isolates of *Lactobacillus acidophilus*, *Escherichia coli*, and *Staphylococcus aureus* (optical density 0.5 McFarland for each) was aspirated into the syringe with the final gel. After adding bacteria, the gel was mixed again through the adapter to ensure uniform microorganism distribution. For demonstration models aimed at better visualization of the cervical canal, 0.3% aqueous methylene blue solution was additionally added to the mucus.

Catheters Used for Sampling

Three types of catheters were used for sampling (Fig. 2): a universal urogenital catheter A2 (Meditsinskie Izdeliya, Russia), Pipelle catheter (Unicornmed, China), Endobrush catheter (Unicornmed, China). The A2 catheter was used to collect samples of cervical mucus from the model cervical canal, while the Pipelle and Endobrush catheters were used to collect air samples after passing through the model cervical canal (simulating a sterile uterine cavity).

Study Design and Sampling Protocol

A total of 36 cervical models were used: 18 with cylindrical and 18 with slit-like canals. For each experimental run, 3 models with cylindrical and 3 models with slit-like canals were used. A total of 3 independent replicate experiments were conducted for both Pipelle and Endobrush catheters. The sampling protocol consisted of two steps.

At the first step, a universal A2 catheter was used to collect a mucus sample from the cervical canal at a depth of 1–1.5 cm, which was then transferred to sterile saline.

At the second step, after cervical sampling, a Pipelle or Endobrush catheter was completely passed through the cervical canal to collect a sample beyond the internal os (simulating the uterine cavity). When using the Pipelle catheter, after exiting 3 cm beyond the canal, an air sample was aspirated. When using the Endobrush catheter, the brush was deployed, several rotational movements were performed, and then it was closed.

After collection, the catheter was removed (with the Endobrush kept in its closed state). Its external surface was wiped with 96% ethanol to remove any adherent cervical mucus and prevent contamination of the sample by cervical microbiota. The sample was then transferred to saline. As a negative control sample at the end of each experiment, an air sample was collected using Pipelle/Endobrush catheters without prior passage through the model system.

Molecular Genetic Analysis

Total DNA extraction from all samples was performed using the 'Proba-NK-PLUS' kit (DNA-Technology LLC, Russia). Quantitative microbiota analysis was performed using the 'Androflor' PCR kit (DNA-Technology LLC, Russia) with detection of the following targets: total bacterial load (TBL), *Lactobacillus* spp., *Staphylococcus* spp., and the *Enterobacteriaceae/Enterococcus group* (EE group). The minimum detection threshold for TBL and all target microorganism groups was 10^3 genome equivalents per sample (GE/sample). For each collected sample, one PCR reaction was performed. Target DNA amplification and amplicon detection were performed in DT-Prime 5M thermocyclers using the manufacturer's standard software (DNA-Technology LLC, Russia). Results are presented as medians across all experimental samples with 1st and 3rd quartile values.

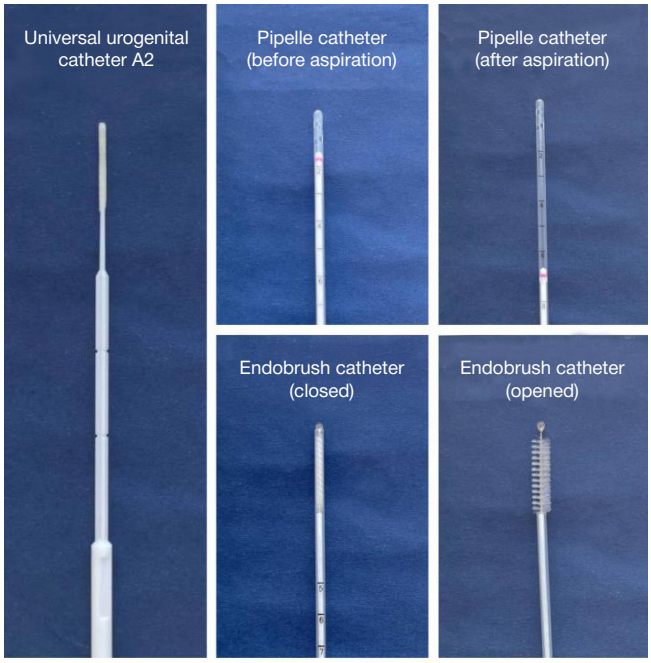


Fig. 2. Catheters used for biomaterial collection. Universal urogenital catheter type A2 for collecting model mucus from the cervical canal. Pipelle and Endobrush catheters used for sampling from the uterine cavity. The Pipelle and Endobrush catheters are shown in two states: before passing through the cervical canal *(central panel)* and after passing through the cervical canal — at the moment of biomaterial collection from the uterine cavity (*right panel*)

Evaluation of Catheter Efficacy in Preventing Contamination

To evaluate catheter efficacy in preventing contamination by cervical microbiota, the percentage transfer of bacterial DNA from 'cervical mucus' to the bacterial DNA-free 'uterine cavity' sample was calculated for each model using the formula:

$$\%\ \text{transfer} = \frac{DNA_{MO,\ \text{uterine cavity (Pipelle/Endobrush)}}}{DNA_{MO,\ \text{cervical mucus (A2)}}} \times 100\%$$

where % transfer — percentage of transferred DNA matrix; $DNA_{MO,\ \text{uterine cavity (Pipelle/Endobrush)}}$ — amount of target microorganism DNA in the 'sterile uterine cavity' sample collected by the investigated Pipelle or Endobrush catheter; $DNA_{MO,\ \text{cervical mucus (A2)}}$ — amount of target microorganism DNA in the cervical mucus of the same model collected by the universal A2 catheter.

Statistical Analysis

Statistical processing and data visualization were performed in R environment, version 4.5.2 (R Foundation for Statistical Computing; Vienna, Austria). Quantitative indicators are presented as median with 1st and 3rd quartile values. For comparison of two independent groups, the non-parametric Mann–Whitney *U*-test was applied. Differences were considered statistically significant at $p < 0.05$.

RESULTS

Initial Microbiota Composition of Models

To assess initial contamination of cervical mucus, samples were collected from all 36 anatomical cervical models (18 with cylindrical and 18 with slit-like canals) using a universal A2

Table 1. Microbial composition of cervical mucus after collection with universal urogenital catheter A2 in models with cylindrical and slit-like canals. Amount of microbial DNA in GE/sample (median, Q_1–Q_3)

Parameter	Cylindrical canal	Slit-like canal	*p*
Total Bacterial Load	$10^{4.9}$ ($10^{4.8}$–10^{5})	10^{5} ($10^{4.9}$–$10^{5.1}$)	0.128
Lactobacillus spp.	$10^{3.5}$ ($10^{3.2}$–$10^{3.9}$)	$10^{3.7}$ ($10^{3.4}$–$10^{3.9}$)	0.375
Staphylococcus spp.	$10^{3.4}$ ($10^{3.1}$–$10^{3.7}$)	$10^{3.6}$ ($10^{3.2}$–$10^{3.9}$)	0.41
EE group	$10^{4.3}$ ($10^{4.1}$–$10^{4.6}$)	$10^{4.5}$ ($10^{4.4}$–$10^{4.7}$)	0.199

catheter. No statistically significant differences were observed in the microbial composition between samples from cylindrical and slit-like canal models (Table 1). Median levels of bacterial DNA were comparable between model groups for all investigated parameters: TBL ($10^{4.9}$ and 10^{5}, $p = 0.128$), *Lactobacillus* spp. ($10^{3.5}$ and $10^{3.7}$, $p = 0.375$), *Staphylococcus* spp. ($10^{3.4}$ and $10^{3.6}$, $p = 0.410$), and EE group ($10^{4.3}$ and $10^{4.5}$, $p = 0.199$).

Efficacy of Pipelle and Endobrush Catheters

Prior to comparative analysis of Pipelle and Endobrush catheter efficacy, the comparability of the initial models intended for their testing was verified. In the models designated for testing the Pipelle catheter, the initial content of *Staphylococcus* spp. was statistically significantly lower ($10^{3.1}$ vs. $10^{3.8}$, $p < 0.001$), while the bacteria of the EE group were significantly higher ($10^{4.6}$ vs. $10^{4.4}$, $p = 0.049$), compared to the group for the Endobrush catheter. At the same time, TBL levels (10^{5} and $10^{4.9}$, $p = 0.612$) and *Lactobacillus* spp. ($10^{3.8}$ and $10^{3.6}$, $p = 0.526$) did not differ significantly between the groups (Table 2).

Pipelle catheters facilitated significant transfer of bacterial DNA from cervical mucus into sterile ‘uterine cavity’ samples. The TBL transfer level ranged from 14% to 172% (median — 81.6%, Q_1–Q_3: 54.4–107%, Table 3). In 12 of 18 models, transfer was less than 100%, while in 6 samples, the TBL amount in sterile ‘uterine cavity’ samples exceeded the initial level in cervical mucus. The DNA transfer level for specific bacterial groups was: for *Lactobacillus* spp. — 25.8% (0–38.7%), for the EE group — 27.6% (11.5–38.7%), and for *Staphylococcus* spp. — 0% (0–0%), below the detection threshold (10^{3} GE/sample) in 100% of cases.

Endobrush catheters demonstrated a statistically significant lower transfer of bacterial DNA (TBL) from cervical mucus into sterile ‘uterine cavity’ samples compared to Pipelle catheters ($p = 0.009$, Table 3). Transfer ranged from 3.9% to 131%, with a median of 29.8% (Q_1–Q_3: 14.8–56.3%). In 12 of 18 models, transfer was less than 50%, in 4 samples — from 50% to 100%, and in 2 samples, the TBL amount in sterile ‘uterine cavity’ samples exceeded the initial level in cervical mucus. Transfer levels for *Lactobacillus* spp. (36.2%; 24.8–61.2%) and the EE group (19%; 9.6–29.4%) were comparable to those observed with Pipelle catheters. In contrast, *Staphylococcus* spp. transfer was significantly higher with Endobrush catheters (14.8%; 0–27.2%) than with Pipelle catheters ($p = 0.004$).

Influence of Canal Shape on Pipelle and Endobrush Catheter Efficacy

The efficacy of Pipelle and Endobrush catheters differed depending on cervical canal shape and microorganism group (Table 4).

For the Pipelle catheter in cylindrical canals, significantly lower contamination levels were observed for *Lactobacillus* spp. (0% vs. 35.2%, $p = 0.032$) and the EE group (19.7% vs. 37.5%, $p = 0.027$). At the same time, no significant differences between canal shapes were detected for *Staphylococcus* spp. (0% vs. 0%, $p = 0.350$) and TBL (71.3% vs. 81.6%, $p = 0.730$).

For the Endobrush catheter, conversely, a trend toward better performance in slit-like canals was noted for TBL contamination level (17.2% vs. 50.8%, $p = 0.052$), while for the remaining parameters, contamination levels were comparable between models with cylindrical and slit-like canals: *Lactobacillus* spp. (41.5% vs. 33.8%, $p = 0.309$), *Staphylococcus* spp. (19.7% vs. 10%, $p = 0.413$), and EE group (19.7% vs. 16.1%, $p = 0.136$).

DISCUSSION

In most endometrial microbiota studies, measures are taken before transcervical sampling to reduce contamination risk, including visual inspection and washing with saline or antiseptics [6, 7, 9–11, 13, 15–22, 27]. However, the efficacy of antiseptics for decontamination is questionable due to short exposure time, particularly in the context of molecular genetic studies that detect DNA from both viable and non-viable microorganisms. Any antimicrobial effect is more likely attributable to mechanical removal of microbial cells rather than true sterilization. Several studies have implemented additional

Table 2. Microbial composition of cervical mucus in models used for evaluation of Pipelle and Endobrush catheter efficacy. Amount of microbial DNA in GE/sample (median, Q_1–Q_3)

Parameter	Pipelle catheter	Endobrush catheter	*p*
Total Bacterial Load	10^{5} ($10^{4.9}$–10^{5})	$10^{4.9}$ ($10^{4.8}$–$10^{5.1}$)	0.612
Lactobacillus spp.	$10^{3.8}$ ($10^{3.4}$–$10^{3.9}$)	$10^{3.6}$ ($10^{3.3}$–$10^{3.8}$)	0.526
Staphylococcus spp.	$10^{3.1}$ ($10^{2.9}$–$10^{3.4}$)	$10^{3.8}$ ($10^{3.5}$–10^{4})	< 0.001
EE group	$10^{4.6}$ ($10^{4.4}$–$10^{4.8}$)	$10^{4.4}$ ($10^{4.2}$–$10^{4.5}$)	0.049

Table 3. Efficacy of Pipelle and Endobrush catheters in preventing contamination by microorganisms of cervical mucus. Contamination level, % DNA transfer from cervical mucus (median, Q_1–Q_3)

Parameter	Pipelle catheter	Endobrush catheter	*p*
Total Bacterial Load	81.6 (54.4–107)	29.8 (14.8–56.3)	0.009
Lactobacillus spp.	25.8 (0–38.7)	36.2 (24.8–61.2)	0.078
Staphylococcus spp.	0 (0–0)	14.8 (0–27.2)	0.004
EE group	27.6 (11.5–38.7)	19 (9.6–29.4)	0.428

Table 4. Efficacy of Pipelle and Endobrush catheters depending on cervical canal shape. Contamination level, % DNA transfer from cervical mucus (median, Q_1–Q_3)

Parameter	Cylindrical canal	Slit-like canal	*p*
Pipelle catheter			
Total Bacterial Load	71.3 (54.4–107)	81.6 (54.4–107)	0.73
Lactobacillus spp.	0 (0–29.6)	35.2 (25.8–67.1)	0.032
Staphylococcus spp.	0 (0–0)	0 (0–0)	0.35
EE group	19.7 (4.7–27.6)	37.5 (32.4–51.7)	0.027
Endobrush catheter			
Total Bacterial Load	50.8 (24.1–100)	17.2 (9.3–33.8)	0.052
Lactobacillus spp.	41.5 (31.6–76.3)	33.8 (22.5–41.5)	0.309
Staphylococcus spp.	19.7 (0–44.4)	10 (0–24.1)	0.413
EE group	19.7 (18.4–62.2)	16.1 (8.2–19.7)	0.136

controls by analyzing vaginal and/or cervical canal microbiota [6, 13, 14, 16, 17, 19, 22]. While this approach may identify gross contamination from distal compartments, it does not adequately address the fundamental problem of admixing microbiota from distinct anatomical niches.

The original clinical application of Pipelle and Endobrush catheters was to obtain endometrial samples for histological or cytological examination [27, 28]. With the Pipelle catheter, sample aspiration occurs only after the device has traversed the cervical canal [29]. The Endobrush catheter incorporates a protective sheath designed to prevent the internal brush from contacting the cervical mucosa during insertion; the brush deploys only within the uterine cavity and retracts before removal. These design features were intended to minimize the inclusion of cervical cells in the sample.

When these catheters are repurposed for microbiological investigation of the endometrium, it is assumed that their design provides adequate protection against contamination by cervical microbiota. However, this assumption overlooks two critical considerations: first, the inherent bacterial load in the uterine cavity is substantially lower than in the cervical canal [4]; second, unlike histological/cytological examination where cell morphology distinguishes endometrial from cervical origin, the anatomical source of detected microorganisms cannot be differentiated.

To assess the actual risk of contamination under controlled conditions that circumvent the limitations of clinical sampling protocols, we developed an experimental *in vitro* model simulating passage through a cervical canal filled with bacterially contaminated mucus (Fig. 1). The spinnbarkeit of the model mucus (1–2 cm) approximated that of genuine cervical mucus during the proliferative phase of the menstrual cycle [29]. The total bacterial DNA load in the model mucus was 10^5 GE/sample, consistent with median levels we have observed in clinical cervical samples using the same PCR assay (unpublished data). Potential background bacterial DNA in the gel matrix did not confound our analysis, as contamination was quantified by calculating the percentage of specific microbial DNA transferred from the cervical mucus sample to the simulated uterine sample within the same model.

The median transfer of bacterial DNA from cervical mucus to simulated uterine cavity samples was 81.6% for Pipelle catheters and 29.8% for Endobrush catheters (Table 3). Given that bacterial DNA levels in genuine endometrial samples typically do not exceed — and are often lower than — those in cervical samples [4, 5], this degree of transfer represents substantial, potentially critical distortion of results. Pipelle catheter sampling, intended for the endometrium, effectively collected cervical mucus instead. In 6 of 18 Pipelle catheter samplings and 2 of 18 Endobrush catheter samplings, the bacterial DNA concentration in the simulated endometrial sample actually exceeded that in the paired cervical sample. This paradoxical finding may reflect more efficient mucus collection by the endometrial sampling catheters compared to the A2 catheter for those specific sample pairs.

DNA transfer levels for *Lactobacillus* spp. and the EE group did not differ significantly between catheter types, with median transfers of 19–36.2%. For *Staphylococcus* spp., transfer was significantly lower with Pipelle catheters (0% vs. 14.8%, $p = 0.004$). However, this difference likely reflects the initially lower *Staphylococcus* spp. concentration in models designated for Pipelle catheter testing ($10^{3.1}$ vs. $10^{3.8}$ GE/sample for Endobrush models, $p < 0.001$) (Table 2). This baseline discrepancy may be attributable to degradation of staphylococcal DNA in the bacterial inoculum, which was refrigerated for three weeks between experimental series (Pipelle catheter experiments followed Endobrush catheter experiments). With the assay's detection limit of 10^3 GE/sample, any reduction from the initial $10^{3.1}$ GE/sample concentration would yield negative results for this bacterial group.

Our results demonstrate a relationship between cervical canal morphology and bacterial DNA transfer (Table 4). With Pipelle catheters, significantly greater transfer of *Lactobacillus* spp. and EE group DNA occurred with slit-like canals (typical of parous women). Conversely, with Endobrush catheters, a trend toward greater total bacterial DNA transfer was observed with cylindrical canals (typical of nulliparous women).

We acknowledge that our model may not fully recapitulate *in vivo* physiology, such as cervical wall tone (resistance), the precise rheological and chemical properties of mucus, or potential microbial gradients along the canal. Consequently, the absolute percentages of DNA transfer should not be directly extrapolated to clinical practice. Nevertheless, our results provide compelling evidence that endometrial sampling with either Pipelle or Endobrush catheters invariably transfers a portion of cervical microbiota into the uterine sample. For the Endobrush catheter, the primary contamination appears to occur after cervical canal transit — during deployment in the uterine cavity, cervical mucus adherent to the protective sheath contacts the brush (Fig. 1, panels E, F). A similar mechanism likely operates with other transcervical sampling devices, as any instrument traversing the cervical canal will inevitably carry cervical mucus into the uterine cavity. Moreover, clinical sampling during the secretory phase may exacerbate this contamination due to increased cervical mucus spinnbarkeit [29].

The demonstration of such contamination when using Pipelle or Endobrush catheters has two major implications: it calls into question the endometrial origin of microbiota detected in such samples, and it confirms the real risk of iatrogenic introduction of microorganisms into the uterine cavity during

these procedures. Given the impossibility of distinguishing the two microbiota sources (cervical canal and endometrium) in transcervical samples, we propose a paradigm shift. Rather than studying a putative 'endometrial microbiota,' research should focus on the combined cervico-endometrial microbial profile obtained from a single sampling procedure.

CONCLUSIONS

In this study, neither Pipelle nor Endobrush intrauterine catheters provided reliable protection against contamination of endometrial samples by cervical microbiota. Both catheter types permitted substantial transfer of bacterial DNA: median transfer levels were 81.6% for Pipelle catheters and 29.8% for Endobrush catheters. Although Endobrush catheters demonstrated 2.5- to 3-fold greater efficacy than Pipelle catheters, a contamination level of 29.8% remains critically significant, particularly given that the bacterial load in the uterine cavity is inherently lower than in the cervical canal for most patients. Catheter efficacy was dependent on both the anatomical configuration of the cervical canal and the specific microbial group analyzed. For Pipelle catheters, efficacy was significantly reduced in slit-like canals for *Lactobacillus* spp. and *Enterococcus/Enterobacteriaceae*, whereas for Endobrush catheters, a trend toward poorer performance was observed in cylindrical canals regarding total bacterial contamination. These findings necessitate a critical reevaluation of studies investigating uterine cavity microbiota using samples obtained with Pipelle or Endobrush catheters, as well as other transcervical sampling methods. As a constructive alternative, we propose reorienting research focus from the analysis of purported 'endometrial microbiota' toward the investigation of the combined cervico-endometrial microbial profile obtained from a single sample collected simultaneously from the cervical canal and uterine cavity. This approach would circumvent the methodological artifacts inherent to contamination-prone sampling techniques.

References

1. Mitchell CM, Haick A, Nkwopara E, Garcia R, Rendi M, Agnew K, et al. Colonization of the upper genital tract by vaginal bacterial species in nonpregnant women. Am J Obstet Gynecol. 2015; 212 (5): 611.e1–611.e9.
2. Polifke A, Schwedler A von, Gulba R, Bensmann R, Dilthey A, Nassar NN, et al. Differential characteristics of vaginal versus endometrial microbiota in IVF patients. Sci Rep. 2024; 14 (1).
3. Franasiak JM, Scott RT. Endometrial microbiome. Curr Opin Obstet Gynecol. 2017; 29 (3): 146–52.
4. Chen C, Song X, Wei W, Zhong H, Dai J, Lan Z, et al. The microbiota continuum along the female reproductive tract and its relation to uterine-related diseases. Nat Commun. 2017; 8: 875.
5. Winters AD, Romero R, Gervasi M, Gomez-Lopez N, Tran MR, Garcia-Flores V, et al. Does the endometrial cavity have a molecular microbial signature? Sci Rep. 2019; 9: 9905.
6. Riganelli L, Iebba V, Piccioni M, Illuminati I, Bonfiglio G, Neroni B, et al. Structural Variations of Vaginal and Endometrial Microbiota: Hints on Female Infertility. Front Cell Infect Microbiol. 2020; 10: 350.
7. Keburiya LK, Smolnikova VYu, Priputnevich TV, Muraveva VV, Trofimov DYu, Shubina ES, i dr. Mikrobiota polosti matki i neudachi implantacii. Est' li svyaz'? Akusherstvo i ginekologiya. 2021; 7: 133–43. Russian.
8. Tapilskaya NI, Budilovskaya OV, Krysanova AA, Tolibova GH, Kopylova AA, Cypurdeeva ND, i dr. Mikrobiota endometriya zhenshchin s hronicheskim endometritom i idiopaticheskim besplodiem. Akusherstvo i ginekologiya. 2020; 4: 72–81. Russian.
9. Qiu T, Liu L, Zhou H, Sheng H, He Y, Liu M, et al. Analysis of endometrial microbiota in intrauterine adhesion by high-throughput sequencing. Ann Transl Med. 2021; 9 (3): 195.
10. Vanakova AI, Dolgushina NV, Denisov PA, Goncharuk OD, Muraveva VV, Priputnevich TV. Osobennosti mikrobioty polosti matki u pacientok s polipami endometriya. Vestnik Rossijskogo gosudarstvennogo medicinskogo universiteta. 2025; 1 (6): 6. Russian.
11. Verstraelen H, Vilchez-Vargas R, Desimpel F, Jauregui R, Vankeirsbilck N, Weyers S, et al. Characterisation of the human uterine microbiome in non-pregnant women through deep sequencing of the V1-2 region of the 16S rRNA gene. Peer J. 2016; 4: e1602.
12. Voroshilina ES, Zornikov DL, Koposova OV, Islamidi DK, Ignatova KYu, Abakumova EI, i dr. Vozmozhnosti ocenki mikrobioty polosti matki s ispol'zovaniem PCR v real'nom vremeni. Vestnik RGMU. 2020; 1: 14–21. Russian.
13. Karahalis LYu, Kononenko TS. Taksonomicheskij profil' mikrobioma endometriya pri hronicheskom endometrite. Akusherstvo i ginekologiya: Novosti. Mneniya. Obucheniya. 2022; 10 (4): 23–30. Russian.
14. Peuranpää P, Holster T, Saqib S, Kalliala I, Tiitinen A, Salonen A, et al. Female reproductive tract microbiota and recurrent pregnancy loss: a nested case-control study. Reproductive BioMedicine Online. 2022; 45 (5): 1021–1031.
15. Bui BN, van Hoogenhuijze N, Viveen M, Mol F, Teklenburg G, de Bruin J-P, et al. The endometrial microbiota of women with or without a live birth within 12 months after a first failed IVF/ICSI cycle. Scientific reports. 2023; 13 (1): 3444.
16. Jain M, Mladova E, Dobychina A, Kirillova K, Shichanina A, Anokhin D, et al. Comparison of microbial profiles and viral status along the vagina-cervix-endometrium continuum of infertile patients. Systems Biology in Reproductive Medicine. 2023; 69 (4): 310–19.
17. Zhang R, Wang M, Zhong J, Xue H. Altered endometrial microbiota profile is associated with poor endometrial receptivity of repeated implantation failure. American Journal of Reproductive Immunology. 2024; 92 (5): e70005.
18. Zhao Y, Liao Y, Xu G, Wang Y. Endometrial microbiota alteration in female patients with endometrial polyps based on 16S rRNA gene sequencing analysis. Front Cell Infect Microbiol. 2024; 14: 1351329.
19. Krysanova AA, Storozheva KV, Budilovskaya OV, Husnutdinova TA, SHalepo KV, Tapilskaya NI, i dr. Arhitektonika mikrobioty endometriya u zhenshchin s besplodiem razlichnogo geneza. Klinicheskaya laboratornaya diagnostika. 2024; 69 (9): 478–86.
20. Ying X, et al. An altered uterine microbiota with endometrial hyperplasia. BMC Microbiol. 2024; 24 (1): 258.
21. Liu Y, Wong KKW, Ko EYL, Chen X, Huang J, Tsui SKW, et al. Systematic comparison of bacterial colonization of endometrial tissue and fluid samples in recurrent miscarriage patients: implications for future endometrial microbiome studies. Clin Chem. 2018; 64 (12): 1743–52.
22. Reschini M, Benaglia L, Ceriotti F, Borroni R, Ferrari S, Castiglioni M, et al. Endometrial microbiome: sampling, assessment, and possible impact on embryo implantation. Sci Rep. 2022; 12: 8467.
23. Moreno I, et al. The first glimpse of the endometrial microbiota in early pregnancy. Am J Obstet Gynecol. 2020; 222 (4): 296–305.
24. Zhang H, Zou H, Zhang C, Li X, Wang Z, Liu C, et al. Chronic endometritis and the endometrial microbiota: implications for reproductive success in patients with recurrent implantation failure. Ann Clin MicrobiolAntimicrob. 2024; 23: 49.
25. Khan KN, Fujishita A, Masumoto H, Muto H, Kitajima M, Masuzaki H, et al. Molecular detection of intrauterine microbial colonization in women with endometriosis. Eur J Obstet Gynecol Reprod Biol. 2016; 199: 69–75.
26. Lee S, et al. The reproductive tract microbiome in women with polycystic ovary syndrome and across different menstrual cycle phases. Hum Reprod. 2025; 40 (3): 518–28.

27. Cornier E. The Pipelle: a disposable device for endometrial biopsy. Am J Obstet Gynecol. 1984; 148 (1): 109–10.
28. Vuopala S, Klemi PJ, Mäenpää J, Salmi T, Mäkäräinen L. Endobrush sampling for endometrial cancer. Acta Obstet Gynecol Scand. 1989; 68 (4): 345350.
29. Cohen MR, Stein IF, Kaye BM. Spinnbarkeit: A Characteristic of Cervical Mucus: Significance at Ovulation Time. Fertil Steril. 1952; 3 (3): 201–09.

Литература

1. Mitchell CM, Haick A, Nkwopara E, Garcia R, Rendi M, Agnew K, et al. Colonization of the upper genital tract by vaginal bacterial species in nonpregnant women. Am J Obstet Gynecol. 2015; 212 (5): 611.e1–611.e9.
2. Polifke A, Schwedler A von, Gulba R, Bensmann R, Dilthey A, Nassar NN, et al. Differential characteristics of vaginal versus endometrial microbiota in IVF patients. Sci Rep. 2024; 14 (1).
3. Franasiak JM, Scott RT. Endometrial microbiome. Curr Opin Obstet Gynecol. 2017; 29 (3): 146–52.
4. Chen C, Song X, Wei W, Zhong H, Dai J, Lan Z, et al. The microbiota continuum along the female reproductive tract and its relation to uterine-related diseases. Nat Commun. 2017; 8: 875.
5. Winters AD, Romero R, Gervasi M, Gomez-Lopez N, Tran MR, Garcia-Flores V, et al. Does the endometrial cavity have a molecular microbial signature? Sci Rep. 2019; 9: 9905.
6. Riganelli L, Iebba V, Piccioni M, Illuminati I, Bonfiglio G, Neroni B, et al. Structural Variations of Vaginal and Endometrial Microbiota: Hints on Female Infertility. Front Cell Infect Microbiol. 2020; 10: 350.
7. Кебурия Л. К., Смольникова В. Ю., Припутневич Т. В., Муравьева В. В., Трофимов Д. Ю., Шубина Е. С. и др. Микробиота полости матки и неудачи имплантации. Есть ли связь? Акушерство и гинекология. 2021; 7: 133–43.
8. Тапильская Н. И., Будиловская О. В., Крысанова А. А., Толибова Г. Х., Копылова А. А., Цыпурдеева Н. Д. и др. Микробиота эндометрия женщин с хроническим эндометритом и идиопатическим бесплодием. Акушерство и гинекология. 2020; 4: 72–81.
9. Qiu T, Liu L, Zhou H, Sheng H, He Y, Liu M, et al. Analysis of endometrial microbiota in intrauterine adhesion by high-throughput sequencing. Ann Transl Med. 2021; 9 (3): 195.
10. Ванакова А. И., Долгушина Н. В., Денисов П. А., Гончарук О. Д., Муравьева В. В., Припутневич Т. В. Особенности микробиоты полости матки у пациенток с полипами эндометрия. Вестник Российского государственного медицинского университета. 2025; 1 (6): 6.
11. Verstraelen H, Vilchez-Vargas R, Desimpel F, Jauregui R, Vankeirsbilck N, Weyers S, et al. Characterisation of the human uterine microbiome in non-pregnant women through deep sequencing of the V1-2 region of the 16S rRNA gene. Peer J. 2016; 4: e1602.
12. Ворошилина Е. С., Зорников Д. Л., Копосова О. В., Исламиди Д. К., Игнатова К. Ю., Абакумова Е. И. и др. Возможности оценки микробиоты полости матки с использованием ПЦР в реальном времени. Вестник РГМУ. 2020; 1: 14–21.
13. Карахалис Л. Ю., Кононенко Т. С. Таксономический профиль микробиома эндометрия при хроническом эндометрите. Акушерство и гинекология: Новости. Мнения. Обучения. 2022; 10 (4): 23–30.
14. Peuranpää P, Holster T, Saqib S, Kalliala I, Tiitinen A, Salonen A, et al. Female reproductive tract microbiota and recurrent pregnancy loss: a nested case-control study. Reproductive BioMedicine Online. 2022; 45 (5): 1021–1031.
15. Bui BN, van Hoogenhuijze N, Viveen M, Mol F, Teklenburg G, de Bruin J-P, et al. The endometrial microbiota of women with or without a live birth within 12 months after a first failed IVF/ICSI cycle. Scientific reports. 2023; 13 (1): 3444.
16. Jain M, Mladova E, Dobychina A, Kirillova K, Shichanina A, Anokhin D, et al. Comparison of microbial profiles and viral status along the vagina-cervix-endometrium continuum of infertile patients. Systems Biology in Reproductive Medicine. 2023; 69 (4): 310–19.
17. Zhang R, Wang M, Zhong J, Xue H. Altered endometrial microbiota profile is associated with poor endometrial receptivity of repeated implantation failure. American Journal of Reproductive Immunology. 2024; 92 (5): e70005.
18. Zhao Y, Liao Y, Xu G, Wang Y. Endometrial microbiota alteration in female patients with endometrial polyps based on 16S rRNA gene sequencing analysis. Front Cell Infect Microbiol. 2024; 14: 1351329.
19. Крысанова А. А., Сторожева К. В., Будиловская О. В., Хуснутдинова Т. А., Шалепо К. В., Тапильская Н. И. и др. Архитектоника микробиоты эндометрия у женщин с бесплодием различного генеза. Клиническая лабораторная диагностика. 2024; 69 (9): 478–86.
20. Ying X, et al. An altered uterine microbiota with endometrial hyperplasia. BMC Microbiol. 2024; 24 (1): 258.
21. Liu Y, Wong KKW, Ko EYL, Chen X, Huang J, Tsui SKW, et al. Systematic comparison of bacterial colonization of endometrial tissue and fluid samples in recurrent miscarriage patients: implications for future endometrial microbiome studies. Clin Chem. 2018; 64 (12): 1743–52.
22. Reschini M, Benaglia L, Ceriotti F, Borroni R, Ferrari S, Castiglioni M, et al. Endometrial microbiome: sampling, assessment, and possible impact on embryo implantation. Sci Rep. 2022; 12: 8467.
23. Moreno I, et al. The first glimpse of the endometrial microbiota in early pregnancy. Am J Obstet Gynecol. 2020; 222 (4): 296–305.
24. Zhang H, Zou H, Zhang C, Li X, Wang Z, Liu C, et al. Chronic endometritis and the endometrial microbiota: implications for reproductive success in patients with recurrent implantation failure. Ann Clin MicrobiolAntimicrob. 2024; 23: 49.
25. Khan KN, Fujishita A, Masumoto H, Muto H, Kitajima M, Masuzaki H, et al. Molecular detection of intrauterine microbial colonization in women with endometriosis. Eur J Obstet Gynecol Reprod Biol. 2016; 199: 69–75.
26. Lee S, et al. The reproductive tract microbiome in women with polycystic ovary syndrome and across different menstrual cycle phases. Hum Reprod. 2025; 40 (3): 518–28.
27. Cornier E. The Pipelle: a disposable device for endometrial biopsy. Am J Obstet Gynecol. 1984; 148 (1): 109–10.
28. Vuopala S, Klemi PJ, Mäenpää J, Salmi T, Mäkäräinen L. Endobrush sampling for endometrial cancer. Acta Obstet Gynecol Scand. 1989; 68 (4): 345350.
29. Cohen MR, Stein IF, Kaye BM. Spinnbarkeit: A Characteristic of Cervical Mucus: Significance at Ovulation Time. Fertil Steril. 1952; 3 (3): 201–09.

CHARACTERISTICS OF SYSTEMIC INFLAMMATION IN PATIENTS WITH ENDOMETRITIS-ASSOCIATED INFERTILITY

Savelieva OE✉, Krivolesova TA, Zhigalina AS, Sigareva LP, Saburov AV, Reznik VA

Saint-Petersburg State Pediatric Medical University, Saint-Petersburg, Russia

Chronic endometritis (CE) is the most significant endometrial disease in terms of its impact on reproductive potential. Thus far, pathogenetically significant inflammatory markers — cytokines, inflammatory proteins, and hematological indices — have not been widely used in medical practice for the diagnosis of CE. This study aimed to evaluate indicators of systemic inflammation, including hematological parameters and inflammatory indices, in patients with infertility, and to determine their diagnostic significance for CE. We analyzed the data of examinations of 50 patients with infertility. The standard hematological method was used to determine the leukocyte count. Based on the blood cell composition, we calculated the inflammatory indices NLR, MLR, PLR, and SII. The concentration of CRP in the blood serum was determined by enzyme immunoassay. In patients with CE-associated infertility, the absolute and relative numbers of lymphocytes were lower ($p = 0.0451$ and $p = 0.0089$, respectively), whereas the relative numbers of monocytes and basophils were higher ($p = 0.0469$ and $p = 0.0005$, respectively) than in patients without CE. In the study group, the concentration of CRP in the blood was almost four times higher than in the control group ($p = 0.0191$), but all indicators remained within the normal range. A comparative analysis of the NLR, MLR, PLR, and SII indices revealed their significant growth in CE-associated infertility cases ($p = 0.0387$, $p = 0.0058$, $p = 0.0335$, and $p = 0.0333$, respectively). ROC analysis established the predictive significance of NLR (0.871 (95% CI: 0.767–0.974); $p < 0.0001$) and MLR (0.848 (95% CI: 0.737–0.958); $p < 0.0001$) indices for detecting CE in infertility patients.

Keywords: chronic endometritis, infertility, inflammatory status, hematological inflammatory indexes

Funding: the work was supported by the Russian Science Foundation grant 24-25-00244.

Author contribution: OE Savelieva — study design, analysis and interpretation of results, article authoring; TA Krivolesova — selection of patients, registration of results, article authoring; AS Zhigalina — data collection and analysis, article authoring; LP Sigareva — literature analysis, statistical processing of results; AV Saburov — selection of patients, registration of results; VA Reznik — research planning and supervision, article editing.

Compliance with ethical standards: the study was approved by the Ethics Committee of St. Petersburg State Medical University (Minutes No. 18/07 of October 27, 2022), conducted in accordance with the federal laws of the Russian Federation (No. 152, 323, etc.) and Declaration of Helsinki 1964, with all subsequent additions and amendments regulating scientific research on biomaterials obtained from humans. All participants signed an informed consent form before participating in the study.

✉ **Correspondence should be addressed:** Olga E. Savelieva
Litovskaya, 2, Saint Petersburg, 194100, Russia; olga_chechina@mail.ru

Received: 29.10.2025 **Accepted:** 03.12.2025 **Published online:** 15.12.2025

DOI: 10.24075/brsmu.2025.071

Copyright: © 2025 by the authors. **Licensee:** Pirogov University. This article is an open access article distributed under the terms and conditions of the Creative Commons Attribution (CC BY) license (https://creativecommons.org/licenses/by/4.0/).

ОСОБЕННОСТИ СИСТЕМНОГО ВОСПАЛИТЕЛЬНОГО СТАТУСА ПАЦИЕНТОК ПРИ ЭНДОМЕТРИТ-АССОЦИИРОВАННОМ БЕСПЛОДИИ

О. Е. Савельева ✉, Т. А. Криволесова, А. С. Жигалина, Л. П. Сигарева, А. В. Сабуров, В. А. Резник

Санкт-Петербургский государственный педиатрический медицинский университет, Санкт-Петербург, Россия

Среди заболеваний эндометрия, снижающих его репродуктивный потенциал, ведущую роль играет хронический эндометрит (ХЭ). Патогенетически значимые воспалительные маркеры, такие как цитокины, воспалительные белки и гематологические индексы, пока не нашли широкого применения в медицинской практике для диагностики ХЭ. Цель исследования — оценить у пациенток с бесплодием показатели системного воспалительного статуса, включая гематологические лабораторные параметры и воспалительные индексы, и определить их диагностическую значимость при ХЭ. Представлены данные исследования 50 пациенток с бесплодием. Подсчет количества лейкоцитов крови проводили стандартным гематологическим методом. На основе клеточного состава крови рассчитывали воспалительные индексы NLR, MLR, PLR и SII. Концентрацию СРБ в сыворотке крови определяли методом иммуноферментного анализа. У пациенток с бесплодием, ассоциированным с ХЭ, абсолютное и относительное количество лимфоцитов было ниже ($p = 0{,}0451$ и $p = 0{,}0089$ соответственно), а относительное количество моноцитов и базофилов было выше ($p = 0{,}0469$ и $p = 0{,}0005$ соответственно), чем у пациенток без ХЭ. У пациенток из исследуемой группы концентрация СРБ в крови была почти в 4 раза выше, чем у пациенток из группы сравнения ($p = 0{,}0191$). При этом все показатели оставались в пределах нормальных значений. Сравнительный анализ индексов NLR, MLR, PLR и SII показал их статистически значимое повышение при бесплодии, ассоциированном с ХЭ ($p = 0{,}0387$, $p = 0{,}0058$, $p = 0{,}0335$ и $p = 0{,}0333$ соответственно). ROC-анализ позволил установить предиктивную значимость у индексов NLR (0,871 (95% ДИ: 0,767–0,974); $p < 0{,}0001$) и MLR (0,848 (95% ДИ: 0,737–0,958); $p < 0{,}0001$) для выявления ХЭ у пациенток с бесплодием.

Ключевые слова: хронический эндометрит, бесплодие, воспалительный статус, гематологические воспалительные индексы

Финансирование: работа выполнена при финансовой поддержке гранта РНФ 24-25-00244.

Вклад авторов: О. Е. Савельева — дизайн исследования, анализ и интерпретация результатов, написание статьи; Т. А. Криволесова — отбор пациентов, получение результатов, написание статьи; А. С. Жигалина — получение и анализ данных, написание статьи; Л. П. Сигарева — анализ литературы, статистическая обработка результатов; А. В. Сабуров — отбор пациентов, получение результатов; В. А. Резник — планирование и руководство исследованием, редактирование статьи.

Соблюдение этических стандартов: исследование одобрено этическим комитетом СПбГПМУ (протокол №18/07 от 27 октября 2022 г.), проведено в соответствии с федеральными законами Российской Федерации (№ 152, 323 и др.) и Хельсинкской декларацией 1964 г. со всеми последующими дополнениями и изменениями, регламентирующими научные исследования на биоматериале, полученном у людей. Все участники подписали информированное добровольное согласие на участие в исследовании.

✉ **Для корреспонденции:** Ольга Евгеньевна Савельева
ул. Литовская, д. 2, г. Санкт-Петербург, 194100, Россия; olga_chechina@mail.ru

Статья получена: 29.10.2025 **Статья принята к печати:** 03.12.2025 **Опубликована онлайн:** 15.12.2025

DOI: 10.24075/vrgmu.2025.071

Авторские права: © 2025 принадлежат авторам. **Лицензиат:** РНИМУ им. Н. И. Пирогова. Статья размещена в открытом доступе и распространяется на условиях лицензии Creative Commons Attribution (CC BY) (https://creativecommons.org/licenses/by/4.0/).

Currently, there is a clear upward trend in cases of pelvic inflammatory disease becoming chronic among women, with the immune and endocrine systems involved in the pathological process [1]. This adversely affects the reproductive function of patients and can lead to infertility.

Chronic endometritis (CE) is the most significant endometrial disease in terms of its impact on reproductive potential. According to various sources, from 0.2 to 46.3% of women of reproductive age suffer from CE [2]. The considerable breadth of this range arises from variations in diagnostic approaches among researchers. Chronic endometritis is a persistent low-intensity inflammation of the endometrium with infiltration of the stroma by immunocompetent cells, leading to disruption of its cyclic biotransformation and receptivity [2, 3].

Currently, the diagnosis, prevention, and restoration of reproductive function in patients with CE are considerably complex matters. This pathology is often asymptomatic, or presents with nonspecific symptoms such as chronic pelvic pain, mucous or mucopurulent vaginal discharge, dyspareunia, abnormal uterine bleeding, or recurrent cystitis [1]. An objective assessment of the prevalence of CE is hampered by the said lack of symptoms (in most cases) and the need for a biopsy to verify the diagnosis, as a definitive conclusion requires pathomorphological examination [3].

In recent years, the number of patients with CE-associated infertility has been steadily increasing. It has been established that from 2.8 to 56.8% of women with confirmed CE are diagnosed infertile [4]. In cases of infertility associated with a chronic inflammatory process, laboratory test results may appear normal, clinical symptoms may be absent, yet immune cell function is often disrupted at both local and systemic levels. The resulting destructive immune-inflammatory process requires appropriate anti-inflammatory and immunomodulatory therapy [5–6]. In addition, CE is one of the causes of spontaneous pathological termination of pregnancy and repeated implantation failures in the context of using assisted reproductive technology to treat infertility [7]. Nevertheless, this disease is still not on the list of conditions checked for before in vitro fertilization (IVF).

The foregoing necessitates the development of new methods for diagnosing and treating CE-associated endometrial pathology and disorders of endometrial receptivity. One of the promising areas of research is determination of the inflammatory status of infertile women. Hematological inflammatory indices can be used for this purpose in clinical practice [8]. For example, the NLR inflammatory index, defined as the ratio of neutrophils to lymphocytes, serves as an indicator of systemic inflammation and reflects the overall state of the immune system under various stress conditions [9]. The PLR index is the ratio of platelets to lymphocytes; platelets are a source of TGFb and VEGF, which contribute to the chronicity of the inflammatory process [10]. The use of these indices as markers of chronic inflammation has become increasingly common [8]. The MLR index, which is the ratio of monocytes to lymphocytes, is not as popular. This index is associated with systemic inflammation [11]. Another inflammatory marker that clinicians have begun to use more frequently in recent years is the SII. When its value is high, the patient's immune function is suppressed and inflammatory processes are activated [12].

Thus, hematological inflammatory indices may prove to be highly informative systemic markers of chronic subclinical inflammation associated with CE, which could facilitate the development of new strategies for anti-inflammatory and immunomodulatory therapy and methods of restoration of reproductive function.

This study aimed to evaluate indicators of systemic inflammation, including hematological parameters and inflammatory indices, in patients with infertility, and to determine their diagnostic significance for CE.

METHODS

Patients

We analyzed the examination results of 50 patients aged 24–43 years (median age 37 [32–40] years). The study group included 27 patients diagnosed with CE-associated infertility, while the control group comprised 23 patients without signs of CE, whose infertility was attributed to the male factor. The participants were women preparing for IVF in the Department of Assisted Reproductive Technologies. The patients underwent ultrasound examination with Doppler assessment of the uterine arteries on the 12th day or later of the menstrual cycle, followed by a Pipelle biopsy of the endometrium, and histological and immunohistochemical examination. Furthermore, all patients had urethral, cervical canal, and vaginal secretions examined by bacterioscopy and PCR (for bacterial and viral infections), as well as by light microscopy (for HPV, CMV, and HSV antigens) using an Axio Lab.A1 microscope (Carl Zeiss, Germany). This step was intended to exclude the influence of infectious factors on the overall results of the study. The patients in both groups were comparable in age, weight, and medical history, including menstrual and reproductive function and the presence of chronic somatic diseases. Inclusion criteria: CE-associated female infertility; infertility associated with the male factor (no signs of CE). Exclusion criteria: bacterial and viral infections of the genitourinary tract; other infectious, allergic, autoimmune, inflammatory, oncological, mental diseases; hormonal, anti-inflammatory therapy; malformations of the genitals. The clinical and diagnostic characteristics of the patients are given in Table 1.

Assessment of parameters of systemic inflammatory status, including inflammatory indices

All patients underwent quantitative determination of blood leukocyte subsets by a standard hematological method with a hematology analyzer (Abbott Laboratories, USA).

Based on the cellular composition of peripheral blood, we calculated the following inflammatory indices: NLR (neutrophil-lymphocyte ratio); PLR (platelet-lymphocyte ratio); MLR (monocyte-lymphocyte ratio); SII (systemic inflammatory index) [10–12].

The indices were calculated using these formulas:

NLR = absolute neutrophil count / absolute lymphocyte count;
PLR = absolute platelet count / absolute lymphocyte count;
MLR = absolute monocyte count / absolute lymphocyte count;
SII = absolute platelet count — absolute neutrophil count / absolute lymphocyte count.

The concentration of CRP in blood serum was measured by enzyme immunoassay using the CRP-IFA kit (KHEMA, Russia) in accordance with the manufacturer's instructions and expressed in mg/ml.

Statistical analysis of the data

For statistical data processing, we used IBM SPSS Statistics 22 (Armonk; USA) and GraphPad Prism 8.3.1 (GraphPad Software; USA). The normality of distribution of all the data

Table 1. Characteristics of patients with infertility

Parameter	Parameter value	Patients with CE (n = 27)	Patients without CE (n = 23)
Median age, years		40,0 (34,0–42,0)	34,0 (30,0–38,0)
Median duration of infertility, years		4,0 (2,0–6,0)	3,0 (2,0–5,0)
Ultrasound signs of CE, frequency of occurrence, % (abs.)	yes	59.3% (16)	0% (0)
	no	40.7% (11)	100% (23)
IHC signs of CE, frequency of occurrence, % (abs.)	yes	100% (27)	–
	no	0% (0)	–
History of infectious diseases of the genitourinary tract	yes	33.3% (9)	4.3% (1)
	no	33.7% (18)	95.7% (22)

considered was checked with the Shapiro–Wilk test. The parameters were described using the median (Me) and the interquartile range (Q_1–Q_3). To assess the differences in the parameters, we used the Mann-Whitney test. The differences were considered significant at $p < 0.05$ (5%).

We used ROC to establish diagnostic significance of the systemic inflammatory status parameters in predicting the presence of CE. The cut-off value for the quantitative marker was the one that maximized Youden's index. The differences were considered significant at $p < 0.05$ (5%).

RESULTS

A comparative analysis of systemic inflammatory parameters — including ESR, total platelet count, leukocyte count, and the absolute and relative numbers of leukocyte subsets — revealed significant differences between patients with and without CE (Table 2). In patients with CE-associated infertility, the absolute and relative lymphocyte counts were significantly lower than those in patients without CE ($p = 0.0451$ and $p = 0.0089$, respectively). At the same time, the relative number of monocytes and basophils in the study group significantly exceeded that in the control group ($p = 0.0469$ and $p = 0.0005$, respectively). In addition, blood CRP levels in the study group were about four times those in the control group ($p = 0.0191$) (Table 2). All indicators in both groups remained within the reference ranges.

A comparative analysis of hematological inflammatory indices in patients with CE-associated infertility and patients without CE also revealed significant intergroup differences. In the study group, the NLR ($p = 0.0387$), MLR ($p = 0.0058$), PLR ($p = 0.0335$) and SII ($p = 0.0333$) indices were significantly higher than those of the control group (Table 3).

We performed ROC analysis and determined the optimal threshold values of the evaluated parameters to assess the diagnostic significance of hematological inflammatory indices in detecting subclinical endometrial inflammation.

The analysis demonstrated a significant association of NLR and MLR indices with chronic endometrial inflammation among infertile patients. NLR values above the threshold of 1.56 absolute units were associated with the probability of CE (Table 4; Fig. 1). The area under curve was 0.871 (95% CI: 0.767–0.974), sensitivity — 87.0%, specificity — 73.7%. The resulting model was statistically significant ($p < 0.0001$).

A similar relationship was found for the MLR index. ROC analysis showed that MLR values exceeding 0.24 absolute units are an independent sign of a high risk of CE in patients with infertility (Table 4; Fig. 2). The area under curve was 0.848 (95% CI: 0.737–0.958), sensitivity — 80.0%, specificity — 75.0%. The resulting model was statistically significant ($p < 0.0001$).

Our assessment of the diagnostic applicability of the PLR and SII indices revealed no significant association between their values and the presence of chronic endometrial inflammation ($p > 0.05$) (Table 4). In addition, we found no diagnostic significance for such cellular parameters of systemic inflammation as the total platelet and leukocyte counts, the absolute and relative numbers of different leukocyte subsets, or ESR and CRP ($p > 0.05$).

Table 2. Hematological parameters of systemic inflammation in patients with infertility (Me (Q_1–Q_3))

Indicator	Patients with CE (n = 27)	Patients without CE (n = 23)	p
ESR, mm/h	6.0 (3.0–15.0)	10.0 (2.0–15.0)	0.8879
CRP, mg/l	2.25 (1.03–3.80)	0.60 (0.06–0.82)	0.0191
Absolute cell count, 10^9/l			
Platelets	255.0 (226.0–287.0)	262.0 (235.0–297.0)	0.2633
Leukocytes	5.7 (4.8–6.8)	6.0 (5.3–6.7)	0.7392
Neutrophils	3.4 (2.6–3.9)	3.1 (2.7–3.8)	0.7028
Lymphocytes	1.6 (1.4–2.2)	2.0 (1.7–2.4)	0.0451
Monocytes	0.50 (0.40–0.50)	0.40 (0.33–0.49)	0.0963
Eosinophils	0.10 (0.10–0.20)	0.11 (0.07–0.17)	0.9635
Basophils	0.00 (0.00–0.10)	0.02 (0.00–0.03)	0.8979
Relative cell count, %			
Neutrophils	58.1 (54.1–61.9)	56.1 (49.5–59.3)	0.1012
Lymphocytes	29.5 (26.8–34.1)	36.0 (31.0–40.0)	0.0089
Monocytes	8.3 (7.1–9.7)	7.4 (5.5–8.4)	0.0469
Eosinophils	2.1 (1.7–2.7)	2.1 (1.5–3.1)	0.7098
Basophils	0.7 (0.5–1.0)	0.4 (0.1–0.5)	0.0005

Table 3. Parameters of systemic inflammatory status in patients with infertility (Me (Q_1–Q_3))

Indicator	Patients with CE (n = 27)	Patients without CE (n = 23)	p
Inflammatory indices, abs. u.			
NLR	1.93 (1.50–2.38)	1.55 (1.30–1.93)	0.0387
MLR	0.27 (0.23–0.30)	0.20 (0.14–0.27)	0.0058
PLR	148.7 (122.6–183.0)	126.8 (111.1–138.7)	0.0335
SII	469.9 (385.3–628.0)	396.4 (329.8–511.7)	0.0333

DISCUSSION

Inflammation plays a key role in the pathogenesis of endometritis-associated infertility and contributes to the risk of adverse reproductive outcomes. It has been shown to suppress the expression of estrogen and progesterone receptors in the endometrium, thereby delaying its maturation and hindering embryo implantation [13].

The diagnosis of CE is a complicated process: the disease is often asymptomatic, ultrasound examination is insufficiently effective, and there are no uniform diagnostic criteria. The absence of signs of CE on ultrasonography cannot be interpreted as the absence of endometrial inflammation; this limitation necessitates an invasive and costly procedure, aspiration biopsy, to obtain pathomorphological confirmation of the diagnosis [14].

Recently, hematological inflammatory indices have been proposed as new biomarkers for various socially significant diseases accompanied by a subclinical inflammation. There is evidence of the usefulness of these indices in the prognosis of cardiovascular [15], oncological [16], and mental [17] diseases, as well as systemic inflammatory diseases of connective tissue [18]. Hematological inflammatory indices are non-invasive, inexpensive, easy to calculate, and require no specialized equipment.

In the context of non-malignant gynecological pathologies, the diagnostic and predictive significance of hematological inflammatory indices has been largely unstudied. Recent studies in the field of obstetrics and gynecology have demonstrated their benefits in the cases of endometriosis, ovarian hyperstimulation syndrome, as well as the adverse course and complications of pregnancy (in particular, preeclampsia) [8]. However, neither Russian nor foreign sources contain any data on the applicability of the said indices in CE cases. Thus, it is reasonable to continue investigating their prognostic significance in patients with chronic inflammatory diseases of the endometrium, particularly in the context of infertility treatment using assisted reproductive technologies.

When the inflammation is subclinical and chronic, the clinical significance of hematological cellular and molecular parameters is low. Earlier, we found significant differences in the concentrations of CRP and the counts of lymphocytes, monocytes, and basophils between the study and control groups; however, these indicators were ultimately deemed uninformative, as their values remained within the reference range.

At the same time, the values of the inflammatory hematological indices NLR, PLR, MLR and SII in these groups were significantly different (Table 3), and NLR and MLR (Table 4, Figures 1 and 2) were deemed diagnostically significant. NLR reflects the balance of the innate and adaptive immune response to various stressors. Its value characterizes the severity of the systemic inflammatory reaction [19]. The increase of the said value in women with CE-associated infertility may be caused by the dropping number of lymphocytes in the blood as they are constantly recruited to the locus of chronic inflammation. A declining NLR may reflect attenuation of the inflammatory response and can be associated with a more favorable prognosis. MLR is the ratio of monocytes to lymphocytes in the blood. Monocytes do not circulate in the blood for long; they migrate into tissues, replenishing the pool of tissue macrophages. In addition, they can differentiate into dendritic cells and tissue-specific phagocytes [20]. Monocytes/macrophages are responsible for phagocytosis and removal of damaged cells, processing of antigens, stimulation of T- and B-cell immune responses, and also secrete regulatory and effector cytokines that ensure the development of a systemic inflammatory response [21]. In patients with CE-associated infertility, a high MLR may have two causes: first, an insufficient rate of monocyte migration from the blood to the site of chronic inflammation; and second, as mentioned above, redistribution of lymphocytes between the blood and the inflamed endometrium. This theory is supported by the decreased lymphocyte counts and increased monocyte counts observed in the blood of patients with CE (Table 2).

Introduction of the inflammatory indices to the laboratory testing and clinical practice requires further validation of the discriminatory levels of these indicators in an independent sample of patients suffering from various forms of infertility. However, it can already be argued that the NLR and MLR indices are applicable in the treatment of infertile women to identify those with asymptomatic CE even if they have normal hematological parameters and no signs of the inflammatory process on the ultrasonography. For such patients, it is feasible to perform additional immunohistochemical examination of the endometrium to confirm the diagnosis and prescribe anti-inflammatory therapy before IVF.

CONCLUSIONS

Patients with infertility associated with chronic endometrial inflammation had a higher relative number of monocytes and basophils, and a lower absolute and relative number of lymphocytes than patients without signs of chronic endometritis, but the values of these indicators remained within the normal

Table 4. Characteristics of the predictive significance of inflammatory hematological indices for detecting the presence of chronic endometrial inflammation in patients with infertility

Indicator	cut-off	AUC	95% CI	p	Sensitivity, %	Specificity, %
NLR	1.56	0.871	0.767–0.974	< 0.0001	87	73.7
MLR	0.24	0.848	0.737–0.958	< 0.0001	80	75
PLR	130.4	0.679	0.528–0.831	0.0339	61.5	54.6
SII	469	0.683	0.531–0.837	0.0333	52	61.9

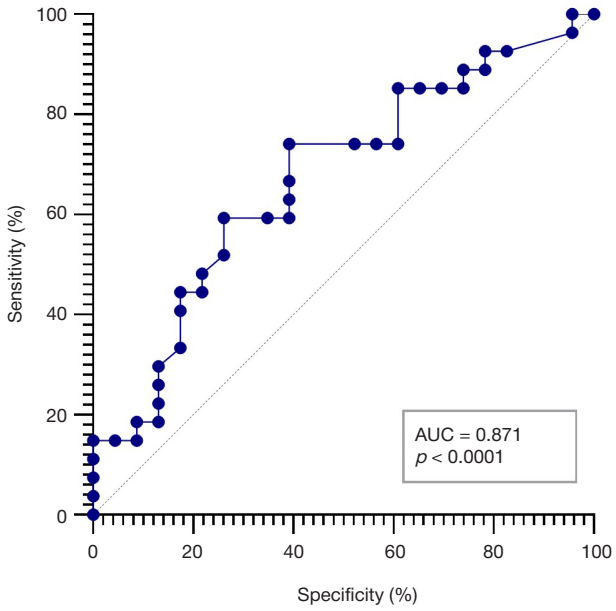


Fig. 1. ROC curve of predictive significance of the NLR index for detecting the presence of chronic endometritis in patients with infertility

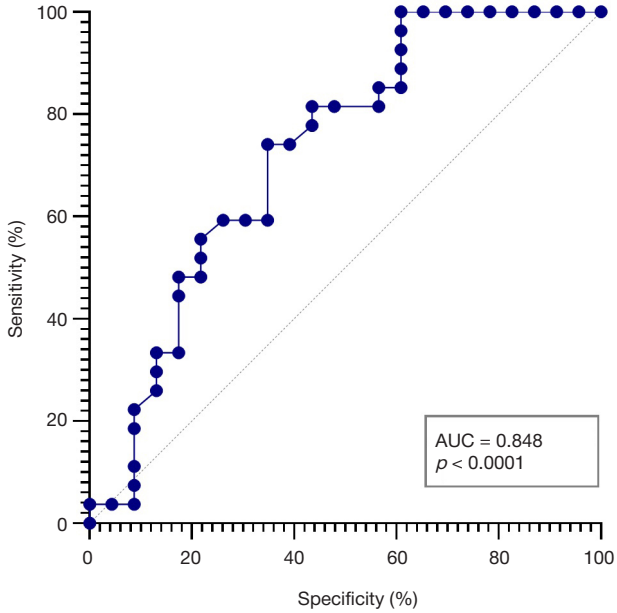


Fig. 2. ROC curve of predictive significance of the MLR index for detecting the presence of chronic endometritis in patients with infertility

range. A comparative analysis of hematological inflammatory indices showed a significant increase in their value in cases of CE-associated infertility. However, ROC analysis allowed establishing that only NLR and MLR indices can be used as predictors of CE in infertile patients, as other inflammatory markers remain within normal values. Ultimately, it should be noted that even when hematological cellular parameters are normal and ultrasound signs of endometritis are absent, infertile patients may still have chronic subclinical endometrial inflammation — a condition that can be ruled out by assessing the NLR and MLR indices. These markers may be useful in clinical practice for screening IVF patients. The assessment of these indices will make it possible to identify individuals at high risk of asymptomatic chronic endometritis, refer them for further immunohistochemical examination, and, if necessary, provide appropriate treatment before IVF. This approach may help reduce the risk of IVF failure.

References

1. Klinicheskie rekomendacii. Vospalitel`ny`e bolezni zhenskix tazovy`x organov. 2024-2025-2026 (24.09.2024). Utverzhdeny` Minzdravom RF. 28 s. Russian.
2. Singh N, Sethi A. Endometritis — Diagnosis,Treatment and its impact on fertility — A Scoping Review. JBRA Assisted Reproduction. 2022; 26 (3): 538–46.
3. Kolmyk VA, Nasyrov RA, Kutusheva GF, Petrov VV, Grigoryev SG. Immunohistochemical value to treat patients with chronic endometritis. Pediatrician (St Petersburg), 2016; 7 (3): 17–22. Russian.
4. Sukhanov AA, Dikke GB, Kukarskaya II. Epidemiology of female infertility and the experience of recovery of reproductive function in patients with chronic endometritis in the tyumen region. Russian Journal of Human Reproduction. 2023; 29 (3): 98–07. Russian.
5. Konoplya AA, Gavrish SA, Konoplya AI, Loktionov AL. The application of intravascular laser irradiation of blood for the correction of the immune disturbances in patients presenting with chronic endometritis. Problems of Balneology, Physiotherapy and Exercise Therapy. 2016; 93 (5): 19–22. Russian.
6. Trunova LA, Trunov AN, Marinkin IO, Kuleshov VM, Obuxova OO, Gorbenko OM i dr. Disbalans citokinov i aktivnost` immunovospalitel`nogo processa u zhenshhin s besplodiem. Allergologiya i immunologiya. 2014; 15 (1): 22–25. Russian.
7. Kimura F, Takebayashi A, Ishida M, Nakamura A, Kitazawa J, Morimuneet A, et al. Review: Chronic endometritis and its effect on reproduction. J Obstet Gynaecol Res. 2019; 45 (5): 951–60.
8. Ivanov DO, Krivolesova TA, Sigareva LP, Reznik VA, Savelieva OE. Prognostic potential of hematological inflammatory indexes for in vitro fertilization. Pediatrician (St. Petersburg). 2025; 16 (1): 88–99. Russian.
9. Shibutani M, Maeda K, Nagahara H, Noda E, Ohtani H, Nishiguchi Y, et al. A high preoperative neutrophil-to-lymphocyte ratio is associated with poor survival in patients with colorectal cancer. Anticancer Res. 2013; 33: 3291–4.
10. Yodying H, Matsuda A, Miyashita M, Matsumoto S, Sakurazawa N, Yamada M, et al. Prognostic Significance of Neutrophil-to-Lymphocyte Ratio and Platelet-to-Lymphocyte Ratio in Oncologic Outcomes of Esophageal Cancer: A Systematic Review and Meta-analysis. Ann Surg Oncol. 2016; 23: 646–54.
11. Naess A, Nilssen SS, Mo R, Eide GE, Sjursen H. Role of neutrophil to lymphocyte and monocyte to lymphocyte ratios in the diagnosis of bacterial infection in patients with fever. Infection. 2017; 45 (3): 299–307.
12. Xu T, Zhang S-M, Wu H-M, Wen X-M, Qiu D-Q, et al. Prognostic significance of prognostic nutritional index and systemic immune-inflammation index in patients after curative breast cancer resection: a retrospective cohort study. BMC Cancer. 2022; 22 (1): 1128.
13. Mishra K, Wadhwa N, Guleria K, Agarwal S. ER, PR and Ki-67 expression status in granulomatous and chronic non-specific endometritis. J Obstet Gynaecol Res. 2008; 34(3): 371–378.
14. Savelieva OE, Krivolesova TA, Sigareva LP, Shlyakhova AD, Gurina OP, Reznik VA. Local and systemic immune status of women with infertility associated with chronic endometritis. Pediatrician (St. Petersburg). 2025; 16 (2): 56–65. Russian.
15. Topolyanskaya SV, Eliseeva TA, Turna OI, Vakulenko ON, Bubman LI, Romanova MA, et al. Hematological indices — a possible marker of subclinical inflammation in very elderly patients and centenarians. Clinical review for general practice. 2022; 6: 6–13. Russian.
16. Shibutani M, Maeda K, Nagahara H, Fukuoka T, Matsutani S, Kimura K, et al. The prognostic significance of the advanced lung cancer inflammation index in patients with unresectable

metastatic colorectal cancer: A retrospective study. BMC Cancer. 2019; 19: 241.
17. Gorbunova AP, Rukavishnikov GV, Kasyanov ED, Mazo GE. The role of hematological coefficients of systemic inflammation in the diagnosis and risk assessment of affective disorders. V. M. Bekhterev Review of psychiatry and medical psychology. 2024; 58 (1): 47–55. Russian.
18. Manzyuk AV, Morozova TE, Gertsog AA, Litvinova MA. The prognostic value of hematological indices in systemic inflammatory diseases of connective tissue. Meditsinskiy sovet. 2024; 12: 136–42. Russian.
19. Lowsby R, Gomes C, Jarman I, Lisboa P, Nee PA, Vardhan M, et al. Neutrophil to lymphocyte count ratio as an early indicator of blood stream infection in the emergency department. Emerg Med J. 2015; 32: 531–4.
20. Dalton HJ, Armaiz-Pena G, Gonzalez-Villasana V, Lopez-Berestein G, Bar-Eli M, Sood AK. Monocyte Subpopulations in Angiogenesis. Cancer Res. 2014; 74 (5): 1287–93.
21. Titov LP. Monocytes, macrophages, dendritic and myeloid suppressor cells: genesis, classification, immunobiological properties. Proceedings of the National Academy of Sciences of Belarus, Medical series. 2018; 15 (3): 363–82.

Литература

1. Клинические рекомендации. Воспалительные болезни женских тазовых органов. 2024-2025-2026 (24.09.2024). Утверждены Минздравом РФ. 28 с.
2. Singh N, Sethi A. Endometritis — Diagnosis,Treatment and its impact on fertility — A Scoping Review. JBRA Assisted Reproduction. 2022; 26 (3): 538–46.
3. Колмык В. А., Насыров Р. А., Кутушева Г. Ф., Петров В. В., Григорьев С. Г. Значение иммуногистохимического контроля для лечения пациенток с хроническим эндометритом. Педиатрия. 2016; 7 (3): 17–22.
4. Суханов А. А., Дикке Г. Б., Кукарская И. И. Эпидемиология женского бесплодия и опыт восстановления репродуктивной функции у пациенток с хроническим эндометритом в Тюменском регионе. Проблемы репродукции. 2023; 29 (3): 98–107.
5. Конопля А. А., Гавриш С. А., Конопля А. И., Локтионов А. Л. Применение внутривенного лазерного облучения крови в коррекции иммунных нарушений у пациенток с хроническим эндометритом. Вопросы курортологии, физиотерапии и лечебной физической культуры. 2016; 5: 19–22.
6. Трунова Л. А., Трунов А. Н., Маринкин И. О., Кулешов В. М., Обухова О. О., Горбенко О. М. и др. Дисбаланс цитокинов и активность иммуновоспалительного процесса у женщин с бесплодием. Аллергология и иммунология. 2014; 15 (1): 22–25.
7. Kimura F, Takebayashi A, Ishida M, Nakamura A, Kitazawa J, Morimuneet A, et al. Review: Chronic endometritis and its effect on reproduction. J Obstet Gynaecol Res. 2019; 45 (5): 951–60.
8. Иванов Д. О., Криволесова Т. А., Сигарева Л. П., Резник В. А., Савельева О. Е. Прогностический потенциал воспалительных гематологических индексов при экстракорпоральном оплодотворении. Педиатрия. 2025; 16 (1): 88–99.
9. Shibutani M, Maeda K, Nagahara H, Noda E, Ohtani H, Nishiguchi Y, et al. A high preoperative neutrophil-to-lymphocyte ratio is associated with poor survival in patients with colorectal cancer. Anticancer Res. 2013; 33: 3291–4.
10. Yodying H, Matsuda A, Miyashita M, Matsumoto S, Sakurazawa N, Yamada M, et al. Prognostic Significance of Neutrophil-to-Lymphocyte Ratio and Platelet-to-Lymphocyte Ratio in Oncologic Outcomes of Esophageal Cancer: A Systematic Review and Meta-analysis. Ann Surg Oncol. 2016; 23: 646–54.
11. Naess A, Nilssen SS, Mo R, Eide GE, Sjursen H. Role of neutrophil to lymphocyte and monocyte to lymphocyte ratios in the diagnosis of bacterial infection in patients with fever. Infection. 2017; 45 (3): 299–307.
12. Xu T, Zhang S-M, Wu H-M, Wen X-M, Qiu D-Q, et al. Prognostic significance of prognostic nutritional index and systemic immune-inflammation index in patients after curative breast cancer resection: a retrospective cohort study. BMC Cancer. 2022; 22 (1): 1128.
13. Mishra K, Wadhwa N, Guleria K, Agarwal S. ER, PR and Ki-67 expression status in granulomatous and chronic non-specific endometritis. J Obstet Gynaecol Res. 2008; 34(3): 371–378.
14. Савельева О. Е., Криволесова Т. А., Сигарева Л. П., Шляхова А. Д., Гурина О. П., Резник В. А. Локальный и системный иммунный статус женщин с бесплодием, ассоциированным с хроническим эндометритом. Педиатрия. 2025; 16 (2): 56–65.
15. Тополянская С. В., Елисеева Т. А., Турна О. И., Вакуленко О. Н., Бубман Л. И., Романова М. А. и др. Гематологические индексы — возможный маркер субклинического воспаления у больных ишемической болезнью сердца старческого возраста и долгожителей. Клинический разбор в общей медицине. 2022; 6: 6–13.
16. Shibutani M, Maeda K, Nagahara H, Fukuoka T, Matsutani S, Kimura K, et al. The prognostic significance of the advanced lung cancer inflammation index in patients with unresectable metastatic colorectal cancer: A retrospective study. BMC Cancer. 2019; 19: 241.
17. Горбунова А. П., Рукавишников Г. В., Касьянов Е. Д., Мазо Г. Э. Роль гематологических коэффициентов системного воспаления в диагностике и оценке риска аффективных расстройств. Обозрение психиатрии и медицинской психологии им. В. М. Бехтерева. 2024; 58 (1): 47–55.
18. Манзюк А. В., Морозова Т. Е., Герцог А. А., Литвинова М. А. Прогностическая ценность гематологических индексов при системных воспалительных заболеваниях соединительной ткани. Медицинский совет. 2024; 18 (12): 136–42.
19. Lowsby R, Gomes C, Jarman I, Lisboa P, Nee PA, Vardhan M, et al. Neutrophil to lymphocyte count ratio as an early indicator of blood stream infection in the emergency department. Emerg Med J. 2015; 32: 531–4.
20. Dalton HJ, Armaiz-Pena G, Gonzalez-Villasana V, Lopez-Berestein G, Bar-Eli M, Sood AK. Monocyte Subpopulations in Angiogenesis. Cancer Res. 2014; 74 (5): 1287–93.
21. Титов Л. П. Моноциты, макрофаги и дендритные клетки: генез, классификация, иммунобиологические свойства. Известия Национальной академии наук Беларуси. Серия медицинских наук. 2018; 15 (3): 363–82.

RIBOSOMAL GENE COPY NUMBER IN PERIPHERAL LEUKOCYTES OF WOMEN WITH NORMAL AND COMPLICATED PREGNANCY

Ershova ES[1], Veiko NN[1], Kostyuk EV[2], Poletkina AA[3], Rozhnova TM[6], Nizyaeva NV[5] ✉, Muzaffarov DU[2], Klimenko PA[4], Kostyuk SV[1]

[1] Longevity Institute, Petrovsky Russian Research Centre of Surgery, Moscow, Russia
[2] Kurnakov Institute of General and Inorganic Chemistry, Moscow, Russia
[3] Institute of Immunology of the Federal Medical-Biological Agency, Moscow, Russia
[4] Pirogov Russian National Research Medical University, Moscow, Russia
[5] Avtsyn Research Institute of Human Morphology, Petrovsky Russian Research Centre of Surgery, Moscow, Russia
[6] Sechenov First Moscow State Medical University, Moscow, Russia

Pregnancy requires the cells of the woman's body to ensure increased ribosomal biogenesis in order to enhance the protein synthesis intensity. The number of ribosomes depends on the copy number of ribosomal genes (rDNA) in the genome. The study aimed to test the hypothesis about the association of the rDNA copy number in the woman's genome with the course of normal and complicated pregnancy. The sample of 488 pregnant women (25–39 weeks) included the following groups: 1) normal pregnancy (control); 2) impaired uteroplacental blood flow and fetoplacental insufficiency; 3) congenital malformations; 4) isthmic-cervical insufficiency; 5) early placental maturation; 6) dichorionic diamniotic twins; 7) polyhydramnios; 8) macrosomia. The rDNA copy number was determined by the quantitative hybridization method in the DNA extracted from peripheral leukocytes. The rDNA copy number varied between 226 and 800 (n = 488). DNA samples with the rDNA copy number below 290 were lacking in groups 3–8. Groups 5–8 included no samples with the rDNA copy number exceeding 520; these in total differed from group 1 by low rDNA copy number values (the average values were 360–381 for groups 3–8 and 452 for group 1; $p < 10–7$). The rDNA copy number range of 290–520 in the woman's genome (the adaptive norm typical for long-lived individuals) is optimal in terms of successful completion of pregnancy in the presence of pregnancy complications. The low rDNA copy number (200–290) in the genome is associated with the failure to complete embryogenesis when there are some fetal abnormalities/features. A high rDNA content (over 600 copies) indicates the presence of genetic variants in the woman's genome that can interfere with the complicated pregnancy course. Determining the rDNA copy number in the genome of married couples may be useful for planning and predicting the course of pregnancy.

Keywords: pregnancy, pregnancy pathology, ribosomal genes, rDNA

Funding: the study was conducted under the State Task on the topic "Molecular mechanisms of abnormal cell-cell communication in atypical placentation, proliferative diseases of the reproductive system, and tumor growth" No. 123030700104-3 FURG-2023-0049.

Author contribution: Ershova ES — experimental procedure, manuscript writing; Veiko NN, Kostyuk SV — study concept, manuscript writing; Kostyuk EV — biomaterial collection, describing the disorder; Poletkina AA — material collection, experimental procedure; Rozhnova TM — statistical data processing; Muzaffarov DU — experimental procedure; Nizyaeva NV — study concept, manuscript editing; Klimenko PA — classification of material, describing the disorder.

Compliance with ethical standards: the study was approved by the Ethics Committee of the Pirogov Russian National Research Medical University (protocol No. 228 dated 17 April 2023). The informed consent was submitted by all study participants.

✉ **Correspondence should be addressed:** Natalia V. Nizyaeva
Abrikosovsky pereulok, 2, k. 1, Moscow, 119435, Russia; niziaeva@gmail.com

Received: 23.10.2025 **Accepted:** 28.11.2025 **Published online:** 12.12.2025

DOI: 10.24075/brsmu.2025.075

Copyright: © 2025 by the authors. **Licensee:** Pirogov University. This article is an open access article distributed under the terms and conditions of the Creative Commons Attribution (CC BY) license (https://creativecommons.org/licenses/by/4.0/).

КОЛИЧЕСТВО КОПИЙ РИБОСОМНЫХ ГЕНОВ В ЛЕЙКОЦИТАХ ПЕРИФЕРИЧЕСКОЙ КРОВИ У ЖЕНЩИН С ФИЗИОЛОГИЧЕСКОЙ И ОСЛОЖНЕННОЙ БЕРЕМЕННОСТЬЮ

Е. С. Ершова[1], Н. Н. Вейко[1], Э. В. Костюк[2], А. А. Полеткина[3], Т. М. Рожнова[6], Н. В. Низяева[5] ✉, Д. У. Музаффаров[2], П. А. Клименко[4], С. В. Костюк[1]

[1] Институт биологии старения и медицины здорового долголетия с клиникой превентивной медицины, Российский научный центр хирургии имени Б. В. Петровского, Москва, Россия
[2] Институт общей и неорганической химии имени. Н. С. Курнакова, Москва, Россия
[3] Институт иммунологии, Федеральное медико-биологическое агентство, Москва, Россия
[4] Российский национальный исследовательский медицинский университет имени Н. И. Пирогова, Москва, Россия
[5] Научно-исследовательский институт морфологии человека имени А. П. Авцына, Российский научный центр хирургии имени Б. В. Петровского, Москва, Россия
[6] Первый Московский государственный медицинский университет имени И. М. Сеченова, Москва, Россия

Беременность требует от клеток организма женщины повышенного уровня биогенеза рибосом для увеличения интенсивности синтеза белка. Количество рибосом зависит от числа копий рибосомных генов в геноме (ЧК рДНК). Целью исследования было проверить гипотезу об ассоциации ЧК рДНК в геноме женщины с протеканием нормальной и осложненной беременности. Выборка 488 беременных (25–39 недель) включала группы: 1) беременность без патологии (контроль); 2) нарушение маточно-плацентарного кровотока и фетоплацентарная недостаточность; 3) врожденные пороки развития; 4) истмико-цервикальная недостаточность; 5) преждевременное созревание плаценты; 6) дихориальная диамниотическая двойня; 7) многоводие; 8) крупный плод. ЧК рДНК определяли методом количественной гибридизации в ДНК, выделенной из лейкоцитов периферической крови. ЧК рДНК варьировало от 226 до 800 (n = 488). В группах 3–8 отсутствовали образцы ДНК с ЧК рДНК менее 290. Группы 5–8 не содержали образцов с ЧК рДНК более 520 и суммарно отличались от группы 1 низкими значениями ЧК рДНК (средние значения 360–381 для групп 3–8 и 452 копии для группы 1; $p < 10–7$). Диапазон ЧК рДНК от 290 до 520 в геноме женщины (адаптивная норма, характерная для долгожителей) является оптимальным с точки зрения успешного завершения беременности при наличии осложнений. Низкое ЧК рДНК (200–290) в геноме ассоциировано с невозможностью реализации эмбриогенеза при наличии патологии/особенности плода. Большое содержание рДНК (более 600 копий) указывает на наличие в геноме женщины генетических вариантов, которые могут препятствовать протеканию осложненной беременности. Определение ЧК рДНК в геноме супружеских пар может быть полезным для планирования и прогнозирования течения беременности.

Ключевые слова: беременность, патология беременности, рибосомные гены, рДНК

Финансирование: работа выполнена в рамках Государственного задания: по теме «Молекулярные механизмы нарушений межклеточных взаимодействий при атипической плацентации, пролиферативных заболеваниях органов репродуктивной системы и опухолевом росте» № 123030700104-3 FURG-2023-0049

Вклад авторов: Е. С. Ершова — экспериментальная работа, написание статьи; Н. Н. Вейко, С. В. Костюк — идея исследования, написание статьи; Э. В. Костюк — сбор биологического материала, описание патологии; А. А. Полеткина — сбор материала, экспериментальная работа; Т. М. Рожнова — статистическая обработка данных; Д. У. Музаффаров — экспериментальная работа; Н. В. Низяева — идея исследования, редактирование статьи; П. А. Клименко — классификация материала, описание патологии.

Соблюдение этических стандартов: исследование одобрено этическим комитетом РНИМУ им. Н. И. Пирогова (протокол № 228 от 17 апреля 2023 г.). Все участницы исследования подписали добровольное информированное согласие.

✉ **Для корреспонденции:** Наталья Викторовна Низяева
Абрикосовский переулок, д. 2, к. 1, г. Москва, 119435, Россия; niziaeva@gmail.com

Статья получена: 23.10.2025 **Статья принята к печати:** 28.11.2025 **Опубликована онлайн:** 12.12.2025

DOI: 10.24075/vrgmu.2025.075

Авторские права: © 2025 принадлежат авторам. **Лицензиат:** РНИМУ им. Н. И. Пирогова. Статья размещена в открытом доступе и распространяется на условиях лицензии Creative Commons Attribution (CC BY) (https://creativecommons.org/licenses/by/4.0/).

The study of the impact of maternal genetic features on the reproductive function and embryogenesis processes are of great importance for addressing the issue of increasing birth rate. Pregnancy and delivery need the cells of the woman's body to effectively respond to stress and to be capable of significantly enhancing protein synthesis in the body. Protein synthesis is a central event of the eukaryotic cell functioning, including in response to stress of any origin. This process referred to as translation is implemented by specific molecular machinery: ribosomes. A human ribosome consists of two components: ribosomal RNA (rRNA) and 70–80 ribosomal proteins [1]. The 28S, 5,8S, and 18S rRNA (rDNA) genes in the human genome are represented by multiple copies. The rDNA copies are arranged into tandem repeats sized 43 kbp in five pairs of acrocentric chromosomes. Each single repeat comprises a transcribed region sized 13.3 kbp (47S rRNA), which contains the 28S, 5,8S, 18S rRNA genes, the transcribed spacers (5′ETS and 3′ETS), and a non-transcribed intergenic spacer (IGS). Together with the 5S rRNA (the genes are located on the first chromosome) these rRNA form ribosomes [2]. The rRNA synthesis for ribosomes is the main function of ribosomal repeats. The rDNA transcription is accomplished by RNA polymerase I in the nucleolus, a specific cell structure in the nucleus (Fig. 1A).

The human genome contains about 200–1000 copies of tandem ribosomal repeats [3–5]. The number of rDNA copies in the genomes of cells of various types within the same body is constant; it does not change with age or under exposure to stress. The rDNA copy number is also the same within the same population of cells. In other words, the rDNA copy number can be considered as a stable genetic trait that remains unchanged throughout human life [3]. In recent years, there are more and more reports suggesting the role of the rDNA copy number in the genome in the human body functioning, as well

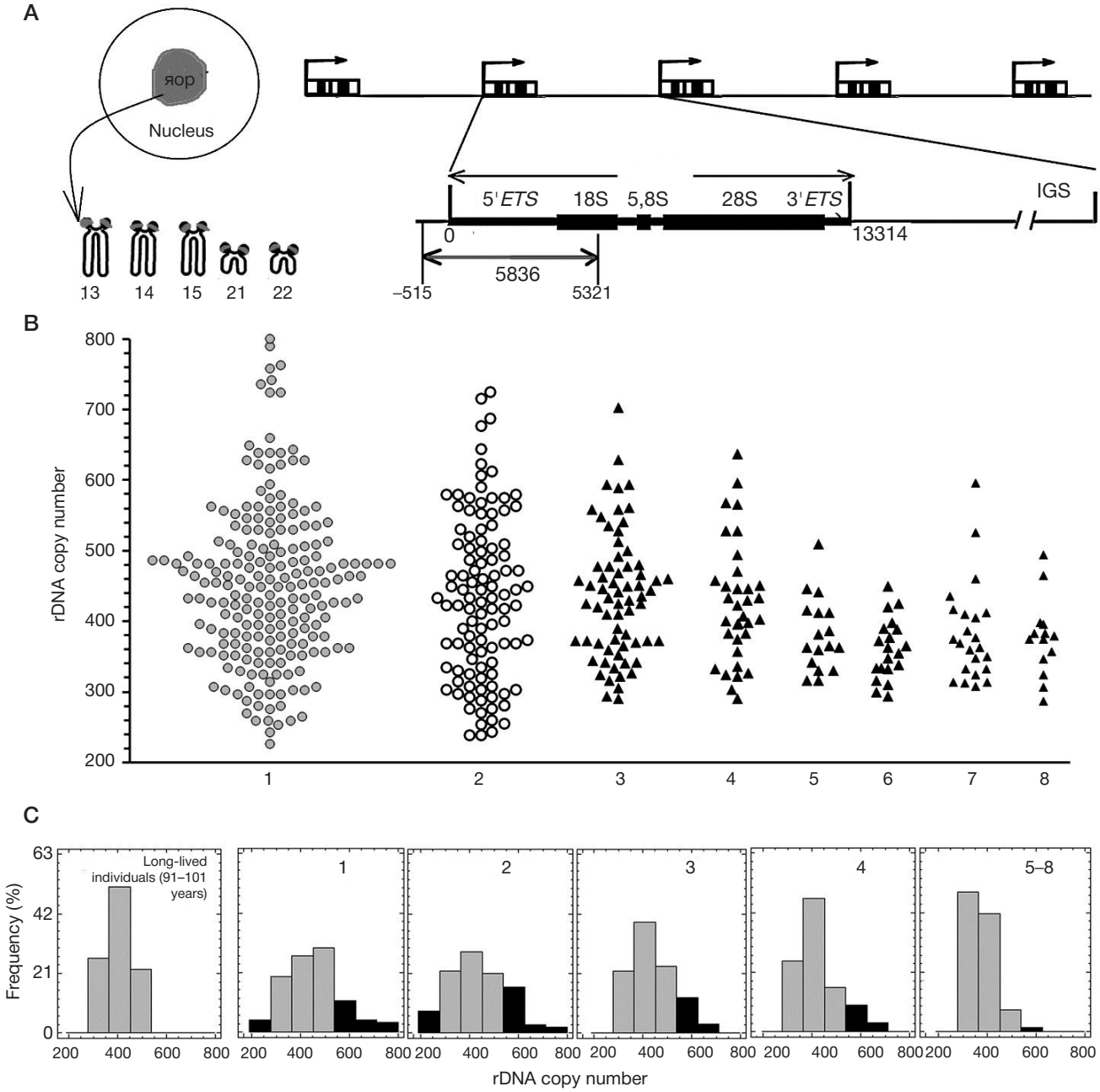


Fig. 1. Ribosomal repeat copy number variation in the genomes of pregnant women. **A**. Ribosomal repeat scheme. The repeat fragment determined with the DNA probe by hybridization is shown. **B**. Experimental data reflecting the rDNA repeat content in the studied groups. C. Distribution of DNA samples in the groups by the rDNA copy number in the genome

Table 1. Characteristics of the groups of women, for whom the rDNA copy number was determined. Descriptive statistics are provided

№	Group	N	Mean ± SD	I min–max	CI (95%)	Median	C_{var}
1	Control (normal pregnancy)	207	452 ± 113	226–800	436–467	450	0.25
2	Impaired uteroplacental blood flow and fetoplacental insufficiency	107	436 ± 115	237–724	413–457	432	0.26
3	Congenital malformations, ch. a.	66	436 ± 88	290–702	414–459	434	0.2
4	Isthmic-cervical insufficiency	34	423 ± 88	290–637	395–459	415	0.21
5	Early placental maturation	17	381 ± 53	316–509	356–416	365	0.14
6	Dichorionic diamniotic twins	20	360 ± 43	294–449	338–382	358	0.12
7	Polyhydramnios	23	379 ± 74	289–596	348–415	363	0.19
8	Macrosomia	14	375 ± 57	287–494	332–415	374	0.15
D	Long-lived individuals (91–101 years) [3]	103	404 ± 55	290–519	393–414	403	0.13

as the association of this trait with disorders and aging. It has been shown that the rDNA copy number is associated with the chronic inflammation level, kiney disease [6], body weigh [7], as well as with the fact of having a monogenic (cystic fibrosis) or polygenic (schizophrenia) disorder [3]. The low rDNA copy number is associated with cognitive impairment in the elderly [8], slower metabolism, and low human cells' resistance to stress [7, 9]. The rDNA content of blood cells in long-lived individuals varies within a narrow range: from about 290 to 530 copies. People with the lower or higher rDNA copy number values don't live to the age of 90 or older [10].

Approximately one-third of all rDNA copies, which are referred to as active copies, are transcribed in the nucleolus. These copies are not methylated, in contrast to the transcriptionally inactive copies, in which the transcribed region of rDNA is methylated. The number of active rDNA copies is proportional to the total number of copies in the genome [11]. The data are provided that are consistent with the hypothesis about the stabilizing selection occurring at the zygote and/or early embryogenesis level and aimed at maintaining the number of active rDNA copies between ~ 94 and ~ 277 copies (beyond the specified threshold values, the cell is not viable). The zygotic loss rate has been determined for this trait (about 10%) [11, 12]. The data obtained suggest that the loss of zygotes/embryos under conditions of insufficient or excess active copies of ribosomal genes in the genome can be one of the factors determining reduced fertility in some married couples [13].

The impact of the rDNA copy number in the woman's genome on the reproductive function and embryogenesis has not yet been adequately studied. The literature provides only the data of the authors, who have revealed a positive association between the IVF success and the rDNA copy number in the women's leukocytes [14]. It has been also shown that silent miscarriage is associated with severe imbalance of the rDNA content in the embryo's genome and maternal genome. In most cases, the genome of a non-developing embryo contains significantly fewer rDNA copies, than the maternal genome and genomes of other embryos, the development of which has not been spontaneously interrupted [15].

It should be noted that the quantitative PCR method widely used for analysis of genes is poorly applicable to the analysis of multicopy ribosomal repeats due to a number of reasons discussed in detail earlier [16]. The tandem nature of repeats, large number of self-complementary regions, various copy methylation levels, increased oxidative modification of multiple Gn-rich rDNA regions result in the fact that rDNA represents a very bad matrix for Taq polymerase. We observed a nonlinear relationship between the amplification reaction effectiveness and the rDNA concentration and oxidation, in contrast to other genome sequences. The non-radioactive quantitative hybridization (NQH) method, that does not depend on the DNA methylation, oxidation, and fragmentation levels since it does not involve PCR, has been developed specifically for rDNA quantification. The alkali-denatured DNA fragments immobilized on the filter are through hybridization with a long biotin-labeled DNA probe. Several calibration DNA samples with the known ribosomal repeat content are used as standards. The results obtained using NQH when studying rDNA in the sample of healthy donors were fully confirmed by later studies by the authors, who used a new long DNA fragment analysis method not involving the amplification reaction (Oxford Nanopore sequencing [17]).

The study aimed to assess the association of the ribosomal gene copy number in the maternal genome with the risk of various pregnancy complications. For that we determined the rDNA copy number by NQH in the leukocyte genomes of women with normal pregnancy and pregnancy with the complications/specific features caused by various factors.

METHODS

Blood samples of women with normal pregnancy and complicated pregnancy were obtained through collaboration with the department of obstetrics and gynecology at the Pediatric Faculty, Pirogov Russian National Research Medical University.

The venous blood samples for analysis of the rDNA copy number in leukocytes were collected from 488 pregnant women aged 18–45 years (average age 32 ± 5 years, gestational age 25–39 weeks) living in Moscow (RF) in the same social environment. Furthermore, the previously published data on the rDNA content in the genomes of long-lived individuals (n = 103, females 84%) aged 91–101 years were taken for comparison [3]. Groups 1–8 were formed (Table 1).

Inclusion criteria: group 1 (control group) — women with the normal course of pregnancy without any disorder identified, who gave birth to healthy children showing no signs of hypoxia and hypotrophy; groups 2–8 — women with the abnormal course of pregnancy diagnosed with the disorders specified in Table 1.

Exclusion criteria: patients having chronic (diabetes, autoimmune diseases, cardiovascular diseases, cancer) and hereditary disorders; acute infection at the time of blood collection; smoking, drinking alcohol, taking drugs or medications; history of unsuccessful pregnancies.

Special tests

DNA was isolated from 1 mL of blood by phenol extraction. Red blood cells were lysed (0.25% ammonium chloride), leukocytes were precipitated by centrifugation at 400 g for 10 min, the sediment was added 1 mL of the lysis buffer (1% sodium lauroyl

sarcosinate, 0.02 M EDTA, pH 7) and treated with RNAse A at a concentration of 0.075 mg/mL (Sigma; USA) for 45 min (37 °C). Then the mixture was treated with proteinase K, 0.2 mg/mL (Promega; USA) for 24 h at 37 °C. After two cycles of extraction with the saturated phenol solution, DNA was precipitated by adding two volumes of ethanol in the presence of 2 M ammonium acetate. Then the sediment was twice washed with the 75% ethanol, dried and dissolved in water.

The phase of determining DNA concentration in the sample is critical for analysis. The concentration was determined by two methods: spectrophotometry (the absorption spectrum was acquired using the Shimadzu UV-160A system) and fluorometry. The PicoGreen fluorescent dye was used (Sigma; USA). Fluorescence was recorded using the LS-55 system (Perkin Elmer; USA).

The ribosomal repeat copy number in the DNA extracted from blood was determined by the non-radioactive quantitative dot-blot hybridization with the biotinylated DNA probes that had been described in detail earlier [16]. Equal quantities (20 ng) of the DNA samples denatured with the 0.1M NaOH, the set of calibration DNA samples with the known rDNA content, and the negative control for non-specific binding were in several repetitions applied onto nitrocellulose filters and then, after thermal immobilization, incubated with the biotinylated DNA probe (Fig 1A). The p(5′ETS-18S) probe represented a rDNA fragment comprising the ribosomal repeat fragment (positions — 515 to 5321 relative to the transcription starting point) cloned into the pBR322 plasmid (HSU 13369; GenBank accession No.U13369). The fragment comprises a small fragment of the non-transcribed spacer, the external transcribed spacer (5′ETS), and a part of the 18S rRNA gene. The probe was biotinylated using the Biotin NT Labeling Kit (Jena Bioscience GmbH, Jena, Germany) for nick translation.

After completing hydridization, the signal was visualized using the streptavidin-alkaline phosphatase conjugate (Merck) and the colorimetric substrate. To quantify rDNA based on the spot signal intensity, the Imager 6 software tool was used allowing one to calculate integral intensity of the signal from each spot. Signals from all the spots corresponding to the same sample were summed up, and the mean and standard error were calculated for each sample. The abundance of ribosomal repeat copies was calculated using a calibration curve showing the signal as a function of the rDNA copy number in the control DNA samples, which were applied onto the filter in the same amount as the test DNA samples. The analysis relative error was 5 ± 3%.

Statistical processing

The descriptive statistics for quantitative variables are provided in Table 1 in the format of the mean and standard deviation (±SD), the median and range of variation (l), confidence interval values (CI 95%) and variation coefficient (Cvar: standard deviation divided by the mean). Two groups were compared using the nonparametric Mann–Whitney test (p). The Kruskal–Wallis test (H, p) was used to compare several groups. Distributions of the measured parameter in the groups were compared using the Kolmogorov–Smirnov test (D, α). The critical significance level was specified as 0.05. When applying Bonferroni correction for multiple comparisons, the differences were considered significant at $p \leq 0.0062$. The StatPlus2007 (http://www.analystsoft.com/) software was used for calculation.

RESULTS

A total of 488 DNA samples isolated from blood leukocytes of pregnant women aged 18–45 years were analyzed. The rDNA copy number was determined by the non-radioactive quantitative hybridization method that had been specially developed for the analysis of tandem ribosomal repeats in the human genome [16]. A biotinylated DNA probe that was homologous to the 5836-nucleotide ribosomal repeat fragment was used for hybridization (Fig. 1A). The rDNA quantity was presented as the repeat copy number per diploid genome.

The quantitative data for the entire sample divided into eight groups are presented in Fig. 1B. Table 1 provides characteristics of the groups and descriptive statistics. Fig. 1C presents distributions of DNA samples in the groups by the rDNA copy number in the genomes. In the studied sample of 88 DNA samples, the rDNA content varies between 226 and 800 copies per diploid genome. The rDNA content in a population of generally healthy people without any obvious genetic pathology aged up to 70 years varies within the same range [3].

By comparison, Fig. 1C presents the DNA sample distribution by the rDNA copy number in the group of long-lived individuals (the data had been published earlier [3]). The rDNA copy number in the genomes of long-lived individuals varies within the narrow range: between ~ 290 and~ 520 copies. This range represents some adaptive norm for the population. People with the higher rDNA copy number (over 550) and low copy number (below 280) do not live to the age of 90 years or more. In the younger sample (3–75 years), DNA samples with the rDNA copy number outside the range of long-lived individuals constitutes about one third [3].

Comparison of the eight studied groups of pregnant women based on the rDNA copy number in the blood leukocyte genome using the nonparametric Kruskal–Wallis test revealed significant intergroup differences ($H = 30.2$; $p < 10–4$, $n = 8$). Then we used the nonparametric Mann–Whitney test to compare group 1 (women with the normal course of pregnancy, without any abnormality detected, who gave birth to children showing no signs of hypoxia and hypotrophy) with the groups 2–8. The data of comparing distributions (Kolmogorov–Smirnov test) and rDNA quantities in the groups (Mann–Whitney test) are provided in Table 2.

Considering Bonferroni correction, group 2 (impaired uteroplacental blood flow and fetoplacental insufficiency) and group 1 (control) showed no significant differences in the rDNA copy number ($p > 0.006$) and no differences in the distribution of this parameter ($D = 0.12$, $\alpha = 0.29$). However, the analysis of distributions (Fig. 1C) showed that group 2 comprised twice more low-copy rDNA variants (8%), than group 1 (4%).

Group 3 (congenital malformations and chromosomal abnormalities) and group 4 (isthmic-cervical insufficiency) also showed no differences from group 1 in the rDNA copy content ($p > 0.006$) and the DNA sample distribution by the parameter values in the groups. However, in these groups there are no DNA samples with the low rDNA copy number (below 290), in contrast to groups 1 and 2.

The analysis using the Kruskal–Wallis test has shown that groups 1–4 do not differ from each other in the rDNA copy number ($H = 2.9$, $p = 0.41$, $n = 4$).

Groups 5 (early placental maturation), 6 (dichorionic diamniotic twins), 7 (polyhydramnios), and 8 (macrosomia) do not differ from each other in the rDNA copy number ($H = 1.27$; $p = 0.74$, $n = 4$). Each of the groups 5–8 is significantly different from the control group 1 in the rDNA copy number and/or trait distribution. The groups comprise lower quantities of rDNA copies in the DNA compared to the control (Table 2). These groups comprise no DNA samples with the low rDNA copy number values and no samples with the large (over 600 copies) rDNA quantities. In group 1 with the normal pregnancy, the number of such samples is 12 and 18%, respectively.

Table 2. Pairwise comparison of the control group 1 (normal pregnancy without any abnormalities) and the sample D (adaptive norm, long-lived individuals) with other groups of pregnant women based on the rDNA copy number in the DNA and the distribution of this parameter

Groups compared		Kolmogorov–Smirnov test		*U*-test
X1	X2	D	α	*p*
1	2	0.12	0.29	0.2
1	3	0.14	0.24	0.34
1	4	0.19	0.23	0.25
1	5	0.4	0.008	0.005*
1	6	0.5	0.0001*	0.0001 *
1	7	0.42	0.001*	0.002*
1	8	0.45	0.006*	0.008
1	∑(5–8)	0.45	3·10–9	10–8
D	1	–0.29	0.00002*	0.0002*
D	2	–0.26	0.001*	0.12
D	3	–0.23	0.02	0.02
D	4	–0.21	0.21	0.34
D	5	0.2	0.5	0.09
D	6	0.34	0.04	0.002*
D	7	0.25	0.2	0.02
D	8	0.29	0.33	0.08

Note: * — significant differences ($p \leq 0.0062$)

In terms of the the rDNA content in the genome and distribution of this parameter, groups 5–8 are most close to the adaptive norm of the rDNA copy number in the group of long-lived individuals (Fig. 1; Tables 1 and 2). The relatively low parameter values, low variation coefficients (0.12–0.19) compared to group 1 (C_{var} = 0.25) and the lack of low-copy (less than 290 copies per genome) rDNA variants are typical for these groups.

DISCUSSION

Human ribosomal repeats located in the r-regions of five pairs of acrocentric chromosomes are characterized by the pronounced quantitative polymorphism. In the sample we have studied, the range of rDNA variation is 595 copies, which confirms the earlier reported data on the ribosomal repeat variability [3, 5, 11]. In humans, the rDNA copy number is a stable genetic trait that is similar in all cells of the body and is not changed during life and under exposure to stress factors [3]. The fact of getting pregnant is also not likely to change the overall rDNA copy number in the genome of the woman's leukocytes.

We studied the rDNA copy number variation in the group of women with the normal course of pregnancy (group 1; Table 1) compared to the women, whose pregnancy was accompanied by various complications. The entire sample was divided into two parts after assessing the rDNA copy number in the genome.

Impaired uteroplacental blood flow and fetoplacental insufficiency (group 2), congenital malformations and chromosomal abnormalities (group 3), isthmic-cervical insufficiency (group 4) — these complications are not associated with alteration of the rDNA copy number in the women's genomes compared to the genomes of women with normal pregnancy without any complications (group 1). However, one nuance that had no effect on the overall analysis was reported for groups 3 and 4. In these groups, there were no DNA samples with the very low (below 290 copies) rDNA content. In groups 1 and 2, such samples accounted for 4 and 8%.

Groups 5–8, which include women with early placental maturation, dichorionic diamniotic twins, polyhydramnios and macrosomia, also comprise no low-copy rDNA variants, in contrast to the control group and group 2 (Fig. 1C). This can indicate that the maternal genome must contain more than 290 rDNA copies to ensure realization of embryogenesis complicated by the factors specified for groups 3–8. The woman's body with the lower rDNA copy number is likely to be unable to ensure acceptable ribosomal biogenesis to respond to the complicated pregnancy-induced stress.

This is confirmed by the data on the association of the rDNA copy number with the IVF procedure effectiveness. Women with the low rDNA copy number in their genomes (average number 305 ± 57) failed to get pregnant after several attempts, while women with the higher rDNA copy number (499 ± 62) successfully got pregnant on the first try [14].

We believe that the lack of low-copy rDNA variants in the genomes of women in groups 3–8 is associated with selection during early embryogenesis. The fact of an abnormality/specific feature in the embryo probably requires the maternal genome to ensure enhanced ribosomal biogenesis to realize the embryo development. Low rDNA quantity in the maternal genome can be associated with the arrest of the development of the embryo having the abnormality/specific feature at early stage. That is why in groups 3–8 at the 25–39th week of gestation no low-copy variants are found. Furthermore, low rDNA copy number in a mother can be inherited by the embryo, especially when the number of copies in the paternal genome is also low. It has been shown that embryos with the low rDNA copy number significantly more often fail to develop (silent miscarriage) compared to the embryos with the normal rDNA copy number [15]. The negative role of the low rDNA copy number in the paternal genome has been demonstrated earlier [18]. The authors have found that the total rDNA copy number in sperm is correlated to the rDNA methylation level and, therefore, to the number of transcriptionally active rDNA copies that ensure the required ribosomal biogenesis level. Sperm of males with idiopathic infertility contained the significantly lower total rDNA copy number and, therefore, the lower number of active copies, than sperm of males with normal fertility.

It is interesting to note that low rDNA copy number in associated with not only insufficient ribosomal biogenesis. The

functions of ribosomal repeats being parts of the nucleoli are not limited to production of subunits for ribosomes [19, 20]. The nucleolus is a center, where the synthesis of ribosomes, cell cycle progress, and the cells' response to various types of stress are coordinated. The research has shown that the epigenetic status of ribosomal genes and the nucleolar structure integrity can modulate cellular homeostasis [21–23]. The discovery of structural and functional links between the nucleolus and other genome of the cell made it possible to hypothesize that the nucleolus plays a key role in the nuclear architecture organization. The low rDNA copy number destabilizes heterochromatin and increases the likelihood of chromosomal rearrangements [24]. The ribosomal repeat copy number variation alters the cells' response to DNA damage. Cells with the low rDNA content are more susceptible to various stress factors [25].

The fact seems paradoxical that the average rDNA content in the group with abnormal pregnancy/specific features of pregnancy is lower compared to the control group, despite the lack of low-copy rDNA variants (Fig. 1B, C; Table 1). In these groups the lack of low-copy DNA samples is accompanied by the reduced number of high-copy samples. The variation interval and variation coefficient of these groups are considerably lower compared to group 1 (normal pregnancy). It would seem that a large number of rDNA copies in the genome should provide a greater number of ribosomes and a better response to stress associated with abnormalities. To answer this question we brought the earlier published data on the rDNA copy number variation associated with genetic abnormalities in the group of long-lived individuals [3]. According to these data, the larger number of rDNA copies in the human genome is associated with genetic abnormalities. During embryogenesis the embryo's genome requires the more intense protein synthesis to respond to the abnormality-induced stress. When the rDNA quantity is insufficient to maintain the ribosomal biogenesis level that is appropriate for genome realization, the embryogenesis failure occurs. The high rDNA copy number have been found in the genomes of patients with monogenic (cystic fibrosis) and polygenic (hereditary forms of schizophrenia) disorders [3], as well as in the genomes of people with renal failure and chronic inflammation [6]. Thus, the high rDNA copy number in the genome is a special marker of the presence of mutations/polymorphic DNA sequence variants in the genome affecting many body's processes, longevity, and probably successful reproductive function realization.

In people who have lived to the age of centenarians (over 90 years), the rDNA copy number varies within a narrow range; it is slightly lower relative to the population of people under the age of 70. The genomes of long-lived individuals comprise neither high-copy, nor low-copy rDNA variants [3]. It is interesting to note that the distribution of DNA samples by the rDNA copy number in groups 5–8 shows no differences from the distribution in the group of long-lived individuals (Table 2). It is likely that only the genome containing the rDNA quantity that is large enough for normal ribosomal biogenesis and not containing any DNA sequence variants that are harmful in terms of normal cell functioning (the abnormally high rDNA content is a marker) allows the woman to nurture the fetus, despite early placental maturation, polyhydramnios, twin pregnancy, or macrosomia.

Study limitations

It should be noted that the conclusions about small groups of women (5, 6, and 8; $n < 20$) are preliminary, these should be verified in the larger cohorts.

CONCLUSIONS

The rDNA copy number ranging from ~ 300 to 500 in the woman's genome (the adaptive norm typical for long-lived individuals) is likely to be optimal in terms of successful completion of pregnancy, even when complications occur. The low rDNA copy number in the woman's genome is associated with the impossibility of embryogenesis realization when there are fetal abnormalities/specific features. The high rDNA content suggests that the woman's genome contains genetic variants that can impede the complicated pregnancy course. Determining the rDNA copy number in the genomes of females and males can be useful for planning and predicting the course of pregnancy. This approach should be further tested for possible introduction into clinical practice.

References

1. Khatter H, Myasnikov AG, Natchiar SK, Klaholz BP. Structure of the human 80S ribosome. Nature. 2015; 520 (7549): 640–5. PubMed PMID: 25901680. DOI: 10.1038/nature14427.
2. McStay B, Grummt I. The epigenetics of rRNA genes: from molecular to chromosome biology. Annu Rev Cell Dev Biol. 2008; 24: 131–57. PubMed PMID: 616426. DOI: 10.1146/annurev.cellbio.24.110707.175259.
3. Veiko NN, Ershova ES, Kondratyeva EI, Porokhovnik LN, Zinchenko RA, Melyanovskaya YL et al. Copy Number Variations of Human Ribosomal Genes in Health and Disease: Role and Causes. Front Biosci (Landmark Ed). 2025; 30 (2): 25765. PubMed PMID: 40018927. DOI: 10.31083/FBL25765.
4. Razzaq A, Bejaoui Y, Alam T, Saad M, El Hajj N. Ribosomal DNA Copy Number Variation is Coupled with DNA Methylation Changes at the 45S rDNA Locus. Epigenetics. 2023; 18 (1): 2229203. PubMed PMID: 37368968. PMCID: PMC10305490. DOI: 10.1080/15592294.2023.2229203.
5. Hori Y, Shimamoto A, Kobayashi T. The human ribosomal DNA array is composed of highly homogenized tandem clusters. Genome Res. 2021; 31 (11): 1971–82. PubMed PMID: 34407983; PMCID: PMC8559705. DOI: 10.1101/gr.275838.121.
6. Rodriguez-Algarra F, Evans DM, Rakyan VK. Ribosomal DNA copy number variation associates with hematological profiles and renal function in the UK Biobank. Cell Genomics. 2024; 4: 100562. PubMed PMID: 38749448; PMCID: PMC11228893. Available from: https://doi.org/10.1016/j.xgen.2024.100562.
7. Law PP, Mikheeva LA, Rodriguez-Algarra F, Asenius F, Gregori M, Seaborne RAE, et al. Ribosomal DNA copy number is associated with body mass in humans and other mammals. Nat Commun. 2024; 15 (1): 5006. PubMed PMID: 38866738; PMCID: PMC11169392. DOI: 10.1038/s41467-024-49397-5.
8. Veiko NN, Ershova ES, Veiko RV, Umriukhin PE, Kurmyshev MV, Kostyuk GP, et al. Mild cognitive impairment is associated with low copy number of ribosomal genes in the genomes of elderly people. Front Genet. 2022; 13: 967448. PubMed PMID: 36199570; PMCID: PMC9527325. DOI: 10.3389/fgene.2022.967448.
9. Vejko NN, Terekhov SM, SHubaeva NO, Smirnova TD, Ivanova SM, Egolina NA, i dr. «Rannij» i «pozdnij» otvet kul'tiviruemyh fibroblastov kozhi zdorovyh donorov i bol'nyh revmatoidnym artritom na okislitel'nyj stress. Vzaimosvyaz' mezhdu intensivnost'yu gibeli kletok i kolichestvom aktivnyh kopij ribosomnyh genov. Molekulyarnaya biologiya. 2005; 39 (2): 264–75. Russian.
10. Ershova ES, Umriukhin PE, Zinchenko RA, Vasilieva TP, Kostyuk SE,

Shabalin NY, et al. Variation in the Content of Three Tandem Repeats of the Human Genome (Ribosomal, Satellite III, and Telomere) in Peripheral Blood Leukocyte DNA of People of Different Ages (5–101 Years). J Aging Res. 2025; 2025: 8847073. PubMed PMID: 40979377; PMCID: PMC12446595. DOI: 10.1155/jare/8847073.
11. Geisen ABC, Santana Acevedo N, Oshima J, Dittrich M, Potabattula R, Haaf T. rDNA Copy Number Variation and Methylation During Normal and Premature Aging. Aging Cell. 2025; 24 (5): e14497. PubMed PMID: 39853912; PMCID: PMC12073889. DOI: 10.1111/acel.14497.
12. Porohovnik LN, Viktorov VV, Egolina NA, i dr. Polimorfizm razmerov klasterov aktivnyh ribosomnyh genov u cheloveka i modelirovanie uslovij ego stabil'nosti v ryadu pokolenij. Genetika. 2011; 47 (12): 1666. Russian.
13. Porohovnik LN, Egolina NA, Kosyakova NV, i dr. Zigoticheskij i embrional'nyj otbor po genomnoj doze aktivnyh ribosomnyh genov kak odin iz vozmozhnyh faktorov snizhennoj plodovitosti supruzheskih par. Medicinskaya genetika. 2012; 11: 6 (120): 31–34. Russian.
14. Veiko NN, Ershova ES, Porokhovnik LN, Klimenko MP, Klimenko PA, Umriukhin PE, et al. Ribosomal, Telomere, and Mitochondrial Repeat Copy Number Variations in Female Genomes during Ovarian Stimulation and the Prediction of In Vitro Fertilization Outcome: A Pilot Study. Front Biosci (Schol Ed). 2023; 15 (3): 9. PubMed PMID: 37806951. DOI: 10.31083/j.fbs1503009.
15. Vejko NN, Ershova ES, Kostyuk SV, Porohovnik LN, Kostyuk EV, Klimenko MP, i dr. Variaciya chisla kopij ribosomnogo povtora v kletkah materi i ploda pri normal'noj i nerazvivayushchejsya beremennosti. Voprosy ginekologii, akusherstva i perinatologii. 2024; 23 (5): 25–31. DOI: 10.20953/1726-1678-2024-5-25-31. Russian.
16. Chestkov IV, Jestkova EM, Ershova ES, Golimbet VE, Lezheiko TV, Kolesina NY, et al. Abundance of ribosomal RNA gene copies in the genomes of schizophrenia patients. Schizophr Res. 2018; 197: 305–14. PubMed PMID: 29336872. DOI: 10.1016/j.schres.2018.01.001.
17. Hori Y, Shimamoto A, Kobayashi T. The human ribosomal DNA array is composed of highly homogenized tandem clusters. Genome Res. 2021; 31 (11): 1971–82. DOI: 10.1101/gr.275838.121. PMID: 34407983; PMCID: PMC8559705.
18. Michler A, Kießling S, Durackova J, Hahn T, Schorsch M, Haaf T. Sperm rDNA Copy Number and Methylation Are Associated with Male-Factor Infertility. Int J Mol Sci. 2025; 26 (21): 10657. DOI: 10.3390/ijms262110657. PMID: 41226693; PMCID: PMC12609593.
19. Boisvert FM, van Koningsbruggen S, Navascués J, Lamond AI. The multifunctional nucleolus. Nat Rev Mol Cell Biol. 2007; 8 (7): 574–85. DOI: 10.1038/nrm2184.
20. Pederson T, Tsai RY. In search of nonribosomal nucleolar protein function and regulation. J Cell Biol. 2009; 184 (6): 771–6. DOI: 10.1083/jcb.200812014.
21. Pestov DG, Strezoska Z, Lau LF. Evidence of p53-dependent cross-talk between ribosome biogenesis and the cell cycle: effects of nucleolar protein Bop1 on G(1)/S transition. Mol Cell Biol. 2001; 21 (13): 4246–55. DOI: 10.1128/MCB.21.13.4246-4255.2001.
22. Bursac S, Brdovcak MC, Donati G, Volarevic S. Activation of the tumor suppressor p53 upon impairment of ribosome biogenesis. Biochim Biophys Acta. 2014; 1842 (6): 817–30. DOI: 10.1016/j.bbadis.2013.08.014.
23. Boulon S, Westman BJ, Hutten S, Boisvert FM, Lamond AI. The nucleolus under stress. Mol Cell. 2010; 40 (2): 216–27. DOI: 10.1016/j.molcel.2010.09.024.
24. Chubb JR, Boyle S, Perry P, Bickmore WA. Chromatin motion is constrained by association with nuclear compartments in human cells. Curr Biol. 2002; 12 (6): 439–45. DOI: 10.1016/s0960-9822(02)00695-4.
25. Kobayashi T. Regulation of ribosomal RNA gene copy number and its role in modulating genome integrity and evolutionary adaptability in yeast. Cell Mol Life Sci. 2011; 68 (8): 1395–403. DOI: 10.1007/s00018-010-0613-2.

Литература

1. Khatter H, Myasnikov AG, Natchiar SK, Klaholz BP. Structure of the human 80S ribosome. Nature. 2015; 520 (7549): 640–5. PubMed PMID: 25901680. DOI: 10.1038/nature14427.
2. McStay B, Grummt I. The epigenetics of rRNA genes: from molecular to chromosome biology. Annu Rev Cell Dev Biol. 2008; 24: 131–57. PubMed PMID: 616426. DOI: 10.1146/annurev.cellbio.24.110707.175259.
3. Veiko NN, Ershova ES, Kondratyeva EI, Porokhovnik LN, Zinchenko RA, Melyanovskaya YL et al. Copy Number Variations of Human Ribosomal Genes in Health and Disease: Role and Causes. Front Biosci (Landmark Ed). 2025; 30 (2): 25765. PubMed PMID: 40018927. DOI: 10.31083/FBL25765.
4. Razzaq A, Bejaoui Y, Alam T, Saad M, El Hajj N. Ribosomal DNA Copy Number Variation is Coupled with DNA Methylation Changes at the 45S rDNA Locus. Epigenetics. 2023; 18 (1): 2229203. PubMed PMID: 37368968. PMCID: PMC10305490. DOI: 10.1080/15592294.2023.2229203.
5. Hori Y, Shimamoto A, Kobayashi T. The human ribosomal DNA array is composed of highly homogenized tandem clusters. Genome Res. 2021; 31 (11): 1971–82. PubMed PMID: 34407983; PMCID: PMC8559705. DOI: 10.1101/gr.275838.121.
6. Rodriguez-Algarra F, Evans DM, Rakyan VK. Ribosomal DNA copy number variation associates with hematological profiles and renal function in the UK Biobank. Cell Genomics. 2024; 4: 100562. PubMed PMID: 38749448; PMCID: PMC11228893. Available from: https://doi.org/10.1016/j.xgen.2024.100562.
7. Law PP, Mikheeva LA, Rodriguez-Algarra F, Asenius F, Gregori M, Seaborne RAE, et al. Ribosomal DNA copy number is associated with body mass in humans and other mammals. Nat Commun. 2024; 15 (1): 5006. PubMed PMID: 38866738; PMCID: PMC11169392. DOI: 10.1038/s41467-024-49397-5.
8. Veiko NN, Ershova ES, Veiko RV, Umriukhin PE, Kurmyshev MV, Kostyuk GP, et al. Mild cognitive impairment is associated with low copy number of ribosomal genes in the genomes of elderly people. Front Genet. 2022; 13: 967448. PubMed PMID: 36199570; PMCID: PMC9527325. DOI: 10.3389/fgene.2022.967448.
9. Вейко Н. Н., Терехов С. М., Шубаева Н. О., Смирнова Т. Д., Иванова С. М., Еголина Н. А. и др. «Ранний» и «поздний» ответ культивируемых фибробластов кожи здоровых доноров и больных ревматоидным артритом на окислительный стресс. Взаимосвязь между интенсивностью гибели клеток и количеством активных копий рибосомных генов. Молекулярная биология. 2005; 39 (2): 264–75.
10. Ershova ES, Umriukhin PE, Zinchenko RA, Vasilieva TP, Kostyuk SE, Shabalin NY, et al. Variation in the Content of Three Tandem Repeats of the Human Genome (Ribosomal, Satellite III, and Telomere) in Peripheral Blood Leukocyte DNA of People of Different Ages (5–101 Years). J Aging Res. 2025; 2025: 8847073. PubMed PMID: 40979377; PMCID: PMC12446595. DOI: 10.1155/jare/8847073.
11. Geisen ABC, Santana Acevedo N, Oshima J, Dittrich M, Potabattula R, Haaf T. rDNA Copy Number Variation and Methylation During Normal and Premature Aging. Aging Cell. 2025; 24 (5): e14497. PubMed PMID: 39853912; PMCID: PMC12073889. DOI: 10.1111/acel.14497.
12. Пороховник Л. Н., Викторов В. В., Еголина Н. А. и др. Полиморфизм размеров кластеров активных рибосомных генов у человека и моделирование условий его стабильности в ряду поколений. Генетика. 2011; 47 (12): 1666.
13. Пороховник Л. Н., Еголина Н. А., Косякова Н. В. и др. Зиготический и эмбриональный отбор по геномной дозе активных рибосомных генов как один из возможных факторов сниженной плодовитости супружеских пар. Медицинская генетика. 2012; 11: 6 (120): 31–34. EDN QYNYKR.
14. Veiko NN, Ershova ES, Porokhovnik LN, Klimenko MP, Klimenko PA, Umriukhin PE, et al. Ribosomal, Telomere, and Mitochondrial Repeat Copy Number Variations in Female Genomes during Ovarian Stimulation and the Prediction of In Vitro Fertilization Outcome: A Pilot Study. Front Biosci (Schol Ed). 2023; 15 (3): 9.

PubMed PMID: 37806951. DOI: 10.31083/j.fbs1503009.
15. Вейко Н. Н., Ершова Е. С., Костюк С. В., Пороховник Л. Н., Костюк Э. В., Клименко М. П. и др. Вариация числа копий рибосомного повтора в клетках матери и плода при нормальной и неразвивающейся беременности. Вопросы гинекологии, акушерства и перинатологии. 2024; 23 (5): 25–31. DOI: 10.20953/1726-1678-2024-5-25-31.
16. Chestkov IV, Jestkova EM, Ershova ES, Golimbet VE, Lezheiko TV, Kolesina NY, et al. Abundance of ribosomal RNA gene copies in the genomes of schizophrenia patients. Schizophr Res. 2018; 197: 305–14. PubMed PMID: 29336872. DOI: 10.1016/j.schres.2018.01.001.
17. Hori Y, Shimamoto A, Kobayashi T. The human ribosomal DNA array is composed of highly homogenized tandem clusters. Genome Res. 2021; 31 (11): 1971–82. DOI: 10.1101/gr.275838.121. PMID: 34407983; PMCID: PMC8559705.
18. Michler A, Kießling S, Durackova J, Hahn T, Schorsch M, Haaf T. Sperm rDNA Copy Number and Methylation Are Associated with Male-Factor Infertility. Int J Mol Sci. 2025; 26 (21): 10657. DOI: 10.3390/ijms262110657. PMID: 41226693; PMCID: PMC12609593.
19. Boisvert FM, van Koningsbruggen S, Navascués J, Lamond AI. The multifunctional nucleolus. Nat Rev Mol Cell Biol. 2007; 8 (7): 574–85. DOI: 10.1038/nrm2184.
20. Pederson T, Tsai RY. In search of nonribosomal nucleolar protein function and regulation. J Cell Biol. 2009; 184 (6): 771–6. DOI: 10.1083/jcb.200812014.
21. Pestov DG, Strezoska Z, Lau LF. Evidence of p53-dependent cross-talk between ribosome biogenesis and the cell cycle: effects of nucleolar protein Bop1 on G(1)/S transition. Mol Cell Biol. 2001; 21 (13): 4246–55. DOI: 10.1128/MCB.21.13.4246-4255.2001.
22. Bursac S, Brdovcak MC, Donati G, Volarevic S. Activation of the tumor suppressor p53 upon impairment of ribosome biogenesis. Biochim Biophys Acta. 2014; 1842 (6): 817–30. DOI: 10.1016/j.bbadis.2013.08.014.
23. Boulon S, Westman BJ, Hutten S, Boisvert FM, Lamond AI. The nucleolus under stress. Mol Cell. 2010; 40 (2): 216–27. DOI: 10.1016/j.molcel.2010.09.024.
24. Chubb JR, Boyle S, Perry P, Bickmore WA. Chromatin motion is constrained by association with nuclear compartments in human cells. Curr Biol. 2002; 12 (6): 439–45. DOI: 10.1016/s0960-9822(02)00695-4.
25. Kobayashi T. Regulation of ribosomal RNA gene copy number and its role in modulating genome integrity and evolutionary adaptability in yeast. Cell Mol Life Sci. 2011; 68 (8): 1395–403. DOI: 10.1007/s00018-010-0613-2.

PREPARATION AND PROCEDURE FOR SCANNING ELECTRON MICROSCOPY EXAMINATION OF CELLS ADHERED TO BIOCERAMIC SURFACES

Danilko KV ✉, Solntsev VA, Plotnitsky RV, Mikhailova AV, Bilyalov AR, Chugunov SS, Galautdinov MF, Akbashev VN, Akhatov ISh

Bashkir State Medical University, Ufa, Russia

Scanning electron microscopy (SEM) enables the analysis of surfaces of various materials, including eukaryotic cells. The ability of cells of various body tissues to attach and grow on the surface of implantation materials is an important characteristic of their biocompatibility. SEM visualizes how cells adhere to the surfaces. However, sample preparation for SEM analysis traditionally requires extensive dehydration and the use of toxic osmium tetroxide. This study aimed to optimize the process of preparing animal cells grown on the surface of bioceramic samples for SEM analysis. We propose a new SEM analysis preparation method for mesenchymal stem cells derived from human adipose tissue cultured on the surface of three types of bioceramics. The method includes fixation with aldehyde, alcohol dehydration, staining with Giemsa dye, drying, and gold spraying. We also propose an algorithm for detecting cells attached to the surface of a porous and rough material. This approach accelerates the preparation of cells for SEM analysis and eliminates the need for highly toxic reagents.

Keywords: bioceramics, scanning electron microscopy, sample preparation, sputtering, mesenchymal stem cells

Funding: the work was supported by grant No. 23-15-20042 from the Russian Science Foundation. The study utilized the equipment purchased under the "Priority 2030" program.

Author contribution: Danilko KV — study planning, development of study protocols, analysis of results, conducting SEM analysis, manuscript drafting; Solntsev VA, Plotnitsky RV — cell culturing, preparation for SEM; Mikhailova AV — conducting SEM analysis, analysis of results; Bilyalov AR — study planning, literature analysis, interpretation of data, manuscript drafting; Chugunov SS — study planning, literature analysis; Galautdinov MF — data collection, analysis, interpretation; Akbashev VN — literature analysis, manuscript drafting; Akhatov IS — study planning, manuscript editing.

✉ **Correspondence should be addressed:** Ksenia V. Danilko
Lenina, 3, Ufa, 450008, Russia; kse-danilko@yandex.ru

Received: 13.11.2025 **Accepted:** 04.12.2025 **Published online:** 17.12.2025

DOI: 10.24075/brsmu.2025.072

Copyright: © 2025 by the authors. **Licensee:** Pirogov University. This article is an open access article distributed under the terms and conditions of the Creative Commons Attribution (CC BY) license (https://creativecommons.org/licenses/by/4.0/).

ПОДГОТОВКА И АЛГОРИТМ ИССЛЕДОВАНИЯ АДГЕЗИРОВАННЫХ НА ПОВЕРХНОСТИ БИОКЕРАМИКИ КЛЕТОК МЕТОДОМ СКАНИРУЮЩЕЙ ЭЛЕКТРОННОЙ МИКРОСКОПИИ

К. В. Данилко ✉, В. А. Солнцев, Р. В. Плотницкий, А. В. Михайлова, А. Р. Билялов, С. С. Чугунов, М. Ф. Галаутдинов, В. Н. Акбашев, И. Ш. Ахатов

Башкирский государственный медицинский университет, Уфа, Россия

Метод сканирующей электронной микроскопии (СЭМ) в настоящее время позволяет анализировать поверхности различных материалов, в том числе эукариотических клеток. Способность клеток различных тканей организма прикрепляться и расти на поверхности материалов для имплантации служит важной характеристикой их биосовместимости. СЭМ позволяет напрямую визуализировать характер контакта клеток с поверхностью. Однако методика подготовки проб к анализу традиционно требует высокой степени обезвоживания образца и применения токсичного тетраоксида осмия. Целью работы было провести оптимизацию методики подготовки животных клеток, растущих на поверхности биокерамических образцов, к анализу с помощью СЭМ. В работе предложена методика подготовки мезенхимальных стволовых клеток жировой ткани человека, выращенных на поверхности трех типов биокерамических образцов, к анализу с помощью СЭМ. Она включает фиксацию с помощью альдегида, спиртовое обезвоживание, подкрашивание красителем Гимзы и высушивание с последующим напылением золота. Предложен также алгоритм поиска прикрепленных клеток на поверхности пористого и шероховатого материала. Данный подход позволяет быстро подготовить клетки к СЭМ-анализу без использования высокотоксичных реагентов.

Ключевые слова: биокерамика, сканирующая электронная микроскопия, пробоподготовка, напыление, мезенхимальные стволовые клетки

Финансирование: работа выполнена при поддержке гранта Российского научного фонда № 23-15-20042. Работа выполнена на оборудовании, приобретенном за счет средств программы «Приоритет 2030».

Вклад авторов: К. В. Данилко — планирование исследования, разработка протоколов исследования, анализ результатов, проведение СЭМ, подготовка черновика рукописи; В. А. Солнцев, Р. В. Плотницкий — культивирование клеток, подготовка к СЭМ; А. В. Михайлова — проведение СЭМ, анализ результатов; А. Р. Билялов — планирование исследования, анализ литературы, интерпретация данных, подготовка черновика рукописи; С. С. Чугунов — планирование исследования, анализ литературы; М. Ф. Галаутдинов — сбор, анализ, интерпретация данных; В. Н. Акбашев — анализ литературы, подготовка рукописи; И. Ш. Ахатов — планирование исследования, редактирование рукописи.

✉ **Для корреспонденции:** Ксения Владимировна Данилко
ул. Ленина, д. 3, г. Уфа, 450008, Россия; kse-danilko@yandex.ru

Статья получена: 13.11.2025 **Статья принята к печати:** 04.12.2025 **Опубликована онлайн:** 17.12.2025

DOI: 10.24075/vrgmu.2025.072

Авторские права: © 2025 принадлежат авторам. **Лицензиат:** РНИМУ им. Н. И. Пирогова. Статья размещена в открытом доступе и распространяется на условиях лицензии Creative Commons Attribution (CC BY) (https://creativecommons.org/licenses/by/4.0/).

Scanning electron microscopy (SEM) enables visualization of surfaces of various materials. Recently, this method has been increasingly used to study biological objects and the nature of the interaction of eukaryotic cells with organic and inorganic materials, in particular ceramic implants [1].

Bioceramic materials occupy an important place among modern biocompatible structures used in regenerative medicine, traumatology, orthopedics, neurosurgery, and maxillofacial surgery. Due to their chemical non-reactivity, biocompatibility, and osseointegration capacity, they are a common choice for bone implants, osteoplastic compositions, and tissue engineering frameworks. The best-studied bioceramic materials today are hydroxyapatite, tricalcium phosphate, and various compositions based on these compounds [2]. The morphology and microrelief of a bioceramic surface largely determine the nature of cell adhesion, proliferation, and differentiation, all of which directly affect the quality of implant integration with body tissues [3].

Evaluating the interaction of cells with the surface of a bioceramic material requires the use of high-precision imaging techniques capable of reproducing the topography of a sample at the micron and submicron levels. Traditional light and fluorescence microscopy enable only indirect assessment of the condition of cells and their distribution; they give no understanding of the nature of the contact between the cell membrane and the surface of the material. In this regard, scanning electron microscopy (SEM) is the optimal tool for visualizing cellular structures with high spatial resolution and depth of field. It provides a detailed view of cell morphology, the condition of their cytoplasmic extensions, the nature of their adhesion to the surface, and the extent of extracellular matrix formation [4].

However, there are some methodological difficulties associated with the use of SEM for the analysis of biological samples. Mainly, the limitations arise from the cells' high water content, poor electrical conductivity, and their tendency to degrade upon drying [5]. Preventing deformation of the cellular structure requires fixation and gradual dehydration. Traditionally, these steps involve the use of toxic substances, such as glutaraldehyde and osmium tetraoxide, and multi-stage critical drying procedures. Osmium tetraoxide is a highly toxic compound; using it necessitates special safety precautions and conditions. The critical point drying protocol must be optimized for each specific material and cell type, and typically takes about 24 hours. In addition, most existing protocols focus on flat glass or metal substrates, whereas bioceramic materials possess a pronounced microrelief and porous surface, which complicates cell localization and reduces the reproducibility of results [6, 7].

The toxicity of the reagents, the time-consuming preparation, and the high cost of equipment — particularly carbon dioxide drying units — make such protocols impractical for routine laboratory use. At the same time, preserving the morphological features of cells and ensuring high-quality visualization with minimal changes in the initial structure remain critical for the correct interpretation of data [8]. Therefore, it is necessary to develop a simpler, more economical, and safer approach for SEM sample preparation of cells that guarantees reproducible results and high image quality without using toxic reagents or expensive equipment.

An especially important task is the development of an algorithm that allows reliable fixation and visualization of cells cultivated on the surface of a bioceramic material without compromising their shape, membrane integrity, and cytoskeleton elements. The resulting technique should be adapted to the specific properties of the material, require no complex equipment, and remain technologically simple. Meeting these conditions will significantly expand the possibilities for routine morphological assessment of biocompatible materials and improve the accessibility of SEM analysis in laboratory practice.

This study aimed to optimize the preparation of animal cells cultured on bioceramic surfaces for SEM analysis.

METHODS

Preparation of bioceramic samples

We described the method of manufacturing bioceramic samples in an earlier work [10]. For this experiment, we used three types of samples of bioceramic materials. The material for 3D printing was derived from an allograft obtained from human bone tissue. It was calcined, ground into a micron-sized powder, suspended in a photopolymerizable medium, and used in an additive manufacturing process involving light curing. The 3D-printed hydroxyapatite and tricalcium phosphate samples were sintered at various temperatures to eliminate moisture and organic residues from the bonding system. All samples were cylinders with a diameter of 3.6-4.5 mm and a height of 1.9–2.6 mm.

Sterilization

The samples were sterilized in a dry oven at 180 °C for 60 minutes. After sterilization, the samples were placed in the wells of a culture plate inside a Class II biosafety cabinet (Laminar Systems, Russia).

Cell preparation

Human mesenchymal stem cells from adipose tissue (MSC AT) (Biolot, Russia) were cultured in DMEM (Capricorn, Germany) supplemented with 10% fetal bovine serum (Biowest, France) and 2% L-glutamine (Servicebio, China) until they reached 90% confluence. Next, the cells were detached using a 0.25% trypsin solution (Biolot, Russia), washed once with phosphate-buffered saline (PBS) without calcium and magnesium (Paneco, Russia), and resuspended in complete culture medium.

Seeding cells into plates

After resuspension, MSCs were seeded at a density of 5000 cells per well in a 96-well plate, corresponding to a concentration of 100000 cells/ml. For this purpose, 50 µl of the suspension was applied to the center of a cylindrical sample and incubated for 30 minutes at 37 °C in a humidified atmosphere containing 5% CO_2 to allow cells to attach to the surface. Two wells of the plate were prepared for each type of sample. After the adhesion time had elapsed, 150 µl of complete culture medium was added to each well and cells were left to proliferate on the bioceramic samples for 7 days in a CO_2 incubator.

Thus, mesenchymal stem cells that adhered to the surface after cultivation were prepared for SEM analysis.

Preparation of cells on the bioceramic sample surfaces for SEM

Washing of samples

Necessary reagents: PBS without calcium and magnesium.

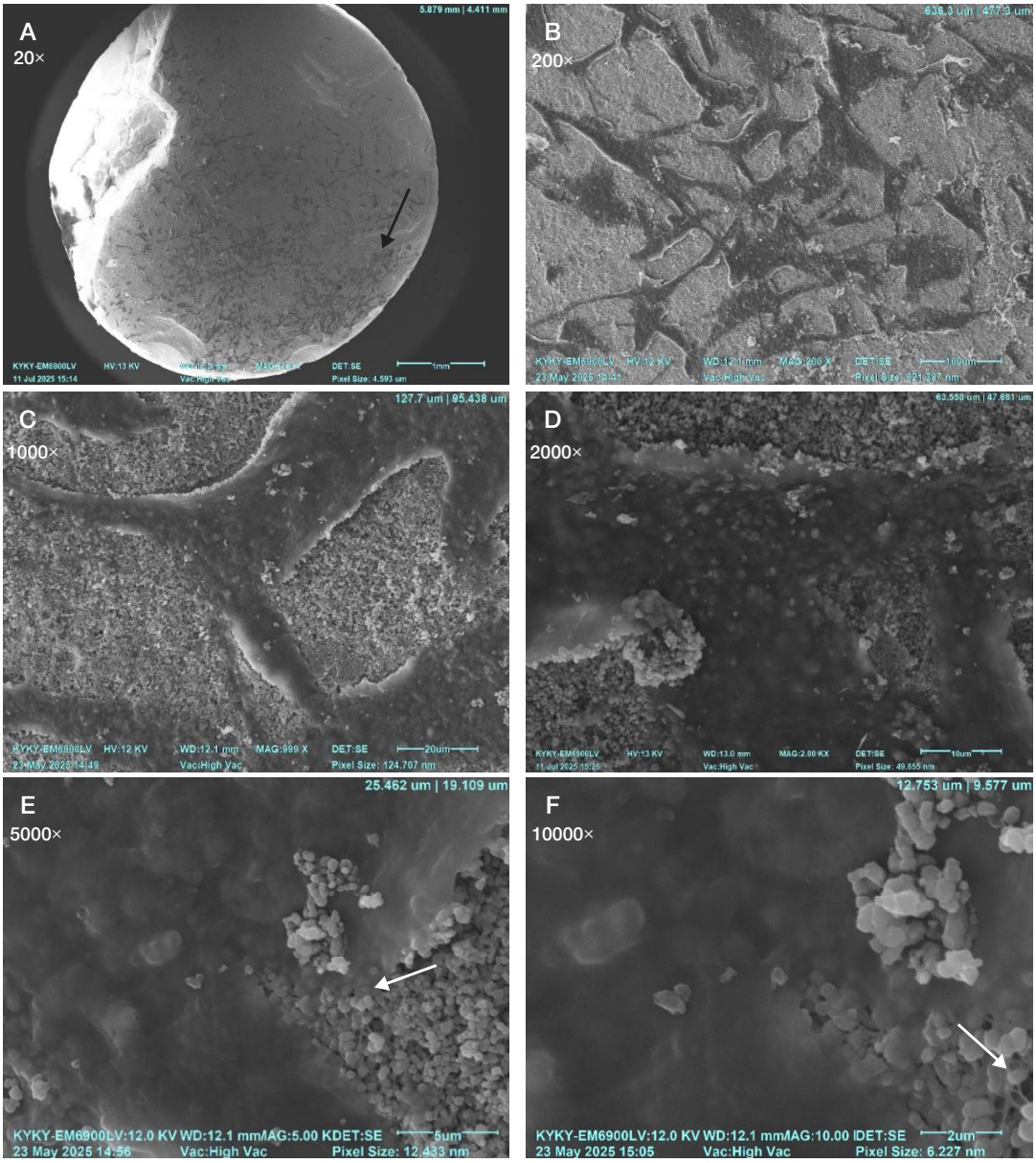


Fig. 1. Scans of the surface of tricalcium phosphate samples after sintering at 800 °C with growing mesenchymal stem cells from adipose tissue, 7 days of cultivation. The black arrow shows dark cells on the surface of a cylindrical tricalcium phosphate sample, and the white arrow shows thin extensions of the membrane. The cells are large, form a cluster, are strongly spread out, in contact with each other by wide extensions; the the cell surface is smooth, there are thin extensions of the membrane visible under the cell body and along the periphery. Magnification from 20× to 10000×

Stages of washing

1. At the end of the cultivation period, 500 µl of PBS were added to each analyzed well to wash the ceramic samples and remove the remaining nutrient medium.
2. The liquid carefully removed.
3. The procedure repeated twice.

Fixation and dehydration of samples

Necessary reagents: 2.5% (w/v) glutaraldehyde in deionized water; saline solution (NaCl, 0.9%); 50% ethanol (prepared by diluting 95% ethanol with deionized water by volume; subsequent dilutions were made similarly); 70% ethanol; 80% ethanol; 90% ethanol; 95% ethanol; 99% ethanol.

Stages of fixation

1. Three hundred µl of 2.5% glutaraldehyde added to each well for 30 minutes. The volume of glutaraldehyde was ten times the volume of the sample.
2. Glutaraldehyde removed, and a 10-fold volume of saline added to the samples for washing.
3. Then liquid completely removed.
4. The procedure of washing repeated twice.

Stages of dehydration

5. The removal of the liquid was followed by the dehydration of the cells. The first stage involved adding 50% ethanol until it covered the sample completely.
6. The samples were kept in this solution for 60 seconds at room temperature.
7. Next, 50% ethanol was removed, and 70% ethanol was added until it completely covered the sample.

At this stage, the protocol can be paused, and the samples may be stored at +4 °C in closed containers to prevent alcohol evaporation.

8. The samples were kept in this solution for 60 seconds at room temperature.

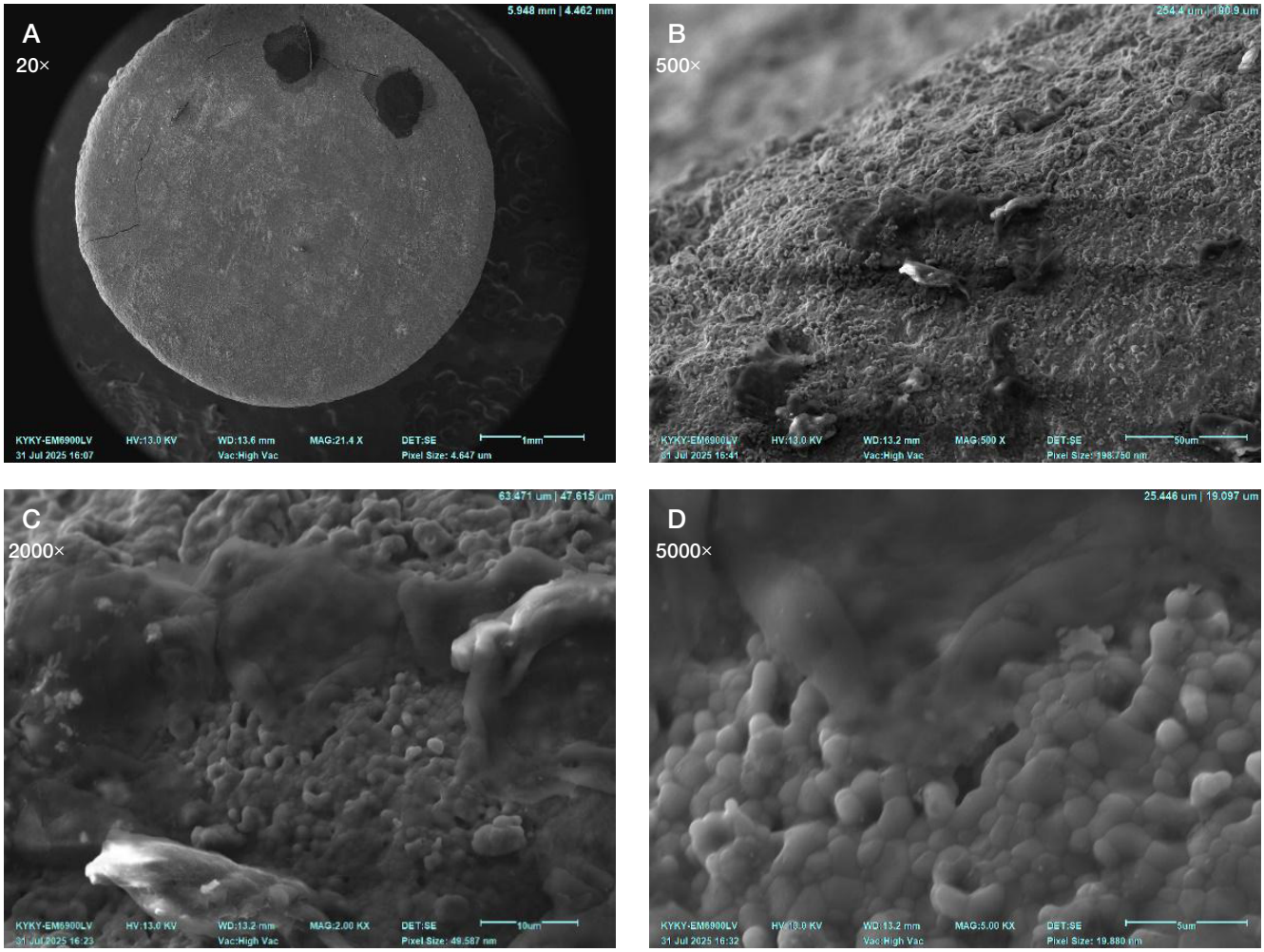


Fig. 2. Scans of the surface of hydroxyapatite samples after sintering at 1250 °C with growing mesenchymal stem cells from adipose tissue, 7 days of cultivation. The surface of the cells is folded, smooth, the cell body is creeping. Magnification from 20× to 5000×

9. Next, 70% ethanol was removed, and 80% ethanol was added until it completely covered the sample.

10. The samples were kept in this solution for 60 seconds at room temperature.

11. Next, 80% ethanol was removed, and 90% ethanol was added until it completely covered the sample.

12. The samples were kept in this solution for 60 seconds at room temperature.

13. Next, 90% ethanol was removed, and 95% ethanol was added until it completely covered the sample.

14. The samples were kept in this solution for 60 seconds at room temperature.

15. Next, 95% ethanol was removed, and 99% ethanol was added until it completely covered the sample.

16. The samples were kept in this solution for 60 seconds at room temperature.

17. After fixation, the samples were air-dried. The next stage involved staining; samples not selected for this stage were stored.

Staining

Staining of cells cultured on a bioceramic surface enables their visualization, which is necessary because during cultivation, washing, and fixation, the samples may shift or overturn in the wells. The cells will mainly be located on the surface of the sample facing the liquid in the well, not its bottom. Orienting the stained cells for SEM can be done with or without visual aids (a light microscope).

Necessary reagents: Giemsa dye, Paneco, Russia.

Stages of staining

1. The sample was completely coated with a solution of Giemsa dye.

2. Incubated for 2 minutes at room temperature.

3. The well was filled with deionized water for washing.

4. The plate was rocked for 2 minutes.

5. The liquid was completely removed and the wells were rinsed with a large volume of tap water until the liquid cleared.

6. The liquid was completely removed and the sample was rinsed again with deionized water for 2 minutes.

7. The liquid was removed, and the stained sample was air-dried and stored in a sealed plate until use.

Spraying

Necessary equipment: DSR1 Desk Sputter Coater (Nanostructured coatings Co, Iran)

Stages of spraying

1. The samples of bioceramic materials secured on aluminum tables (1 cm in diameter) for SEM using electrically conductive tape.

2. Giemsa staining turned areas with cells blue-violet. Colored surfaces were oriented upwards, uncolored — downwards, and secured on an electrically conductive tape.

3. Next, the samples received a 20–30 — layer of gold, which was applied using an automatic spraying system.

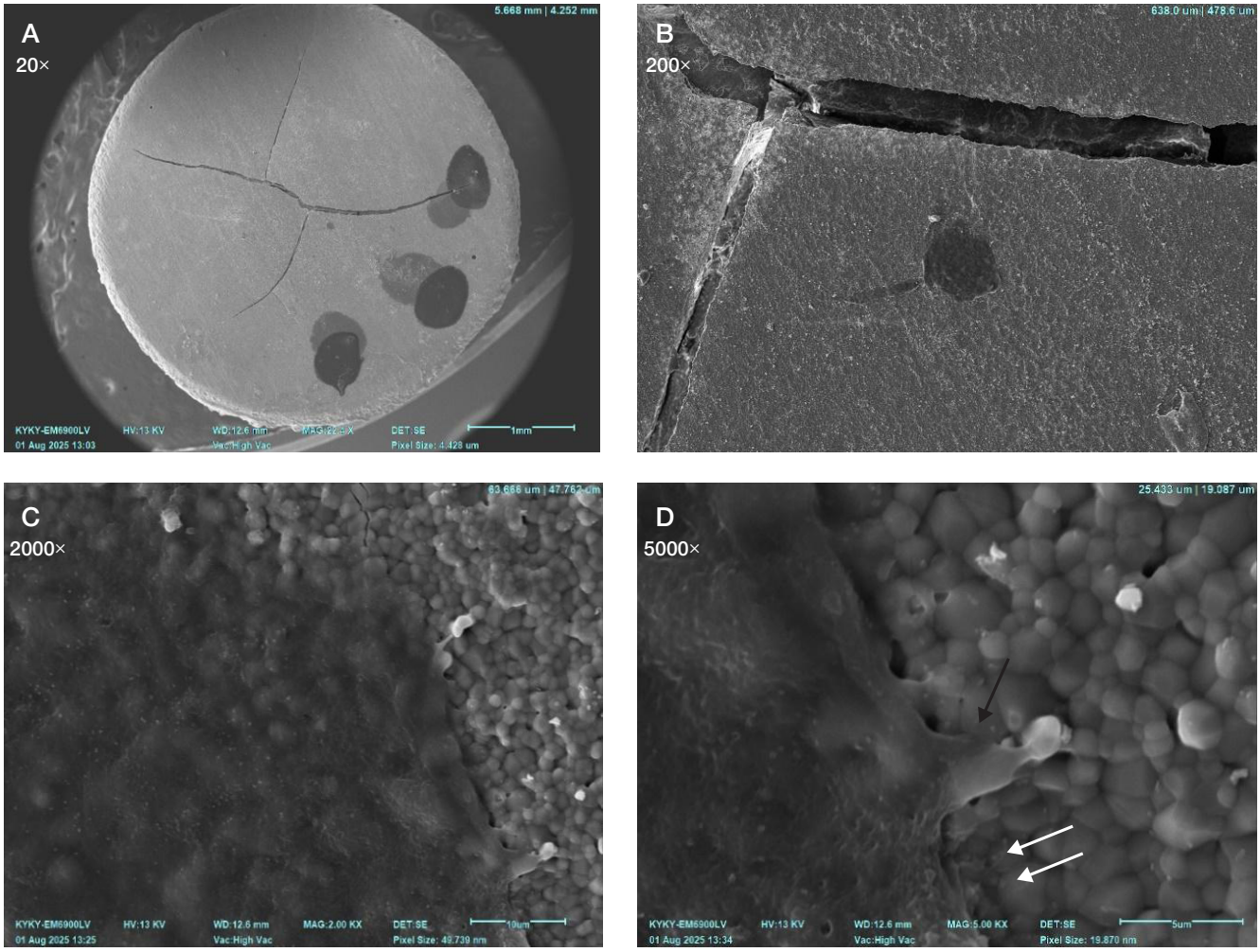


Fig. 3. Scans of the surface of tricalcium phosphate samples after sintering at 1250 °C with growing mesenchymal stem cells from adipose tissue, 7 days of cultivation. The black arrow point to a wide pseudopod. The white arrow — to a thin extension that widens at the end. Magnification 20x–5000x. The cell has a high degree of adhesion, it fits firmly to the surface, is strongly flattened; underneath, the contour of the material granules are visible, the surface has small depressions, extensions of various thicknesses are seen along the perimeter of the cell and are visible under its body

Surface analysis using SEM

Necessary equipment: KYKY-EM6900LV Scanning Electron Microscope (KYKY Technology Co., Ltd. China)

Stages of analysis

1. Tables with secured samples placed in the chamber of the microscope.

2. Settings: high vacuum mode; voltage 11–13 kV; working distance 10–14 mm; use of the electron detector.

3. Search for the sample, centering at minimum magnification (Fig. 1A).

4. Cells stained with Giemsa dye appear as darker structures on the surface (Fig. 1A, black arrow).

5. We selected individual darkest areas on the surfaces of the samples, set the magnification of 2000× or 5000×, and studied them to confirm the presence of cells there. This step is necessary because the color of the bioceramic material may be not uniform, with some spots appearing darker than the surrounding parts of the surface.

6. Having found morphologies untypical for the particles of the material, we set a smaller magnification (200× or 500×) and searched for objects with parameters of a cell (Fig. 1B).

7. This algorithm allowed finding individual cells and groups of cells. In both cases, we observed structures with a dark membrane, an almost flat surface, with outlines of ceramic particles, extensions, and strands of different lengths seen underneath and by the edges. The surface of the cell could be less smooth depending on the nature of its growth and how well the material was dehydrated (Fig. 1–4).

8. Having found the cells, we scanned them and generated images at the conditional magnifications of 200×, 500×, 2000×, 5000×, 10000× (Fig. 1–4).

RESULTS

To study biocompatibility using SEM, we prepared 15 samples from three types of materials: treated human bone allogeneic material, hydroxyapatite, and tricalcium phosphate. The approach underpinning this work enabled detection of cells on the surface of all samples (Fig. 1–5). SEM analysis of the sample surfaces allowed characterization of cell morphology, including cell size and shape, surface uniformity and roughness, the presence and length of marginal extensions, extensions beneath the cell body, and the number of cells on each sample.

Among the cells we detected, there can be identified several morphological variants that characterize the degree of cell attachment to the surface of the material (Fig. 5): 1) high degree of adhesion — large cells spread over the surface with very fine folds, under which the outlines of particles of the surface material can be distinguished, with long thin extensions of the plasma membrane along the edges of the

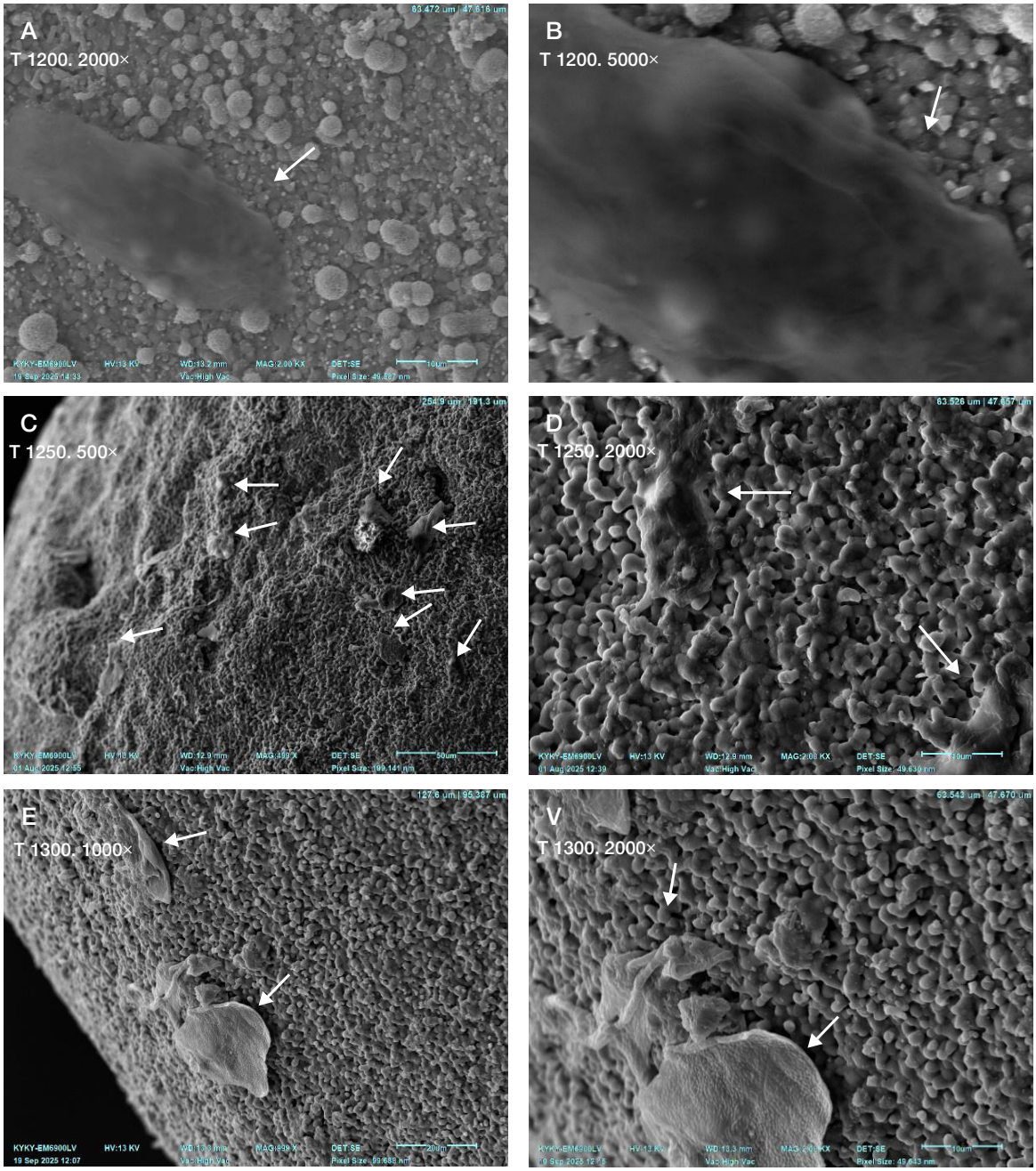


Fig. 4. The nature of cell growth on bone allograft samples with different physical processing parameters. Scans. T1200 — sintering temperature of 1200 ° C, T1250 — sintering temperature of 1250 °C, T1300 — sintering temperature of 1300 °C. The degree of cell adhesion to the material is different. The white arrows point to the cells on the surface of the allograft material. **A**, **B**. Maximum adhesion: the cells adhere tightly to the surface, they are strongly flattened, the contour of the granules of the material is visible under the cell body, the surface is smooth, with faintly noticeable folds, there are extensions of varying thicknesses (mostly thin, around the perimeter of the cell, visible under its body). **C**, **D**. Moderate adhesion: the cells adhere to the surface, in some areas the edges of the cell are raised, the surface has clearly visible folds, and the extensions are predominantly wide. **E**, **F**. Low adhesion: the cells are slightly spread out, the edges of the cells are noticeably raised around the perimeter, the cell surface has small bumps, there are no extensions

cell and under its body; 2) medium degree of adhesion — cells spread out, with small surface irregularities, of medium size, with a small number of wide and thin extensions of the membrane mainly along the periphery of the cell; 3) low degree of adhesion — relatively small, flat cells with well-marked folds, well-marked regular surface irregularities, without extensions of the membrane under the cell body and along the periphery, no material particles visible.

DISCUSSION

The results of the study demonstrate that the proposed algorithm for preparing cell cultures on the surface of bioceramic samples preserves cell morphology and enables reliable visualization of their interaction zones with the material using SEM. Unlike conventional sample preparation protocols that require sophisticated equipment, extended processing time, and toxic reagents, this approach uses sequential fixation and gentle dehydration, making it feasible in a standard laboratory setting. The previously described techniques, despite the use of a similar dehydration scheme [11], often led to membrane deformation and loss of cellular pseudopods due to changes in surface tension during sample processing. Modern studies indicate that even minimal differences in microrelief and porosity of bioceramics can significantly affect cell adhesion and spatial orientation [12]. In our study, fixation with sequential

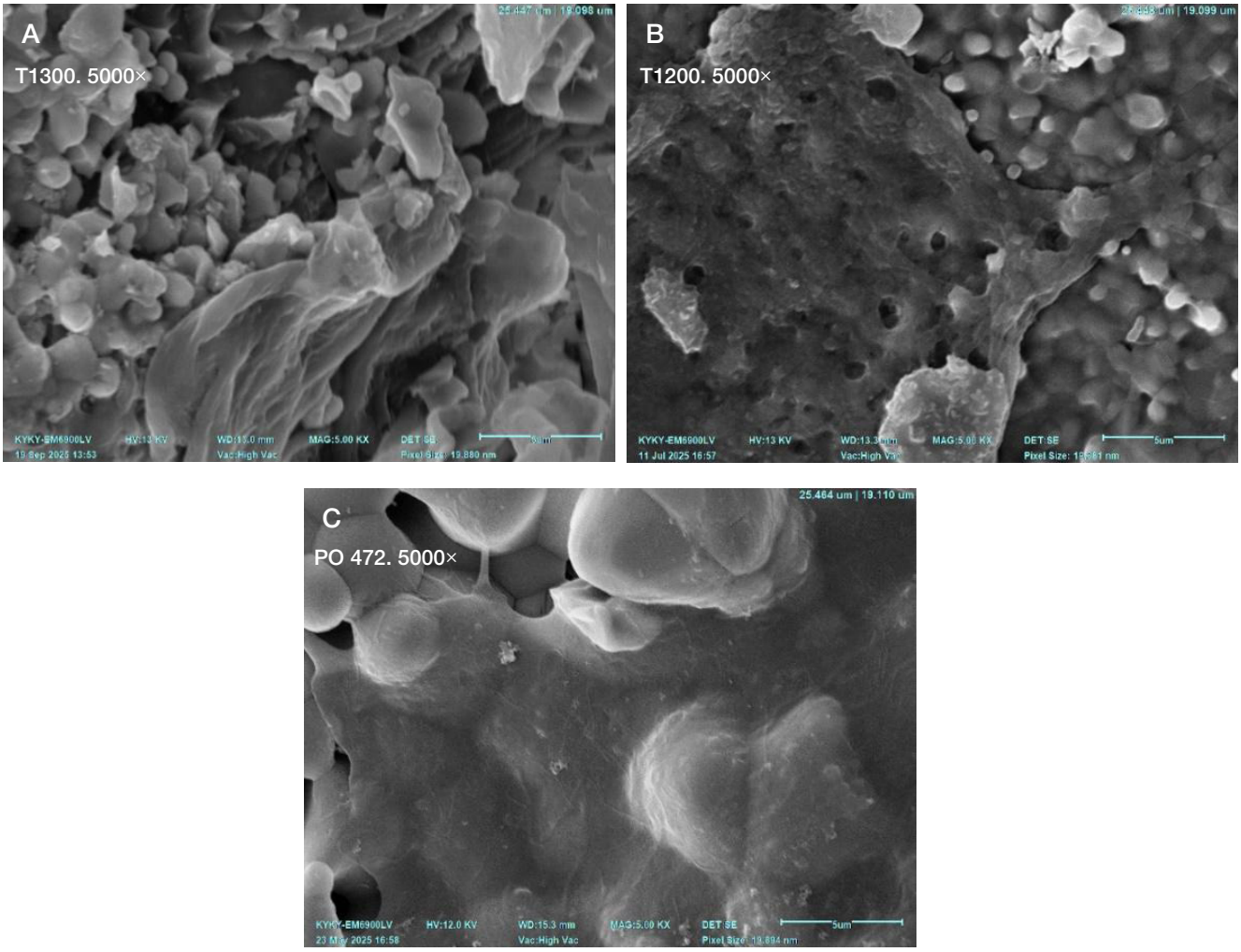


Fig. 5. Morphological features of mesenchymal stem cells from adipose tissue on the surface of tricalcium phosphate samples. Scans. **A**. Folded surface of the cell, smooth, low degree of spreading, adhesion at individual points, no extensions of the cell body. **B**. The cell is spread out, almost completely adhered, the surface is bumpy, there are several wide and separate thin extensions along the periphery. **C**. The cell is strongly spread out, fully adhered, the surface is smooth, there are many wide and thin extensions under the cell body and along the periphery. T1200, T1300 — the sintering temperature of the material during the manufacture of samples in °C. RO 472 — laboratory sample marking

dehydration in an ethanol gradient at room temperature allowed avoiding such distortions and preserving the natural contours of cells and the microstructure of the material. Critical point drying, a commonly used sample preparation technique, is relatively laborious and time-consuming [13]. In this study, sample preparation was limited to dehydration followed by plasma spraying of gold to ensure sample conductivity.

A particularly important step is the staining with a Giemsa dye before spraying: this step ensured accurate positioning of the sample surfaces with attached cells and significantly reduced the search time for areas of interest during the SEM analysis. Such a combination of techniques has not previously been described for bioceramic substrates; it may be useful in morphological studies of other types of materials.

The analysis of microscopic images showed that the mesenchymal stem cells preserve the shape characteristic for them, grow extensions, and form pronounced contact zones with the ceramic surface. On tricalcium phosphate samples, cells demonstrated tighter adhesion and longer membrane extensions, which is consistent with data on the high biocompatibility of calcium-phosphate materials and their stimulating effect on osteogenic differentiation [14]. As for the allogeneic allogeneic material, the cells exhibited considerable shape variability, which depended on the processing temperature of the material and was probably also caused by the heterogeneity of the surface structure.

The proposed protocol combines reproducibility, technological simplicity, and safety. It can be adapted for analyzing other types of cells and substrates, thereby broadening the scope of morphological assessments of cell–material interfaces in biomedical research and the development of osteointegrating implants

Study Limitations

The study has a number of limitations. First of all, the analysis was primarily qualitative in nature and did not include quantitative morphometry of cellular structures, which could increase the objectivity of the assessment. In addition, the work was performed on one cell model, human mesenchymal adipose tissue stem cells; to confirm the universality of the method, testing on other cell types is required.

This was an in vitro study, which may limit the applicability of the resulting data to *in vivo* models. We also did not consider the influence of individual physico-chemical parameters of bioceramics on the quality of visualization and the preservation of cellular morphology; it may become the subject of further research.

CONCLUSIONS

This work describes a new SEM analysis preparation method for mesenchymal stem cells derived from human adipose tissue cultured on the surface of bioceramic samples, and the flow of the analysis itself. The approach proposed in this paper requires no more than one hour to prepare cells for SEM analysis, including the sample drying stage. Moreover, it eliminates the need for toxic heavy metal salts and ensures stable, reproducible results. The use of Giemsa staining greatly facilitates the search for cells on the sample surfaces and allows orienting the samples correctly for examination. The described sample preparation method can also be applied to other animal cells adhering to the surface of any material that is resistant to glutaraldehyde and ethanol treatment.

References

1. Zhang Y, Shen Y, Peng F, Jiang C, Li W, Miao H, Huang F, Zeng Y. Method for acquiring accurate coordinates of the source point in electron backscatter diffraction. J Microsc. 2021; 284 (3): 233–243. DOI: 10.1111/jmi.13055. PubMed PMID: 34383320.
2. Eliaz N, Metoki N. Calcium Phosphate Bioceramics: A Review of Their History, Structure, Properties, Coating Technologies and Biomedical Applications. Materials (Basel). 2017; 10 (4): 334. DOI: 10.3390/ma10040334. PubMed PMID: 28772697.
3. Kim SE, Park K. Recent Advances of Biphasic Calcium Phosphate Bioceramics for Bone Tissue Regeneration. Adv Exp Med Biol. 2020; 1250: 177–88. DOI: 10.1007/978-981-15-3262-7_12. PubMed PMID: 32601945.
4. Koga D, Kusumi S, Shibata M, Watanabe T. Applications of Scanning Electron Microscopy Using Secondary and Backscattered Electron Signals in Neural Structure. Front Neuroanat. 2021; 15: 759804. DOI: 10.3389/fnana.2021.759804. PubMed PMID: 34955763; PMCID: PMC8693767.
5. Qu Y, Pan H, Peng R, Niu J, Li C. Interference illumination of three nonzero-order beams for LCOS-based structured illumination microscopy. J Microsc. 2019; 275 (2): 97–106. DOI: 10.1111/jmi.12806.. PubMed PMID: 31087655.
6. Bray DF, Bagu J, Koegler P. Comparison of hexamethyldisilazane (HMDS), Peldri II, and critical-point drying methods for scanning electron microscopy of biological specimens. Microsc Res Tech. 1993; 26 (6): 489–95. DOI: 10.1002/jemt.1070260603. PubMed PMID: 8305726.
7. Fakhrullin R, Nigamatzyanova L, Fakhrullina G. Dark-field/hyperspectral microscopy for detecting nanoscale particles in environmental nanotoxicology research. Sci Total Environ. 2021; 772: 145478. DOI: 10.1016/j.scitotenv.2021.145478. PubMed PMID: 33571774.
8. Orhan EO, Bahadır D, Akgün C, Aktaş S. Scanning electron microscopic evaluation of the efficacy of 5% ethylenediaminetetraacetic acid for smear layer removal. Microsc Res Tech. 2021; 84 (2): 253–60. DOI: 10.1002/jemt.23582. PMID: 32905662.
9. Teixeira S, Ferraz MP, Monteiro FJ. Biocompatibility of highly macroporous ceramic scaffolds: cell adhesion and morphology studies. J Mater Sci Mater Med. 2008; 19 (2): 855–9. DOI: 10.1007/s10856-007-3005-x. Epub 2007 Aug 1. PubMed PMID: 17665126.
10. Bilyalov A, Piatnitskaia S, Rafikova G, et al. The effect of sterilization methods on the cytotoxicity of ceramic medical implants. Bulletin of Russian State Medical University. 2025; 1: 77–84. DOI: 10.24075/brsmu.2025.009.
11. Ullah N, Guhar D, Khan S. Preparation and topographical studies of various biological specimens using alternate method to critical point drying: Scanning electron microscopy. J Microsc. 2025; 299 (1): 25–35. DOI: 10.1111/jmi.13412. PubMed PMID: 40171741.
12. Skliarenko Y, Kolomiiets VV, Balatskyi VV, et al. The impact of the physicochemical properties of calcium phosphate ceramics on biocompatibility and osteogenic differentiation of mesenchymal stem cells. BMC Res Notes. 2024; 17, 295. DOI: 10.1186/s13104-024-06937-y.
13. Parisi L, Toffoli A, Ghezzi B, Lagonegro P, Trevisi G, et al. Preparation of hybrid samples for scanning electron microscopy (SEM) coupled to focused ion beam (FIB) analysis: A new way to study cell adhesion to titanium implant surfaces. PLOS ONE. 2022; 17 (8): e0272486. DOI: 10.1371/journal.pone.0272486.
14. Gou Y, Qi K, Wei Y, Gu Z, Xie H. Advances of calcium phosphate nanoceramics for the osteoinductive potential and mechanistic pathways in maxillofacial bone defect repair. Nano TransMed. 2024; 3: 100033. DOI: 10.1016/j.ntm.2024.100033.

Литература

1. Zhang Y, Shen Y, Peng F, Jiang C, Li W, Miao H, Huang F, Zeng Y. Method for acquiring accurate coordinates of the source point in electron backscatter diffraction. J Microsc. 2021; 284 (3): 233–243. DOI: 10.1111/jmi.13055. PubMed PMID: 34383320.
2. Eliaz N, Metoki N. Calcium Phosphate Bioceramics: A Review of Their History, Structure, Properties, Coating Technologies and Biomedical Applications. Materials (Basel). 2017; 10 (4): 334. DOI: 10.3390/ma10040334. PubMed PMID: 28772697.
3. Kim SE, Park K. Recent Advances of Biphasic Calcium Phosphate Bioceramics for Bone Tissue Regeneration. Adv Exp Med Biol. 2020; 1250: 177–88. DOI: 10.1007/978-981-15-3262-7_12. PubMed PMID: 32601945.
4. Koga D, Kusumi S, Shibata M, Watanabe T. Applications of Scanning Electron Microscopy Using Secondary and Backscattered Electron Signals in Neural Structure. Front Neuroanat. 2021; 15: 759804. DOI: 10.3389/fnana.2021.759804. PubMed PMID: 34955763; PMCID: PMC8693767.
5. Qu Y, Pan H, Peng R, Niu J, Li C. Interference illumination of three nonzero-order beams for LCOS-based structured illumination microscopy. J Microsc. 2019; 275 (2): 97–106. DOI: 10.1111/jmi.12806.. PubMed PMID: 31087655.
6. Bray DF, Bagu J, Koegler P. Comparison of hexamethyldisilazane (HMDS), Peldri II, and critical-point drying methods for scanning electron microscopy of biological specimens. Microsc Res Tech. 1993; 26 (6): 489–95. DOI: 10.1002/jemt.1070260603. PubMed PMID: 8305726.
7. Fakhrullin R, Nigamatzyanova L, Fakhrullina G. Dark-field/hyperspectral microscopy for detecting nanoscale particles in environmental nanotoxicology research. Sci Total Environ. 2021; 772: 145478. DOI: 10.1016/j.scitotenv.2021.145478. PubMed PMID: 33571774.
8. Orhan EO, Bahadır D, Akgün C, Aktaş S. Scanning electron microscopic evaluation of the efficacy of 5% ethylenediaminetetraacetic acid for smear layer removal. Microsc Res Tech. 2021; 84 (2): 253–60. DOI: 10.1002/jemt.23582. PMID: 32905662.
9. Teixeira S, Ferraz MP, Monteiro FJ. Biocompatibility of highly macroporous ceramic scaffolds: cell adhesion and morphology studies. J Mater Sci Mater Med. 2008; 19 (2): 855–9. DOI: 10.1007/s10856-007-3005-x. Epub 2007 Aug 1. PubMed PMID: 17665126.
10. Bilyalov A, Piatnitskaia S, Rafikova G, et al. The effect of sterilization methods on the cytotoxicity of ceramic medical implants. Bulletin of Russian State Medical University. 2025; 1: 77–84. DOI: 10.24075/brsmu.2025.009.

11. Ullah N, Guhar D, Khan S. Preparation and topographical studies of various biological specimens using alternate method to critical point drying: Scanning electron microscopy. J Microsc. 2025; 299 (1): 25–35. DOI: 10.1111/jmi.13412. PubMed PMID: 40171741.
12. Skliarenko Y, Kolomiiets VV, Balatskyi VV, et al. The impact of the physicochemical properties of calcium phosphate ceramics on biocompatibility and osteogenic differentiation of mesenchymal stem cells. BMC Res Notes. 2024; 17, 295. DOI: 10.1186/s13104-024-06937-y.
13. Parisi L, Toffoli A, Ghezzi B, Lagonegro P, Trevisi G, et al. Preparation of hybrid samples for scanning electron microscopy (SEM) coupled to focused ion beam (FIB) analysis: A new way to study cell adhesion to titanium implant surfaces. PLOS ONE. 2022; 17 (8): e0272486. DOI: 10.1371/journal.pone.0272486.
14. Gou Y, Qi K, Wei Y, Gu Z, Xie H. Advances of calcium phosphate nanoceramics for the osteoinductive potential and mechanistic pathways in maxillofacial bone defect repair. Nano TransMed. 2024; 3: 100033. DOI: 10.1016/j.ntm.2024.100033.

DEVELOPMENT OF THE VASCULAR CONDITION CLASSIFIER USING SUPERVISED MACHINE LEARNING METHODS

Besedovskaia ZV[1,2] ✉, Korobov AYu[3], Kudriashova NI[4]

[1] Vladimir Zelman Center for Neurobiology and Neurorehabilitation Skolkovo Institute of Science and Technology, Moscow
[2] Artificial Intelligence Center Skolkovo Institute of Science and Technology, Moscow
[3] Center for Photonics and Photonic Technologies Skolkovo Institute of Science and Technology, Moscow
[4] Center for Molecular and Cellular Biology Skolkovo Institute of Science and Technology, Moscow

Quantitative processing of optoacoustic angiograms is an important task, the solution of which will potentially enable the early diagnosis of vascular diseases. The aim of this study is to refine and conduct biomedical validation of a software tool for the analysis of optoacoustic angiograms, focusing on the application of machine learning methods. The work was conducted on an open dataset containing three-dimensional optoacoustic angiograms of an experimental animal (mouse) in three temperature conditions: cold temperature (16 °C), room temperature (23 °C), and body temperature (30 °C), as well as a dataset with basic vascular features obtained by processing using Amira/Avizo (Thermo Fisher Scientific), a general-purpose software for visualization and analysis of scientific and industrial data. Various vascular features missing from previous work were developed and calculated, after which basic methods of unsupervised/supervised clustering and supervised classification were applied to determine different temperature conditions of vessel segments. Supervised classification methods demonstrated high overall accuracy: CatBoost — 98.9%, SGDClassifier — 95.7%, and logistic regression — 99.7%. The results are consistent with existing descriptions of vascular changes during temperature tests. The applied methodology is universal, meaning with minor modifications it can be adapted to patients. Therefore, the results of this study may potentially improve the diagnosis of vascular pathologies.

Keywords: ptoacoustics, classification, clustering of vascular changes, vasodilation, vasoconstriction, angiography, photoacoustics, vessels, vascular features

Acknowledgments: All authors of this article express their gratitude to the authors of article [15] for providing the open data used in this study.

Author contribution: Z. Besedovskaya — development of the pipeline and clustering tools, image preparation for publication, and draft publication. A. Korobov — creation and integration of new vessel segment features into the pipeline and draft publication. N. Kudryashova — medical conceptualization and validation of the vessel segment features and draft publication. All authors contributed equally to this study.

✉ **Correspondence should be addressed:** Zlata Besedovskaia
Bolshoy Bulvar, 30, Building 1, Moscow, 121205; iratnagold@gmail.com

Received: 07.10.2025 **Accepted:** 10.11.2025 **Published online:** 27.11.2025

DOI: 10.24075/brsmu.2025.060

Copyright: © 2025 by the authors. **Licensee:** Pirogov University. This article is an open access article distributed under the terms and conditions of the Creative Commons Attribution (CC BY) license (https://creativecommons.org/licenses/by/4.0/).

РАЗРАБОТКА КЛАССИФИКАТОРА СОСТОЯНИЙ СОСУДОВ С ИСПОЛЬЗОВАНИЕМ МЕТОДОВ КОНТРОЛИРУЕМОГО МАШИННОГО ОБУЧЕНИЯ

З. В. Беседовская[1,2] ✉, А. Ю. Коробов[3], Н. И. Кудряшова[4]

[1] Центр нейробиологии и нейрореабилитации имени Владимира Зельмана, Сколковский институт науки и технологий, Москва, Россия
[2] Центр искусственного интеллекта, Сколковский институт науки и технологий, Москва, Россия
[3] Центр фотоники и фотонных технологий, Сколковский институт науки и технологий, Москва, Россия
[4] Центр молекулярной и клеточной биологии, Сколковский институт науки и технологий, Москва, Россия

Количественная обработка оптоакустических ангиограмм — одна из важных задач, решение которой в перспективе позволит диагностировать сосудистые заболевания на ранних стадиях. Целью исследования было провести доработку и медико-биологическую валидацию программного инструмента для анализа оптоакустических ангиограмм с фокусом на применение методов машинного обучения. Работу проводили на открытом наборе данных, содержащем трехмерные оптоакустические ангиограммы экспериментального животного (мыши) в трех температурных состояниях: температура холодной воды (16 °C), комнатная температура (23 °C) и температура тела (30 °C), а также датасет с базовыми параметрами сосудов, полученных при обработке программным обеспечением общего назначения для визуализации и анализа научных и промышленных данных Amira/Avizo (Thermo Fisher Scientific). Были разработаны и посчитаны различные параметры сосудов, отсутствующие в предыдущей работе, после чего применены основные методы неконтролируемой/контролируемой кластеризации и контролируемой классификации для определения принадлежности сегментов сосудов к разным температурным состояниям. Методы контролируемой классификации показали высокую общую точность: CatBoost — 98,9%, SGDClassifier — 95,7%, логистическая регрессия — 99,7%. Полученные результаты согласуются с существующими описаниями изменений сосудов при температурных тестах. Примененная методология универсальна, а значит при небольшой модификации может быть адаптирована для пациентов. Таким образом, полученные результаты в перспективе позволят улучшить диагностику сосудистых патологий.

Ключевые слова: оптоакустика, кластеризация васкулярных изменений, вазодилатация, вазоконстрикция, ангиография, фотоакустика

Благодарности: авторы статьи выражают признательность авторам опубликованной ранее работы [15] за предоставление открытых данных, которые были использованы при проведении исследования.

Вклад авторов: З. В. Беседовская — разработка пайплайна и инструментов кластеризации, подготовка изображений для публикации, подготовка драфта публикации; А. Ю. Коробов — создание и интеграция новых дескрипторов сегментов сосудов в пайплайн, подготовка драфта публикации; Н. И. Кудряшова — медицинская концептуализация и валидация дескрипторов сегментов сосудов, подготовка драфта публикации.

✉ **Для корреспонденции:** Злата Валерьевна Беседовская
Большой бульвар, 30, стр. 1, Москва, 121205, Россия; iratnagold@gmail.com

Статья получена: 07.10.2025 **Статья принята к печати:** 10.11.2025 **Опубликована онлайн:** 27.11.2025

DOI: 10.24075/vrgmu.2025.060

Авторские права: © 2025 принадлежат авторам. **Лицензиат:** РНИМУ им. Н.И. Пирогова. Статья размещена в открытом доступе и распространяется на условиях лицензии Creative Commons Attribution (CC BY) (https://creativecommons.org/licenses/by/4.0/).

Optoacoustic (OA) angiography is a promising new vascular imaging technique applicable in scientific research and clinical practice. It is based on the optoacoustic effect: the acoustic response of materials to intermittent light [1, 2]. Thus, the method combines optical and acoustic approaches, and angiography itself is based on the optical absorption of light by hemoglobin [3].

One of the advantages of OA angiography is its noninvasive nature [1]. In diagnostics, it can complement large-vessel imaging techniques [4]. Compared to small-vessel imaging techniques (capillaroscopy, optical coherence tomography), OA provides greater visualization depth [5, 6] and enables assessment of arterioles, venules, as well as small arteries and veins [5].

OA is successfully used in various fields of both applied medicine and fundamental research. The method's successes can be highlighted in ophthalmology [7, 8], dermatology [9], cardiology [10], oncology [11], and neuroimaging [12].

Preclinical and fundamental biological research play a key role both in the study of basic biological processes and in the further development of OA imaging methodology itself [5].

Despite significant advances in the development of OA imaging technology, its widespread clinical implementation is hampered by a number of significant technological limitations. Limitations of the method include low imaging speed, a fundamental contradiction between spatial resolution and penetration depth, and engineering challenges in integrating light delivery systems and ultrasound (US) transducers [5, 6].

Artificial intelligence (AI) application is dramatically improving OA imaging. Neural networks such as U-Net effectively eliminate artifacts and improve image quality. Furthermore, AI automates data analysis, making diagnostics faster and more objective [13, 14]. Thus, the use of AI helps overcome technological barriers, enables wider clinical adoption of OA imaging, and opens new horizons for noninvasive diagnostics [5].

The goal of this work is to develop a methodology for analyzing various vascular features and validate it on an open dataset containing mouse optoacoustic 3D angiograms. The developed software will be suitable not only for the specific task described above, but also (with minor modifications) for a wide range of studies involving OA angiograms, including the diagnosis of various vascular diseases in patients.

METHODS

In this work, we used the set of features mentioned in [15] for calculations, as well as features calculated by Amira/Avizo (Thermo Fisher Scientific, USA), a general-purpose software for visualization and analysis of scientific data. We also developed new features to describe segmental spatial characteristics and improve the accuracy of machine learning (ML) models (Table 1).

Obtaining initial open data

One Balb/C nu/nu mouse was used for OA angiography. Skin vessels in the animal's left thigh were visualized in a chamber filled with distilled water. Three technical replicates were obtained (Fig. 1A) for each water temperature: body temperature (BT) (30 °C); room temperature (RT) (23 °C); and cold temperature (CT) (16 °C). Each imaging was conducted in 10 minutes after immersion of the mouse's thigh in water to stabilize the tissue and water temperatures.

An OA mesoscopy system (Institute of Applied Physics, Russian Academy of Sciences, Russia) based on an ONDA532 diode laser (wavelength 532 nm) was used for imaging. Ultrasound signals were collected using a scanning module in a sealed immersion chamber filled with distilled water. The scanning range was 10 mm in both axes, the scanning step was 20 μm, the time interval was approximately 5 min, and the signal detection depth was up to 3 mm (Fig. 1B). The acquired signals were converted into 3D angiographic datasets using reconstruction and deconvolution algorithms. The 3D angiographic images were processed using the SKYQUANT 3D tool [15].

Details of the experiment are available in a previous publication, which describes in detail the object, methods, and equipment used to acquire the images [15].

Description of the original open data

The dataset contains 16,619 vessel segments with 9 quantitative features for each segment (based on which 9 new features described in Table 1 were derived and calculated) and 11 quantitative features for each image. The experimental design is described in [15] and included:

Cold temperature (16 °C): 3 images, 10,418 segments;
Room temperature (23 °C): 3 images, 4,663 segments;
Body temperature (30 °C): 3 images, 1,538 segments.

For all subsequent operations, the original dataset was split into training, testing, and validation sets of 60%, 25%, and 15%, respectively (random seed = 42). For ML-based clustering, the features of individual segments were retained, while the features of individual images were used for descriptive statistics and quality control described in [15].

All features were standardized by removing the mean and scaling to unit variance using statistics computed only on the training samples; the same affine transformation was applied to the validation/test splits to prevent information leakage.

Unsupervised clustering based on centroid and density

Before moving on to more complex clusterers, a projection map of multidimensional objects was obtained using the nonlinear dimensionality reduction method UMAP (Uniform Manifold Approximation and Projection) with features n_neighbors = 15 and min_dist = 0.1.

After assessing visual separability of the data, K-means was applied to optimize within-cluster variance.

DBSCAN was used to capture arbitrary cluster shapes and clearly separate "noise" from the "core."

To reduce collinearity and noise while maintaining maximum variance, we applied principal component analysis (PCA) with five principal components extracted.

Following PCA, K-means and DBSCAN were repeated, and internal clustering metrics were compared.

Supervised classification

To test the separability of the data by supervised classifiers, we selected three additional models covering the linear-nonlinear and generative-discriminative families:

1. CatBoost — gradient boosting, which sequentially builds decision trees to minimize the loss function and improve the quality of the model.
2. SGDClassifier — a stochastic gradient descent learning approach that supports loss functions and penalties for classification.
3. Logistic Regression Softmax — adaptation of the logistic regression function to multiclass data.

We used a cross-validation strategy to prepare the dataset with all preprocessing. The metrics used were accuracy,

Table 1. Developed and calculated vessel features to describe the characteristics of vascular segments and their position in the image area

Feature	Formula	Description
Segment Z	Initial feature calculated automatically in Amira/Avizo software	Average depth of the centroid of segment $\mathcal{S}$
Weighted Segment MeanRadius perSegment (a.u.)	$\overline{R}_{ij_{seg}}^{(\omega)} = \frac{\overline{R}_{ij_{seg}} \bullet L_{i_{seg}}}{\sum_{i=0}^{N_j} L_{i_{seg}}}$ $\overline{R}_{ij_{seg}}$: Mean Radius i_{seg} image j; $L_{i_{seg}}$: Vessels segment Curved lenght	The mean radius value calculated for each vessel segment, weighted by the segment tortuosity or segment length
Weighted Segment Volume perSegment (a.u.)	$V_{ij_{seg}}^{(\omega)} = \frac{V_{ij_{seg}} \bullet L_{i_{seg}}}{\sum_{i=0}^{N_j} L_{i_{seg}}}$ $V_{ij_{seg}}$: Mean Radius i_{seg} image j; $L_{i_{seg}}$: Vessels segment Curved lenght	The curved length-weighted volume value calculated for each vessel segment
Features reflecting the pressure of surrounding tissues on the vessels		
Linearity	$Linearity = \frac{\lambda_1 - \lambda_2}{max(\lambda_1, \varepsilon)}$	Assesses the “threadlikeness” of a segment; values close to 1 correspond to elongated, “rod-like” structures
Planarity	$Planarity = \frac{\lambda_2 - \lambda_3}{max(\lambda_1)}$	Assesses the "ribboniness" (two-dimensionality of an object). High values are typical for geometries flattened in a plane
LinearityScore	$Linearity_{score} = \frac{\lambda_1 - \lambda_2}{\tau}$	Normalized metrics are robust to the overall Tensor scale. In practical data, LinearityScore + PlanarityScore + ScatteringScore ≈ 1
PlanarityScore	$Planarity_{score} = \frac{2 \cdot (\lambda_2 - \lambda_3)}{\tau}$	
ScatteringScore	$Scattering_{score} = \frac{3 \cdot \lambda_3}{\tau}$	
VerticalityScore	$Verticality_{score} = \lvert \upsilon_{1z} \rvert \in [0,1]$	The cosine of the angle between the main axis of the segment and the Z axis
VerticalityAngle (rad)	$Verticality_{Angle} = arccos \in [0, \pi/2]$	Angle to the Z-axis in radians

overall accuracy, balanced accuracy, logarithmic loss function Llog, Matthews correlation coefficient (MCC), Cohen's kappa (Cohen's κ), as well as ROC-AUC with macro- and micro-averaging and F1-measure with macro- and weighted averaging. Confusion matrices normalized by true classes are also presented.

RESULTS

Dimensionality reduction using the UMAP method

The UMAP method was used to visualize the multidimensional data structure.

UMAP visualization demonstrated a clear division of the data into three clusters corresponding to the three experimental temperature conditions (Fig. 2). The cold temperature cluster (16 °C) was the most compact, indicating pronounced and uniform changes in vascular architecture under hypothermia. The room temperature cluster (23 °C) occupied an intermediate position between the other two groups, while the body temperature cluster (30 °C) demonstrated a greater dispersion of points, indicating variability in vascular characteristics under physiological conditions.

Unsupervised clustering

To evaluate the effectiveness of unsupervised ML methods in the problem of separating temperature states, the DBSCAN and K-Means algorithms were used both with and without PCA data preprocessing (Table 2).

An analysis of the results showed that the use of PCA did not significantly improve clustering quality. The DBSCAN algorithm demonstrated higher accuracy (0.626) and silhouette coefficient (0.632) compared to K-Means, but showed low values of the macro-averaged F1-measure ($F1_{macro}$) (0.259), indicating unbalanced class recognition. K-Means, in contrast, provided a better balance between classes ($F1_{macro} = 0.367$), but with lower overall accuracy (0.524). The extremely low values of

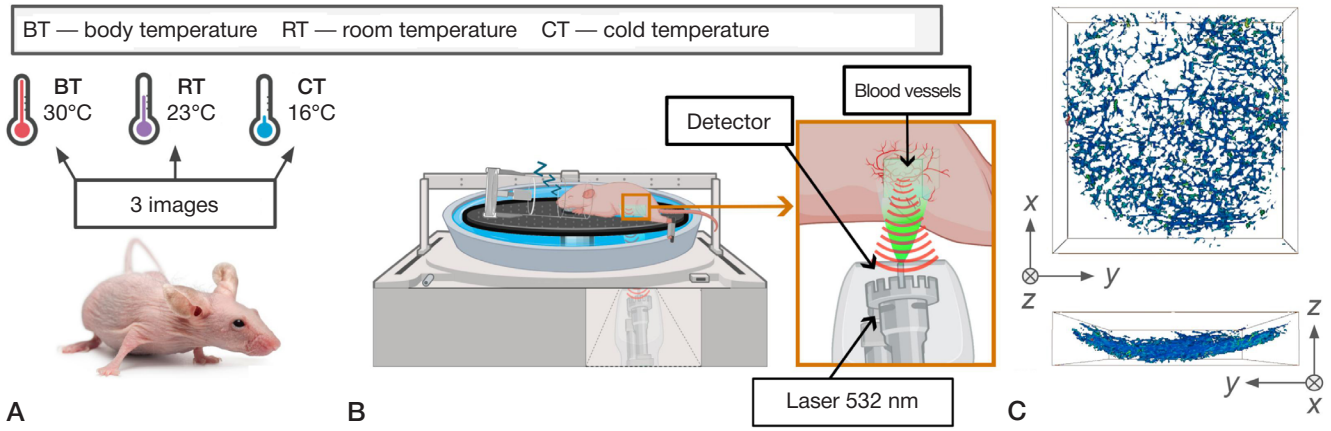


Fig. 1. A. Schematic representation of the experimental design. **B**. Schematic representation of the experimental setup. **C**. Image in the analyzed coordinate plane. Modified from [15]

the adjusted Rand index (ARI < 0.015) and normalized mutual information (NMI < 0.02) for both algorithms indicate a weak correspondence between the resulting clusters and the true temperature groups when using unsupervised approaches.

Despite multi-stage training, the internal clustering evaluation metrics demonstrated insufficient consistency and stability for subsequent interpretation.

Supervised Classification

Classification with the Catboost Model

To solve the problem of supervised classification of temperature states, gradient boosting on decision trees in the Catboost implementation was applied. The classification results are presented in Fig. 2B.

The Catboost model demonstrated exceptional performance in classifying temperature states in the vascular network. Overall accuracy was 98.9%, with a balanced accuracy of 98.5%, indicating correct model performance even with varying numbers of observations in classes. The area under the ROC curve, exceeding 0.999 for all averaging variants, indicates near-perfect separability of the classes in the feature space.

The highest classification recall (recall = 0.997) was achieved for the cold temperature group, consistent with the results of the UMAP analysis, which showed the greatest compactness and isolation of this cluster. The body temperature group demonstrated the highest accuracy (precision = 0.997), but slightly lower recall (0.985). The lowest completeness was observed for the room temperature group (0.971), which may be associated with the transitional nature of this state between hypo- and normothermia.

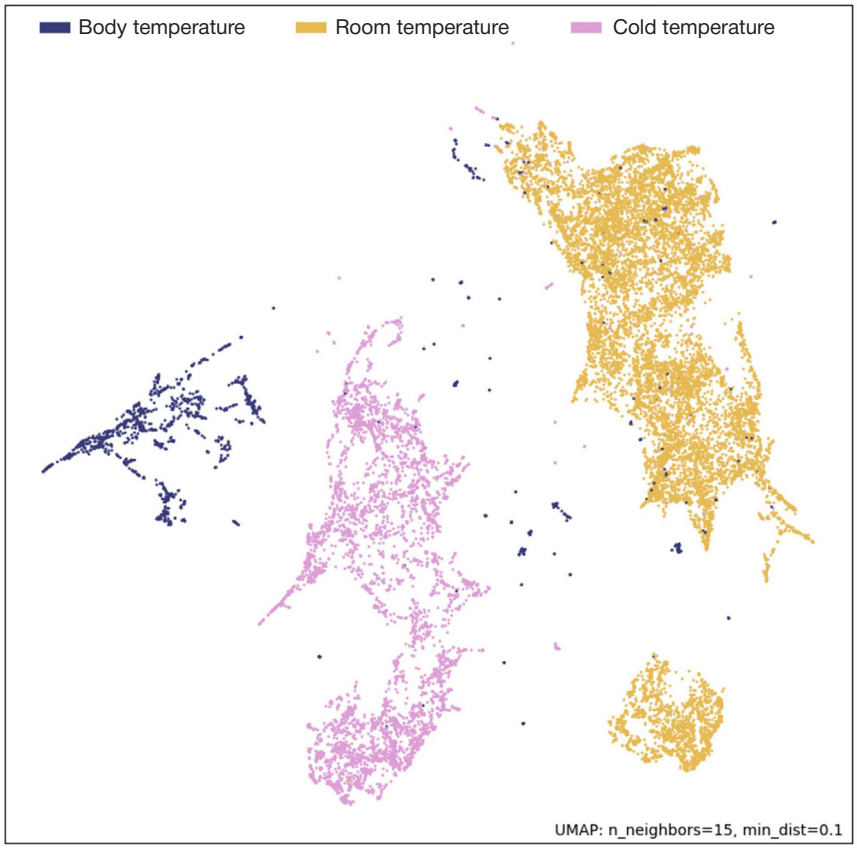


Fig. 2. UMAP clustering of the original data

Table 2. Obtained metrics of unsupervised clustering

Metrics	K-Means	DBSCAN	K-Means (PCA)	DBSCAN (PCA)
accuracy	0.524	0.626	0.524	0.626
$F1_{macro}$	0.367	0.259	0.367	0.259
silhouette	0.326	0.632	0.333	0.628
ARI	0.014	0.005	0.014	0.004
NMI	0.017	0.002	0.017	0.001

Classification by the SGDClassifier model

The SGDClassifier model demonstrated robust performance on the test set (Table 3): overall accuracy was 95.7%, balanced accuracy was 95.1%, $F1_{macro}$ was 0.960, and $F1_{weighted}$ was 0.956. The goodness-of-fit coefficients were also high (MCC = 0.917, Cohen's κ = 0.915), indicating reliable prediction consistency above chance. The area under the ROC curve was high (macro-AUC = 0.988; micro-AUC = 0.994), but it still performed worse than the nonlinear gradient boosting model; the log loss of 0.176 indicates a more conservative probabilities calibration compared to the Catboost model.

Very high recall (recall = 0.997) and very high precision (precision = 0.994) were shown for the body temperature group (F1 = 0.997), indicating clear separability of this condition in the space of all features. For the cold temperature group, the model demonstrated record sensitivity (recall = 0.995) simultaneously with moderately reduced precision (precision = 0.940; F1 = 0.967). The greatest clustering difficulties, as in the previous case, were shown for the room temperature group: despite high precision (precision = 0.988), the recall is shown below (recall = 0.857; F1 = 0.918), indicating frequent assignments of objects from this group to neighboring groups, primarily to the cold temperature group. This effect is typical of linear separators in the case of a transitional class.

Classification by logistic regression model

The logistic regression model, like Catboost, demonstrated near-limit performance on the test set (Table 3). The area under the ROC curve is close to ideal ($ROC\text{-}AUC_{macro}$ = 0.99983; $ROC\text{-}AUC_{micro}$ = 0.99987), while the low logarithmic loss (L_{log} = 0.033) indicates good calibration of the probabilities—better than the other linear and boosted models.

For the body temperature group, extremely high recall values (recall = 0.996) with very high precision (precision = 0.998; F1 = 0.999) are shown, indicating good separability of this condition. For the cold temperature group, the quality is also close to ideal (precision = 0.999; recall = 0.997; F1 = 0.998), meaning that the model makes virtually no errors in classifying segments from images in the cold temperature group. The greatest decrease is observed for the room temperature group: precision = 0.993, recall = 0.996, F1 = 0.995. This indicates rare false positives in favor of the room temperature group for boundary objects.

Assessing the significance of features for three models revealed two stable, highly significant classes (Fig. 3A): topological (tortuosity, verticality/planarity, normalized dispersion, and linearity) and geometric (radii, lengths, volume, and segment Z-coordinate). It is important to note that the linear models (SGDClassifier and logistic regression) base their decisions primarily on topological features.

The confusion matrix (Fig. 3B) allows for a detailed assessment of misclassification patterns for the three models.

For logistic regression, the significance of tortuosity (Fig. 3A) is noteworthy, with its contribution exceeding that of the other features by an order of magnitude. Smaller but consistent contributions are provided by normalized verticality, normalized linearity, planarity, verticality angle, normalized dispersion, and linearity (approximately 0.28–1.07). The scale features — mean radii, length/tortuosity-weighted mean radii, curved and cord length, volume and weighted volume, and segment z-coordinate — are of virtually zero importance.

SGDClassifier follows the same linear weighting pattern: the tortuosity feature contributes the most, followed by normalized verticality, planarity, verticality angle, normalized scattering, and linearity; geometric features remain close to zero.

Unlike linear models, the Catboost model exhibits a different feature hierarchy: the tortuosity-weighted mean radius, volume, and curved length are of maximum importance. Topological features such as tortuosity make a minor contribution.

DISCUSSION

A standard approach for analyzing OA imaging results is the use of AI methods [13]. An example is the work of N. Davoudi et al., who used the U-Net neural network to improve the quality of images distorted by artifacts. The authors trained the model on a hybrid dataset that included simulations, phantoms, and

Table 3. Metrics for assessing the quality of supervised classification models

Метрика	Catboost	LogisticRegression	SGDClassifier
accuracy	0.989	0.997	0.957
balanced accuracy	0.985	0.998	0.951
L_{log}	0.108	0.033	0.176
MCC	0.979	0.994	0.917
Cohen's κ	0.979	0.994	0.915
$ROC\text{-}AUC_{macro}$	0.999	0.999	0.988
$F1_{macro}$	0.988	0.997	0.96
$ROC\text{-}AUC_{micro}$	0.999	0.999	0.994
$F1_{weighted}$	0.989	0.997	0.956

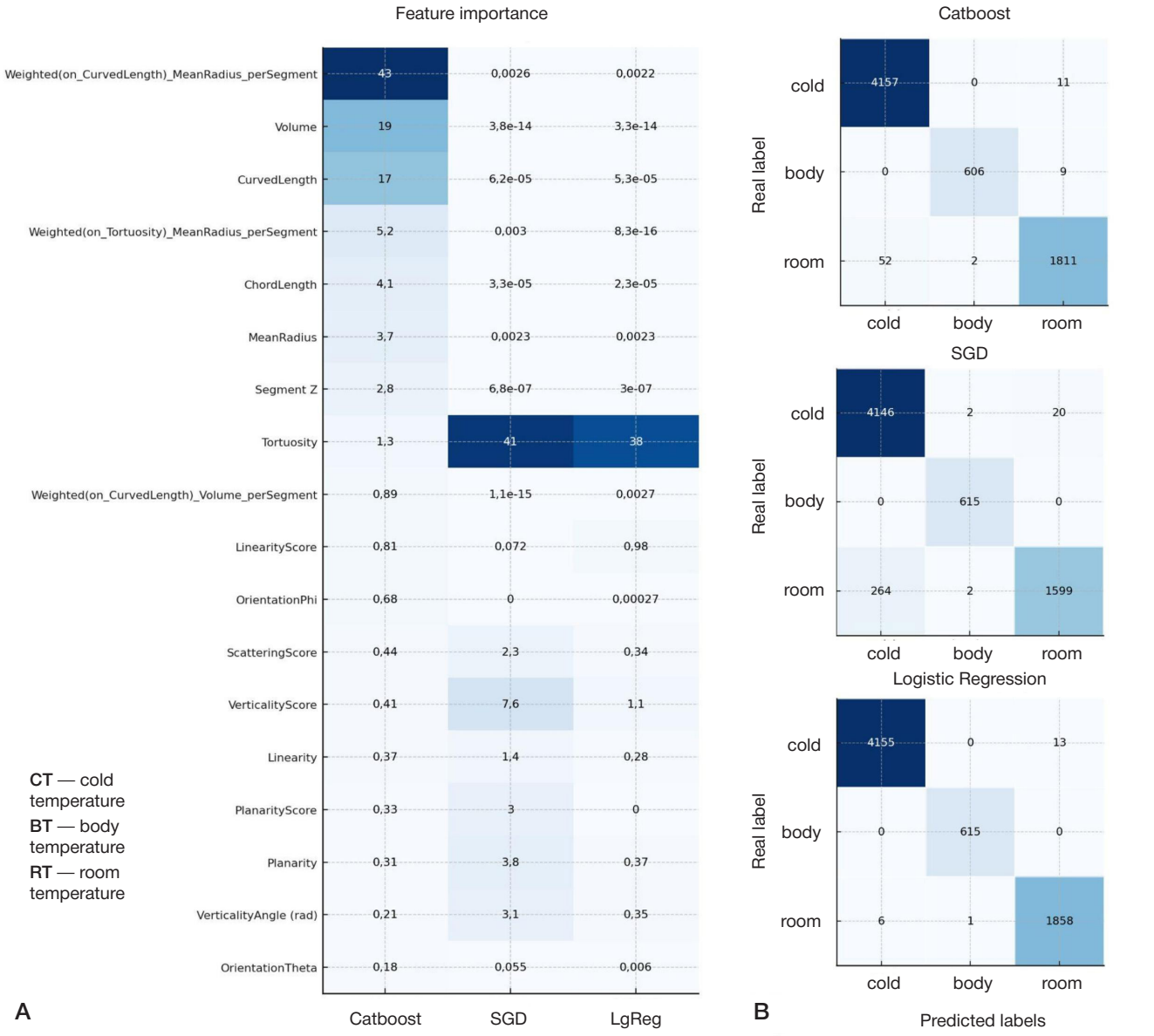


Fig. 3. Characteristics of trained ML models: Catboost, SGDClassifier, LogisticRegression. **A**) Feature weights for individual vessel segments. **B**) Error matrices for the three models

cross-sectional images of mice *in vivo*. The trained network effectively removed artifacts even with a sixfold undersampling of the original data. Validation on an experimental setup confirmed that the algorithm successfully copes with the task, significantly improving image quality [14]. However, it is worth considering that the main limiting factor for the use of artificial intelligence methods is the amount of data being analyzed [16]. In our study, unlike the aforementioned studies, we were able to overcome the data limitation by using a hybrid approach: image filtering and extraction of the analyzed vascular features are performed using a modified SKYQUANT-3D pipeline [15], which does not employ machine learning methods. However, further analysis was performed using various machine learning classifiers and clusterers. The effectiveness of the SKYQUANT-3D pipeline methodology has already been confirmed in tests on a vascular phantom, preclinical experiments, and clinical experiments [15].

The most important step in the analysis of OA angiograms is the selection and calculation of the analyzed vascular features. For example, in [17], 64 microvascular features were obtained, characterizing vessel blood flow, changes in their geometric configuration, branching, spatial localization, and other features [17]. The authors of the study used a random forest-based classifier for feature selection in order to identify the most significant biomarkers from the initial 64 features. By reducing the dataset to 32 key features, they were able to focus on the most informative features for differentiating healthy volunteers from diabetic patients, thereby confirming the importance of selecting significant vascular features for further analysis [17].

In [18], visual assessment of vascular features such as diameter and tortuosity was performed, which enabled effective discrimination between patients with post-thrombotic syndrome and healthy volunteers [18]. In the study [15], vessel radii, lengths, and tortuosity were analyzed in various variations. This made it possible to characterize changes in the vessels of an experimental animal during a temperature test, as well as changes in the vessels of a healthy volunteer during a positional test [15]. Our study uses the features from the article [15], supplementing them with features of branching and spatial localization similar to those mentioned in [17]. The unique features of vessel planarity, verticality, and linearity also deserve

special attention, indicating changes in the microcirculatory bed due to fluid redistribution. In this experiment, fluid redistribution in the body of the experimental animal was associated with temperature changes, but similar processes can occur in humans as a result of the development of vascular disease, such as chronic venous insufficiency [19].

The feature values we obtained reflect changes in the vessels caused by cooling, previously shown by other authors. Cooling causes dilation of small peripheral vessels, leading to a greater volume of blood containing hemoglobin, the main source of contrast in optoacoustics, to pass through them [20–22]. This makes them "visible" to the imaging system. The overall increase in blood volume in the studied area is a direct consequence of the vasodilation process. The peripheral vascular network is inherently more tortuous and branched than the main vessels, so its visibility in the image leads to an increase in the mean tortuosity feature [20–22]. Thus, the effectiveness of the classification is explained by existing biological effects. It is worth noting that many of the analysis components are universal for both animals and humans, which allows the development to be implemented into clinical practice.

CONCLUSIONS

In this study, quantitative vascular features were calculated and analyzed to describe the state of the microcirculatory bed.

Various machine learning methods were compared for determining different temperature states in experimental animals. Supervised classification methods demonstrated the greatest effectiveness, with near-absolute accuracy. The Catboost and logistic regression models demonstrated the greatest success, accounting for the most significant physiological features. Further, the choice between the two models should be made on a case-by-case basis, depending on the specific feature distribution. Feature weights reflect the actual physiology of vascular changes.

The methodology developed in this study will potentially help not only effectively distinguish between experimental conditions but also differentiate pathological vascular changes from each other and from the norm in patients with various diseases. This will help overcome some of the limitations of OA angiography, enabling its wider implementation in clinical practice. This will enable more accurate diagnosis of vascular changes in the early stages of diseases.

References

1. Lin L, Wang LV. The emerging role of photoacoustic imaging in clinical oncology. Nat Rev Clin Oncol. 2022; 19: 365–384. DOI: 10.1038/s41571-022-00615-3.
2. Neprokin A, Broadway C, Myllylä T, Bykov A, Meglinski I. Photoacoustic Imaging in Biomedicine and Life Sciences. Life. 2022; 12: 588. DOI: 10.3390/life12040588.
3. Xia J, Yao J, Wang LHV. Photoacoustic tomography: principles and advances. PIER. 2014; 147: 1–22. DOI: 10.2528/pier14032303.
4. Karlas A, Fasoula N-A, Paul-Yuan K, Reber J, Kallmayer M, Bozhko D, et al. Cardiovascular optoacoustics: From mice to men — A review. Photoacoustics. 2019; 14: 19–30. DOI: 10.1016/j.pacs.2019.03.001.
5. Kye H, Song Y, Ninjbadgar T, Kim C, Kim J. Whole-Body Photoacoustic Imaging Techniques for Preclinical Small Animal Studies. Sensors. 2022; 22: 5130. DOI: 10.3390/s22145130.
6. Wang X, Ku G, Wegiel MA, Bornhop DJ, Stoica G, Wang LV. Noninvasive photoacoustic angiography of animal brains in vivo with near-infrared light and an optical contrast agent. Opt Lett. 2004; 29: 730. DOI: 10.1364/ol.29.000730.
7. Hu S, Rao B, Maslov K, Wang LV. Label-free photoacoustic ophthalmic angiography. Opt Lett. 2009; 35: 1. DOI: 10.1364/ol.35.000001.
8. Zhao H, Li K, Yang F, Zhou W, Chen N, et al. Customized anterior segment photoacoustic imaging for ophthalmic burn evaluation in vivo; OEA. 2021; 4: 200017–200017. DOI: 10.29026/oea.2021.200017.
9. Li D, Humayun L, Vienneau E, Vu T, Yao J. Seeing through the Skin: Photoacoustic Tomography of Skin Vasculature and Beyond. JID Innovations. 2021; 1: 100039. DOI: 10.1016/j.xjidi.2021.100039.
10. Luo Y, Wang LV. Photoacoustic Tomography in Cardiovascular Medicine: Innovations in Assessing Hemodynamics and Metabolic Function. Curr Treat Options Cardio Med. 2025; 27. DOI: 10.1007/s11936-025-01092-4.
11. Leng X, Uddin KMS, Chapman W Jr, Luo H, Kou S, Amidi E, et al. Assessing Rectal Cancer Treatment Response Using Coregistered Endorectal Photoacoustic and US Imaging Paired with Deep Learning. Radiology. 2021; 299: 349–358. DOI: 10.1148/radiol.2021202208.
12. Qiu T, Lan Y, Gao W, Zhou M, Liu S, Huang W, et al. Photoacoustic imaging as a highly efficient and precise imaging strategy for the evaluation of brain diseases. Quant Imaging Med Surg. 2021; 11: 2169–86. DOI: 10.21037/qims-20-845.
13. Brown EL, Lefebvre TL, Sweeney PW, Stolz BJ, Gröhl J, Hacker L, et al. Quantification of vascular networks in photoacoustic mesoscopy. Photoacoustics. 2022; 26: 100357. DOI: 10.1016/j.pacs.2022.100357.
14. Davoudi N, Deán-Ben XL, Razansky D. Deep learning optoacoustic tomography with sparse data. Nat Mach Intell. 2019; 1: 453–60. DOI: 10.1038/s42256-019-0095-3.
15. Korobov A, Besedovskaia Z, Petrova E, Kurnikov A, Glyavina A, Orlova A, et al. SKYQUANT 3D: Quantifying Vascular Anatomy With an Open-Source Workflow for Comprehensive Analysis of Volumetric Optoacoustic Angiography Data. Journal of Biophotonics. 2024; 17. DOI: 10.1002/jbio.202400143.
16. Baeza-Yates R. The Limitations of Data, Machine Learning and Us. Companion of the 2024 International Conference on Management of Data. ACM; 2024. pp. 1–2. DOI: 10.1145/3626246.3656000.
17. Karlas A, Katsouli N, Fasoula N-A, Bariotakis M, Chlis N-K, Omar M, et al. Dermal features derived from optoacoustic tomograms via machine learning correlate microangiopathy phenotypes with diabetes stage. Nat Biomed Eng. 2023; 7: 1667–82. DOI: 10.1038/s41551-023-01151-w.
18. Nemirova S, Orlova A, Kurnikov A, Litvinova Y, Kazakov V, Ayvazyan I, et al. Scanning optoacoustic angiography for assessing structural and functional alterations in superficial vasculature of patients with post-thrombotic syndrome: A pilot study. Photoacoustics. 2024; 38: 100616. DOI: 10.1016/j.pacs.2024.100616.
19. Barajas Colón JÁ, Granados-Romero JJ, Barrera-Mera B, Banegas-Ruiz R, Vargas-Morales JJ, Barrera-Calva E, et al. Chronic venous insufficiency: a review. Int J Res Med Sci. 2021; 9: 1808. DOI: 10.18203/2320-6012.ijrms20211928.
20. Zhang R, Li X, Balasundaram G, Li B, Qi Y, Santosa A, et al. Hybrid Photoacoustic Ultrasound Imaging System for Cold-Induced Vasoconstriction and Vasodilation Monitoring. IEEE Trans Biomed Eng. 2024; 71: 712–6. DOI: 10.1109/tbme.2023.3301013.
21. Chang F, Flavahan S, Flavahan NA. Cooling-induced cutaneous vasodilatation is mediated by small-conductance, calcium-activated potassium channels in tail arteries from male mice. Physiological Reports. 2023; 11. DOI: 10.14814/phy2.15884.
22. Van den Brande P, De Coninck A, Lievens P. Skin Microcirculation Responses to Severe Local Cooling. Int J Microcirc. 1997; 17: 55–60. DOI: 10.1159/000179207.

Литература

1. Lin L, Wang LV. The emerging role of photoacoustic imaging in clinical oncology. Nat Rev Clin Oncol. 2022; 19: 365–384. DOI: 10.1038/s41571-022-00615-3.
2. Neprokin A, Broadway C, Myllylä T, Bykov A, Meglinski I. Photoacoustic Imaging in Biomedicine and Life Sciences. Life. 2022; 12: 588. DOI: 10.3390/life12040588.
3. Xia J, Yao J, Wang LHV. Photoacoustic tomography: principles and advances. PIER. 2014; 147: 1–22. DOI: 10.2528/pier14032303.
4. Karlas A, Fasoula N-A, Paul-Yuan K, Reber J, Kallmayer M, Bozhko D, et al. Cardiovascular optoacoustics: From mice to men — A review. Photoacoustics. 2019; 14: 19–30. DOI: 10.1016/j.pacs.2019.03.001.
5. Kye H, Song Y, Ninjbadgar T, Kim C, Kim J. Whole-Body Photoacoustic Imaging Techniques for Preclinical Small Animal Studies. Sensors. 2022; 22: 5130. DOI: 10.3390/s22145130.
6. Wang X, Ku G, Wegiel MA, Bornhop DJ, Stoica G, Wang LV. Noninvasive photoacoustic angiography of animal brains in vivo with near-infrared light and an optical contrast agent. Opt Lett. 2004; 29: 730. DOI: 10.1364/ol.29.000730.
7. Hu S, Rao B, Maslov K, Wang LV. Label-free photoacoustic ophthalmic angiography. Opt Lett. 2009; 35: 1. DOI: 10.1364/ol.35.000001.
8. Zhao H, Li K, Yang F, Zhou W, Chen N, et al. Customized anterior segment photoacoustic imaging for ophthalmic burn evaluation in vivo; OEA. 2021; 4: 200017–200017. DOI: 10.29026/oea.2021.200017.
9. Li D, Humayun L, Vienneau E, Vu T, Yao J. Seeing through the Skin: Photoacoustic Tomography of Skin Vasculature and Beyond. JID Innovations. 2021; 1: 100039. DOI: 10.1016/j.xjidi.2021.100039.
10. Luo Y, Wang LV. Photoacoustic Tomography in Cardiovascular Medicine: Innovations in Assessing Hemodynamics and Metabolic Function. Curr Treat Options Cardio Med. 2025; 27. DOI: 10.1007/s11936-025-01092-4.
11. Leng X, Uddin KMS, Chapman W Jr, Luo H, Kou S, Amidi E, et al. Assessing Rectal Cancer Treatment Response Using Coregistered Endorectal Photoacoustic and US Imaging Paired with Deep Learning. Radiology. 2021; 299: 349–358. DOI: 10.1148/radiol.2021202208.
12. Qiu T, Lan Y, Gao W, Zhou M, Liu S, Huang W, et al. Photoacoustic imaging as a highly efficient and precise imaging strategy for the evaluation of brain diseases. Quant Imaging Med Surg. 2021; 11: 2169–86. DOI: 10.21037/qims-20-845.
13. Brown EL, Lefebvre TL, Sweeney PW, Stolz BJ, Gröhl J, Hacker L, et al. Quantification of vascular networks in photoacoustic mesoscopy. Photoacoustics. 2022; 26: 100357. DOI: 10.1016/j.pacs.2022.100357.
14. Davoudi N, Deán-Ben XL, Razansky D. Deep learning optoacoustic tomography with sparse data. Nat Mach Intell. 2019; 1: 453–60. DOI: 10.1038/s42256-019-0095-3.
15. Korobov A, Besedovskaia Z, Petrova E, Kurnikov A, Glyavina A, Orlova A, et al. SKYQUANT 3D: Quantifying Vascular Anatomy With an Open-Source Workflow for Comprehensive Analysis of Volumetric Optoacoustic Angiography Data. Journal of Biophotonics. 2024; 17. DOI: 10.1002/jbio.202400143.
16. Baeza-Yates R. The Limitations of Data, Machine Learning and Us. Companion of the 2024 International Conference on Management of Data. ACM; 2024. pp. 1–2. DOI: 10.1145/3626246.3656000.
17. Karlas A, Katsouli N, Fasoula N-A, Bariotakis M, Chlis N-K, Omar M, et al. Dermal features derived from optoacoustic tomograms via machine learning correlate microangiopathy phenotypes with diabetes stage. Nat Biomed Eng. 2023; 7: 1667–82. DOI: 10.1038/s41551-023-01151-w.
18. Nemirova S, Orlova A, Kurnikov A, Litvinova Y, Kazakov V, Ayvazyan I, et al. Scanning optoacoustic angiography for assessing structural and functional alterations in superficial vasculature of patients with post-thrombotic syndrome: A pilot study. Photoacoustics. 2024; 38: 100616. DOI: 10.1016/j.pacs.2024.100616.
19. Barajas Colón JÁ, Granados-Romero JJ, Barrera-Mera B, Banegas-Ruiz R, Vargas-Morales JJ, Barrera-Calva E, et al. Chronic venous insufficiency: a review. Int J Res Med Sci. 2021; 9: 1808. DOI: 10.18203/2320-6012.ijrms20211928.
20. Zhang R, Li X, Balasundaram G, Li B, Qi Y, Santosa A, et al. Hybrid Photoacoustic Ultrasound Imaging System for Cold-Induced Vasoconstriction and Vasodilation Monitoring. IEEE Trans Biomed Eng. 2024; 71: 712–6. DOI: 10.1109/tbme.2023.3301013.
21. Chang F, Flavahan S, Flavahan NA. Cooling-induced cutaneous vasodilatation is mediated by small-conductance, calcium-activated potassium channels in tail arteries from male mice. Physiological Reports. 2023; 11. DOI: 10.14814/phy2.15884.
22. Van den Brande P, De Coninck A, Lievens P. Skin Microcirculation Responses to Severe Local Cooling. Int J Microcirc. 1997; 17: 55–60. DOI: 10.1159/000179207.

DETECTION OF *SALMONELLA ENTERICA* BY LOOP-MEDIATED ISOTHERMAL AMPLIFICATION OF DNA USING A FLUORESCENTLY LABELED LOOP PRIMER

Shamovskaya DV[1], Gordukova MA[2], Smertina MA[1], Galeeva EV[2], Oscorbin IP[1], Khrapov EA[1], Boyarskikh UA[1], Filipenko ML[1,3] ✉

[1] Institute of Chemical Biology and Fundamental Medicine, Siberian Branch of the Russian Academy of Sciences, Novosibirsk, Russia

[2] Speransky City Children's Clinical Hospital No. 9, Moscow, Russia

[3] Institute of Translational Medicine and Biotechnology, Sechenov University, Moscow, Russia

Salmonellosis remains one of the leading causes of bacterial gastrointestinal infections in humans and animals. Molecular diagnostics has dramatically reshaped the diagnostic landscape for Salmonella infection; however, it remains time- and resource-intensive. Isothermal DNA amplification, for example loop isothermal amplification (LAMP), performed at a constant temperature, is the basis for the development of rapid diagnostic tests that can be adapted to the point-of-care (PoC) formats and implemented in resource-limited settings or remote from centralized laboratories. The aim of this study was to develop and validate a novel LAMP-based method for detecting *Salmonella enterica* in human stool samples, wherein amplification results are monitored using a loop primer labeled with a fluorophore and an internal quencher. The proposed method achieves a limit of detection (LoD_{95}) of 250 copies per reaction, with a sensitivity of 86.84% (95% CI: 71.91–95.59%) and specificity of 96.49% (95% CI: 87.89–99.57%) relative to qPCR, and demonstrates increased robustness against DNA amplification inhibitors present in fecal samples. Incorporation of distinct fluorophores into loop primers for FLP-LAMP targeting different genes could potentially enable multiplexing and simultaneous detection of multiple pathogens, thereby expanding the diagnostic utility of isothermal amplification.

Keywords: *Salmonella enterica*, LAMP, fluorescent loop primer, fluorescent probe, analytical validation, DNA amplification inhibitors

Funding: This work was supported by the Russian state-funded project for the Institute of Chemical Biology and Fundamental Medicine, Siberian Branch of the Russian Academy of Sciences (Grant No. 125012300671-8).

Author contribution: Shamovskaya DV, Smertina MA, Khrapov EA — LAMP assay optimization and validation on clinical samples; Gordukova MA, Galeeva EV — collection of clinical specimens and patient data; Oscorbin IP — experimental design for LAMP assays; Boyarskikh UA — LAMP primer design; Filipenko ML — conceptualization, writing, and editing of the manuscript.

Compliance with ethical standards: The study was approved by the Ethics Committees of the Institute of Chemical Biology and Fundamental Medicine, SB RAS (Protocol No. 4, May 25, 2022) and the City Clinical Hospital for Children No. 9 named after G. N. Speransky, Moscow Healthcare Department (Protocol No. 44, April 19, 2022). All patients provided written informed consent.

✉ **Correspondence should be addressed:** Mikhail L. Filipenko
Prospekt Lavrenteva, 8, Novosibirsk, 630090, Russia; mlfilipenko@gmail.com

Received: 23.11.2025 **Accepted:** 13.12.2025 **Published online:** 22.12.2025

DOI: 10.24075/brsmu.2025.066

Copyright: © 2025 by the authors. **Licensee:** Pirogov University. This article is an open access article distributed under the terms and conditions of the Creative Commons Attribution (CC BY) license (https://creativecommons.org/licenses/by/4.0/).

ДЕТЕКЦИЯ *SALMONELLA ENTERICA* ПЕТЛЕВОЙ ИЗОТЕРМАЛЬНОЙ АМПЛИФИКАЦИЕЙ ДНК С ИСПОЛЬЗОВАНИЕМ ФЛУОРЕСЦЕНТНО МЕЧЕНОГО ПЕТЛЕВОГО ПРАЙМЕРА

Д. В. Шамовская[1], М. А. Гордукова[2], М. А. Смертина[1], Е. В. Галеева[2], И. П. Оскорбин[1], Е. А. Храпов[1], У. А. Боярских[1], М. Л. Филипенко[1,3] ✉

[1] Институт химической биологии и фундаментальной медицины Сибирского отделения Российской академии наук, Новосибирск, Россия

[2] Детская городская клиническая больница № 9 им. Г. Н. Сперанского, Москва, Россия

[3] Институт трансляционной медицины и биотехнологий, Сеченовский университет, Москва, Россия

Сальмонеллез остается одной из ведущих причин бактериальных кишечных инфекций человека и животных. Молекулярная диагностика радикально трансформировала диагностический ландшафт сальмонеллезной инфекции, однако остается времени- и ресурсозатратной. Изотермическая амплификация ДНК, например, петлевая изотермальная амплификация (LAMP), выполняемая при постоянной температуре, является основой разработки быстрых диагностических тестов, которые могут быть адаптированы к формату point-of-care (PoC) и выполнены в условиях ограниченных ресурсов и вдали от централизованных лабораторий. Целью исследования было разработать и валидировать новый метод детекции *Salmonella enterica* в образцах кала человека методом LAMP, в котором мониторинг результатов амплификации достигается с помощью петлевого флуоресцентно-меченного праймера, несущего также внутренний гаситель флуоресценции. Предложенный метод имеет предел обнаружения (LoD 95%) 250 копий на реакцию, чувствительность 86,84% (95% ДИ: 71,91–95,59%) и специфичность — 96,49% (95% ДИ: 87,89–99,57%) относительно qPCR, а также показал большую устойчивость к ингибиторам амплификации ДНК в образцах фекалий. Введение разных флуоресцентных меток в петлевые праймеры для FLP-LAMP с разными мишенями потенциально обеспечивает возможность мультиплексирования и одновременного выявления нескольких патогенов, что увеличивает диагностические возможности изотермальной амплификации.

Ключевые слова: *Salmonella enterica*, LAMP, петлевой флуоресцентный праймер, флуоресцентный зонд, аналитическая валидация, ингибиторы ДНК

Финансирование: исследование поддержано в рамках государственного задания ИХБФМ СО РАН № 125012300671-8.

Вклад авторов: Д. В. Шамовская, М. А. Смертина, Е. А. Храпов — оптимизация и валидация LAMP на клинических образцах; М. А. Гордукова, Е. В. Галеева — сбор клинических образцов и данных пациентов; И. П. Оскорбин — планирование экспериментов LAMP; У. А. Боярских — дизайн праймеров LAMP; М. Л. Филипенко — идея исследования, написание и редактирование статьи.

Соблюдение этических стандартов: исследование одобрено этическим комитетом ИХБФМ СО РАН (протокол № 4 от 25 мая 2022 г.), этическим комитетом при ГБУЗ «ДГКБ № 9 им. Г. Н. Сперанского ДЗМ» (протокол № 44 от 19 апреля 2022 г.). Пациенты подписали добровольное информированное согласие.

✉ **Для корреспонденции:** Максим Леонидович Филипенко
ул. Проспект Лаврентьева, д. 8, г. Новосибирск, 630090, Россия; mlfilipenko@gmail.com

Статья получена: 23.11.2025 **Статья принята к печати:** 13.12.2025 **Опубликована онлайн:** 22.12.2025

DOI: 10.24075/vrgmu.2025.066

Авторские права: © 2025 принадлежат авторам. **Лицензиат:** РНИМУ им. Н. И. Пирогова. Статья размещена в открытом доступе и распространяется на условиях лицензии Creative Commons Attribution (CC BY) (https://creativecommons.org/licenses/by/4.0/).

Salmonellosis is one of the most common anthropozoonotic infections caused by Gram-negative bacteria of the genus *Salmonella*, predominantly *Salmonella enterica* subsp. enterica [1]. According to the World Health Organization (WHO), 93–200 million cases of salmonellosis leading to acute gastroenteritis are registered annually, and about 155,000 cases worldwide result in death [2]. Therefore, salmonellosis remains a major public health problem in both developed and developing countries.

Diagnosis of salmonellosis includes the analysis of epidemiological and epizootological data, clinical signs, and pathomorphological changes, which can support a preliminary diagnosis. A definitive diagnosis is established using laboratory methods. *In vivo* diagnostics typically relies on serological, molecular genetic, and microbiological approaches.

In current clinical practice, the gold standard for detecting salmonellosis is microbiological culture, i.e., bacteriological inoculation of patient specimens onto selective media (e.g., *Rappaport–Vassiliadis medium*) [3]. The main drawbacks are the long turnaround time (48–96 hours), which delays timely initiation of targeted therapy, and reduced sensitivity if the patient has received antibiotics before sample collection. Microbiological testing requires dedicated facilities, equipment, and highly trained personnel, has low throughput, and is poorly suited for mass screening and epidemiological surveillance.

Rapid diagnostic methods include allele-specific real-time PCR and ELISA. Quantitative allele-specific PCR can shorten time to result (2–4 hours) and improve analytical sensitivity to 1–10 colony-forming units per milliliter (CFU/mL) [4]. PCR targets include *invA*, *ttr*, *bcfD*, and other conserved *Salmonella*-specific sequences [5]. However, the method is limited in many regions due to expensive equipment (real-time thermocyclers), insufficient personnel qualification in clinical diagnostic laboratories, and relatively high test cost.

Methods of isothermal amplification, in particular loop-mediated isothermal amplification (LAMP) developed by Notomi et al., have become a promising solution for point-of-care diagnostics. LAMP amplifies DNA at a constant temperature of 60–65 °C without thermal cycling, using a thermostable DNA polymerase (e.g., the large fragment of DNA polymerase I from *Geobacillus stearothermophilus*) and a highly specific set of four (less often six) primers recognizing six (or eight) distinct sites within the target DNA. This confers exceptionally high specificity of targeted sequence amplification [6]. Compared with PCR/qPCR, LAMP offers high specificity, rapid amplification (20–30 minutes), increased tolerance to amplification inhibitors in clinical samples, and does not require expensive instrumentation [7]. Various LAMP modifications are used in instrument-free tests or integrated into portable point-of-care devices for field use [8].

Multiple approaches have been proposed to visualize and monitor LAMP results, including turbidimetry, colorimetric assays, intercalating fluorescent dyes (SYTO, SYBR Green I), and modified oligonucleotides carrying fluorophores (primer-probes, molecular beacons, hybridization probes) [9]. The latter approach is particularly attractive due to multiplexing potential via multiple probes labeled with different dyes (FAM, HEX, ROX, Cy5) [8]. Nevertheless, the use of fluorescently labeled loop primers with an internal quencher in LAMP remains underexplored.

Here, we developed and validated a new approach to generate a real-time fluorescent signal in LAMP using a fluorescently labeled loop primer that also carries an internal fluorescence quencher, using diagnostic amplification of a fragment of the *Salmonella enterica bcfD* gene as a model. We hypothesized that loop primer-probes would enable reliable real-time monitoring comparable to intercalating dyes while opening opportunities for future multiplexing.

METHODS

Preparation of Control Material

A 211-nucleotide fragment of the *bcfD* gene (NC_003197, *Salmonella enterica* subsp. enterica) was amplified from *Salmonella* genomic DNA using primers bcfD-F3 and bcfD-B3 and cloned into a vector using the Quick-TA kit (Evrogen, Russia) following the manufacturer's instructions. Plasmid clone structure was confirmed by Sanger sequencing using the BigDye Terminator 3.1 kit (Applied Biosystems, USA) on an ABI 3730 genetic analyzer (Applied Biosystems, USA) at the Molecular Diagnostics Laboratory of ICBFM SB RAS.

The control plasmid (pBCFD) was linearized with BamHI and quantified using the Spectra Q BR kit (Sesana, Russia). The linearized plasmid was serially diluted over a range of 10^0–10^6 copies in buffer containing 10 mM Tris-HCl (pH 8.0), 2.5 µg/mL yeast RNA, and 0.01% NaN3. Copy numbers in dilutions were determined by droplet digital PCR (ddPCR) on the QX200 Droplet Digital PCR system (Bio-Rad, Hercules, CA, USA) according to the manufacturer's instructions using primers Slm1 and Slm2 (600 nM) and the fluorescent probe Slm-PF (200 nM).

LAMP

Standard 20 µL LAMP reactions contained: 1× Gss-Sto polymerase buffer (40 mM Tris-HCl pH 8.9; 10 mM $(NH_4)2SO_4$; 10 mM KCl; 8 mM $MgSO_4$; 2.5% DMSO; 0.1% Triton X-100), 1.5 mM each dNTP, 0.4 µM outer primers (F3/B3), 0.3 µM loop primers (LF/LB), 1.6 µM inner primers (FIP/BIP), DNA template, and 3 units of Gss-Sto polymerase (ICBFM SB RAS). For fluorescence monitoring, either fluorescently labeled loop primers (SLB-LB1F, SLB-LB2F, SLF-LB1H) or the intercalating dye SYTO-13 at 0.5 µM were used. LAMP was performed in a CFX96 Touch thermocycler (Bio-Rad, Hercules, CA, USA) using 120 cycles of amplification at 60 °C with fluorescence acquisition in the HEX/FAM channel every 15–30 seconds.

Specificity was assessed by electrophoresis in 1.8% agarose gel to verify the characteristic LAMP amplicon pattern or its absence in the no-template control (data not shown). Amplification results were evaluated using the Tt (time-to-threshold) parameter, defined as the time required for the fluorescence curve to cross a threshold line set at the mean plus three standard deviations of the negative control.

Real-Time PCR (qPCR)

qPCR reactions (20 µL) contained: 1× PCR buffer (64 mM Tris-HCl pH 8.9; 16 mM $(NH_4)2SO_4$; 0.05% Tween-20; 3 mM $MgCl_2$; 0.002% NaN_3), 0.6 µM forward and reverse primers and 0.15 µM fluorescent probe (Table 1), 2 units of Taq polymerase (SibEnzyme, Russia), and DNA template. Cycling conditions were: Taq activation at 96 °C for 15 min; then 45 cycles of 95 °C for 10 s and 60 °C for 40 s with fluorescence acquisition in the FAM and Cy5 channels. Data were analyzed in CFX Manager (Bio-Rad).

Limit of Detection, Clinical Sensitivity and Specificity

The limit of detection (LoD 95%) was evaluated by varying control plasmid concentration: 65, 125, 250, 500, and 1000 copies per reaction, with 20 technical replicates at each concentration. LoD95% was defined as the concentration at which a positive reaction (Tt of negative control minus Tt of

Table 1. Oligonucleotide primers and fluorescent probes

Name	Sequence (5'–3')
bcfD-FIP	GCACTTTACCGGTACGCTGAATACAGCGGCAATTTCAACCA
bcfD-BIP	CGGTCTGGATTCGCAGGTCAAAGCGATAGCCTGGGGAAC
bcfD-F3	CCGGACAAACGATTCTGGTA
bcfD-B3	CCGACATCGGCATTATCCG
bcfD-LF	TACCCCCTCCGGCTTTTG
bcfD-LB	ACAATGCGTCTTATCGCTACG
SLF-RB1H	HEX-TTTTTTACCCCC(T-BHQ1)CCGGCTTTTG
SLB-LB1F	FAM-AAAAACAATGCGTC(T-BHQ1)TATCGCTACG
SLB-LB2F	FAM-ACAATGCGTCT(T-BHQ1)ATCGCTACG
Slm1	GGCAATTTCAACCATGCAGGC
Slm2	CCAGACCGCTGCACTTTACCG
Slm-PF	FAM-AGCCGGAGGGGGTACGAGCG-BHQ1

sample > 10 min) was observed in at least 95% of technical replicates.

Clinical sensitivity and specificity were evaluated on 95 DNA samples from children's stool collected at G. N. Speransky Children's City Clinical Hospital No. 9. qPCR targeting the *bcfD* gene was used as the reference standard. Samples were considered qPCR-positive if the Cq value was less than 34, corresponding to the system's LoD95% of ≤ 12.5 copies per reaction.

RESULTS

Design and Optimization of a Fluorescently Labeled Loop Primer

Development of the LAMP visualization method using fluorescently labeled loop primers was based on a previously published, well-characterized set of LAMP primers specific to a bcfD gene fragment. We used a concept analogous to TaqMan-like probes that generate fluorescence through hybridization rather than enzymatic hydrolysis [10]. In the free state, such a probe forms a three-dimensional conformation that brings a fluorophore and a quencher into proximity, quenching fluorescence via FRET. Upon hybridization to a complementary target sequence, the probe becomes linear, increasing the distance between the fluorophore and the quencher and increasing fluorescence.

Based on this principle, we synthesized a series of fluorescently labeled loop primer-probes for LAMP (Table 1). Each oligonucleotide contained: (1) a fluorophore (FAM or HEX) at the 5' end; (2) a free 3' OH-end available for elongation; and (3) an internal BHQ1 quencher introduced via a thymidine residue (T-BHQ1) located near the 3' end.

The structures of the conventional loop primers bcfD-LF and bcfD-LB served as starting points for design of the labelled probes. For three oligonucleotides, the distance between the fluorophore and quencher was varied: five deoxyadenosines (5 dA) were added to the 5' end of SLB-LB1F, and five deoxythymidines (5 dT) were added to the 5' end of SLF-LB1H to increase the FRET-pair spacing. The third variant (SLB-LB2F) carried the fluorophore directly at the native 5' end without extension.

Comparison of Fluorescent Loop Primer-Probes

Replacing a conventional loop primer (LF or LB) with a fluorescently labeled loop primer-probe (0.3 μM) in a LAMP reaction using pBCFD template (3000 copies per reaction) produced a clear fluorescence increase curve dependent on the oligonucleotide variant (Fig. 1). All three primer-probe variants generated fluorescence upon incorporation into the growing amplicon.

Signal amplitude was similar across various probes; however, the oligonucleotide with increased fluorophore–

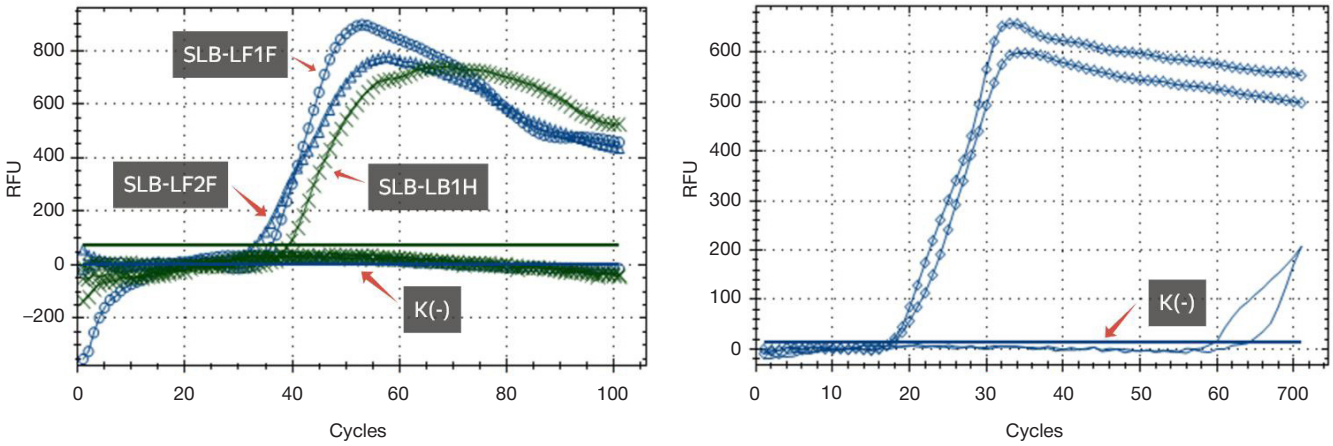


Fig. 1. LAMP fluorescent curves. The left panel depicts various fluorescently-labelled loop primers; the right panel demonstrates results of LAMP with the SYTO-13 intercalating dye

quencher spacing (SLB-LB1F) showed a higher signal amplitude (~35–40% of baseline fluorescence). As expected, using the intercalating dye SYTO-13 yielded a substantially shorter Tt (~9–10 min) compared with the fluorescent loop primer-probes (~16–19 min), likely due to the much larger number of dye molecules binding to the amplicon.

Increasing the concentration of the SLF-LB1H loop primer-probe from 0.3 to 0.6 μM did not substantially affect Tt but markedly improved signal amplitude from ~10–15% to 15–35% of the baseline fluorescence prior to amplification (Fig. 2). Higher concentrations did not notably increase the fluorescence amplitude; therefore, 0.6 μM was selected for subsequent experiments.

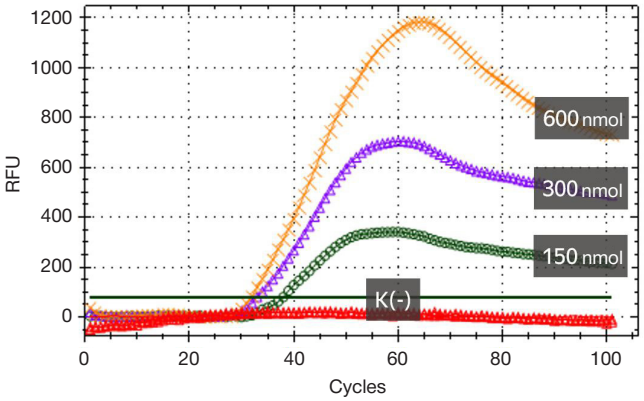


Fig. 2. Influence of a loop probe-primer SLF-LB1H concentration on the fluorescence amplitude

Determination of the Limit of Detection

The LoD95% is a key analytical characteristic defining the minimum amount of target DNA that can be reliably detected. We evaluated LoD for both visualization approaches by titrating DNA template at 65, 125, 250, 500, and 1000 copies per reaction (20 replicates per concentration). For the bcfD-LAMP-SLF-LB1H system, LoD95% was 250 copies per reaction (19/20 replicates positive; Tt = 20.67 ± 2.60 min). In comparison, SYTO-13 produced a slightly lower LoD: 125 copies per reaction (20/20 replicates; Tt = 17.78 ± 2.07 min), corresponding to approximately a twofold difference in sensitivity between the two visualization methods.

A critical parameter for diagnostic LAMP is the assay duration, because amplification time is constrained by the risk of nonspecific product formation in no-template controls (NTC). Prolonged incubation increases the risk of false-positive results and incorrect clinical interpretation. Because no fluorescence increase was observed in negative controls up to 60 minutes or longer, and the largest Tt for positive samples at LoD95% did not exceed 25 minutes for bcfD-LAMP-SLF-LB1H, the diagnostic LAMP duration was set to 30 minutes.

Testing on Clinical Samples

To determine clinical sensitivity and specificity of bcfD-LAMP-SLF-LB1H, 95 DNA samples from children's stool were analyzed. qPCR targeting bcfD with an established LoD95% of ≤ 12.5 copies per reaction (Cq ~34) was used as the reference standard. Samples were considered qPCR-positive if Cq < 34.

Clinical sensitivity of LAMP-SLF-LB1H was 86.84% (95% CI: 71.91–95.59%) and specificity was 96.49% (95% CI: 87.89–99.57%) (Tables 2, 3). For comparison, SYTO-13 yielded higher sensitivity (94.74%) with the same specificity. Cohen's kappa, a measure of agreement between two classification systems, was 0.844 (95% CI: 0.734–0.955) for LAMP-SLF-LB1H versus qPCR, indicating good agreement. For LAMP-SYTO13, kappa was higher (0.912; 95% CI: 0.828–0.996), also reflecting good agreement.

Discordant results and inhibitor tolerance

The main reason for discrepancies between LAMP-SLF-LB1H and qPCR was the difference in LoD: the method using fluorescent loop primers has a higher LoD (i.e., lower sensitivity) than qPCR. Analysis of discordant samples (qPCR-positive, LAMP-negative) showed Cq values in the 31–33 range, close to the positivity threshold of 34, suggesting borderline low amounts of target DNA.

To investigate discordance, two samples that were LAMP-SLF-LB1H-positive but negative in the initial qPCR analysis were retested by qPCR after fivefold dilution of DNA. Dilution is commonly used to reduce the concentration of amplification inhibitors that may be present in stool. After dilution, both samples became qPCR-positive with borderline Cq values (32–33), further supporting greater tolerance of LAMP-SLF-LB1H to fecal DNA amplification inhibitors. This is consistent with the well-known increased resistance of LAMP to inhibitors such as hemoglobin, bilirubin, heme, and other stool components.

DISCUSSION

Interest to isothermal amplification methods such as LAMP continues to grow because of their potential for decentralized diagnostics. Several approaches to generate fluorescent signal in LAMP using modified oligonucleotides have been proposed, including molecular beacons, hybridization probes (TaqMan-like probes operating via hybridization without cleavage), intercalating dyes (SYBR Green, SYTO), and fluorescent nucleotides (FL-dNTPs) incorporated during synthesis [11].

In this study, we developed and evaluated a LAMP test with fluorescent signal detection using fluorescently labeled loop primer-probes that are directly incorporated into the growing amplicon. The key advantage of this approach is that each incorporated primer-probe molecule contributes to

Table 2. Results of testing 95 children's stool DNA samples for *Salmonella* Comparison of LAMP-SLF-LB1H vs qPCR

	qPCR (+)	qPCR (–)	N
LAMP-SLF-LB1H (+)	33	2	35
LAMP-SLF-LB1H (–)	5	55	60
N	38	57	
	qPCR (+)	qPCR (–)	N
LAMP-SYTO13 (+)	36	2	38
LAMP-SYTO13 (–)	2	55	57
N	38	57	

Table 3. Diagnostic performance of LAMP methods compared with qPCR

Metric	LAMP-SLF-LB1H	LAMP-SYTO13
Sensitivity	86.84% (95% CI: 71.91–95.59%)	94.74% (95% CI: 82.25–99.36%)
Specificity	96.49% (95% CI: 87.89–99.57%)	96.49% (95% CI: 87.89–99.57%)
Cohen's kappa	0.844 (95% CI: 0.734–0.955)	0.912 (95% CI: 0.828–0.996)
Positive predictive value	94.29%	94.74%
Negative predictive value	91.67%	96.49%

fluorescence in proportion to the amount of product formed. When a fluorescent loop primer is incorporated into amplicon concatemers, the oligonucleotide becomes linear, substantially increasing the distance between the fluorophore (5' end) and the quencher (T-BHQ1), which restores fluorescence. Increasing fluorophore–quencher distance by adding extra nucleotides (5 dA or 5 dT) increased signal amplitude, although the effect was moderate.

The closest analogue to our system is FLOS-LAMP (fluorescence of loop primer upon self-dequenching) [12, 13]. In that approach, a fluorophore is introduced within the 3′ region of the loop primer in a specific nucleotide context, leading to quenching in the unbound state and increased fluorescence upon incorporation into the amplicon duplex. Our primer design is considerably simpler.

On control samples with known DNA concentrations, LAMP-SLF-LB1H demonstrated LoD95% of 250 copies per reaction, which is twofold higher than LAMP-SYTO13 (125 copies per reaction). This difference is expected because many more intercalating dye molecules bind to the amplicon and generate a stronger fluorescence signal. Nevertheless, LoD95% of 250 copies per reaction remains acceptable for clinical diagnostics, since typical *Salmonella* loads in stool samples from patients with acute gastroenteritis substantially exceed this value [14]. Further optimization of amplification conditions may improve sensitivity and reduce assay time. On a panel of 95 clinical stool DNA samples, LAMP-SLF-LB1H achieved sensitivity of 86.84% and specificity of 96.49% relative to qPCR.

Two samples that were LAMP-SLF-LB1H-positive but initially qPCR-negative became qPCR-positive after dilution, indicating the presence of amplification inhibitors. Isothermal amplification, including LAMP, is known for increased tolerance to inhibitors present in clinical samples [7]. The Gss-Sto DNA polymerase used here contains a DNA-binding domain and shows higher inhibitor tolerance than native enzymes [15]. The observed higher resistance of LAMP-SLF-LB1H to inhibitors compared with qPCR is consistent with the literature and is practically relevant, as it can reduce sample preparation requirements and enable less labor-intensive DNA extraction protocols. This observation should be confirmed more rigorously in larger studies.

A potential advantage of using fluorescently labeled loop primers is the ability to use primers with different fluorophores (FAM, HEX, ROX, Cy5) for simultaneous detection of multiple targets in a single LAMP reaction. This is especially important for mixed infections or panel tests detecting multiple pathogens (e.g., *Salmonella*, *Shigella*, *Vibrio*). A multiplex LAMP system using fluorescent loop primers could serve as the basis for a robust point-of-care diagnostic platform for rapid detection of multiple pathogens [16, 17].

Study limitations include the relatively small clinical panel size for robust diagnostic validation. In addition, although *bcfD* is considered *Salmonella*-specific, cross-testing against other closely related Enterobacteriaceae and intestinal pathogens is required. The study used high-quality instrumentation (CFX96 Touch, Bio-Rad), which may not reflect real-world PoC settings. Finally, intensive optimization was intentionally avoided to assess the reproducibility of the concept under routine LAMP conditions.

Despite these limitations, the results demonstrate the potential of fluorescent loop primers as a visualization system for LAMP. The method can be adapted to portable fluorescence devices for PoC diagnostics. The possibility of using different fluorophores opens prospects for multiplex test development and integration into molecular diagnostic devices for resource-limited settings.

CONCLUSIONS

We developed and validated a new LAMP design using a fluorescently labeled loop primer-probe that generates a real-time fluorescent signal for detection of Salmonella enterica based on the bcfD gene. The method provides acceptable analytical characteristics: LoD95% = 250 copies per reaction, sensitivity of 86.84% (95% CI: 71.91–95.59%) and specificity of 96.49% (95% CI: 87.89–99.57%) compared with qPCR. Using fluorescent loop primers labeled with different fluorophores opens prospects for multiplex LAMP to simultaneously detect several pathogens in a single reaction.

References

1. Hugas M, Beloeil PA. Controlling Salmonella along the food chain in the European Union — progress over the last ten years. Eurosurveillance. 2014; 19 (19): 1–4. DOI: 10.2807/1560-7917.ES2014.19.19.20804.
2. de Jong HK, Parry CM, van der Poll T, Wiersinga WJ. Host-Pathogen Interaction in Invasive Salmonellosis. PLoS Pathog. 2012; 8–10: 1002933. DOI: 10.1371/journal.ppat.1002933.
3. Pimenov NV, Laishevtcev AI. Modern methods of epizootic and epidemiological monitoring in the poultry industry on the example of Salmonella infection. Russ J Agric Socio-Economic Sci. 2017; 64–4: 257–69. DOI: 10.18551/rjoas.2017-04.33.
4. Fu H, Xu W, Huang M, Cong Y. Molecular Detection of Salmonella. J Food Prot. 2025; 88–12:100659. DOI: 10.1016/j.jfp.2025.100659.
5. Chirambo AC, Nyirenda TS, Jambo N, Msefula C, Kamngona A, Molina S, et al. Performance of molecular methods for the detection of Salmonella in human stool specimens. Wellcome Open Res. 2021; 5: 237. DOI: 10.12688/wellcomeopenres.16305.2.
6. Notomi T. Loop-mediated isothermal amplification of DNA. Nucleic Acids Res. 2000; 28–12: 63e–63. DOI: 10.1093/nar/28.12.e63.
7. Garg N, Ahmad FJ, Kar S. Recent advances in loop-mediated isothermal amplification (LAMP) for rapid and efficient detection of pathogens. Curr Res Microb Sci. 2022; 3: 100120. DOI: 10.1016/j.crmicr.2022.100120.
8. Liu N, Zou D, Dong D, Yang Z, Ao D, Liu W, et al. Development of a multiplex loop-mediated isothermal amplification method for the simultaneous detection of Salmonella spp. and Vibrio parahaemolyticus. Sci Rep. 2017; 7–1: 45601. DOI: 10.1038/srep45601.

9. Yang Q, Domesle KJ, Ge B. Loop-Mediated Isothermal Amplification for Salmonella Detection in Food and Feed: Current Applications and Future Directions. Foodborne Pathog. Dis. 2018; 15–6: 309–31. DOI: 10.1089/fpd.2018.2445.
10. Zhuang L, Gong J, Li Q, Zhu C, Yu Y, Dou X, et al. Detection of Salmonella spp. by a loop-mediated isothermal amplification (LAMP) method targeting bcfD gene. Lett Appl Microbiol. 2014; 59–6: 658–64. DOI: 10.1111/lam.12328.
11. Chen S, Wang F, Beaulieu JC, Stein RE, Ge B. Rapid Detection of Viable Salmonellae in Produce by Coupling Propidium Monoazide with Loop-Mediated Isothermal Amplification. Appl Environ Microbiol. 2011; 77–12: 4008–16. DOI: 10.1128/AEM.00354-11.
12. Gadkar VJ, Goldfarb DM, Gantt S, Tilley PAG. Real-time Detection and Monitoring of Loop Mediated Amplification (LAMP) Reaction Using Self-quenching and De-quenching Fluorogenic Probes. Sci Rep. 2018; 8–1: 5548. DOI: 10.1038/s41598-018-23930-1.
13. Lee S-Y, Oh S-W. Point-of-Care Diagnostic System for Viable Salmonella Species via Improved Propidium Monoazide and Recombinase Polymerase Amplification Based Nucleic Acid Lateral Flow. Diagnostics. 2024; 14–8: 831. DOI: 10.3390/diagnostics14080831.
14. Abdullah J, Saffie N, Sjasri FAR, Husin A, Abdul-Rahman Z, Ismail A, et al. Rapid detection of Salmonella Typhi by loop-mediated isothermal amplification (LAMP) method. Brazilian J. Microbiol. 2014; 45–4: 1385–91. DOI: 10.1590/S1517-83822014000400032.
15. Oscorbin IP, Belousova EA, Boyarskikh UA, Zakabunin AI, Khrapov EA, Filipenko ML. Derivatives of Bst-like Gss-polymerase with improved processivity and inhibitor tolerance. Nucleic Acids Res. 2017; 45–16: 9595–10. DOI: 10.1093/nar/gkx645.
16. Pusterla N, Naranatt P, Swadia H, Winfield L, Hartwig A, Barnum S, et al. Multi-Centered Field Evaluation of a Salmonella spp. Point-of-Care PCR Assay Using Equine Feces and Environmental Samples. J Equine Vet Sci. 2023; 126: 104538. DOI: 10.1016/j.jevs.2023.104538.
17. Zhang X, Zhao Y, Zeng Y, Zhang C. Evolution of the Probe-Based Loop-Mediated Isothermal Amplification (LAMP) Assays in Pathogen Detection. Diagnostics. 2023; 13–9: 1530. DOI: 10.3390/diagnostics13091530.

Литература

1. Hugas M, Beloeil PA. Controlling Salmonella along the food chain in the European Union — progress over the last ten years. Eurosurveillance. 2014; 19 (19): 1–4. DOI: 10.2807/1560-7917.ES2014.19.19.20804.
2. de Jong HK, Parry CM, van der Poll T, Wiersinga WJ. Host-Pathogen Interaction in Invasive Salmonellosis. PLoS Pathog. 2012; 8–10: 1002933. DOI: 10.1371/journal.ppat.1002933.
3. Pimenov NV, Laishevtcev AI. Modern methods of epizootic and epidemiological monitoring in the poultry industry on the example of Salmonella infection. Russ J Agric Socio-Economic Sci. 2017; 64–4: 257–69. DOI: 10.18551/rjoas.2017-04.33.
4. Fu H, Xu W, Huang M, Cong Y. Molecular Detection of Salmonella. J Food Prot. 2025; 88–12:100659. DOI: 10.1016/j.jfp.2025.100659.
5. Chirambo AC, Nyirenda TS, Jambo N, Msefula C, Kamngona A, Molina S, et al. Performance of molecular methods for the detection of Salmonella in human stool specimens. Wellcome Open Res. 2021; 5: 237. DOI: 10.12688/wellcomeopenres.16305.2.
6. Notomi T. Loop-mediated isothermal amplification of DNA. Nucleic Acids Res. 2000; 28–12: 63e–63. DOI: 10.1093/nar/28.12.e63.
7. Garg N, Ahmad FJ, Kar S. Recent advances in loop-mediated isothermal amplification (LAMP) for rapid and efficient detection of pathogens. Curr Res Microb Sci. 2022; 3: 100120. DOI: 10.1016/j.crmicr.2022.100120.
8. Liu N, Zou D, Dong D, Yang Z, Ao D, Liu W, et al. Development of a multiplex loop-mediated isothermal amplification method for the simultaneous detection of Salmonella spp. and Vibrio parahaemolyticus. Sci Rep. 2017; 7–1: 45601. DOI: 10.1038/srep45601.
9. Yang Q, Domesle KJ, Ge B. Loop-Mediated Isothermal Amplification for Salmonella Detection in Food and Feed: Current Applications and Future Directions. Foodborne Pathog. Dis. 2018; 15–6: 309–31. DOI: 10.1089/fpd.2018.2445.
10. Zhuang L, Gong J, Li Q, Zhu C, Yu Y, Dou X, et al. Detection of Salmonella spp. by a loop-mediated isothermal amplification (LAMP) method targeting bcfD gene. Lett Appl Microbiol. 2014; 59–6: 658–64. DOI: 10.1111/lam.12328.
11. Chen S, Wang F, Beaulieu JC, Stein RE, Ge B. Rapid Detection of Viable Salmonellae in Produce by Coupling Propidium Monoazide with Loop-Mediated Isothermal Amplification. Appl Environ Microbiol. 2011; 77–12: 4008–16. DOI: 10.1128/AEM.00354-11.
12. Gadkar VJ, Goldfarb DM, Gantt S, Tilley PAG. Real-time Detection and Monitoring of Loop Mediated Amplification (LAMP) Reaction Using Self-quenching and De-quenching Fluorogenic Probes. Sci Rep. 2018; 8–1: 5548. DOI: 10.1038/s41598-018-23930-1.
13. Lee S-Y, Oh S-W. Point-of-Care Diagnostic System for Viable Salmonella Species via Improved Propidium Monoazide and Recombinase Polymerase Amplification Based Nucleic Acid Lateral Flow. Diagnostics. 2024; 14–8: 831. DOI: 10.3390/diagnostics14080831.
14. Abdullah J, Saffie N, Sjasri FAR, Husin A, Abdul-Rahman Z, Ismail A, et al. Rapid detection of Salmonella Typhi by loop-mediated isothermal amplification (LAMP) method. Brazilian J. Microbiol. 2014; 45–4: 1385–91. DOI: 10.1590/S1517-83822014000400032.
15. Oscorbin IP, Belousova EA, Boyarskikh UA, Zakabunin AI, Khrapov EA, Filipenko ML. Derivatives of Bst-like Gss-polymerase with improved processivity and inhibitor tolerance. Nucleic Acids Res. 2017; 45–16: 9595–10. DOI: 10.1093/nar/gkx645.
16. Pusterla N, Naranatt P, Swadia H, Winfield L, Hartwig A, Barnum S, et al. Multi-Centered Field Evaluation of a Salmonella spp. Point-of-Care PCR Assay Using Equine Feces and Environmental Samples. J Equine Vet Sci. 2023; 126: 104538. DOI: 10.1016/j.jevs.2023.104538.
17. Zhang X, Zhao Y, Zeng Y, Zhang C. Evolution of the Probe-Based Loop-Mediated Isothermal Amplification (LAMP) Assays in Pathogen Detection. Diagnostics. 2023; 13–9: 1530. DOI: 10.3390/diagnostics13091530.

ANTI-OPISTHORCHIASIS AND HEPATOPROTECTIVE EFFECTS OF *POPULUS TREMULA* BARK EXTRACT: *IN VITRO* STUDIES

Perina EA[1]✉, Buyko EE[1], Kaidash OA[1], Efimova LV[1], Diksas EB[1], Krivoshchekov SV[1], Ivanov AA[1,2], Ivanov VV[1], Udut EV[1]

[1] Central Research Laboratory, Siberian State Medical University of the Ministry of Health of the Russian Federation, Tomsk
[2] Biolit limited liability company, Tomsk

The problem of opisthorchiasis caused by *Opisthorchis felineus* requires a search for alternative treatments, because the trematode can develop drug resistance and the existing drugs, such as praziquantel, may have undesirable side effects. This study aimed to identify the anti- opisthorchiasis and hepatoprotective properties of *Populus tremula L.* bark extract using *in vitro* methods. The PGF-PT active fraction with a high content of phenol glycosides was obtained though extraction. PGF-PT showed a dose-dependent anti-opisthorchiasis effect: the relative mobility index of maritae decreased from 98.2% at 250 μg/ml to 54.5% at 2000 μg/ml ($p < 0.05$), and the proportion of immobile specimens at 2000 μg/ml was 30% ($p < 0.05$). The probable mechanism of action is focal damage to the cells of the parasite's superficial epithelium (tegument). PGF-PT exhibited a pronounced hepatoprotective effect in a lipotoxicity model based on HepG2 cells, as evidenced by normalized intracellular lipid accumulation and reduced oxidative stress. A high antioxidant activity of PGF-PT was shown in the model system (IC_{50} = 79.3 ± 1.0 μg/ml). Thus, the PGF-PT fraction has a complex effect — eliminating parasites and correcting metabolic disorders in the liver — which makes it a promising basis for new effective anthelmintic drugs.

Keywords: *Opisthorchis felineus*, *Populus tremula* bark extract, anthelmintic therapy, praziquantel, phenol glycosides, antioxidants, tegument

Funding: the project is supported by the state research assignment "720000F.99.1.BN62AB05000 Development of a new drug based on a natural complex of phenol glycosides and arabinogalactanes for the treatment of trematodosis" (Agreement on granting subsidies to a federal budget-supported or autonomous institution as financial support for the state assignment involving provision of public services (implementation of works) of 21.01.2025 No. 056-03-2025-100, supplementary agreement of 04.04.2025 No. 056-03-2025-100/1).

Author contribution: Perina EA — reproduction of opisthorchiasis invasion, assessment of anti- opisthorchiasis effect; Buyko EE — determination of hepatoprotective effect and cytotoxicity of the extract; Kaidash OA — statistical data processing, article authoring, final review and approval of the manuscript; Efimova LV — assessment of damage to the maritae's tegument; Diksas EB — reproduction of opisthorchiasis invasion; Krivoshchekov SV — synthesis of the extract; Ivanov AA — chemical analysis of the extract; Ivanov VV — study design and conceptualization, data analysis and interpretation; Udut EV — study coordination, final review and approval of the manuscript.

Compliance with ethical standards: the study was approved by the Institutional Animal Care and Use Committee of the Preclinical Research Center, Central Research Laboratory, Siberian State Medical University of the Ministry of Health of the Russian Federation (Resolution No. 1 of September 02, 2023). The work was performed in full compliance with current drug circulation regulations, guidelines for the use of laboratory (experimental) animals in preclinical (non-clinical) studies, and sanitary and epidemiological standards.

✉ **Correspondence should be addressed:** Ekaterina Alexandrovna Perina
Moskovsky tract, 2, str. 16, Tomsk, 634050, Russia; catherineperina@gmail.com

Received: 17.10.2025 **Accepted:** 19.11.2025 **Published online:** 02.12.2025

DOI: 10.24075/brsmu.2025.063

Copyright: © 2025 by the authors. **Licensee:** Pirogov University. This article is an open access article distributed under the terms and conditions of the Creative Commons Attribution (CC BY) license (https://creativecommons.org/licenses/by/4.0/).

ПРОТИВООПИСТОРХОЗНАЯ И ГЕПАТОПРОТЕКТОРНАЯ АКТИВНОСТЬ ЭКСТРАКТА КОРЫ ОСИНЫ (*POPULUS TREMULA L.*) В ЭКСПЕРИМЕНТАХ *IN VITRO*

Е. А. Перина[1]✉, Е. Е. Буйко[1], О. А. Кайдаш[1], Л. В. Ефимова[1], Е. Б. Диксас[1], С. В. Кривощеков[1], А. А. Иванов[1,2], В. В. Иванов[1], Е. В. Удут[1]

[1] Центральная научно-исследовательская лаборатория, Сибирский государственный медицинский университет, Томск, Россия
[2] Общество с ограниченной ответственностью «Биолит», Томск, Россия

Для решения проблемы описторхоза, вызванного трематодой *Opisthorchis felineus*, необходим поиск альтернативных терапевтических решений ввиду рисков развития лекарственной устойчивости и возможных побочных эффектов существующих препаратов, таких как празиквантел. Цель исследования — выявить противоописторхозные и гепатопротекторные свойства экстракта коры осины (*Populus tremula* L.) на примере *in vitro*-моделей. Методом экстракции выделена активная фракция PGF-PT с высоким содержанием фенолгликозидов. Выявлен дозозависимый антигельминтный эффект PGF-PT: индекс относительной подвижности марит снизился с 98,2% (250 мкг/мл) до 54,5% (2000 мкг/мл, $p < 0,05$), а доля неподвижных особей при концентрации 2000 мкг/мл достигла 30% ($p < 0,05$). Вероятный механизм действия — индуцированное очаговое повреждение клеток поверхностного эпителия (тегумента) паразита. Выявлен выраженный гепатопротекторный эффект PGF-PT, подтвержденный моделью липотоксичности на клетках HepG2: наблюдались нормализация накопления внутриклеточных липидов и подавление окислительного стресса. В модельной системе показана высокая антиоксидантная активность PGF-PT (IC_{50} = 79,3 ± 1,0 мкг/мл). Таким образом, фракция PGF-PT обладает комплексным действием, направленным на элиминацию паразита и коррекцию метаболических нарушений в печени, что открывает перспективы для создания на ее основе новых эффективных препаратов для антигельминтной терапии.

Ключевые слова: *Opisthorchis felineus*, экстракт коры осины, антигельминтная терапия, празиквантел, фенолгликозиды, антиоксиданты, тегумент

Финансирование: средства субсидии на финансовое обеспечение выполнения государственного задания на проведение научного исследования «720000Ф.99.1.БН62АБ05000 Разработка нового лекарственного средства на основе природного комплекса фенолгликозидов и арабиногалактанов для терапии трематодозов» (Соглашение о предоставлении субсидии федеральному бюджетному или автономному учреждению на финансовое обеспечение выполнения государственного задания на оказание государственных услуг (выполнение работ) от 21.01.2025 № 056-03-2025-100, дополнительное соглашение от 04.04.2025г. № 056-03-2025-100/1).

Вклад авторов: Е. А. Перина — воспроизведение описторхозной инвазии, оценка противоописторхозного действия; Е. Е. Буйко — определение гепатопротекторного действия и цитотоксичности экстракта; О. А. Кайдаш — статистическая обработка данных, написание текста статьи, утверждение рукописи для публикации; Л. В. Ефимова — оценка повреждений тегумента марит; Е. Б. Диксас — воспроизведение описторхозной инвазии; С. В. Кривощеков — синтез экстракта; А. А. Иванов — химический анализ экстракта; В. В. Иванов — разработка концепции и дизайна исследования, анализ и интерпретация данных; Е. В. Удут — координация выполнения исследования, утверждение рукописи для публикации.

Соблюдение этических стандартов: исследование одобрено комиссией по контролю содержания и использования лабораторных животных центра доклинических исследований центральной научно-исследовательской лаборатории (ЦДИ ЦНИЛ) ФГБОУ ВО СибГМУ Минздрава России (протокол № 1 от 2 сентября 2023 г.). Работа выполнена в полном соответствии с действующими нормативно-правовыми документами об обращении лекарственных средств, рекомендациями по работе с лабораторными (экспериментальными) животными при проведении доклинических (неклинических) исследований, соблюдением санитарно-эпидемиологических норм.

✉ **Для корреспонденции:** Екатерина Александровна Перина
Московский тракт, д. 2, стр. 16, г. Томск, 634050, Россия; catherineperina@gmail.com

Статья получена: 17.10.2025 **Статья принята к печати:** 19.11.2025 **Опубликована онлайн:** 02.12.2025

DOI: 10.24075/vrgmu.2025.063

Авторские права: © 2025 принадлежат авторам. **Лицензиат:** РНИМУ им. Н. И. Пирогова. Статья размещена в открытом доступе и распространяется на условиях лицензии Creative Commons Attribution (CC BY) (https://creativecommons.org/licenses/by/4.0/).

The problem of opisthorchiasis caused by the trematodes *Opisthorchis felineus* and *Opisthorchis viverrini* remains extremely urgent in modern medicine, parasitology, and epidemiology [1]. The endemic regions extend across parts of the Russian Federation (Western and Eastern Siberia, Cis-Urals), Eastern Europe, Kazakhstan, and Southeast Asian countries (Thailand, Laos, Vietnam) [2]. According to WHO, more than 80 million people in the world are at risk, and the number of infected is estimated at several tens of millions [3]. The only drug used for etiotropic therapy is praziquantel (PZQ); however, its widespread use poses a potential risk of generating resistant parasite strains, which could render the medicine completely ineffective [4]. In addition, several recent reports suggest that repeated courses of PZQ may increase the risk of cholangiocarcinoma, likely due to the massive release of parasitic antigens associated with the treatment [4, 5]. Therefore, the search for alternative medicines that are both effective and low in toxicity has become particularly urgent.

Extracts derived from parts of trees in the Populus family, particularly their buds and bark, are traditionally used due to their anti-inflammatory, antioxidant, and hepatoprotective properties confirmed by studies [6, 7]. Since oxidative stress and chronic inflammation play key roles in the development of opisthorchiasis complications, and plant extracts with similar structures — such as artesunate — have already proven effective in treating other trematodes [8], the bark extract of *Populus tremul*a L. (*P. tremula*) appears to be a promising subject for further study. The pharmacological activity of aspen (*P. tremula* L.) bark extracts mainly stems from the high content of phenol glycosides of the salicinoid class [9]. Studies have shown that these phytochemical components have a pronounced antiparasitic effect against a wide range of etiological agents causing trematodiasis (e.g., *Opisthorchis spp.*, *Psilostomum*) and helminthiasis (including nematodosis and protozoal infections such as giardiasis) [10, 11].

The purpose of this study was to investigate the properties of *P. tremula* bark extract that is rich in phenol glycosides.

METHODS

The object of the study was the *P. tremula* bark extract with a high content of phenol glycosides.

At the facilities of Biolit, a research and production company, we made a liquid extract with the feedstock to product ratio of 1:1. The feedstock was the bark of *P. tremula* harvested in autumn and winter, naturally dried to a residual humidity of 8–10%; the extraction was performed in a 2000 L industrial extractor (Hubei weihua machinery co., ltd, China) using the repercolation method. The extractant was water; the resulting liquid extract was condensed in an SX-250 vacuum evaporation system (Hubei weihua machinery co., ltd, China) to a residual moisture content of 25–40%.

The phenol glycoside–rich fraction (PGF-PT) was prepared in the Quality Control Laboratory of the Central Research Laboratory, Siberian State Medical University, as follows: the thick extract was reconstituted with purified water at a ratio of 1:15, mixed for 30 minutes, and enriched with a threefold (v/v) excess of 96% ethanol. After allowing the sediment to settle at 4°C for 12 hours, the supernatant was decanted and centrifuged at 4000 rpm for 3 minutes (Eppendorf 5702, Eppendorf, USA). The decanted solution was combined with the supernatant and concentrated to one-tenth of its original volume using a Rotavapor V-3 rotary evaporator (Buchi, Switzerland) equipped with a PC 500 vacuum pumping station (Vacuubrand, Germany) at a water bath temperature of 40 °C. The concentrated solution was then dried by convection. The yield of PGF-PT was 71.65 ± 13.4%. Using HPLC, we standardized PGF-PT by quantifying its salicin phenol glycoside content in an Ultimate 3000 chromatograph (Dionex, Thermo, Germany) equipped with a DAD3000 diode matrix detector on a Zorbax Eclipse plus C18 3.0 × 150 mm, 3.5 µm column, mobile phase A — 0.1% trifluoroacetic acid in water, mobile phase B — acetonitrile. The elution was gradient, the volume of the introduced sample was 20 µl, and the temperature of the column thermostat — 30 °C. We identified the salicin peak by spectral features: absorption maxima at wavelengths of 194 and 269 nm, and the shoulder at a wavelength of 215 nm. The salicin content was determined by the external standard method. The salicin peak retention time was 7.544 minutes. Tannin content, representing polyphenolic compounds, was quantified permanganometrically as specified in applicable regulations; it equaled 8.16 ± 0.41%, and the content of salicin was 4.7 ± 0.6%.

The anti-opisthorchiasis activity of PGF-PT was evaluated at the Preclinical Research Center of the Central Research Laboratory using maritae of the hepatic fluke *O. felineus*. Praziquantel (PZQ, TCI, Japan) at a dose of 600 µg/ml was used as a comparison drug [11]. The experimental animals were infected using the described method [12]. A total of 40 specific pathogen-free (SPF) female golden hamsters (*Mesocricetus auratus*), weighing 130–150 g, were used in the experiment. The animals were obtained from the Federal Research Center, Institute of Cytology and Genetics, Siberian Branch of the Russian Academy of Sciences. Three months after infection, the animals were euthanized in a CO_2 atmosphere. Maritae were extracted from the hepatobiliary tract, washed with 0.9% NaCl solution, and incubated at 37 °C in a 5% CO_2 atmosphere for 2 hours in RPMI 1640 culture medium containing 2× penicillin–streptomycin [13]. The maritae were placed in a six-well culture plate, ten specimens per well, containing RPMI 1640 medium supplemented with 1× penicillin-streptomycin, 10 g/L glucose, and 2 g/L sodium bicarbonate.

Solutions of the PGF-PT and PZQ fractions were prepared in dimethyl sulfoxide (DMSO), followed by dilution in an incubation medium. The studied PGF-PT fraction was tested at final concentrations of 250, 500, 1000, and 2000 µg/ml. As a negative control, we used samples incubated in a medium containing a similar volume of DMSO (up to 0.5%) to exclude the possible nonspecific effects of the solvent itself on the metabolism and behavior of the maritae. The incubation of maritae with the substances lasted 24 hours in a CO_2 incubator.

The efficacy of anthelmintic drugs is tested *in vitro*, by assessing the mobility and morphology of parasites [10, 11]. Thus, we assessed the antiparasitic activity of the studied agent by analyzing changes in the mobility and tegument morphology of the maritae using a NE910 microscope (Ningbo Yongxin Optics Co., Ltd., China) equipped with a Digital Sight 1000 camera (Nikon, China). Mobility was assessed visually using a 4-point scale [14]: 4 — very active movements, similar to those of control flukes; 3 — regularly active movements, less energetic than the control, but involving the entire body; 2 — low activity, with limited movement; 1 — immobile worms. The mobility indicators measured in the wells were normalized to the values of the control group.

The relative mobility index (RM) was calculated by the following formulas [14]:

$$RM\ \% = \frac{MI\ experiment}{MI\ control}$$

$$MI = \frac{\Sigma n \times Nn}{\Sigma Nn},$$

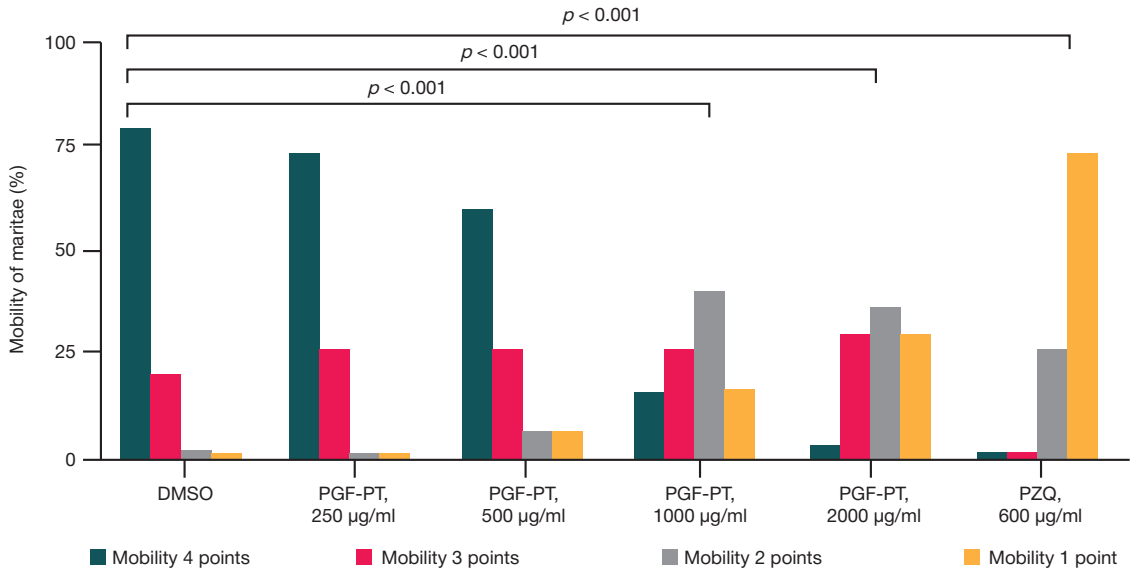


Fig. 1. The effect of the PGF-PT fraction on the mobility of *O. felineus* maritae

where *MI* — the index of mobility of the worm group, *n* — mobility score (points), Nn — the number of trematodes given n points.

To determine the effect of the extract on the functional state of the liver fluke's tegument, we studied the specimens using propidium iodide (PI), a fluorescent intercalating dye that binds to DNA and stains the nuclei of dead cells. The maritae were incubated with PI (2 μg/ml) for 20 minutes, then washed with saline solution. The images were made with a Leica DM6 fluorescence microscope (Leica Microsystems GmbH, Germany) [15].

The hepatoprotective activity of PGF-PT was evaluated in vitro using a lipotoxicity model induced by a mixture of oleate and sodium palmitate in HepG2 hepatocellular carcinoma cells, by measuring intracellular lipid levels and reactive oxygen species (ROS). The lipid content was assessed after staining with Nile red fluorescent dye [16]. For positive control, we used 100 μM of gemfibrozil, a lipid-lowering compound (Sigma-Aldrich, USA). The lipid droplets were visualized using a Leica DM6 fluorescence microscope (Leica Microsystems GmbH, Germany). The level of ROS in cells was measured using 2.7'-dichloro-dihydro-fluorescein diacetate (DCFH-DA) [17]. The safe concentrations of PGF-PT for use in this model (31.25, 62.5, and 125 μg/ml) were selected by testing with a neutral red vital dye [18].

To evaluate the degree of contribution of the direct anti-radical effect to the fraction's ability to influence ROS levels in cells, we set up an experiment in the model system that involved a stable radical of 1.1-diphenyl-2-picrylhydrazyl (DPPH), as described previously [19]. The activity was expressed as the IC50 index, which reflects the effective concentration of PGF-PT at which 50% of the free radicals of DPPH are reduced.

Statistical data analysis was performed in GraphPad Prism 8.0 (GraphPad Software, USA). Pearson's chi-square test (χ^2) was used to analyze the ordered data. For pairwise group comparisons, we applied the Bonferroni correction. The normality of the distribution of the quantitative variables was assessed using the Shapiro–Wilk test. The mean values of several independent groups were compared using one-way analysis of variance (ANOVA). The threshold of statistical significance was $p < 0.05$.

RESULTS

The PGF-PT fraction had a dose-dependent effect on the mobility of *O. felineus* maritae (Fig. 1).

In the control group, the maritae maintained their mobility and integrity of the tegument. Treatment with the PGF-PT fraction at a concentration of 1000 μg/ml reduced the mobility of 40% of adult worms to a minimum value (2 points on the mobility scale), and 17% of the parasites became completely motionless (1 point on the mobility scale). An increased concentration of 2000 μg/ml increased the proportion of motionless specimens to 30%. PZQ, the comparison drug, completely immobilized 73% of maritae at a concentration of 600 μg/ml.

In the control group, the parasite mobility index was 3.8. As the concentration of the PGF-PT fraction increased from 250 to 2000 μg/ml, the index decreased from 3.7 to 2.1, and the relative mobility of the worms dropped from 98.2% to 54.5%. PZQ, in turn, reduced parasite activity to 28.5%, inducing spastic paralysis (Table).

Examination of tegument integrity in the control group showed that the PI fluorescent dye failed to penetrate the cells of the maritae. After treatment with PZQ, the fluorescent glow localized in the areas of tegument syncytium. These results are consistent with the published studies that report PZQ's capability to induce peeling of tegument and destruction of *O. viverrini* [15]. Application of PGF-PT at concentrations of 500, 1000, and 2000 μg/ml allowed PI to partially penetrate deep into the tegument syncytium in certain areas of the worm's body, indicating local cell membrane disruptions and breach of tissue integrity (Fig. 2).

Table. The effect of PGF-PT on the mobility index (MI) and relative mobility index (RM) of *O. felineus* maritae

	DMSO	PGF-PT, 250 μg/ml	PGF-PT, 500 μg/ml	PGF-PT, 1000 μg/ml	PGF-PT, 2000 μg/ml	PZQ, 600 μg/ml
MI	3.8	3.7	3.4	2.4	2.1	1.1
RM, %		98.2	89.5	64	54.5	28.5

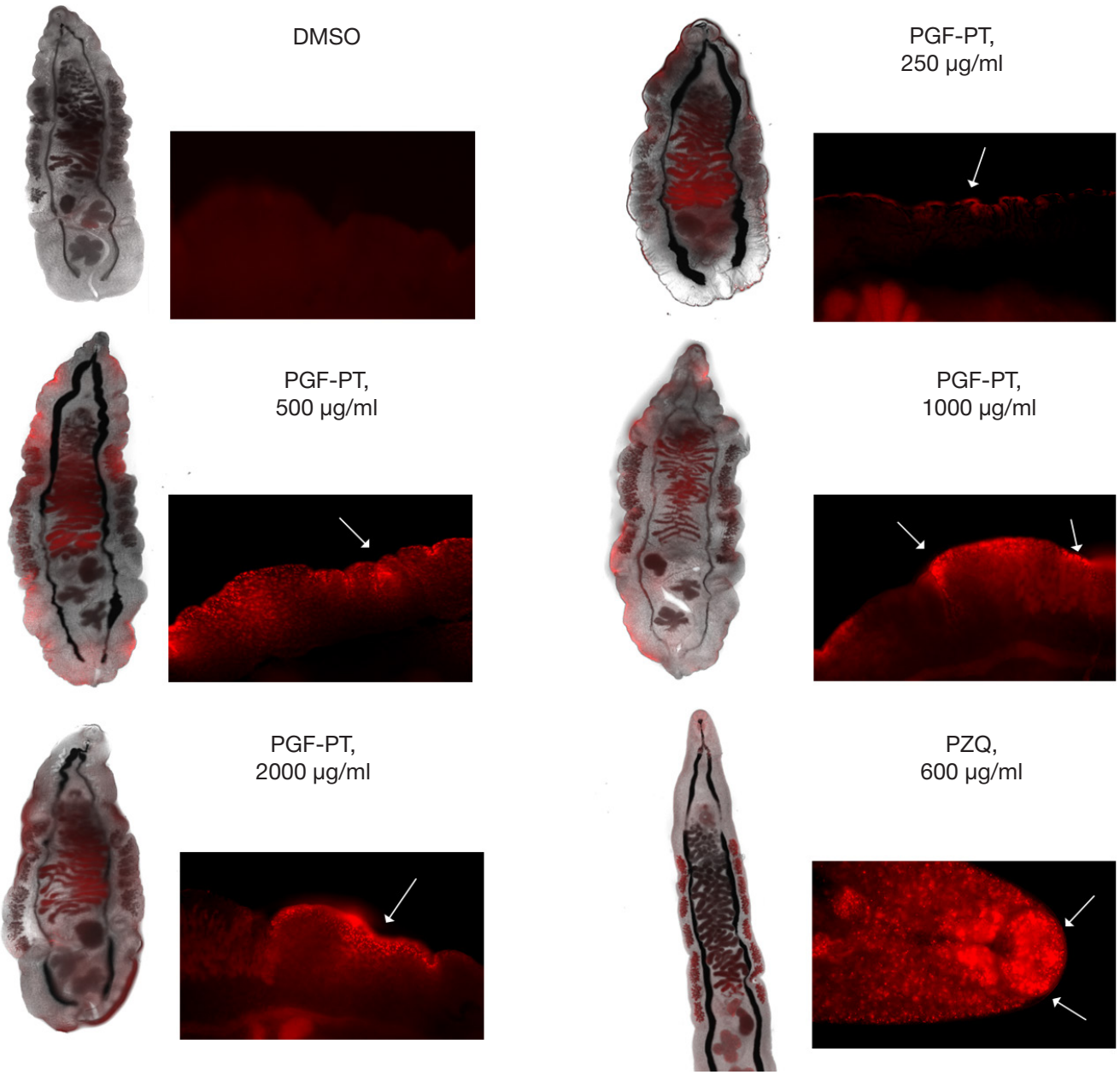


Fig. 2. Assessment of damage to the *O. felineus* maritae tegument by fluorescent staining

Thus, exposure to PGF-PT caused partial degradation of the tegument cells but did bring complete functional destruction of the parasite's organism and loss of mobility in all the cases considered.

Light microscopy confirmed significant damage to the surface structures of the maritae's bodies after incubation with high concentrations of PGF-PT (1000 and 2000 μg/ml): massive peeling of the epithelium and edema of the tegument (see appendix).

Incubation of HepG2 cells in a medium with oleic and palmitic fatty acids (FA) induced hepatotoxicity. According to the assessment of changes in the fluorescence intensity of the lipophilic dye (Fig. 3A), which was consistent with microscopy data (Fig. 3B), the intracellular lipid content increased by 55% ($p < 0.05$). The fluorescence intensity of DCFH-DA also increased by 57% ($p < 0.05$), following the growth of the level of ROS in the cells (Fig. 3B).

At concentrations of 62.5 and 125 μg/ml, PGF-PT pushed the lipid levels down by 32.9% ($p < 0.05$) and 48.9% ($p < 0.05$), respectively; this effect was comparable to that of gemfibrozil, a lipid-lowering compound ($p < 0.05$) (Fig. 3A). Meanwhile, the PGF-PT fraction reduced oxidative stress in FA-treated HepG2 cells (Fig. 3B). The introduction of PGF-PT at concentrations of 31.25, 62.50, and 125.00 μg/ml reduced the intensity of fluorescence of DCFH-DA ROS probe by 12.6% ($p < 0.05$), 28.2% ($p < 0.05$) and 36.2% ($p < 0.05$), respectively.

The decrease of intracellular ROS levels may also result from the PGF-PT's direct anti-radical properties, the assessment of which in the model system is shown in Figure 4A.

Based on the data obtained, we calculated the concentration of the PGF-PT fraction that ensures inhibition of 50% of DPPH free radicals (IC50): 79.3 ± 1.0 μg/ml (Fig. 4B). Thus, the results of the study indicate the pronounced anti-radical and hepatoprotective properties of the PGF-PT fraction.

DISCUSSION

This study demonstrates pronounced anti-opisthorchiasis and hepatoprotective potentials of the *P. tremula* bark extract with high content of phenol glycosides (PGF-PT fraction).

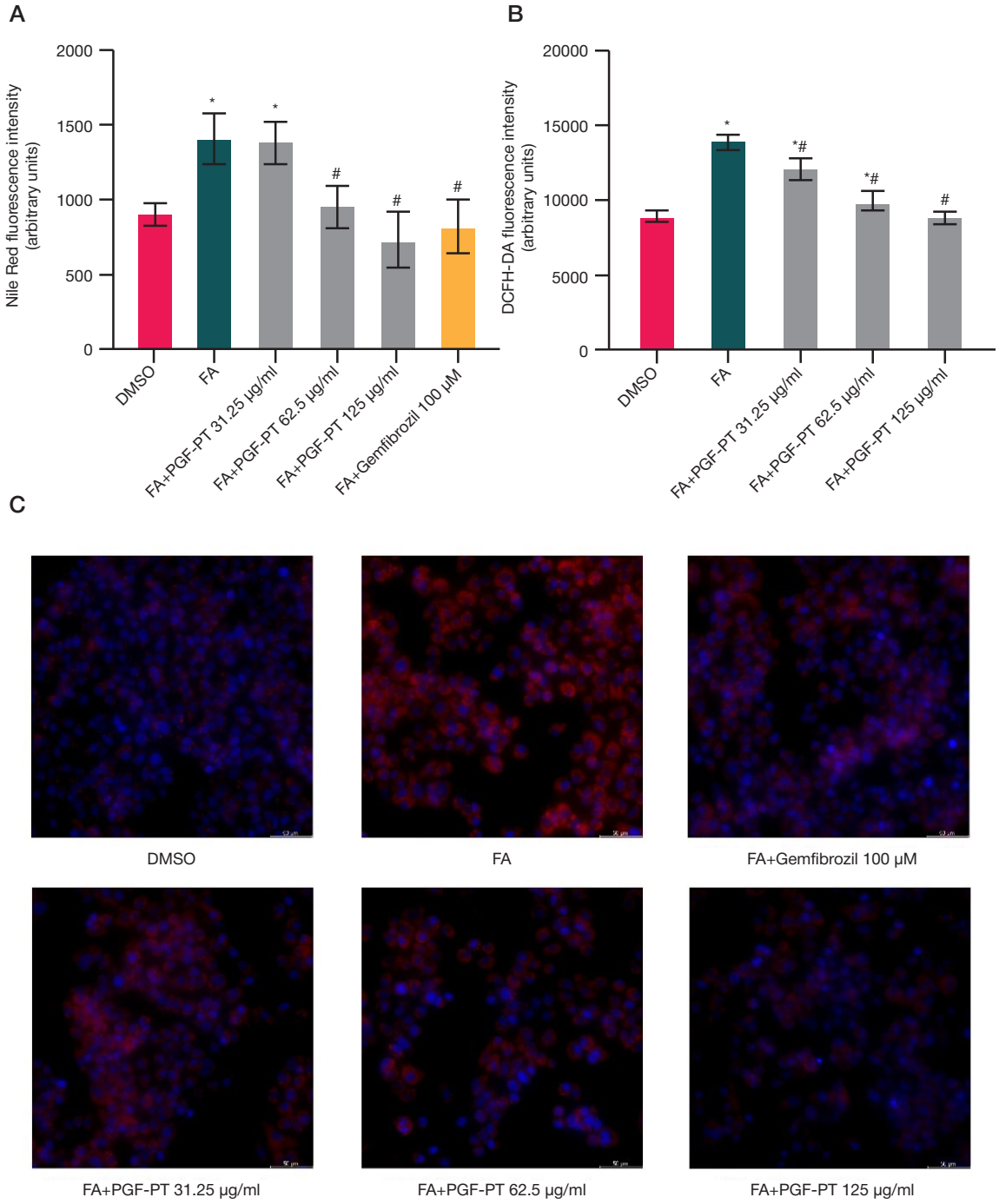


Fig. 3. Hepatoprotective activity of PGF-PT, estimated by the level of intracellular lipids and reactive oxygen species (ROS) in HepG2 cells after incubation in a medium containing oleic (1 mM) and palmitic (0.5 mM) fatty acids (FA): **A** — intensity of Nile red fluorescence (intracellular lipids), **B** — intensity of 2,7'-dichlorodihydrofluorescein diacetate fluorescence (ROS), and **C** — fluorescence images of cells (magnification x40) stained with Nile red and Hoechst 33342 (cell nuclei). The data is presented as M ± SD. * — the differences from the DMSO group are significant ($p < 0.05$); # — the differences from the FA group are significant ($p < 0.05$))

We found that this fraction exhibited a dose-dependent ability to reduce the mobility of *O. felineus* maritae. At the highest tested concentration (2000 µg/ml), 30% of the worms became completely motionless. Although this effect was lower than that achieved with PZQ (73% of specimens motionless), it indicates that developing a drug based on PGF-PT is a promising direction.

Microscopic examination confirmed that exposure to PGF-PT causes partial degradation of the tegument cells, which limits the functional capabilities of the parasite. However, the destruction was incomplete, and the parasite retained the ability to move to a certain degree, which underscores the need to continue research to enhance the anthelmintic effect. Tegument antigens from this multinucleated syncytium, approximately 4 µm thick and performing key functions like immune evasion, are promising for anthelmintic drug or vaccine development. Interestingly, anthelmintic drugs with different mechanisms of action cause damage to the parasite tegument [11]. This indicates that the drugs, along with their direct effect on molecular targets, disrupt the surface of the parasite, which activates the antibody-dependent cellular cytotoxicity and provokes an effective immune response of the host organism.

These data on the dose-dependent suppression of *O. felineus* mobility and focal tegumental damage align with prior reports of strong antiparasitic effects from phenol glycosides in *Populus spp*. Recent studies describe the anti-opisthorchiasis effect of crude

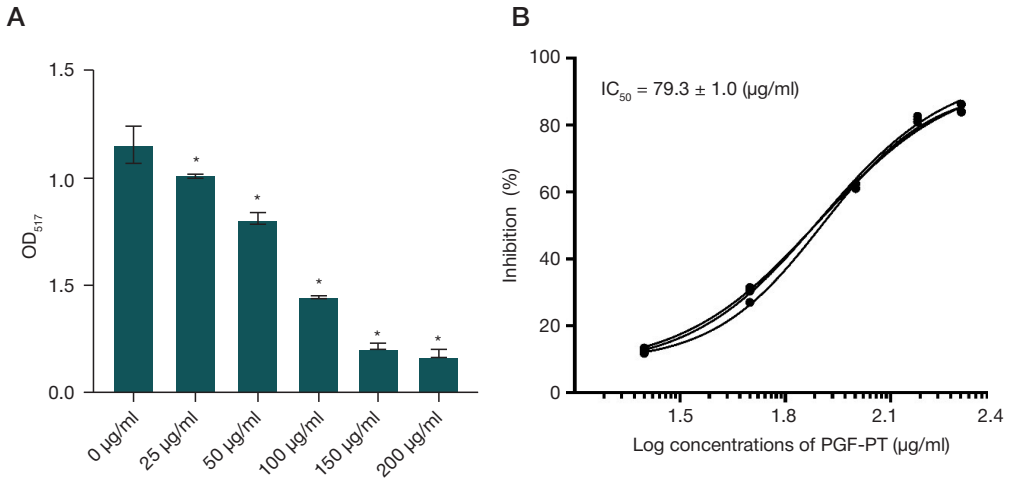


Fig. 4. The effect of the PGF-PT fraction on the optical density of a 2,2-diphenyl-1-picrylhydrazyl solution (DPPH, 100 µm) (**A**) and the semi-logarithmic dependence of the DPPH radical reaction inhibition effectiveness and the concentration of the PGF-PT fraction (**B**). The data is presented as M ± SD. * — the differences from the control group (0 µg/ml) are significant ($p < 0.05$)

extracts of *Allium sativum* L. [11] and Thunbergia laurifolia Lindl. [20]. Other works investigate the anthelmintic properties of flavonoid quercetin, a polyphenolic compound; it is capable of suppressing mobility of the parasites and damaging their tegument [21, 22]. A milder mechanism of action may help reduce the risk of severe immunopathological reactions associated with mass death and destruction of parasites.

The hepatoprotective effect of PGF-PT — manifested as decreased lipotoxicity and oxidative stress in the HepG2 cell model — is supported by current data on the properties of phenol glycosides and other bioflavonoids. The hepatoprotective effect of polyphenols was shown to rely on a complex of activities, including enhancement of antioxidant action, metabolism, and immunomodulation [23]. This suggests that therapy with this extract not only reduces the parasitic load, but also protects the liver from damage, which is especially important in chronic forms of opisthorchiasis and in view of the risk of cholangiocarcinoma.

CONCLUSIONS

The PGF-PT fraction from the *Populus tremula* bark shows a pronounced anthelmintic activity against *Opisthorchis felineus in vitro*. The effect is dose-dependent; the fraction suppresses mobility of the parasite and damages its tegument. In addition, PGF-PT protects the liver, reducing lipotoxicity and oxidative stress in hepatocytes, and, as opposed to praziquantel, offers a lower risk of immunopathological complications due to milder action. These data highlight the potential of PGF-PT as a promising component of new anti-opisthorchiasis drugs with additional hepatoprotective effect. *In vitro* systems have significant limitations in terms of reproduction of a real multicomponent "parasite-host" system, but they can give important information about the basic mechanisms of pharmacological action. The results of this study serve as the basis for further *in vivo* investigation aimed at evaluating the efficacy and safety of the PGF-PT fraction in real biological conditions.

References

1. Liu L, Lu LD, Yang GJ, Qian MB, Yang K, Tan F, et al. Global, regional and national disease burden of food-borne trematodiases: projections to 2030 based on the Global Burden of Disease Study 2021. Infect Dis Poverty. 2024; 13 (1): 95.
2. Fedorova OS, Kovshirina YV, Kovshirina AE, Fedotova MM, Deev IA, Petrovskiy FI, et al. Opisthorchis felineus infection and cholangiocarcinoma in the Russian Federation: A review of medical statistics. Parasitol Int. 2017; (4): 365–71.
3. World Health Organization. Ending the neglect to attain the sustainable development goals: a road map for neglected tropical diseases 2021–2030. Geneva: World Health Organization, 2020. Available from: https://iris.who.int/handle/10665/338565. Accessed 9 July, 2024.
4. Lvova MN, Ponomarev DV, Tarasenko AA, Kovner AV, Minkova GA, Tsyganov MA, et al. Curcumin and its supramolecular complex with disodium glycyrrhizinate as potential drugs for the liver fluke infection caused by Opisthorchis felineus. Pathogens. 2023; 12 (6): 819.
5. Kamsa-Ard S, Luvira V, Pugkhem A, Luvira V, Thinkhamrop B, Suwanrungruang K, et al. Association between praziquantel treatment and cholangiocarcinoma: a hospital-based matched case-control study. BMC Cancer. 2015; 15: 776.
6. Debbache-Benaida N, Atmani-Kilani D, Schini-Keirth VB, Djebbli N, Atmani D. Pharmacological potential of Populus nigra extract as antioxidant, anti-inflammatory, cardiovascular and hepatoprotective agent. Asian Pacific Journal of Tropical Biomedicine. 2013; 3 (9): 697–704.
7. Urbanchik EA, Kurkin VA, Agapov AI. The pharmacognostic study of some species of the genus poplar (Populus l.) growing in the Samara Region. Aspirantskiy Vestnik Povolzhiya. 2021; (5–6): 92–97.
8. Gouveia MJ, Brindley PJ, Gärtner F, Costa JMCD, Vale N. Drug Repurposing for Schistosomiasis: Combinations of Drugs or Biomolecules. Pharmaceuticals (Basel). 2018; 11 (1): 15.
9. Rashmi SP, Yogendra P, Motamarri VNLC, Avijit M, Navneet K, Prabin KT. Discerning the multi-dimensional role of Salicin: bioactive glycoside beyond analgesic: different perspectives. Current Drug Therapy. 2024; 19 (7): e221123223716.
10. V. Devi Rajeswari. Anthelmintic Activity of Plants: A Review. Research Journal of Phytochemistry. 2014; 8: 57–63.
11. Sangkam W, Arunsan P, Pechdee P, Boonsuya A, Thanchonnang C, Chatdumrong W, et al. Anthelmintic activity and pathophysiological effect of anthelmintic drugs against carcinogenic liver fluke, Opisthorchis viverrini. Trop Biomed. 2024; 41 (2): 196–205.
12. Pershina AG, Saltykova IV, Ivanov VV, Perina EA, Demin AM, Shevelev OB, et al. Hemozoin "knobs" in Opisthorchis felineus infected liver. Parasit Vectors. 2015; (8): 459.
13. Wong Y, Pearson MS, Fedorova O, Ivanov V, Khmelevskaya E,

Tedla B. Secreted and surface proteome and transcriptome of Opisthorchis felineus. Frontiers in Parasitology. 2023; (2): 1195457.
14. Ponomarev D, Lvova M, Mordvinov V, Chidunchi I, Dushkin A, Avgustinovich D. Anti-Opisthorchis felineus effects of artemisinin derivatives: An in vitro study. Acta Trop. 2024; 254: 107196.
15. Pakharukova MY, Shilov AG, Pirozhkova DS, Katokhin AV, Mordvinov VA. The first comprehensive study of praziquantel effects in vivo and in vitro on European liver fluke Opisthorchis felineus (Trematoda). Int J Antimicrob Agents. 2015; 46 (1): 94–100.
16. Yao HR, Liu J, Plumeri D, Cao YB, He T, Lin L, et al. Lipotoxicity in HepG2 cells triggered by free fatty acids. American journal of translational research. 2011; 3 (3); 284.
17. Zhang M, Lai J, Wu Q, Lai J, Su J, Zhu B. Naringenin induces HepG2 cell apoptosis via ROS-mediated JAK-2/STAT-3 signaling pathways. Molecules. 2023; 28 (11): 4506.
18. Repetto G, del Peso A, Zurita JL. Neutral red uptake assay for the estimation of cell viability/cytotoxicity. Nat Protoc. 2008; 3 (7): 1125–13.
19. Lee SE, Ju EM, Kim JH. Free radical scavenging and antioxidant enzyme fortifying activities of extracts from Smilax china root. Experimental & molecular medicine. 2001; 33 (4): 263–8.
20. Pechdee P, Arunsan P, Boonsuya A, Thanchonnang C, Phinsiri S, Rattanapitoon N, et al. Efficacy of Thunbergia laurifoliacrude extracts against carcinogenic liver fluke, Opisthorchis viverrini. Tropical Biomedicine. 2025; 42 (1): 65–75.
21. Elmahy RA, Radwan NA. In vitro evaluation of the nematicidal efficacy of quercetin on adult toxocara canis. Acta Parasitol. 2025; 70 (3): 96.
22. Ray MS, Mondal C, Saha S, Mandal S, Lyndem LM. Quercetin: An anthelmintic potential against zoonotic tapeworm Hymenolepis diminuta (Rudolphi, 1819). J Helminthol. 2025; (99): e9.
23. Brzhozovskiy AG, Semenov SD, Zherebker AY, Bugrova AE, Yurova MN, Zhernov YV. Hepatoprotective activity of nature-derived polyphenols studied by mass spectrometry based multi-OMICS approach. Int J Mol Sci. 2025; 26 (4): 1604.

Литература

1. Liu L, Lu LD, Yang GJ, Qian MB, Yang K, Tan F, et al. Global, regional and national disease burden of food-borne trematodiases: projections to 2030 based on the Global Burden of Disease Study 2021. Infect Dis Poverty. 2024; 13 (1): 95.
2. Fedorova OS, Kovshirina YV, Kovshirina AE, Fedotova MM, Deev IA, Petrovskiy FI, et al. Opisthorchis felineus infection and cholangiocarcinoma in the Russian Federation: A review of medical statistics. Parasitol Int. 2017; (4): 365–71.
3. World Health Organization. Ending the neglect to attain the sustainable development goals: a road map for neglected tropical diseases 2021–2030. Geneva: World Health Organization, 2020. Available from: https://iris.who.int/handle/10665/338565. Accessed 9 July, 2024.
4. Lvova MN, Ponomarev DV, Tarasenko AA, Kovner AV, Minkova GA, Tsyganov MA, et al. Curcumin and its supramolecular complex with disodium glycyrrhizinate as potential drugs for the liver fluke infection caused by Opisthorchis felineus. Pathogens. 2023; 12 (6): 819.
5. Kamsa-Ard S, Luvira V, Pugkhem A, Luvira V, Thinkhamrop B, Suwanrungruang K, et al. Association between praziquantel treatment and cholangiocarcinoma: a hospital-based matched case-control study. BMC Cancer. 2015; 15: 776.
6. Debbache-Benaida N, Atmani-Kilani D, Schini-Keirth VB, Djebbli N, Atmani D. Pharmacological potential of Populus nigra extract as antioxidant, anti-inflammatory, cardiovascular and hepatoprotective agent. Asian Pacific Journal of Tropical Biomedicine. 2013; 3 (9): 697–704.
7. Urbanchik EA, Kurkin VA, Agapov AI. The pharmacognostic study of some species of the genus poplar (Populus l.) growing in the Samara Region. Aspirantskiy Vestnik Povolzhiya. 2021; (5–6): 92–97.
8. Gouveia MJ, Brindley PJ, Gärtner F, Costa JMCD, Vale N. Drug Repurposing for Schistosomiasis: Combinations of Drugs or Biomolecules. Pharmaceuticals (Basel). 2018; 11 (1): 15.
9. Rashmi SP, Yogendra P, Motamarri VNLC, Avijit M, Navneet K, Prabin KT. Discerning the multi-dimensional role of Salicin: bioactive glycoside beyond analgesic: different perspectives. Current Drug Therapy. 2024; 19 (7): e221123223716.
10. V. Devi Rajeswari. Anthelmintic Activity of Plants: A Review. Research Journal of Phytochemistry. 2014; 8: 57–63.
11. Sangkam W, Arunsan P, Pechdee P, Boonsuya A, Thanchonnang C, Chatdumrong W, et al. Anthelmintic activity and pathophysiological effect of anthelmintic drugs against carcinogenic liver fluke, Opisthorchis viverrini. Trop Biomed. 2024; 41 (2): 196–205.
12. Pershina AG, Saltykova IV, Ivanov VV, Perina EA, Demin AM, Shevelev OB, et al. Hemozoin "knobs" in Opisthorchis felineus infected liver. Parasit Vectors. 2015; (8): 459.
13. Wong Y, Pearson MS, Fedorova O, Ivanov V, Khmelevskaya E, Tedla B. Secreted and surface proteome and transcriptome of Opisthorchis felineus. Frontiers in Parasitology. 2023; (2): 1195457.
14. Ponomarev D, Lvova M, Mordvinov V, Chidunchi I, Dushkin A, Avgustinovich D. Anti-Opisthorchis felineus effects of artemisinin derivatives: An in vitro study. Acta Trop. 2024; 254: 107196.
15. Pakharukova MY, Shilov AG, Pirozhkova DS, Katokhin AV, Mordvinov VA. The first comprehensive study of praziquantel effects in vivo and in vitro on European liver fluke Opisthorchis felineus (Trematoda). Int J Antimicrob Agents. 2015; 46 (1): 94–100.
16. Yao HR, Liu J, Plumeri D, Cao YB, He T, Lin L, et al. Lipotoxicity in HepG2 cells triggered by free fatty acids. American journal of translational research. 2011; 3 (3); 284.
17. Zhang M, Lai J, Wu Q, Lai J, Su J, Zhu B. Naringenin induces HepG2 cell apoptosis via ROS-mediated JAK-2/STAT-3 signaling pathways. Molecules. 2023; 28 (11): 4506.
18. Repetto G, del Peso A, Zurita JL. Neutral red uptake assay for the estimation of cell viability/cytotoxicity. Nat Protoc. 2008; 3 (7): 1125–13.
19. Lee SE, Ju EM, Kim JH. Free radical scavenging and antioxidant enzyme fortifying activities of extracts from Smilax china root. Experimental & molecular medicine. 2001; 33 (4): 263–8.
20. Pechdee P, Arunsan P, Boonsuya A, Thanchonnang C, Phinsiri S, Rattanapitoon N, et al. Efficacy of Thunbergia laurifoliacrude extracts against carcinogenic liver fluke, Opisthorchis viverrini. Tropical Biomedicine. 2025; 42 (1): 65–75.
21. Elmahy RA, Radwan NA. In vitro evaluation of the nematicidal efficacy of quercetin on adult toxocara canis. Acta Parasitol. 2025; 70 (3): 96.
22. Ray MS, Mondal C, Saha S, Mandal S, Lyndem LM. Quercetin: An anthelmintic potential against zoonotic tapeworm Hymenolepis diminuta (Rudolphi, 1819). J Helminthol. 2025; (99): e9.
23. Brzhozovskiy AG, Semenov SD, Zherebker AY, Bugrova AE, Yurova MN, Zhernov YV. Hepatoprotective activity of nature-derived polyphenols studied by mass spectrometry based multi-OMICS approach. Int J Mol Sci. 2025; 26 (4): 1604.

BLOOD EXPRESSION OF CD39 AND CD73 ECTONUCLEOTIDASES IN PATIENTS WITH VARIOUS FORMS OF METABOLIC-ASSOCIATED FATTY LIVER DISEASE

Zhulai GA[1]✉, Kurbatova IV[1], Dudanova OP[1,2]

[1] Institute of Biology, Karelian Research Centre, Russian Academy of Sciences, Petrozavodsk, Russia

[2] Petrozavodsk State University, Petrozavodsk, Russia

Experimental studies have demonstrated the protective role of ectonucleotidases — particularly CD39 and CD73 — in limiting inflammation connected to a liver pathology. However, their expression in metabolic-associated fatty liver disease (MAFLD) has not been thoroughly investigated. This study aimed to evaluate the mRNA levels of the *ENTPD1* and *NT5E* genes, which encode CD39 and CD73, respectively, in patients with different forms of MAFLD (liver steatosis (LS) and metabolic-associated steatohepatitis (MASH)), and to assess the expression of CD39- and CD73-positive cells following immune cell activation *in vitro*. The sample included 29 healthy donors and 56 MAFLD patients. We measured the mRNA levels of the *ENTPD1* and *NT5E* genes, pro-inflammatory cytokines (IL-6, TNFα), fragmented cytokeratin-18, and the blood content of $CD39^+$ cells. Another parameter measured in vitro was the effect of immune cell activation on the proportion of $CD39^+$ and $CD73^+$ cells in patients with MASH and healthy donors. The expression of the *ENTPD1* gene ($p = 0.007$ vs. control group; $p = 0.010$ vs. LS group) and the proportion of $CD39^+$ cells among monocytes ($p = 0.004$ vs. control group; $p = 0.003$ vs. LS group) and lymphocytes ($p = 0.034$ vs. control group) were lower in the MASH group compared with both the control and LS groups. Activation of cells from MASH patients increased the proportion of $CD39^+$ lymphocytes, but not that of $CD14^+$ monocytes. It also increased the proportion of $CD73^+$ cells among both lymphocytes and $CD14^+$ monocytes. Thus, further investigation into the roles of CD39 and CD73 in the context of MAFLD progression represents a promising avenue for future research.

Keywords: metabolic-associated fatty liver disease, metabolic-associated steatohepatitis, CD39, CD73, $CD14^+$ monocytes, $CD4^+$ T cells

Funding: the work was supported by grant No. 25-25-00534 of the Russian Science Foundation and used equipment of the Collective Use Centre of Karelian Research Centre of the Russian Academy of Sciences.

Author contribution: Zhulai GA, Kurbatova IV — study planning, collection, processing and analysis of material, statistical processing, article authoring; Dudanova OP — formation of clinical groups, analysis of clinical data, article editing.

Compliance with ethical standards: the study was approved by the Ethics Committee of the Ministry of Health of the Republic of Karelia and Petrozavodsk State University (Minutes No. 48 of March 10, 2023). All participants signed the voluntary informed consent form and the consent form for personal data processing.

✉ **Correspondence should be addressed:** Galina A. Zhulai
Pushkinskaya, 11, Petrozavodsk, Russia; zhgali-111@yandex.ru

Received: 11.11.2025 **Accepted:** 12.12.2025 **Published online:** 21.12.2025

DOI: 10.24075/brsmu.2025.079

Copyright: © 2025 by the authors. **Licensee:** Pirogov University. This article is an open access article distributed under the terms and conditions of the Creative Commons Attribution (CC BY) license (https://creativecommons.org/licenses/by/4.0/).

ЭКСПРЕССИЯ ЭКТОНУКЛЕОТИДАЗ CD39 И CD73 В КРОВИ БОЛЬНЫХ РАЗНЫМИ ФОРМАМИ МЕТАБОЛИЧЕСКИ АССОЦИИРОВАННОЙ ЖИРОВОЙ БОЛЕЗНИ ПЕЧЕНИ

Г. А. Жулай[1]✉, И. В. Курбатова[1], О. П. Дуданова[1,2]

[1] Институт биологии, Карельский научный центр Российской академии наук, Петрозаводск, Россия

[2] Петрозаводский государственный университет, Петрозаводск, Россия

Экспериментальные исследования показали защитную роль экспрессии эктонуклеотидаз, в частности CD39 и CD73, в ограничении воспаления при патологии печени, но их экспрессия у больных метаболически ассоциированной жировой болезнью печени (МАЖБП) мало изучена. Целью работы было оценить уровни мРНК генов *ENTPD1* и *NT5E*, кодирующих CD39 и CD73 соответственно, у пациентов с разными формами МАЖБП: стеатозом печени (СП) и метаболически ассоциированным стеатогепатитом (МАСГ), а также оценить содержание CD39- и CD73-экспрессирующих клеток при активации иммунных клеток *in vitro*. Обследовали 29 здоровых доноров и 56 пациентов с МАЖБП. Проводили оценку уровня мРНК генов *ENTPD1* и *NT5E*, уровня провоспалительных цитокинов (ИЛ-6, ФНОα), уровня фрагментированного цитокератина-18 и содержания $CD39^+$ клеток в крови обследованных людей. Кроме того, оценивали влияние активации иммунных клеток на содержание $CD39^+$ и $CD73^+$-клеток у пациентов с МАСГ и здоровых доноров *in vitro*. Установлено, что экспрессия гена ENTPD1 ($p = 0{,}007$ при сравнении с контролем; $p = 0{,}010$ — с СП) и содержание $CD39^+$-клеток в популяции моноцитов ($p = 0{,}004$ — с контролем; $p = 0{,}003$ — с СП) и лимфоцитов ($p = 0{,}034$ — с контролем) снижены при МАСГ относительно групп контроля и СП. Показано, что активация клеток пациентов с МАСГ увеличивает уровень $CD39^+$-лимфоцитов, но не $CD14^+$-моноцитов, а $CD73^+$-клеток — среди лимфоцитов и $CD14^+$-моноцитов. Таким образом, представляется перспективным дальнейшее изучение CD39 и CD73 в механизмах прогрессирования МАЖБП.

Ключевые слова: метаболически ассоциированная жировая болезнь печени, метаболически ассоциированный стеатогепатит, CD39, CD73, $CD14^+$-моноциты, $CD4^+$ Т-клетки

Финансирование: работа выполнена при финансовой поддержке Российского научного фонда (грант № 25-25-00534) на научном оборудовании ЦКП КарНЦ РАН.

Вклад авторов: Г. А Жулай, И. В. Курбатова — планирование работы, сбор, обработка и анализ материала, статистическая обработка, написание текста; О. П. Дуданова — формирование клинических групп, анализ клинических данных, редактирование текста.

Соблюдение этических стандартов: исследование одобрено этическим комитетом Министерства здравоохранения Республики Карелия и Петрозаводского государственного университета (протокол № 48 от 10 марта 2023 г.). От участников исследования получено добровольное информированное согласие и согласие на обработку данных.

✉ **Для корреспонденции:** Галина Анатольевна Жулай
ул. Пушкинская, д. 11, г. Петрозаводск, Республика Карелия, Россия; zhgali-111@yandex.ru

Статья получена: 11.11.2025 **Статья принята к печати:** 12.12.2025 **Опубликована онлайн:** 21.12.2025

DOI: 10.24075/vrgmu.2025.079

Авторские права: © 2025 принадлежат авторам. **Лицензиат:** РНИМУ им. Н. И. Пирогова. Статья размещена в открытом доступе и распространяется на условиях лицензии Creative Commons Attribution (CC BY) (https://creativecommons.org/licenses/by/4.0/).

Metabolic-associated fatty liver disease (MAFLD) is a chronic, non-communicable, slowly progressing multifactorial disease that is extremely common in the world and in Russia in particular. In the recent reports, the prevalence of MAFLD among the adult population in Russia and worldwide is put at 29–35% [1, 2].

According to current concepts, the complex pathogenesis of MAFLD involves insulin resistance, impaired autophagy, lipotoxicity, inflammation, imbalances in cytokines and adipokines, activation of innate immunity and the microbiota, as well as environmental and genetic factors [3, 4]. Several clinical and morphological forms of MAFLD are distinguished according to the disease stage: steatosis, metabolic-associated steatohepatitis (MASH) with or without fibrosis, and liver cirrhosis (LC) [3]. Liver steatosis (LS) typically follows a benign clinical course, whereas MASH may have a progressive course and develop into LC and hepatocellular carcinoma. Early MASH is often asymptomatic for a long time, but ultimately, even with only minimal abnormalities in routine liver function tests, it can lead to several comorbidities — such as type 2 diabetes mellitus, hypertension, and chronic kidney disease — that adversely affect both the employability and quality of life of patients. At the same time, the mechanisms of progression of MAFLD remain poorly understood [4]. One of the key problems of modern gastroenterology is that of finding alternatives to liver biopsy to differentiate MASH from LS [5].

MAFLD involves a complex interaction among inflammation, apoptosis, and fibrosis, in which immune cells and cytokines are crucial mediators of these interconnected processes [6-8]. Many authors have convincingly demonstrated the relationship of fragmented cytokeratin-18 (FCK-18) with laboratory and histological signs of inflammation in MASH [9, 10].

Currently, one promising avenue for controlling inflammation is the study and therapeutic targeting of the ATP–adenosine balance. Extracellular ATP is released from the cell during necrosis, apoptosis, or hypoxia; it directs phagocytes to the inflammation loci, thus activating the inflammasome, which is followed by the release of pro-inflammatory cytokines. Extracellular adenosine then acts as a limiter of inflammation and tissue damage, exerting an anti-inflammatory effect [11]. The key enzymes in extracellular adenosine formation are ectonucleoside triphosphate diphosphohydrolase 1 (ENTPD1, also known as CD39), which hydrolyzes ATP and ADP to AMP, and ecto-5'-nucleotidase (NT5E, also known as CD73), which converts AMP to adenosine.

Accumulating evidence suggests that CD39 and CD73 play an important role in liver diseases [12–14]. In experimental models, the deletion of CD39 was shown to lead to insulin resistance and exacerbation of inflammation in the liver [15]. In another study, CD39 deficiency contributed to bile duct damage and fibrosis by attracting cytotoxic T cells [16]. Deficiency of the adenosine A2A receptor in both macrophages and hepatocytes was associated with increased severity of MAFLD, likely due to enhanced inflammation and lipogenesis [17]. By dephosphorylating ATP to adenosine, CD39 and CD73 ectonucleotidases play a protective role and prevent local and systemic inflammation. The significance of this mechanism in MAFLD has not been investigated. This study aimed to evaluate the mRNA levels of the *ENTPD1* and *NT5E* genes, which encode CD39 and CD73, respectively, in patients with different forms of MAFLD (LS, MASH), and to assess the expression of CD39- and CD73-positive cells following immune cell activation *in vitro*.

METHODS

We examined 56 patients with MAFLD: 31 with simple liver steatosis (LS group) and 25 with moderate to high activity MASH (MASH group). The control group consisted of 29 healthy people.

The inclusion criteria for the control group were a normal BMI, normal liver function test results, normal liver sonographic structure, and normal liver stiffness.

The exclusion criteria for the control group were the presence of cardiometabolic risk factors, a diagnosis of NAFLD, or the use of medications.

The exclusion criteria common to all study groups included infectious or inflammatory diseases within the past month, pregnancy or lactation, smoking, and alcohol consumption.

The inclusion criteria for the treatment group were an established diagnosis of NAFLD (LS or NASH), and presence of at least one cardiometabolic risk factor.

The criteria for exclusion of NAFLD patients were as follows: viral genesis of liver damage as proven by the absence of serological markers of HBV, HCV infection; autoimmune genesis, as proven by the absence of autoantibodies to hepatocyte structures; alcoholic genesis, as proven by anamnestic, clinical data, data from the CAGE, AUDIT scales; drug genesis, as proven by anamnestic data; diabetes mellitus types 1 and 2; liver cirrhosis; active course of hepatotropic or other therapy at the time of sampling the material for the study.

Healthy donors and MAFLD patients were examined by general practitioners at *RZD-medicine* clinical hospital (Petrozavodsk). The diagnosis of MAFLD, including determination of its form (LS or MASH), was established based on traditional clinical, laboratory, instrumental, and histological data in accordance with clinical guidelines [3]. All non-healthy participants (patients) had signs of metabolic syndrome and at least one cardiometabolic risk factor, most often — dyslipidemia (in 64% of LS and 93% of MASH patients) and visceral obesity (all patients, BMI > 25 kg/m^2). The patients underwent an ultrasound examination of the abdominal organs using a Vivid Pro-7 system (General Electric, USA), which revealed increased echogenicity of the liver tissue exceeding that of the right kidney. Liver stiffness was assessed by ARFI shear wave elastometry using a Mindray DC-80 device (Mindray, China). None of the patients showed signs of portal hypertension: there was no ascites, and esophagogastroscopy did not reveal esophageal or gastric varices. The patients underwent a blind percutaneous liver biopsy, and histological activity and fibrosis were assessed according to the method of Brunt et al. [18]. Based on these findings, the form of MAFLD was verified as either steatosis (≥5% of hepatocytes) without inflammation and hepatocellular ballooning, or as steatohepatitis characterized by active injury, including hepatocellular balloon degeneration and lobular inflammation (predominantly lymphocytic with some neutrophils), along with varying degrees of steatosis. According to the results of histological examination, fibrosis in all patients did not exceed stage F2.

For the study, fasting venous blood was drawn from the ulnar vein into K_2EDTA tubes. Clinical evaluation of liver function tests, isolation of peripheral blood leukocytes (PBLs) and plasma, as well as analysis of CD39-expressing cells, were performed within one hour after blood sampling. Blood plasma, total RNA isolated from PBLs, and peripheral blood mononuclear cells (PBMCs) obtained by Ficoll density gradient centrifugation (density = 1.077 g/cm^3; Biolot) were placed in a biobank for storage at –80 °C for no more than 3 months. The collection of samples took place after the patients had been admitted to the hospital but before therapy was prescribed, approximately 2–3 days prior to liver biopsy and elastography.

Assessment of liver function parameters — alanine aminotransferase (ALT), aspartate aminotransferase (AST), total

bilirubin, alkaline phosphatase (ALP), glucose, total cholesterol (TCH), high-density lipoprotein (HDL), triglycerides, and C-reactive protein (CRP) — was carried out using a Random Access F-15 analyzer (BioSystems, Spain) with reagents from Vector-Best (Russia). LDL levels were calculated using the Friedewald formula. The erythrocyte sedimentation rate (ESR) was determined by the Westergren method.

The ELISA method was used to determine the concentration of tissue polypeptide-specific antigen (hepatocyte apoptosis index FCK-18), tumor necrosis factor alpha (TNF) and interleukin-6 (IL-6) in blood plasma on a SuPerMax 3100 tablet multimodal reader (Flash Spectrum, China). The test systems used were TPS ELISA (Biotech, Sweden), Human TNFa Platinum ELISA (eBioscience, Austria), Interleukin-6 — IFA – Best (Vector-Best, Russia).

Total RNA from PBLs was isolated using ExtractRNA reagent (Eurogen, Russia). The relative expression level of the *ENTPD1* and *NT5E* genes in PBLs was assessed by real-time PCR using a LightCycler instrument (Roche, Germany) and the qPCRmix-HS SYBR kit (Eurogen, Russia) Primers for amplification of the *ENTPD1* gene are forward 5'-AGCAGCTGAAATATGCTGGC-3', reverse 5'-GAGACAGTATCTGCCGAAGTCC-3'; for the *NT5E* gene, forward 5'- ATTGCAAAGTGGTTCAAAGTCA-3', reverse 5'-ACTTGGCCAGTAAAATAGGG-3'. The *18S rRNA* gene was used as a reference, with forward primer 5'-AGAAACGGCTACCACATCCA-3' and reverse primer 5'-CACCAGACTTGCCCTCCA-3'. The PCR conditions were as follows: cDNA denaturation for 5 min 95 °C; 40 cycles: denaturation at 95 °C for 30 seconds, annealing at 64 °C for 30 seconds, elongation at 72 °C for 30 seconds. The specificity of the amplification products was verified by melting curve analysis. Each PCR analysis was performed in triplicate to assess repeatability. The relative level of transcripts was assessed by Livak and Schmittgen [19].

The relative cell content of the studied populations was determined using a Cytomics FC500 flow cytometer (Beckman Coulter, USA). Blood samples or cell suspensions were stained with FITC-, PE-, PerCP, and PE-Cy7–labeled monoclonal antibodies against CD39, CD4, CD25, CD161, and CD14 antigens, as well as with appropriate isotypic controls (Sony Biotechnology, USA; eBioscience, USA). The erythrocytes were lysed with the FACS Lysing Solution reagent (BD Biosciences, USA). FMO (fluorochrome minus one) control was used to identify CD39- and CD73-expressing cells. The absolute number of cells was determined based on the data of a clinical blood test.

To assess the effect of activation on the proportions of $CD39^+$ and $CD73^+$ cells, PBMCs isolated from MASH patients ($n = 6$) and healthy donors ($n = 6$) were seeded in 48-well plates (3.5×10^5 cells per well) in RPMI-1640 medium (Servicebio) supplemented with 10% heat-inactivated ETS (Biolot), 2 mM L-glutamine, 100 U/ml penicillin, and 100 µg/ml streptomycin (Servicebio). The cultures were incubated at 37°C in a humidified atmosphere containing 5% CO_2 for 24 hours. The cells were activated with classical stimulants: lymphocytes with PHA at a final concentration of 10 µg/ml (Biolot), and monocytes with LPS (Pyrogenal, MEDGAMAL of N. F. Gamaleya National Center of Epidemiology and Microbiology) at a concentration of 1 µg/ml.

Statistical analysis was performed using GraphPad Prism v.8 (GraphPad Software Inc.; San Diego, CA, USA). The data on the graphs are given as Me (Q_1–Q_3). The differences were considered significant at $p < 0.05$. Due to non-normal distributions of indicators in the groups (confirmed by the Shapiro-Wilk test), nonparametric tests were used for analysis. To compare the studied indicators across groups, we used the Kruskal–Wallis test, and for pairwise comparisons, the Mann–Whitney *U* test. A paired comparison of related indicators was performed using the Wilcoxon signed-rank test. The relationship of the indicators was assessed by calculating the Spearman's rank correlation coefficient (*r*). The strength of the correlation between the two variables was evaluated using the Chaddock scale.

RESULTS

Table 1 shows the clinical and laboratory characteristics of patients with LS, MASH, and healthy participants. In MASH patients, compared with LS patients, blood aminotransferase activity, clinical markers of inflammation (CRP, ESR), LDL levels, and FCK-18 concentrations were increased (Tables 1 and 2). The blood plasma levels of the main pro-inflammatory cytokines (TNF-α and IL-6) in patients with MAFLD were higher than in healthy controls and similar between subgroups with different forms of the disease (Table 2).

We performed a comparative analysis of the mRNA expression levels of the *ENTPD1* gene (which encodes CD39) and the *NT5E* gene (which encodes CD73) in PBLs obtained from patients with MAFLD and healthy donors. As shown by the Kruskal–Wallis ANOVA, the study groups differ significantly in the mRNA levels of *ENTPD1* ($H = 8.830$, $p = 0.012$), but not in the mRNA levels of *NT5E* ($H = 0.618$, $p = 0.734$) (Fig. 1). It has been established that the expression level of the *ENTPD1* gene in MASH patients is lower than in healthy people and LS patients. At the same time, the mRNA level of the *ENTPD1* gene does not differ from the control in LS (Fig. 1A).

Since we found that *ENTPD1* expression differed significantly between the study groups, the next step was to perform a correlation analysis of *ENTPD1* mRNA levels in MAFLD patients and healthy donors with blood biochemical parameters, including routine clinical indicators, FCK-18 concentrations, and the pro-inflammatory cytokines TNFα and IL-6 (Tables 1 and 2). This analysis revealed a moderate positive correlation between the relative mRNA expression level of *ENTPD1* and the blood LDL level in LS patients ($r = 0.379$, $p = 0.039$).

As shown in Table 1, the blood levels of lymphocytes and monocytes did not differ between the MAFLD groups and the control group. However, the data obtained earlier in this study (Fig. 1) necessitated the evaluation of CD39 ectonucleotidase expression on PBLs in MAFLD patients. This enzyme is known to be expressed on the surface of various immune cells [20]. We therefore assessed the frequency of $CD39^+$ granulocytes, monocytes, and lymphocytes. Among lymphocytes, the focus was on the proportion of $CD39^+$ T cells within the $CD4^+$ T helper population as a whole, as well as within its subpopulations — immunosuppressive Treg cells ($CD4^+CD25^{hi}$) and pro-inflammatory Th17 cells ($CD4^+CD161^+$). The data is presented in Table 3 and Fig. 2.

We found that the relative content of $CD39^+$ monocytes in the MASH group was significantly reduced compared with the control and with the LS group (Table 3, Fig. 2). The granulocytes from both MAFLD patients and healthy donors were almost all CD39- positive (Table 3). In MASH patients, we also observed a reduced relative and absolute count of $CD39^+$ lymphocytes compared with controls (Table 3). The content of $CD39^+$ Treg cells was higher in the MASH group compared to healthy donors (Fig. 2). A noteworthy fact: the count of Treg cells themselves in LS and MASH patients ($p = 0.007$ and $p = 0.013$, respectively) was lower than in the control group.

To determine whether the expression of the ectonucleotidases CD39 and CD73 on monocytes and lymphocytes from MASH

Table 1. Clinical and laboratory characteristics of the study groups

Indicator	Control (*n* = 29)	LS (*n* = 31)	MASH (*n* = 25)
Age, years	43.72 ± 1.12 (44.81)	48.43 ± 1.63 (48.10)	46.29 ± 2.27 (47.50)
Male/Female (*n*)	14/15	15/16	12/13
ALT, units/l	16.04 ± 1.25 (14.76)	23.16 ± 1.74 (21.90)	116.80 ± 27.67 (84.85)*#
AST, units/l	20.60 ± 0.86 (20.35)	23.92 ± 0.90 (23.90)	75.01 ± 8.48 (65.95)*#
Total bilirubin, mmol/l	15.14 ± 2.20 (12.20)	15.40 ± 1.38 (13.30)	16.85 ± 2.23 (15.92)*
ALP, units/l	96.37 ± 11.12 (83.20)	141.24 ± 16.17 (143.21)*	173.21 ± 16.54 (165.43)*
CRP, mg/l	1.06 ± 0.17 (0.95)	1.18 ± 0.40 (1.25)	4.87 ± 0.11 (4.87)*#
ESR, mm/h	8.65 ± 1.94 (6.00)	10.87 ± 2.06 (7.00)	17.38 ± 4.77 (12.00)*#
Glucose, mmol/l	5.12 ± 0.07 (5.02)	5.20 ± 0.10 (5.20)	5.31 ± 0.11 (5.28)
TC, mmol/l	5.04 ± 0.16 (4.96)	5.09 ± 0.19 (5.03)	5.56 ± 0.22 (5.60)*
HDL, mmol/l	1.40 ± 0.06 (1.30)	1.36 ± 0.13 (1.11)	1.22 ± 0.12 (1.03)
LDL, mmol/l	3.01 ± 0.18 (2.56)	2.74 ± 0.15 (2.68)	3.81 ± 0.24 (3.80)*#
Triglycerides, mmol/l	1.22 ± 0.12 (1.09)	1.81 ± 0.19 (1.55)	1.91 ± 0.14 (1.94)*
BMI, kg/m^2	23.88 ± 1.10 (23.77)	33.81 ± 0.78 (33.10)*	34.40 ± 1.13 (34.25)*
Lymphocytes, %	33.33 ± 0.99 (33.00)	31.36 ± 1.34 (31.00)	32.09 ± 1.1 (31.07)
Lymphocytes, ×10^9/l	2.11 ± 0.10 (2.23)	2.09 ± 0.12 (1.92)	1.91 ± 2.17 (0.14)
Monocytes, %	7.06 ± 0.35 (6.80)	7.63 ± 0.44 (7.35)	7.68 ± 0.46 (7.55)
Monocytes, ×10^9/l	0.44 ± 0.03 (0.41)	0.51 ± 0.03 (0.46)	0.50 ± 0.01 (0.45)

Note: the data are presented as M ± *m*, median in parentheses; * — significant difference from the control group, # — significant difference from the LS group (Mann–Whitney *U*–test with Bonferroni correction).

patients was associated with cellular activation, their cells and those from healthy donors (controls) were stimulated and analyzed by flow cytometry after 24 hours. We assessed the expression levels of CD39- and CD73-positive cells within lymphocyte gates, CD4$^+$ T cells, and CD14$^+$ monocytes. In addition, the median fluorescence intensity (MFI) for CD39 and CD73 was determined, which reflects the density of antigen expression on cells. Fig. 3 shows the results.

It is known that the activation of lymphocytes, particularly T cells, is usually accompanied by an increase in CD39 enzymatic activity and in the number of CD39$^+$ cells [21]. In our study, we observed an increase in the number of CD39$^+$ cells in lymphocyte cultures — particularly among CD4$^+$ T cells — following the addition of a mitogen in the control and MASH groups. (Fig. 3A). Changes in CD39 MFI were noted only in the lymphocyte gate, in both of these groups (Fig. 3B). The presence of LPS had no effect on the content of CD14$^+$CD39$^+$ monocytes (Fig. 3A).

The analysis of CD73$^+$ cell numbers after activation of PBMCs from patients with MASH and healthy donors (Fig. 3B) revealed significant differences. Upon stimulation, the proportion of CD73$^+$ lymphocytes and CD14$^+$ monocytes increased in MASH patients, whereas in healthy donors, significant changes in CD73$^+$ cell numbers were observed only among CD4$^+$ T cells. Both MASH patients and healthy donors showed an increase in CD73 MFI within the lymphocyte gate after activation (Fig. 3G).

DISCUSSION

The progression of hepatocellular dysfunction in MAFLD results from immuno-inflammatory processes, in which leukocytes play a central role [6, 8]. It is known that CD39 and CD73 ectonucleotidases are expressed on the surface of various immune cells in peripheral blood. In addition, enzyme expression can start from exposure to oxidative stress and hypoxia, as well as pro-inflammatory cytokines [22]. The levels of ectonucleotidases, determined mainly using experimental models, have been described in certain acute and chronic liver pathologies [22]. However, the expression of CD39 and CD73 in the blood of MAFLD patients and on individual populations of immune cells has not been investigated. Therefore, we conducted a comparative assessment of ectonucleotidase expression at both the mRNA level and on the surface of PBLs in patients with different forms of MAFLD (LS and MASH).

We discovered that in a simple LS case, the mRNA ENTPD1 levels of and the count of the enzyme on the surface of the PBLs are similar to those seen in the control group. In MASH cases, CD39 expression — both at the mRNA level in PBLs and at the protein level on the surface of monocytes — is significantly lower than in LS cases and in samples from healthy donors (Fig. 1, Fig. 2, Table 3). In addition, it was found that the number of CD39$^+$ cells changes among monocytes as well as Treg cells in MASH patients. We observed a higher proportion of CD39$^+$ cells among Treg cells in patients with MASH compared with the control group, although the overall number of Treg cells

Table 2. Cytokine content and FCK-18 levels in the blood plasma of patients with MAFLD and healthy donors

Indicator	Control (*n* = 29)	LS (*n* = 31)	MASH (*n* = 25)
FCK-18, units/l	80.36 ± 10.06 (83.80)	130.60 ± 13.83 (129.00)*	423.90 ± 84.60 (269.70)*#
TNFα, pg/ml	4.01 ± 0.35 (3.58)	5.86 ± 0.33 (5.89)*	6.50 ± 0.35 (6.67)*
IL-6, pg/ml	1.79 ± 0.18 (1.75)	5.31 ± 0.88 (4.25)*	6.89 ± 1.28 (6.71)*

Note: the data are presented as M ± *m*, median in parentheses; * — significant difference from the control group, # — significant difference from the LS group (Mann–Whitney *U* test with Bonferroni correction).

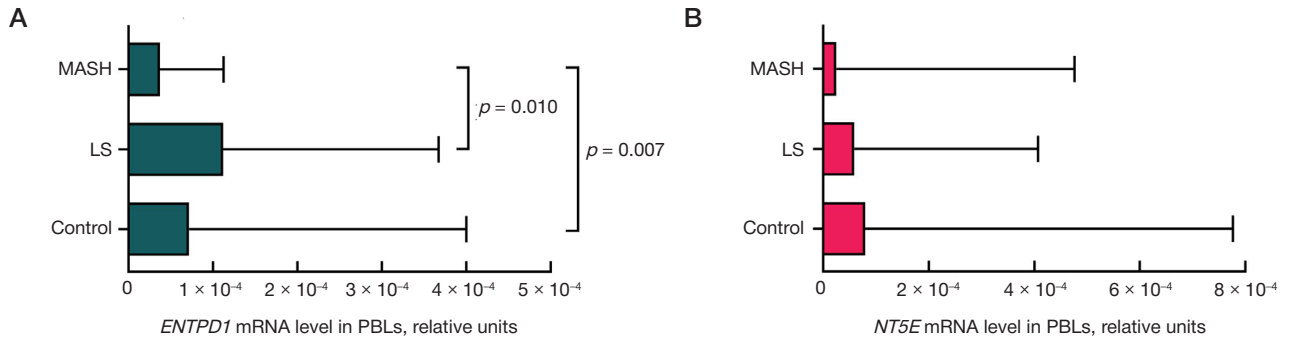


Fig. 1. The mRNA levels of *ENTPD1* (**A**) and *NT5E* (**B**) in the PBLs of MAFLD patients and healthy donors, Me and interquartile range; the differences are significant according to the Mann-Whitney *U* test with Bonferroni correction.

Table 3. Relative and absolute levels of CD39-expressing cells in blood cell populations of patients with MAFLD and healthy donors

	Control	LS	MASH
Lymphocytes CD39⁺ cells, % CD39⁺ cells, x10⁹/l	 12.40 (11.05–14.78) 0.33 (0.26–0.42)	 11.25 (9.84–12.59) 0.24 (0.18–0.30)	 10.65 (9.85–12.10)* 0.20 (0.19–0.30)*
Monocytes CD39⁺ cells, % CD39⁺ cells, x10⁹/l	 80.17 (70.98–88.41) 0.37 (0.31–0.49)	 76.95 (68.88–81.54) 0.35 (0.28–0.40)	 61.46 (53.64–71.94)*# 0.33 (0.24–0.41)
Granulocytes CD39⁺ cells, %	 94.65 (90.68–97.14)	 95.65 (92.49–97.90)	 94.65 (90.68–94.65)

Note: the data are given as Me (Q_1–Q_3). * — significant difference from the control group, # — significant difference from the LS group (Mann–Whitney *U* test with Bonferroni correction). Cell populations were isolated using forward scatter (FSC/FS) and side scatter (SSC/SS).

in these patients was reduced. It is likely that the increased CD39 expression on the surface of these cells is associated with compensation for their low number, since the generation of extracellular adenosine through CD39 production is one of the main mechanisms of Treg-associated immunosuppression [20]. Moreover, their concentrations in the blood of patients with MASH are insufficient to modulate pro-inflammatory cell function.

In addition, we have shown that, upon in vitro activation, the level of CD14⁺CD39⁺ monocytes in MASH patients remains lower than that observed in healthy donors (Fig. 3). It is noted in the literature that low CD39 expression on monocytes may be a poor prognostic sign. For example, a reduced CD39⁺ monocyte count is described as a potential diagnostic biomarker and predictor of an unfavorable prognosis in patients with sepsis [23].

A decrease in CD39 expression in MASH cases can lead to reduced extracellular degradation of ATP and ADP, resulting in lower levels of anti-inflammatory adenosine, which may contribute to the progression of inflammation and insulin resistance. This assumption is supported by data on the pathological effect of ENTPD1/CD39 deficiency on these processes in liver damage [15, 16].

A study of CD39 activity in the platelets of patients with hypercholesterolemia [21] showed that hypercholesterolemia, including elevated LDL levels, is associated with an increased inflammatory response, oxidative stress, and enhanced hydrolysis of ATP and ADP. The authors attributed the increase in CD39 activity to a compensatory response to the inflammatory and pro-oxidant conditions associated with hypercholesterolemia [24]. Interestingly, in cases of LS — the early stage of MAFLD characterized by lipid accumulation in hepatocytes and low-level subclinical inflammation — we did not observe a decrease in CD39 expression in peripheral blood compared with the control group. However, we found a moderate positive correlation between *ENTPD1* gene mRNA

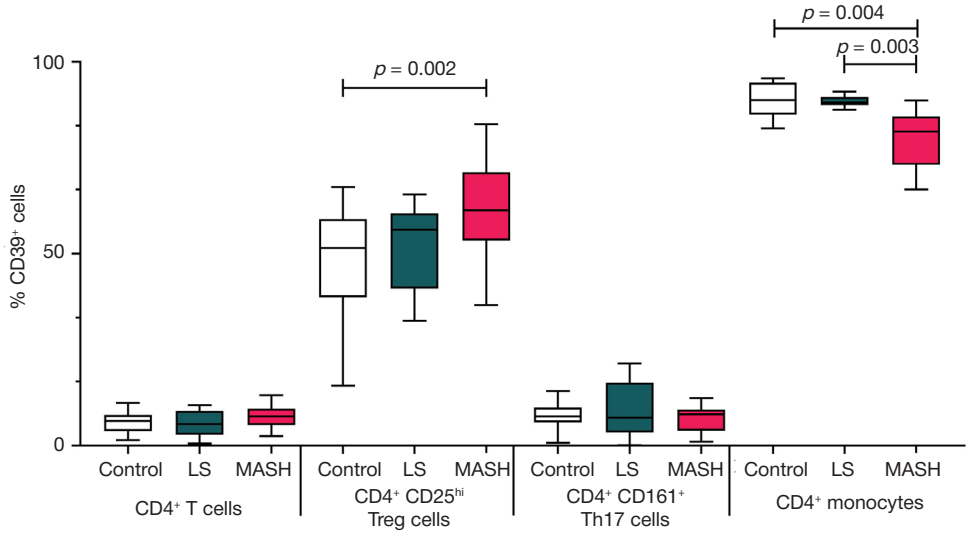


Fig. 2. Relative levels of CD39-expressing cells in blood cell populations of patients with MAFLD and healthy donors. Me, interquartile range, minimum and maximum values

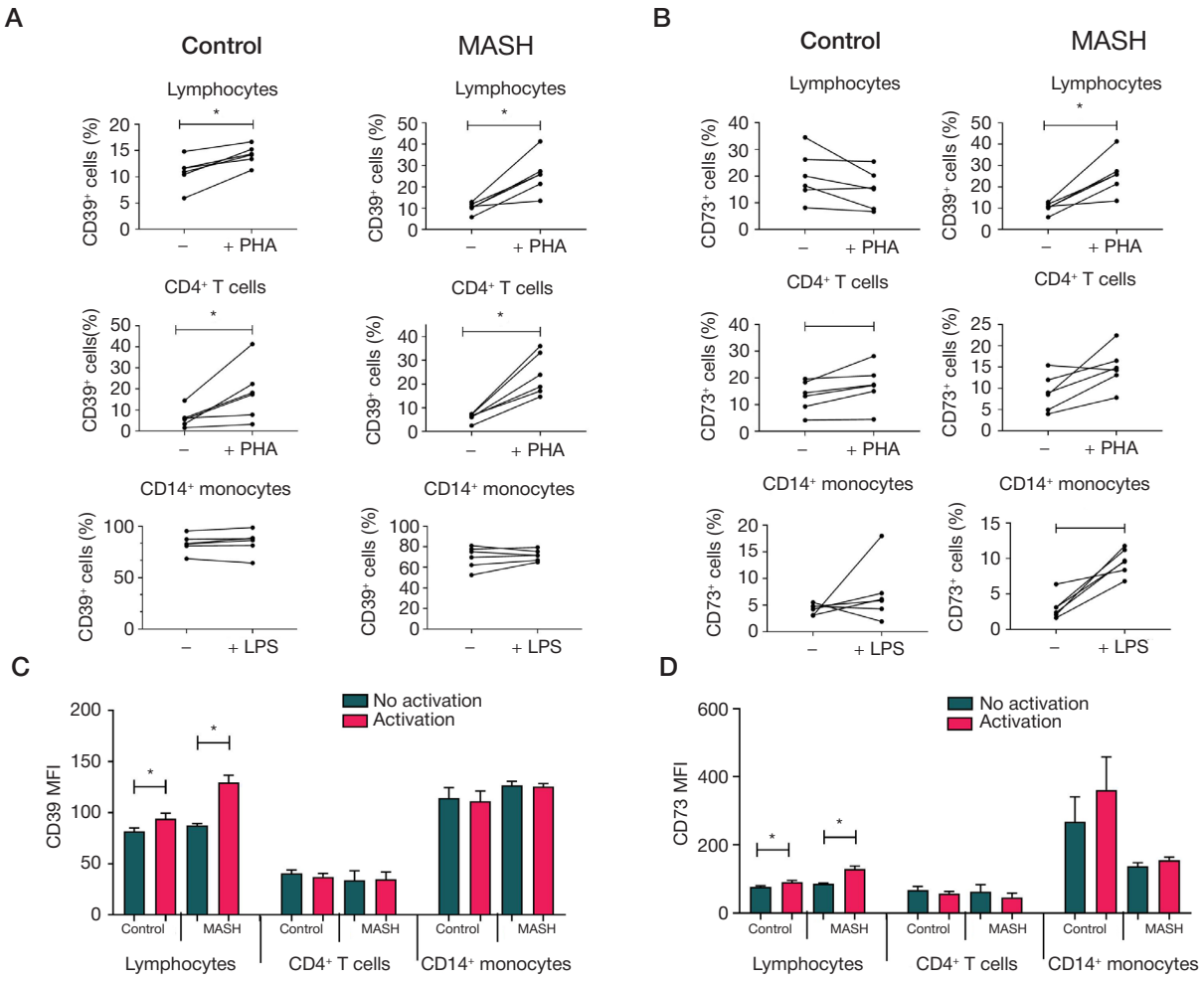


Fig. 3. Changes in the content of cells expressing CD39 and CD73 ectonucleotidases after activation in healthy donors (n = 6) and patients with MASH (n = 6). **A**. The content of CD39⁺ cells, % of the studied population. **B**. The content of CD73⁺ cells, % of the studied population. **C**. MFI of CD39 expression on activated vs. unactivated cells. **D**. MFI of CD73 expression on activated vs. unactivated cells. The data are presented as M ± SE, * — significant differences from inactive cells (Wilcoxon T test)

levels and LDL levels. Previously, evidence of a link between cholesterol metabolism and CD39 activity was identified. *In vitro*, it has been shown that a decrease in the level of cholesterol in the cell membrane leads to inhibition of the enzymatic and antiplatelet activity of CD39, and treatment of membranes with cholesterol completely restores the function of the enzyme [25]. However, unlike in LS patients, no correlation was detected between *ENTPD1* gene mRNA levels and blood lipid concentration in patients with MASH, likely due to severe inflammation and altered lipid status. Nevertheless, a decrease in CD39 expression in peripheral blood was observed relative to both the control group and LS patients. Probably, in MASH, progressive inflammation disrupts compensatory mechanisms that support the dephosphorylation of ATP to adenosine in liver damage. Changes in CD39 ectonucleotidase expression can also be detected for other immune cell populations; this work did not consider B cells that predominantly express CD39 among lymphocytes, as well as NK cells and CD8⁺ T cells.

CONCLUSIONS

Thus, in patients with MASH, the levels of inflammatory indicators (ESR, CRP, IL-6, and TNF-α) are higher than in healthy donors. Along with this, this study as shown that in MASH, the expression of CD39 ectonucleotidase is reduced both at the mRNA level in PBLs and at the enzyme level on the surface of monocytes and lymphocytes. The lack of the enzyme on the surface of immune cells can lead to the accumulation of extracellular ATP and thus support the process of inflammation. Based on the data obtained, it seems promising to further investigate CD39 ectonucleotidase as a diagnostic and prognostic marker in MAFLD.

References

1. Younossi ZM, Golabi P, Paik JM, Henry A, Van Dongen C, Henry L. The global epidemiology of nonalcoholic fatty liver disease (NAFLD) and nonalcoholic steatohepatitis (NASH): a systematic review. Hepatology. 2023; 77 (4): 1335–47. DOI: 10.1097/HEP.0000000000000004.
2. Maev IV, Andreev DN, Kucheryavyj YuA. Rasprostranennost' nealkogol'noj zhirovoj bolezni pecheni v Rossii: meta-analiz. Consilium Medicum. 2023; 25 (5): 313–9. DOI: 10.26442/20751753.2023.5.202155. Russian.
3. Ivashkin VT, Drapkina OM, Maevskaya MV, Rajhelson KL, Okovityj SV, Zharkova MS, i dr. Klinicheskie rekomendacii Rossijskogo obshchestva po izucheniyu pecheni, Rossijskoj gastroenterologicheskoj associacii, Rossijskogo obshchestva profilaktiki neinfekcionnyh zabolevanij,

Rossijskoj associacii endokrinologov, Rossijskogo nauchnogo medicinskogo obshchestva terapevtov, Nacional'nogo obshchestva profilakticheskoj kardiologii, Rossijskoj associacii gerontologov i geriatrov po nealkogol'noj zhirovoj bolezni pecheni. Rossijskij zhurnal gastroenterologii, gepatologii, koloproktologii. 2025; 35 (1): 94–152. DOI: 10.22416/1382-4376-2025-35-1-94-152. Russian.
4. Loomba R, Friedman SL, Shulman GI. Mechanisms and disease consequences of nonalcoholic fatty liver disease. Cell. 2021; 184 (10): 2537–64. DOI: 10.1016/j.cell.2021.04.015.
5. Di Mauro S, Scamporrino A, Filippello A, Di Pino A, Scicali R, Malaguarnera R, et al. Clinical and molecular biomarkers for diagnosis and staging of NAFLD. Int J Mol Sci. 2021; 22 (21): 11905. DOI: 10.3390/ijms222111905.
6. Peiseler M, Schwabe R, Hampe J, Kubes P, Heikenwälder M, Tacke F. Immune mechanisms linking metabolic injury to inflammation and fibrosis in fatty liver disease — novel insights into cellular communication circuits. J Hepatol. 2022; 77 (4): 1136–60. DOI: 10.1016/j.jhep.2022.06.012.
7. Kurbatova IV, Topchieva LV, Dudanova OP, Shipovskaya AA. The role of the soluble interleukin-6 receptor in the progression of nonalcoholic fatty liver disease. Bull Exp Biol Med. 2023; 174 (5): 628–33. DOI: 10.1007/s10517-023-05759-5.
8. Topchieva LV, Kurbatova IV, Dudanova OP, Vasileva AV, Zhulai GA. Immune cell balance as potential biomarker of progressing non-alcoholic fatty liver disease. Genes & Cells. 2024; 19 (1): 105–25. DOI: 10.17816/gc610252.
9. Shipovskaya AA, Dudanova OP, Kurbatova IV. Inflammatory cytokines, soluble interleukin-6 receptors, and fragmented cytokeratin-18 as indicators of non-alcoholic steatohepatitis. Ter Arkh. 2025; 97 (2): 115–20. DOI: 10.26442/00403660.2025.02.203123.
10. Eguchi A, Iwasa M, Yamada M, Tamai Y, Shigefuku R, Hasegawa H, et al. A new detection system for serum fragmented cytokeratin 18 as biomarker reflecting histological activities of human nonalcoholic steatohepatitis. Hepatol Commun. 2022; 6 (8): 1987–99. DOI: 10.1002/hep4.1971.
11. Pasquini S, Contri C, Borea PA, Vincenzi F, Varani K. Adenosine and Inflammation: Here, There and Everywhere. Int J Mol Sci. 2021; 22: 7685. DOI: 10.3390/ijms22147685.
12. Jain S, Jacobson KA. Purinergic signaling in liver pathophysiology. Front Endocrinol (Lausanne). 2021; 12: 718429. DOI: 10.3389/fendo.2021.718429.
13. Snider NT, Griggs NW, Singla A, Moons DS, Weerasinghe SV, Lok AS, et al. CD73 (ecto-5'-nucleotidase) hepatocyte levels differ across mouse strains and contribute to mallory-denk body formation. Hepatology. 2013; 58 (5): 1790–800. DOI: 10.1002/hep.26525.
14. Wang S, Gao S, Zhou D, Qian X, Luan J, Lv X. The role of the CD39-CD73-adenosine pathway in liver disease. J Cell Physiol. 2021; 236 (2): 851–62. DOI: 10.1002/jcp.29932.
15. Sun X, Imai M, Nowak-Machen M, Guckelberger O, Enjyoji K, Wu Y, et al. Liver damage and systemic inflammatory responses are exacerbated by the genetic deletion of CD39 in total hepatic ischemia. Purinergic Signal. 2011; 7 (4): 427–34. DOI: 10.1007/s11302-011-9239-6.
16. Peng ZW, Rothweiler S, Wei G, Ikenaga N, Liu SB, Sverdlov DY, et al. The ectonucleotidase ENTPD1/CD39 limits biliary injury and fibrosis in mouse models of sclerosing cholangitis. Hepatol Commun. 2017; 1 (9): 957–72. DOI: 10.1002/hep4.1084.
17. Cai Y, Li H, Liu M, Qian X, Luan J, Lv, X. Disruption of adenosine 2A receptor exacerbates NAFLD through increasing inflammatory responses and SREBP1c activity. Hepatology. 2018; 68 (1): 48–61. DOI:10.1002/jcp.29932.
18. Brunt EM, Janney CG, Di Bisceglie AM, Neuschwander-Tetri BA, Bacon BR. Nonalcoholic steatohepatitis: a proposal for grading and staging the histological lesions. Am J Gastroenterol. 1999; 94 (9): 2467–74. DOI: 10.1111/j.1572-0241.1999.01377.x.
19. Livak KJ, Schmittgen TD. Analysis of relative gene expression data using Real-Time quantitative PCR and the 2–ΔΔCT method. Methods. 2001. 25 (4): 402–8. DOI: 10.1006/meth.2001.1262.
20. Timperi E, Barnaba V. CD39 Regulation and Functions in T Cells. International Journal of Molecular Sciences. 2021; 22 (15): 8068. DOI: 10.3390/ijms22158068.
21. Pulte ED, Broekman MJ, Olson KE, Drosopoulos JH, Kizer JR, Islam N, et al. CD39/NTPDase-1 activity and expression in normal leukocytes. Thrombosis research. 2007; 121 (3): 309–17. DOI: 10.1016/j.thromres.2007.04.008.
22. Vuerich M, Robson SC, Longhi MS. Ectonucleotidases in intestinal and hepatic inflammation. Front Immunol. 2019; 10: 507. DOI: 10.3389/fimmu.2019.00507.
23. Li H, Ding P, Nan Y, Wu Z, Hua N, Luo L, et al. Low expression of CD39 on monocytes predicts poor survival in sepsis patients. J intensive care. 2025; 13: 12. DOI: 10.1186/s40560-025-00784-0.
24. Duarte MM, Loro VL, Rocha JB, Leal DB, Bem AF, Dorneles A, et al. Enzymes that hydrolyze adenine nucleotides of patients with hypercholesterolemia and inflammatory processes. FEBS J. 2007; 274 (11): 2707–14. DOI: 10.1111/j.1742-4658.2007.05805.x.
25. Papanikolaou A, Papafotika A, Murphy C, Papamarcaki T, Tsolas O, Drab M, et al. Cholesterol-dependent lipid assemblies regulate the activity of the ecto-nucleotidase CD39. J Biol Chem. 2005; 280 (28): 26406–14. DOI: 10.1074/jbc.M413927200014.

Литература

1. Younossi ZM, Golabi P, Paik JM, Henry A, Van Dongen C, Henry L. The global epidemiology of nonalcoholic fatty liver disease (NAFLD) and nonalcoholic steatohepatitis (NASH): a systematic review. Hepatology. 2023; 77 (4): 1335–47. DOI: 10.1097/HEP.0000000000000004.
2. Маев И. В., Андреев Д. Н., Кучерявый Ю. А. Распространенность неалкогольной жировой болезни печени в России: мета-анализ. Consilium Medicum. 2023; 25 (5): 313–9. DOI: 10.26442/20751753.2023.5.202155.
3. Ивашкин В. Т., Драпкина О. М., Маевская М. В., Райхельсон К. Л., Оковитый С. В., Жаркова М. С. и др. Клинические рекомендации Российского общества по изучению печени, Российской гастроэнтерологической ассоциации, Российского общества профилактики неинфекционных заболеваний, Российской ассоциации эндокринологов, Российского научного медицинского общества терапевтов, Национального общества профилактической кардиологии, Российской ассоциации геронтологов и гериатров по неалкогольной жировой болезни печени. Российский журнал гастроэнтерологии, гепатологии, колопроктологии. 2025; 35 (1): 94–152. DOI: 10.22416/1382-4376-2025-35-1-94-152.
4. Loomba R, Friedman SL, Shulman GI. Mechanisms and disease consequences of nonalcoholic fatty liver disease. Cell. 2021; 184 (10): 2537–64. DOI: 10.1016/j.cell.2021.04.015.
5. Di Mauro S, Scamporrino A, Filippello A, Di Pino A, Scicali R, Malaguarnera R, et al. Clinical and molecular biomarkers for diagnosis and staging of NAFLD. Int J Mol Sci. 2021; 22 (21): 11905. DOI: 10.3390/ijms222111905.
6. Peiseler M, Schwabe R, Hampe J, Kubes P, Heikenwälder M, Tacke F. Immune mechanisms linking metabolic injury to inflammation and fibrosis in fatty liver disease — novel insights into cellular communication circuits. J Hepatol. 2022; 77 (4): 1136–60. DOI: 10.1016/j.jhep.2022.06.012.
7. Kurbatova IV, Topchieva LV, Dudanova OP, Shipovskaya AA. The role of the soluble interleukin-6 receptor in the progression of nonalcoholic fatty liver disease. Bull Exp Biol Med. 2023; 174 (5): 628–33. DOI: 10.1007/s10517-023-05759-5.
8. Topchieva LV, Kurbatova IV, Dudanova OP, Vasileva AV, Zhulai GA. Immune cell balance as potential biomarker of progressing non-alcoholic fatty liver disease. Genes & Cells. 2024; 19 (1): 105–25. DOI: 10.17816/gc610252.
9. Shipovskaya AA, Dudanova OP, Kurbatova IV. Inflammatory cytokines, soluble interleukin-6 receptors, and fragmented cytokeratin-18 as indicators of non-alcoholic steatohepatitis. Ter Arkh. 2025; 97 (2): 115–20. DOI: 10.26442/00403660.2025.02.203123.
10. Eguchi A, Iwasa M, Yamada M, Tamai Y, Shigefuku R, Hasegawa H, et al. A new detection system for serum fragmented cytokeratin 18 as

biomarker reflecting histological activities of human nonalcoholic steatohepatitis. Hepatol Commun. 2022; 6 (8): 1987–99. DOI: 10.1002/hep4.1971.
11. Pasquini S, Contri C, Borea PA, Vincenzi F, Varani K. Adenosine and Inflammation: Here, There and Everywhere. Int J Mol Sci. 2021; 22: 7685. DOI: 10.3390/ijms22147685.
12. Jain S, Jacobson KA. Purinergic signaling in liver pathophysiology. Front Endocrinol (Lausanne). 2021; 12: 718429. DOI: 10.3389/fendo.2021.718429.
13. Snider NT, Griggs NW, Singla A, Moons DS, Weerasinghe SV, Lok AS, et al. CD73 (ecto-5'-nucleotidase) hepatocyte levels differ across mouse strains and contribute to mallory-denk body formation. Hepatology. 2013; 58 (5): 1790–800. DOI: 10.1002/hep.26525.
14. Wang S, Gao S, Zhou D, Qian X, Luan J, Lv X. The role of the CD39-CD73-adenosine pathway in liver disease. J Cell Physiol. 2021; 236 (2): 851–62. DOI: 10.1002/jcp.29932.
15. Sun X, Imai M, Nowak-Machen M, Guckelberger O, Enjyoji K, Wu Y, et al. Liver damage and systemic inflammatory responses are exacerbated by the genetic deletion of CD39 in total hepatic ischemia. Purinergic Signal. 2011; 7 (4): 427–34. DOI: 10.1007/s11302-011-9239-6.
16. Peng ZW, Rothweiler S, Wei G, Ikenaga N, Liu SB, Sverdlov DY, et al. The ectonucleotidase ENTPD1/CD39 limits biliary injury and fibrosis in mouse models of sclerosing cholangitis. Hepatol Commun. 2017; 1 (9): 957–72. DOI: 10.1002/hep4.1084.
17. Cai Y, Li H, Liu M, Qian X, Luan J, Lv, X. Disruption of adenosine 2A receptor exacerbates NAFLD through increasing inflammatory responses and SREBP1c activity. Hepatology. 2018; 68 (1): 48–61. DOI:10.1002/jcp.29932.
18. Brunt EM, Janney CG, Di Bisceglie AM, Neuschwander-Tetri BA, Bacon BR. Nonalcoholic steatohepatitis: a proposal for grading and staging the histological lesions. Am J Gastroenterol. 1999; 94 (9): 2467–74. DOI: 10.1111/j.1572-0241.1999.01377.x.
19. Livak KJ, Schmittgen TD. Analysis of relative gene expression data using Real-Time quantitative PCR and the 2–ΔΔCT method. Methods. 2001. 25 (4): 402–8. DOI: 10.1006/meth.2001.1262.
20. Timperi E, Barnaba V. CD39 Regulation and Functions in T Cells. International Journal of Molecular Sciences. 2021; 22 (15): 8068. DOI: 10.3390/ijms22158068.
21. Pulte ED, Broekman MJ, Olson KE, Drosopoulos JH, Kizer JR, Islam N, et al. CD39/NTPDase-1 activity and expression in normal leukocytes. Thrombosis research. 2007; 121 (3): 309–17. DOI: 10.1016/j.thromres.2007.04.008.
22. Vuerich M, Robson SC, Longhi MS. Ectonucleotidases in intestinal and hepatic inflammation. Front Immunol. 2019; 10: 507. DOI: 10.3389/fimmu.2019.00507.
23. Li H, Ding P, Nan Y, Wu Z, Hua N, Luo L, et al. Low expression of CD39 on monocytes predicts poor survival in sepsis patients. J intensive care. 2025; 13: 12. DOI: 10.1186/s40560-025-00784-0.
24. Duarte MM, Loro VL, Rocha JB, Leal DB, Bem AF, Dorneles A, et al. Enzymes that hydrolyze adenine nucleotides of patients with hypercholesterolemia and inflammatory processes. FEBS J. 2007; 274 (11): 2707–14. DOI: 10.1111/j.1742-4658.2007.05805.x.
25. Papanikolaou A, Papafotika A, Murphy C, Papamarcaki T, Tsolas O, Drab M, et al. Cholesterol-dependent lipid assemblies regulate the activity of the ecto-nucleotidase CD39. J Biol Chem. 2005; 280 (28): 26406–14. DOI: 10.1074/jbc.M41392720014.

ANTIVIRAL ACTIVITY OF mRNAS ENCODING INTRACELLULAR SCFV ANTIBODIES AGAINST CONSERVED INFLUENZA VIRUS EPITOPES

Plotnikova MA, Oleynik VA, Klotchenko SA ✉

Smorodintsev Research Institute of Influenza, St. Petersburg, Russia

Monoclonal antibody therapy is one of the most promising approaches for effective influenza control. In this study, we evaluated the antiviral activity of exogenous mRNA-encoded single-chain variable fragment (scFv) antibodies, which are capable of binding viral antigens inside the cell with high affinity. Two influenza virus proteins, hemagglutinin (antibody FI6) and nucleoprotein (antibody 2/3), were chosen as targets. Each scFv encoded by mRNA was produced in two variants: one containing a signal peptide (SP) to direct secretion into the extracellular space (scFv-SP) and one lacking the signal peptide (scFv-WO) for cytosolic localization and function. These variants showed distinct intracellular localization patterns: scFv-SP localized to regions characteristic of the endoplasmic reticulum and the Golgi complex, whereas scFv-WO was distributed diffusely throughout the cytoplasm. mRNAs encoding scFv-FI6-SP, scFv-2/3-SP, and scFv-2/3-WO exhibited antiviral activity against influenza A virus *in vitro*. The scFv-FI6-SP mRNA showed the strongest antiviral effect, reducing viral load by approximately tenfold compared to the control. For influenza B virus, both scFv-2/3 mRNA variants, with and without the signal peptide, reduced viral load by an average of 50%. These findings highlight the antiviral potential of intracellular antibodies and point to new opportunities for targeting viral components that are not accessible to conventional antiviral therapies.

Keywords: influenza virus, antiviral agents, broadly neutralizing antibodies, passive immunotherapy, mRNA therapeutics, mRNA-encoded antibodies, intrabodies, scFv fragments, virus neutralization

Funding: This study was funded by the Russian Science Foundation, project no. 24-25-00488 'Study of the antiviral potential of intracellular scFv antibodies against influenza virus' (principal investigator — S. A. Klotchenko); https://rscf.ru/project/24-25-00488/

Author contribution: Plotnikova MA — design of structures, conducting experiments, registration and analysis of results, statistical processing, manuscript authoring and formatting; Oleynik VA — conducting experiments, registration of results; Klotchenko SA — study design, preparation and characterization of mRNA preparations, conducting experiments, registration and analysis of results, manuscript editing.

✉ **Correspondence should be addressed:** Sergey A. Klotchenko
Prof. Popova, 15/17, Saint Petersburg, 197022, Russia; fosfatik@mail.ru

Received: 27.11.2025 **Accepted:** 10.12.2025 **Published online:** 26.12.2025

DOI: 10.24075/brsmu.2025.077

Copyright: © 2025 by the authors. **Licensee:** Pirogov University. This article is an open access article distributed under the terms and conditions of the Creative Commons Attribution (CC BY) license (https://creativecommons.org/licenses/by/4.0/).

ПРОТИВОВИРУСНАЯ АКТИВНОСТЬ мРНК, КОДИРУЮЩИХ ВНУТРИКЛЕТОЧНЫЕ SCFV-ФРАГМЕНТЫ АНТИТЕЛ К КОНСЕРВАТИВНЫМ ЭПИТОПАМ ВИРУСА ГРИППА

М. А. Плотникова, В. А. Олейник, С. А. Клотченко ✉

Научно-исследовательский институт гриппа имени А. А. Смородинцева, Санкт-Петербург, Россия

Один из перспективных подходов к эффективной борьбе с гриппом — терапия с использованием моноклональных антител. Целью работы было провести оценку противовирусного действия внутриклеточных scFv-фрагментов антител, которые были трансфицированы в клетку в виде экзогенной мРНК, транслировались и были способны к высокоаффинному связыванию с вирусными антигенами непосредственно внутри клетки. В качестве вирусных мишеней были выбраны два белка вируса гриппа — гемагглютинин (антитело FI6) и нуклеопротеин (антитело 2/3). Каждый из scFv-фрагментов, кодируемых мРНК, был получен в двух формах: с сигнальным пептидом (SP) для секреции во внеклеточное пространство (scFv-SP) и без него (scFv-WO) — для внутриклеточного функционирования в цитозоле. Показана различная локализация этих белков в клетке: scFv-SP обнаруживались в областях, характерных для эндоплазматического ретикулума и комплекса Гольджи, в то время как scFv-WO были диффузно распределены по цитоплазме. Продемонстрировано, что мРНК, кодирующие scFv-FI6-SP и scFv-2/3-SP, а также мРНК, кодирующая scFv-2/3-WO, проявляли противовирусное действие в отношении вируса гриппа А на клеточной модели. Наибольшим противовирусным эффектом обладала мРНК scFv-FI6-SP: она приводила к снижению вирусной нагрузки относительно контроля примерно в 10 раз. В отношении вируса гриппа В обе мРНК, кодирующие scFv-2/3 (как с SP, так и без него), приводили к снижению вирусной нагрузки в среднем на 50% относительно контроля. Таким образом, показано, что внутриклеточные антитела обладают высоким противовирусным потенциалом и открывают возможности для воздействия на новые, перспективные вирусные мишени, которые ранее были недоступны для лекарственной терапии.

Ключевые слова: вирус гриппа, противовирусные препараты, антитела широкого спектра действия, пассивная иммунотерапия, технологии терапевтических мРНК, мРНК-кодируемые антитела, внутриклеточные антитела, scFv-фрагменты антител, вируснейтрализующая активность

Финансирование: исследование выполнено при финансовой поддержке Российского научного фонда, Соглашение № 24-25-00488: «Изучение противовирусного потенциала внутриклеточных scFv антител к гриппу» (руководитель — С. А. Клотченко), https://rscf.ru/project/24-25-00488/.

Вклад авторов: М. А. Плотникова — разработка конструкций, проведение экспериментов, регистрация и анализ результатов, статистическая обработка, написание и оформление рукописи; В. А. Олейник — проведение экспериментов, регистрация результатов; С. А. Клотченко — дизайн исследования, получение и характеристика препаратов мРНК, проведение экспериментов, регистрация и анализ результатов, редактирование рукописи.

✉ **Для корреспонденции:** Сергей Анатольевич Клотченко
ул. Профессора Попова, 15/17, г. Санкт-Петербург, 197022, Россия; fosfatik@mail.ru

Статья получена: 27.11.2025 **Статья принята к печати:** 10.12.2025 **Опубликована онлайн:** 26.12.2025

DOI: 10.24075/vrgmu.2025.077

Авторские права: © 2025 принадлежат авторам. **Лицензиат:** РНИМУ им. Н. И. Пирогова. Статья размещена в открытом доступе и распространяется на условиях лицензии Creative Commons Attribution (CC BY) (https://creativecommons.org/licenses/by/4.0/).

According to the World Health Organization, influenza was the third leading cause of death from infectious diseases until 2021, accounting for up to 350,000 deaths worldwide [1]. Although the COVID-19 pandemic has changed the epidemiology of respiratory viral infections, influenza remains a frequent cause of severe pneumonia, especially in children and adults over 70 years of age. In addition, influenza viruses have a high zoonotic potential and the capacity to cross species barriers, posing a persistent threat of future pandemics.

Current strategies for combating influenza rely largely on vaccination. However, its effectiveness is limited, as it is difficult to accurately predict which viral strains will dominate in an upcoming epidemic season. This uncertainty emphasizes the need for new therapeutic approaches.

Monoclonal antibodies, which can specifically bind molecular targets and modulate biological functions — including the disruption of protein-protein interactions — are promising candidates for antiviral drug development. To date, most monoclonal antibody-based therapies have been restricted to extracellular targets. Advances in genetic engineering now make it possible to explore the therapeutic potential of recombinant antibodies or their fragments expressed inside cells. This enables targeting conservative and functionally critical viral antigens that are typically inaccessible to conventional therapies.

Studies from the 1980s and 1990s demonstrated that mature exogenous antibodies can remain stable and functional when introduced directly into the cytosol [2–4], opening new possibilities for suppressing antigen function within living cells. For example, monoclonal antibodies directed against α-tubulin or β-tubulin were shown to induce microfilament destruction and aggregation within 1.5 hours of microinjection into living cells [3].

Nevertheless, the systemic delivery of relatively large proteins, such as antibodies, into cells is still a major challenge [5]. One promising strategy to overcome this limitation is the stable, mRNA-mediated intracellular expression of monoclonal antibodies in non-immune mammalian cells, which enables direct inactivation of target antigens [6].

Proper antibody folding is known to depend on chaperones localized in the endoplasmic reticulum (ER), to which antibody chains are directed by signal sequences that facilitate their translocation [7]. It is during protein synthesis on the ribosome that N-terminal signal peptides (SPs), typically 5–30 amino acids in length, are recognized by the signal-recognition particle, which directs the nascent polypeptide chain into the ER lumen [8, 9]. Upon translocation across the ER membrane, the signal peptide is cleaved by signal peptidase.In the absence of a signal peptide, the heavy and light chains of recombinant immunoglobulins remain in the cytosol, where misfolding is likely to occur, leading to loss of antibody function [10, 11].

More compact antibody formats, such as single-chain variable fragments (scFvs) of ~28 kDa, can retain both functional activity and target specificity. Functional studies have demonstrated that scFvs can fold and assemble correctly in the cytosol, despite the absence of ER-resident chaperones that usually support protein folding, and the reducing environment of the cytosol, which is unfavorable for disulfide bond formation [12].

In this study, we designed synthetic mRNAs encoding high-affinity scFv antibody fragments and evaluated their antiviral activity against influenza virus. Two key viral proteins of different subcellular localizations were selected as targets: the surface hemagglutinin and the internal nucleoprotein. The mRNAs were designed either to promote secretion of scFv fragments for neutralization of viral particles or to drive their accumulation in the cytoplasm to suppress viral replication within infected cells.

METHODS

Design of scFv antibody fragments

We previously developed expression constructs encoding scFv fragments of antibodies FI6 and 2/3 [13]. To generate exogenous mRNAs, DNA sequences encoding scFvs of the desired length were amplified using appropriate primers (Eurogen, Russia) and inserted by restriction cloning at the BstPA I and Bmt I sites (Sibenzyme, Russia). The resulting inserts were then ligated into the pIVTS3 vector system, developed at the Smorodintsev Research Institute of Influenza and based on the PIVOT vector (NovoPro Bioscience, China). The pIVTS3 vector contains a T7 promoter region, 5' and 3' UTRs, and a poly(dA/dT) sequence. Ligation mixtures were used to transform competent *E. coli* cells (NEB Stable strain, New England Biolabs, UK), which were then plated onto selective agar medium supplemented with 100 μg/mL ampicillin. After 24 hours, the resulting colonies were screened by RT-PCR. Plasmids containing inserts of the expected size were propagated in liquid LB medium and purified using the Plasmid Miniprep 2.0 kit (Eurogen, Russia). The sequences of the plasmid constructs used for *in vitro* transcription of exogenous mRNAs were verified by Sanger sequencing performed by Eurogen (Russia).

In vitro transcription (IVT)

Exogenous mRNAs were synthesized using the *in vitro* mRNA Synthesis Kit containing ΨTP, m^5CTP, and m^7GmAmG (Biolabmix, Russia). Plasmid DNA (1 μg) pre-linearized at the AhlI site (Sibenzyme, Russia) served as the template. The IVT reaction was carried out according to the manufacturer's instructions. After completion of transcription, 2 units of TURBO DNase (Thermo Fisher Scientific, USA) were added to the reaction mixture and incubated for 30 minutes at 37°C to cleave residual double-stranded plasmid DNA. The resulting mRNA preparations were purified by lithium chloride precipitation. mRNA concentrations were measured using a NanoDrop ND-1000 spectrophotometer and a Qubit 4 fluorimeter (Thermo Fisher Scientific, USA).

Agarose gel electrophoresis

Plasmid DNA, including linearized forms, was analyzed by electrophoresis on a 0.8% agarose gel prepared in 1× TAE buffer containing 0.5 μg/mL ethidium bromide. DNA samples were mixed with 6× loading buffer and loaded into gel wells.mRNA integrity and quality were assessed by electrophoresis under denaturing conditions in a 1% agarose gel. For sample preparation, 200–500 ng of mRNA was mixed with Gel Loading Buffer II (Invitrogen, USA) and denatured at 70 °C for 5 minutes before loading onto the gel containing ethidium bromide. Electrophoresis was performed in MOPS buffer at room temperature. Gel images were acquired using a Gel Doc EZ Imager (Bio-Rad, USA).

Exogenous mRNA transfection

Established cell lines were used in this study: A549 human lung carcinoma cells (American Type Culture Collection (ATCC), USA; #CCL-185) and Madin-Darby canine kidney (MDCK) cells (International Reagent Resource (IRR), USA; #FR58). A549 cells were cultured in F-12K nutrient medium (Gibco, USA) supplemented with 10% fetal bovine serum, SC-Biol (Gibco, USA). MDCK cells were cultured in α-MEM medium (Biolot, Russia) supplemented with 5% SC-Biol. All cultures were maintained and used in experiments without antibiotics.

For transfection with exogenous mRNAs, cells were grown to a 90–100% confluent monolayer, and the growth medium was replaced with serum-free medium immediately before mRNA delivery. Transfections were performed using GenJector-U (Molekta, Russia) according to the manufacturer's instructions. Lipoplexes containing 100 ng mRNA and 0.3 µL transfection reagent were prepared and added to wells of a 96-well plate at a volume of 10 µL per well. Depending on the experimental design, transfected cells were incubated for 2–48 hours at 37 °C in a humidified atmosphere containing 5% CO_2.

Immunofluorescence

Immunofluorescence staining was performed 24 hours after transfection of eukaryotic cells with exogenous mRNAs. Cells were seeded onto Lab-Tek II chamber slides (Nunc, USA). Monolayers were washed with DPBS, fixed with 4% paraformaldehyde for 10 minutes, and permeabilized with 0.1% Triton X-100 (Sigma-Aldrich, USA). Blocking was performed overnight at 4 °C in DPBS containing 1% bovine serum albumin. The nuclei were stained with DAPI (AppliChem, USA), and the actin cytoskeleton was visualized using rhodamine-conjugated phalloidin (Thermo Fisher Scientific, USA). scFv antibody fragments were detected using primary mouse monoclonal against the 6×His-tag sequence (Penta-His; Qiagen, USA) at a dilution of 1 : 1000, followed by secondary goat anti-mouse antibodies conjugated to Alexa Fluor 488 at a final concentration of 0.5 µg/mL. Cells were imaged sequentially using a Cytell cell imaging system (GE Healthcare, USA) with blue, green, and orange fluorescence channels.

ELISA

Levels of scFv antibody fragments in cell culture medium were quantified by ELISA. Purified viral concentrates of influenza A/California/07/09 (H1N1pdm) and influenza B/Phuket/3073/13 (Yamagata), diluted in PBS to a final concentration of 2 µg/mL, were used as capture ligands. Aliquots of 100 µL of ligand solution were added to wells of a 96-well Microlon High Binding plate (Greiner Bio-One, Germany) and incubated overnight (12–18 hours) at 4 °C. Plates were then washed three times with PBST (PBS containing 0.05% Tween 20) using an ELx405 automatic plate washer (BioTek, USA). Wells were blocked with 200 µL per well of a 5% skimmed milk in PBST (Blotting-Grade Blocker; Bio-Rad, USA) using an MB100-4A thermoshaker (Allsheng, China) at 37 °C for 1 hour. After washing, 100 µL of test culture medium, diluted 1 : 2 in blocking reagent, was added to each well and incubated at 37 °C for 2 hours. Plates were then washed, and bound scFv fragments were detected using horseradish peroxidase-conjugated anti-6×His-tag antibodies (His17-HRP; Hytest, Russia), diluted 1 : 2000 in blocking reagent, and incubated at 37 °C for 1 hour (100 µL per well). After washing, the peroxidase reaction was initiated by adding 100 µL of tetramethylbenzidine (TMB) substrate (Khema, Russia) to each well. The reaction was stopped by adding 100 µL of 2H H_2SO_4, and absorbance (optical density, OD) was measured at 450 nm (OD_{450}) and 620 nm (OD_{620}) using a Multiskan SkyHigh Microplate Spectrophotometer (Thermo Fisher Scientific, USA). Primary data were analyzed in Microsoft Office Excel 2010 (Microsoft, USA) and GraphPad Prism 8 (GraphPad Software, USA).

Western blotting

MDCK cell lysates were prepared using a two-component extraction system consisting of Extraction Buffer 5× PTR and Extraction Enhancer Buffer 50× (Abcam, USA). Fifty microliters of freshly prepared, ice-cold 1× extraction buffer were added to each well containing a cell monolayer pre-washed with DBPS. Plates were incubated on ice for 30 minutes, after which lysates were collected into microcentrifuge tubes and clarified by centrifugation at 13,800×g for 30 minutes at 4 °C using a 5415R centrifuge (Eppendorf, Germany). Clarified supernatants were mixed with Laemmli sample buffer, heated at 95 °C for 10 minutes, and separated under denaturing conditions on Any kD Mini-PROTEAN TGX Stain-Free Protein Gels (Bio-Rad, USA). Next, proteins were transferred to 0.2 µm nitrocellulose membranes using a Trans-Blot Turbo semi-dry transfer system and Trans-Blot Turbo Mini 0.2 µm nitrocellulose transfer packs (Bio-Rad, USA). After transfer, membranes were blocked overnight at 4 °C and incubated for 2 hours at 37 °C with mouse monoclonal anti-6×His-tag antibodies (Penta-His; Qiagen, USA) diluted 1:2000 in blocking reagent. After washing with PBST, membranes were incubated for 1 hour at 37 °C with horseradish peroxidase-conjugated goat anti-mouse secondary antibodies (GAM-HRP; Bio-Rad; USA) diluted 1 : 2000 in blocking reagent. Protein bands were visualized using Clarity Western ECL substrate (Bio-Rad, USA) and imaged with a ChemiDoc MP system (Bio-Rad, USA). Lysates from cells transfected with mRNA encoding the heavy chain of an immunoglobulin specific to an irrelevant antigen were used as a negative control.

Antiviral activity assessment

A combined prophylactic–therapeutic protocol was used to evaluate the antiviral activity of exogenous mRNAs encoding scFv antibody fragments. Confluent MDCK cell monolayers were washed with sterile DPBS to remove serum components that inhibit viral replication. Fresh α-MEM medium (Biolot; Russia; 100 µL) containing 10 µL of lipoplexes prepared with the commercial transfection reagent GenJector-U (Molekta; Russia) was then added to each well according to the manufacturer's instructions. Each well of a 96-well plate contained 100 ng of mRNA and 0.3 µL of transfection reagent (approximately 5×10^4 cells). Next, cells were incubated for 6 hours at 37 °C in a humidified atmosphere containing 5% CO_2.

Cells were subsequently infected by exposure to 50 µL of virus-containing medium for 1 hour at 37 °C and 5% CO_2. Reference strains of human influenza viruses from the collection of the Smorodintsev Research Institute of Influenza were used: A/California/07/09 (H1N1pdm), A/Cambodia/e0826360/2020 (H3N2), B/Phuket/3073/13 (Yamagata), and B/Malaysia/2506/2004 (Victoria), with initial titers of 6×10^8 TCID50/mL, 3.16 × 107 $TCID_{50}$/mL, 3.16×10^6 $TCID_{50}$/mL, and 1.0×10^8 $TCID_{50}$/mL, respectively. Cells were infected at MOIs ranging from 0.1 to 1, corresponding to virus dilutions of up to 1:1000.

After incubation, the virus-containing medium was removed and replaced with the original transfection medium containing lipoplexes. Cells were then incubated for an additional 24 hours at 37 °C and 5% CO_2. Viral particles were subsequently detected in culture medium using a hemagglutination assay performed according to a standard protocol [14] and in infected cells using in-cell ELISA.

In-cell ELISA

Viral particles in infected cells were detected using the ELISA protocol described above, with minor modifications. Briefly, infected cells in 96-well plates were fixed with 80% acetone

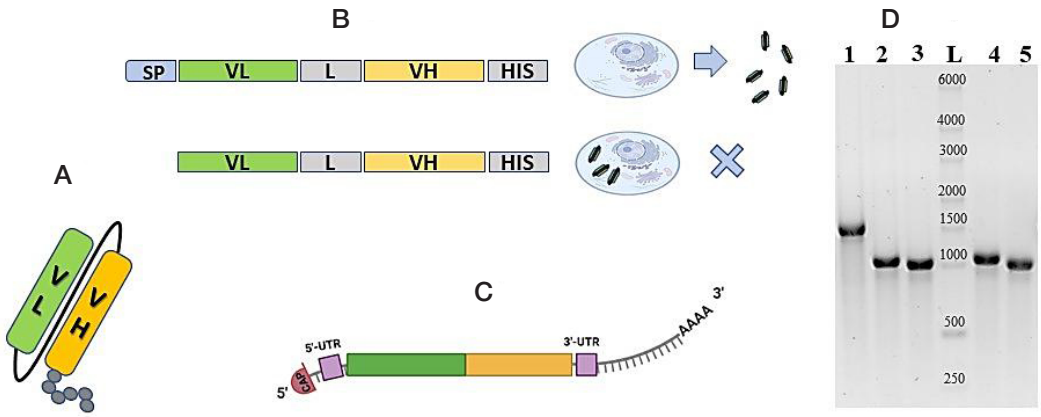


Fig. 1. Basic structure of the developed scFv antibody fragments against influenza A and B viruses and the exogenous mRNAs encoding them. **A**. Structure of scFvs composed of variable domains of the light (green) and heavy (orange) chains. The black line indicates the linker peptide $(G_4S)_4$. Gray circles indicate the C-terminal 6×His-tag sequence. **B**. Structure of the coding regions of secreted and cytosolic scFv antibodies. The key difference is the presence of a signal peptide (SP) at the N terminus in the secreted variant. VL and VH denote the variable domains of the light and heavy chains, respectively; L, the linker peptide; HIS, the 6'His tag sequence. **C**. Structure of the exogenous mRNA used for intracellular scFv translation. The 5' cap (m^7GmAmG) is shown at the 5' terminus; the 5' UTR and 3'UTR regulatory regions are shown in lilac; green and yellow blocks represent the scFv coding region; the extended gray line with notches represents the poly(A) tail. **D**. Agarose gel electrophoretic analysis of purified exogenous mRNA preparations: lane 1, negative control mRNA encoding the heavy chain of an immunoglobulin against an irrelevant antigen (NC-RNA), estimated length 1792 nt; lane 2, mRNA encoding scFv-FI6-SP, 1219 nt; lane 3, mRNA encoding scFv-FI6-WO, 1162 nt; lane 4, mRNA encoding scFv-2/3-SP, 1201 nt; lane 5, mRNA encoding scFv-2/3-WO, 1138 nt. L, RNA molecular weight marker (RiboRuler High Range RNA Ladder; Thermo Fisher Scientific, USA). Marker sizes (nt) are indicated on the lane

in DPBS (50 µL per well) for 30 minutes at 4 °C. After washing with PBST, wells were incubated with blocking reagent (200 µL per well) for 1 hour at 37 °C and then washed. Mouse monoclonal antibodies against the nucleoprotein of influenza A and B viruses [15] were added at a final concentration of 0.5 µg/mL in blocking reagent (100 µL per well) and incubated for 1 hour at 37 °C. Plates were washed, and bound antibodies were detected using horseradish peroxidase-conjugated goat anti-mouse secondary antibodies (GAM-HRP; Bio-Rad, USA), diluted 1 : 2000 in blocking reagent (100 µL per well) and incubated for 1 hour at 37 °C. After washing, signal development and data acquisition were performed as described for the ELISA protocol above.

Statistical data analysis

Statistical analyses were performed using GraphPad Prism 8 (GraphPad Software, USA). Differences between groups were evaluated using one-way ANOVA followed by Holm-Šídák multiple comparison test. Differences were considered statistically significant at $p < 0.05$.

RESULTS

Design and production of exogenous mRNAs encoding scFv antibodies

This study further explored antigen-binding regions of antibodies in the scFv format that we had developed previously [13]. One of these fragments, scFv-FI6, specifically recognized the stem region of hemagglutinin (HA), which is conserved among influenza A viruses (IAV) of both major phylogenetic groups [16]. The second fragment, scFv-2/3, specifically binds the nucleoprotein (NP) of influenza B viruses (IBV) from both genetic lineages [17].

Each scFv consisted of variable domains derived from the corresponding full-length recombinant antibody, with the variable regions of the heavy and light chains connected by a linker composed of four tandem repeats of the G_4S motif. To enable secretion into the extracellular space, the N terminus of each scFv contained a signal peptide (SP) derived from the light chain of the original antibody; these constructs are referred to as scFv-SP. The following signal peptide sequences were used: MKSQTQVLVFLLCVSGAHG for scFv-FI6-SP and MDFQVQIFSFLLISASVIISRG for scFv-2/3-SP. To promote intracellular accumulation, we also generated versions of each scFv without the signal peptide (scFv-WO). In these constructs, the ORF begins with an ATG codon encoding methionine, immediately followed by the sequence of the light-chain variable domain.

The scFv-SP and scFv-WO constructs differed only in the presence or absence of the N-terminal signal peptide. All recombinant scFv antibodies were engineered with C-terminal hexahistidine tags to facilitate detection (Fig. 1A, B). On the basis of this sequence design, plasmid constructs containing a T7 promoter were generated for *in vitro* transcription of mRNA.

mRNA technology was used to translate intracellular scFv antibodies in non-immune eukaryotic cells. The mRNAs was generated by *in vitro* transcription and consisted of five standard elements: an optimized cap analogue at the 5' terminus (CleanCap m7GmAmG; TriLink BioTechnologies, USA), followed by a 5' untranslated region (UTR), the scFv ORF, a 3' UTR, and a poly(A) tail encoded by a poly(dA/dT) sequence embedded in the plasmid (Fig. 1B). To reduce immunogenicity and increase stability, the mRNAs incorporated modified nucleotides: pseudouridine (ΨTP) and 5-methylcytidine (m5CTP).

The resulting purified preparations included four mRNAs encoding scFv antibody fragments FI6 and 2/3 against IAV and IBV, each produced with or without a signal peptide, as well as a control mRNA encoding the heavy chain of an immunoglobulin specific to an irrelevant antigen. All mRNAs were characterized by spectrophotometry and agarose gel electrophoresis (Fig. 1G). The observed transcript lengths matched the predicted sizes, and the purity and integrity of the mRNA preparations were sufficient to support intracellular translation of the target proteins.

Functional properties of scFv antibodies encoded by exogenous mRNAs

We evaluated the translational activity of exogenous mRNAs encoding scFv fragments of antibodies in the eukaryotic cell lines MDCK and A549. The mRNA-containing culture medium was removed 24 hours after transfection, and the cells were

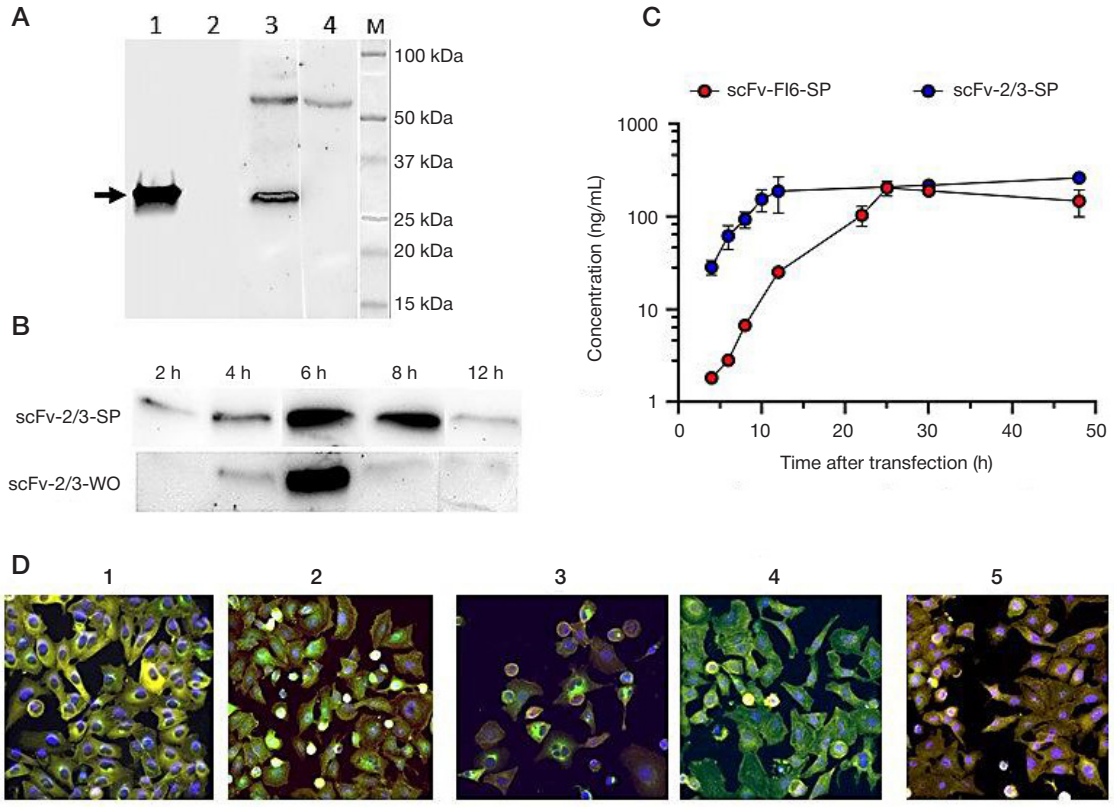


Fig. 2. Translational activity of exogenous mRNAs encoding cytosolic (WO) and secreted (SP) forms of scFv antibody fragments against influenza A and B viruses. **A**. Western blot analysis of scFv-2/3 antibody fragments in culture medium and MDCK cell lysates using antibodies specific to the 6'His tag sequence. Similar results were obtained for scFv-FI6 but are not shown. Lanes 1 and 2 show culture medium from MDCK cells transfected with mRNAs encoding scFv-2/3-SP and scFv-2/3-WO, respectively; lanes 3 and 4 show cell lysates from MDCK cells transfected with mRNAs encoding scFv-2/3-SP and scFv-2/3-WO, respectively. M, molecular weight marker (Precision Plus Protein Kaleidoscope Preferred Protein Standards; Bio-Rad, USA); corresponding molecular weights (kDa) are indicated to the right. All samples were collected 24 h after mRNA cell transfection. **B**. Western blot analysis of scFv-2/3 antibody fragments in MDCK cell lysates at different time points using anti–6'His-tag antibodies. The upper panel shows intracellular production of scFv-2/3-SP, and the lower panel shows scFv-2/3-WO. Sampling times after mRNA transfection are indicated at the top (hours). **C**. ELISA analysis of scFv concentrations in culture medium after transfection of A549 cells with mRNAs encoding scFv-FI6-SP (*red*) and scFv-2/3-SP (*blue*). Data points represent mean values from two biological replicates ± SD. **D**. Representative fluorescence microscopy images of fixed A549 cells transfected with exogenous mRNAs encoding: (1) scFv-FI6-SP, (2) scFv-FI6-WO, (3) scFv-2/3-SP, (4) scFv-2/3-WO, and (5) NC-RNA. The actin cytoskeleton (yellow) was visualized using rhodamine-conjugated phalloidin, and nuclei (blue) were stained with DAPI. scFv fragments (*green*) were detected using primary mouse monoclonal anti-6'His-tag antibodies followed by Alexa Fluor 488-conjugated goat anti-mouse secondary antibodies. Images were acquired and processed using a Cytell cell imaging system (40× objective); individual channels were pseudocolored in RGB during image processing. Enlarged views of the processed images are shown

then lysed, and the levels of histidine-tagged proteins in the lysates were analyzed by Western blotting.

At 24 hours after transfection of MDCK cells with mRNAs encoding scFv-SP, proteins of the expected molecular weight (~28 kDa), corresponding to monomeric scFv antibody fragments, were readily detected using antibodies against the 6×His tag (Fig. 2A). By contrast, detection of scFv products in cell lysates proved challenging. For both scFv-SP and scFv-WO constructs, nonspecific high-molecular-weight bands (~55 kDa) were observed, which were also present in the negative control. Enzymatic signal amplification combined with extended exposure time allowed us to identify intracellular scFv-SP (Fig. 2A, lane 3), whereas scFv-WO remained undetectable (Fig. 2A, lane 4). Thus, transfection with mRNA encoding scFv-SP resulted in the secretion of mature monomeric scFv fragments within 24 hours, which were detected both in the culture medium and in cell lysates.

Assuming that intracellular scFvs may be unstable and have short half-lives of only a few hours, we next examined their expression kinetics in cell lysates at 2, 4, 6, 8, and 12 hours after transfection with exogenous mRNAs. For both SP and WO variants, maximal translation was observed at 6 hours post-transfection (Fig. 2B). Notably, intracellular stability of scFvs varied significantly depending on the presence or absence of the signal peptide. scFv-SP antibodies were detectable as early as 2 hours after transfection, and their production increased by 6 hours and then dropped by 12 hours. In contrast, scFv-WO was first detected in cells at near-threshold levels at 4 hours after transfection, reached peak abundance at 6 hours, and decreased to the detection limit by 8 hours.

Next, we evaluated the kinetics of scFv-SP accumulation in the culture medium of A549 cells transfected with the corresponding exogenous mRNAs (Fig. 2B). To this end, we performed an ELISA using purified inactivated influenza A and B virus concentrates as capture ligands and horseradish peroxidase–conjugated antibodies to detect the 6×His tags. scFv fragment concentrations were quantified using a calibration curve generated with purified recombinant scFv preparations [13].

Functional scFv fragments of antibodies were detected in the culture medium as early as 2 hours after transfection of A549 cells with scFv-SP mRNA, at analytically detectable levels. scFv levels increased steadily over the subsequent 24 hours, reaching approximately 200 ng/mL for both scFv-FI6-SP and scFv-2/3-SP. Saturation of protein accumulation occurred at around 24 hours post-transfection, after which scFv levels reached a plateau maintained throughout the rest of the 48-hour observation period.

To assess the intracellular localization of proteins encoded by scFv-SP and scFv-WO constructs, we performed immunofluorescence staining of A549 cells transfected with the corresponding mRNAs (Fig. 2D). Immunocytochemical analysis showed that scFv-FI6-WO and scFv-2/3-WO were diffusely

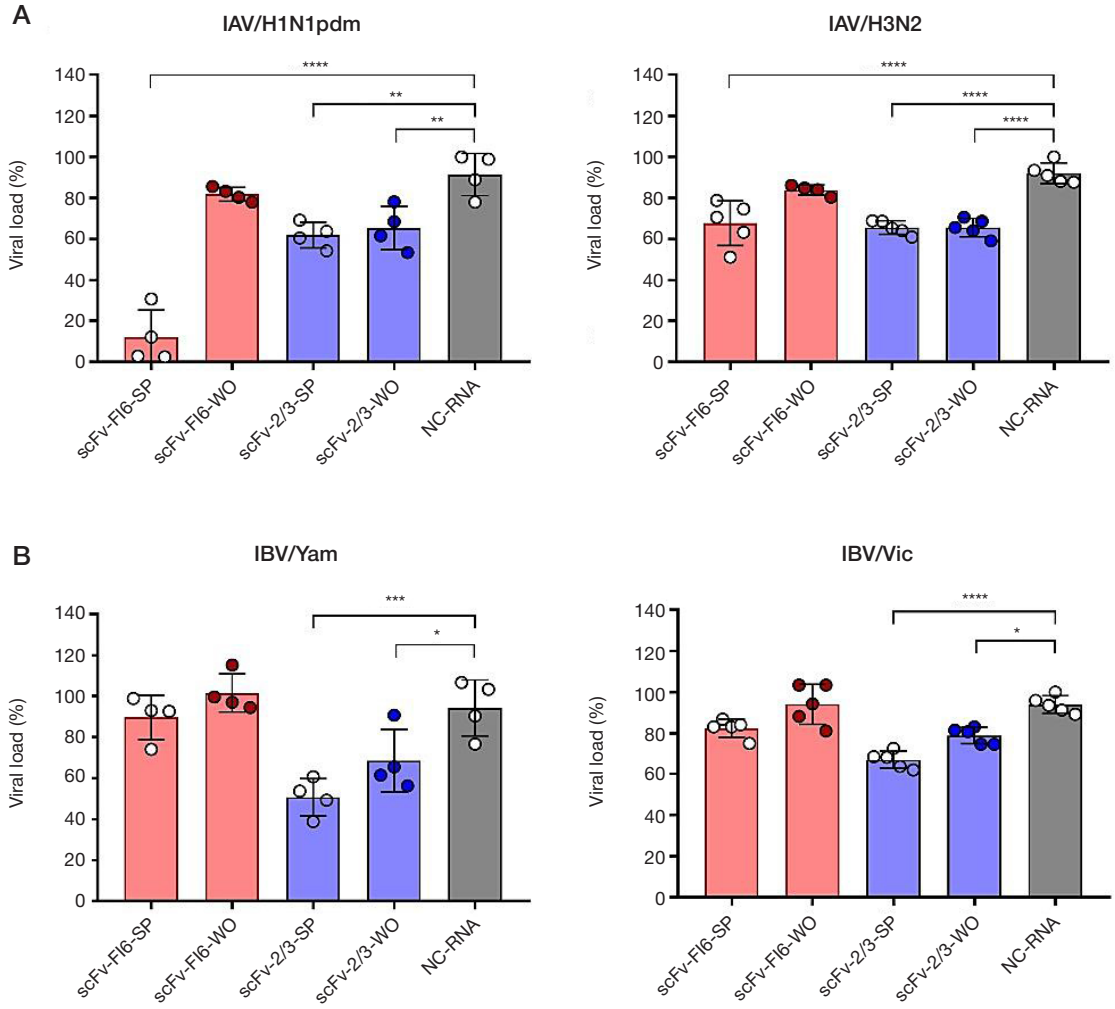


Fig. 3. In-cell ELISA analysis of the antiviral activity of exogenous mRNAs encoding cytosolic (WO) and secreted (SP) forms of scFv antibody fragments against influenza A and B viruses. **A**. Intracellular levels of influenza A virus (IAV) after infection with A/California/07/09 (H1N1pdm) (left) and A/Cambodia/e0826360/2020 (H3N2) (right) strains. **B**. Intracellular levels of influenza B virus (IBV) after infection with B/Phuket/3073/13 (Yamagata) (left) and B/Malaysia/2506/2004 (Victoria) (right) strains. Data points represent mean values for four samples ± SD. Red bars indicate therapeutic administration of exogenous mRNAs encoding scFv fragments against IAV hemagglutinin; blue bars indicate administration of exogenous mRNAs encoding scFv fragments against IBV nucleoprotein. Gray bars show mean values for cells transfected with exogenous mRNA encoding the heavy chain of an immunoglobulin specific to an irrelevant antigen (negative control). Statistical significance was determined using one-way ANOVA followed by Holm-Šídák multiple comparison test. *Asterisks* indicate significant differences compared with the negative control (NC-RNA): * — p_{value} < 0.0332; ** — p_{value} < 0.0021; *** — p_{value} < 0.0002; **** — p_{value} < 0.0001

distributed throughout the cytoplasm, with no distinct subcellular localization. scFv-FI6-SP and scFv-2/3-SP, on the contrary, were distinctly localized in the perinuclear region, consistent with their accumulation primarily in the ER (not labeled directly).

In the final stage of the study, we evaluated the antiviral activity of the exogenous mRNAs against influenza A and B viruses. As a negative control, we used an mRNA encoding the heavy chain of an immunoglobulin specific to an irrelevant antigen (NC-RNA).

Experiments were conducted using the combined prophylactic–therapeutic protocol involving mRNA transfection both before and after a 1-hour exposure to the virus. Three mRNAs — encoding scFv-FI6-SP, scFv-2/3-SP, and scFv-2/3-WO — were found to have antiviral activity against IAV (Fig. 3A). For the H1N1pdm strain, scFv-FI6-SP mRNA produced the strongest antiviral effect, decreasing viral load by approximately tenfold relative to the control. No such enhancement was observed in the case of the H3N2: all three mRNAs showed comparable antiviral effects, reducing viral load to 60–70% of control levels. It is noteworthy that scFv-FI6-WO mRNA, which specifically binds IAV hemagglutinin, did not affect IAV replication.

For IBV, both mRNAs encoding scFv-2/3 (SP and WO) demonstrated antiviral activity. Prophylactic transfection decreased viral load to 50–70% of that observed in control samples, with similar effects against IBV strains of the Yamagata and Victoria lineages. Importantly, neither the original full-length monoclonal antibody 2/3 [17] nor the derived scFv-2/3 fragment was previously shown to neutralize IBV [13].

DISCUSSION

Modern passive immunotherapy based on neutralizing monoclonal antibodies can provide broad protection against infections caused by influenza viruses [16, 18, 19]. Most currently available therapeutic immunoglobulins target hemagglutinin or neuraminidase, the major surface antigens of influenza virus. Yet, reliance on antibodies directed against these highly variable proteins has inherent limitations and risks [20, 21], underscoring the value of strategies that target more conserved viral antigens.

This study aimed to evaluate the potential of intracellular therapeutic antibodies directed against two distinct influenza virus targets: surface hemagglutinin, which is accessible to neutralizing antibodies, and the internal nucleoprotein, which is shielded from antibody recognition in mature virions. Efforts to introduce monoclonal antibodies into the cytosol of living cells

and to study their functional activity date back to the 1970s [22–24]. However, the practical therapeutic application of intracellular antibodies has only become feasible in the past decade, supported by advances in mRNA technologies that enable direct intracellular expression of antibody constructs.

Full-length immunoglobulins comprise not only antigen-binding regions but also an Fc domain that mediates effector functions through interactions with immune cells [25, 26]. Such functions are unnecessary for specific antigen recognition within the intracellular environment. Accordingly, to evaluate intracellular antibody activity, we chose the scFv antibody format [27, 28] that comprises only the variable domains.

For each antibody — scFv-FI6 targeting IAV hemagglutinin and scFv-2/3 targeting IBV nucleoprotein, we designed two types of constructs. One included a signal peptide (SP) sequence to direct nascent polypeptide into the ER, followed by transport through the Golgi apparatus and secretion into the extracellular space. The second construct lacked the signal peptide or any additional targeting sequences, such as nuclear localization signals or ER retention motifs (for example, KDEL) [8, 9]. We reasoned that the protein product translated from such exogenous mRNA would remain in the cytosol, where it could interact effectively with target proteins, thus suppressing viral replication.

Consistent with the design principles, observed distinct intracellular distribution patterns for the two scFv variants. scFv-SP fragments were mainly concentrated in regions with highly curved smooth membranes characteristic of the ER-Golgi interface. In contrast, scFv-WO fragments had no distinct subcellular localization and were distributed diffusely throughout the cytoplasm. This likely reflects cytosolic retention of this variant and a lack of involvement in vesicular transport.

Notably, Western blot analysis of cell lysates 24 hours after transfection with mRNA encoding scFv-WO failed to detect monomeric scFv antibody fragments (~28 kDa), in contrast to scFv-SP. At the same time, after transfection with either scFv-FI6-SP or scFv-2/3-SP mRNAs, proteins of the expected molecular weight were readily detected in the culture medium.

We further established that intracellular scFv antibodies have a short half-life. Products encoded by mRNA lacking a signal peptide (scFv-WO) remained detectable for only 4 hours, which indicates their rapid degradation, likely mediated by the ubiquitin-proteasome system. Numerous studies have shown that cytosolic scFv fragments often have low stability and are prone to dimerization and degradation [29]. This instability can be attributed to suboptimal conditions for antibody folding in the cytosol, including a lack of chaperones, low pH, and a reducing environment that prevents the formation of stabilizing disulfide bonds [11, 12, 30]. As a result, the effectiveness of scFvs operating in the cytosol can be substantially limited by impaired folding and the inability to adopt a stable, functional conformation [31]. Importantly, scFv antibodies containing a secretion signal showed an earlier and more sustained intracellular production, suggesting that routing through the secretory pathway can enhance both folding efficiency and protein stability.

We next assessed the antiviral activity of the exogenous mRNAs encoding scFv antibody fragments in a cellular model of influenza infection. It is known that exogenous mRNAs can suppress viral replication due to their intrinsic immunogenicity and activation of cellular nucleic-acid-sensing pathways [32, 33]. To control for these non-specific effects, we used an mRNA encoding the heavy chain of an immunoglobulin targeting an irrelevant antigen and containing a signal peptide sequence, which was produced and purified using the same protocol as the experimental mRNAs.

Of the two constructs encoding scFv-FI6, which specifically binds IAV hemagglutinin, only the mRNA encoding the secreted form (scFv-FI6-SP) showed antiviral activity. The therapeutic application of this mRNA reduced viral load after infection with the H1N1pdm strain by nearly tenfold compared to the control treatment. We detected no antiviral activity of the cytosolic form, scFv-FI6-WO. These findings suggest that intracellular antibodies are more effective when their intracellular trafficking mirrors that of their viral targets. Indeed, an intracellular human scFv antibody against hemagglutinin, expressed from plasmid DNA, has been shown to suppress H5N1 influenza virus replication *in vitro*. Moreover, its *in vivo* efficacy significantly increased when combined with an extracellular IgG1 containing identical variable domains [34].

In contrast, the results obtained with scFv-2/3, which targets IBV nucleoprotein and lacks neutralizing activity [13], were unexpected. Both the cytosolic and secreted variants showed antiviral activity, reducing IBV viral load by approximately twofold relative to the control. In addition, transfection of exogenous mRNAs encoding scFv-2/3 also suppressed IAV replication. As the original full-length monoclonal 2/3 antibody does not exhibit neutralizing activity [17], it is challenging to identify its epitope on the IBV nucleoprotein. It is therefore plausible that this epitope is highly conserved between influenza A and B viruses. Overall, expression of exogenous mRNAs encoding scFv-2/3 reduced replication of both IAV and IBV by an average of ~50% relative to the control.

The use of intracellular antibodies targeting IAV nucleoprotein has been described previously. Such antibodies inhibit viral replication by blocking interactions between nucleoprotein and the viral polymerase subunits PB1 and PB2, which are essential for viral transcription and replication [35]. In another study, single-domain llama antibodies directed against various IAV nucleoprotein epitopes were shown to suppress viral replication by inhibiting nuclear import of ribonucleoprotein complexes responsible for nuclear transport, transcription, replication, and packaging of the viral genome into newly formed virions [36]. It is important to emphasize that, in both cases, intracellular antibodies were expressed via transfection with plasmid constructs rather than through the delivery of exogenous mRNAs.

Our findings indicate that the antiviral efficacy of structurally distinct intracellular scFv antibody fragments depends on the intracellular trafficking of their viral target proteins. The data suggest that effective inhibition of certain viral functions requires antibody-antigen interactions to occur within specific cellular compartments.

Thus, the use of exogenous mRNAs encoding high-affinity scFv antibody fragments to conserved intracellular viral proteins, particularly influenza virus nucleoprotein, is a promising strategy for suppressing viral replication. The main advantage of this approach is its ability to target internal viral components, including intracellular viral replication-transcription complexes, which are substantially more conserved and less susceptible to antigenic drift than viral surface glycoproteins [37].

CONCLUSIONS

In this work: (1) single-chain variable fragments (scFv) of antibodies targeting influenza A hemagglutinin and influenza B nucleoprotein were constructed; (2) exogenous mRNAs encoding these scFvs in both cytosolic and secreted forms were generated; (3) efficient translation of scFv proteins was confirmed following transfection of exogenous mRNAs into eukaryotic cells; (4) the cytosolic forms showed diffuse

intracellular distribution, whereas the secreted forms localized predominantly within the endoplasmic reticulum; and (5) the antiviral activity of exogenous mRNAs encoding scFv fragments against influenza A and B viruses was demonstrated.

References

1. Bender RG, et al. Global, regional, and national incidence and mortality burden of non-COVID-19 lower respiratory infections and aetiologies, 1990–2021: a systematic analysis from the Global Burden of Disease Study 2021. The Lancet Infectious Diseases. 2024; 24 (9): 974–1002. Available from: https://doi.org/10.1016/S1473-3099(24)00176-2.
2. Lin JJ, Feramisco JR. Disruption of the in vivo distribution of the intermediate filaments in fibroblasts through the microinjection of a specific monoclonal antibody. Cell. 1981; 24 (1): 185–93. Available from: https://doi.org/10.1016/0092-8674(81)90514-6.
3. Blose SH, Meltzer DI, Feramisco JR. 0-nm Filaments Are Induced to Collapse in Living Cells Microinjected with Monoclonal and Polyclonal Antibodies Against Tubulin. Journal of Cell Biology. 1984; 98: 847–58. Available from: https://doi.org/10.1083/jcb.98.3.847.
4. Kallajoki M, et al. Microinjection of a monoclonal antibody against SPN antigen, now identified by peptide sequences as the NuMA protein, induces micronuclei in PtK2 cells. Journal of Cell Science. 1993; 104 (1): 139–50. Available from: https://doi.org/10.1242/jcs.104.1.139.
5. Rabbitts TH. Intracellular Antibodies for Drug Discovery and as Drugs of the Future. Antibodies. 2023; 12 (1). Available from: https://doi.org/10.3390/antib12010024.
6. Biocca S, Neuberger MS, Cattaneo A. Expression and targeting of intracellular antibodies in mammalian cells. The EMBO Journal. 1990; 9 (1): 101–8. Available from: https://doi.org/10.1002/j.1460-2075.1990.tb08085.x.
7. Marschall ALJ, Dübel S, Böldicke T. Recent advances with ER targeted intrabodies. Advances in Experimental Medicine and Biology. 2016; 917: 77–93. Available from: https://doi.org/10.1007/978-3-319-32805-8_5.
8. Gerondopoulos A, et al. A signal capture and proofreading mechanism for the KDEL-receptor explains selectivity and dynamic range in ER retrieval. eLife. 2021; 10. Available from: https://doi.org/10.7554/eLife.68380.
9. Johnson AE, Van Waes MA. The Translocon: A Dynamic Gateway at the ER Membrane. Annual review of cell and developmental biology. 1999; 15 (1): 799–842. Available from: https://doi.org/10.1146/annurev.cellbio.15.1.799.
10. Haryadi R, et al. Optimization of Heavy Chain and Light Chain Signal Peptides for High Level Expression of Therapeutic Antibodies in CHO Cells. PloS one. 2015; 10 (2). Available from: http://dx.doi.org/10.1371/journal.pone.0116878.
11. Marschall ALJ, et al. Targeting antibodies to the cytoplasm. mAbs. 2011; 3 (1): 3–16. Available from: https://doi.org/10.4161/mabs.3.1.14110.
12. Richardson JH, Wayne MA. Intracellular antibodies: development and therapeutic potential. Trends in biotechnology. 1995; 13 (8): 306–10. Available from: https://doi.org/10.1016/S0167-7799(00)88970-2.
13. Плотникова М. А., и др. scFv-фрагменты рекомбинантных антител к вирусу гриппа: получение и характеристика функциональной активности. БИОпрепараты. Профилактика, диагностика, лечение. Принято к публикации 12.12.2025. Available from: https://doi.org/10.30895/2221-996X-2025-728.
14. Killian ML. Hemagglutination assay for influenza virus. Animal influenza virus. Animal Influenza Virus. Methods in Molecular Biology. 2014; 1161: 3–9. Available from: https://doi.org/10.1007/978-1-4939-0758-8_1.
15. Plotnikova MA, et al. Antibody microarray immunoassay for screening and differential diagnosis of upper respiratory tract viral pathogens. Journal of Immunological Methods. 2020; 478: 112712. Available from: https://doi.org/10.1016/j.jim.2019.112712.
16. Corti D, et al. A neutralizing antibody selected from plasma cells that binds to group 1 and group 2 influenza A hemagglutinins. Science. 2011; 333 (6044): 850–6. Available from: https://doi.org/10.1126/science.1205669.
17. Krivitskaya VZ, et al. Detection and Differentiation of Current Influenza B Viruses by the Microculture Enzyme-Linked Immunosorbent Assay Using Monoclonal Antibodies. Applied Biochemistry and Microbiology. 2023; 59 (7): 1039–46. Available from: https://doi.org/10.1134/S0003683823070037.
18. Biswas M, et al. Broadly neutralizing antibodies for influenza: Passive immunotherapy and intranasal vaccination. Vaccines. 2020; 8 (3): 424. Available from: https://doi.org/10.3390/vaccines8030424.
19. Momont C, et al. A pan-influenza antibody inhibiting neuraminidase via receptor mimicry. Nature. 2023; 618 (7965): 590–7. Available from: https://doi.org/10.1038/s41586-023-06136-y.
20. Heaton NS, et al. Genome-wide mutagenesis of influenza virus reveals unique plasticity of the hemagglutinin and NS1 proteins. Proceedings of the National Academy of Sciences. 2013; 110 (50): 20248–53. Available from: https://doi.org/10.1073/pnas.1320524110.
21. Klasse PJ. Neutralization of Virus Infectivity by Antibodies: Old Problems in New Perspectives. Advances in biology. 2014; 2014 (1): 157895. Available from: https://doi.org/10.1155/2014/157895.
22. Yamaizumi M, et al. Neutralization of diphtheria toxin in living cells by microinjection of antifragment A contained within resealed erythrocyte ghosts. Cell. 1978; 13 (2): 227–32. Available from: https://doi.org/10.1016/0092-8674(78)90191-5.
23. Tonegawa S. Somatic generation of antibody diversity. Nature. 1983; 302 (5909): 575–81. Available from: https://doi.org/10.1038/302575a0.
24. Burke B, Warren G. Microinjection of mRNA coding for an anti-golgi antibody inhibits intracellular transport of a viral membrane protein. Cell. 1984; 36 (4): 847–56. Available from: https://doi.org/10.1016/0092-8674(84)90034-5.
25. Cottignies-Calamarte A, Tudor D, Bomsel M. Antibody Fc-chimerism and effector functions: When IgG takes advantage of IgA. Frontiers in immunology. 2023; 14: 1037033. Available from: https://doi.org/10.3389/fimmu.2023.1037033.
26. Tiller KE, Tessier PM. Advances in Antibody Design. Annual review of biomedical engineering. 2015; 17 (1): 191–216. Available from: https://doi.org/10.1146/annurev-bioeng-071114-040733.
27. Helfrich W, et al. A rapid and versatile method for harnessing scFv antibody fragments with various biological effector functions. Journal of Immunological Methods. 2000; 237 (1–2): 131–45. Available from: https://doi.org/10.1016/s0022-1759(99)00220-3.
28. Ahmad ZA, et al. scFv antibody: Principles and clinical application. Journal of Immunology Research. 2012; 2012 (1): 980250. Available from: https://doi.org/10.1155/2012/980250.
29. Le Gall F, et al. Di-, tri- and tetrameric single chain Fv antibody fragments against human CD19: Effect of valency on cell binding. FEBS letters. 1999; 453 (1–2): 164–8. Available from: https://doi.org/10.1016/S0014-5793(99)00713-9.
30. Kabayama H, et al. An ultra-stable cytoplasmic antibody engineered for in vivo applications. Nature communications. 2020; 11 (1): 336. Available from: https://doi.org/10.1038/s41467-019-13654-9.
31. Marschall ALJ, Dübel S, Böldicke T. Specific in vivo knockdown of protein function by intrabodies. MAbs. 2015; 7 (6): 1010–35. Available from: https://doi.org/10.1080/19420862.2015.1076601.
32. Karikó K, et al. Suppression of RNA recognition by Toll-like receptors: the impact of nucleoside modification and the evolutionary origin of RNA. Immunity. 2005; 23 (2): C. 165–75. Available from: https://doi.org/10.1016/j.immuni.2005.06.008.
33. Sahin U, Karikó K, Türeci Ö. mRNA-based therapeutics-developing a new class of drugs. Nature reviews Drug discovery. 2014; 13 (10): 759–80. Available from: https://doi.org/10.1038/nrd4278.
34. Jin Q, et al. The protective effect of a combination of human intracellular and extracellular antibodies against the highly pathogenic avian influenza H5N1 virus. Human Vaccines & Immunotherapeutics. 2022; 18 (1): 2035118. Available from: https://doi.org/10.1080/21645515.2022.2035118.
35. Mukhtar MM, et al. Single-chain intracellular antibodies inhibit

influenza virus replication by disrupting interaction of proteins involved in viral replication and transcription. The international journal of biochemistry & cell biology. 2009; 41 (3): 554–60. Available from: https://doi.org/10.1016/j.biocel.2008.07.001.
36. Ashour J, et al. Intracellular expression of camelid single-domain antibodies specific for influenza virus nucleoprotein uncovers distinct features of its nuclear localization. Journal of virology. 2015; 89 (5): 2792–800. Available from: https://doi.org/10.1128/JVI.02693-14.
37. Blavier J, et al. Targeting viral replication complexes with mRNA-encoded nanobodies: a new frontier for antiviral design. Drug Discovery Today. 2025; 104531. Available from: https://doi.org/10.1016/j.drudis.2025.104531.

Литература

1. Bender RG, et al. Global, regional, and national incidence and mortality burden of non-COVID-19 lower respiratory infections and aetiologies, 1990–2021: a systematic analysis from the Global Burden of Disease Study 2021. The Lancet Infectious Diseases. 2024; 24 (9): 974–1002. Available from: https://doi.org/10.1016/S1473-3099(24)00176-2.
2. Lin JJ, Feramisco JR. Disruption of the in vivo distribution of the intermediate filaments in fibroblasts through the microinjection of a specific monoclonal antibody. Cell. 1981; 24 (1): 185–93. Available from: https://doi.org/10.1016/0092-8674(81)90514-6.
3. Blose SH, Meltzer DI, Feramisco JR. 0-nm Filaments Are Induced to Collapse in Living Cells Microinjected with Monoclonal and Polyclonal Antibodies Against Tubulin. Journal of Cell Biology. 1984; 98: 847–58. Available from: https://doi.org/10.1083/jcb.98.3.847.
4. Kallajoki M, et al. Microinjection of a monoclonal antibody against SPN antigen, now identified by peptide sequences as the NuMA protein, induces micronuclei in PtK2 cells. Journal of Cell Science. 1993; 104 (1): 139–50. Available from: https://doi.org/10.1242/jcs.104.1.139.
5. Rabbitts TH. Intracellular Antibodies for Drug Discovery and as Drugs of the Future. Antibodies. 2023; 12 (1). Available from: https://doi.org/10.3390/antib12010024.
6. Biocca S, Neuberger MS, Cattaneo A. Expression and targeting of intracellular antibodies in mammalian cells. The EMBO Journal. 1990; 9 (1): 101–8. Available from: https://doi.org/10.1002/j.1460-2075.1990.tb08085.x.
7. Marschall ALJ, Dübel S, Böldicke T. Recent advances with ER targeted intrabodies. Advances in Experimental Medicine and Biology. 2016; 917: 77–93. Available from: https://doi.org/10.1007/978-3-319-32805-8_5.
8. Gerondopoulos A, et al. A signal capture and proofreading mechanism for the KDEL-receptor explains selectivity and dynamic range in ER retrieval. eLife. 2021; 10. Available from: https://doi.org/10.7554/eLife.68380.
9. Johnson AE, Van Waes MA. The Translocon: A Dynamic Gateway at the ER Membrane. Annual review of cell and developmental biology. 1999; 15 (1): 799–842. Available from: https://doi.org/10.1146/annurev.cellbio.15.1.799.
10. Haryadi R, et al. Optimization of Heavy Chain and Light Chain Signal Peptides for High Level Expression of Therapeutic Antibodies in CHO Cells. PloS one. 2015; 10 (2). Available from: http://dx.doi.org/10.1371/journal.pone.0116878.
11. Marschall ALJ, et al. Targeting antibodies to the cytoplasm. mAbs. 2011; 3 (1): 3–16. Available from: https://doi.org/10.4161/mabs.3.1.14110.
12. Richardson JH, Wayne MA. Intracellular antibodies: development and therapeutic potential. Trends in biotechnology. 1995; 13 (8): 306–10. Available from: https://doi.org/10.1016/S0167-7799(00)88970-2.
13. Плотникова М. А., и др. scFv-фрагменты рекомбинантных антител к вирусу гриппа: получение и характеристика функциональной активности. БИОпрепараты. Профилактика, диагностика, лечение. Принято к публикации 12.12.2025. Available from: https://doi.org/10.30895/2221-996X-2025-728.
14. Killian ML. Hemagglutination assay for influenza virus. Animal influenza virus. Animal Influenza Virus. Methods in Molecular Biology. 2014; 1161: 3–9. Available from: https://doi.org/10.1007/978-1-4939-0758-8_1.
15. Plotnikova MA, et al. Antibody microarray immunoassay for screening and differential diagnosis of upper respiratory tract viral pathogens. Journal of Immunological Methods. 2020; 478: 112712. Available from: https://doi.org/10.1016/j.jim.2019.112712.
16. Corti D, et al. A neutralizing antibody selected from plasma cells that binds to group 1 and group 2 influenza A hemagglutinins. Science. 2011; 333 (6044): 850–6. Available from: https://doi.org/10.1126/science.1205669.
17. Krivitskaya VZ, et al. Detection and Differentiation of Current Influenza B Viruses by the Microculture Enzyme-Linked Immunosorbent Assay Using Monoclonal Antibodies. Applied Biochemistry and Microbiology. 2023; 59 (7): 1039–46. Available from: https://doi.org/10.1134/S0003683823070037.
18. Biswas M, et al. Broadly neutralizing antibodies for influenza: Passive immunotherapy and intranasal vaccination. Vaccines. 2020; 8 (3): 424. Available from: https://doi.org/10.3390/vaccines8030424.
19. Momont C, et al. A pan-influenza antibody inhibiting neuraminidase via receptor mimicry. Nature. 2023; 618 (7965): 590–7. Available from: https://doi.org/10.1038/s41586-023-06136-y.
20. Heaton NS, et al. Genome-wide mutagenesis of influenza virus reveals unique plasticity of the hemagglutinin and NS1 proteins. Proceedings of the National Academy of Sciences. 2013; 110 (50): 20248–53. Available from: https://doi.org/10.1073/pnas.1320524110.
21. Klasse PJ. Neutralization of Virus Infectivity by Antibodies: Old Problems in New Perspectives. Advances in biology. 2014; 2014 (1): 157895. Available from: https://doi.org/10.1155/2014/157895.
22. Yamaizumi M, et al. Neutralization of diphtheria toxin in living cells by microinjection of antifragment A contained within resealed erythrocyte ghosts. Cell. 1978; 13 (2): 227–32. Available from: https://doi.org/10.1016/0092-8674(78)90191-5.
23. Tonegawa S. Somatic generation of antibody diversity. Nature. 1983; 302 (5909): 575–81. Available from: https://doi.org/10.1038/302575a0.
24. Burke B, Warren G. Microinjection of mRNA coding for an anti-golgi antibody inhibits intracellular transport of a viral membrane protein. Cell. 1984; 36 (4): 847–56. Available from: https://doi.org/10.1016/0092-8674(84)90034-5.
25. Cottignies-Calamarte A, Tudor D, Bomsel M. Antibody Fc-chimerism and effector functions: When IgG takes advantage of IgA. Frontiers in immunology. 2023; 14: 1037033. Available from: https://doi.org/10.3389/fimmu.2023.1037033.
26. Tiller KE, Tessier PM. Advances in Antibody Design. Annual review of biomedical engineering. 2015; 17 (1): 191–216. Available from: https://doi.org/10.1146/annurev-bioeng-071114-040733.
27. Helfrich W, et al. A rapid and versatile method for harnessing scFv antibody fragments with various biological effector functions. Journal of Immunological Methods. 2000; 237 (1–2): 131–45. Available from: https://doi.org/10.1016/s0022-1759(99)00220-3.
28. Ahmad ZA, et al. scFv antibody: Principles and clinical application. Journal of Immunology Research. 2012; 2012 (1): 980250. Available from: https://doi.org/10.1155/2012/980250.
29. Le Gall F, et al. Di-, tri- and tetrameric single chain Fv antibody fragments against human CD19: Effect of valency on cell binding. FEBS letters. 1999; 453 (1–2): 164–8. Available from: https://doi.org/10.1016/S0014-5793(99)00713-9.
30. Kabayama H, et al. An ultra-stable cytoplasmic antibody engineered for in vivo applications. Nature communications. 2020; 11 (1): 336. Available from: https://doi.org/10.1038/s41467-019-13654-9.
31. Marschall ALJ, Dübel S, Böldicke T. Specific in vivo knockdown of protein function by intrabodies. MAbs. 2015; 7 (6): 1010–35. Available from: https://doi.org/10.1080/19420862.2015.1076601.
32. Karikó K, et al. Suppression of RNA recognition by Toll-like receptors: the impact of nucleoside modification and the evolutionary origin of RNA. Immunity. 2005; 23 (2): C. 165–75. Available from: https://doi.org/10.1016/j.immuni.2005.06.008.
33. Sahin U, Karikó K, Türeci Ö. mRNA-based therapeutics-developing a new class of drugs. Nature reviews Drug discovery. 2014; 13 (10): 759–80. Available from: https://doi.org/10.1038/nrd4278.
34. Jin Q, et al. The protective effect of a combination of human intracellular and extracellular antibodies against the highly

pathogenic avian influenza H5N1 virus. Human Vaccines & Immunotherapeutics. 2022; 18 (1): 2035118. Available from: https://doi.org/10.1080/21645515.2022.2035118.

35. Mukhtar MM, et al. Single-chain intracellular antibodies inhibit influenza virus replication by disrupting interaction of proteins involved in viral replication and transcription. The international journal of biochemistry & cell biology. 2009; 41 (3): 554–60. Available from: https://doi.org/10.1016/j.biocel.2008.07.001.

36. Ashour J, et al. Intracellular expression of camelid single-domain antibodies specific for influenza virus nucleoprotein uncovers distinct features of its nuclear localization. Journal of virology. 2015; 89 (5): 2792–800. Available from: https://doi.org/10.1128/JVI.02693-14.

37. Blavier J, et al. Targeting viral replication complexes with mRNA-encoded nanobodies: a new frontier for antiviral design. Drug Discovery Today. 2025; 104531. Available from: https://doi.org/10.1016/j.drudis.2025.104531.

HMGB1 AND ANTI-HMGB1 ANTIBODIES IN SYSTEMIC LUPUS ERYTHEMATOSUS AND OTHER RHEUMATIC DISEASES

Melamud MM[1], Ermakov EA[1,2], Tolmacheva AS[1], Sizikov AE[1,3], Klyaus NA[4], Nevinsky GA[1], Buneva VN[1,2]✉

[1] Institute of Chemical Biology and Fundamental Medicine, Siberian Branch of the Russian Academy of Sciences, Novosibirsk, Russia
[2] Department of Natural Sciences, Novosibirsk State University, Novosibirsk, Russia
[3] Research Institute of Fundamental and Clinical Immunology, Siberian Branch of the Russian Academy of Sciences, Novosibirsk, Russia
[4] Almazov National Medical Research Centre, Saint Petersburg, Russia

The high-mobility group protein B1 (HMGB1) belongs to alarmins — a group of molecules involved in inflammatory responses. HMGB1 is actively studied in the context of certain rheumatic diseases (RDs), including systemic lupus erythematosus (SLE), rheumatoid arthritis (RA), ankylosing spondylitis (AS), and psoriatic arthritis (PsA), but the accumulated knowledge remains insufficient. HMGB1 can also act as an antigen, yet the level of anti-HMGB1 antibodies is poorly understood in RDs. The aim of this study was to investigate the concentrations of HMGB1 and anti-HMGB1 antibodies in four RDs. Using enzyme-linked immunosorbent assay (ELISA), plasma samples from patients with RA (n = 60), AS (n = 60), SLE (n = 24), PsA (n = 30), and healthy donors (HD) (n = 60) were analyzed. After adjustment for age and disease duration, it was shown that the concentration of HMGB1 was significantly increased in SLE ($p < 0.01$), RA ($p < 0.01$), and AS ($p = 0.017$), while a statistically non-significant increase in HMGB1 was observed in PsA ($p = 0.07$) compared to HD. Among the four diseases, the highest level of HMGB1 was found in SLE ($p < 0.01$). The concentration of anti-HMGB1 antibodies was also elevated in SLE ($p < 0.01$), RA ($p = 0.026$), and AS ($p = 0.028$). Using correlation and regression analysis, a strong direct association was established between the level of HMGB1 and the DAS28 index in RA ($p < 0.01$ for both analyses). The results of the study describe characteristic changes in HMGB1 and anti-HMGB1 antibody levels in RDs and indicate the involvement of HMGB1 in the pathogenesis of these diseases.

Keywords: rheumatoid arthritis, ankylosing spondylitis, psoriatic arthritis, systemic lupus erythematosus, HMGB1, anti-HMGB1 antibodies

Funding: this work was supported by the Russian Science Foundation (Grant No. 23-15-00357).

Author contribution: Melamud MM — data analysis, manuscript writing; Ermakov EA — study design, manuscript writing and editing; Tolmacheva AS — experimental work, data analysis; Sizikov AE, Klyaus NA — material collection and preparation, data analysis; Nevinsky GA, Buneva VN — project supervision, editing. The contributions of Melamud MM and Ermakov EA were equal.

Compliance with ethical standards: The study was approved by the Ethics Committee of the Institute of Chemical Biology and Fundamental Medicine, Siberian Branch of the Russian Academy of Sciences (Protocol No. 3 dated June 19, 2023) and was conducted in accordance with the principles of the Declaration of Helsinki. All study participants provided written informed consent.

✉ **Correspondence should be addressed:** Valentina N. Buneva
prospekt Akademika Lavrentieva, 8, Novosibirsk, 630090, Russia; buneva@1bio.ru

Received: 29.10.2025 **Accepted:** 06.12.2025 **Published online:** 14.12.2025

DOI: 10.24075/brsmu.2025.074

Copyright: © 2025 by the authors. **Licensee:** Pirogov University. This article is an open access article distributed under the terms and conditions of the Creative Commons Attribution (CC BY) license (https://creativecommons.org/licenses/by/4.0/).

HMGB1 И АНТИ-HMGB1 АНТИТЕЛА ПРИ СИСТЕМНОЙ КРАСНОЙ ВОЛЧАНКЕ И ДРУГИХ РЕВМАТИЧЕСКИХ ЗАБОЛЕВАНИЯХ

М. М. Меламуд[1], Е. А. Ермаков[1,2], А. С. Толмачева[1], А. Э. Сизиков[1,3], Н. А. Кляус[4], Г. А. Невинский[1], В. Н. Бунева[1,2]✉

[1] Институт химической биологии и фундаментальной медицины Сибирского отделения Российской академии наук, Новосибирск, Россия
[2] Новосибирский национальный исследовательский государственный университет, Новосибирск, Россия
[3] Научно-исследовательский институт фундаментальной и клинической иммунологии, Новосибирск, Россия
[4] Национальный медицинский исследовательский центр имени В. А. Алмазова, Санкт-Петербург, Россия

Белок B1 группы высокой подвижности (англ. high-mobility group protein B1, HMGB1) относится к аларминам — группе молекул, участвующих в воспалительных реакциях. HMGB1 активно изучают в контексте некоторых ревматических заболеваний (РЗ), включая системную красную волчанку (СКВ), ревматоидный артрит (РА), анкилозирующий спондилит (АС) и псориатический артрит (ПсА), однако накопленных знаний недостаточно. HMGB1 может также выступать антигеном, но уровень анти-HMGB1 антител плохо изучен при РЗ. Целью работы было изучить концентрации HMGB1 и анти-HMGB1 антител при четырех РЗ. Методом иммуноферментного анализа проанализированы образцы плазмы пациентов с РА (n = 60), АС (n = 60), СКВ (n = 24), ПсА (n = 30) и здоровых доноров (ЗД) (n = 60). После поправки на возраст и длительность заболевания показано, что концентрация HMGB1 достоверно повышалась при СКВ ($p < 0,01$), РА ($p < 0,01$) и АС ($p = 0,017$), а при ПсА выявлено статистически незначимое повышение HMGB1 ($p = 0,07$) по сравнению с ЗД. Среди четырех заболеваний наибольший уровень HMGB1 выявлен при СКВ ($p < 0,01$). Концентрация анти-HMGB1 антител оказалась также выше при СКВ ($p < 0,01$), РА ($p = 0,026$) и АС ($p = 0,028$). Методами корреляционного и регрессионного анализа установлена выраженная прямая ассоциация между уровнем HMGB1 и индексом DAS28 при РА ($p < 0,01$ для обоих анализов). Результаты работы описывают характерные изменения уровня HMGB1 и анти-HMGB1 антител при РЗ и указывают на вовлеченность HMGB1 в патогенез этих заболеваний.

Ключевые слова: ревматоидный артрит, анкилозирующий спондилит, псориатический артрит, системная красная волчанка, HMGB1, анти-HMGB1 антитела

Финансирование: работа выполнена при финансовой поддержке Российского научного фонда (грант № 23-15-00357).

Вклад авторов: М. М. Меламуд — обработка результатов, написание статьи; Е. А. Ермаков — планирование исследования, написание и редактирование статьи; А. С. Толмачёва — экспериментальная работа, анализ данных; А. Э. Сизиков, Н. А. Кляус — сбор и подготовка материала, анализ данных; Г. А. Невинский, В. Н. Бунева — курирование работы, редактирование; вклад М. М. Меламуда и Е. А. Ермакова был равнозначным.

Соблюдение этических стандартов: исследование одобрено этическим комитетом Института химической биологии и фундаментальной медицины Сибирского отделения РАН (протокол № 3 от 19 июня 2023 г.), проведено в соответствии с принципами Хельсинкской декларации; все участники исследования подписали добровольное информированное согласие.

✉ **Для корреспонденции:** Валентина Николаевна Бунева
пр. Академика Лаврентьева, д. 8, г. Новосибирск, 630090, Россия; buneva@1bio.ru

Статья получена: 29.10.2025 **Статья принята к печати:** 06.12.2025 **Опубликована онлайн:** 14.12.2025

DOI: 10.24075/vrgmu.2025.074

Авторские права: © 2025 принадлежат авторам. **Лицензиат:** РНИМУ им. Н. И. Пирогова. Статья размещена в открытом доступе и распространяется на условиях лицензии Creative Commons Attribution (CC BY) (https://creativecommons.org/licenses/by/4.0/).

Rheumatic diseases (RD) are an important medical and social problem due to their prevalence, impact on quality of life, and high economic costs of treatment. Systemic lupus erythematosus (SLE) is one of the most common autoimmune diseases, predominantly affecting young women aged 15–45 years, thereby indirectly worsening the demographic situation in addition to its direct effect on patients' lives. The global prevalence of SLE varies from 3 to 517 cases per 100,000 people; in recent decades, the incidence has been growing [1]. Another common RD is rheumatoid arthritis (RA): approximately 200 cases per 100,000 persons, and the incidence is steadily increasing and is projected to almost double by 2050 [2]. Ankylosing spondylitis (AS) occurs in 9–30 people per 100,000 persons [3]. Unlike most RDs, AS affects men more often than women (the approximate ratio is 2–3 to 1), typically — men of working age; 92% of patients experience the first symptoms of the disease before the age of 45 [4]. Compared to other diseases, psoriatic arthritis (PsA) has been studied much less, even though it is fairly common (more than 100 cases per 100,000 population) and significantly affects patients' quality of life [5]. Treatment of RDs increases the financial burden on the healthcare system each year [6]. The high prevalence and social significance of RDs necessitate the search for new biomarkers that would enable early diagnosis and timely therapy. In addition, a comparison of biomarkers among RDs can reveal the characteristic pathophysiological mechanisms of each RD and potential markers for differential diagnosis.

The pathogenesis of RDs is associated with the activation of inflammatory pathways of both innate and acquired immunity. Damage-associated molecular patterns (DAMPs), also known as alarmins, greatly contribute to the development of inflammatory responses [7]. Alarmins of nuclear origin play an important role in the pathogenesis of RDs [8–10]. One of them is high-mobility group protein B1 (HMGB1), which consists of box A, considered anti-inflammatory, box B, exhibiting pro-inflammatory functions, and an acid tail limiting the activity of this protein within the nucleus [11]. HMGB1 acts as a chemoattractant, bringing immune cells to the lesion site. The protein acts synergistically with DNA, triggering a powerful proinflammatory response that enables autoimmunity, including in cases of RDs [12]. The changes in HMGB1 concentrations associated with SLE and RA have been well studied [12, 13], but there is relatively little information in the literature regarding such changes in AS and PsA. Moreover, both the relationship between HMGB1 level and disease manifestations and the comparison of these parameters across various RDs remain largely uninvestigated.

The pathogenesis of RDs involves not only innate, but also adaptive immunity. Autoantibodies, especially antinuclear antibodies, are considered biomarkers of SLE. Antibodies to cyclic citrullinated polypeptide (ACCP) and rheumatoid factor (RF) are often found in RA patients. Some of these autoantibodies are included in the criteria for diagnosis [14, 15]. HMGB1 is known to also induce production of antibodies that can participate in the pathogenetic processes of RDs [16, 17]. However, very few studies have focused on anti-HMGB1 antibodies in RD cases, even though this protein plays an active role in the inflammatory response and the development of autoimmune reactions.

This study aimed to analyze blood concentrations of HMGB1 and anti-HMGB1 antibodies in patients with SLE, RA, PsA, and AS, as well as in healthy donors (controls), and to assess the relationship between these markers and the clinical characteristics of the diseases.

METHODS

Patients and healthy donors

The study was conducted from July 2023 to July 2025 in two establishments: Institute of Chemical Biology and Fundamental Medicine, Siberian Branch of the Russian Academy of Sciences, Novosibirsk; Research Institute of Fundamental and Clinical Immunology, Siberian Branch of the Russian Academy of Sciences, Novosibirsk.

The study included 60 patients with rheumatoid arthritis (RA) diagnosed according to the 2010 ACR/EULAR criteria; 60 patients with ankylosing spondylitis (AS) or axial spondyloarthritis diagnosed according to the modified New York and ASAS criteria; 30 patients with psoriatic arthritis (PsA) diagnosed according to the CASPAR criteria; 24 patients with systemic lupus erythematosus (SLE) diagnosed according to the 2019 ACR/EULAR criteria; and 60 healthy controls without active somatic pathology. The diagnoses and medical histories were established and collected by qualified rheumatologists at the Research Institute of Fundamental and Clinical Immunology, where the participating patients donated blood samples. Healthy controls gave their blood for the study at the Institute of Chemical Biology and Fundamental Medicine. The indices used to evaluate the clinical condition of the patients were as follows: for RA — the DAS28 index; for AS — the ASDAS-CRP/ASDAS-ESR and BASDAI indices; for PsA — the DAPSA index; and for SLE — the SELENA-SLEDAI index.

To participate in the study, patients had to sign a voluntary informed consent form, be 18 years or older, have an established diagnosis of RA, PsA, SLE or AS. The exclusion criteria included the presence of other autoimmune diseases, a history of cancer, severe liver or kidney damage, acute inflammatory diseases within two weeks before blood sampling, surgical operations within the last two months, HIV infection, and pregnancy. Healthy donors had to sign an informed consent form, be over the age of 18, and not meet any of the exclusion criteria.

The blood samples were collected in vacuum tubes with K3EDTA (VACUETTE, Greiner Bio-One GmbH, Austria). Blood plasma was separated by centrifugation at 2000 × g for 30 minutes at 4 °C, then aliquoted and stored at –20 °C until analysis.

Determination of the concentration of HMGB1 and anti-HMGB1 antibodies

The concentration of HMGB1 was determined by enzyme immunoassay (ELISA) using the Human HMGB1 ELISA Kit (Cat. No.: E-EL-H1554, Elabscience, USA). The sensitivity of this kit was 18.75 pg/ml, the measuring range — 31.25–2000 pg/ml. The blood plasma was preliminarily diluted 10 times for analysis. The concentration of anti-HMGB1 antibodies was determined using the ELISA Kit for anti-HMGB1 antibody (Cat. No.: AEA399Hu, Cloud-Clone Corp., China). The sensitivity of this kit was 1.17 ng/ml, the measuring range — 3.12–200 ng/ml. Participants with concentrations below the sensitivity threshold were considered to have no anti-HMGB1 antibodies. The blood plasma used for anti-HMGB1 antibody analysis was diluted 1 : 100. Optical density was measured on a Multiskan™ FC Microplate Photometer (Thermo Fisher Scientific Inc., USA) at a wavelength of 450 nm according to the instructions of the manufacturer.

Table 1. Clinical and medical history data of the participants (patients with RDs and healthy individuals)

Parameter*	RA (*n* = 60) (1)	AS (*n* = 60) (2)	PsA (*n* = 30) (3)	SLE (*n* = 24) (4)	Healthy (*n* = 60) (5)	*p***
Sex (m/w), %	22/78	69/31	30/70	0/100	30/70	< 0.01
Age, years	52 (38; 61)	46 (38; 52)	44 (34; 56)	44 (31; 54)	45 (29; 51)	H.3.
Duration of the disease, years	9 (5; 17.5)	12 (7.8; 22.3)	12.5 (3; 21.3)	6 (3; 14)	–	2 vs. 4: < 0.01
BMI	26 (23; 29)	25.8 (21.5; 28.1)	25.9 (21.2; 30)	25.2 (21; 28)	23.5 (20.2; 26.3)	IS
ESR, mm/h	2.6 (0.8; 11.5)	2.8 (1.1; 6.2)	4.3 (2.4; 9.8)	2.2 (0.8; 8.9)	–	IS
CRP, mg/l	14.5 (6.8; 28)	10 (4; 18)	16 (10; 26)	15 (8.5; 38)	–	IS
Clinical index	DAS28: 3.4 (2.6; 4.6)	ASDAS-CRP: 1.7 (1.3; 2.5); ASDAS-ESR: 1.8 (1.31; 2.6); BASDAI: 1.9 (1.0; 3.2)	DAS28: 3.5 (1; 9.4); DAPSA: 14 (6; 22)	SELENA-SLEDAI: 4 (2; 8)	–	–

Note: * — the data are given as Me (Q_1; Q_3). ** — Yates-corrected chi-square test, or the Kruskal–Wallis test with Dunn's post-hoc test. BMI — body mass index, ESR — erythrocyte sedimentation rate, CRP — C-reactive protein, IS — insignificant

Statistical analysis

Statistical analysis and data visualization were performed using OriginPro 2021 and the Google Colab environment with Python 3.13.0, employing the NumPy (v2.3.3), SciPy (v1.16.2), and Matplotlib (v3.10.6) libraries. The type of distribution of data in individual samples was determined with the Shapiro–Wilk test. Since the data mostly did not distribute normally, the results are presented as a median (Q_1–Q_3). The values between the samples were compared using a rank ANCOVA followed by a post-hoc Dunn's test, with the covariates (age and duration of the disease) factored in. Categorical variables (frequency of occurrence of the trait) were evaluated using the chi-square test. The difference in the frequency of occurrence of the trait was estimated by calculating the odds ratio (OR). Spearman's rank correlation coefficient enabled the assessment of correlation. Multiple linear regression was used to evaluate the relationship between the dependent variable (DAS28) and the predictors. Before performing multiple regression, all data were normalized by logarithmization (log10).

RESULTS

Sample characteristics

A total of 234 people participated in the study: 60 patients with RA, 60 with AS, 30 with PsA, 24 with SLE, and 60 healthy individuals. Table 1 gives the clinical and medical history data of the participants. According to DAS28, most RA patients exhibited moderate disease activity. Eighty percent of them had a positive RF value, and 82% were found to have ACCP. Patients with AS mostly had low disease activity according to the ASDAS-CRP and ASDAS-ESR indices, but moderate activity according to the BASDAI index. Seventy-six percent of them carried the HLA-B27 allele. The majority of PsA patients had moderate disease activity according to the DAS28 and DAPSA indices. Among patients with SLE, more than half had low disease activity. The sex distribution of participants varied across disease subgroups, and patients with RA tended to be older, reflecting the typical age and sex characteristics of each disease. In addition, AS patients had a longer duration of the disease than SLE patients (Table 1).

All patients were undergoing therapy. In particular, 56% of patients with RA, 90% with AS, and 50% with PsA were taking biologic disease-modifying antirheumatic drugs (bDMARDs). Patients with SLE did not take bDMARDs. As for other drugs, 43% of patients with RA, 32% with AS, 40% with PsA, and 8% with SLE were taking methotrexate. For SLE, the most common drug was hydroxychloroquine (71%).

Concentration of HMGB1 and anti-HMGB1 antibodies

Analyzing the concentrations of HMGB1 and anti-HMGB1 antibodies, we included age and disease duration as covariates to account for the respective trends observed in the sample, particularly within the RA and AS subgroups. The analysis was performed using the ANCOVA rank method followed by a post-hoc Dunn's test. For the control group, only the age covariate was factored in. The analysis showed that after adjusting for age and duration of the disease, the plasma concentration of HMGB1 in patients with SLE (Me [Q_1–Q_3]: 22.6 [12.8–33.5] ng/ml), RA (15 [9–23]), and AS (12.5 [7.6–18.9]) was significantly higher than in healthy controls (8.6 [5.7–12.2]) (Fig. 1A). The HMGB1 level in PsA cases (11.6 [5.9–20.1]) did not significantly differ from that in the controls. In SLE cases, the concentration of this protein was higher than in patients with AS and PsA. In the ANCOVA model, age and duration of the disease did not significantly affect the indicators. Thus, the highest level of HMGB1 was found in patients with SLE.

The levels of HMGB1 among subgroups did not differ significantly depending on the clinical features of the diseases. In particular, the difference in concentrations of the protein in RF-positive (17.5 [9–25.2]) and RF-negative (13.6 [6.1–23.4]) RA patients was insignificant (p = 0.33), same as in ACCP-positive (17.5 [9–25.4]) and ACCP-negative (9.7 [6.9–22.1]) RA patients (p = 0.26). In AS, there was a statistically insignificant trend towards an increase in HMGB1 levels in HLA-B27-positive patients (12.8 [9.6–18.9]) compared with HLA-B27-negative (9 [6.2–13.7]) patients (p = 0.07).

Analysis of the concentration of anti-HMGB1 antibodies adjusted for age and duration of the disease showed a significant increase in the level of these antibodies in SLE (Me [Q_1–Q_3]: 1121 [691–2859] ng/ml), RA (737 [104–1219]) and AS (543 [55–1546]) cases compared with healthy individuals (167 [0–602]) (Fig. 1B). In PsA patients, the concentration of anti-HMGB1 antibodies (550 [0–1158]) did not differ from that in the control group. The highest median level of anti-HMGB1 antibodies was observed in patients with SLE, but no significant differences were found for the four diseases considered. Age and duration of the disease were insignificant in the ANCOVA model.

The level of anti-HMGB1 antibodies varied among the participants. Based on the sensitivity of the ELISA kit (1.17 ng/ml),

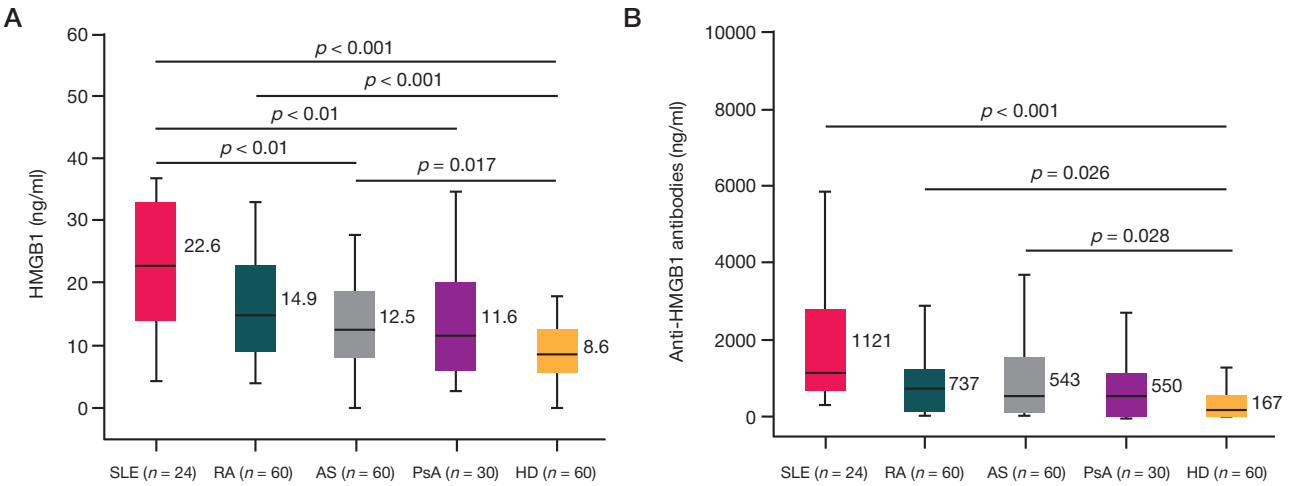


Fig. 1. The blood plasma concentration of HMGB1 (**A**) and anti-HMGB1 antibodies (**B**) in patients with systemic lupus erythematosus (SLE), rheumatoid arthritis (RA), ankylosing spondylitis (AS), psoriatic arthritis (PsA) and healthy donors (HD). The analysis was performed using the ANCOVA rank method followed by a post-hoc Dunn's test, adjusted for age and duration of the disease. The median values are shown to the right of the boxes

the participants were divided into anti-HMGB1-negative (below the threshold) and anti-HMGB1-positive (above the threshold) (Fig. 2). We identified the smallest number of anti-HMGB1–positive participants in the control group. Among patients with RDs, the frequency of this status decreased progressively from SLE to RA, AS, and PsA. Anti-HMGB1 antibodies were detected in SLE cases 40.2 times more often (95%CI: 2.3–692, p = 0.0003) than in healthy individuals. In RA and AS, such antibodies were also detected 2.7 (1.23–5.9, p = 0.02) and 2.45 (1.13–5.33, p = 0.04) times more often, respectively, than in the controls. Among the group of participants with RDs, anti-HMGB1 antibodies were detected in patients with SLE 15.3 (0.87–267, p = 0.04) times more often than in RA cases, 16.6 (0.96–291, p = 0.03) times more often than in AS patients, and 25.1 (1.38–455, p = 0.008) times more often than in participants with PsA. Thus, the incidence of anti-HMGB1 antibodies in SLE is higher than in other RDs.

No significant differences were found among the clinical subgroups. In particular, the levels of anti-HMGB1 antibodies in RF-positive RA patients (784 [23–1219]) and in RF-negative patients (717 [502–1051]) did not differ (p = 0.69), same as between ACCP-positive (679 [32–1117]) and ACCP-negative patients (1117 [542–1431]) (p = 0.12). In AS, the levels of anti-HMGB1 antibodies in HLA-B27-positive (584 [32–1388]) and HLA-B27-negative (369 [13–1383]) participants also did not differ significantly (p = 0.62).

Correlations

Correlation analysis revealed a direct link between HMGB1 levels and CRP and ESR parameters in RA, AS, and PsA (Fig. 3). Antibodies to HMGB1 positively correlated only with CRP in patients with RA and with ESR in patients with AS. Unexpectedly, in patients with SLE, neither HMGB1 nor anti-HMGB1 antibodies correlated with ESR and CRP (Fig. 3A), which is probably due to the small sample size. These findings highlight the pro-inflammatory role of HMGB1 in RA, AS, and PsA.

An analysis of the correlation between HMGB1 levels and the DAS28 index in patients with RA showed a strong positive association (Rs = 0.56, p = 8.4e–6) (Fig. 3B). In patients with PsA, HMGB1 levels positively correlated with the DAPSA index (Rs = 0.38, p = 0.04), but not with the DAS28 index (Fig. 3C). In the same subgroup of participants, the level of antibodies to HMGB1 positively correlated with both the DAS28 index (Rs = 0.52, p = 0.005) and the DAPSA index (Rs = 0.52, p = 0.005). No statistically significant correlations with the studied markers and clinical indices were found in patients with AS and SLE (Fig. 3).

Regression analysis

In this study, multiple regression analysis was used to assess the relationship between the concentrations of HMGB1 and anti-HMGB1 antibodies (as independent predictors) and clinical indices (as dependent variables). For RA, the DAS28 score was used; for AS, the ASDAS-CRP, ASDAS-ESR, and BASDAI scores; for PsA, the DAS28 and DAPSA scores; and for SLE, the SELENA-SLEDAI score. Of the seven regression models built, only the model for RA turned out to be significant (Table 2). This model explains the 31.1% variation of the logarithmic DAS28 index. It has been shown that a 1% increase in HMGB1 concentration is associated with a 0.49% increase in DAS28 (p < 0.001). As for anti-HMGB1 antibodies, there were no significant associations established (p = 0.145) (Table 2).

Since ESR is one of the variables used to calculate the DAS28 index, a regression model was also built in which ESR and CRP served as predictors of DAS28. The model turned out to be significant (R2adj. = 0.351; F = 15.31; p < 0.001). As expected, ESR, unlike CRP, was a significant predictor

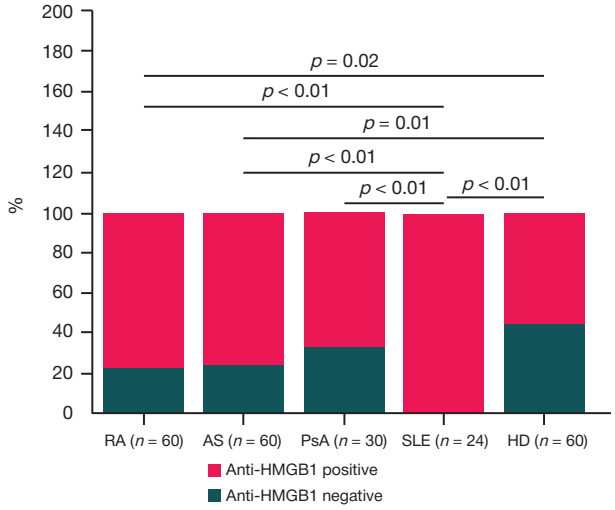


Fig. 2. The frequency of occurrence of anti-HMGB1 antibodies in patients with RA, AS, PsA, SLE, and healthy donors (HD). Statistical significance was assessed using the chi-square test

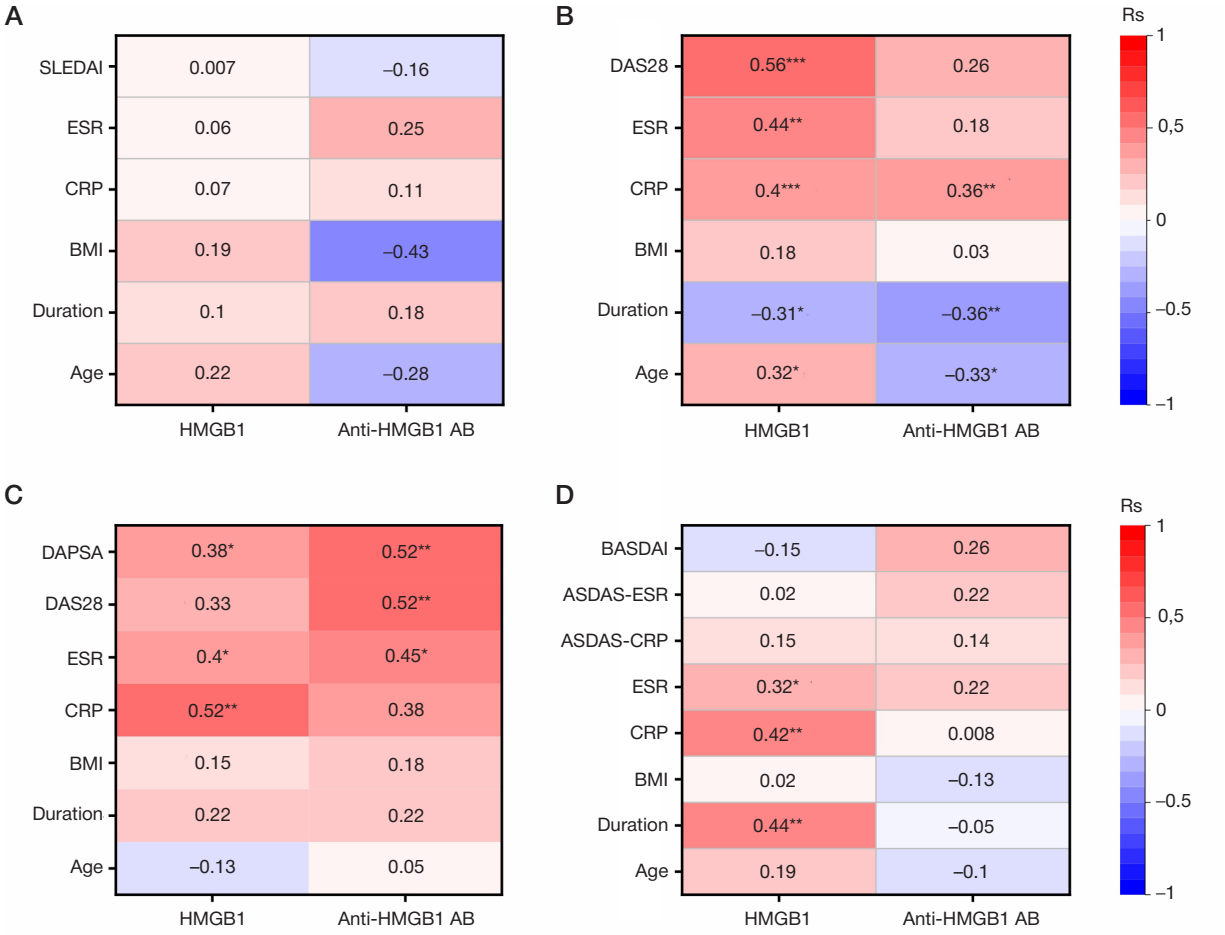


Fig. 3. Correlation of the concentration of HMGB1 and anti-HMGB1 antibodies with the clinical characteristics of SLE (**A**), RA (**B**), PsA (**C**) and AS (**D**). Spearman's rank correlation coefficients (Rs) are color-coded. * — $p < 0.05$, ** — $p < 0.01$, *** — $p < 0.001$

of DAS28. In the regression model, a 1% increase in ESR is associated with a 0.265% increase in DAS28. Thus, HMGB1, along with ESR, was a predictor of DAS28.

DISCUSSION

Previous studies have shown that blood HMGB1 concentrations are elevated in patients with RA [18], AS [19], PsA [20] and SLE [21, 22] compared with healthy individuals. In this work, the recorded increase in HMGB1 levels in SLE, RA, and AS (Fig. 1A) is consistent with the data reported in the literature [18–20]. However, we observed only an upward trend — a 1.39-fold increase in HMGB1 concentration — in PsA, which may be attributable to the small sample size and treatment effects. Therefore, it is necessary to continue investigation of HMGB1 levels and its role in PsA.

Previous studies have focused on the analysis of HMGB1 concentrations in certain RDs [18–21]. In this work, we compare four RDs. The highest level of HMGB1 was detected in SLE (Fig. 1A), which may indicate that the inflammation is most pronounced in SLE compared with other considered diseases, since HMGB1 is an inflammatory mediator [12]. Nevertheless, given the detected increase in HMGB1 levels and the association with DAS28 (Fig. 1A, Fig. 3B, Table 2), it can be assumed that HMGB1 is also involved in the pathogenesis of RA. Therefore, existing therapeutic strategies targeting HMGB1, including monoclonal antibodies [12], may be effective for treating patients with SLE and RA; however, further studies are needed to evaluate the effects of HMGB1 suppression in these diseases.

The regression (Table 2) and correlation (Fig. 3B) analyses revealed association of HMGB1 level with DAS28 in RA, which seemed intriguing. We have shown that a 1% increase in HMGB1 concentration is associated with a 0.49% increase in DAS28 (Table 2). Moreover, in a regression model using ESR as a predictor of DAS28, we found that a 1% increase in ESR was associated with a 0.265% increase in DAS28. Thus, the level of HMGB1 turned out to be a comparable predictor of DAS28 in RA, same as ESR, which is used to calculate this index. Therefore, HMGB1 may serve as a potential biomarker for RA disease activity. However, HMGB1 is a non-specific marker of inflammation, which reduces its diagnostic and predictive value in the context of RA.

The positive correlation of HMGB1 with ESR and CRP in RA, AS, and PsA (Fig. 3) highlights the pro-inflammatory role of this protein in these diseases. This is consistent with

Table 2. Multiple regression analysis for DAS28 as a dependent variable, and HMGB1 and anti-HMGB1 antibodies as predictors

Variable	β	St. error	*t*	*p*	Model
Constant	–1.6808	0.468	–3.588	< 0.001	$R^2_{корр.} = 0.311$; F = 11.13; $p < 0.001$
HMGB1	0.4878	0.108	4.51	< 0.001	
Anti-HMGB1 antibodies	0.0646	0.043	1.495	0.145	

the data reported in the literature. For example, HMGB1 has been shown to correlate with ESR and CRP in AS [19]. In our work, no such association was found for SLE, although it was recorded earlier [22]. The possible reasons for this is the small sample size or the effects of anti-inflammatory therapy.

The appearance of HMGB1 in the bloodstream may be associated with both active secretion and cell death [11]. In various variants of the latter, the protein can be released with other nuclear components, including DNA [11]. Evidence suggests an increase in circulating extracellular DNA levels in SLE [9, 23], RA [24], and AS [25, 26]. These data are consistent with our findings showing elevated HMGB1 levels in SLE, RA, and AS (Fig. 1A), as circulating extracellular DNA can be isolated in complex with this protein. It is feasible to further investigate the mechanisms of HMGB1 release in RDs.

The elevated level of HMGB1 may be associated with the formation of antibodies to HMGB1 [16]. In this study, high concentration of anti-HMGB1 antibodies were detected in SLE, RA, and AS (Fig. 1B). Such antibodies were most often found in patients with SLE (Fig. 2), who also had the highest level of HMGB1 (Fig. 1A). Interestingly, in PsA, the antibody level did not differ from the control, which is consistent with the low concentration of HMGB1 in these cases. However, these patients unexpectedly showed a positive correlation of anti-HMGB1 antibodies with DAS28 and DAPSA (Fig. 3C), which requires further study. The elevated level of anti-HMGB1 antibodies in SLE we have registered is consistent with the literature data [16]. However, there is no previously reported findings about the antibodies in RA, AS, and PsA, so this study fills this knowledge gap.

The limitations of this work include a relatively small sample size, a trend towards a higher age of RA patients, differences in the duration of the disease, and an unbalanced sex ratio due to the characteristics of the analyzed RDs. We adjusted for age and duration of the disease, but further studies should find out the influence of sex on the considered indicators.

CONCLUSIONS

This study revealed an increase in the blood plasma concentration of HMGB1 in SLE, RA and AS, while in PsA there was only an increase trend compared with healthy donors. Among the four rheumatic diseases, the greatest increase in HMGB1 was found in patients with SLE. The level of anti-HMGB1 antibodies was also significantly increased in patients with SLE, and to a lesser extent in RA and AS. However, there were no pronounced associations with the clinical parameters of SLE. On the contrary, in RA, the level of these markers was associated with the clinical characteristics of patients, which was confirmed both by the correlation analysis and the regression model. These data indicate that HMGB1 may be involved in complex pathogenetic mechanisms primarily in RA, which confirms the relevance of this molecule as a therapeutic target. Anti-HMGB1 antibodies were associated with clinical indices in patients with PsA, which necessitates further investigation of the contribution of these antibodies to the pathogenesis of PsA.

References

1. Carter EE, Barr SG, Clarke AE. The global burden of SLE: prevalence, health disparities and socioeconomic impact. Nat Rev Rheumatol. 2016; 12: 605–20. Available from: https://doi.org/10.1038/nrrheum.2016.137.
2. Black RJ, Cross M, Haile LM, Culbreth GT, Steinmetz JD, Hagins H, et al. Global, regional, and national burden of rheumatoid arthritis, 1990–2020, and projections to 2050: a systematic analysis of the Global Burden of Disease Study 2021. The Lancet Rheumatology. 2023; 5: e594–610. Available from: https://doi.org/10.1016/S2665-9913(23)00211-4.
3. Wang R, Ward MM. Epidemiology of axial spondyloarthritis: an update. Current Opinion in Rheumatology. 2018; 30: 137–43. Available from: https://doi.org/10.1097/BOR.0000000000000475.
4. Boel A, López-Medina C, Van Der Heijde DMFM, Van Gaalen FA. Age at onset in axial spondyloarthritis around the world: data from the Assessment in SpondyloArthritis international Society Peripheral Involvement in Spondyloarthritis study. Rheumatology. 2022; 61: 1468–75. Available from: https://doi.org/10.1093/rheumatology/keab544.
5. Lembke S, Macfarlane GJ, Jones GT. The worldwide prevalence of psoriatic arthritis — a systematic review and meta-analysis. Rheumatology. 2024; 63: 3211–20. Available from: https://doi.org/10.1093/rheumatology/keae198.
6. Lila AM, Lila VA. Social'naya znachimost' i ekonomicheskie posledstviya revmaticheskih zabolevanij. Gigiena i sanitariya. 2017; 96: 387–92. Available from: https://doi.org/10.47470/0016-9900-2017-96-4-387-392. Russian.
7. Danieli MG, Antonelli E, Piga MA, Claudi I, Palmeri D, Tonacci A, et al. Alarmins in autoimmune diseases. Autoimmunity Reviews. 2022; 21: 103142. Available from: https://doi.org/10.1016/j.autrev.2022.103142.
8. Ermakov EA, Tolmacheva AS, Kon'kov VV, Melamud MM, Sizikov AE, Klyaus NA, et al. Plasma high-mobility group nucleosome-binding domain 1 (HMGN1) protein levels in four common rheumatic diseases: A potential biomarker of rheumatoid arthritis. The Egyptian Rheumatologist. 2025; 47: 51–5. Available from: https://doi.org/10.1016/j.ejr.2024.12.003.
9. Truszewska A, Wirkowska A, Gala K, Truszewski P, Krzemień-Ojak Ł, Perkowska-Ptasińska A, et al. Cell-free DNA profiling in patients with lupus nephritis. Lupus. 2020; 29: 1759–72. Available from: https://doi.org/10.1177/0961203320957717.
10. Duvvuri B, Lood C. Cell-Free DNA as a Biomarker in Autoimmune Rheumatic Diseases. Front Immunol. 2019; 10: 502. Available from: https://doi.org/10.3389/fimmu.2019.00502.
11. Chen R, Kang R, Tang D. The mechanism of HMGB1 secretion and release. Exp Mol Med. 2022; 54: 91–102. Available from: https://doi.org/10.1038/s12276-022-00736-w.
12. Dong Y, Ming B, Dong L. The Role of HMGB1 in Rheumatic Diseases. Front Immunol. 2022; 13: 815257. Available from: https://doi.org/10.3389/fimmu.2022.815257.
13. Liu T, Son M, Diamond B. HMGB1 in Systemic Lupus Erythematosus. Front Immunol. 2020; 11: 1057. Available from: https://doi.org/10.3389/fimmu.2020.01057.
14. Infantino M, Nagy E, Bizzaro N, Fischer K, Bossuyt X, Damoiseaux J. Anti-dsDNA antibodies in the classification criteria of systemic lupus erythematosus. Journal of Translational Autoimmunity. 2022; 5: 100139. Available from: https://doi.org/10.1016/j.jtauto.2021.100139.
15. Sokolova MV, Schett G, Steffen U. Autoantibodies in Rheumatoid Arthritis: Historical Background and Novel Findings. Clinic Rev Allerg Immunol. 2021; 63: 138–51. Available from: https://doi.org/10.1007/s12016-021-08890-1.
16. Abdulahad DA, Westra J, Bijzet J, Limburg PC, Kallenberg CG, Bijl M. High mobility group box 1 (HMGB1) and anti-HMGB1 antibodies and their relation to disease characteristics in systemic lupus erythematosus. Arthritis Res Ther. 2011; 13: R71. Available from: https://doi.org/10.1186/ar3332.
17. Wirestam L, Schierbeck H, Skogh T, Gunnarsson I, Ottosson L, Erlandsson-Harris H, et al. Antibodies against High Mobility Group Box protein-1 (HMGB1) versus other anti-nuclear antibody fine-specificities and disease activity in systemic lupus erythematosus. Arthritis Res Ther. 2015; 17: 338. Available from: https://doi.org/10.1186/s13075-015-0856-2.

18. Goldstein RS, Bruchfeld A, Yang L, Qureshi AR, Gallowitsch-Puerta M, Patel NB, et al. Cholinergic anti-inflammatory pathway activity and High Mobility Group Box-1 (HMGB1) serum levels in patients with rheumatoid arthritis. Mol Med. 2007; 13: 210–5. Available from: https://doi.org/10.2119/2006–00108.Goldstein.
19. Wang C, Miao Y, Wu X, Huang Y, Sun M, Zhu Y, et al. Serum HMGB1 Serves as a Novel Laboratory Indicator Reflecting Disease Activity and Treatment Response in Ankylosing Spondylitis Patients. Journal of Immunology Research. 2016; 2016: 1–8. Available from: https://doi.org/10.1155/2016/6537248.
20. Yildirim D, Baykul M, Edek YC, Gulengul M, Alp GT, Eroglu FS, et al. Could Serum HMGB1 Levels be a Predictor Associated with Psoriatic Arthritis? Biomark Med. 2023; 17: 871–80. Available from: https://doi.org/10.2217/bmm-2023-0490.
21. Lu M, Yu S, Xu W, Gao B, Xiong S. HMGB1 Promotes Systemic Lupus Erythematosus by Enhancing Macrophage Inflammatory Response. Journal of Immunology Research. 2015; 2015: 1–12. Available from: https://doi.org/10.1155/2015/946748.
22. Tanaka A, Ito T, Kibata K, Inagaki-Katashiba N, Amuro H, Nishizawa T, et al. Serum high-mobility group box 1 is correlated with interferon-α and may predict disease activity in patients with systemic lupus erythematosus. Lupus. 2019; 28: 1120–7. Available from: https://doi.org/10.1177/0961203319862865.
23. Lee H-T, Lin C-S, Pan S-C, Chen W-S, Tsai C-Y, Wei Y-H. The Role of Plasma Cell-Free Mitochondrial DNA and Nuclear DNA in Systemic Lupus Erythematosus. Front Biosci (Landmark Ed). 2022; 27: 333. Available from: https://doi.org/10.31083/j.fbl2712333.
24. Rykova E, Sizikov A, Roggenbuck D, Antonenko O, Bryzgalov L, Morozkin E, et al. Circulating DNA in rheumatoid arthritis: pathological changes and association with clinically used serological markers. Arthritis Res Ther. 2017; 19: 85. Available from: https://doi.org/10.1186/s13075-017-1295-z.
25. Li Z, Lin J, Su Z, Zeng Y, Zhou Y, Li J, et al. Neutrophil Extracellular Traps–Associated RNA Impedes CD4+ Treg Differentiation by TLR7 – IRF7 Axis in Ankylosing Spondylitis. Arthritis & Rheumatology. 2025; 77: 1242–53. Available from: https://doi.org/10.1002/art.43166.
26. Peng Y, Wu Y, Chen S, Liu Y, Qian H, He Y, et al. Circulating cell-free DNA correlate to disease activity and treatment response of patients with radiographic axial spondyloarthritis. Sci Rep. 2024; 14: 178. Available from: https://doi.org/10.1038/s41598-023-50543-0.

Литература

1. Carter EE, Barr SG, Clarke AE. The global burden of SLE: prevalence, health disparities and socioeconomic impact. Nat Rev Rheumatol. 2016; 12: 605–20. Available from: https://doi.org/10.1038/nrrheum.2016.137.
2. Black RJ, Cross M, Haile LM, Culbreth GT, Steinmetz JD, Hagins H, et al. Global, regional, and national burden of rheumatoid arthritis, 1990–2020, and projections to 2050: a systematic analysis of the Global Burden of Disease Study 2021. The Lancet Rheumatology. 2023; 5: e594–610. Available from: https://doi.org/10.1016/S2665-9913(23)00211-4.
3. Wang R, Ward MM. Epidemiology of axial spondyloarthritis: an update. Current Opinion in Rheumatology. 2018; 30: 137–43. Available from: https://doi.org/10.1097/BOR.0000000000000475.
4. Boel A, López-Medina C, Van Der Heijde DMFM, Van Gaalen FA. Age at onset in axial spondyloarthritis around the world: data from the Assessment in SpondyloArthritis international Society Peripheral Involvement in Spondyloarthritis study. Rheumatology. 2022; 61: 1468–75. Available from: https://doi.org/10.1093/rheumatology/keab544.
5. Lembke S, Macfarlane GJ, Jones GT. The worldwide prevalence of psoriatic arthritis — a systematic review and meta-analysis. Rheumatology. 2024; 63: 3211–20. Available from: https://doi.org/10.1093/rheumatology/keae198.
6. Лила А. М., Лила В. А. Социальная значимость и экономические последствия ревматических заболеваний. Гигиена и санитария. 2017; 96: 387–92. Available from: https://doi.org/10.47470/0016-9900-2017-96-4-387-392.
7. Danieli MG, Antonelli E, Piga MA, Claudi I, Palmeri D, Tonacci A, et al. Alarmins in autoimmune diseases. Autoimmunity Reviews. 2022; 21: 103142. Available from: https://doi.org/10.1016/j.autrev.2022.103142.
8. Ermakov EA, Tolmacheva AS, Kon'kov VV, Melamud MM, Sizikov AE, Klyaus NA, et al. Plasma high-mobility group nucleosome-binding domain 1 (HMGN1) protein levels in four common rheumatic diseases: A potential biomarker of rheumatoid arthritis. The Egyptian Rheumatologist. 2025; 47: 51–5. Available from: https://doi.org/10.1016/j.ejr.2024.12.003.
9. Truszewska A, Wirkowska A, Gala K, Truszewski P, Krzemień-Ojak Ł, Perkowska-Ptasińska A, et al. Cell-free DNA profiling in patients with lupus nephritis. Lupus. 2020; 29: 1759–72. Available from: https://doi.org/10.1177/0961203320957717.
10. Duvvuri B, Lood C. Cell-Free DNA as a Biomarker in Autoimmune Rheumatic Diseases. Front Immunol. 2019; 10: 502. Available from: https://doi.org/10.3389/fimmu.2019.00502.
11. Chen R, Kang R, Tang D. The mechanism of HMGB1 secretion and release. Exp Mol Med. 2022; 54: 91–102. Available from: https://doi.org/10.1038/s12276-022-00736-w.
12. Dong Y, Ming B, Dong L. The Role of HMGB1 in Rheumatic Diseases. Front Immunol. 2022; 13: 815257. Available from: https://doi.org/10.3389/fimmu.2022.815257.
13. Liu T, Son M, Diamond B. HMGB1 in Systemic Lupus Erythematosus. Front Immunol. 2020; 11: 1057. Available from: https://doi.org/10.3389/fimmu.2020.01057.
14. Infantino M, Nagy E, Bizzaro N, Fischer K, Bossuyt X, Damoiseaux J. Anti-dsDNA antibodies in the classification criteria of systemic lupus erythematosus. Journal of Translational Autoimmunity. 2022; 5: 100139. Available from: https://doi.org/10.1016/j.jtauto.2021.100139.
15. Sokolova MV, Schett G, Steffen U. Autoantibodies in Rheumatoid Arthritis: Historical Background and Novel Findings. Clinic Rev Allerg Immunol. 2021; 63: 138–51. Available from: https://doi.org/10.1007/s12016-021-08890-1.
16. Abdulahad DA, Westra J, Bijzet J, Limburg PC, Kallenberg CG, Bijl M. High mobility group box 1 (HMGB1) and anti-HMGB1 antibodies and their relation to disease characteristics in systemic lupus erythematosus. Arthritis Res Ther. 2011; 13: R71. Available from: https://doi.org/10.1186/ar3332.
17. Wirestam L, Schierbeck H, Skogh T, Gunnarsson I, Ottosson L, Erlandsson-Harris H, et al. Antibodies against High Mobility Group Box protein-1 (HMGB1) versus other anti-nuclear antibody fine-specificities and disease activity in systemic lupus erythematosus. Arthritis Res Ther. 2015; 17: 338. Available from: https://doi.org/10.1186/s13075-015-0856-2.
18. Goldstein RS, Bruchfeld A, Yang L, Qureshi AR, Gallowitsch-Puerta M, Patel NB, et al. Cholinergic anti-inflammatory pathway activity and High Mobility Group Box-1 (HMGB1) serum levels in patients with rheumatoid arthritis. Mol Med. 2007; 13: 210–5. Available from: https://doi.org/10.2119/2006–00108.Goldstein.
19. Wang C, Miao Y, Wu X, Huang Y, Sun M, Zhu Y, et al. Serum HMGB1 Serves as a Novel Laboratory Indicator Reflecting Disease Activity and Treatment Response in Ankylosing Spondylitis Patients. Journal of Immunology Research. 2016; 2016: 1–8. Available from: https://doi.org/10.1155/2016/6537248.
20. Yildirim D, Baykul M, Edek YC, Gulengul M, Alp GT, Eroglu FS, et al. Could Serum HMGB1 Levels be a Predictor Associated with Psoriatic Arthritis? Biomark Med. 2023; 17: 871–80. Available from: https://doi.org/10.2217/bmm-2023-0490.
21. Lu M, Yu S, Xu W, Gao B, Xiong S. HMGB1 Promotes Systemic Lupus Erythematosus by Enhancing Macrophage Inflammatory Response. Journal of Immunology Research. 2015; 2015: 1–12. Available from: https://doi.org/10.1155/2015/946748.
22. Tanaka A, Ito T, Kibata K, Inagaki-Katashiba N, Amuro H, Nishizawa T, et al. Serum high-mobility group box 1 is correlated with interferon-α and may predict disease activity in patients with systemic lupus erythematosus. Lupus. 2019; 28: 1120–7. Available from: https://doi.org/10.1177/0961203319862865.
23. Lee H-T, Lin C-S, Pan S-C, Chen W-S, Tsai C-Y, Wei Y-H. The Role of Plasma Cell-Free Mitochondrial DNA and Nuclear DNA in Systemic Lupus Erythematosus. Front Biosci (Landmark Ed). 2022;

27: 333. Available from: https://doi.org/10.31083/j.fbl2712333.
24. Rykova E, Sizikov A, Roggenbuck D, Antonenko O, Bryzgalov L, Morozkin E, et al. Circulating DNA in rheumatoid arthritis: pathological changes and association with clinically used serological markers. Arthritis Res Ther. 2017; 19: 85. Available from: https://doi.org/10.1186/s13075-017-1295-z.
25. Li Z, Lin J, Su Z, Zeng Y, Zhou Y, Li J, et al. Neutrophil Extracellular Traps–Associated RNA Impedes CD4+ Treg Differentiation by TLR7 – IRF7 Axis in Ankylosing Spondylitis. Arthritis & Rheumatology. 2025; 77: 1242–53. Available from: https://doi.org/10.1002/art.43166.
26. Peng Y, Wu Y, Chen S, Liu Y, Qian H, He Y, et al. Circulating cell-free DNA correlate to disease activity and treatment response of patients with radiographic axial spondyloarthritis. Sci Rep. 2024; 14: 178. Available from: https://doi.org/10.1038/s41598-023-50543-0.

FOLLICULAR T CELLS IN PERIPHERAL BLOOD: INCREASING COMPLEXITY AND KEY QUESTIONS

Grigorova IL ✉

Pirogov Russian National Research Medical University, Moscow, Russia

Follicular helper (Tfh) and follicular regulatory (Tfr) T cells play critical roles in inducing and controlling B cell responses, including the generation of high-affinity humoral immunity, the antibody class-switching, and the prevention of autoreactivity. Successful Tfh responses are linked to robust vaccine-induced neutralizing antibody production and efficient clearance of various pathogens. Conversely, dysregulation of follicular T cells is often linked to autoimmune diseases and allergic reactions. Furthermore, these cells are implicated in the formation of ectopic lymphoid structures (ELS), contribute to certain vascular pathologies, and hold prognostic value in several cancers. Consequently, the analysis of follicular T cell subpopulations in human peripheral blood is increasingly utilized to investigate the mechanisms underlying various diseases. In this opinion article, the current understanding of follicular T cell subsets, their functions, and the evolving methods for analyzing their circulating counterparts in human blood are discussed. In the author's opinion, the central unresolved questions remaining in the field are the precise phenotypic definition of circulating Tfr cell subpopulations, the elucidation of their developmental trajectory from precursors cells to mature regulatory forms, and the identification of their anatomical differentiation niches. The collection and translation of these essential data into reliable cellular signatures for peripheral blood analysis are critical for advancing personalized patient prognosis and developing tailored therapies.

Keywords: follicular helper T cells (Tfh), follicular regulatory T cells (Tfr), circulating follicular T cells, infectious diseases, vaccines, allergies, autoimmune diseases, oncology

Funding: this research was supported by the Russian Science Foundation (Grant No. 24-15-00545).

Acknowledgments: the author is grateful to I. V. Zvyagin for assistance with editing the article.

✉ **Correspondence should be addressed:** Irina L. Grigorova
Ostrovityanova, 1, Moscow, 117997, Russia; grig76@gmail.com

Received: 10.12.2025 **Accepted:** 12.12.2025 **Published online:** 23.12.2025

DOI: 10.24075/brsmu.2025.076

Copyright: © 2025 by the authors. **Licensee:** Pirogov University. This article is an open access article distributed under the terms and conditions of the Creative Commons Attribution (CC BY) license (https://creativecommons.org/licenses/by/4.0/).

ФОЛЛИКУЛЯРНЫЕ Т-КЛЕТКИ ПЕРИФЕРИЧЕСКОЙ КРОВИ: НАРАСТАЮЩАЯ СЛОЖНОСТЬ И ПЕРВООЧЕРЕДНЫЕ ВОПРОСЫ

И. Л. Григорова ✉

Российский национальный исследовательский медицинский университет имени Н. И. Пирогова, Россия, Москва

Фолликулярные Т-хелперы (Tfh) и фолликулярные регуляторные Т-клетки (Tfr) играют ключевую роль в индукции и контроле В-клеточных ответов, включая формирование высокоаффинного гуморального иммунитета, переключение классов антител и предотвращение аутореактивности. Успешный ответ Tfh ассоциирован с эффективной выработкой нейтрализующих антител после вакцинации и эффективной элиминацией различных патогенов. В то же время дизрегуляция фолликулярных Т-клеток часто связана с аутоиммунными заболеваниями и аллергическими реакциями. Нарушение их нормального функционирования связано также с формированием эктопических лимфоидных структур (ЭЛС), способствует развитию некоторых сосудистых патологий и имеет прогностическое значение при ряде онкологических заболеваний. В связи с этим анализ субпопуляций фолликулярных Т-клеток в периферической крови человека все чаще используют при изучении механизмов различных заболеваний. В данной статье обсуждаются современные данные о разных типах фолликулярных Т-клеток, их функциях и методах анализа субпопуляций фолликулярных Т-клеток, циркулирующих в крови человека. Согласно мнению автора, центральными нерешенными вопросами остаются точное фенотипическое определение циркулирующих субпопуляций Tfr-клеток, выяснение иерархии их развития от клеток-предшественников до зрелых регуляторных форм и установление их анатомических ниш дифференцировки. Накопление необходимых сведений и их преобразование в надежные сигнатуры для клеток периферической крови необходимы для развития подходов прогнозирования исхода заболевания у отдельных пациентов и разработки персонализированных терапевтических подходов.

Ключевые слова: фолликулярные хелперные Т-клетки, Tfh, фолликулярные регуляторные Т-клетки, Tfr, циркулирующие фолликулярные Т-клетки, инфекционные заболевания, вакцины, аллергия, аутоиммунные заболевания, онкологические заболевания

Финансирование: исследование выполнено при финансовой поддержке Российского научного фонда (грант № 24-15-00545).

Благодарности: автор выражает признательность И. В. Звягину за помощь с редактированием статьи.

✉ **Для корреспонденции:** Ирина Леонидовна Григорова
ул. Островитянова, д. 1, г. Москва, 117997, Россия; grig76@gmail.com

Статья получена: 10.12.2025 **Статья принята к печати:** 12.12.2025 **Опубликована онлайн:** 23.12.2025

DOI: 10.24075/vrgmu.2025.076

Авторские права: © 2025 принадлежат авторам. **Лицензиат:** РНИМУ им. Н.И. Пирогова. Статья размещена в открытом доступе и распространяется на условиях лицензии Creative Commons Attribution (CC BY) (https://creativecommons.org/licenses/by/4.0/).

Follicular T cells, which localize in B cell follicles and specifically assist in regulating B cell and antibody responses, were first reported in 1999 [1]. Since that time, they have attracted considerable scientific interest, gradually evolving into a field integrated with the understanding of various diseases and pathologies. Association analysis of the risk of development and progression of various diseases with impaired function and imbalance of follicular T cell subpopulations circulating in peripheral blood is increasingly becoming an important tool for prognosis and for establishing potential treatment targets for multiple diseases [2, 3].

The central feature of follicular T cells is that they are driven by the master transcription factor Bcl6 and have elevated levels of the G-protein coupled receptor CXCR5 (Figure, Table). The CXCR5 receptor enables T cells to migrate into B cell follicles of secondary lymphoid organs (SLOs), where stromal

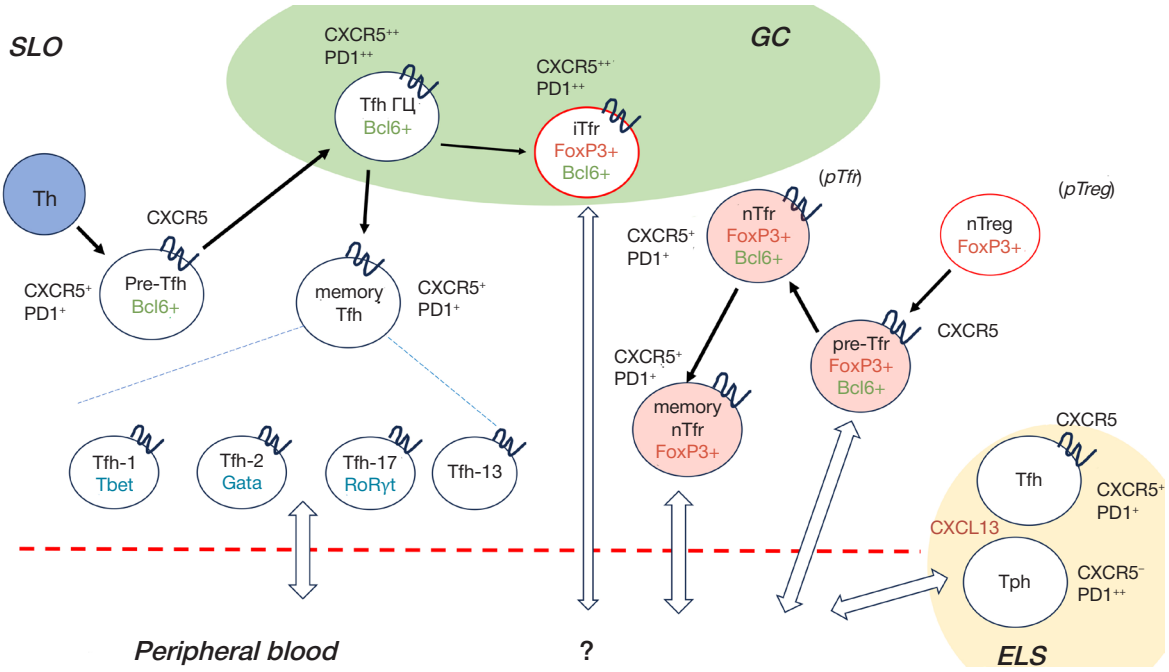


Fig. Major follicular and follicular-like T cells in humans. A schematic describing the generation in secondary lymphoid organs (SLOs) and possible recirculation into peripheral blood of the main follicular T cell subpopulations: helper (Tfh) and regulatory (Tfr). GC — germinal centers. ELS — ectopic lymphoid structures. Memory follicular T cells that acquire the ability to enter the circulation downregulate Bcl6 expression and surface levels of CXCR5 and PD1 compared to T cells in GCs. Peripheral helper T cells (Tph) and, to some extent, Tfh accumulate in ELS, where they produce the chemokine CXCL13, which can recruit B cells

cells express the CXCR5 chemokine ligand CXCL13. Two major types of follicular T cells that differentiate in response to antigenic challenge from CD4⁺ helper T cells (Th) and regulatory T cells (Tregs) are called follicular helper T cells (Tfh) and follicular regulatory T cells (Tfr) correspondingly.

Tfh cells are critical for supporting long-term, high-affinity B cell and antibody responses, as they are essential for germinal center (GC) reactions in SLOs. Tfh cells selectively help GC B cells that present the highest density of cognate peptide–MHCII complexes via T cell receptor recognition, delivering essential signals (CD40L, cytokines IL-21, and IL-4). These interactions ensure the survival and proliferation of high-affinity B cell clones and therefore drives GC B cells affinity maturation. Furthermore, Tfh support immunoglobulin class-switching, memory B-cell formation, and differentiation of B cells into plasma cells [4].

In contrast to Tfh, Tfr cells are involved in the tolerance control of B cell responses. In addition, Tfr cells suppress B cell isotype switching to IgA and IgE as well as differentiation into plasma cells. They also play an important role in fine-tuning B cell affinity maturation [5].

While the majority of Tfh cells are known to differentiate from foreign antigen-specific Th cells, the precursors of Tfr cells have long been suggested to be thymically-derived Tregs that express transcription factor FoxP3 and are specific to autoantigens or in some cases peripheral Tregs (pTregs, Th cells that upregulate FoxP3 in the periphery). However, more recent studies have also demonstrated the upregulation of FoxP3 and the formation of Tfr cells from Tfh cells in mice and human tonsils. These cells are now called induced Tfr (iTfr) [6, 7] (Figure, Table).

Given the critical role of Tfh and Tfr cells in regulating B cell responses, forming memory B cells, and generating high-affinity humoral immunity, their contribution is extensively studied in both animal models and in human diseases. The functions of Tfh cells have been studied in detail using animal models of various chronic and acute infections [2, 3]. In parallel, human studies have examined their roles in infections including Streptococcus pyogenes, malaria, HIV, flaviviruses, COVID-19, and other infections [2, 3, 8]. Vaccination studies in humans, particularly following seasonal influenza and SARS-CoV-2 mRNA immunization, have further assessed Tfh cell responses in relation to neutralizing antibody outcomes [2, 3, 9]. Dysregulation of follicular T cells is also a major focus of investigation in autoimmune diseases, spanning both autoantibody-mediated and T cell-dependent pathologies, as well as in allergies. Furthermore, Tfh cells have been linked to the development of a number of cardiovascular pathologies, as well as to a positive prognosis in certain cancers when present within the tumor [2, 3, 9, 10].

The analysis of follicular T cell dynamics in humans during the normal or pathological immune responses has been carried out predominantly on the subpopulations that circulate in peripheral blood. Since GC Tfh cells are confined to SLOs, the majority of blood-circulating CXCR5⁺ T cells represent Bcl6- memory Tfh cells that have partially downregulated expression of CXCR5 (Figure, Table). These circulating Tfh (cTfh) can be further classified into functional subsets Th1-, Th2-, and Th17-associated, based on chemokine receptor expression (CCR6, CXCR3) and their underlying transcription factor profiles (Table) [11]. Additionally, cytokine profiling has identified IL-13⁺ cTfh cells, a subset associated with IgE with high-affinity to allergens [12].

Notably, human cTfh cells themselves express high levels of CXCL13. This has led to the hypothesis that cTfh cells that access peripheral tissues may help initiate ectopic lymphoid structures (ELS) by creating a chemokine gradient, which attracts B cells and promotes further lymphoid organization. However, recent studies have also revealed enrichment of a distinct CXCL13⁺ T-cell subpopulation with a CXCR5⁻ PD1^{high} IL-21⁺ phenotype in ELS. These cells, named peripheral helper T cells (Tph), are phenotypically similar to Tfh and can also support B-cell responses despite lacking the CXCR5 receptor. Furthermore, a strong association has been established between the circulating Tph and diseases such as rheumatoid arthritis and systemic lupus erythematosus. Current evidence does not clarify the cellular origin of Tph [2, 3]. Nevertheless, Tph have now become a standard component in the analysis

Table 1. Major types of follicular and follicular-like T cells that regulate B cell responses.

Cell type	Precursor cells	antigen	Major TF	Cytokines	Surface markers	Localization	Peripheral Blood
Pre-Tfh	Th	foreign antigen	Bcl6+		CXCR5+ PD1+ ICOS+	SLO	None
Tfh GC	Pre-Tfh	foreign antigen	Bcl6+	IL21 IL4 CXCL13	CXCR5++ PD1++ ICOS++	GC in SLO	None
Tfh memory cells	Tfh GC	foreign antigen	Bcl6-	CXCL13	CXCR5+ PD1+ ICOS+	follicles in SLO/ELS	cTfh
Tfh-1			Tbet+	IFNγ	CXCR3+ CCR6-	SLO	cTfh-1
Tfh-2			Gata+	IL4, IL5	CXCR3- CCR6-		cTfh-2
Tfh-17			RoRγt+	IL17, IL22	CXCR3- CCR6+		cTfh-17
Tfh-13		allergen		IL4, IL13			cTfh-13
Tph			Blimp1+ MAF	IL21 CXCL13	CXCR5- PD1++ CR2	ELS/inflamed tissues	cTph
Pre-Tfr	nTreg	auto-antigen	Bcl6+ FoxP3+		CXCR5+ PD1+ ICOS+ CD45RA+	SLO	None
Pre-Tfr memory cells	Pre-Tfr?		Bcl6- FoxP3+		CXCR5+ PD1+ ICOS+ CD45RA+	SLO	cPre-Tfr
nTfr	Pre-Tfr	auto-antigen	Bcl6+ FoxP3+ Blimp1+	IL10	CXCR5+ PD1+ ICOS+ CD45RA- CD25high	follicles in SLO, around GC	None
nTfr memory cells	nTfr	auto-antigen	Bcl6- FoxP3+		CXCR5+ PD1+ ICOS+ CD45RA- CD25high	SLO	cTfr?
iTfr	Tfh GC	auto-antigen	Bcl6+ FoxP3+		CXCR5++ PD1++ CD38+	GC	?

Note: GC — germinal centers, TF — transcription factors, SLO — secondary lymphoid organs, ELS — ectopic lymphoid structures.

of peripheral blood follicular T lymphocytes in various conditions [11].

The somewhat delayed discovery of FoxP3$^+$ Tfr cells necessitated reassessment of the earlier analysis of circulating follicular T cells, in which all CXCR5$^+$ T cells were presumed to be of Tfh origin. CD4$^+$ CXCR5$^+$ FoxP3$^+$ circulating Tfr cells were first identified in murine blood shortly after immunization [13]. Similarly, human studies have demonstrated a significant increase in circulating Tfr frequency following vaccination [9]. These cells are now understood to represent a circulating memory Tfr population (cTfr), capable of long-term persistence *in vivo* and potential recruitment into SLO upon rechallenge. The important role of Tfr in immune response regulation warrants significant attention to their abundance in peripheral blood. A key predictive parameter is believed to be the cTfr/cTfh ratio, which has been shown in some studies to be more predictive of dysregulated antibody responses than either subset alone [14].

More in-depth analysis of circulating Tfr has now revealed that a significant fraction of CD4$^+$CXCR5$^+$FoxP3$^+$ cells in the blood are CD45RA$^+$ cells that formed in SLOs in response to immunological challenge but represent an intermediate, not fully differentiated form of Tfr. Referred to as "pre-Tfr," these long-lived, recirculating cells can, upon stimulation, mature into potent regulators of B cell responses and also acquire some capacity for wound repair [9]. In addition to these pre-Tfr, more mature "effector-like" CD45RA$^-$CD4$^+$CXCR5$^+$FoxP3$^+$ cTfr cells are found in peripheral blood (Figure, Table).

One of the recent studies has separately assessed these Tfr subpopulations in the peripheral blood of COVID-19 patients. This was achieved using high-dimensional mass cytometry (CyTOF), which enabled the simultaneous analysis of multiple immune cell types in patient samples. The approach revealed extensive correlative networks between various cellular parameters, including the negative associations between cTfr levels and populations such as plasma cells or Tph cells [10]. Collectively, accumulating evidence supports the establishment of multiparametric signatures describing the diversity of follicular T cells in the blood, which have prognostic value and are indicative of specific dysfunctions in B cell and antibody responses. Initially, generating such signatures will require data from single-cell transcriptomics/proteomics, potentially combined with CyTOF. This could later be adapted into a reduced panel for flow cytometry analysis.

While increasing resolution of analysis of follicular T cells in peripheral blood deepens our understanding of ongoing disease processes, the portrait of circulating Tfr cells remains

incomplete. The recent identification of iTfr cells, which arise in SLOs from Tfh cells and help contract GC responses, raises important questions. Does this foreign antigen-specific Tfr subset enter the circulation? If this is the case, how can we differentiate between iTfr, which suppress foreign antigen/pathogen-driven B-cell responses, and nTfr (of nTreg origin), which are biased toward autoantigen recognition and control of autoreactive B-cell responses? We propose that future studies should explicitly investigate the presence of iTfr in human blood and define a molecular signature to distinguish circulating iTfr from their nTfr counterparts. Furthermore, research is needed to determine the stability of the Treg phenotype in iTfr cells.

Another key question is whether circulating Tfr cells retain a molecular imprint of their tissue of origin or a homing bias toward specific organs. Tissue-resident Tregs have been shown to acquire specialized receptor profiles that guide their localization [15]. Profiling the chemokine receptor and adhesion molecule signatures imprinted during Tfr differentiation in SLO could reveal their site of formation and predict their preferred tissue destinations. Such insight would further clarify Tfr specialization and function across different physiological and pathological contexts.

CONCLUSION

To summarize, within the past decade, significant progress has been made in dissecting various types of follicular T cells, their development, function, and association with humoral responses to pathogens, allergies, and various autoimmune diseases. However, despite accumulated knowledge, it is evident that intensive research is required to develop a phenotypic and functional profile of human peripheral blood follicular T cells and their interactions with other immune cell types. In particular, two key questions remain unresolved: defining the molecular signatures of various Tfr cell subpopulations in blood that originate from different precursor cells, and elucidating their tissue of origin. It is anticipated that the development of such cellular biomarker signatures could improve the prediction of immune status and enable personalized therapy selection for each patient.

References

1. Ansel KM, McHeyzer-Williams LJ, Ngo VN, McHeyzer-Williams MG, Cyster JG. In vivo-activated CD4 T cells upregulate CXC chemokine receptor 5 and reprogram their response to lymphoid chemokines. J Exp Med. 1999; 190: 1123–34.
2. Crotty S. T Follicular Helper Cell Biology: A Decade of Discovery and Diseases. Immunity. 2019; 50: 1132–48.
3. Yu D, Walker LSK, Liu Z, Linterman MA, Li Z. Targeting TFH cells in human diseases and vaccination: rationale and practice. Nat Immunol. 2022; 23: 1157–68.
4. Victora GD, Nussenzweig MC. Germinal Centers. Annu Rev Immunol. 2022; 40: 413–42.
5. Sokolova S, Grigorova IL. Follicular regulatory T cell subsets in mice and humans: origins, antigen specificity and function. Int Immunol. 2023; dxad031.
6. Le Coz C, Oldridge DA, Herati RS, De Luna N, Garifallou J, Cruz Cabrera E, et al. Human T follicular helper clones seed the germinal center-resident regulatory pool. Sci Immunol. 2023; 8: eade8162.
7. Jacobsen JT, Hu W, R Castro TB, Solem S, Galante A, Lin Z, et al. Expression of Foxp3 by T follicular helper cells in end-stage germinal centers. Science. 2021; 373: eabe5146.
8. Flores-Pérez PN, Collazo-Llera JA, Rodríguez-Alvarado FA, Rivera-Amill V. The Emerging Role of Circulating T Follicular Helper Cells in Dengue Virus Immunity: Balancing Protection and Pathogenesis. Viruses. 2025; 17: 652.
9. Tulyeu J, Søndergaard JN, Priest DG, Ebihara T, Matsumoto H, Llamas-Covarrubias MA,et al. Human precursor T follicular regulatory cells are primed for differentiation into mature Tfr and disrupted during severe infections. Sci Adv. 2025; 11: eadv6939.
10. Søndergaard JN, Tulyeu J, Edahiro R, Shirai Y, Yamaguchi Y, Murakami T, et al. A sex-biased imbalance between Tfr, Tph, and atypical B cells determines antibody responses in COVID-19 patients. Proc Natl Acad Sci USA. 2023; 120: e2217902120.
11. Song W, Craft J. T Follicular Helper Cell Heterogeneity. Annual Review of Immunology. 2024; 42: 127–52.
12. Gowthaman U, Chen JS, Zhang B, Flynn WF, Lu Y, Song W, et al. Identification of a T follicular helper cell subset that drives anaphylactic IgE. Science. 2019; 365: eaaw6433.
13. Sage PT, Alvarez D, Godec J, von Andrian UH, Sharpe AH. Circulating T follicular regulatory and helper cells have memory-like properties. J Clin Invest. 2014; 124: 5191–204.
14. Su R, Wang Y, Hu F, Li B, Guo Q, Zheng X, et al. Altered Distribution of Circulating T Follicular Helper-Like Cell Subsets in Rheumatoid Arthritis Patients. Front Med (Lausanne). 2021; 8: 690100.
15. Jugder B-E, Park E, Du L, Jawale C, Popov N, Guo Z, et al. Tissue-specific roles of regulatory T cells: mechanisms of suppression and beyond along with emerging therapeutic insights in autoimmune indications. Front Immunol. 2025; 16: 1650451.

Литература

1. Ansel KM, McHeyzer-Williams LJ, Ngo VN, McHeyzer-Williams MG, Cyster JG. In vivo-activated CD4 T cells upregulate CXC chemokine receptor 5 and reprogram their response to lymphoid chemokines. J Exp Med. 1999; 190: 1123–34.
2. Crotty S. T Follicular Helper Cell Biology: A Decade of Discovery and Diseases. Immunity. 2019; 50: 1132–48.
3. Yu D, Walker LSK, Liu Z, Linterman MA, Li Z. Targeting TFH cells in human diseases and vaccination: rationale and practice. Nat Immunol. 2022; 23: 1157–68.
4. Victora GD, Nussenzweig MC. Germinal Centers. Annu Rev Immunol. 2022; 40: 413–42.
5. Sokolova S, Grigorova IL. Follicular regulatory T cell subsets in mice and humans: origins, antigen specificity and function. Int Immunol. 2023; dxad031.
6. Le Coz C, Oldridge DA, Herati RS, De Luna N, Garifallou J, Cruz Cabrera E, et al. Human T follicular helper clones seed the germinal center-resident regulatory pool. Sci Immunol. 2023; 8: eade8162.
7. Jacobsen JT, Hu W, R Castro TB, Solem S, Galante A, Lin Z, et al. Expression of Foxp3 by T follicular helper cells in end-stage germinal centers. Science. 2021; 373: eabe5146.
8. Flores-Pérez PN, Collazo-Llera JA, Rodríguez-Alvarado FA, Rivera-Amill V. The Emerging Role of Circulating T Follicular Helper Cells in Dengue Virus Immunity: Balancing Protection and Pathogenesis. Viruses. 2025; 17: 652.
9. Tulyeu J, Søndergaard JN, Priest DG, Ebihara T, Matsumoto H, Llamas-Covarrubias MA,et al. Human precursor T follicular regulatory cells are primed for differentiation into mature Tfr and disrupted during severe infections. Sci Adv. 2025; 11: eadv6939.
10. Søndergaard JN, Tulyeu J, Edahiro R, Shirai Y, Yamaguchi Y, Murakami T, et al. A sex-biased imbalance between Tfr, Tph, and atypical B cells determines antibody responses in COVID-19

patients. Proc Natl Acad Sci USA. 2023; 120: e2217902120.
11. Song W, Craft J. T Follicular Helper Cell Heterogeneity. Annual Review of Immunology. 2024; 42: 127–52.
12. Gowthaman U, Chen JS, Zhang B, Flynn WF, Lu Y, Song W, et al. Identification of a T follicular helper cell subset that drives anaphylactic IgE. Science. 2019; 365: eaaw6433.
13. Sage PT, Alvarez D, Godec J, von Andrian UH, Sharpe AH. Circulating T follicular regulatory and helper cells have memory-like properties. J Clin Invest. 2014; 124: 5191–204.
14. Su R, Wang Y, Hu F, Li B, Guo Q, Zheng X, et al. Altered Distribution of Circulating T Follicular Helper-Like Cell Subsets in Rheumatoid Arthritis Patients. Front Med (Lausanne). 2021; 8: 690100.
15. Jugder B-E, Park E, Du L, Jawale C, Popov N, Guo Z, et al. Tissue-specific roles of regulatory T cells: mechanisms of suppression and beyond along with emerging therapeutic insights in autoimmune indications. Front Immunol. 2025; 16: 1650451.

ETIOLOGICAL STRUCTURE OF ENTEROVIRUS INFECTION IN CHILDREN IN THE MOSCOW REGION

Polyakova VA[1], Davydova EE[1] ✉, Luparev AR[1], Matsvay AD[1], Gnusareva NI[1], Gordukova MA[2], Galeeva EV[2], Tolokonceva AA[1], Shipulin GA[1]

[1] Center for Strategic Planning and Management of Medical and Biological Health Risks of the Federal Medical Biological Agency, Moscow, Russia

[2] Speransky Children's City Clinical Hospital No. 9, Moscow, Russia

The diversity and succession of epidemiologically significant enteroviruses (EV) lead to constant changes in the clinical presentation and morbidity levels. The aim of the study is to investigate cases of EV infection in hospitalized children during the resurgence of the epidemic process following the COVID-19 pandemic. We collected clinical samples from 156 patients with EV infection across a range of ages. Virus genotyping was performed using the Sanger sequencing of the 5'UTR-VP2 and VP1 genome fragments. Sixteen types of enteroviruses were identified, with one additional case identified only to the species level (EV-C). The dominant EV type was Coxsackie CV-A6, with a share of 80.6% (95% CI: 66.7–95.5) in 2021 and 36.1% (95% CI: 27.5–44.6) in 2022. Most commonly, CV-A6 caused skin lesions (exanthema or HFMD) and respiratory manifestations. In 2022, the proportion of CV-A10 cases increased considerably to 27.0% (95% CI: 19.2–34.9) compared with 6.4% (95% CI: 0–15.1) in 2021. The most common clinical manifestation of CV-A10 was herpangina. The most severe EV infection cases were associated with ECHO 6 — four out of 11 patients were diagnosed with meningitis, while the remaining patients exhibited neurological symptoms (meningism, intense headache, vomiting) accompanied by fever. We observed a large number of EV cases accompanied by the presence of other infectious agents in biological samples, which may result from immune suppression during EV infection development. The most common of these agents was human herpesvirus 6 (HHV-6). The nucleotide sequences of the characterized enteroviruses have been deposited in the NCBI database to enable subsequent epidemiological analysis of enterovirus circulation in the Russian Federation.

Keywords: enterovirus infection, epidemiologically significant enteroviruses, hand, foot and mouth disease (HFMD), herpangina, Coxsackie viruses, Echoviruses, co-infection, Sanger sequencing

Author contribution: Polyakova VA, Luparev AR, Matsvay AD, Gnusareva NI, Gordukova MA, Galeeva EV, Tolokonceva AA — conducting the research; Davydova EE, Polyakova VA, Luparev AR — literature analysis; Davydova EE, Luparev AR — data interpretation; Gordukova MA, Galeeva EV — collection of biological samples; Polyakova VA — article authoring; Davydova EE — manuscript editing; Polyakova VA — preparation of illustrations; Shipulin GA — supervision and procurement of funding.

Compliance with ethical standards: the study was approved by the Ethics Committee of the Children's City Clinical Hospital No. 9 named after G.N. Speransky (Minutes No. 44 of April 19, 2022), conducted in accordance with the principles of the Declaration of Helsinki. All participants submitted signed informed consent forms prior to participation in the study.

✉ **Correspondence should be addressed:** Ekaterina E. Davydova
Pogodinskaya, 10, Moscow, 119121, Russia, edavydova@cspfmba.ru

Received: 24.11.2025 **Accepted:** 13.12.2025 **Published online:** 25.12.2025

DOI: 10.24075/brsmu.2025.082

Copyright: © 2025 by the authors. **Licensee:** Pirogov University. This article is an open access article distributed under the terms and conditions of the Creative Commons Attribution (CC BY) license (https://creativecommons.org/licenses/by/4.0/).

ЭТИОЛОГИЧЕСКАЯ СТРУКТУРА ЭНТЕРОВИРУСНОЙ ИНФЕКЦИИ У ДЕТЕЙ В МОСКОВСКОМ РЕГИОНЕ

В. А. Полякова[1], Е. Е. Давыдова[1] ✉, А. Р. Лупарев[1], А. Д. Мацвай[1], Н. И. Гнусарева[1], М. А. Гордукова[2], Е. В. Галеева[2], А. А. Толоконцева[1], Г. А. Шипулин[1]

[1] Центр стратегического планирования и управления медико-биологическими рисками здоровью Федерального медико-биологического агентства, Москва, Россия

[2] Детская городская клиническая больница № 9 имени Г. Н. Сперанского, Москва, Россия

Разнообразие и смена эпидемически значимых энтеровирусов (EV) приводит к постоянному изменению характера клинической картины и уровня заболеваемости. Цель работы — изучить случаи энтеровирусной инфекции (ЭВИ) у госпитализированных детей в период восстановление эпидемического процесса после пандемии COVID-19. Был собран клинический материал от 156 пациентов с ЭВИ различных возрастных групп. Проведено генотипирование вирусов методом секвенирования по Сэнгеру 5'UTR-VP2 и VP1 фрагментов генома. Выявлено 16 типов энтеровирусов, для одного удалось установить только вид (EV-C). Доминирующим типом EV оказался Коксаки CV-A6 — доля составила 80,6% (95% ДИ: 66,7–95,5) в 2021 г. и 36,1% (95% ДИ: 27,5–44,6) в 2022 г. Чаще всего CV-A6 вызывал кожные поражения (экзантемы и энтеровирусный везикулярный стоматит с экзантемой) и респираторные инфекции. В 2022 г. наблюдался рост доли CV-A10 — 27,0% (95% ДИ: 19,2–34,9) в 2022 г. против 6,4% (95% ДИ: 0–15,1) в 2021 г., наиболее частым проявлением CV-A10 была герпетическая ангина. Самые тяжелые случаи ЭВИ наблюдались при ECHO 6 и далее — у четверых из 11 пациентов диагностирован менингит, у остальных проявлялись неврологические симптомы (менингизм, интенсивная головная боль, рвота) на фоне лихорадки. Отмечено большое количество случаев ЭВИ, сопровождающихся присутствием в биоматериале других инфекционных агентов, что может быть связано с ослаблением иммунитета при развитии ЭВИ, чаще всего выявляли вирус герпеса 6-го типа. Нуклеотидные последовательности охарактеризованных энтеровирусов размещены в базе NCBI для возможности последующего эпидемиологического анализа циркуляции энтеровирусов на территории РФ.

Ключевые слова: энтеровирусная инфекция, эпидемически значимые энтеровирусы, вирусы Коксаки, эховирусы, энтеровирусный везикулярный стоматит с экзантемой, герпангина, коинфекция, секвенирование по Сэнгеру

Вклад авторов: В. А. Полякова, А. Р. Лупарев, А. Д. Мацвай, Н. И. Гнусарева, М. А. Гордукова, Е. В. Галеева, А. А. Толоконцева — проведение исследований; Е. Е. Давыдова, В. А. Полякова, А. Р. Лупарев — анализ литературы; Е. Е. Давыдова, А. Р. Лупарев — интерпретация данных; М. А. Гордукова, Е. В. Галеева — коллекция биоматериала; В. А. Полякова — написание текста; Е. Е. Давыдова — редактирование рукописи; В. А. Полякова — подготовка иллюстраций; Г. А. Шипулин — руководство и получение финансирования.

Соблюдение этических стандартов: исследование одобрено этическим комитетом Детской городской клинической больницы № 9 им. Г. Н. Сперанского (протокол № 44 от 19 апреля 2022 г.,), проведено в соответствии с принципами Хельсинкской декларации. У всех участников исследования было получено информированное согласие.

✉ **Для корреспонденции:** Екатерина Евгеньевна Давыдова
ул. Погодинская, д. 10, г. Москва, 119121, Россия, edavydova@cspfmba.ru

Статья получена: 24.11.2025 **Статья принята к печати:** 13.12.2025 **Опубликована онлайн:** 25.12.2025

DOI: 10.24075/vrgmu.2025.082

Авторские права: © 2025 принадлежат авторам. **Лицензиат:** РНИМУ им. Н. И. Пирогова. Статья размещена в открытом доступе и распространяется на условиях лицензии Creative Commons Attribution (CC BY) (https://creativecommons.org/licenses/by/4.0/).

Enteroviruses are a diverse group of small non-enveloped viruses with an non-segmented (+)-RNA genome, including pathogenic and opportunistic human viruses of the species *Enterovirus alphacoxsackie* (EV-A), *Enterovirus betacoxsackie* (EV-B), *Enterovirus coxsackiepol* (EV-C), *Enterovirus deconjuncti* (EV-D). *Polioviruses* belonging to the *Enterovirus coxsackiepol* species, capable of causing severe forms of neuropathogenesis, are on the verge of elimination. However, non-poliomyelitic enteroviruses of various types, including Coxsackie viruses, echoviruses and numbered enteroviruses, are widespread, and they cause various clinical forms of enterovirus infection, including hand, foot and mouth disease (HFMD), various types of exanthema, herpangina (enterovirus vesicular pharyngitis), diseases of the upper and lower respiratory tract, hemorrhagic conjunctivitis, infections of the gastrointestinal tract, epidemic myalgia, myopericarditis, neuroinfections (encephalitis, meningitis, acute flaccid myelitis) and other diseases.

A certain correlation has been established between the species of enteroviruses and their characteristic clinical manifestations: EV-A enteroviruses predominantly cause HFMD and herpangina; EV-B enteroviruses (Coxsackie B, ECHO) are the dominant pathogens of enterovirus meningitis; EV-D enteroviruses (D68) mainly affect the upper and lower respiratory tract. However, even for a single type of enterovirus, the clinical picture can vary significantly depending on the state of immunity and other individual characteristics of the patient. Approximately 85 % of EV infection cases are asymptomatic, about 12–14 % are diagnosed as mild forms, and only 1–3 % exhibit a severe course [1, 2]. Clinical manifestations are also associated with certain age groups: in adult patients, the disease often occurs as a mild respiratory or intestinal infection, younger patients develop HFMD, herpangina, and exanthema, and children aged 3–14 years are predisposed to severe neurological forms, such as enterovirus meningitis [2].

Monitoring of EV infections reveals that distinct circulation patterns exist for individual enterovirus types; for example, ECHO 9, ECHO 30, and EV-D68 tend to cause outbreaks, whereas CV-B4 and several other types exhibit relatively stable circulation [2, 3].

The regular replacement of epidemiologically important enterovirus may stem from different factors, but it always affects the incidence rate and the nature of the clinical picture. Monitoring the activity and prevalence of different EV types allows predicting the emergence of outbreaks or an increase in severe disease cases. [1, 4].

In 2020, the COVID-19-related anti-epidemic measures slowed the circulation of enteroviruses. Consequently, in the subsequent years, the proportion of the population without immunity to enterovirus infection increased, which contributed to a more active spread of EV infection. Thus, according to official statistics in the Russian Federation, in 2024, there were 21491 EV cases recorded, which is 14.69 per 100 thousand population. This is 1.5 times more than the long-term baseline incidence rate [5].

Before the pandemic, EV-B enteroviruses, including ECHO 30, posed a significant threat in the Russian Federation, being a major cause of meningitis. However, following the decline in enterovirus circulation in 2020, the proportion of EV-B decreased significantly. At the same time the incidence of infections associated with EV-A, primarily A6 and A10, has increased [2, 6]. According to the data of molecular genetic monitoring in the Russian Federation, in some years, the share of CV-A6 reached 40% [2, 7]. In this regard, the clinical presentation of EV infections has also changed, cases of herpangina and exanthema becoming more frequent, especially among children in their early years [6]. For example, in the Irkutsk region in 2023, the main clinical form of EV infection was herpangina (39.9%) and HFMD (28.9%) [8].

The aim of the study is to investigate cases of EV infection in children admitted to hospitals in the Moscow region during the period of epidemic process recovery (2021–2023), in order to assess the circulation of various enterovirus types taking into account the associated clinical manifestations.

METHODS

Samples

Clinical samples were collected from 156 patients of various ages at the Children's City Clinical Hospital No. 9 named after G. N. Speransky (Moscow, Russia). The participants had to have a diagnosed enterovirus infection to be included in the study. The children were aged 0–17 years; 78% of them were under six years of age. Most of the samples (n = 122) were collected in 2022, with additional 31 and 3 samples taken in 2021 and 2023.

Oropharyngeal and nasopharyngeal swab samples (n = 137) were collected from patients with symptoms of EV or respiratory infection, feces (n = 18) were taken from patients with acute intestinal infection. A cerebrospinal fluid sample was taken from one patient diagnosed with meningitis (n = 1). Only one type of clinical specimen was analyzed per patient. Clinical specimens were stored at –70 °C until the start of the analysis.

Study locations

PCR testing of samples for the presence of enterovirus RNA and other infectious agents was performed in the Laboratory Diagnostic Department of Children's City Clinical Hospital No. 9 named after G. N. Speransky. Enterovirus genotyping was performed in the Center for Postgenomic Technologies of the Center for Strategic Planning and Management of Medical and Biological Health Risks (FMBA of Russia).

Sample preparation

Swab and cerebrospinal fluid samples did not require any preparation before RNA extraction. To prepare the fecal extract, approximately 0.1 g (0.1 ml) of feces was resuspended in 0.8 ml of phosphate buffer (VWR International, LLC, USA). The homogeneous suspension was centrifuged at 10000 g on a MiniSpin centrifuge (Eppendorf, Germany) for 5 minutes, 300–400 µl of supernatant was collected above the surface of the precipitate, and stored at –70 °C for further use.

Confirmation of the presence of enterovirus and other infectious agents in clinical samples

To confirm the presence of enteroviruses and other infectious agents in clinical samples, we used PCR kits AmpliTest® Neuroviruses (Center for Strategic Planning and Management of Medical and Biological Health Risks, FMBA of Russia, Russia), AmpliSens® EBV/CMV/HHV6A/B-screen-FL, AmpliSens® HSV I, II-FL, AmpliSens® OKI-screen-FL, AmpliSens® ARVI-screen-FL, AmpliSens® MRSA-screen-titer-FL, AmpliSens® Streptococcus pyogenes-screen/monitor-FL (Central Research Institute of Epidemiology of Rospotrebnadzor, Russia).

RNA extraction

For nucleic acid extraction from clinical samples, the *in vitro* diagnostic reagent kit AmpliTest® Magno-Sorb-Combo (Center

for Strategic Planning and Management of Medical and Biological Health Risks FMBA of Russia, Russia) was used. The set extracts nucleic acids using magnetized silica particles. RNA isolation was performed using the Auto-Pure 96 device (Hangzhou Allsheng Instruments Co., Ltd., China). For extraction, 10 µl IC-R was added to all the samples.

Obtaining cDNA

Reverse transcription of RNA was performed using the AmpliTest® Reverta kit (CSP of FMBA of Russia, Russia).

Amplification of 5'UTR-VP2 and VP1 regions of the enterovirus genome

The VP1 region was amplified using universal primers recommended for genotyping human enteroviruses EV-A, EV-B, EV-C, and EV-D. The process involved two-round thermal cycling: the first round with a pair of primers SO222 5'-CICCIGGIGGIAYRWACAT-3' and SO224 5'-GCIATGYTIGGIACICAYRT-3', and the second round with AN88 5'-TACTGGACCACCTGGNGGNAYRWAC AT-3' and AN89 5'-CCAGCACTGACAGCAGGARAYNGG-3' [9]. To amplify the 5'UTR-VP2 region of the enterovirus genome, we used oligonucleotide primers of our own design — EV_S_for 5'-GTGTAGMTYRGGYYGATGAG-3' and EV_S_rev 5'-RTCHGGRAAYTTCCAVYACCA-3'.

Electrophoretic analysis of PCR products and their purification

Electrophoresis of PCR products was carried out in 2% agarose gel. For purification of PCR products, we used KAPA Pure Beads (KAPA Biosystems, Wilmington, MA, USA). Nucleic acid concentrations were measured using a NanoDrop 2000C spectrophotometer (Thermo Scientific, Waltham, MA, USA).

Sequencing of sections of the enterovirus genome

The Sanger PCR reaction was carried out using the BigDye™ Terminator v3.1 Cycle Sequencing Kit (Thermo Fisher Scientific) in accordance with the manufacturer's protocol on a SimpliAmp Thermal Cycler (Thermo Fisher Scientific). For sequencing of VP1 and 5'UTR-VP2 PCR products, we used internal primers AN232 5' CCAGCACTGACAGCA 3' [9] and EV_S_in 5' CATGGTGYGAAGYCTATTGAGC 3' respectively. The Sanger sequencing was performed on an Applied Biosystems 3500 Genetic Analyzer (Thermo Fisher Scientific).

Enterovirus RNA was found in 156 clinical samples. Genotyping in two genome regions was performed for 96 samples; the results of VP1 and 5'UTR-VP2 typing were the same for all of them. For 40 samples, genotyping was performed only in the 5'UTR-VP2 region, and for 20 samples in the VP1 region of the genome.

The nucleotide sequences of fragment VP1 (PX468781–PX468895) and region 5'UTR-VP2 (PX491339–PX491474) were uploaded to the NCBI GenBank database.

Identification of enterovirus types

We used the resources of Enterovirus Genotyping Tool Version 0.1, National Institute for Public Health and the Environment, Bilthoven, The Netherlands) [10] and NCBI BLAST [11].

Statistical data processing

We used the Medcals resource [12] and the standard functions of Microsoft Excel (Microsoft Corporation). To compare the frequency of symptoms between the groups, the two-tailed Fisher's exact test was performed. Differences were considered statistically significant at $p < 0.05$. For samples with a small number of observations ($n < 10$), no statistical comparison was performed.

RESULTS

Genotyping of enteroviruses in biological samples from children revealed 16 different types, for one sample only the EV-C enterovirus species could be established. The majority of the studied enteroviruses were of the EV-A CV-A6 type: among the samples from 2021, their share was 80.6%, from 2022 — 36.1%. CV-A10 was the second most common enterovirus detected in EV patients, accounting for 6.5% of the 2021 sample batch and 27.0% of the 2022 batch. Other EV-A enteroviruses were found much less frequently. The CV-A16 virus was detected in only one patient (2022 sample batch).

EV-B viruses of types CV-A9, CV-B2, CV-B3, CV-B5, ECHO 6, ECHO 9, ECHO 11 were identified in 16.0% of patients (in 2021–2022). ECHO 6 dominated among them, with a 9.0% share in the 2022 sample batch.

In addition, we identified three samples of enterovirus of the EV-C species (two cases of CV-A19 and one case of EV-C of unidentified type) and four cases of enterovirus EV-D68 of the EV-D type. The results of enterovirus genotyping are shown in Table 1.

We analyzed the relationship of symptoms in patients infected with enteroviruses of various types. Those of the EV-A species (CV-A2, CV-A3, CV-A4, CV-A5, CV-A6, CV-A10, CV-A16) caused similar symptoms: HFMD, exanthema, diseases of the upper and lower respiratory tract, herpangina, gastrointestinal infections, acute hemorrhagic conjunctivitis. Enteroviruses of the EV-B type (CV-A9, CV-B2, CV-B3, CV-B5, ECHO 6, ECHO 9, ECHO 11) mainly manifested as neurological disorders (meningism, intense headache, vomiting) against a background of fever, respiratory and/or intestinal symptoms. Four of the 11 patients with ECHO6 infection were diagnosed with meningitis (Fig. 1).

Enteroviruses of types CV-A6 ($n = 69$) and CV-A10 ($n = 35$) were represented sufficiently to allow a comparison of the frequency of various clinical manifestations (Table 2). It was reliably shown that in this study, exanthema developed more often in patients with CV-A6 infection than in CV-A10 cases (65.2% vs 25.7%), and herpangina, on the contrary, was more often observed when the disease was brought by a CV-A10 infection (62.9% vs 23.2%).

We have also investigated the frequency of detection of other infectious agents in patients, including those causing a clinical picture similar to an EV infection (exanthema, respiratory, intestinal, or neuroinfections). The specific RNA and DNA pathogens tested for were as follows: herpes simplex viruses type 1 and 2 (HSV-1/2), human herpesvirus 6 (HHV-6), Epstein–Barr virus (EBV), cytomegalovirus (HCMV), rhinoviruses (HRV), respiratory syncytial virus (RSV), human metapneumovirus (HMPV), human parainfluenza viruses types 1–4 (HPIV-1 to HPIV-4), human bocavirus (HBoV), adenoviruses species B, C, E, and F (HAdV-B, -C, -E, -F), human coronaviruses OC43, 229E, NL63, and HKU1 (HCoVs), rotavirus A, norovirus genogroup II, astroviruses, *Shigella* spp./enteroinvasive *Escherichia coli* (EIEC), *Salmonella* spp., *Campylobacter* spp., *Streptococcus pyogenes*, *Staphylococcus* spp., and *Candida albicans*.

The total number of EV infection cases concomitant with other infectious agents in various combinations was 29.5%, but in most cases, those agents did not significantly affect disease

Table 1. Results of typing of enteroviruses in biological material collected from children in 2021–2023 in Moscow

Type of enterovirus	2021		2022		2023	Total
	Number of patients, *n* = 31	Proportion *n*, % (95% CI)	Number of patients, *n* = 122	Proportion *n*, % (95% CI)	Number of patients, *n* = 3	156
Enterovirus alphacoxsackie, EV-A						
CV-A2	1	3.2 (0–9.4)	1	0.8 (0–2.4)	–	2
CV-A3	–	–	1	0.8 (0–2.4)	–	1
CV-A4	1	3.2 (0–9.4)	7	5.7 (1.6–9.9)	1	9
CV-A5	1	3.2 (0–9.4)	6	4.9 (1.1–8.8)	–	7
CV-A6	25	80.6 (66.7–95.5)	44	36.1 (27.5–44.6)	–	69
CV-A10	2	6.5 (0–15.1)	33	27.0 (19.2–34.9)	–	35
CV-A16	–	–	1	0.8 (0–2.4)	–	1
Enterovirus betacoxsackie, EV-B						
CV-A9	–	–	4	3.3 (0.12–6.4)	–	4
CV-B2	–	–	1	0.8 (0–2.4)	–	1
CV-B3	1	3.2 (0–9.4)	–	–	–	1
CV-B5	–	–	4	3.3 (0.12–6.4)	–	4
ECHO 6	–	–	11	9.0 (3.9–14.1)	–	11
ECHO 9	–	–	3	2.5 (0–5.2)	–	3
ECHO 11	–	–	1	0.8 (0–2.4)	–	1
Enterovirus coxsackiepol, EV-C						
CV-A19	–	–	1	0.8 (0–2.4)	1	2
Unknown	–	–	1	0.8 (0–2.4)	–	1
Enterovirus deconjuncti, EV-D						
EV-D68	–	–	3	2.5 (0–5.2)	1	4

severity. Herpes virus type 6 (HHV-6) was detected most often (in up to 17% of all studied cases of EV infection). In 7% of cases, we observed infections involving multiple pathogens — either mixed viral infections (e.g., CV-A10, HHV-6, EBV, HCMV) or bacterial–viral co-infections (e.g., CV-A6, *Astrovirus*, *Shigella* spp.,) (Fig. 2).

DISCUSSION

Genotyping of enteroviruses in biological samples collected from children in the Moscow region in 2021–2022 showed that the dominant type was CV-A6. This type has been widely distributed across European countries since 2008 and subsequently spread to Asia and North America. There are atypical forms of CV-A6 that cause unusual skin manifestations: exanthema, rash, eczema, blisters, onychomadesis [13, 14]. In 2017, the prevalence of CV-A6 in some countries reached 71.1% [15], with large-scale outbreaks reported in Brazil, Vietnam, France, and China [16–20]. The dominant position of the CV-A6 in Russia is confirmed by the data of the Reference Center: the prevalence of this type among patients with EV infection was 13% in 2018, 29% in 2019, 40% in 2021, 19% in 2022, 34% in 2023, 17% in 2024 [2]. Compared to the classic Coxsackie virus CV-A16, which was previously a common cause of HFMD [2, 21], CV-A6 infection is characterized by a longer duration, atypical skin manifestations, and neurological symptoms [15, 18].

In this study, CV-A6 predominantly caused exanthema and diseases of the upper and lower respiratory tract, less often — HFMD, herpangina, gastrointestinal infections, and acute hemorrhagic conjunctivitis. In four cases (patients under 3 years old, accounting for about 6% of the CV-A6 sample), the infection was severe and accompanied by seizures and loss of consciousness in the context of febrile fever. A concomitant agent, HHV-6, was detected only in one case of these four, therefore, the complicated course is probably not associated with coinfection.

It is shown that compared to 2021, in 2022, the proportion of CV-A6 decreased from 80.6% to 36.1%, while the share of CV-A10 cases increased from 6.5% to 27.0%. This is consistent with the reports of the growing numbers of CV-A10 infection cases in the regions of the Russian Federation and other countries [2, 22, 23]. The symptoms of CV-A10 infection were generally similar to those of CV-A6 infection, except that herpangina was more frequent and various exanthemas were less common. Six patients aged 0–6 years (17% of patients with CV-A10) had seizures and/or loss of consciousness with febrile fever in the background, and only two of them had associated infectious agents (HHV-6, HAdV). In this study, we did not observe any cases of meningitis associated with CV-A10, although such cases have been reported previously. Moreover, according to published data, CV-A10 infection tends to be more severe than those caused by CV-A6 or CV-A16 [22].

Separately, it should be noted that two patients with CV-A10 and CV-A3 had a rather rare complication — urinary tract infections. The cytopathogenic effect of enteroviruses on renal tissue cells was described earlier, which indicates the possibility of involvement of organs of the urinary system in the pathological process [24].

Among EV-B enteroviruses, ECHO 6 was the most common type. It was detected exclusively in the 2022 sample batch, correlating with the epidemic rise of this type observed across the Russian Federation that year [2]. Symptoms of neuroinfection were noted, some patients had meningitis, the rest had neurological symptoms (meningism, intense headache, vomiting) against the background of fever, respiratory and/or intestinal disorders. One of the cases of ECHO 6 infection manifested in a child as enterovirus vesicular pharyngitis,

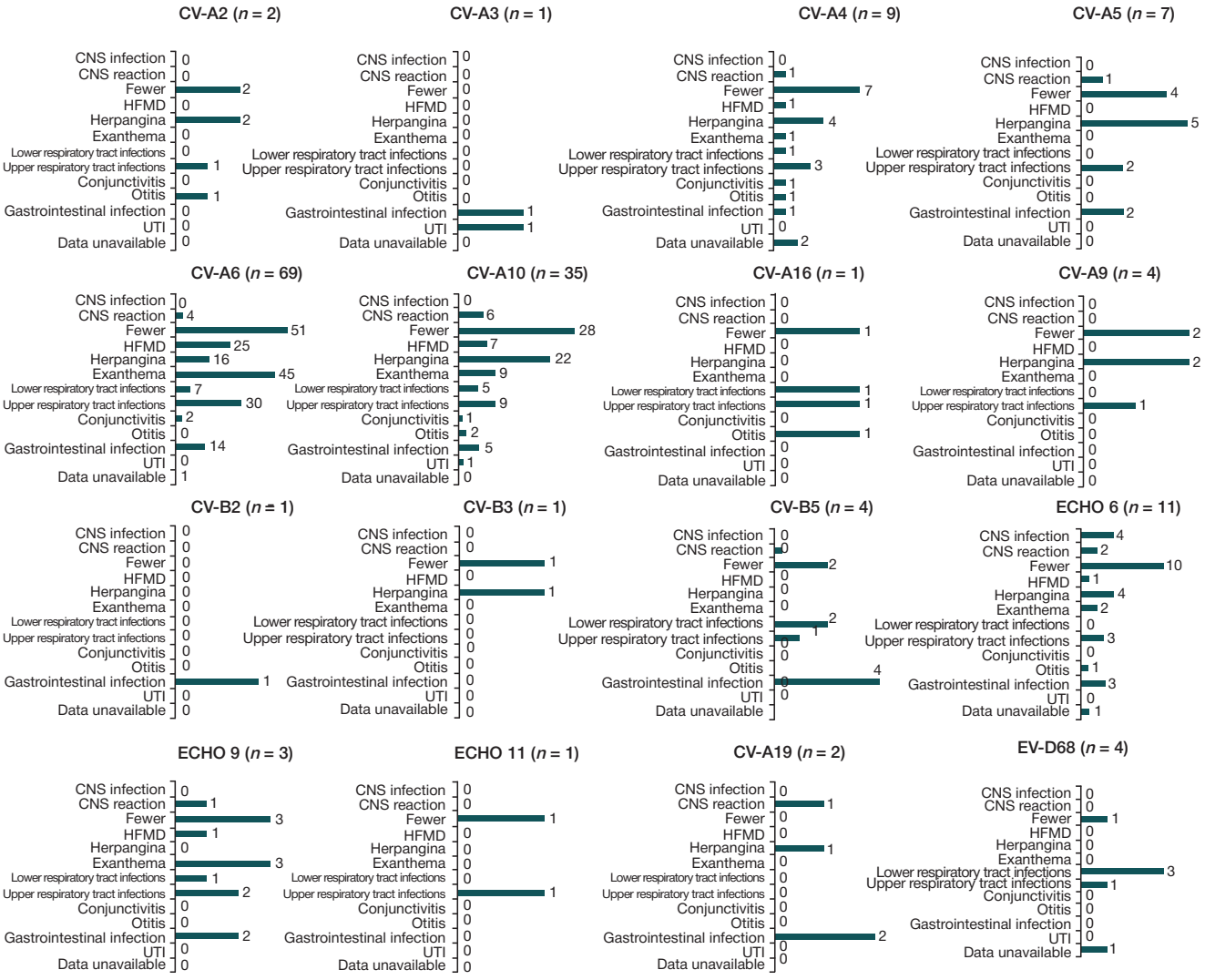


Fig. 1. The relationship of clinical symptoms with the type of enterovirus. CNS infection — infection of the central nervous system (meningitis); CNS reaction — reaction of the central nervous system (encephalopathy, meningism, seizures, impaired consciousness, apnea); fever (subfebrile, febrile, pyretic fever); HFMD — hand, foot and mouth disease — enterovirus vesicular stomatitis with exanthema; herpangina — enterovirus vesicular pharyngitis; lower respiratory tract infections — bronchitis, pneumonia; upper respiratory tract infections — rhinitis, pharyngitis, tonsillitis, tracheitis; gastrointestinal infection — infectious gastritis, enteritis, colitis; UTI — urinary tract infection

however, the mother of this child had it as enterovirus meningitis. This example does not agree with the typical clinical model of EV infection, in which adults carry the infection in a milder or asymptomatic form, because in the described case the parent experienced a more severe course of the disease.

In other cases of EV-B infections, the symptoms involved intestinal (gastroenteritis, enterocolitis) and respiratory (rhinitis, bronchitis) disorders without affecting the central nervous system. In some cases, we also observed herpangina (CV-B3, ECHO 6) and HFMD (ECHO 6, ECHO 9). ECHO 11, which is associated with neonatal sepsis in infants, was detected only in a three-year-old patient with symptoms of respiratory infection. The ECHO 30 virus, which has been the predominant causative agent of enteroviral meningitis in the Russian Federation for many years, was not detected in this study. This finding is consistent with the enterovirus monitoring data from the Reference Center: since the onset of the COVID-19 pandemic, ECHO 30 has been rarely detected in the Russian Federation during 2021–2022. However, ECHO 30 showed an upward trend later; in 2024, it accounted for 8% of all EV infection cases [2].

Two cases of EV-C CV-A19 virus infection have also been identified. According to the literature, CV-A19 is a fairly rare infection agent; it can cause various respiratory and intestinal disorders, herpangina, as well as meningitis and acute flaccid myelitis [25–26]. In the first case, the patient developed a herpangina with infectious enterocolitis. In the second case, against the background of norovirus and astrovirus coinfection, the child had acute infectious gastroenteritis, toxicosis, exicosis and acidosis, along with speech disorder and logoneurosis. Electroencephalography has also detected epileptiform activity. The effects affecting the central nervous system are probably associated with severe intestinal coinfection.

Epidemiologically significant enteroviruses include EV-D68, which was also identified in this study. This type commonly brings respiratory symptoms, but since 2014, it has been associated with acute flaccid myelitis, the symptoms of which include damage to the lower motor neurons in the gray matter of the spinal cord, impaired reflexes, respiratory failure, and sudden muscle weakness [27]. Outbreaks of EV-D68 infection, accompanied by acute flaccid paralysis, myelitis, myocarditis, pericarditis, neonatal sepsis, and pneumonia, have been recorded in the United States and Europe. In the Russian Federation, isolated cases of EV-D68 have been registered since 2018. The cases of EV-D68 infection identified in this study in children aged 5–12 years were associated with respiratory tract diseases, including rhinopharyngitis, obstructive bronchitis, and pneumonia.

Table 2. Comparison of clinical symptoms, CV-A6 and CV-A10 types

	CV-A6 (n = 69)			CV-A10 (n = 35)			OR (95% CI)	p-value
Symptom	Quantity	Proportion of patients with the symptom, % (95% CI)		Quantity	Proportion of patients with the symptom, % (95% CI)			
CNS reaction	4	5.8	(0.3–11.3)	6	17	(4.7–29.6)	0.3 (0.1–1.1)	0.08
Fever	51	73.9	(63.5–84.3)	28	80	(66.7–93.2)	0.7 (0.3–1.9)	0.63
HFMD	25	36.2	(24.9–47.6)	7	20	(6.7–33.2)	2.3 (0.9–5.9)	0.12
Herpangina	16	23.2	(13.2–33.1)	22	62.9	(46.8–78.8)	0.2 (0.1–0.4)	< 0.001
Exanthema	45	65.2	(53.9–76.4)	9	25.7	(11.2–40.2)	5.4 (2.2–13.4)	< 0.001
Lower respiratory tract infections	7	10.1	(3.0–17.3)	5	14.3	(2.7–25.9)	0.7 (0.2–2.3)	0.53
Upper respiratory tract infections	30	43.5	(31.8–55.2)	9	25.7	(11.2–40.2)	2.2 (0.9–5.4)	0.09
Conjunctivitis	2	2.9	(0–6.9)	1	2.9	(0–8.4)	1.0 (0.1–11.6)	1
Gastrointestinal infection	14	20.3	(10.8–29.8)	5	14.3	(2.7–25.9)	1.5 (0.5–4.6)	0.59

Our data show a high proportion of cases of EV infection accompanied by other infectious agents (up to 30% of all cases), which confirms previously published data on cases of coinfections in various forms of EV infection. The literature describes cases of coinfections such as EV/HSV-1 in neonatal meningitis; CV-A6/EV-D68/HPeV/HHV-6/parvovirus in acute encephalopathy; EV/Pasteurella multocida in meningitis and sepsis; EV/HSV-1, CV-A6/HHV-7, and CV-A6 / CMV in hand, foot, and mouth disease (HFMD) syndrome; and EV / *Escherichia coli* in urinary tract infections [33].

According to our data, in most cases, coinfection with EV was associated with pathogens that can remain latent in the body and become active under conditions of weakened immunity — such as herpes simplex virus types 1 and 2,

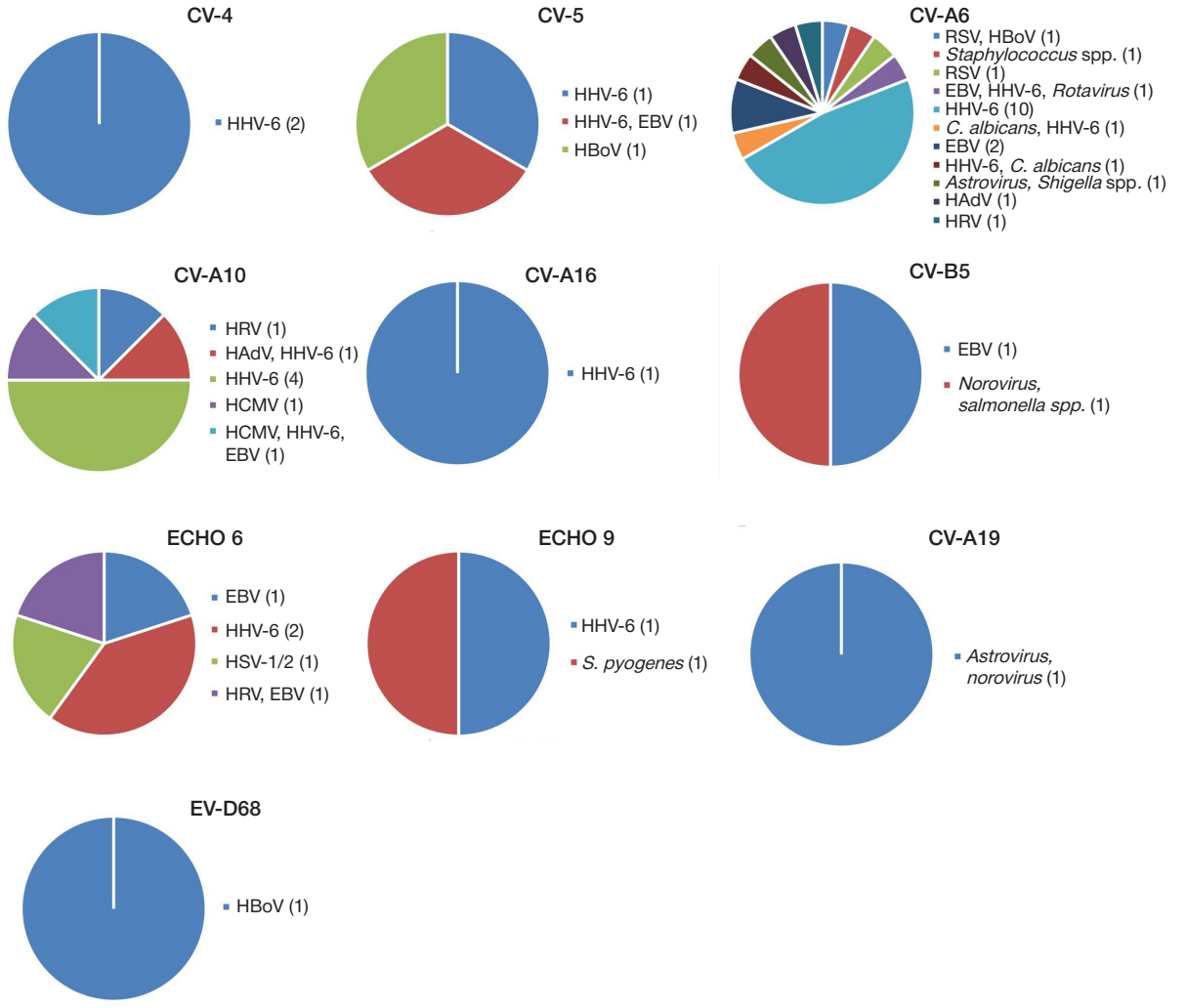


Fig. 2. Identification of various concomitant infectious agents in patients with EV infection

cytomegalovirus, Epstein–Barr virus, and human herpesvirus 6 — accounting for up to 74% of all cases in which additional infectious agents were detected.

CONCLUSIONS

It was determined that among the enteroviruses detected in children in the Moscow region in 2021–2022, CV-A6 was dominant, primarily causing skin lesions in patients. In 2022, there was an increase in the number of CV-A10 cases, for which there was a large proportion of cases with a severe course of the disease compared to CV-A6. Among EV-B viruses, the largest proportion belonged to ECHO 6; several patients were diagnosed with meningitis. A large number of EV infectious cases showed the presence of other viral and bacterial pathogens in patients' biomaterials, which may be due to immune suppression during the course of EV infectious. The nucleotide sequences of all characterized enteroviruses are publicly available in the NCBI database, which makes it possible to use them for future epidemiological analyses of enterovirus circulation in the Russian Federation.

References

1. Alimov AV, Feldblyum IV, Akimkin VG, Zaharova Yu.A, Sergeev AG, Piterskij MV. Epidemiologicheskij nadzor i kontrol' enterovirusnoj (nepolio) infekcii: aktual'nye problemy i puti resheniya. Ekaterinburg: YUnika, 2021; 181 s, ISBN 978-5-6045184-4-1. Russian.
2. Informacionnye byulleteni FBUN «Nizhegorodskij nauchno-issledovatel'skij institut epidemiologii i mikrobiologii im. akademika I. N. Blohinoj». Zabolevaemost' i etiologicheskaya struktura enterovirusnoj (nepolio) infekcii. 2021–2025. Russian.
3. Khetsuriani N, Lamonte-Fowlkes A, Oberst S, Pallansch MA. Centers for Disease Control and Prevention. Enterovirus surveillance — United States, 1970–2005. MMWR Surveill Summ. 2006; 55 (8): 1–20. Available from: https://www.cdc.gov/mmwr/preview/mmwrhtml/ss5508a1.htm.
4. Midgley CM, Watson JT, Nix WA, Curns AT, Rogers SL, Brown BA, et al. Severe respiratory illness associated with a nationwide outbreak of enterovirus D68 in the USA (2014): a descriptive epidemiological investigation. Lancet Respir Med. 2015; 3 (11): 879–87. DOI: 10.1016/S2213-2600(15)00335-5.
5. O sostoyanii sanitarno-epidemiologicheskogo blagopoluchiya naseleniya v Rossijskoj Federacii v 2024 godu: Gosudarstvennyj doklad. M.: Federal'naya sluzhba po nadzoru v sfere zashchity prav potrebitelej i blagopoluchiya cheloveka, 2025; 2025. Russian.
6. Starikova PK, Bykov RO, Itani TM, CHalapa VI, Sergeev AG, Olen'kova OM, i dr. V. Etiologicheskaya struktura enterovirusnogo meningita v Ekaterinburge do i posle pandemii COVID 19. Ural'skij medicinskij zhurnal. 2024; 23 (3): 26–35. Dostupno po ssylke: https://doi.org/10.52420/umj.23.3.26. Russian.
7. Butakova LV, Sapega EYu, Trocenko OE. Enterovirusy — vozbuditeli gerpanginy u naseleniya Dal'nego Vostoka Rossii. Byulleten' fiziologii i patologii dyhaniya. 2025; (97): 57–68. Dostupno po ssylke: https://doi.org/10.36604/1998-5029-2025-97-57-68. Russian.
8. Sapega EYu, Butakova LV, Trocenko OE. Osobennosti epidemicheskogo processa enterovirusnoj infekcii v Irkutskoj oblasti v 2023 godu. Zdorov'e naseleniya i sreda obitaniya — ZNiSO. 2024; 32 (8): 77–84. Dostupno po ssylke: https://doi.org/10.35627/2219-5238/2024-32-8-77-84. Russian.
9. Nix WA, Oberste MS, Pallansch MA. Sensitive, seminested PCR amplification of VP1 sequences for direct identification of all enterovirus serotypes from original clinical specimens. J Clin Microbiol. 2006; 44 (8): 2698–704. DOI: 10.1128/JCM.00542-06.
10. Kroneman A, Vennema H, Deforche K, Avoort H, Penaranda S, Oberste MS, et al. An automated genotyping tool for enteroviruses and noroviruses. J Clin Virol. 2011; 51 (2): 121–5. DOI: 10.1016/j.jcv.2011.03.006.
11. Altschul SF, Gish W, Miller W, Myers EW, Lipman DJ. Basic local alignment search tool. J Mol Biol. 1990; 215 (3): 403–10. DOI: 10.1016/S0022-2836(05)80360-2.
12. MedCalc Software Ltd. Fisher exact probability. Available from: https://www.medcalc.org/en/calc/fisher.php (Version 23.4.5; accessed December 12, 2025).
13. Gaunt E, Harvala H, Österback R, Sreenu VB, Thomson E, Waris M, Simmonds P. Genetic characterization of human coxsackievirus A6 variants associated with atypical hand, foot and mouth disease: a potential role of recombination in emergence and pathogenicity. J Gen Virol. 2015; 96 (5): 1067–79. DOI: 10.1099/vir.0.000062.
14. Puenpa J, Vongpunsawad S, Österback R, Waris M, Eriksson E, Albert J, et al. Molecular epidemiology and the evolution of human coxsackievirus A6. J Gen Virol. 2016; 97 (12): 3225–31. DOI: 10.1099/jgv.0.000619.
15. Li X, Chen S, Chen Y, Han S, Dai B, Li T, et al. Epidemiological and genetic characterizations of hand, foot, and mouth disease and acute respiratory infections due to CV-A6 infection in Henan Province, China between 2021 and 2022. BMC Pediatr. 2025; 25 (1): 264. DOI: 10.1186/s12887-025-05527-6.
16. Justino MCA, da S Mesquita D, Souza MF, Farias FP, Dos S Alves JC, Ferreira JL, et al. Atypical hand-foot-mouth disease in Belém, Amazon region, Northern Brazil, with detection of coxsackievirus A6. J Clin Virol. 2020; 126: 104307. DOI: 10.1016/j.jcv.2020.104307.
17. Anh NT, Nhu LNT, Van HMT, Hong NTT, Thanh TT, Hang VTT, et al. Emerging coxsackievirus A6 causing hand, foot and mouth disease, Vietnam. Emerg Infect Dis. 2018; 24 (4): 654–62. DOI: 10.3201/eid2404.171298.
18. Mirand A, Cohen R, Bisseux M, Tomba S, Sellem FC, Gelbert N, et al. A large-scale outbreak of hand, foot and mouth disease, France, as at 28 September 2021. Euro Surveill. 2021; 26 (43): 2100978. DOI: 10.2807/1560-7917.ES.2021.26.43.2100978.
19. Hu L, Maimaiti H, Zhou L, Gao J, Lu Y. Changing serotypes of hand, foot and mouth disease in Shanghai, 2017–2019. Gut Pathog. 2022; 14 (1): 12. DOI: 10.1186/s13099-022-00485-1.
20. Xu S, Li H, Qiao P, Xu G, Zhao D, Lin X, et al. Neonatal hand, foot, and mouth disease due to coxsackievirus A6 in Shanghai. BMC Pediatr. 2020; 20 (1): 364.
21. Zhu P, Ji W, Li D, Li Z, Chen Y, Dai B, et al. Current status of hand-foot-and-mouth disease. J Biomed Sci. 2023; 30 (1): 15. DOI: 10.1186/s12929-023-00908-4.
22. Chen L, Yao XJ, Yang H, Zhang HL, Shi XL, Peng B, et al. Molecular Epidemiology of Coxsackievirus A10 Associated With Hand, Foot and Mouth Disease From 2021 to 2024 in Shenzhen, China. J Med Virol. 2025; 97 (8): e70552. DOI: 10.1002/jmv.70552.
23. Lv S, Zhou Y, Ji J, Yan Y, Zhu G. Epidemiological and genetic characteristics of enteroviruses associated with hand, foot, and mouth disease in Jiaxing, China from 2019 to 2022. Sci Rep. 2025; 15 (1): 14546. DOI: 10.1038/s41598-025-99251-x.
24. Kokoreva SP, Kazarceva NV. Izmeneniya mochevoj sistemy u detej pri enterovirusnoj infekcii. Rossijskij pediatricheskij zhurnal. 2021; 24 (3): 193–6. Dostupno po ssylke: https://doi.org/10.46563/1560-9561-2021-24-3-193-196. Russian.
25. Tapparel C, Siegrist F, Petty TJ, Kaiser L. Picornavirus and enterovirus diversity with associated human diseases. Infect Genet Evol. 2013; 14: 282–93. DOI: 10.1016/j.meegid.2012.10.016.
26. Apostol LN, Suzuki A, Bautista A, Galang H, Paladin FJ, Fuji N, et al. Detection of non-polio enteroviruses from 17 years of virological surveillance of acute flaccid paralysis in the Philippines. J Med Virol. 2012; 84 (4): 624–31. DOI: 10.1002/jmv.23242.
27. Holm-Hansen CC, Midgley SE, Fischer TK. Global emergence of enterovirus D68: a systematic review. Lancet Infect Dis. 2016; 16 (5): e64–75. DOI: 10.1016/S1473-3099(15)00543-5.

28. Coramusi C, Rizzoli A, Alegiani C, Bonafoni S, Auriti C, Parisi P, et al. Neonatal Meningitis Due to Herpes Simplex Virus Type 1 and Enterovirus Coinfection: Case Report and Review of the Literature. Viruses. 2025; 17 (6): 790. DOI: 10.3390/v17060790.
29. Nakata K, Kashiwagi M, Masuda M, Shigehara S, Oba C, Murata S, et al. A child with acute encephalopathy associated with quadruple viral infection. Front Pediatr. 2015; 3: 26. DOI: 10.3389/fped.2015.00026.
30. Aguado I, Calvo C, Wilhelmi I, Pablo-Hernando ME, Medina MJ, Sáez-Nieto JA, et al. Sepsis and meningitis caused by Pasteurella multocida and echovirus 9 in a neonate. Pediatr Infect Dis J. 2014; 33 (12): 1308–9. DOI: 10.1097/INF.0000000000000504.
31. Ndiaye N, Teixeira DD, Dia N, Da Silva Leite CC, Fall G, Furtado UD, et al. An outbreak of atypical hand, foot and mouth disease associated Coxsackievirus A6 in children from Cape Verde, 2023. Virol J. 2025; 22 (1): 48. DOI: 10.1186/s12985-025-02621-0.
32. Hooi PS, Chua BH, Lee CS, Lam SK, Chua KB. Hand, foot and mouth disease: University Malaya Medical Centre experience. Med J Malaysia. 2002; 57 (1): 88–91. PMID: 14569726.
33. Calvo C, Gallardo P, Torija P, et al. Enterovirus neurological disease and bacterial coinfection in very young infants with fever. J Clin Virol. 2016; 85: 37–39. DOI: 10.1016/j.jcv.2016.10.020.

Литература

1. Алимов А. В., Фельдблюм И.В., Акимкин В.Г., Захарова Ю.А., Сергеев А.Г., Питерский М.В. Эпидемиологический надзор и контроль энтеровирусной (неполио) инфекции: актуальные проблемы и пути решения. Екатеринбург: Юника, 2021; 181 с, ISBN 978-5-6045184-4-1.
2. Информационные бюллетени ФБУН «Нижегородский научно-исследовательский институт эпидемиологии и микробиологии им. академика И. Н. Блохиной». Заболеваемость и этиологическая структура энтеровирусной (неполио) инфекции. 2021–2025.
3. Khetsuriani N, Lamonte-Fowlkes A, Oberst S, Pallansch MA. Centers for Disease Control and Prevention. Enterovirus surveillance — United States, 1970–2005. MMWR Surveill Summ. 2006; 55 (8): 1–20. Available from: https://www.cdc.gov/mmwr/preview/mmwrhtml/ss5508a1.htm.
4. Midgley CM, Watson JT, Nix WA, Curns AT, Rogers SL, Brown BA, et al. Severe respiratory illness associated with a nationwide outbreak of enterovirus D68 in the USA (2014): a descriptive epidemiological investigation. Lancet Respir Med. 2015; 3 (11): 879–87. DOI: 10.1016/S2213-2600(15)00335-5.
5. О состоянии санитарно-эпидемиологического благополучия населения в Российской Федерации в 2024 году: Государственный доклад. М.: Федеральная служба по надзору в сфере защиты прав потребителей и благополучия человека, 2025; 2025.
6. Старикова П. К., Быков Р. О., Итани Т. М., Чалапа В. И., Сергеев А. Г., Оленькова О. М., и др. В. Этиологическая структура энтеровирусного менингита в Екатеринбурге до и после пандемии COVID-19. Уральский медицинский журнал. 2024; 23 (3): 26–35. Доступно по ссылке: https://doi.org/10.52420/umj.23.3.26.
7. Бутакова Л. В., Сапега Е. Ю., Троценко О. Е. Энтеровирусы — возбудители герпангины у населения Дальнего Востока России. Бюллетень физиологии и патологии дыхания. 2025; (97): 57–68. Доступно по ссылке: https://doi.org/10.36604/1998-5029-2025-97-57-68.
8. Сапега Е. Ю., Бутакова Л. В., Троценко О. Е. Особенности эпидемического процесса энтеровирусной инфекции в Иркутской области в 2023 году. Здоровье населения и среда обитания — ЗНиСО. 2024; 32 (8): 77–84. Доступно по ссылке: https://doi.org/10.35627/2219-5238/2024-32-8-77-84.
9. Nix WA, Oberste MS, Pallansch MA. Sensitive, seminested PCR amplification of VP1 sequences for direct identification of all enterovirus serotypes from original clinical specimens. J Clin Microbiol. 2006; 44 (8): 2698–704. DOI: 10.1128/JCM.00542-06.
10. Kroneman A, Vennema H, Deforche K, Avoort H, Penaranda S, Oberste MS, et al. An automated genotyping tool for enteroviruses and noroviruses. J Clin Virol. 2011; 51 (2): 121–5. DOI: 10.1016/j.jcv.2011.03.006.
11. Altschul SF, Gish W, Miller W, Myers EW, Lipman DJ. Basic local alignment search tool. J Mol Biol. 1990; 215 (3): 403–10. DOI: 10.1016/S0022-2836(05)80360-2.
12. MedCalc Software Ltd. Fisher exact probability. Available from: https://www.medcalc.org/en/calc/fisher.php (Version 23.4.5; accessed December 12, 2025).
13. Gaunt E, Harvala H, Österback R, Sreenu VB, Thomson E, Waris M, Simmonds P. Genetic characterization of human coxsackievirus A6 variants associated with atypical hand, foot and mouth disease: a potential role of recombination in emergence and pathogenicity. J Gen Virol. 2015; 96 (5): 1067–79. DOI: 10.1099/vir.0.000062.
14. Puenpa J, Vongpunsawad S, Österback R, Waris M, Eriksson E, Albert J, et al. Molecular epidemiology and the evolution of human coxsackievirus A6. J Gen Virol. 2016; 97 (12): 3225–31. DOI: 10.1099/jgv.0.000619.
15. Li X, Chen S, Chen Y, Han S, Dai B, Li T, et al. Epidemiological and genetic characterizations of hand, foot, and mouth disease and acute respiratory infections due to CV-A6 infection in Henan Province, China between 2021 and 2022. BMC Pediatr. 2025; 25 (1): 264. DOI: 10.1186/s12887-025-05527-6.
16. Justino MCA, da S Mesquita D, Souza MF, Farias FP, Dos S Alves JC, Ferreira JL, et al. Atypical hand-foot-mouth disease in Belém, Amazon region, Northern Brazil, with detection of coxsackievirus A6. J Clin Virol. 2020; 126: 104307. DOI: 10.1016/j.jcv.2020.104307.
17. Anh NT, Nhu LNT, Van HMT, Hong NTT, Thanh TT, Hang VTT, et al. Emerging coxsackievirus A6 causing hand, foot and mouth disease, Vietnam. Emerg Infect Dis. 2018; 24 (4): 654–62. DOI: 10.3201/eid2404.171298.
18. Mirand A, Cohen R, Bisseux M, Tomba S, Sellem FC, Gelbert N, et al. A large-scale outbreak of hand, foot and mouth disease, France, as at 28 September 2021. Euro Surveill. 2021; 26 (43): 2100978. DOI: 10.2807/1560-7917.ES.2021.26.43.2100978.
19. Hu L, Maimaiti H, Zhou L, Gao J, Lu Y. Changing serotypes of hand, foot and mouth disease in Shanghai, 2017–2019. Gut Pathog. 2022; 14 (1): 12. DOI: 10.1186/s13099-022-00485-1.
20. Xu S, Li H, Qiao P, Xu G, Zhao D, Lin X, et al. Neonatal hand, foot, and mouth disease due to coxsackievirus A6 in Shanghai. BMC Pediatr. 2020; 20 (1): 364.
21. Zhu P, Ji W, Li D, Li Z, Chen Y, Dai B, et al. Current status of hand-foot-and-mouth disease. J Biomed Sci. 2023; 30 (1): 15. DOI: 10.1186/s12929-023-00908-4.
22. Chen L, Yao XJ, Yang H, Zhang HL, Shi XL, Peng B, et al. Molecular Epidemiology of Coxsackievirus A10 Associated With Hand, Foot and Mouth Disease From 2021 to 2024 in Shenzhen, China. J Med Virol. 2025; 97 (8): e70552. DOI: 10.1002/jmv.70552.
23. Lv S, Zhou Y, Ji J, Yan Y, Zhu G. Epidemiological and genetic characteristics of enteroviruses associated with hand, foot, and mouth disease in Jiaxing, China from 2019 to 2022. Sci Rep. 2025; 15 (1): 14546. DOI: 10.1038/s41598-025-99251-x.
24. Кокорева С. П., Казарцева Н. В. Изменения мочевой системы у детей при энтеровирусной инфекции. Российский педиатрический журнал. 2021; 24 (3): 193–6. Доступно по ссылке: https://doi.org/10.46563/1560-9561-2021-24-3-193-196.
25. Tapparel C, Siegrist F, Petty TJ, Kaiser L. Picornavirus and enterovirus diversity with associated human diseases. Infect Genet Evol. 2013; 14: 282–93. DOI: 10.1016/j.meegid.2012.10.016.
26. Apostol LN, Suzuki A, Bautista A, Galang H, Paladin FJ, Fuji N, et al. Detection of non-polio enteroviruses from 17 years of virological surveillance of acute flaccid paralysis in the Philippines. J Med Virol. 2012; 84 (4): 624–31. DOI: 10.1002/jmv.23242.
27. Holm-Hansen CC, Midgley SE, Fischer TK. Global emergence of enterovirus D68: a systematic review. Lancet Infect Dis. 2016; 16 (5): e64–75. DOI: 10.1016/S1473-3099(15)00543-5.
28. Coramusi C, Rizzoli A, Alegiani C, Bonafoni S, Auriti C, Parisi P, et al. Neonatal Meningitis Due to Herpes Simplex Virus Type 1

and Enterovirus Coinfection: Case Report and Review of the Literature. Viruses. 2025; 17 (6): 790. DOI: 10.3390/v17060790.
29. Nakata K, Kashiwagi M, Masuda M, Shigehara S, Oba C, Murata S, et al. A child with acute encephalopathy associated with quadruple viral infection. Front Pediatr. 2015; 3: 26. DOI: 10.3389/fped.2015.00026.
30. Aguado I, Calvo C, Wilhelmi I, Pablo-Hernando ME, Medina MJ, Sáez-Nieto JA, et al. Sepsis and meningitis caused by Pasteurella multocida and echovirus 9 in a neonate. Pediatr Infect Dis J. 2014; 33 (12): 1308–9. DOI: 10.1097/INF.0000000000000504.
31. Ndiaye N, Teixeira DD, Dia N, Da Silva Leite CC, Fall G, Furtado UD, et al. An outbreak of atypical hand, foot and mouth disease associated Coxsackievirus A6 in children from Cape Verde, 2023. Virol J. 2025; 22 (1): 48. DOI: 10.1186/s12985-025-02621-0.
32. Hooi PS, Chua BH, Lee CS, Lam SK, Chua KB. Hand, foot and mouth disease: University Malaya Medical Centre experience. Med J Malaysia. 2002; 57 (1): 88–91. PMID: 14569726.
33. Calvo C, Gallardo P, Torija P, et al. Enterovirus neurological disease and bacterial coinfection in very young infants with fever. J Clin Virol. 2016; 85: 37–39. DOI: 10.1016/j.jcv.2016.10.020.

COMPARATIVE IMAGING OF THE HAEE-CY5 AND EEAH-CY5 TETRAPEPTIDE BINDING TO THE Aβ AGGREGATES ON THE SH-SY5Y CELLS

Ivanova AV[1,2] ✉, Chmelyuk NS[1,2], Kuzmichev IA[1], Shilyaeva MI[1], Abakumov MA[1,2]

[1] Research Institute of Translational Medicine, Pirogov Russian National Research Medical University, Moscow, Russia

[2] Institute of Biomedical Engineering, MISIS University of Science and Technology, Moscow, Russia

Due to high diagnostic value of β-amyloid aggregates, the target ligands capable of specific binding to abnormal Aβ aggregates are of special interest. The study aimed to perform comparative characterization of the HAEE-Cy5 (Ac-His-Ala-Glu-Glu-Gly-Gly-Gly-Gly-Lys(ε-Cy5)-NH2) and EEAH-Cy5 (Ac-Glu-Glu-Ala-His-Gly-Gly-Gly-Gly-Lys(ε-Cy5)-NH2) tetrapeptide capability of binding to the Aβ aggregates in the SH-SY5Y human neuroblastoma cell line by confocal microscopy. It has been shown that the HAEE-Cy5 tetrapeptide demonstrates specific binding yielding typical cytoplasmic clusters and clear co-localization with the amyloid aggregates, while the EEAH-Cy5 peptide with the inverted sequence totally loses the binding capability. Quantification has confirmed high specificity of the HAEE-Cy5 binding to the Aβ aggregates (Manders' colocalization coefficient 0.58 ± 0.03). It has been found that the histidine N-terminal position is a critical determinant of the interaction specificity. The findings offer the prospects of using the HAEE peptide as a platform for the development of targeted disgnostic systems for amyloid disorder imaging.

Keywords: HAEE peptide, EEAH peptide, Aβ aggregates, SH-SY5Y, Alzheimer's disease

Funding: the work was carried out under the State Assignment "Development of a radiopharmaceutical for the diagnosis of Alzheimer's disease using the HAEE tetrapeptide as a vector molecule", EGISU R&D registration number 1024110600012-8-3.2.25;3.2.26;3.2.12.

Author contribution: Ivanova AV — literature review, manuscript writing; Chmelyuk NS — fixation, cell sample preparation for microscopic imaging, image acquisition and analysis using a confocal microscope; Kuzmichev IA — synthesis of Ac-HAEEGGGGK(ε-Cy5)-NH2 and Ac-EEAHGGGGK(ε-Cy5)-NH2 fluorescent peptides; Shilyaeva MI — cell sample preparation; Abakumov MA — goal setting, developing the study design, manuscript writing; all the authors contributed to preparation of the paper equally, they confirmed compliance of their authorship with the international ICMJE criteria.

✉ **Correspondence should be addressed:** Anna V. Ivanova
Ostrovityanova, 1, str.1, Moscow, 117513, Russia; super.fosforit@yandex.ru

Received: 15.10.2025 **Accepted:** 13.11.2025 **Published online:** 24.11.2025

DOI: 10.24075/brsmu.2025.061

Copyright: © 2025 by the authors. **Licensee:** Pirogov University. This article is an open access article distributed under the terms and conditions of the Creative Commons Attribution (CC BY) license (https://creativecommons.org/licenses/by/4.0/).

СРАВНИТЕЛЬНАЯ ВИЗУАЛИЗАЦИЯ СВЯЗЫВАНИЯ ТЕТРАПЕПТИДОВ HAEE-CY5 И EEAH-CY5 С АГРЕГАТАМИ Aβ НА КЛЕТКАХ SH-SY5Y

А. В. Иванова[1,2] ✉, Н. С. Чмелюк[1,2], И. А. Кузьмичев[1], М. И. Шиляева[1], М. А. Абакумов[1,2]

[1] Научно-исследовательский институт трансляционной медицины, Российский национальный исследовательский медицинский университет имени Н. И. Пирогова, Москва, Россия

[2] Институт биомедицинской инженерии, Университет науки и технологий МИСИС, Москва, Россия

В связи с высокой диагностической значимостью β-амилоидных агрегатов при болезни Альцгеймера особый интерес представляют целевые лиганды, способные к специфическому связыванию с патологическими агрегатами Aβ. Целью исследования было провести методом конфокальной микроскопии сравнительную характеристику связывающей способности тетрапептидов HAEE-Cy5 (Ac-His-Ala-Glu-Glu-Gly-Gly-Gly-Gly-Lys(ε-Cy5)-NH2) и EEAH-Cy5 (Ac-Glu-Glu-Ala-His-Gly-Gly-Gly-Gly-Lys(ε-Cy5)-NH2) с агрегатами Aβ на клеточной линии нейробластомы человека SH-SY5Y. Показано, что тетрапептид HAEE-Cy5 демонстрирует специфическое связывание с образованием характерных цитоплазматических скоплений и четкой колокализации с амилоидными агрегатами, в то время как пептид EEAH-Cy5 с обращенной последовательностью полностью утрачивает способность к связыванию. Количественный анализ подтвердил высокую специфичность связывания HAEE-Cy5 с агрегатами Aβ (коэффициент колокализации Мандерса 0.58 ± 0.03). Установлено, что N-концевое положение гистидина является критическим детерминантом специфичности взаимодействия. Результаты работы открывают перспективы применения пептида HAEE в качестве платформы для разработки целевых диагностических систем визуализации амилоидной патологии.

Ключевые слова: пептид HAEE, пептид EEAH, агрегаты Aβ, SH-SY5Y, болезнь Альцгеймера

Финансирование: работы выполнены в рамках Государственного задания «Создание радиофармацевтического лекарственного препарата для диагностики болезни Альцгеймера с использованием тетрапептида HAEE в качестве векторной молекулы», регистрационный номер ЕГИСУ НИОКТР 1024110600012-8-3.2.25;3.2.26;3.2.12.

Вклад авторов: А. В. Иванова — обзор литературы, подготовка рукописи; Н. С. Чмелюк — фиксация, подготовка клеточных образцов для съемки на микроскопе, получение и анализ изображений на конфокальном микроскопе; И. А. Кузьмичев — синтез флуоресцентных пептидов Ac-HAEEGGGGK(ε-Cy5)-NH2 и Ac-EEAHGGGGK(ε-Cy5)-NH2; М. И. Шиляева — подготовка образцов клеток; М. А. Абакумов — постановка цели, разработка дизайна исследования, подготовка рукописи; все авторы внесли равнозначный вклад в подготовку публикации, подтверждают соответствие своего авторства международным критериям ICMJE.

✉ **Для корреспонденции:** Анна Валерьевна Иванова
ул. Островитянова, д. 1, стр.1, г. Москва, 117513, Россия; super.fosforit@yandex.ru

Статья получена: 15.10.2025 **Статья принята к печати:** 13.11.2025 **Опубликована онлайн:** 24.11.2025

DOI: 10.24075/vrgmu.2025.061

Авторские права: © 2025 принадлежат авторам. **Лицензиат:** РНИМУ им. Н. И. Пирогова. Статья размещена в открытом доступе и распространяется на условиях лицензии Creative Commons Attribution (CC BY) (https://creativecommons.org/licenses/by/4.0/).

Alzheimer's disease (AD) is the most globally prevalent neurodegenerative disorder that usually results in the neuronal death and brain atrophy. It is accompanied by accumulation of abnormal deposits: senile plaques consisting of the aggregated β-amyloid (Aβ) and neurofibrillary tangles formed by the hyperphosphorylated tau protein [1, 2]. Despite decades of research, the amyloid hypothesis remains one of the central to explain the AD pathogenesis. Accumulation of the oligomeric Aβ forms and their subsequent aggregation into mature, stable fibrils is considered to be the key event triggering the neurotoxicity and neuroinflammation cascade [3–5]. Since Aβ aggregates represent the main structural component of senile plaques, these are a priority target for the development of the diagnosis and treatment methods. One promising approach is the search for compounds capable of inhibiting the Aβ aggregation. Currently, various classes of such compounds are being developed, including small molecules [6, 7], monoclonal antibodies (aducanumab, lecanemab) [8, 9], peptides [10], natural ligands [11], multifunctional hybrid molecules [12], however, many of these face the problems of low bioavailability and limited efficacy in late-stage AD, or serious adverse effects, such as ARIA (amyloid-related imaging abnormalities), in cases of antibody therapy [13, 14]. In this context, of special interest are the short peptides conbining targeted effects and the fundamentally better penetration capacity. The HAEE tetrapeptide is a candidate compound. According to some data [15], HAEE acts as a specific molecular tool selectively binding to the metal-binding domain of the Aβ peptide (11EVHH14) to form a stable complex in the presence of Zn^{2+}. Such interaction confirmed by the surface plasmon resonance, nuclear magnetic resonance, and molecular modeling methods significantly disturbes the Zn^{2+}-dependent Aβ monomer dimerization, thereby preventing production of toxic oligomers. The *in vivo* experiments on the blood-brain barrier (BBB) provided important evidence of the HAEE efficacy: the peptide not only inhibited the Zn^{2+}-induced amyloid accumulation, but completely prevented the associated abnormal phenotypes, including paralysis and shortened lifespan of transgenic nematodes [15]. No signs of the peptide toxicity were reported in these experiments, which suggested the peptide beneficial safety profile in this model system. Furthermore, one more key property was reported for HAEE: pharmacokinetic studies and molecular modeling suggest that it was capable of crossing the BBB [15]. It should be noted that HAEE is a peptide derived from the sequence of the nicotinic acetylcholine receptor α4-subunit (nAChRα4) [16]. Thus, HAEE has properties of the unique candidate for AD therapy: it has a determined mechanism of action targeting the key pathogenesis link and demonstrates its efficacy at the whole-body level. The direct detection of the HAEE binding to the Aβ aggregates under the cell culture conditions can be a simple and clear method to further confirm this mechanism. Fluorescence microscopy, specifically when combined with immunocytochemistry analysis, is among the most popular and accessible methods to complete the task.

Thus, the study aimed to perform direct imaging and confirm binding of the HAEE-Cy5 fluorescent conjugate to the Aβ aggregates in the SH-SY5Y human neuroblastoma cell line by fluorescence microscopy in order to assess its specificity and the prospects of using the HAEE peptide as a target ligand for the AD diagnosis and treatment.

METHODS

All the experiments were conducted at the laboratory of the Deparment of Medical Nanobiotechnology of the Research Institute of Translational Medicine, Pirogov Russian National Research Medical University. Confocal microscopy was performed at the Biomedical Nanomaterials laboratory of the Bioengineering Institute, MISIS University of Science and Technology.

The following compounds were tested in the experiment: HAEE-Cy5 (Ac-His-Ala-Glu-Glu-Gly-Gly-Gly-Gly-Lys(ε-Cy5)-NH_2, EEAH-Cy5 (Ac-Glu-Glu-Ala-His-Gly-Gly-Gly-Gly-Lys(ε-Cy5)-NH_2, Cy5-NH2. The test peptides HAEE-Cy5 and EEAH-Cy5 (purity > 95% based on the HPLC data) were synthesized and provided by the laboratory of the Department of Medical Nanobiotechnology, Research Institute of Translational Medicine, Pirogov Russian National Research Medical University. The peptides cosist of the tetrapeptide “head” (HAEE or EEAH) connected to the Cy5 fluorescent dye via a linker of four glycine residues (GGGG).

The L-lysine residue (K) in the linker provides a conjugation site for the dye. The chemical structure of the test compounds is provided in Fig. 1.

The lyophilized peptides were dissolved in the sterile deionized water to the concentration of 5–10 mM, and aliquots of solutions were stored at –20 °C for no longer than 3 months. Before applying the peptides to the cells the solutions were

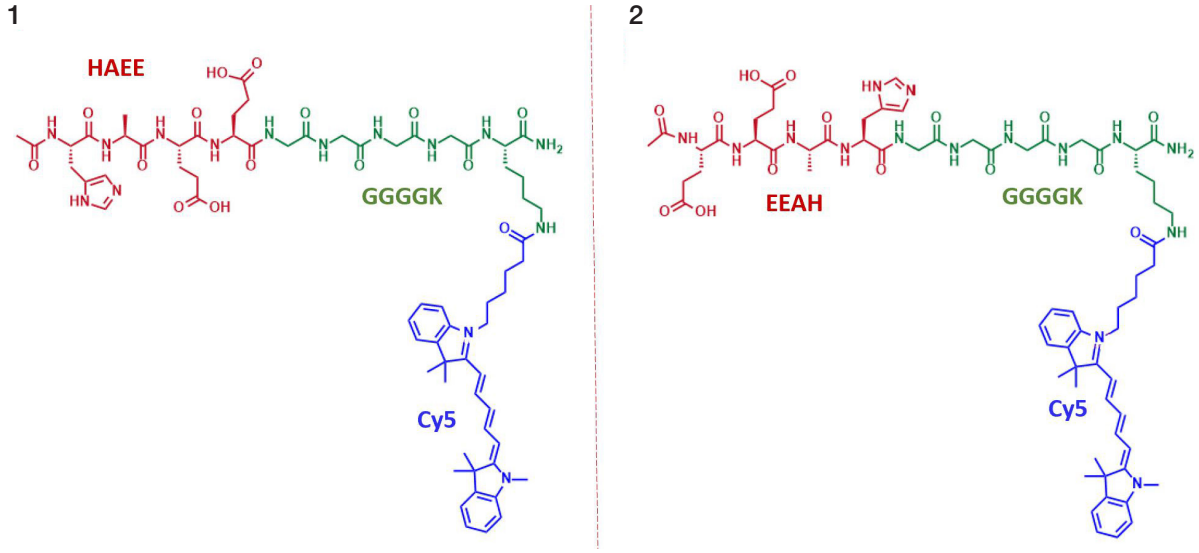


Fig. 1. Chemical structure of the test conjugated peptides

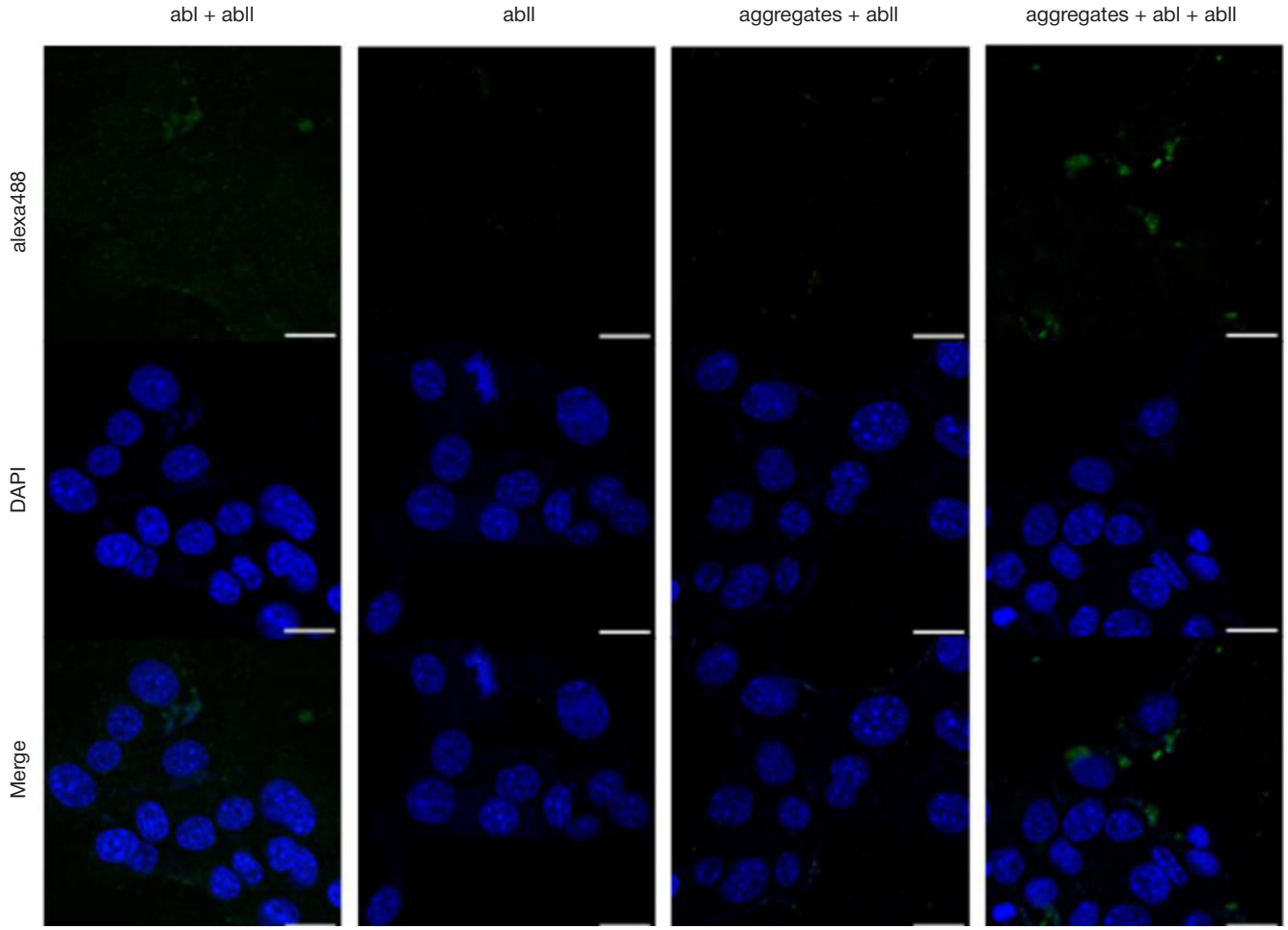


Fig. 2. Control of immunofluorescence staining specificity in the SH-SY5Y cells. Alignment of channels demonstrates localization of the alexa 488-stained target antigens (*green*) on the Aβ aggregates. The nuclei are DAPI stained (*blue*). Scale bar 20 μm

diluted in the DMEM/F12 cell culture medium containing no fetal bovine serum (FBS) to the concentration of 5 μM.

SH-SY5Y cell culturing

The SH-SY5Y human neuroblastoma cells (ATCC, USA) were grown in the cell culture flasks with the growth medium comprising DMEM/F12 (ServiceBio, China) supplemented with the 10% FBS (Cytiva (GE Healthcare Life Sciences HyClone), USA), antibiotic mixture (penicillin — 100 μg/mL, streptomycin — 100 μg/mL) (ServiceBio, China), and L-glutamine (100 mM) (ServiceBio, China) at 37 °C in the 5% CO_2 atmosphere.

Beta-amyloid preparations

The lyophilized Aβ (Amyloid β-Protein (1–42) (E-PP-0428), Elabscience, China) was dissolved in the 1% NH_4OH to the concentration of 1 mg/mL in the ultrasonic bath without heating for 10 min. Then the solution was aliquoted (10 μL) and stored at –80 °C. Before applying to the cells, the solution was ultrasound-treated again for 30 min at 37 °C in the final concentration (20 μg/mL).

Immunofluorescence analysis

To assess localization of the compounds, the SH-SY5Y cells were sown in the wells of the 24-well plate, 200 × 10^3 cells per well. After 24 h the cells were treated with the Aβ preparations (20 μg/mL) in the medium containing no FBS and incubated for 4 h. Then the cells were twice washed with the Hanks' solution, added the test compounds (HAEE-Cy5, EEAH-Cy5, NH2-Cy5) in a concentration of 5 μM, and incubated for 2 h. Then the cells were fixed for 15 min in the 4% paraformaldehyde at +4 °C. Permeabilization was performed in the blocking buffer of 0.2% Twin-20, 0.2% Triton X-100, and 2% goat serum for 30 min at room temperature. Then incubation with the primary antibody (mouse IgG1 antibody against himan beta-amyloid protein, abl, clone 6E10 BioLegend) diluted 1:100 000 (0.01 μg/mL) in the buffer (0.2% Twin-20, 0.2% Triton X-100, 0.2% goat serum, FBS) was performed for 60 min. After that the cells were triple washed with the solutions of 0.2% Twin-20, 0.2% Triton X-100 for 5 min. Then the cells were incubated with the secondary antibody (abll, goat antibody against IgG(H+L) conjugated with alexa 488 (E-AB-1056, Elabscience, China). Incubation with the secondary antibody was also conducted for 60 min; then the cells were triple washed with the solutions of 0.2% Twin-20, 0.2% Triton X-100 for 5 min and stained with the DAPI nuclear dye.

Confocal microscopy

Cell imaging was accomplished with the Nikon Eclipse Ti2 microscope (Nikon, Tokyo, Japan) equipped with the laser scanning system (ThorLabs, Newton, New Jersey, USA) and the Apo 60×/0.5–1.25 oil immersion lens. Scanning was performed using the ThorImageLS software (version 2.4) (Thorlabs, Newton, New Jersey, USA); images were processed using the Fiji 2.9.0 software tool.

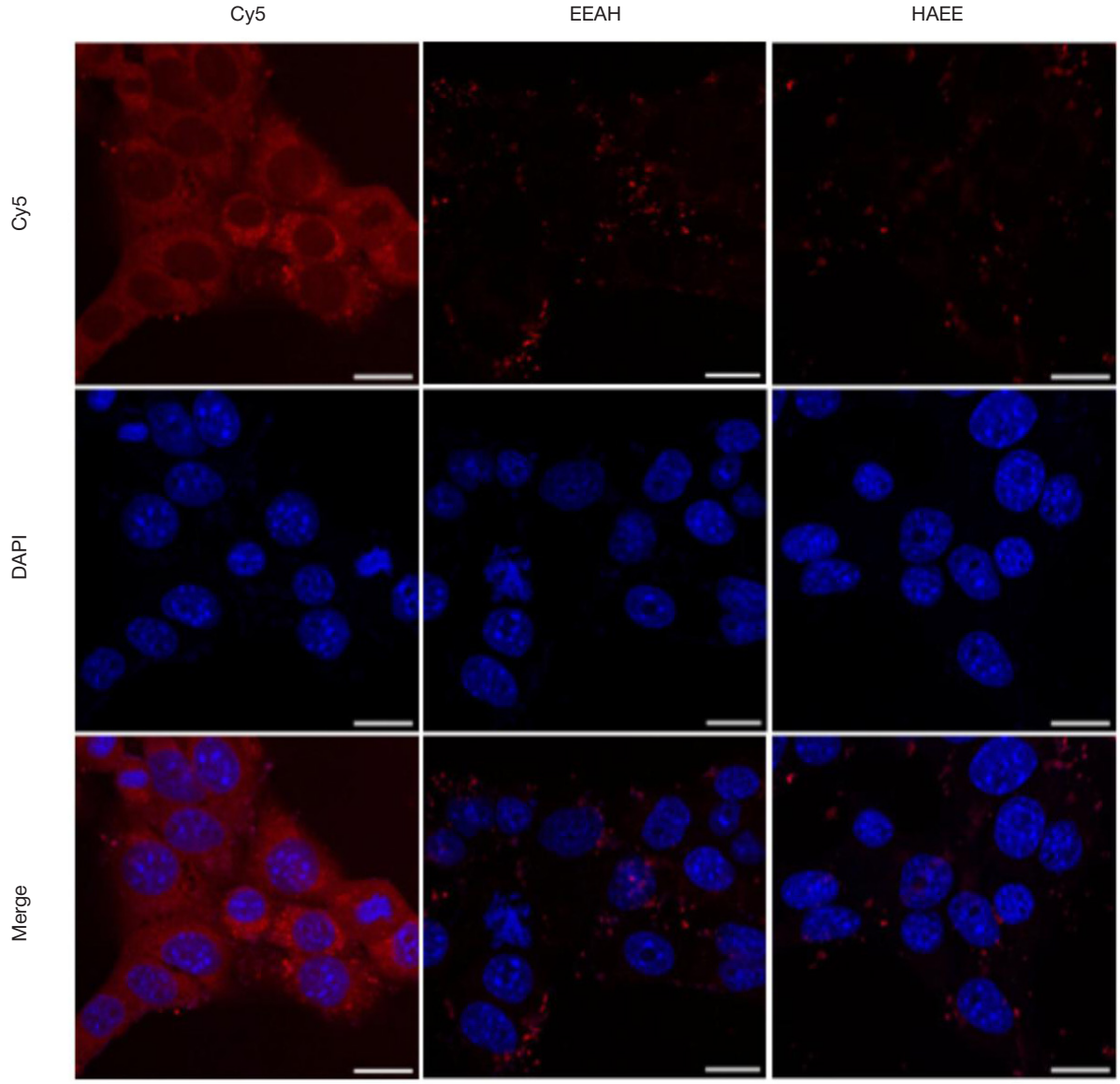


Fig. 3. Localization of the EEAH-Cy5 and HAEE-Cy5 compounds in the SH-SY5Y cells. Signal of the Cy5-labeled compounds (*red*). The nuclei are DAPI stained (*blue*). Scale bar 20 μm

Statistical analysis

Colocalization of images in the alexa488 and Cy5 channels was calculated using the Fiji software tool and Manders' coefficient; images (n = 6) were used for analysis.

RESULTS

To confirm immunofleorescence staining specificity in the SH-SY5Y cells, a number of control experiments was conducted (Fig. 2). When using only secondary antibodies conjugated with the alexa 488 (abII) fluorescent label, no significant fluorescent signal was detected. Likewise, incubation of cells with Aβ in the absence of primary antibody (abI) did not result in specific staining. Treatment of cells with abI or abII without Aβ yielded no significant fluorescent signal. Intense fluorescent staining was observed only when there were Aβ, abI, and abII at once; this corresponded to the expected localization of target antigens. The results obtained confirm that specific staining requires the presence of all system components and indicate specificity of the antibodies used.

Then the HAEE-Cy5 and EEAH-Cy5 localization of the cells was assessed. In the control experiment involving the use of the free Cy5-NH2 dye, the nonspecific internalization of the dye manifested by a diffuse signal on the cell membrane and in the cytoplasm was reported. The fact that such a hydrophobic compound is localized partially in the cytoplasm can be explained by permeabilization of the cells during the analysis. In contrast, the intense and structurally organized signal that was qualitatively different from the control was reported for the EEAH-Cy5 and HAEE-Cy5 compounds: this was characterized by the prominent membrane-bound component and formation of discrete clusters in the cytoplasm (Fig. 3). This suggests specific interaction of the test substances with the cell structures, which is not limited to non-specific accumulation of the dye.

Due to the detected specific EEAH-Cy5 and HAEE-Cy5 localization, direct verification of their capability of binding to the Aβ aggregates was performed. The analysis of confocal microscopy images showed the clear and intense colocalization of the HAEE-Cy5 signal (red) with the signal of Aβ deposits (alexa 488, green) visualized as large yellow regions in the combined image (Fig. 4), which unambiguously indicated the HAEE-Cy5 tetrapeptide high-affinity binding to amyloid aggregates. In contrast to HAEE-Cy5, no significant signal in

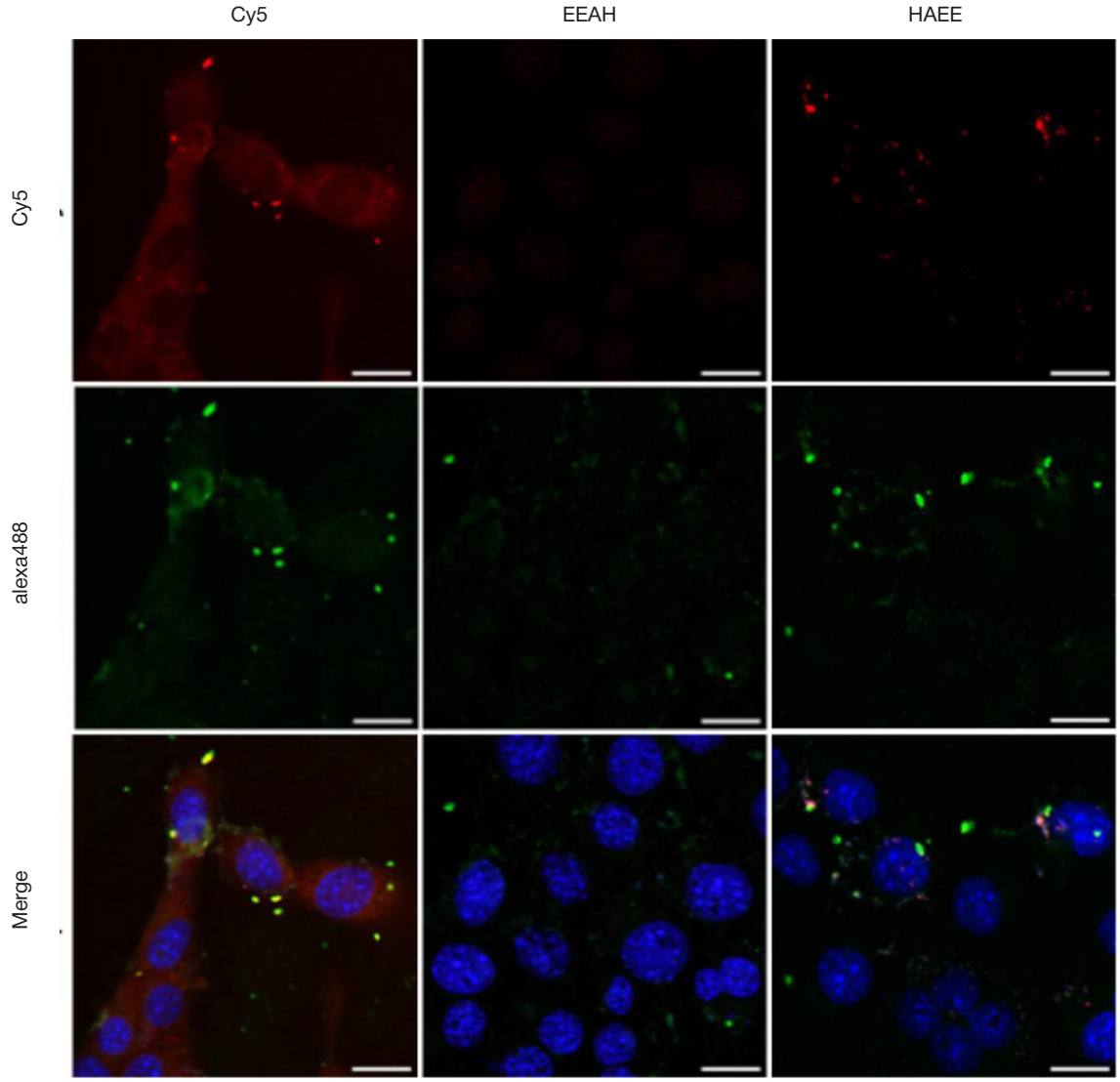


Fig. 4. Visualization of the HAEE-Cy5 and EEAH-Cy5 binding to the Aβ aggregates in the SH-SY5Y cells. Signal of the Cy5-labeled tetrapeptides (*red*). The alexa 488-labeled antibodies on Aβ (*green*). *Yellow* on the combined image indicates colocalization of peptides with Aβ aggregates. The nuclei are DAPI stained (*blue*). Scale bar 20 μm

the Cy5 channel was reported for the EEAH-Cy5 peptide, which suggested that it was unable to specifically interact with the studied target. Despite the fact that the source Cy5 dye showed some capability of binding to amyloid deposits, it was to the greater extent nonspecifically localized, which also confirmed high HAEE-Cy5 affinity for Aβ aggregates. To further confirm colocalization of the channels, the Manders' coefficient was calculated (between the channels of the Aβ aggregate images and test compounds for the images acquired): the highest coefficient value was reported for the HAEE-Cy5 compound and Aβ aggregates (0.58 ± 0.03), while the values between the Aβ and Cy5 channels and Aβ and EEAH-Cy5 channels were 0.22 ± 0.05 and 0.19 ± 0.02, respectively, which suggested no Cy5 and EEAH-Cy5 colocalization and higher extent of the HAEE-Cy5 binding to Aβ. The extremely low EEAH-Cy5 fluorescence signal can be associated with with its low capability of staying on the Aβ aggregates and in other cell compartments. At the same time, the Cy5 signal is significant, it is enhanced in the areas of Aβ aggregates, however, a large amount of fluorescence is distributed across the membrane and cytoplasm, which suggests low specificity of the Cy5 binding to Aβ.

DISCUSSION

The study conducted has made it possible to identify fundamental differences in the HAEE-Cy5 and EEAH-Cy5 capability of binding to the Aβ aggregates in the SH-SY5Y cells, which are likely to result from their structural features. Despite identical amino acid composition, the reversed EEAH-Cy5 sequence led to the complete functional activity loss, while HAEE-Cy5 showed high specificity for the studied target. The data obtained suggest that the histidine N-terminal position in the HAEE-Cy5 sequence is critically important for formation of specific interaction with Aβ. Our data clearly demonstrate that the histidine (His, H) shift from the first to fourth position in the tetrapeptide “head” of the ligand results in the rapidly decreased capability of binding to Aβ. It is well known that the Aβ peptide N-terminal domain comprises the main binding centers, specifically the His6, His13, His14 residues being the good σ-donors that are involved in coordination with metals [17], as well as the aromatic Phe4 and Tyr10 residues responsible for the π π interaction [17, 18]. It can be assumed that histidine being part of HAEE is involved in similar interaction with these sites. As for the inactive EEAH peptide, the presence of two negatively charged glutamic acid residues (Glu, E) in

the N-terminal position, as well as the presence of the Cy5 fluorescent dye in the ε-end of lysine (Lys, K), can cause the peptide chain folding or create steric hindrances disrupting spatial orientation and the key histidine residue availability. In such a configuration, histidine can be sterically unavailable for interaction with the Aβ binding sites.

The quantitative evidence to substantiate high specificity of the HAEE-Cy5 binding to amyloid aggregates is calculation of the Manders' colocalization coefficient. The coefficient value of 0.58 ± 0.03 for the HAEE-Cy5/Aβ pair is considerably higher compared to the values of control compounds (Cy5-NH2/Aβ and EEAH-Cy5/Aβ), which are close to zero. Quantification clearly demonstrates that the intense colocalization signal is not random, it confirms high HAEE peptide affinity specifically for the target Aβ aggregates, which is fully consistent with visual observation and demonstrates critical importance of the correct amino acid sequence for effective interaction.

The lack of the EEAH-Cy5 fluorescence signal upon clear detection of HAEE-Cy5 to extracellular Aβ aggregates suggests that it is not capable of specific interaction with the target. This difference resulting from suboptimal primary structure of the control peptide can be due to several factors: impaired binding to Aβ, increased susceptibility to proteolytic degradation, worse cellular permeability or accelerated removal from the cell. Thus, in contrast to HAEE-Cy5, the EEAH-Cy5 peptide fails to fulfill the target function, which confirms critical importance of certain amino acid sequence for effective binding. It is worth noting that in the absence of Aβ both peptides demonstrate similar intracellular localization, which suggests their stability and capability of entering the cell. However, the HAEE-Cy5 peptide intense and structurally organized signal manuifested by discrete cytoplasmic clusters suggests that it is capable of entering the cell and interacting with intracellular structures. Furthermore, according to the literature data [19], the reported colocalization with Aβ (Fig. 4) occurs in the extracellular space, which confirms the binding specificity. It is important to note that the HAEE-Cy5 distribution observed was qualitatively different from the diffuse signal of the free Cy5-NH2 dye, which precludes explanation by simple dye accumulation and emphasizes the role of peptide sequence in the targeted binding.

The findings are of high practical importance. The HAEE-Cy5 specificity for Aβ aggregates detected allows one to consider it is a promising ligand for the development of diagnostic means. In particular, it can be used as a foundation for the development of the following: MRI contrast agents for *in vivo* imaging of amyloid plaques, fluorescent probes for intraoperative detection of amyloid deposits, theranostic platforms for targeted delivery of drugs. In contrast to HAEE-Cy5, the EEAH-Cy5 peptide shows the total lack of binding activity. This clearly demonstrates that biological function is determined by not only amino acid composition, but also strict amino acid order. Further development of this research area requires the following: 1) thorough investigation of the HAEE interaction with Aβ by molecular docking and spectroscopy methods; 2) *in vitro* assessment of the HAEE capability of inhibiting the Aβ aggregation; 3) *in vivo* study of the HAEE distribution and bioavailability in transgenic AD models. Thus, the study results have not only identified the highly specific Aβ ligand, but also demonstrated that minimal changes in the peptide structure can have a dramatic effect on its functional properties, which is of fundamental importance for the design of peptide drugs.

CONCLUSIONS

In the study, we successfully validated the method to detect Aβ aggregates and visualized specific binding of the Cy5-conjugated HAEE tetrapeptide to amyloid aggregates in the SH-SY5Y cells, which was quantitatively confirmed by high Manders' colocalization coefficient (0.58 ± 0.03). The amino acid sequence critical importance for such interaction was determined based on the fact that the EEAH-Cy5 peptide with the reversed sequence showed the total lack of binding activity. Thus, it has been found that it is N-terminal position of histidine that is critical for formation of specific interaction with Aβ aggregates. The findings confirm the prospects of using HAEE as a target ligand for the development of diagnostic and theranostic agents for AD and emphasize the importance of stereochemical factors for construction of peptide drugs. To further develop the research area it is necessary to study molecular mechanisms of interaction and assess the peptide distribution *in vivo*.

References

1. Kolobova EA, Petrushanko IY, Mitkevich VA, Makarov AA, Grigorova IL. Novel method for detection of Aβ and Iso-D7-Aβ N-terminus-specific B cells and Iso-D7-Aβ-specific antibodies. Biol Methods Protoc. 2025; 10 (1).
2. Knopman DS, Amieva H, Petersen RC, Chételat G, Holtzman DM, Hyman BT, et al. Alzheimer disease. Nat Rev Dis Primers. 2021; 7 (1): 33.
3. Harris JR, Marles-Wright J, editors. Macromolecular Protein Complexes II: Structure and Function. Subcell Biochem. 2019; 93.
4. Walsh DM, Selkoe DJ. Amyloid β-protein and beyond: the path forward in Alzheimer's disease. Curr Opin Neurobiol. 2020; 61: 116–24.
5. Katzmarski N, Ziegler-Waldkirch S, Scheffler N, Witt C, Abou-Ajram C, Nuscher B, et al. Aβ oligomers trigger and accelerate Aβ seeding. Brain Pathol. 2020; 30 (1): 36–45.
6. Wilcock GK, Gauthier S, Frisoni GB, Jia J, Hardlund JH, Moebius HJ, et al. Potential of low dose leuco-methylthioninium bis(hydromethanesulphonate) monotherapy for treatment of mild Alzheimer's disease: cohort analysis as modified primary outcome in a phase III clinical trial. J Alzheimers Dis. 2018; 61 (1): 435–57.
7. Paul A, Viswanathan GKK, Huber A, Arad E, Engel H, Jelinek R, et al. Inhibition of tau amyloid formation and disruption of its preformed fibrils by naphthoquinone-dopamine hybrid. FEBS J. 2021; 288 (13): 4267–90.
8. Fedele E. Anti-amyloid therapies for Alzheimer's disease and the amyloid cascade hypothesis. Int J Mol Sci. 2023; 24 (19): 14499.
9. Kepp KP, Robakis NK, Høilund-Carlsen PF, Sensi SL, Vissel B. The amyloid cascade hypothesis: an updated critical review. Brain. 2023; 146 (9): 3969–90.
10. Tucker M, Liao GY, Park JY, Rosenfeld M, Wezeman J, Mangalindan R, et al. Behavioral and neuropathological features of Alzheimer's disease are attenuated in 5xFAD mice treated with intranasal GHK peptide. bioRxiv. 2023; 20: 2023.11.20.567908.
11. Kryscio RJ, Abner EL, Caban-Holt A, Lovell M, Goodman P, Darke AK, et al. Association of antioxidant supplement use and dementia in the Prevention of Alzheimer's Disease by Vitamin E and Selenium Trial (PREADViSE). JAMA Neurol. 2017; 74 (5): 567–73.
12. Ramesh M, Govindaraju T. Multipronged diagnostic and therapeutic strategies for Alzheimer's disease. Chem Sci. 2022; 13 (46): 13657–89.
13. Salloway S, Sperling R, Fox NC, Blennow K, Klunk W, Raskind M, et al. Two phase 3 trials of bapineuzumab in mild-to-moderate Alzheimer's disease. N Engl J Med. 2014; 370 (4): 322–33.

14. Ivanova AV, Kutuzova AD, Kuzmichev IA, Abakumov MA. Alzheimer's disease: from molecular mechanisms to promising therapeutic strategies. Int J Mol Sci. 2025; 26 (19): 9444.
15. Mitkevich VA, Barykin EP, Eremina S, Pani B, Katkova-Zhukotskaya O, Polshakov VI, et al. Zn-dependent β-amyloid aggregation and its reversal by the tetrapeptide HAEE. Aging Dis. 2023; 14 (2): 309–14.
16. Barykin EP, Garifulina AI, Tolstova AP, Anashkina AA, Adzhubei AA, Mezentsev YV, et al. Tetrapeptide Ac-HAEE-NH2 protects α4β2 nAChR from inhibition by Aβ. Int J Mol Sci. 2020; 21 (24): 1–18.
17. Silva DES, Cali MP, Pazin WM, Carlos-Lima E, Salles Trevisan MT, Venâncio T, et al. Luminescent Ru(II) phenanthroline complexes as a probe for real-time imaging of Aβ self-aggregation and therapeutic applications in Alzheimer's disease. J Med Chem. 2016; 59 (19): 9215–27.
18. Yao S, Cherny RA, Bush AI, Masters CL, Barnham KJ. Characterizing bathocuproine self-association and subsequent binding to Alzheimer's disease amyloid β-peptide by NMR. J Pept Sci. 2004; 10 (4): 210–7.
19. Petrushanko IY, Mitkevich VA, Anashkina AA, Adzhubei AA, Burnysheva KM, Lakunina VA, et al. Direct interaction of beta-amyloid with Na, K-ATPase as a putative regulator of the enzyme function. Sci Rep. 2016; 6: 27738.

Литература

1. Kolobova EA, Petrushanko IY, Mitkevich VA, Makarov AA, Grigorova IL. Novel method for detection of Aβ and Iso-D7-Aβ N-terminus-specific B cells and Iso-D7-Aβ-specific antibodies. Biol Methods Protoc. 2025; 10 (1).
2. Knopman DS, Amieva H, Petersen RC, Chételat G, Holtzman DM, Hyman BT, et al. Alzheimer disease. Nat Rev Dis Primers. 2021; 7 (1): 33.
3. Harris JR, Marles-Wright J, editors. Macromolecular Protein Complexes II: Structure and Function. Subcell Biochem. 2019; 93.
4. Walsh DM, Selkoe DJ. Amyloid β-protein and beyond: the path forward in Alzheimer's disease. Curr Opin Neurobiol. 2020; 61: 116–24.
5. Katzmarski N, Ziegler-Waldkirch S, Scheffler N, Witt C, Abou-Ajram C, Nuscher B, et al. Aβ oligomers trigger and accelerate Aβ seeding. Brain Pathol. 2020; 30 (1): 36–45.
6. Wilcock GK, Gauthier S, Frisoni GB, Jia J, Hardlund JH, Moebius HJ, et al. Potential of low dose leuco-methylthioninium bis(hydromethanesulphonate) monotherapy for treatment of mild Alzheimer's disease: cohort analysis as modified primary outcome in a phase III clinical trial. J Alzheimers Dis. 2018; 61 (1): 435–57.
7. Paul A, Viswanathan GKK, Huber A, Arad E, Engel H, Jelinek R, et al. Inhibition of tau amyloid formation and disruption of its preformed fibrils by naphthoquinone-dopamine hybrid. FEBS J. 2021; 288 (13): 4267–90.
8. Fedele E. Anti-amyloid therapies for Alzheimer's disease and the amyloid cascade hypothesis. Int J Mol Sci. 2023; 24 (19): 14499.
9. Kepp KP, Robakis NK, Høilund-Carlsen PF, Sensi SL, Vissel B. The amyloid cascade hypothesis: an updated critical review. Brain. 2023; 146 (9): 3969–90.
10. Tucker M, Liao GY, Park JY, Rosenfeld M, Wezeman J, Mangalindan R, et al. Behavioral and neuropathological features of Alzheimer's disease are attenuated in 5xFAD mice treated with intranasal GHK peptide. bioRxiv. 2023; 20: 2023.11.20.567908.
11. Kryscio RJ, Abner EL, Caban-Holt A, Lovell M, Goodman P, Darke AK, et al. Association of antioxidant supplement use and dementia in the Prevention of Alzheimer's Disease by Vitamin E and Selenium Trial (PREADViSE). JAMA Neurol. 2017; 74 (5): 567–73.
12. Ramesh M, Govindaraju T. Multipronged diagnostic and therapeutic strategies for Alzheimer's disease. Chem Sci. 2022; 13 (46): 13657–89.
13. Salloway S, Sperling R, Fox NC, Blennow K, Klunk W, Raskind M, et al. Two phase 3 trials of bapineuzumab in mild-to-moderate Alzheimer's disease. N Engl J Med. 2014; 370 (4): 322–33.
14. Ivanova AV, Kutuzova AD, Kuzmichev IA, Abakumov MA. Alzheimer's disease: from molecular mechanisms to promising therapeutic strategies. Int J Mol Sci. 2025; 26 (19): 9444.
15. Mitkevich VA, Barykin EP, Eremina S, Pani B, Katkova-Zhukotskaya O, Polshakov VI, et al. Zn-dependent β-amyloid aggregation and its reversal by the tetrapeptide HAEE. Aging Dis. 2023; 14 (2): 309–14.
16. Barykin EP, Garifulina AI, Tolstova AP, Anashkina AA, Adzhubei AA, Mezentsev YV, et al. Tetrapeptide Ac-HAEE-NH2 protects α4β2 nAChR from inhibition by Aβ. Int J Mol Sci. 2020; 21 (24): 1–18.
17. Silva DES, Cali MP, Pazin WM, Carlos-Lima E, Salles Trevisan MT, Venâncio T, et al. Luminescent Ru(II) phenanthroline complexes as a probe for real-time imaging of Aβ self-aggregation and therapeutic applications in Alzheimer's disease. J Med Chem. 2016; 59 (19): 9215–27.
18. Yao S, Cherny RA, Bush AI, Masters CL, Barnham KJ. Characterizing bathocuproine self-association and subsequent binding to Alzheimer's disease amyloid β-peptide by NMR. J Pept Sci. 2004; 10 (4): 210–7.
19. Petrushanko IY, Mitkevich VA, Anashkina AA, Adzhubei AA, Burnysheva KM, Lakunina VA, et al. Direct interaction of beta-amyloid with Na, K-ATPase as a putative regulator of the enzyme function. Sci Rep. 2016; 6: 27738.

DETERMINING TARGETS FOR PERSONALIZED MULTITARGET NONINVASIVE STIMULATION OF THE FRONTOPARIETAL CONTROL NETWORK

Poydasheva AG ✉, Sinitsyn DO, Bakulin IS, Zabirova AH, Lagoda DYu, Suponeva NA, Piradov MA

Russian Center of Neurology and Neurosciences, Moscow, Russia

Personalization of selecting a target for rTMS is a problem, solving which can significantly increase the method efficacy. Stimulation of the key hubs of individual-level resting-state networks represents an approach to personalization. The study aimed to develop an rTMS personalization method based on the selection of individual frontoparietal control network (FPCN) hubs and assessment of their localization variability. To determine the FPCN hubs, individual maps were built using the FPCN group mask as a seed. The searchlight algorithm with the sphere radius of 5 mm was used to select targets within the dorsolateral prefrontal cortex (DLPFC) and posterior parietal cortex (PPC). The target spatial localization variability and correctness of using the routine "5 cm rule" for the DLPFC localization were analyzed. In 24 healthy volunteers (9 males, average age 29±7 years), high interindividual variability of targets was demonstrated. In no area is there a universal position of the stimulation coil that would effectively stimulate targets in all volunteers. Spatial dispersion of points is higher in the DLPFC (volumes of the polyhedra containing the point sets are 2095 mm^3 in the DLPFC and 739 mm^3 in the PPC). All individual targets in the DLPFC are located within the FPCN mask, while in the PPC some targets are outside this mask. The average distance between the M1 zones and DLPFC is 64±13 mm. In 75% of the subjects, this exceeds 5 cm, which confirms that it was incorrect to use the routine "5 cm rule" for coil positioning in the majority of subjects. An algorithm to select personalized targets for rTMS based on the resting-state fMRI data in the DLPFC and PPC being the key FPCN hubs has been developed.

Keywords: multitarget transcranial magnetic stimulation, personalization, resting-state networks, frontoparietal control network

Funding: the study was conducted as part of the project "Developing a Transcranial Magnetic Stimulation Method to Improve Cognitive Functions in Healthy Individuals" implemented within the framework of the National Project "New Health Preservation Technologies" (registration number 1025020400006-8-3.2.25).

Author contribution: Poydasheva AG, Sinitsyn DO, Bakulin IS — study planning and design; Poydasheva AG, Zabirova AH — literature review; Bakulin IS, Zabirova AH, Lagoda DYu — data acquisition; Sinitsyn DO, Poydasheva AG — data analysis; Poydasheva AG, Sinitsyn DO — manuscript writing; all authors — data interpretation, manuscript editing.

Compliance with ethical standards: the study was approved by the Ethics Committee of the Russian Center of Neurology and Neurosciences (protocol No. 5-1/25 dated 19 May 2025). All the volunteers signed the informed consent form.

✉ **Correspondence should be addressed:** Alexandra G. Poydasheva
Volokolamskoye shosse, 80, Moscow, 125310, Russia; poydasheva@neurology.ru

Received: 14.11.2025 **Accepted:** 10.12.2025 **Published online:** 20.12.2025

DOI: 10.24075/brsmu.2025.081

ОПРЕДЕЛЕНИЕ МИШЕНЕЙ ДЛЯ ПЕРСОНАЛИЗИРОВАННОЙ МУЛЬТИТАРГЕТНОЙ НЕИНВАЗИВНОЙ СТИМУЛЯЦИИ ЛОБНО-ТЕМЕННОЙ СЕТИ КОНТРОЛЯ

А. Г. Пойдашева ✉, Д. О. Синицын, И. С. Бакулин, А. Х. Забирова, Д. Ю. Лагода, Н. А. Супонева, М. А. Пирадов

Российский центр неврологии и нейронаук, Москва, Россия

Персонализация выбора мишени для рТМС — актуальная задача, решение которой может значительно увеличить эффективность метода. Один из подходов к персонализации — стимуляция ключевых хабов индивидуальных сетей покоя. Цель исследования — разработка методологии персонализации рТМС на основе выделения индивидуальных хабов фронто-париетальной контрольной сети (FPCN) с оценкой вариабельности их локализации. Для определения хабов FPCN были построены индивидуальные карты с использованием в качестве seed групповой маски сети FPCN. С помощью алгоритма прожектора с радиусом сферы 5 мм были выбраны мишени в пределах дорсолатеральной префронтальной коры (ДЛПФК) и задней теменной коры (ЗТК). Анализировали вариабельность пространственной локализации мишеней и корректность применения рутинного «правила 5 см» для локализации ДЛПФК. У 24 здоровых добровольцев (9 мужчин, средний возраст 29±7 лет) продемонстрирована высокая межиндивидуальная вариабельность мишеней. Ни в одной из областей не существует универсального положения стимулирующей катушки, позволившего бы эффективно стимулировать мишени у всех добровольцев. Пространственный разброс точек выше в ДЛПФК (объемы многогранников, содержащих множества точек равны 2095 $мм^3$ в ДЛПФК и 739 $мм^3$ в ЗТК). Все индивидуальные мишени в ДЛПФК лежат в пределах маски FPCN, а для ЗТК ряд мишеней находится вне этой маски. Среднее расстояние между зоной кисти первичной моторной коры (М1) и ДЛПКК составило 64±13 мм. У 75% участников это расстояние превышало 5 см, что подтверждает некорректность применения рутинного «правила 5 см» позиционирования катушки для большинства испытуемых. Разработан алгоритм выбора персонализированных мишеней для рТМС по данным фМРТ покоя в ДЛПФК и ЗТК, которые являются ключевыми хабами FPCN.

Ключевые слова: мультитаргетная транскраниальная магнитная стимуляция, персонализация, сети покоя, лобно-теменная сеть контроля

Финансирование: исследование выполнено в рамках проекта «Разработка методики транскраниальной магнитной стимуляции для улучшения когнитивных функций у здоровых лиц», выполняемого в ходе Национального проекта «Новые технологии сбережения здоровья» (рег. №1025020400006-8-3.2.25).

Вклад авторов: А. Г. Пойдашева, Д. О. Синицын, И. С. Бакулин — планирование и дизайн исследования; А. Г. Пойдашева, А. Х. Забирова — анализ литературы; И. С. Бакулин, А. Х. Забирова, Д. Ю. Лагода — сбор данных; Д. О. Синицын, А. Г. Пойдашева — анализ данных; А. Г. Пойдашева, Д. О. Синицын — подготовка статьи; все авторы — интерпретация данных, редактирование статьи.

Соблюдение этических стандартов: исследование одобрено этическим комитетом ФГБНУ РЦНН (протокол № 5-1/25 от 19 мая 2025 г.). Все добровольцы подписали форму добровольного информированного согласия.

✉ **Для корреспонденции:** Александра Георгиевна Пойдашева
Волоколамское шоссе, д. 80, г. Москва, 125367, Россия; poydasheva@neurology.ru

Статья получена: 14.11.2025 **Статья принята к печати:** 10.12.2025 **Опубликована онлайн:** 20.12.2025

DOI: 10.24075/vrgmu.2025.081

Repetitive transcranial magnetic stimulation (rTMS) is a noninvasive neuromodulation method widely used in research and clinical practice [1]. The rTMS protocols have long-term effects similar to the synaptic plasticity mechanisms: high-frequency protocols and intermittent theta-burst stimulation have an effect similar to the long-term potentiation (LTP-like), increasing the stimulated cortex area excitability, while low-frequency protocols and continuous theta-burst stimulation have an effect similar to the long-term depression (LTD-like), decreasing the stimulated area excitability [2]. In recent years, the rTMS neural network effects represented by the possibility of modulating activity of not only the stimulated zone, but also distant brain areas structurally or functionally connected to this zone, are extensively discussed [3, 4].

The high effect variability, one of the possible reasons for which is considered to be suboptimal selection of a target for stimulation, is an important issue of using rTMS in both clinical and research practice. The size of most stimulated anatomical regions is larger than the size of the focus of the magnetic field generated by the stimulation coil, which results in a large number of possible variants of coil positioning within the region. Furthermore, various zones located within these anatomical regions can have different cytoarchitecture, as well as structural and functional connectivity, which is especially important in the context of the rTMS neural network effects [5, 6].

The emergence of TMS neuronavigation systems and algorithms to calculate the TMS-induced electric field maximum made it possible to control the stimulation coil position relative to individual structural data of the patient's MRI in real time, as well as to considerably increase the coil positioning accuracy [7]. Moreover, neuronavigation systems allowed one to use functional MRI data (both group and individual) for targeting, thereby opening up new opportunities for the personalized identification and influence on the selected targets [8]. Various approaches to personalized target identification based on functional MRI in the resting state and with different paradigms are being explored. The personalized determination of the localization of "hubs" of a particular resting-state network represents one such approach. In this case the main hypothesis is that there is a possibility of providing the TMS neural network effects and modulating the activity of a certain network when stimulating one or more network "hubs".

There are a number of methodological issues related to both individual allocation of the resting-state networks and determination of the target itself based on the activation maps identified. For example, several algorithms for allocation of individual resting-state networks were proposed: iterative (see [9] for details), Infomap algorithm [10], multi-session hierarchical Bayesian model (MS-HBM) [11], independent component analysis (ICA), etc. A point, the signal of which reaches the maximum of the functional connectivity characteristic of interest, can be specified as a target within the selected connectivity map [12], or a number of approaches can be used considering connectivity of the zones surrounding this point. For example, the searchlight algorithm selects the point with the maximum average value of the functional connectivity characteristic of interest over the sphere with the specified radius having the center in this point [13], while the cluster algorithm uses the specified threshold to cut off the cluster with the maximum signal and use the coordinates of the center of mass of this cluster [14].

The fronto-parietal control network (FPCN) is one of the networks most consistently identified in resting-state fMRI, the activity of which is associated with cognitive activity [15, 16]. The major FPCN hubs located superficially and accessible for rTMS are the dorsolateral prefrontal cortex (DLPFC) and posterior parietal cortex (PPC). The studies have shown the possibility of modulating cognitive functions in the population of healthy subjects and patients when conducting rTMS of these regions without using a personalized approach, however, the results of these studies are heterogeneous due to high effect variability [17–19].

The objective of this study was to develop a method for personalized identification of the targets for transcranial magnetic stimulation based on the identification of individual FPCN hubs within the DLPFC and PPC with assessment of variability of localization of such targets in healthy volunteers.

METHODS

The study was conducted at the Russian Center of Neurology and Neurosciences in 2025. Medical history and demographic data were collected for all healthy volunteers.

Subjects

Inclusion criteria: the informed consent availability; age 20–50 years. Exclusion criteria: refusal to participate in the study; contraindications for MRI; a neurological disorder affecting cognitive functions or a mental disorder at the time of enrollment or a history of such disorders; a chronic severe somatic disorder, decompensated chronic disorder or acute phase of the disease (for example, ARVI).

A total of 24 healthy volunteers aged 21–48 years (9 males, average age 29 years, standard deviation 7 years) were included in the study.

All volunteers underwent neuroimaging assessment on a 3 T Siemens MAGNETOM Prisma scanner (Germany).

MRI data acquisition and pre-processing

The neuroimaging assessment protocol included the T1-weighted imaging mode with the Multi-Planar Reconstruction (MPR) option for structural data acquisition (TR 2300 ms, voxel 1 × 1 × 1 mm^3) and the Multiplanar Gradient Echo mode (TR 1500 ms, voxel 2 × 2 × 2.2 mm^3) to record the resting-state fMRI signal for analysis of functional connectivity.

The MRI data were analyzed using the CONN (Functional Connectivity SPM Toolbox 2017, McGovern Institute for Brain Research, Massachusetts Institute of Technology (http://www.nitrc.org/projects/conn), Cambridge, USA) version 22.v2407, and SPM12 (Functional Imaging Laboratory, Wellcome Department of Imaging Neuroscience, Institute of Neurology (http://www.fil.ion.ucl.ac.uk/spm/software), London, UK) software packages. Functional images were subjected to realignment with susceptibility distortion correction using field maps, slice timing correction, outlier identification. The structural data were segmented into tissues and normalized into the MNI (Montreal Neurological Institute) space, while functional data were normalized using the deformation field calculated for structural data (indirect normalization). Spatial smoothing was applied to functional data with a Gaussian filter with the full width at half maximum (FWHM) kernel size of 8 mm. Furthermore, the average signal for the region, the connectivity with which was calculated (in the seed-to-voxel procedure described below), was determined based on the unsmoothed data in order to avoid mixing with the signal from adjacent regions.

Furthermore, regression was used to delete contributions of artifacts proportional to the signal of white matter (five principal

Table. Individual coordinates of targets in the left dorsolateral prefrontal cortex and posterior parietal cortex

No	Cortical area						Distance between M1 and the target in the DLPFC, mm
	DLPFC			PPC			
	X-axis coordinate	*Y*-axis coordinate	*Z*-axis coordinate	*X*-axis coordinate	*Y*-axis coordinate	*Z*-axis coordinate	
1	–41	51	14	–27	–69	59	75
2	–45	48	6	–46	–57	52	76
3	–47	28	36	–39	–60	57	44
4	–41	47	21	–46	–48	58	68
5	–41	34	36	–54	–40	52	50
6	–43	48	14	–51	–53	50	72
7	–44	47	14	–51	–48	52	71
8	–49	28	32	–51	–47	52	46
9	–43	47	13	–55	–42	51	72
10	–51	21	34	–38	–72	46	39
11	–50	25	30	–39	–64	54	44
12	–46	46	9	–50	–52	52	72
13	–44	39	28	–56	–42	50	57
14	–47	43	8	–50	–51	53	71
15	–45	24	42	–45	–61	51	39
16	–42	52	6	–52	–48	51	80
17	–48	43	9	–51	–51	51	70
18	–41	40	30	–46	–57	54	59
19	–45	46	11	–60	–29	44	72
20	–40	35	37	–58	–42	46	51
21	–44	47	12	–57	–49	43	72
22	–40	51	17	–43	–54	57	73
23	–46	47	6	–46	–49	58	75
24	–45	48	6	–45	–54	56	76

Note: DLPFC — dorsolateral prefrontal cortex, PPC — posterior parietal cortex, M1 — primary motor cortex.

components), cerebrospinal fluid (five principal components), motion parameters and their first order derivatives (12 regressors), outlier scans, session effect and its first-order derivative (two regressors), as well as the linear trend (two regressors) from functional data, with subsequent band-pass filtering in the 0.008–0.09 Hz range.

Resting-state fMRI data analysis aimed at selecting targets for stimulation

The literature dedicated to solving the problem of finding an invidual parcellation of the cortical surface into functional resting-state networks and selecting an optimal point in the zones available within this network fragment was reviewed. An optimal set of approaches was identified at each stage of data analysis, which was later combined into an algorithm for selecting personalized targets for rTMS. The main steps of this algorithm are provided below.

Algorithm to select personalized targets for rTMS belonging to the fronto-parietal control network (FPCN)

Step 1. Construction of the map of the degree to which points in the brain belong to the FPCN.

The seed-to-voxel method is used: calculation of connectivity of the given region (referred to as seed region) with other voxels of the brain. The method is applied to individual resting-state fMRI data. The FPCN mask generated in the study [20] based on the average connectivity of the group of 1000 healthy volunteers is used as the seed region. The resulting seed connectivity map is used as a map of the degree to which points in the brain belong to the FPCN.

Step 2. Creating a set of candidate voxels for selection of targets located on the brain surface.

Voxels located on the brain surface are selected. For that the function spm_erode is applied to the intracranial volume mask from the SPM package transformed into the specific subject's individual space. This function calculates the region obtained from the specified region by removing one layer of voxels from its surface. Voxels removed by this function are calculated by subtraction of intracranial volume masks before and after the spm_erode application. The set of these voxels is taken as the intracranial volume margin; targets are further selected among these voxels.

Step 3. Selection of the candidate voxels located within the specified target regions.

The ones located within the target regions, DLPFC and PPC, are selected among the voxels obtained in the previous step. The left DLPFC was defined as the portion of the left middle frontal gyrus, excluding the premotor cortex. The mask of the left middle frontal gyrus was taken from the atlas created by A. Hammers and colleagues [21]. The mask of the premotor

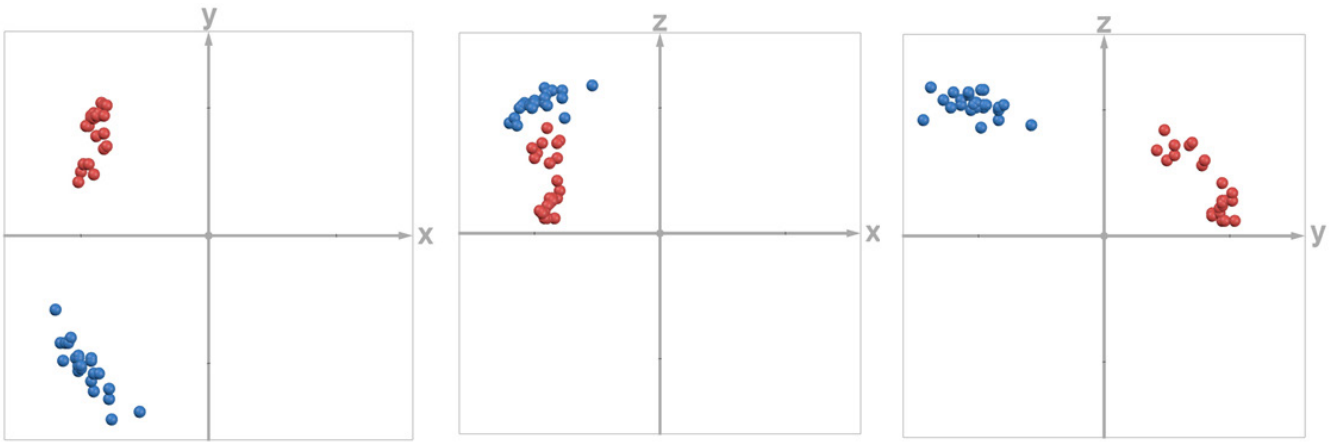


Fig. 1. Projections of targets in 24 subjects on coordinate planes. Red are targets in the DLPFC, blue are targets in the posterior parietal cortex

cortex was obtained by merging areas of the left dorsal and ventral premotor cortex from the HMAT (Human Motor Area Template, [22]). The left posterior parietal cortex was defined as the union of the left supramarginal and angular gyri and the superior parietal lobule from the atlas by A. Hammers.

Step 4. Selection of targets by the searchlight method [13, 14].

The quality measure equal to the mean of the values of the above seed connectivity map within the sphere with the center in a given voxel and the 5 mm radius is calculated for each voxel selected in the previous steps (to consider the effect of stimulation on a certain cortical region surrounding the target point). Voxels with the maximum quality measure values within each target region are selected as targets.

Analysis of the target spatial localization

Individual targets for each subject were transformed into the MNI space using the deformation field transforming the structural image into this space that was generated during MRI data pre-processing. Group mean values and standard deviations of the coordinates of these targets were calculated to describe the distribution of their localization in different subjects. Distances between the targets in the DLPFC and the motor cortex in the hand muscle cortical representation area were calculated. For that the group map of activation (for 486 subjects) upon moving the right fingers based on the Human Connectome Project data [21] was used, downloaded from the Neurovault database (dataset ID https://identifiers.org/neurovault.image:3162). This map was binarized with the threshold Z > 22 selected in such a way as to highlight the cluster in the precentral gyrus region, without including other nearby clusters. The distance to the closest voxel in the resulting binarized activation map was calculated for each target in the DLPFC.

RESULTS

An algorithm for determining the coordinates of points within individual FPCN hubs in the DLPFC and PPC that could be used as targets for rTMS was developed based on the literature review.

Coordinates of targets in two cortical regions were determined for each volunteer (Table).

After transforming each target to the MNI space the group-mean coordinates of targets in the DLPFC are –44.6, 41.1, 19.7 mm, standard deviations are 3.1, 9.5, 12.0 mm. The mean coordinates of targets in the PPC are –48.2, –51.7, 52.0 mm, standard deviations are 7.6, 9.6, 4.2 mm. For the DLPFC, the mean distance between the target and its midpoint is 14.3 mm, the maximum distance is 28.3 mm, for PPC these are 10.4 mm and 28 mm, respectively. The maximum distance

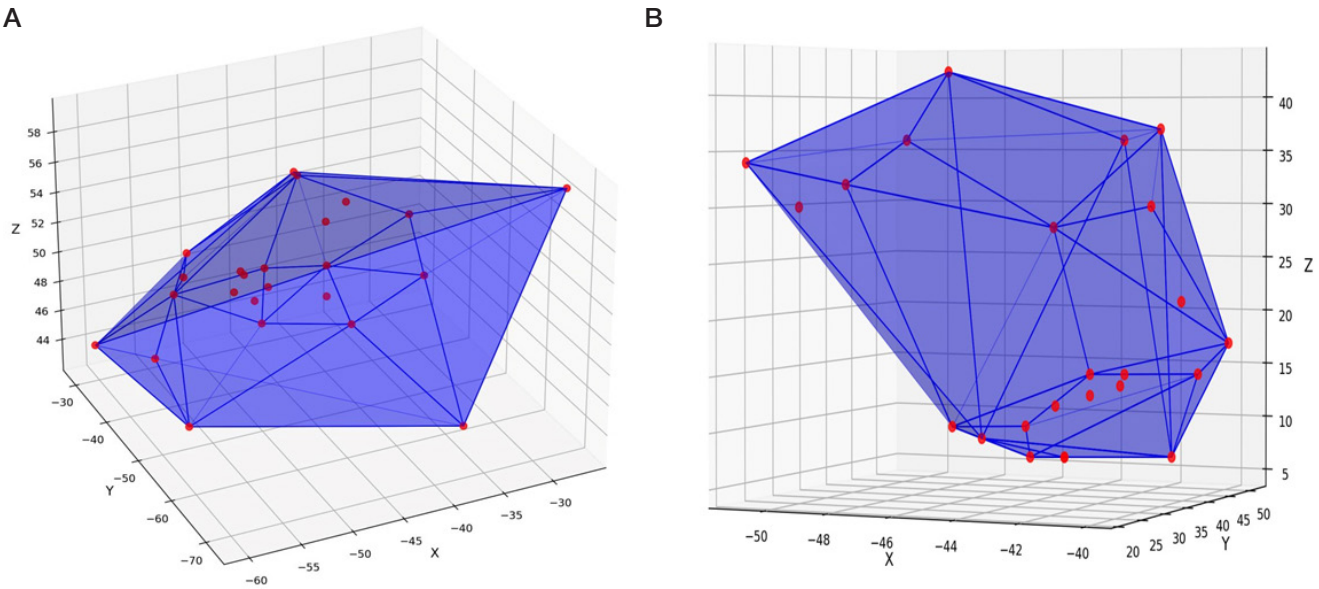


Fig. 2. Convex hulls of sets of points with the coordinates of targets in the PPC (Fig. A) and DLPFC (Fig. B)

between pairs of targets is 45.9 mm in the DLPFC, 54.1 mm in the PPC (Fig. 1).

Despite comparable linear measures of target dispersion, the volumes of polyhedra calculated by the convex hull method and containing sets of points for each of the assessed regions reported for the DLPFC turned out to be almost 3 times higher than that reported for the PPC (2095 and 739 mm^3, respectively) (Fig. 2).

When superimposing targets on the FPCN mask used as a seed region for individual connectivity calculations, in the DLPFC all targets were within the mask, while in the PPC some targets were beyond the mask (Fig. 3).

When estimating distances from individual targets in the DLPFC to the primary motor cortex (M1), the mean value was 64 mm, standard deviation was 13 mm (Table 1). Furthermore, only 6 volunteers had distances (25%) not exceeding 50 mm.

DISCUSSION

In the study, we proposed a personalized target selection algorithm based on selection of individual FPCN hubs within the DLPFC and PPC. High interindividual variability of targets was demonstrated. Furthermore, spatial dispersion of points was higher in the DLPFC, but all individual targets in the DLPFC were within the applied FPCN mask, while in PPC some targets turned out to be beyond this mask. The analysis of the determined target localization variability allows us to state that in none of the specified areas there is a single universal position of the stimulating coil that would allow for effective stimulation of the targets in all volunteers. Moreover, according to the data obtained, the distance between the M1 zones and the DLPFC did not exceed 5 cm only in 25% of subjects, which confirmed that it was incorrect to use the routine “5 cm rule” for coil positioning, at least in the population of healthy individuals.

The personalized target selection algorithm developed allows one to determine individual localization of targets in two key FPCN hubs. The resulting target localization in volunteers was variable in both DLPFC and PPC. Moreover, the size of the stimulated area for most figure-of-eight coils most frequently used for rTMS (for the details of calculations see [22]) is smaller, than the size of the individual target dispersion area in both DLPFC and PPC. Thus, it is clear that there is no single universal stimulation coil position that would allow for effective stimulation of targets in all volunteers in any specified region. These data challenge the “one-fits-all” concept widely used in both scientific research and clinical practice, implying the use of the universal approach (the same for all subjects/patients) to determine the target in the region of interest based on the structural (for example, specified coordinates in the MNI space) or surface (for example, the “5 cm rule”) landmarks. The data showing that in the highly heterogeneous regions, such as DLPFC, the same anatomical zone can be part of different networks, so the neural network effects resulting from stimulation of this zone would be different, suggest that the concept is incorrect [23].

Comparison with the available literature data showed similarity of localization of targets in the DLPFC as a FPCN hub. Thus, the average of the targets corresponding to the peaks of the left FPCN independent component, identified visually among the independent component analysis (ICA) results, obtained in the study [24], was located at coordinates (–38, –39, 17) in the MNI space. This point is located at a distance of 7.4 mm from the midpoint obtained in our study in the direction into the depth of the brain (Fig. 4). The more superficial location of targets reported in our study is explained by methodological

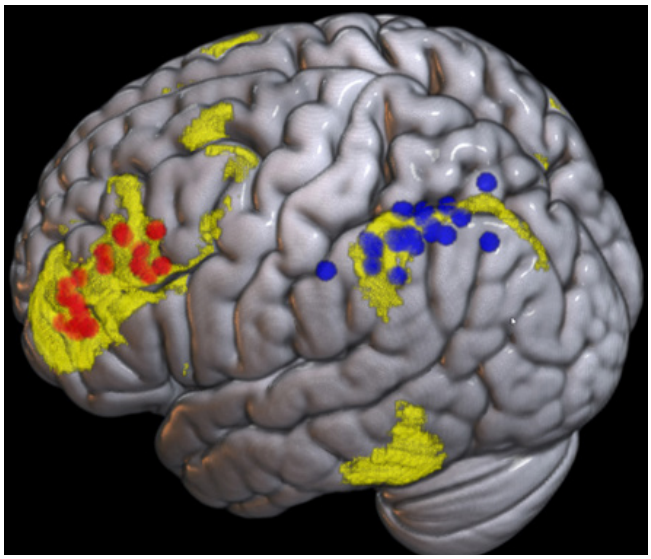


Fig. 3. Positions of targets for all subjects in the MNI space. Shown in yellow is the group-derived mask of the frontoparietal control network (FPCN) from [20] used as a seed region in the calculations of individual connectivity. Shown in red are the individual targets in DLPFC (defined as the part of the middle frontal gyrus excluding the premotor cortex), shown in blue are the targets in the posterior parietal cortex (defined as the union of the supramarginal and angular gyri and the superior parietal lobule). The data is shown on the mni152 template from the MRIcroGL software

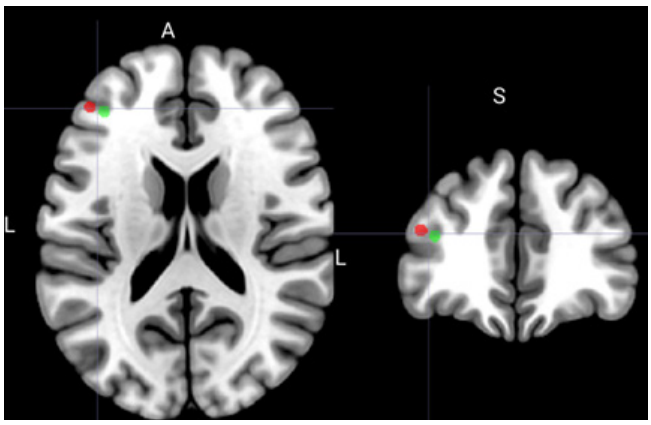


Fig. 4. Comparison of the mean target locations in the DLPFC in MNI space from this study (red) and the paper [24] (green). In the study [24], the point was calculated as the mean of targets defined as peaks of independent components of the individual resting-state fMRI signal visually identified as the FPCN.

features. Considering the limited depth of the magnetic field effect in rTMS, we limited the depth at which the targets were located by the intracranial volume margin found using the spm_erode function of the SPM package.

We have found that the mean distance between the hand zone of primary motor cortex (M1) and targets in the DLPFC exceeds 6 cm. The data obtained are important in the context of assessing the “5 cm rule” validity as an approach to localization of the rTMS target in the DLPFC. Such an approach was originally proposed in the studies focused on therapy for treatment-resistant depression [25]. However, later it became widely used for localization of targets in the DLPFC and for other disorders, as well as in the studies involving healthy volunteers due to simplicity and convenience. According to our data, the distance between the target in the DLPFC and the hand zone in M1 did not exceed 5 cm only in 25% of subjects. Furthermore, it’s important to note that we assessed the shortest distance between two points, while the “5 cm rule” implies estimation of the distance between the projections of those on the convex scalp surface. These data confirm the results of multiple studies

showing that when using the "5 cm rule" the resulting target is displaced caudally relative to the targets obtained by using neuronavigation systems based on the structural and functional data, and the target is often located within the premotor cortex, i.e. another anatomical zone having different functions and connections [26–28].

When comparing the regions formed by sets of targets in two specified regions with each other and with the FPCN mask used as a seed region, it has been shown that with comparable linear target dispersion metrics, the volume of the polyhedron, at the vertices of which the obtained individual targets lie, is significantly higher for the DLPFC than for the PPC. At the same time, all individual targets in the DLPFC are within the FPCN mask, while in the PPC some targets are beyond this mask. The findings suggest high interindividual variability of the topography of both FPCN hubs, which only emphasizes the need for the personalized approach to target selection.

The proposed algorithm for determining targets needs to be discussed separately. To find the cortical surface individual parcellation into functional resting-state network, we used an algorithm similar to the first step of the iterative method [9]: the group mask of the fronto-parietal control network from the paper [20] was used as a seed region when assessing individual resting-state fMRI data. The initial literature review showed that the MS-HBM method [11] allowing one to select the most homogeneous signal in the regions obtained seemed optimal for the task of individual determination of resting-state networks. However, this method does not allow one to assess the degree of confidence in the belonging of each point to the specified network, which is required to select the optimal point within a specified network fragment. We rejected the approaches involving the independent component analysis due to the need to match the components obtained from individual data to the known networks previously obtained using group data. Furthermore, such matching can be accomplished by both visual topography comparison [24] and automated methods [29, 30], but in both cases there can be situations with high uncertainty in the assignment of networks making it difficult to interpret the results.

The searchlight method allowing one to consider heterogeneity of the signal from neighboring voxels within the areas of interest was used to select the target based on this connectivity map. However, in this case the target localization depended on the sphere size specified by the researcher. We used a sphere radius of 5 mm, taking into account the size of the area stimulated during rTMS [22]. Thus, the algorithm developed was designed to identify individual targets for rTMS based on the FPCN hub identification.

Study limitations

The small size of the sample of subjects represents a limitation of this study. However, heterogeneity in the rTMS target location justifying the importance of a personalized approach was demonstrated even in such sample. Inclusion of healthy young and middle-aged volunteers only is another limitation, due to which in future studies it will be necessary to conduct a similar analysis in healthy older and elderly individuals, as well as in patients with cognitive impairment of different origin. It should be also noted that in this study neuroimaging was conducted in a 3 T MRI scanner. It seems reasonable to validate the proposed algorithm using data from 1–1.5 T MRI scanners, which are much more accessible. Furthermore, in this study we did not assess stability between sessions for the determined individual FPCN and the targets in the DLPFC and PPC selected based on this network. It should be noted that after the first iteration of the algorithm [9], which is conceptually similar to our method, the individual parcellation into resting-state networks for the Human Connectome Project data had a reproducibility of about 0.9, which was measured as the proportion of voxels found in the same network upon retest (though the data had approximately twice longer duration and twice higher temporal resolution).

CONCLUSIONS

Personalization of the target selection for rTMS is an important problem, the solution of which can significantly increase the effectiveness of using the method in clinical practice and scientific research. The analysis of individual resting-state network maps makes it possible to obtain personalized targets, the localization of which is characterized by high interindividual variability. At the same time it should be noted, that such analysis is associated with a number of methodological problems and requires a justified choice of one or another approach at each stage. During the study we proposed an algorithm for personalized selection of targets for rTMS based on the resting-state fMRI in the DLPFC and PPC, being the key FPCN hubs and the main rTMS targets in both patients with cognitive impairment and healthy individuals in studies of cognitive function modulation. The development of automated algorithms for the resting-state fMRI analysis accounting for the specifics of the task (determination of targets for rTMS) may further facilitate the wider spread of personalized rTMS. It is necessary to confirm the increase in rTMS effectiveness when using the developed approach to personalized target selection in further randomized controlled trials.

References

1. Chen M, Zhao G, Peng L. Transcranial Magnetic Stimulation Applications in the Study of Executive Functions: A Review. Brain Behav. 2024; 14 (11): e70099.
2. Sun W, Wu Q, Gao L, Zheng Z, Xiang H, Yang K, et al. Advancements in Transcranial Magnetic Stimulation Research and the Path to Precision. Neuropsychiatr Dis Treat. 2023; 19: 1841–51.
3. Tik M, Hoffmann A, Sladky R, Tomova L, Hummer A, Navarro de Lara L, et al. Towards understanding rTMS mechanism of action: Stimulation of the DLPFC causes network-specific increase in functional connectivity. Neuroimage. 2017; 162: 289–96.
4. Ørbo MC, Høier S, Vangberg TR, Csifcsak G, Grønli OK, Aslaksen PM. The cerebral and cognitive changes after intermittent theta burst stimulation (iTBS) treatment for depression: study protocol for a randomized double-blind sham-controlled trial. Trials. 2024; 25 (1): 752.
5. Smith S, Duff E, Groves A, Nichols TE, Jbabdi S, Westlye LT, et al. Structural Variability in the Human Brain Reflects Fine-Grained Functional Architecture at the Population Level. J Neurosci.; 39 (31): 6136–49.
6. Lioumis P, Roine T, Granö I, Aydogan DB, Ukharova E, Souza VH, et al. Optimization of TMS target engagement: current state and future perspectives. Front Neurosci. 2025; 19: 1517228.
7. Caulfield KA, Fleischmann HH, Cox CE, Wolf JP, George MS, McTeague LM. Neuronavigation maximizes accuracy and precision in TMS positioning: Evidence from 11,230 distance, angle, and electric field modeling measurements. Brain Stimul. 2022; 15 (5):

1192–205.
8. Cash RFH, Zalesky A. Personalized and Circuit-Based Transcranial Magnetic Stimulation: Evidence, Controversies, and Opportunities. Biol Psychiatry. 2024; 95 (6): 510–22.
9. Wang D, Buckner RL, Fox MD, Holt DJ, Holmes AJ, Stoecklein S, et al. Parcellating cortical functional networks in individuals. Nat Neurosci. 2015; 18 (12): 1853–60.
10. Gordon EM, Laumann TO, Gilmore AW, Newbold DJ, Greene DJ, Berg JJ, et al. Precision Functional Mapping of Individual Human Brains. Neuron. 2017; 95 (4): 791–807.e7.
11. Kong R, Li J, Orban C, Sabuncu MR, Liu H, Schaefer A, et al. Spatial Topography of Individual-Specific Cortical Networks Predicts Human Cognition, Personality, and Emotion. Cereb Cortex. 2019; 29 (6): 2533–51.
12. Ning L, Makris N, Camprodon JA, Rathi Y. Limits and reproducibility of resting-state functional MRI definition of DLPFC targets for neuromodulation. Brain Stimul. 2019; 12 (1): 129–38.
13. Fox MD, Liu H, Pascual-Leone A. Identification of reproducible individualized targets for treatment of depression with TMS based on intrinsic connectivity. Neuroimage. 2013; 66: 151–60.
14. Cash RFH, Cocchi L, Lv J, Wu Y, Fitzgerald PB, Zalesky A. Personalized connectivity-guided DLPFC-TMS for depression: Advancing computational feasibility, precision and reproducibility. Hum Brain Mapp. 2021; 42 (13): 4155–72.
15. Menon V, D'Esposito M. The role of PFC networks in cognitive control and executive function. Neuropsychopharmacology. 2022; 47 (1): 90–103.
16. Xia H, He Q, Chen A. Understanding cognitive control in aging: A brain network perspective. Front Aging Neurosci. 2022; 14: 1038756.
17. Ebrahimzadeh E, Sadjadi SM, Asgarinejad M, Dehghani A, Rajabion L, Soltanian-Zadeh H. Neuroenhancement by repetitive transcranial magnetic stimulation (rTMS) on DLPFC in healthy adults. Cogn Neurodyn. 2025; 19 (1): 34.
18. Zhang Y, Dong K, Yang J, Guo Q, Zhao Y, Zhu X, et al. Comparative efficacy of rTMS on different targets in Alzheimer's disease: a systematic review and meta-analysis. Front Aging Neurosci. 2025; 17: 1536573.
19. Xu M, Nikolin S, Samaratunga N, Chow EJH, Loo CK, Martin DM. Cognitive Effects Following Offline High-Frequency Repetitive Transcranial Magnetic Stimulation (HF-rTMS) in Healthy Populations: A Systematic Review and Meta-Analysis. Neuropsychol Rev. 2024; 34 (1): 250–76.
20. Yeo BT, Krienen FM, Sepulcre J, Sabuncu MR, Lashkari D, Hollinshead M, et al. The organization of the human cerebral cortex estimated by intrinsic functional connectivity. J Neurophysiol. 2011; 106 (3): 1125–65.
21. Hammers A, Allom R, Koepp MJ, Free SL, Myers R, et al. Three-dimensional maximum probability atlas of the human brain, with particular reference to the temporal lobe. Hum Brain Mapp. 2003;19(4):224-47.
22. Mayka MA, Corcos DM, Leurgans SE, Vaillancourt DE. Three-dimensional locations and boundaries of motor and premotor cortices as defined by functional brain imaging: a meta-analysis. Neuroimage. 2006;31(4):1453-74.
23. Van Essen DC, Smith SM, Barch DM, Behrens TE, Yacoub E, Ugurbil K; et al. The WU-Minn Human Connectome Project: an overview. Neuroimage. 2013; 80: 62–79.
24. Drakaki M, Mathiesen C, Siebner HR, Madsen K, Thielscher A. Database of 25 validated coil models for electric field simulations for TMS. Brain Stimul. 2022; 15 (3): 697–706.
25. Lynch CJ, Elbau IG, Ng TH, Wolk D, Zhu S, Ayaz A, et al. Automated optimization of TMS coil placement for personalized functional network engagement. Neuron. 2022; 110 (20): 3263–77.
26. Sayalı C, Gogulski J, Granö I, Lioumis P, Barrett F. Test-retest reliability of TMS-evoked potentials over fMRI-based definitions of non-motor cortical targets. bioRxiv 2024.12.20.629675.
27. Pascual-Leone A, Rubio B, Pallardó F, Catalá MD. Rapid-rate transcranial magnetic stimulation of left dorsolateral prefrontal cortex in drug-resistant depression. Lancet. 1996; 348 (9022): 233–7.
28. Tsukuda B, Ikeda S, Minami S, Katsura K, Shimizu T, Kame T, et al. Targeting Method for rTMS for Treating Depression in Japanese Patients: A Comparison of the Standard, F3, and Neuronavigation Approaches. Neuropsychobiology. 2024; 83 (3–4): 170–8.
29. Fitzgerald PB. Targeting repetitive transcranial magnetic stimulation in depression: do we really know what we are stimulating and how best to do it? Brain Stimul. 2021; 14 (3): 730–6.
30. Ahdab R, Ayache SS, Brugières P, Goujon C, Lefaucheur JP. Comparison of "standard" and "navigated" procedures of TMS coil positioning over motor, premotor and prefrontal targets in patients with chronic pain and depression. Neurophysiol Clin. 2010; 40 (1): 27–36.
31. Bagattini C, Brignani D, Bonnì S, Quattrini G, Gasparotti R, Pievani M. Functional Imaging to Guide Network-Based TMS Treatments: Toward a Tailored Medicine Approach in Alzheimer's Disease. Front Neurosci. 2021; 15: 687493.
32. Castrillon G, Sollmann N, Kurcyus K, Razi A, Krieg SM, Riedl V. The physiological effects of noninvasive brain stimulation fundamentally differ across the human cortex. Sci Adv. 2020; 6 (5): eaay2739.

Литература

1. Chen M, Zhao G, Peng L. Transcranial Magnetic Stimulation Applications in the Study of Executive Functions: A Review. Brain Behav. 2024; 14 (11): e70099.
2. Sun W, Wu Q, Gao L, Zheng Z, Xiang H, Yang K, et al. Advancements in Transcranial Magnetic Stimulation Research and the Path to Precision. Neuropsychiatr Dis Treat. 2023; 19: 1841–51.
3. Tik M, Hoffmann A, Sladky R, Tomova L, Hummer A, Navarro de Lara L, et al. Towards understanding rTMS mechanism of action: Stimulation of the DLPFC causes network-specific increase in functional connectivity. Neuroimage. 2017; 162: 289–96.
4. Ørbo MC, Høier S, Vangberg TR, Csifcsak G, Grønli OK, Aslaksen PM. The cerebral and cognitive changes after intermittent theta burst stimulation (iTBS) treatment for depression: study protocol for a randomized double-blind sham-controlled trial. Trials. 2024; 25 (1): 752.
5. Smith S, Duff E, Groves A, Nichols TE, Jbabdi S, Westlye LT, et al. Structural Variability in the Human Brain Reflects Fine-Grained Functional Architecture at the Population Level. J Neurosci.; 39 (31): 6136–49.
6. Lioumis P, Roine T, Granö I, Aydogan DB, Ukharova E, Souza VH, et al. Optimization of TMS target engagement: current state and future perspectives. Front Neurosci. 2025; 19: 1517228.
7. Caulfield KA, Fleischmann HH, Cox CE, Wolf JP, George MS, McTeague LM. Neuronavigation maximizes accuracy and precision in TMS positioning: Evidence from 11,230 distance, angle, and electric field modeling measurements. Brain Stimul. 2022; 15 (5): 1192–205.
8. Cash RFH, Zalesky A. Personalized and Circuit-Based Transcranial Magnetic Stimulation: Evidence, Controversies, and Opportunities. Biol Psychiatry. 2024; 95 (6): 510–22.
9. Wang D, Buckner RL, Fox MD, Holt DJ, Holmes AJ, Stoecklein S, et al. Parcellating cortical functional networks in individuals. Nat Neurosci. 2015; 18 (12): 1853–60.
10. Gordon EM, Laumann TO, Gilmore AW, Newbold DJ, Greene DJ, Berg JJ, et al. Precision Functional Mapping of Individual Human Brains. Neuron. 2017; 95 (4): 791–807.e7.
11. Kong R, Li J, Orban C, Sabuncu MR, Liu H, Schaefer A, et al. Spatial Topography of Individual-Specific Cortical Networks Predicts Human Cognition, Personality, and Emotion. Cereb Cortex. 2019; 29 (6): 2533–51.
12. Ning L, Makris N, Camprodon JA, Rathi Y. Limits and reproducibility of resting-state functional MRI definition of DLPFC targets for neuromodulation. Brain Stimul. 2019; 12 (1): 129–38.
13. Fox MD, Liu H, Pascual-Leone A. Identification of reproducible individualized targets for treatment of depression with TMS based on intrinsic connectivity. Neuroimage. 2013; 66: 151–60.
14. Cash RFH, Cocchi L, Lv J, Wu Y, Fitzgerald PB, Zalesky A. Personalized connectivity-guided DLPFC-TMS for depression:

Advancing computational feasibility, precision and reproducibility. Hum Brain Mapp. 2021; 42 (13): 4155–72.
15. Menon V, D'Esposito M. The role of PFC networks in cognitive control and executive function. Neuropsychopharmacology. 2022; 47 (1): 90–103.
16. Xia H, He Q, Chen A. Understanding cognitive control in aging: A brain network perspective. Front Aging Neurosci. 2022; 14: 1038756.
17. Ebrahimzadeh E, Sadjadi SM, Asgarinejad M, Dehghani A, Rajabion L, Soltanian-Zadeh H. Neuroenhancement by repetitive transcranial magnetic stimulation (rTMS) on DLPFC in healthy adults. Cogn Neurodyn. 2025; 19 (1): 34.
18. Zhang Y, Dong K, Yang J, Guo Q, Zhao Y, Zhu X, et al. Comparative efficacy of rTMS on different targets in Alzheimer's disease: a systematic review and meta-analysis. Front Aging Neurosci. 2025; 17: 1536573.
19. Xu M, Nikolin S, Samaratunga N, Chow EJH, Loo CK, Martin DM. Cognitive Effects Following Offline High-Frequency Repetitive Transcranial Magnetic Stimulation (HF-rTMS) in Healthy Populations: A Systematic Review and Meta-Analysis. Neuropsychol Rev. 2024; 34 (1): 250–76.
20. Yeo BT, Krienen FM, Sepulcre J, Sabuncu MR, Lashkari D, Hollinshead M, et al. The organization of the human cerebral cortex estimated by intrinsic functional connectivity. J Neurophysiol. 2011; 106 (3): 1125–65.
21. Hammers A, Allom R, Koepp MJ, Free SL, Myers R, et al. Three-dimensional maximum probability atlas of the human brain, with particular reference to the temporal lobe. Hum Brain Mapp. 2003;19(4):224-47.
22. Mayka MA, Corcos DM, Leurgans SE, Vaillancourt DE. Three-dimensional locations and boundaries of motor and premotor cortices as defined by functional brain imaging: a meta-analysis. Neuroimage. 2006;31(4):1453-74.
23. Van Essen DC, Smith SM, Barch DM, Behrens TE, Yacoub E, Ugurbil K; et al. The WU-Minn Human Connectome Project: an overview. Neuroimage. 2013; 80: 62–79.
24. Drakaki M, Mathiesen C, Siebner HR, Madsen K, Thielscher A. Database of 25 validated coil models for electric field simulations for TMS. Brain Stimul. 2022; 15 (3): 697–706.
25. Lynch CJ, Elbau IG, Ng TH, Wolk D, Zhu S, Ayaz A, et al. Automated optimization of TMS coil placement for personalized functional network engagement. Neuron. 2022; 110 (20): 3263–77.
26. Sayalı C, Gogulski J, Granö I, Lioumis P, Barrett F. Test-retest reliability of TMS-evoked potentials over fMRI-based definitions of non-motor cortical targets. bioRxiv 2024.12.20.629675.
27. Pascual-Leone A, Rubio B, Pallardó F, Catalá MD. Rapid-rate transcranial magnetic stimulation of left dorsolateral prefrontal cortex in drug-resistant depression. Lancet. 1996; 348 (9022): 233–7.
28. Tsukuda B, Ikeda S, Minami S, Katsura K, Shimizu T, Kame T, et al. Targeting Method for rTMS for Treating Depression in Japanese Patients: A Comparison of the Standard, F3, and Neuronavigation Approaches. Neuropsychobiology. 2024; 83 (3–4): 170–8.
29. Fitzgerald PB. Targeting repetitive transcranial magnetic stimulation in depression: do we really know what we are stimulating and how best to do it? Brain Stimul. 2021; 14 (3): 730–6.
30. Ahdab R, Ayache SS, Brugières P, Goujon C, Lefaucheur JP. Comparison of "standard" and "navigated" procedures of TMS coil positioning over motor, premotor and prefrontal targets in patients with chronic pain and depression. Neurophysiol Clin. 2010; 40 (1): 27–36.
31. Bagattini C, Brignani D, Bonnì S, Quattrini G, Gasparotti R, Pievani M. Functional Imaging to Guide Network-Based TMS Treatments: Toward a Tailored Medicine Approach in Alzheimer's Disease. Front Neurosci. 2021; 15: 687493.
32. Castrillon G, Sollmann N, Kurcyus K, Razi A, Krieg SM, Riedl V. The physiological effects of noninvasive brain stimulation fundamentally differ across the human cortex. Sci Adv. 2020; 6 (5): eaay2739.

DIFFERENTIATION OF iPSCs INTO CORNEAL EPITHELIAL PRECURSORS IN THREE-DIMENSIONAL *IN VITRO* CULTURE

Zhigmitova EB[1], Kosykh AV[1], Gurskaya NG[1,2] ✉

[1] Pirogov Russian National Research Medical University, Moscow, Russia.

[2] Shemyakin–Ovchinnikov Institute of Bioorganic Chemistry, Moscow, Russia

Diseases associated with limbal stem cell deficiency, such as chronic epithelial erosion and corneal scarring, require new therapeutic approaches rooted in regenerative medicine. This study aimed to develop a protocol for obtaining progenitor cells of the epithelium of the limb and cornea from induced pluripotent stem cells (iPSCs). We differentiated iPSCs toward eye organoids to obtain three-dimensional heterogeneous structures within three weeks. The resulting organoids contain corneal epithelial progenitor cells expressing keratin 3 and collagen 7, which confirms the possibility of generating functional epithelium in vitro. The protocol enables the generation of isogenic, patient-specific cell lines for treating limbal insufficiency and dystrophic epidermolysis bullosa, including applications following preliminary genome editing of iPSCs.

Keywords: iPSCs, spheroid, differentiation, eye organoid, epithelium, limbus, cornea, collagen 7

Funding: the work was supported by a grant from the Ministry of Health of the Russian Federation, project No. 124021000001-09.

Acknowledgements: the authors thank M. A. Lagarkova, Corresponding Member of the Russian Academy of Sciences, Professor, for fruitful discussion of the work and critical comments.

Author contribution: Zhigmitova EB — design and conduct of the experiment, Kosykh AV — material processing, micrography, preparation of the article, Gurskaya NG — concept, design of the work, primary manuscript editing.

✉ **Correspondence should be addressed:** Nadezhda G. Gurskaya
Ostrovityanova, 1, str. 1, Moscow, 117997, Russia; ngurskaya@mail.ru

Received: 25.11.2025 **Accepted:** 12.12.2025 **Published online:** 27.12.2025

DOI: 10.24075/brsmu.2025.070

Copyright: © 2025 by the authors. **Licensee:** Pirogov University. This article is an open access article distributed under the terms and conditions of the Creative Commons Attribution (CC BY) license (https://creativecommons.org/licenses/by/4.0/).

ДИФФЕРЕНЦИРОВКА иПСК В ПРЕДШЕСТВЕННИКИ ЭПИТЕЛИЯ РОГОВИЦЫ В ТРЕХМЕРНЫХ УСЛОВИЯХ *IN VITRO*

Е. Б. Жигмитова[1], А. В. Косых[1], Н. Г. Гурская[1,2] ✉

[1] Российский национальный исследовательский медицинский университет имени Н. И. Пирогова, Москва, Россия

[2] Институт биоорганической химии имени М. М. Шемякина и Ю. А. Овчинникова, Москва, Россия

Заболевания, связанные с дефицитом лимбальных стволовых клеток (хронические эрозии, рубцевание роговицы), требуют новых подходов регенеративной медицины. Цель исследования — разработать протокол получения клеток-предшественников эпителия лимба и роговицы из индуцированных плюрипотентных стволовых клеток (иПСК). Использовали метод дифференцировки иПСК в направлении органоида глаза для получения трехмерных гетерогенных структур за три недели. Полученные органоиды содержат клетки-предшественники эпителия роговицы, экспрессирующие кератин 3 и коллаген 7, что подтверждает возможность генерации функционального эпителия *in vitro*. Протокол позволяет создавать изогенные пациент-специфичные линии для терапии лимбальной недостаточности и дистрофического буллезного эпидермолиза, в том числе после предварительного редактирования генома иПСК.

Ключевые слова: иПСК, сфероид, дифференцировка, органоид глаза, эпителий, лимб, роговица, коллаген 7

Финансирование: работа выполнена при поддержке гранта Министерства здравоохранения РФ, проект №124021000001-09.

Благодарности: члену-корреспонденту РАН, профессору М. А. Лагарьковой за обсуждение работы, плодотворную дискуссию и критические замечания.

Вклад авторов: Е. Б. Жигмитова — дизайн и проведение эксперимента; А. В. Косых — обработка материала, микросъемка и подготовка статьи; Н. Г. Гурская — концепция, дизайн работы, редактирование первичной рукописи.

✉ **Для корреспонденции:** Надежда Георгиевна Гурская
ул. Островитянова, д. 1, стр. 1, г. Москва, 117997, Россия; ngurskaya@mail.ru

Статья получена: 25.11.2025 **Статья принята к печати:** 12.12.2025 **Опубликована онлайн:** 27.12.2025

DOI: 10.24075/vrgmu.2025.070

Авторские права: © 2025 принадлежат авторам. **Лицензиат:** РНИМУ им. Н. И. Пирогова. Статья размещена в открытом доступе и распространяется на условиях лицензии Creative Commons Attribution (CC BY) (https://creativecommons.org/licenses/by/4.0/).

Blindness and eyesight disorders are a global health problem affecting at least 2.2 billion people worldwide (according to WHO), of whom 6.17 million have severe visual impairments caused by corneal pathologies [1]. Corneal transplantation (keratoplasty) restores vision in such cases by replacing the damaged area with a donor transplant. This is one of the most common and successful transplantation surgeries in the world: over 180,000 such operations are performed annually [2]. However, the demand for donor corneas far exceeds their availability, particularly in countries with limited resources. Therefore, the scientific community looks for alternative corneal allotransplantation solutions, from the use of decellularized corneal xenografts to the introduction of tissue engineering and regenerative medicine methods using differentiated stem cells [3, 4].

The eye is a complex organ consisting of highly specialized tissues originating from different rudiments [5]. The retina develops from the neuroectoderm through the optic vesicle, the

corneal epithelium originates from the superficial ectoderm, and the iris and corneal stroma originate from the neural crest. The development of methods that enable the differentiation of stem cells into specialized eye cells provides a promising resource for new studies of morphogenesis and eye development.

Induced pluripotent human stem cells (iPSCs) are a unique model that allows using the advantages of regenerative medicine. iPSCs are similar in properties to embryonic stem cells; they can differentiate into a wide variety of cell types. There are various methods for obtaining iPSCs, and there are many sources of somatic cells for their reprogramming to ultimately produce an autologous material, from keratinocytes and dermal fibroblasts obtained during skin biopsy to peripheral blood mononuclear cells or donor urine cells.

iPSCs differentiation protocols can be conditionally divided into two groups: those stemming from standard protocols for suspended cell culture management and those based on three-dimensional models [6, 7].

According to a report [8], the number of clinical studies on retinal pigment epithelium (RPE) transplants derived from iPSC differentiation has increased significantly in recent years. The mammalian retina is devoid of significant regenerative potential in adulthood, it does not restore its function when degenerative processes begin. Congenital and acquired degenerative diseases of the retina are accompanied by the loss of photoreceptors in it, which leads to severe and irreversible vision loss. Against the background of significant progress in understanding the pathogenesis of degenerative retinal diseases, the task becoming especially important is that of the development of methods of cell generation (RPE) from progenitor cells. Promising sources are allogeneic cells and autologous cells obtained from patient-specific progenitor cells of RPE, which can potentially compensate for functional defects [6].

Unlike the retina, the anterior corneal epithelium of the adult body is capable of reparative regeneration, although the rate and type of replacement tissue depend on the severity of traumatic injuries. With deep defects, not only the epithelium is affected, but also the Bowman's membrane, which consists of collagen fibers, as well as the underlying part of the corneal stroma. During the repair of lesions, the epithelium covering the wound multiplies, and the resulting epithelial layer is often thicker than normal. The defects of the underlying layers are replaced by coarse fibrous (scar) tissue [9]. In addition to injury, various diseases and genetic disorders can lead to damage and degenerative changes in the cornea. Among the diseases affecting the functioning of the limb and cornea, those deserving a special mention are the limbal insufficiency syndrome (LIS), bullous keratopathy (endothelial-epithelial dystrophy of the cornea), and symblepharon, in which the fusion of the bulbar conjunctiva (from the eye) with the palpebral conjunctiva (from the inner surface of the eyelid) leads to scarring of the cornea. For example, ophthalmological complications are common in patients with epidermolysis bullosa (EB) in general, but their frequency varies significantly depending on the subtype of the disease. The most severe manifestations are observed in recessive dystrophic epidermolysis bullosa (RDEB) and borderline subtypes. As a result of impaired synthesis of type VII collagen, patients with RDEB experience, inter alia, recurrent corneal erosions, blisters, and scarring, which may lead to complications such as exposure keratitis and symblepharon [10].

This study aimed to develop a protocol that combines the advantages of various approaches for generating eye organoids and corneal epithelium, particularly through the three-dimensional culture of differentiable cells.

METHODS

Culturing

iPSCs (KYOU-DXR0109B) were cultured at 37 °C (5% CO_2) in mTESR medium (85850, STEMCELL Technologies Inc., Canada) on plastic Petri dishes coated with matrigel (356234, Corning, USA). For individual iPSC colonies, we seeded 3,800 cells per cm^2. After 5 days, the iPSC colonies were collected following treatment with 0.4 mg/ml dispase (17105041, Gibco, Thermo Fisher Scientific, USA), which detaches the colonies from the culture surface without dissociating them into single cells.

For the subsequent cultivation of non-adhesive cultures, we used the ultra low attachment Petri dishes (3261, Corning, USA).

The transition between different types of culture media was always done in stages over 4–5 days, as follows:

– 1st day: –1 ml/+1 ml;

– 2nd day: –1.5 ml/+1.5 ml;

– 3rd day: –2 ml/+2 ml, etc.

where "–" indicates the removed volume of the current culture medium, and "+" indicates the added volume of the differentiation medium of the next stage.

The medium for embryoid body (EB) formation consisted of DMEM/F12 (C470p, PanEco, Russia) supplemented with 20% fetal bovine serum (F800820, GlobeKang, China), 100 μM β-mercaptoethanol (21985023, Thermo Fisher Scientific, USA), 100 μM MEM non-essential amino acids (F115/100, PanEco, Russia), 1 mM sodium pyruvate (11360070, Thermo Fisher Scientific, USA), 50 U/mL penicillin-streptomycin (15140122, Thermo Fisher Scientific, USA), and 2 mM GlutaMAX (35050061, Thermo Fisher Scientific, USA) [11].

XF-KO-SR (xeno-free KnockOut serum medium) consisted of DMEM (C455p, PanEco, Russia) supplemented with 15% KnockOut SR XenoFree CTS (12618012, Thermo Fisher Scientific, USA), 100 μM β-mercaptoethanol (21985023, Thermo Fisher Scientific, USA), 100 μM MEM non-essential amino acids (F115/100, PanEco, Russia), 2 mM GlutaMAX (35050061, Thermo Fisher Scientific, USA), 50 U/mL penicillin-streptomycin (15140122, Thermo Fisher Scientific, USA), and 10 μM ROCK inhibitor (ab120129, Abcam, USA) [12].

At subsequent stages of the differentiation protocol, 50 ng/mL Noggin4 (PSG100-10, SciStore, Russia), 50 ng/mL bFGF (PSG060-10, SciStore, Russia), and then 25 ng/mL BMP4 (PCH9534, Thermo Fisher Scientific, USA) were added to the XF-KO-SR medium.

Human corneal epithelial cells (hCEpCs) were cultured in DMEM/F12 medium (C470p, PanEco, Russia) supplemented with 10% KnockOut SR XenoFree CTS (12618012, Thermo Fisher Scientific, USA), 2 mM GlutaMAX (35050061, Thermo Fisher Scientific, USA), 10 μM ROCK inhibitor (ab120129, Abcam, USA), 0.4 μg/mL hydrocortisone (H0888, Sigma-Aldrich, USA), 5 μg/mL insulin (F062, PanEco, Russia), 1.4 ng/mL 3,3′,5-triiodo-L-thyronine (100-0548, STEMCELL Technologies Inc., Canada), 24 μg/mL adenine sulfate (A0013500100, SUVCHEM, India), 10 μM forskolin (F6886, Sigma-Aldrich, USA), 10 ng/mL EGF (PSG130, SciStore, Russia), 10 ng/mL KGF (PSG230-10, SciStore, Russia), and 50 U/mL penicillin-streptomycin (15140122, Thermo Fisher Scientific, USA) [13].

The composition of these media was developed based on the referenced literature sources with partial modifications due to the unavailability of some components. The replacement substances, according to the literature, had similar mechanisms of action.

Photographs of whole organoids were taken with a Leica M205 stereomicroscope.

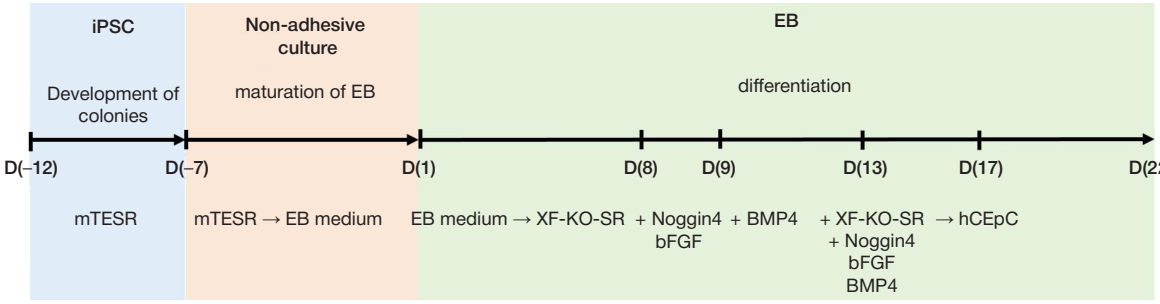


Fig. 1. Protocol for generating EBs and their subsequent differentiation into corneal epithelial cells. D(–12) — the beginning of the experiment. D(1) — the first day of the differentiation protocol. D(22) — the last day of differentiation; collection of organoids for subsequent analysis

Histological examination

The organoids were fixed in 10% neutral buffered formalin (00020709, Histoline, Russia) for 30 minutes, washed with DPBS (P060p-1, PanEco, Russia) to remove the fixative, and then incubated for 1 hour in DPBS containing sucrose solutions (170764, Lenreactive, Russia) of increasing concentrations (10%, 20%, and 30%) to prevent deformation of the organoids. The organoids were collected, drained of excess solution, embedded in Tissue-Tek O.C.T. Compound (4583, Electron Microscopy Sciences, USA), and snap-frozen in liquid nitrogen.

We prepared 10 µm-thick sections using a Thermo Scientific Microm HM 525 cryostat, dried them, and further fixed them in 10% neutral buffered formalin (00020709, Histoline, Russia) for 15 minutes at room temperature. The sections were then washed three times in DPBS (5 minutes each), followed by incubation in DPBS containing 1% hydrogen peroxide (153142, Lenreactive, Russia) for 30 minutes, and subsequently in DPBS containing 2.5% BSA (A7906, Sigma-Aldrich, USA).

Immunohistochemistry

For subsequent immunohistochemical staining, the sections were incubated overnight at +4 °C with primary antibodies against keratin 3 (PAA490Hu01, Cloud-Clone, USA) and collagen VII (pA5-18390, Invitrogen, Thermo Fisher Scientific, USA), diluted 1:100 and 1:300, respectively, in DPBS blocking solution containing 2% BSA (A7906, Sigma-Aldrich, USA), 1% Triton X-100 (1001776062, Sigma-Aldrich, USA), and 1% Tween 20 (P7949, Sigma-Aldrich, USA). The next day, the sections were washed in DPBS and incubated overnight at +4 °C with secondary antibodies: Alexa 594–conjugated anti–rabbit IgG (A11012, Invitrogen, Thermo Fisher Scientific, USA) and Alexa 488–conjugated anti–goat IgG (A32814, Invitrogen, Thermo Fisher Scientific, USA), both diluted 1 : 1000 in blocking solution. The next day, the sections were washed with DPBS and mounted in VectaSHIELD Antifade medium containing DAPI (H-1200-10, Vector Laboratories, USA).

Using a Nikon Eclipse Ni upright microscope equipped with a DS-Ri2 camera (Nikon Corporation, Japan), we analyzed the sections and acquired a series of images using the microscope's set of optical filters, which enabled detection of fluorescence emission. The images were processed using the ImageJ software package (NIH, USA) and converted into microphotographs.

RESULTS

There were two stages to the formation of the initial EB (Fig. 1). At the first stage, which began on D(–12), iPSC colonies were cultured under adhesive conditions; on D(–7), they were transitioned to a non-adhesive form. After 7 days of cultivation under non-adhesive conditions, the EBs matured, and the colonies acquired a more rounded shape with smooth edges. Subsequently, we switched to the differentiation protocol for corneal epithelial cells (D(1)).

From day 8 of the differentiation protocol, Noggin4 and bFGF factors were injected into the XF-KO-SR medium, blocking TGFß and Wnt signaling and activating FGF signaling to induce ectodermal differentiation. Additionally, we introduced BMP4, as it was shown that this factor promotes the differentiation of iPSCs into corneal epithelial cells [14].

On day 13, we began to gradually replace the XF-KO-SR medium with a medium for culturing human corneal epithelial cells (hCEpCs).

By day 22, both monospheres (Fig. 2A) and complex formations were observed among the organoids, likely resulting from the aggregation of several individual elements (Fig. 2B, C). Most of the organoids became optically translucent in transmitted light, but some objects had pigmented areas (Fig. 2).

To analyze the expression patterns of differentiation markers, we prepared cryosections of the organoids and examined them

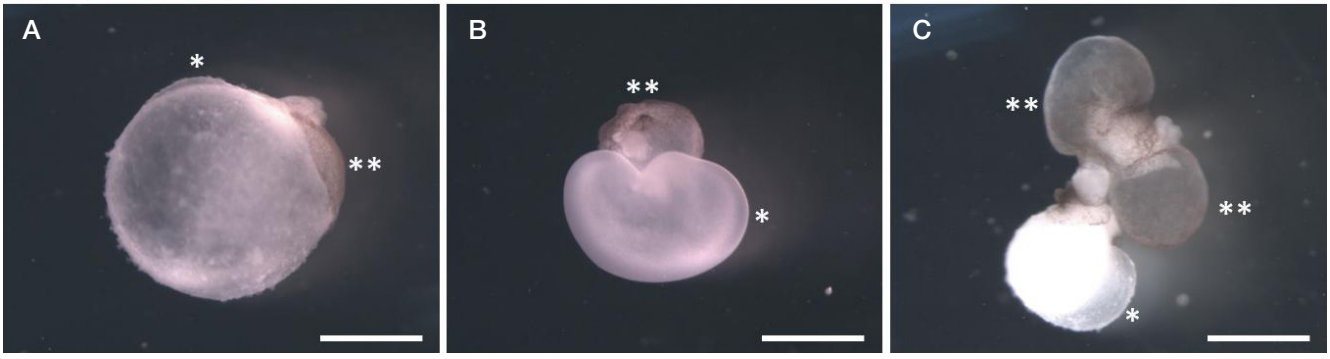


Fig. 2. Darkfield photo of organoids on the 22nd day of differentiation. There are both translucent spheres and pigmented areas. * — translucent zones at the periphery of the organoid, presumably corresponding to corneal regions; ** — pigmented areas of the organoid, presumably corresponding to retinal pigment epithelium (RPE) regions. Each scale division is 1 mm

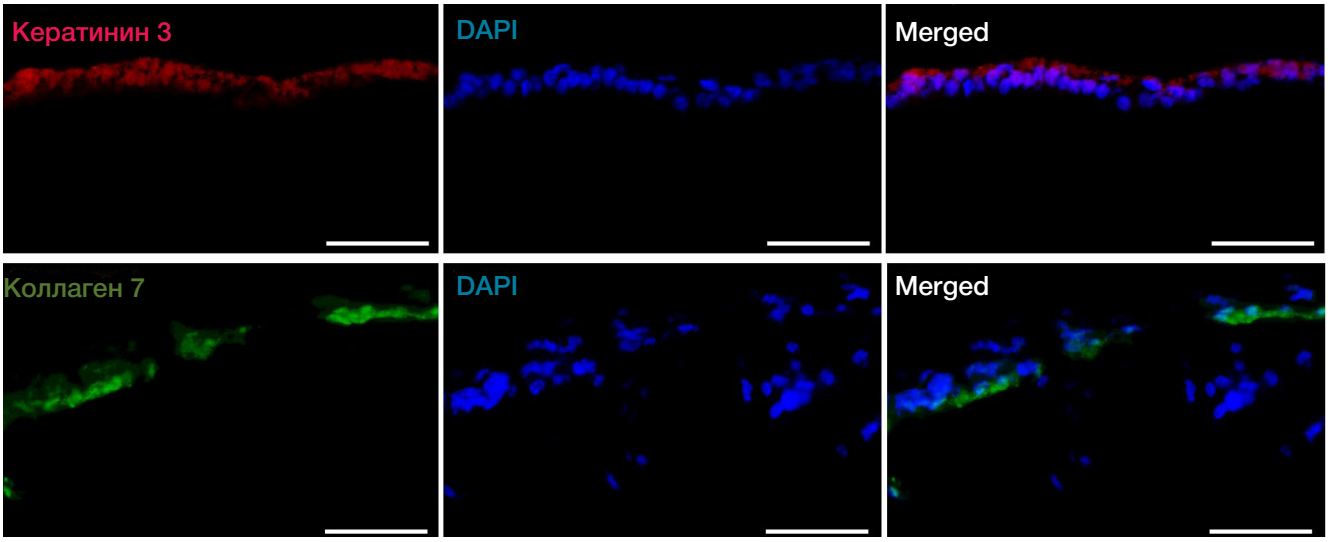


Fig. 3. Immunohistochemical staining of cryopresections of organoids on the 22nd day of differentiation. Reaction with antibodies to keratin 3 (red) and reaction with antibodies to type VII collagen (green). The cores were additionally colored with DAPI. The scale segment is 50 μm

by immunohistochemistry. In view of the corneal epithelium staining positive for the keratin markers K3, K7, and K19, we analyzed the expression levels of the corresponding corneal and conjunctival biomarkers [15].

The corneal epithelium is supported by a specialized basement membrane complex that anchors it to Bowman's layer. This attachment is mediated by a network of anchoring fibrils composed of type VII collagen and associated anchoring plaques that interact with the dense collagen matrix of Bowman's layer [16].

Figure 3 shows photographs of organoid sections that are a sphere with translucent contents bordered by cellular layers, with positive staining for markers of epithelial differentiation (K3) and basement membrane (type VII collagen). Cells positively stained for keratin 3 were observed on the periphery in the outer cell layer of the organoid. The expression of type VII collagen was seen in the underlying cell layers.

DISCUSSION

Corneal transplantation is one of the most successful organ transplantations in human beings. The orthotopic corneal allografts are used frequently (and successfully) in both humans and experimental animals because of the so-called immune privilege of the eye: any inflammatory processes is suppressed in order to preserve visual function. In case of corneal transplantation, this privilege is believed to be supported by three factors: 1) anatomical, cellular, and molecular barriers in the cornea; 2) tolerance associated with the presence of regulatory T cells and immune abnormalities in the anterior chamber of the eye; 3) immunosuppressive intraocular microenvironment [17].

We describe a protocol for differentiating functional corneal epithelium from human iPSCs in vitro. Under this protocol, some cells spontaneously form round colonies, spheroids, or embryoid bodies, which, during successive stages of the differentiation process that involves gradual change the culture medium and addition of growth factors and inhibitors of the WNT cascade, produce structures with the properties of the organoid of the eye. Our protocol was based on the methodology described in the Isla-Magrané article [18]. In this work, we also used a three-dimensional model of differentiation with forced aggregation of EB during cultivation and prevention of cell adhesion to the plastic surface. The advantages of this protocol include the possibility of co-cultivation of cells of various types, and the production of single three-dimensional models of controllable size [19]. The cells aggregate and form spheroids due to intercellular adhesion and the lack of adhesion to the culture plastic [20]. The differentiation protocol published in this paper can potentially be useful to researchers interested in eye development and/or regeneration of the eye surface, as well as specialists in the field of translational regenerative medicine.

The development of methods for the directed differentiation of iPSCs in RPE enabled some approaches allowing generation of the epithelium of the limb and cornea. Small molecules, inhibitors of the WNT/β-catenin cascade, or recombinant proteins and factors are used to produce RPE cells from iPSCs [22, 23].

When iPSC colonies differentiate under adhesive conditions, concentric SEAM (self-earned autonomous multi-zone) zones gradually form, in which cells begin to acquire different morphologies and a specific set of markers. This protocol has a distinct advantage. During cultivation, homogeneous cell types can be mechanically isolated and then sorted by flow cytometry to yield a population of progenitor cells analogous to the epithelial cells of the limb. Cells of this type can be multiplied and differentiated to form an epithelial layer expressing keratin markers 3 and 12, PAX6. The researchers confirmed the functionality of the obtained cells in an animal model of corneal epithelial dysfunction through surgical xenotransplantation. In 2024, the results of the first successful clinical trials on allogeneic transplantation of corneal epithelial cells differentiated from iPSCs using the SEAM protocol in four patients were published. Two patients suffered from limbal insufficiency syndrome, one from ocular mucosal pemphigoid, and one from toxic epidermal necrosis [24]. In all cases, after 52 weeks of follow-up, the researchers notes improved eye condition, better visual acuity, and a decrease in corneal opacity. Corneal epithelial defects, subjective symptoms, quality of life indicators, and corneal neovascularization have mostly improved or remained unchanged. Through the follow-up period, there were no serious adverse events observed, including tumor formation or clinical rejection.

Obtaining an eye organoid from iPSCs using the developed protocol allowed the detection of type VII collagen expression in the area adjacent to the basal membrane. The attachment fibrils formed by type VII collagen are an important structural element that supports the integrity of the tissue. Patients

affected by hereditary disorders involving defects in type VII collagen, such as recessive dystrophic epidermolysis bullosa, are classified as disabled from childhood due to chronic inflammation of the skin and epithelial linings of internal organs. Current clinical treatments for ophthalmological manifestations thereof, such as contact lenses, lubricants, and antibiotics, may reduce symptoms but fail to prevent corneal scarring [10].

In such cases, allogeneic transplants of the epithelium of the limb and cornea, differentiated from iPSCs of healthy donors, may be applicable for cell therapy. The creation of stem cell banks with homozygous human leukocyte antigen (HLA) cell lines can provide an effective and cost-effective resource for this type of therapy.

Autologous iPSC-based treatments can be prohibitively expensive and time-consuming. However, patient-specific iPSCs (RDEB-iPSCs) can be differentiated into eye organoids to create disease models for testing new drugs and evaluating gene therapy approaches.

CONCLUSIONS

This study describes a protocol for obtaining an organoid of an eye with a formed corneal epithelium by differentiating iPSCs. The development of various methods for the generation of corneal and limb epithelial tissues contributes to the development of regenerative medicine in ophthalmology. Although a single type of corneal transplant is unlikely to provide a universal solution, combining different approaches may help address the shortage of donor corneas, support the development of bioengineered matrices — implantable with or without cells — to stimulate tissue repair and regeneration, and enable new treatments for diseases that cannot be cured with currently available methods.

References

1. Porth JM, Deiotte E, Dunn M, Bashshur R. A Review of the Literature on the Global Epidemiology of Corneal Blindness. Cornea. 2019; 38 (12): 1602–9.
2. Gain P, Jullienne R, He Z, et al. Global Survey of Corneal Transplantation and Eye Banking. JAMA Ophthalmol. 2016; 134 (2): 167–73.
3. Hernández J, Panadero-Medianero C, Arrázola MS, Ahumada M. Mimicking the Physicochemical Properties of the Cornea: A Low-Cost Approximation Using Highly Available Biopolymers. Polymers (Basel). 2024; 16 (8): 1118.
4. Griffith M, Polisetti N, Kuffova L, Gallar J, Forrester J, Vemuganti GK, Fuchsluger TA. Regenerative approaches as alternatives to donor allografting for restoration of corneal function. Ocul Surf. 2012; 10 (3): 170–83.
5. Ludwig PE, Lopez MJ, Czyz CN. Embryology, Eye Malformations. [Updated 2023 Apr 3]. In: StatPearls [Internet]. Treasure Island (FL): StatPearls Publishing; 2025 Jan [cited 2025 Nov 19]. Available from: https://www.ncbi.nlm.nih.gov/books/NBK482496/#.
6. Hirami Y, Mandai M, Sugita S, Maeda A, Maeda T, Yamamoto M, et al. Safety and stable survival of stem-cell-derived retinal organoid for 2 years in patients with retinitis pigmentosa. Cell Stem Cell. 2023; 30 (12): 1585–1596.
7. Hirayama M, Hatou S, Nomura M, Hokama R, Hirayama OI, Inagaki E, et al. A first-in-human clinical study of an allogenic iPSC-derived corneal endothelial cell substitute transplantation for bullous keratopathy. Cell Rep Med. 2025; 6 (1): 101847.
8. Haritonov AE, Surdina AV, Lebedeva OS, Bogomazova AN, Lagarkova MA. Vozmozhnosti ispol'zovaniya plyuripotentnyh stvolovyh kletok dlya vosstanovleniya povrezhdennogo pigmentnogo epiteliya setchatki glaza. Acta Naturae. 2018; 10 (3): 30–39. Russian.
9. Chandran C, Santra M, Rubin E, Geary ML, Yam GH. Regenerative Therapy for Corneal Scarring Disorders. Biomedicines. 2024; 12 (3): 649.
10. Tong L, Hodgkins PR, Denyer J, Brosnahan D, Harper J, Russell-Eggitt I, et al. The eye in epidermolysis bullosa. Br J Ophthalmol. 1999; 83 (3) :323–6.
11. Hayashi R, Ishikawa Y, Ito M, Kageyama T, Takashiba K, Fujioka T, et al. Generation of corneal epithelial cells from induced pluripotent stem cells derived from human dermal fibroblast and corneal limbal epithelium. PLoS One. 2012; 7 (9): e45435.
12. Hongisto H, Ilmarinen T, Vattulainen M, Mikhailova A, Skottman H. Xeno- and feeder-free differentiation of human pluripotent stem cells to two distinct ocular epithelial cell types using simple modifications of one method. Stem Cell Res Ther. 2017; 8 (1): 291.
13. Ahmad S, Stewart R, Yung S, Kolli S, Armstrong L, Stojkovic M, et al. Differentiation of human embryonic stem cells into corneal epithelial-like cells by in vitro replication of the corneal epithelial stem cell niche. Stem Cells. 2007; 25 (5): 1145–55.
14. Lee HS, Mok J, Joo CK. Bone Morphogenetic Protein 4 (BMP4) enhances the differentiation of human induced pluripotent stem cells into limbal progenitor cells. Curr Issues Mol Biol. 2021; 43 (3): 2124–34.
15. Poli M, Burillon C, Auxenfans C, Rovere MR, Damour O. Immunocytochemical Diagnosis of Limbal Stem Cell Deficiency: Comparative Analysis of Current Corneal and Conjunctival Biomarkers. Cornea. 2015; 34 (7): 817–23.
16. Forrester JV, Dick AD, McMenamin PG, Roberts F, Pearlman E, editors. The Eye. 2016; p. 1–102.
17. Hori J, Yamaguchi T, Keino H, Hamrah P, Maruyama K. Immune privilege in corneal transplantation. Prog Retin Eye Res. 2019; 72: 100758.
18. Isla-Magrané H, Veiga A, García-Arumí J, Duarri A. Multiocular organoids from human induced pluripotent stem cells displayed retinal, corneal, and retinal pigment epithelium lineages. Stem Cell Res Ther. 2021; 12 (1): 581.
19. Chen X, Sun G, Tian E, Zhang M, Davtyan H, Beach TG, et al. Modeling Sporadic Alzheimer's Disease in Human Brain Organoids under Serum Exposure. Adv Sci (Weinh). 2021; 8 (18): e2101462.
20. Sakalem ME, De Sibio MT, da Costa FADS, de Oliveira M. Historical evolution of spheroids and organoids, and possibilities of use in life sciences and medicine. Biotechnol J. 2021; 16 (5): e2000463.
21. Maliszewska-Olejniczak K, Brodaczewska KK, Bielecka ZF, Solarek W, Kornakiewicz A, Szczylik C, Porta C, et al. Development of extracellular matrix supported 3D culture of renal cancer cells and renal cancer stem cells. Cytotechnology. 2019; 71 (1): 149–63.
22. Buchholz DE, Pennington BO, Croze RH, Hinman CR, Coffey PJ, Clegg DO. Rapid and efficient directed differentiation of human pluripotent stem cells into retinal pigmented epithelium. Stem Cells Transl Med. 2013; 2 (5): 384–93.
23. Zhu J, Reynolds J, Garcia T, Cifuentes H, Chew S, Zeng X, et al. Generation of Transplantable Retinal Photoreceptors from a Current Good Manufacturing Practice-Manufactured Human Induced Pluripotent Stem Cell Line. Stem Cells Transl Med. 2018; 7 (2): 210–19.
24. Soma T, Oie Y, Takayanagi H, Matsubara S, Yamada T, Nomura M, Yoshinaga Y, et al. Induced pluripotent stem-cell-derived corneal epithelium for transplant surgery: a single-arm, open-label, first-in-human interventional study in Japan. Lancet. 2024; 404 (10466): 1929–39.

Литература

1. Porth JM, Deiotte E, Dunn M, Bashshur R. A Review of the Literature on the Global Epidemiology of Corneal Blindness. Cornea. 2019; 38 (12): 1602–9.
2. Gain P, Jullienne R, He Z, et al. Global Survey of Corneal Transplantation and Eye Banking. JAMA Ophthalmol. 2016; 134 (2): 167–73.
3. Hernández J, Panadero-Medianero C, Arrázola MS, Ahumada M. Mimicking the Physicochemical Properties of the Cornea: A Low-Cost Approximation Using Highly Available Biopolymers. Polymers (Basel). 2024; 16 (8): 1118.
4. Griffith M, Polisetti N, Kuffova L, Gallar J, Forrester J, Vemuganti GK, Fuchsluger TA. Regenerative approaches as alternatives to donor allografting for restoration of corneal function. Ocul Surf. 2012; 10 (3): 170–83.
5. Ludwig PE, Lopez MJ, Czyz CN. Embryology, Eye Malformations. [Updated 2023 Apr 3]. In: StatPearls [Internet]. Treasure Island (FL): StatPearls Publishing; 2025 Jan [cited 2025 Nov 19]. Available from: https://www.ncbi.nlm.nih.gov/books/NBK482496/#.
6. Hirami Y, Mandai M, Sugita S, Maeda A, Maeda T, Yamamoto M, et al. Safety and stable survival of stem-cell-derived retinal organoid for 2 years in patients with retinitis pigmentosa. Cell Stem Cell. 2023; 30 (12): 1585–1596.
7. Hirayama M, Hatou S, Nomura M, Hokama R, Hirayama OI, Inagaki E, et al. A first-in-human clinical study of an allogenic iPSC-derived corneal endothelial cell substitute transplantation for bullous keratopathy. Cell Rep Med. 2025; 6 (1): 101847.
8. Харитонов А. Е., Сурдина А. В., Лебедева О. С., Богомазова А. Н., Лагарькова М. А. Возможности использования плюрипотентных стволовых клеток для восстановления поврежденного пигментного эпителия сетчатки глаза. Acta Naturae. 2018; 10 (3): 30–39.
9. Chandran C, Santra M, Rubin E, Geary ML, Yam GH. Regenerative Therapy for Corneal Scarring Disorders. Biomedicines. 2024; 12 (3): 649.
10. Tong L, Hodgkins PR, Denyer J, Brosnahan D, Harper J, Russell-Eggitt I, et al. The eye in epidermolysis bullosa. Br J Ophthalmol. 1999; 83 (3) :323–6.
11. Hayashi R, Ishikawa Y, Ito M, Kageyama T, Takashiba K, Fujioka T, et al. Generation of corneal epithelial cells from induced pluripotent stem cells derived from human dermal fibroblast and corneal limbal epithelium. PLoS One. 2012; 7 (9): e45435.
12. Hongisto H, Ilmarinen T, Vattulainen M, Mikhailova A, Skottman H. Xeno- and feeder-free differentiation of human pluripotent stem cells to two distinct ocular epithelial cell types using simple modifications of one method. Stem Cell Res Ther. 2017; 8 (1): 291.
13. Ahmad S, Stewart R, Yung S, Kolli S, Armstrong L, Stojkovic M, et al. Differentiation of human embryonic stem cells into corneal epithelial-like cells by in vitro replication of the corneal epithelial stem cell niche. Stem Cells. 2007; 25 (5): 1145–55.
14. Lee HS, Mok J, Joo CK. Bone Morphogenetic Protein 4 (BMP4) enhances the differentiation of human induced pluripotent stem cells into limbal progenitor cells. Curr Issues Mol Biol. 2021; 43 (3): 2124–34.
15. Poli M, Burillon C, Auxenfans C, Rovere MR, Damour O. Immunocytochemical Diagnosis of Limbal Stem Cell Deficiency: Comparative Analysis of Current Corneal and Conjunctival Biomarkers. Cornea. 2015; 34 (7): 817–23.
16. Forrester JV, Dick AD, McMenamin PG, Roberts F, Pearlman E, editors. The Eye. 2016; p. 1–102.
17. Hori J, Yamaguchi T, Keino H, Hamrah P, Maruyama K. Immune privilege in corneal transplantation. Prog Retin Eye Res. 2019; 72: 100758.
18. Isla-Magrané H, Veiga A, García-Arumí J, Duarri A. Multiocular organoids from human induced pluripotent stem cells displayed retinal, corneal, and retinal pigment epithelium lineages. Stem Cell Res Ther. 2021; 12 (1): 581.
19. Chen X, Sun G, Tian E, Zhang M, Davtyan H, Beach TG, et al. Modeling Sporadic Alzheimer's Disease in Human Brain Organoids under Serum Exposure. Adv Sci (Weinh). 2021; 8 (18): e2101462.
20. Sakalem ME, De Sibio MT, da Costa FADS, de Oliveira M. Historical evolution of spheroids and organoids, and possibilities of use in life sciences and medicine. Biotechnol J. 2021; 16 (5): e2000463.
21. Maliszewska-Olejniczak K, Brodaczewska KK, Bielecka ZF, Solarek W, Kornakiewicz A, Szczylik C, Porta C, et al. Development of extracellular matrix supported 3D culture of renal cancer cells and renal cancer stem cells. Cytotechnology. 2019; 71 (1): 149–63.
22. Buchholz DE, Pennington BO, Croze RH, Hinman CR, Coffey PJ, Clegg DO. Rapid and efficient directed differentiation of human pluripotent stem cells into retinal pigmented epithelium. Stem Cells Transl Med. 2013; 2 (5): 384–93.
23. Zhu J, Reynolds J, Garcia T, Cifuentes H, Chew S, Zeng X, et al. Generation of Transplantable Retinal Photoreceptors from a Current Good Manufacturing Practice-Manufactured Human Induced Pluripotent Stem Cell Line. Stem Cells Transl Med. 2018; 7 (2): 210–19.
24. Soma T, Oie Y, Takayanagi H, Matsubara S, Yamada T, Nomura M, Yoshinaga Y, et al. Induced pluripotent stem-cell-derived corneal epithelium for transplant surgery: a single-arm, open-label, first-in-human interventional study in Japan. Lancet. 2024; 404 (10466): 1929–39.

DEVELOPMENT AND ASSESSMENT OF THE BONE ALLOGRAFT-BASED MATERIAL FOR DLP 3D PRINTING

Bilyalov AR ✉, Chugunov SS, Akhatov ISh, Tikhonov AA, Shangina OR, Pavlov VN, Danilko KV, Galautdinov MF, Akbashev VN

Bashkir State Medical University, Ufa, Russia

The use of allogenic bone material as a ceramic filler for DLP printing makes it possible to obtain personalized complex-shaped implants combining the matrix biomimetic nature with the additive technology benefits. The study aimed to assess the possibility of using the calcined cortical bone allograft powder as part of photopolymerizable suspension for DLP printing and producing bioceramics with the characteristics comparable to that of synthetic hydroxyapatite by sintering. The bone allograft was subjected to multi-stage specialized treatment involving complete removal of cells with preservation of the intercellular matrix and collagen fiber structure. The calcined medical allograft was crushed, introduced into a photopolymerizable matrix, and used for DLP printing of the samples that were further sintered and analyzed by X-ray diffraction and energy-dispersive spectroscopy methods before and after additive production. The sintered material specific gravity was 81.5%, compressive strength — 75.8 MPa, tensile strength — 12 MPa, Young's modulus — 3.08 GPa, and Vickers hardness — 0.55 GPa, which was within the range of values for porous hydroxyapatite. After DLP printing and sintering the sample phase and elemental composition did not change considerably compared to the source calcined material. The calcined bone allograft powder is suitable for preparing photopolymerizable suspensions and subsequent DLP printing of ceramic samples without deteriorating the material phase and chemical stability. The resulting mechanical properties make it possible to consider this allogenic bone material as a promising candidate for production of personalized implants with sophisticated geometry.

Keywords: hydroxyapatite, 3D printing, bioceramics, allograft, alloplant, biomedical application, firing, ceramics

Funding: the study was supported by the Russian Science Foundation grant No. 23-15-20042.

Author contribution: Bilyalov AR, Chugunov SS — study planning, literature review, data interpretation, manuscript writing; Akhatov ISh — study planning, data interpretation, manuscript writing; Tikhonov AA — study planning, literature review, data acquisition, analysis, and interpretation; Shangina OR — study planning, data analysis and interpretation; Pavlov VN — study planning; Danilko KV — study planning, data acquisition, analysis, and interpretation; Galautdinov MF — data acquisition; Akbashev VN — literature review.

✉ **Correspondence should be addressed:** Azat R. Bilyalov
Lenina, 3, Ufa, 450008, Russia; azat.bilyalov@gmail.com

Received: 03.11.2025 **Accepted:** 29.11.2025 **Published online:** 18.12.2025

DOI: 10.24075/brsmu.2025.068

Copyright: © 2025 by the authors. **Licensee:** Pirogov University. This article is an open access article distributed under the terms and conditions of the Creative Commons Attribution (CC BY) license (https://creativecommons.org/licenses/by/4.0/).

РАЗРАБОТКА И ИССЛЕДОВАНИЕ МАТЕРИАЛА НА ОСНОВЕ КОСТНОГО АЛЛОТРАНСПЛАНТАТА ДЛЯ DLP-3D-ПЕЧАТИ

А. Р. Билялов ✉, С. С. Чугунов, И. Ш. Ахатов, А. А. Тихонов, О. Р. Шангина, В. Н. Павлов, К. В. Данилко, М. Ф. Галаутдинов, В. Н. Акбашев

Башкирский государственный медицинский университет, Уфа, Россия

Использование аллогенного костного материала как керамического наполнителя для DLP-печати позволяет получать индивидуализированные имплантаты сложной формы, совмещающие биомиметичную природу матрицы с преимуществами аддитивных технологий. Целью работы было оценить возможность использования прокаленного порошка кортикального костного аллотрансплантата в составе фотополимеризуемой суспензии для DLP-печати и получения после спекания биокерамики с характеристиками, сопоставимыми с синтетическим гидроксиапатитом. Костный аллотрансплантат подвергали многоэтапной специализированной обработке с полным удалением клеток при сохранении структуры межклеточного матрикса и коллагеновых волокон. Прокаленный медицинский аллотрансплантат измельчали, вводили в фотополимеризуемую матрицу и использовали для DLP-печати образцов, которые затем спекали и анализировали методами рентгеновской дифракции и энергодисперсионной спектроскопии до и после аддитивного производства. Относительная плотность спеченного материала составила 81,5%, прочность на сжатие — 75,8 МПа, прочность на растяжение — 12 МПа, модуль Юнга — 3,08 ГПа и твердость по Виккерсу — 0,55 ГПа, что находится в диапазоне значений для пористого гидроксиапатита. Фазовый и элементный состав образцов после DLP-печати и спекания не претерпевал существенных изменений по сравнению с исходным прокаленным материалом. Прокаленный порошок костного аллотрансплантата пригоден для приготовления фотополимеризуемых суспензий и последующей DLP-печати керамических образцов без ухудшения фазовой и химической стабильности материала. Полученные механические свойства позволяют рассматривать данный аллогенный костный материал в качестве перспективного кандидата для изготовления индивидуализированных имплантатов сложной геометрии.

Ключевые слова: гидроксиапатит, 3D-печать, биокерамика, аллографт, аллоплант, биомедицинское применение, обжиг, керамика

Финансирование: работа выполнена при поддержке гранта Российского научного фонда № 23-15-20042.

Вклад авторов: А. Р. Билялов, С. С. Чугунов — планирование исследования, анализ литературы, интерпретация данных, подготовка рукописи; И. Ш. Ахатов — планирование исследования, интерпретация данных, подготовка рукописи; А. А. Тихонов — планирование исследования, анализ литературы, сбор, анализ, интерпретация данных; О. Р. Шангина — планирование исследования, анализ, интерпретация данных; В. Н. Павлов — планирование исследования; К. В. Данилко — планирование исследования, сбор, анализ, интерпретация данных; М. Ф. Галаутдинов — сбор данных; В. Н. Акбашев — анализ литературы.

✉ **Для корреспонденции:** Азат Ринатович Билялов
ул. Ленина, д. 3, г. Уфа, 450008, Россия; azat.bilyalov@gmail.com

Статья получена: 03.11.2025 **Статья принята к печати:** 29.11.2025 **Опубликована онлайн:** 18.12.2025

DOI: 10.24075/vrgmu.2025.068

Авторские права: © 2025 принадлежат авторам. **Лицензиат:** РНИМУ им. Н. И. Пирогова. Статья размещена в открытом доступе и распространяется на условиях лицензии Creative Commons Attribution (CC BY) (https://creativecommons.org/licenses/by/4.0/).

The annual number of trauma and orthopedic surgical procedures in Russia exceeded 1.2 million by 2023. The most popular treatment methods include the use of orthopedic bone cement and plastic material for treatment of bone injuries. In the field of orthobiologic procedures, bone grafts and substitutes made up the largest share in 2022 [1].

Autografts are commonly used as effective implants for substitution of bone defects [2], especially in orthopedic and dental surgery. Autografts obtained from the patient, usually from his/her iliac crest, show high biocompatibility, low risk of rejection, and considerable osteogenic potential [3]. When assessing the autograft strengths and weaknesses, allografts turn out to be a promising alternative [4]. Allografts obtained from donors, usually cadaver ones, eliminate the need for additional surgical aggression, thereby reducing the risk of complications. Furthermore, the use of allografts can reduce both surgery and anesthesia time, since there is no need for additional surgical intervention. Moreover, the allograft size and shape can be modified for the implantation area long before the operation, in the preoperative planning phase.

However, allografts are not without drawbacks. Practically, the complexity of creating volumetric bone blocks to match the size of the bone defect is the problem associated with using allografts [5].

The importance of using the DLP ceramic printing technology for medical purposes results from the possibility of creating complex-shaped and functional biocompatible products for implants and reconstructive surgery. DLP provides high processing resolution and precision, which are critical for products made of bioinert or bioactive ceramic materials. This makes it possible to produce porous structures mimicking the bone tissue that contribute to osseointegration and biological function restoration [6].

Traditional ceramic production methods are hampered by the complexity of processing and shaping, while DLP printing allows one to obtain complex geometric shapes without significant expenditure of time and materials. Modern research also reports the importance of optimizing rheological properties of photopolymer suspensions for successful printing and achieving the required mechanical characteristics of products [7].

The ceramic materials used in DLP, such as hydroxyapatite, aluminum oxide, and zirconium oxide, show excellent biocompatibility and bioinertness, which reduce the risk of rejection and inflammatory responses in patients. The technology allows for control of the surface microstructure, which improves the implant adhesion to tissues [6].

The DLP printing works well with other additive production and post-processing methods, thereby expanding the possibilities for the creation of multifunctional and composite materials for medical use [8].

In this study we assess applicability of the digital light processing (DLP)-based additive production method to the hydroxyapatite material obtained from cortical bones of the cadaver bone allograft. As far as we know, no studies devoted specifically to additive production of ceramic products using human bone allografts have been presented in the literature to date.

The material used in this study represents the commercially available medical bone allograft in the form of blocks (Alloplant® allografts for surgery according to MS 9398-001-04537642-2011; registration certificate for a medical product FSR 2011/12012; manufacturer — Bashkir State Medical University, Russia). This commercially available material is widely used in medical practice; more than 2,000 orthopedic surgeries are performed in medical clinics every year.

The study was initiated in response to requests from practicing surgeons concerning the development of advanced technologies for production of allografts. The main purpose of using this allograft material in 3D printing is to achieve high precision of geometry parameters with deviations within hundreds microns, allowing for adaptation of products to the irregularly shaped bone defects while maintaining high biomedical properties.

The study aimed to assess applicability of the digital light processing (DLP)-based additive production technology for forming high-precision complex-shaped implants made of the bone allograft-derived material.

METHODS

Allograft material processing and photopolymerizable suspension preparation

The cadaver bone material is through a number of chemical treatment and radiation sterilization procedures to remove immunogenic components and induce lysis of membrane tissues; collagen and some elements of the amorphous bone matrix are preserved [9]. The study design is presented in Fig. 1.

The bone blocks sized 0.5–6 cm were calcined in the Kittec CLL15 laboratory kiln (Kittec, Germany) at a temperature of 900 °C for 5 h in order to remove organic content. There were yellowish and grayish deposits on the surface of approximately 15% of the calcined blocks. Both clean calcined blocks and blocks with deposits were analyzed using the Jeol JSM-6390LV scanning electron microscope (JEOL, Japan) equipped with the energy-dispersive X-ray analyzer (EX-230 BU).

After calcination the allograft material was through the two-stage grinding procedure involving the zirconium grinding cups and zirconium balls in the Retsch PM400 planetary ball mill (Retsch, Germany). Stage 1 aimed to grind the allograft blocks into the millimeter-sized powder. Stage 2 aimed to grind into particles sized 1–5 μm. Such grinding included wet grinding in isopropanol (IPA). Then the ground material was dried in the Binder ED56 drying oven (Binder GmbH, Germany) at 115 °C for 2 h to eliminate the remaining IPA.

After stage 1 of grinding the powder fraction was obtained using the laboratory sieves with the mesh size of 400 μm and 315 μm. Sample A consisted of the 315–400 μm powder fraction. Sample B was obtained from the resulting powder after stage 2 of grinding.

The micron-sized allograft powder was mixed with the Dysperbyk-180 dispersing additive (BYK GmbH, Germany) at a mass concentration of 2% in the Retsch PM400 planetary ball mill using the 8-mm zirconium balls with the speed of 200 rpm for 1 h. To produce a photopolymerizable suspension, the CB2-DLP-GM/2 organic binder (Vundertech LLC, Russia) was mixed with the E104 dye at a mass concentration of 0.24% and then added to the dispersed allograft powder to achieve the powder load with the mass concentration of 68.9%, which corresponded to the concentration of 42.6% v/v. The dye was included to minimize light scattering by ceramic particles during 3D printing. Finally, the suspension was homogenized in the Retsch PM400 planetary ball mill using the 20-mm zirconium balls with the speed of 200 rpm for 5 h.

Tesing the photopolymerizable suspension and 3D printing operations

All the tests involving the photopolymerizable suspension were conducted using the Creality Mage Pro 8K DLP 3D printer (Creality, China).

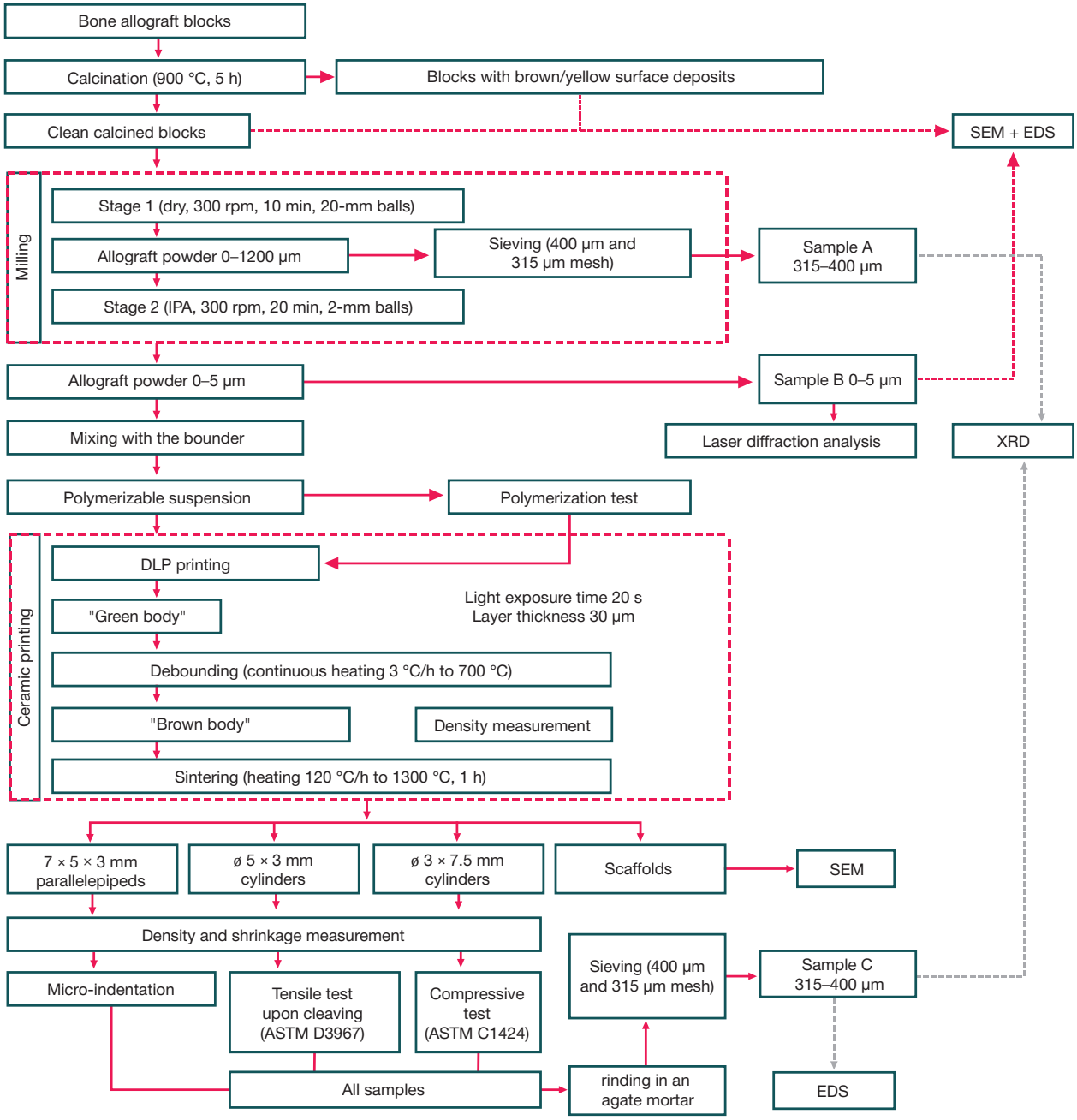


Fig 1. Study design

First, the syspension polymerization effectiveness was assessed. The square objects sized 1 × 1 cm were polymerized at different light energy of 0.12, 0.2, 0.24, 0.8, and 16 J/cm^2, which corresponded to the exposure time of 15, 25, 30, 100, and 2000 s, respectively. In each case, the 2 mm-thick suspension layer was placed in the printer bath, and the experiment was repeated four times. After polymerization the polymerized layer thickness was measured using the Interapid thickness gauge (Schut, Switzerland) with an accuracy of 0.001 mm. Such evaluation yielded two important results: a) confirmation that the allograft-based suspension was suitable for DLP printing; b) determination of the relationship between light energy and polymerization depth.

Optimal 3D printing parameters were determined based on this relationship: exposure time of 20 s and layer thickness of 30 μm. 3D printing was conducted in two series. The first series involved production of the cylinders sized 3–7.5 mm for mechanical compressive testing (ASTM C1424) [10] and X-ray diffraction analysis (ISO 10993-14) [11] and parallelepipeds sized 7 × 5 × 3 mm for measurement of the density, shrinkage during sintering, porosity, Vickers hardness (ISO 10993-14).

The second series involved evaluation of the possibility of printing complex ceramic structures in the form of a mesh or scaffold. After 3D printing all the objects were subjected to thermal debounding in the Kittec CLL15 kiln through heating to 700 °C with the rate of 3 °C/h in air. The object size was measured using the Topex 31C628 caliper (Group Topex, Poland) with an accuracy of 0.02 mm, while mass measurement was performed using the AND HR250-AZG laboratory scales (AD Company, Japan) with an accuracy of 0.001 g. This measurement allowed us to accurately estimate the samples' density and porosity at the non-sintered product (raw material) stage.

After the bounder removal (debounding) the samples showed porosity of 58% and were characterized as loosely consolidated and mechanically weak. These were sintered in

the Kittec CLL15 kiln in air at a temperature of 1300 °C with the heating rate of 120 °C/h and subsequently conditioned for 1 h.

After the end of testing physical and mechanical characteristics of the sintered allograft material the previously fractioned samples, cylinders and parallelepipeds, were grinded in the agate mortar and sieved to obtain the 315–400 μm powdery fraction. Sample C was collected from the resulting powder.

Laboratory assessment of the material properties

Assessment of the non-sintered allograft material

The energy-dispersive spectroscopy was used to assess chemical composition of the calcined allograft blocks, specifically of the clean fragments and yellowish and grayish surface deposits. This method was also used for Sample B to assess chemical composition of the target powdery material for 3D printing. It was expected that the Sample B composition would reflect the effects of calcination and grinding, including potential chemical activation or degradation of chemical compounds. The powdery sample was evenly distributed over the area of 1 × 1 cm of the sample holder in the scanning electron microscope (SEM) and examined at two different sites using the voltage of 20 kV and the exposure time of 120 s.

The particle size distribution in Sample B was assessed using the Fritsch Analysette 22 NanoTec laser particle sizer (Fritsch GmbH, Idar-Oberstein, Germany) to make sure that most particles in the powder were smaller than 10 μm, in accordance with the requirements of the digital light processing (DLP) technique.

Assessment of physical and mechanical properties of the additively manufactured sintered allograft material

The density and porosity of green, calcined, and sintered objects were calculated based on the measured size and mass. Measurement was performed for each object individually. The size was measured using the Topex 31C628 caliper, while mass measurement was performed using the AND HR250-AZG scales. The relative density was calculated based on the hydroxyapatite theoretical density (3.16 g/cm^3).

The coefficients of shrinkage due to thermal sintering were calculated by assessing changes in size between the object's green and sintered states. It is important to note that the shrinkage coefficients in the X, Y, and Z directions were different due to the 3D printing anisotropic nature.

Hardness of the parallelepiped objects was assessed using the Nanovea PB1000 mechanical tester (Nanovea, USA) equipped with the Vickers hardness tester. The compressive and tensile tests upon cleaving were performed using the Instron 5969 dual column testing system (Instron, USA). Compressive tests were compliant with the ASTM C1424 standards, and the test samples were cylinders sized 3–7.5 mm. These samples were produced in accordance with the X2 chapter of the ASTM C1424 test standard [10], but these were proportionally reduced in size by 40%. Evolution of the two-dimentional deformation field during loading was recorded using the Vic-3D Digital Image Correlation (DIC) measurement system (Correlated Solutions Inc., USA).

Parameters of the sintered allograft material tension were obtained from the tensile tests upon cleaving conducted in accordance with ASTM D3967.

The additively manufactured sintered scaffold was tested for potential structural artifacts using the Helios G4 PFIB ThermoFisher Scientific scanning electron microscope (ThermoFisher Scientific, USA).

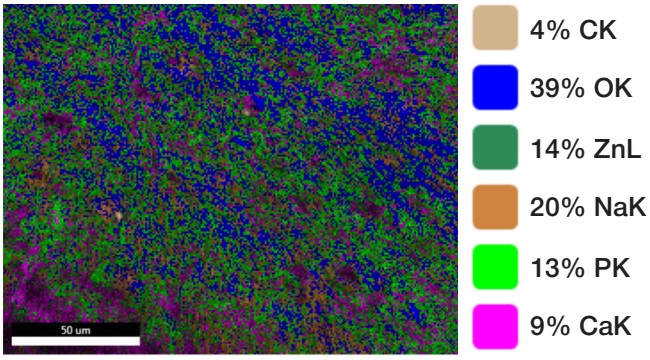


Fig. 2. Results of the EDS analysis of colored deposits on the surface of calcined allografts: distribution of chemical elements across the yellowish deposit area, several colors of some compounds correspond to the same set of chemical components appearing in different orders in the EDS results, for example Ca/P/O/Na/Zn or Ca/P/O/Zn/Na

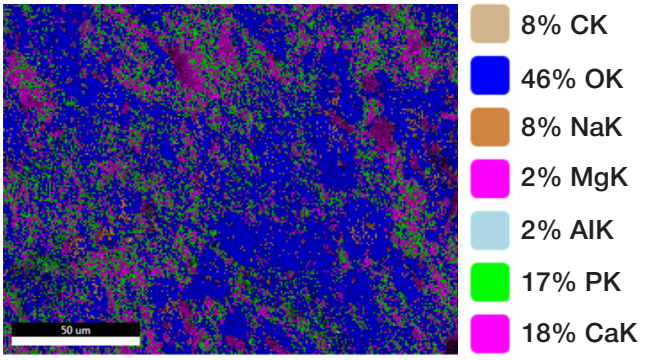


Fig. 3. Results of the EDS analysis of the surface of the calcined allograft with no identifiable deposits: distribution of chemical elements across the allograft area. Several colors of some compounds correspond to the same set of chemical components appearing in different orders in the EDS results, for example Ca/P/O/C or Ca/C/P/O

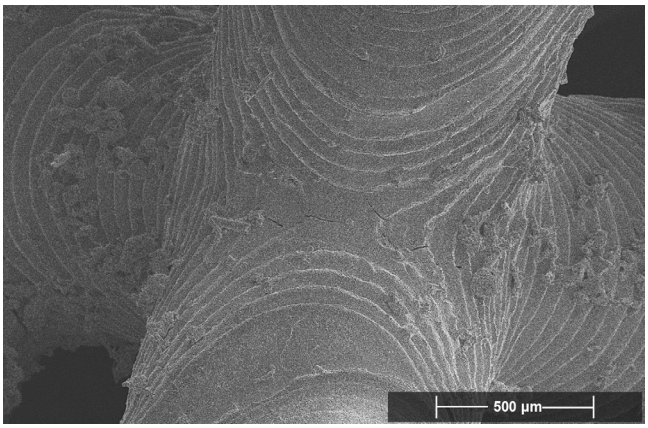


Fig. 4. Allograft-derived 3D-printed complex-shaped sintered scaffold. Convex and concave areas of the object and the layered structure are visible; microcracks in the layered structure of the object emerged during heat treatment

Assessment of evolution of the allograft phase in additive manufacturing processes

Assessment of the material phase evolution at various stages of the production process was performed for samples A, B, and C using the Guinier camera coupled with the Huber G670 X-ray diffractometer (Huber Diffraktionstechnik GmbH Co. KG, Germany). Powdery samples were applied on the Mylar film using acetone before transfer for testing. Measurement was performed using the Ge (111) curved monochromator and the image plate detector using CoKα1 (λ = 1.78892 Å). The assessed 2θ range was 4–100° with the 0.01° angular step.

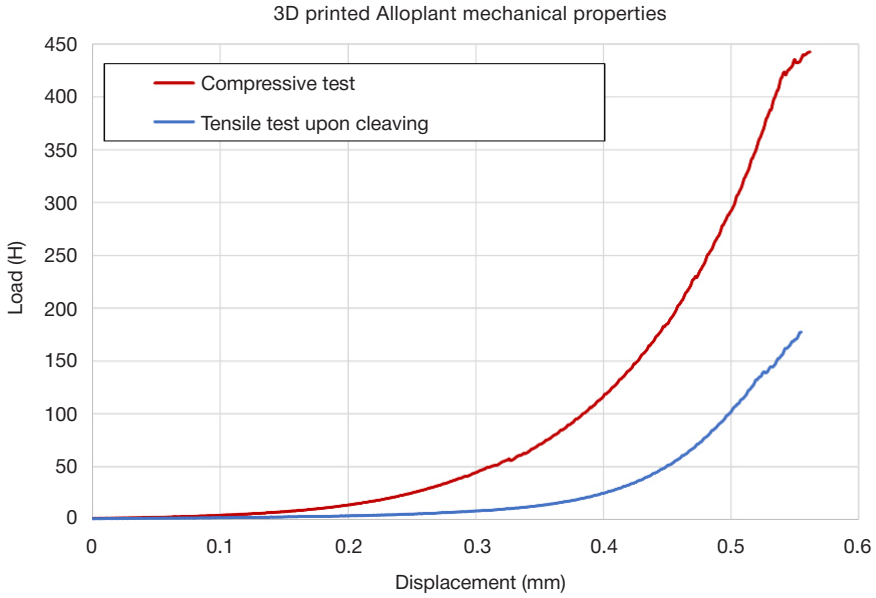


Fig. 5. Mechanical behavior of the 3D-printed allograft material sintered at 1300 — during the mechanical compressive test (6 samples) and tensile test upon cleaving (6 samples)

The analysis of the X-ray diffraction (XRD) testing results was conducted using the ICDD PDF-2 database (The International Centre for Diffraction Data Powder Diffraction File-2). The XRD testing results for samples A, B, and C were compared to assess the impact of the material grinding and heat treatment.

RESULTS

Assessment of the non-sintered allograft material

Calcination of the allograft bulk samples eliminates residual organic content and ethanol from the allograft material yielding the dry, brittle ceramic matrix. The mass loss during calcination was 41.9%.

In our analysis of the processed allograft bulk samples, about 15% of bone blocks showed visible surface deposits. These deposits included the zinc-rich yellowish substances and the grayish matter containing a considerable amount of carbon. Some yellowish deposits also showed traces of the grayish matter. Other samples looked clean and white, with no visible signs of deposits.

The analysis of the deposit chemical composition by EDS revealed high zinc concentrations, probably in the form of yellow-brown hopeite crystals, in the yellowish deposits (Fig. 2). The analysis revealed the calcium, phosphorus, oxygen, sodium and zinc atoms, which together accounted for up to 82% of the area examined. The remaining 18% included similar chemical components along with additional carbon atoms, possibly indicating a limited amount of soot formed from the decomposition of organic matter.

Significant amounts of carbon, probably in the form of soot, were found in the greyish deposits. The EDS results showed that there were no detectable calcium atoms in these grayish areas, and 84% of the area analyzed also contained no phosphorus.

The EDS analysis of visually clean calcined allograft samples revealed atoms of calcium, phosphorus, and oxygen in all the areas examined. Up to 93% of these areas were still covered with a thin layer of carbon deposits, while 27% contained sodium atoms (Fig. 3). It was impossible to accurately determine the Ca/P ratio based on the EDS data on the calcined sample surfaces, since during thermal decomposition the organic matter was likely to diffuse through the porous structure of the inorganic matrix causing uneven distribution of elements across the surface.

The scanning electron microscopy (SEM) has shown that the calcined allograft consists of the tightly packed grains of calcium phosphate ceramics sized 130 nm–2.2 μm. The grains have a rounded morphology typical for sintered ceramics.

After calcination the allograft organic content decomposed, which increased fragility and made grinding easier. At the first stage the calcined bone was ground to powder with the particle size below 1.2 mm and sieved through the 1200 μm sieve. At the second stage powder with the particle size 0–5 μm was obtained. According to the laser diffractometry results, the particle size is 300 nm–5 μm, the average value is 2.57 μm. The secondary peak of the distribution (5–25 μm) is due to agglomerates of small particles, which is confirmed by SEM. Such agglomerates do not interfere with DLP processes, as these are destroyed during the suspension preparation.

Assessment of physical and mechanical properties of the additively manufactured sintered allograft material

Based on polymerization tests of the photopolymerizable suspension we determined the relationship between light energy and polymerization depth. According to the method by Jacobs [12], the critical energy required for effective polymerization is Ec = 3.51 mJ/cm^2, which is in line with the capabilities of the 3D printer used. The minimum exposure time ensuring polymerization was determined as 15 s (layer thickness 122 μm), but such samples were soft and unstable. With the 20 s exposure, solid and durable “green bodies” without defects were produced. Simple-shaped objects and scaffolds were successfully printed by the DLP method, cleared of binder, and sintered.

The scaffold was examined by SEM (Fig. 4). The layered structure was clearly visible. During heat treatment microcracks with the holes sized about 10–15 μm emerged in the contact zones of the protruding structures, which suggests the need to optimize sintering. Internal surfaces of the cracks contained the densely packed grains sized 5–10 μm, while the source powder had the 0.3–5 μm grains, which suggests rearrangement and growth of grains during sintering.

The lack of nanoporous voids in the corners of conjugated grains, typical for high-temperature sintering, is noteworthy. The material contains intergranular microcracks, which can form a porous system in the absence of nanopores. With the relative density of 82%, the expected porosity of 19% is consistent with the observations. Porosity results from intergranular microcracks and large voids between clusters of grains, which is typical for low-density materials.

The allograft compaction during sintering resulted in reduction of the linear dimensions and geometric features. The average linear shrinkage of the allograft was 24%. Such anisotropic shrinkage typical for 3D printing can be associated with uneven application of the source material both inside and outside the layer formation plane.

The EDS results obtained for Sample C give an idea about the ratio of calcium and phosphorus (Ca/P), since these cover the data on both surface and bulk of material. The EDS analysis shows that the main sintered allograft material components are calcium (Ca), phosphorus (P), and oxygen (O), as well as trace amounts of sodium (Na), magnesium (Mg), strontium (Sr), aluminum (Al), and potassium (K).

The Ca/P ratio varied between 1.6 and 1.7 in the eight samples tested.

The results of compressive and tensile tests upon cleaving are provided in Fig. 5. The sintered allograft material compressive strength varied between 50 and 100 MPa, with the average value of 76 MPa. The tensile strength obtained from the tensile test upon cleaving varied between 4 and 23 MPa, with the average value of 12 MPa. Furthermore, the Young's modulus turned out to be between 2.9 and 3.3 GPa.

The sintered allograft material Vickers hardness varied between 0.3 and 0.8 GPa.

Such a high local hardness value can be associated with the ZrO_2 incorporation resulting from grinding. Except for this outlier, the average Vickers hardness was approximately 0.6 GPa.

Assessment of the allograft phase evolution due to milling and additive production processes

The X-ray diffraction (XRD) analysis results for samples A, B, and C fit closely with the control peaks for the "[9–432] Hydroxyapatite" record of the ICDD PDF-2 database. All the test samples were calcined at 900 °C before XRD analysis, which reflects the effects of such treatment. Small amorphous phase amounts were found in Sample A and Sample B, which was indicated by wider peaks and small deviations from the baseline. Sample C, on the contrary, showed narrower and sharper peaks, which suggests the reduced amorphous phase content. Moreover, new peaks corresponding to CaO ($2\theta \approx 43°$) and ZrO_2 ($2\theta \approx 34°$) were identified in Sample C. The presence of CaO inclusions can be explained by mechanical activation and potential degradation of hydroxyapatite and amorphous calcium phosphate compounds. The ZrO_2 peaks are related to the zirconium dioxide inclusions that contaminated the allograft material at the second stage of milling.

DISCUSSION

The allograft material obtained from cadaver human cortical bones showed potential for successful use in the digital light processing (DLP)-based additive procedure. We have found no studies focused on using bone allografts for 3D printing in the scientific literature. We have shown that the bone allograft-based material can be effectively used together with the additive production methods showing the behavior similar to that of synthetic hydroxyapatite during 3D printing.

The printing and heat treatment protocols optimized for synthetic calcium phosphate ceramics did not ensure the required properties of the bone-derived allograft. The sign of this were cracks in the sintered samples caused by low density of brown bodies and suboptimal sintering. The density can be increased by increasing the amount of powder in the photopolymerizable suspension. Optimization of sintering will require a series of parametric tests and laboratory analysis of material properties.

Despite the fact that the process of producing the samples manufactured by the additive method from the allograft was not optimized, it made it possible to obtain the relatively high sintering density on a microscale, which suggests the potential for further improvement. It is noteworthy that there were no voids in the corners of conjugated grains, and the natural chemical inclusions in the material structure, such as sodium (Na), magnesium (Mg), strontium (Sr), aluminum (Al), and potassium (K), were preserved in the amounts typical for human bones. These factors indicate that the allograft properties are superior to that of synthetic alternatives.

The milling operations contributed to effective homogenization of the allograft chemical composition. However, due to low powder filling coefficient of the source material, the "brown body" baseline density was not enough, which resulted in the unnecessary stress and insufficient compaction during thermal sintering. As a result, intergranular microcracks and large intergranular voids emerged, which contributed to the sintered material porosity in 15.8%. The calcium phosphate crystals in the intact bone represent the plate-shaped particles sized 40 × 3 × 7.5 nm intertwined with the collagen fibers [12]. The lack of such nanoplates in the calcined sample indicates sintering and transformation of those into roundish grains during calcination.

No significant changes in the material phases or chemical composition were observed throughout the production process. The commercially available human bone allograft contains about 60–70% minerals and 30–40% organic components (by mass) [13–15]. Thorough analysis confirmed the calcium-deficient nature of the bone-derived mineral with the average calcium to phosphorus ratio (Ca/P) of 1.65. The calcium phosphate ceramics resorb faster as the Ca/P ratio decreases. That is why it is expected that bioresorption of allograft materials will proceed faster than that of synthetic hydroxyapatite. This ratio is consistent with expectations for the calcium-deficient hydroxyapatite phase, confirmed by the X-ray diffraction (XRD) results [16]. Some studies report that the human bone average Ca/P ratio is about 1.67 [17], while according to the results of other studies [18], the bone mineral usually has the Ca/P ratio below 1.67 due to calcium deficiency.

The sintered material mechanical properties are critical for determination of its overall strength and hardness, especially considering the non-oprimized material microstructure. Therefore, the material properties can be improved through optimization of processing and production technologies.

CONCLUSIONS

The allograft material used in this study was obtained from the cadaver human cortical bone tissue. This material was calcined and then ground into the micron-sized powder to produce a photopolymerizable suspension and to be later used for the DLP-based additive production. The results confirmed high compatibility of the allograft material with the additive production technologies. Polymerization tests and 3D printing operations demonstrated stability of the bone allograft-derived material at every stage of additive production. Further research

is necessary to clarify the characteristics of the additively manufactured allograft implants and compare these with synthetic analogues. This includes optimization of the additive production process preparation stages and assessment of their potential aimed to regulate osteoinduction, osteoconduction, and mechanical stability both in vitro and in vivo.

References

1. GlobalData Plc, United States (US) Orthopedic Procedures Count By Segments And Forecast To 2030, GlobalData Plc, John Carpenter House, John Carpenter Street, London, EC4Y 0AN, UK, 2023. Available from: https://www.globaldata.com/store/report/usa-orthopedic-procedures-analysis/#:~:text=US%20Orthopedic%20Market%20Report%20Overview,US%20was%2018%2C577%2C953%20in%202022.
2. Rogers GF, Greene AK, Autogenous bone graft: basic science and clinical implications, J Craniofac Surg. 2012; 23: 323–7. Available from: https://doi.org/10.1097/SCS.0b013e318241dcba
3. Dutta SR, Passi D, Singh P, Bhuibhar A, Ceramic and non-ceramic hydroxyapatite as a bone graft material: a brief review. Ir J Med Sci. 1971; 184 (2015): 101–06. Available from: https://doi.org/10.1007/s11845-014-1199-8.
4. Yang C, Zhuo W, Li Q, Huang C, Yan H, Jin D, Preliminary outcomes of allograft and hydroxyapatite as substitutes for autograft in anterior cervical discectomy and fusion with self-locking standalone cages. J Orthop Surg. 2021; 16: 123. Available from: https://doi.org/10.1186/s13018-021-02257-0.
5. Rasch A, Naujokat H, Wang F, Seekamp A, Fuchs S, Klüter T, Evaluation of bone allograft processing methods: Impact on decellularization efficacy, biocompatibility and mesenchymal stem cell functionality. PLOS ONE. 2019; 14: e0218404. Available from: https://doi.org/10.1371/journal.pone.0218404.
6. Buj-Corral I, Tejo-Otero A. 3D Printing of Bioinert Oxide Ceramics for Medical Applications. J Funct Biomater. 2022; 13 (3): 155. DOI: 10.3390/jfb13030155. PMID: 36135590; PMCID: PMC9505679. Available from: https://doi.org/10.3390/jfb13030155.
7. Thakur N, Carretta M, Komissarenko D, Blugan G. Advancements in DLP 3D printing: High strength alumina toughened zirconia ceramics for biomedical applications. Open Ceramics. 2024; 18: 100601. Available from: https://doi.org/10.1016/j.oceram.2024.100601.
8. Sadaf Bashir Khan, Syed Irfan, Zhengjun Zhang, Weifeng Yuan. ACS Applied Bio Materials. 2025; 8 (8): 6470–525. Available from: https://doi.org/10.1021/acsabm.4c01923.
9. Muldashev ER, Muslimov SA, Vyalkov VA, Galimova VU, Nigmatullin RT, Salikhov AY, et al. Biomaterial alloplant dlja regenerativnoj hirurgii, RU2189257C1. 2002.
10. American Society for Testing and Materials, ASTM C1424 -Standard Test MEthod for Monolithic Compressive Strength of Advanced Ceramics at Ambient Temperature. 2004.
11. International Organization for Standardization, ISO 10993-14:2001(E): Biological evaluation of medical devices — Part 14: Identification and quantification of degradation products from ceramics. 2001.
12. Jacobs PF. Fundamentals of Stereolithography. 1992.
13. Dey P. Bone Mineralisation. In: Churchill DG, Dutour Sikirić M, Čolović B, Füredi H. Milhofer, editors. Contemp Top Phosphorus Biol Mater. IntechOpen. 2020. Available from: https://doi.org/10.5772/intechopen.92065.
14. Pietrzak WS, Woodell-May J, The Composition of Human Cortical Allograft Bone Derived from FDA/AATB-Screened Donors. J Craniofac Surg. 2005; 16: 579–85. Available from: https://doi.org/10.1097/01.SCS.0000159086.44801.C7.
15. Wang W, Yeung KWK, Bone grafts and biomaterials substitutes for bone defect repair: A review. Bioact Mater. 2017; 2: 224–47. Available from: https://doi.org/10.1016/j.bioactmat.2017.05.007.
16. Kuhn LT, Grynpas MD, Rey CC, Wu Y, Ackerman JL, Glimcher MJ. A Comparison of the Physical and Chemical Differences Between Cancellous and Cortical Bovine Bone Mineral at Two Ages. Calcif Tissue Int. 2008; 83: 146–54. Available from: https://doi.org/10.1007/s00223-008-9164-z.
17. Ishikawa K, Ducheyne P, Radin S, Determination of the Ca/P ratio in calcium-deficient hydroxyapatite using X-ray diffraction analysis. J Mater Sci Mater Med. 1993; 4: 165–8. Available from: https://doi.org/10.1007/BF00120386.
18. Gotoh Y, Hiraiwa K, Nagayama M. In vitro mineralization of osteoblastic cells derived from human bone. Bone Miner. 1990; 8: 239–50. Available from: https://doi.org/10.1016/0169-6009(90)90109-s.

Литература

1. GlobalData Plc, United States (US) Orthopedic Procedures Count By Segments And Forecast To 2030, GlobalData Plc, John Carpenter House, John Carpenter Street, London, EC4Y 0AN, UK, 2023. Available from: https://www.globaldata.com/store/report/usa-orthopedic-procedures-analysis/#:~:text=US%20Orthopedic%20Market%20Report%20Overview,US%20was%2018%2C577%2C953%20in%202022.
2. Rogers GF, Greene AK, Autogenous bone graft: basic science and clinical implications, J Craniofac Surg. 2012; 23: 323–7. Available from: https://doi.org/10.1097/SCS.0b013e318241dcba
3. Dutta SR, Passi D, Singh P, Bhuibhar A, Ceramic and non-ceramic hydroxyapatite as a bone graft material: a brief review. Ir J Med Sci. 1971; 184 (2015): 101–06. Available from: https://doi.org/10.1007/s11845-014-1199-8.
4. Yang C, Zhuo W, Li Q, Huang C, Yan H, Jin D, Preliminary outcomes of allograft and hydroxyapatite as substitutes for autograft in anterior cervical discectomy and fusion with self-locking standalone cages. J Orthop Surg. 2021; 16: 123. Available from: https://doi.org/10.1186/s13018-021-02257-0.
5. Rasch A, Naujokat H, Wang F, Seekamp A, Fuchs S, Klüter T, Evaluation of bone allograft processing methods: Impact on decellularization efficacy, biocompatibility and mesenchymal stem cell functionality. PLOS ONE. 2019; 14: e0218404. Available from: https://doi.org/10.1371/journal.pone.0218404.
6. Buj-Corral I, Tejo-Otero A. 3D Printing of Bioinert Oxide Ceramics for Medical Applications. J Funct Biomater. 2022; 13 (3): 155. DOI: 10.3390/jfb13030155. PMID: 36135590; PMCID: PMC9505679. Available from: https://doi.org/10.3390/jfb13030155.
7. Thakur N, Carretta M, Komissarenko D, Blugan G. Advancements in DLP 3D printing: High strength alumina toughened zirconia ceramics for biomedical applications. Open Ceramics. 2024; 18: 100601. Available from: https://doi.org/10.1016/j.oceram.2024.100601.
8. Sadaf Bashir Khan, Syed Irfan, Zhengjun Zhang, Weifeng Yuan. ACS Applied Bio Materials. 2025; 8 (8): 6470–525. Available from: https://doi.org/10.1021/acsabm.4c01923.
9. Muldashev ER, Muslimov SA, Vyalkov VA, Galimova VU, Nigmatullin RT, Salikhov AY, et al. Biomaterial alloplant dlja regenerativnoj hirurgii, RU2189257C1. 2002.
10. American Society for Testing and Materials, ASTM C1424 -Standard Test MEthod for Monolithic Compressive Strength of Advanced Ceramics at Ambient Temperature. 2004.
11. International Organization for Standardization, ISO 10993-14:2001(E): Biological evaluation of medical devices — Part 14: Identification and quantification of degradation products from ceramics. 2001.
12. Jacobs PF. Fundamentals of Stereolithography. 1992.
13. Dey P. Bone Mineralisation. In: Churchill DG, Dutour Sikirić M, Čolović B, Füredi H. Milhofer, editors. Contemp Top Phosphorus Biol Mater. IntechOpen. 2020. Available from: https://doi.org/10.5772/

intechopen.92065.
14. Pietrzak WS, Woodell-May J, The Composition of Human Cortical Allograft Bone Derived from FDA/AATB-Screened Donors. J Craniofac Surg. 2005; 16: 579–85. Available from: https://doi.org/10.1097/01.SCS.0000159086.44801.C7.
15. Wang W, Yeung KWK, Bone grafts and biomaterials substitutes for bone defect repair: A review. Bioact Mater. 2017; 2: 224–47. Available from: https://doi.org/10.1016/j.bioactmat.2017.05.007.
16. Kuhn LT, Grynpas MD, Rey CC, Wu Y, Ackerman JL, Glimcher MJ. A Comparison of the Physical and Chemical Differences Between Cancellous and Cortical Bovine Bone Mineral at Two Ages. Calcif Tissue Int. 2008; 83: 146–54. Available from: https://doi.org/10.1007/s00223-008-9164-z.
17. Ishikawa K, Ducheyne P, Radin S, Determination of the Ca/P ratio in calcium-deficient hydroxyapatite using X-ray diffraction analysis. J Mater Sci Mater Med. 1993; 4: 165–8. Available from: https://doi.org/10.1007/BF00120386.
18. Gotoh Y, Hiraiwa K, Nagayama M. In vitro mineralization of osteoblastic cells derived from human bone. Bone Miner. 1990; 8: 239–50. Available from: https://doi.org/10.1016/0169-6009(90)90109-s.

EXPRESSION OF microRNA MIR146A IN THE BLOOD PLASMA OF RATS WITH OBESITY AND KNEE ARTHROSIS AFTER ADMINISTRATION OF DEXAMETHASONE

Ivanov AS[1,2] ✉, Tananakina TP[1], Kashchenko SA[1], Pogorelova IA[1]

[1] Federal State Budgetary Educational Institution of Higher Education “LSMU named St. Luke”, Russia
[2] Non-governmental private institusion Scientific Diagnostic Center "Policlinic on Smolenskaya"

MicroRNAs are resistant to RNases and are highly specific for various pathological conditions, particularly inflammation, allowing them to be considered inflammation biomarkers. They were detected in all body fluids, and miR146a plays a key role in the pathogenesis of inflammation. A total of 180 male white Wistar rats were selected for the study. All animals were 8–10 weeks old and weighed 200–250 grams. The animals were divided into five groups of 36 each. The first received saline solution intramuscularly, while the others underwent experimental modeling of obesity and knee arthrosis. The second group received 1.0 ml of saline solution intramuscularly, while the third, fourth, and fifth groups received dexamethasone at doses of 1 ng/ml, 10 ng/ml, and 100 ng/ml, respectively. Blood samples for the study were collected on days 3, 5, and 10. The obtained parameters were analyzed at the statistical significance level ($p < 0.05$). Increased miR146a levels were observed in animals in the second group compared to the others, due to the development of inflammation associated with obesity and concomitant gonarthrosis. In the third group, expression levels decreased slightly, remaining high. In the fourth group, with the use of 10 ng/ml dexamethasone, miR146a expression levels decreased most significantly on days 3 and 5. In the fifth group, virtually no changes were observed, with the parameter decreasing only slightly. The 10 ng/ml dexamethasone dose demonstrated the greatest efficacy during the experiment, possessing the greatest anti-inflammatory activity compared to the other doses.

Keywords: gonarthrosis, dexamethasone, microRNA, inflammation, rats, obesity, expression, miR146a

Author contribution: Ivanov AS — study design development, experimental design; Tananakina TP — study design development, participation in the experimental design, and scientific supervision; Kashchenko SA — scientific editing, scientific supervision, and participation in the experimental design; Pogorelova IA — technical proofreading, participation in the experimental design.

Compliance with ethical standards: the study was approved by the Ethics Committee of the St. Luke's Lugansk State Medical University of the Russian Ministry of Health (protocol No 1 dated 23 September 2025). When working with laboratory animals, the conditions of care and experimentation were fully compliant with the standards of Order No. 199n of the Russian Ministry of Health "On Approval of the Rules of Good Laboratory Practice" 1, adhering to the principles of the European Convention for the Protection of Vertebrate Animals used for Experimental and other Scientific Purposes, and strictly adhering to the Directive of the European Parliament and of the Council of the European Union on the Protection of Animals used for Scientific Purposes.

✉ **Correspondence should be addressed:** Aleksey S. Ivanov
A. Dikogo, 16A, kv. 73, 111396, Moskva, Rossiya: sashatravmatolog1985@mail.ru

Received: 04.10.2025 **Accepted:** 30.10.2025 **Published online:** 11.11.2025

DOI: 10.24075/brsmu.2025.056

Copyright: © 2025 by the authors. **Licensee:** Pirogov University. This article is an open access article distributed under the terms and conditions of the Creative Commons Attribution (CC BY) license (https://creativecommons.org/licenses/by/4.0/).

ЭКСПРЕССИЯ микроРНК MIR146A В ПЛАЗМЕ КРОВИ КРЫС С ОЖИРЕНИЕМ И АРТРОЗОМ КОЛЕННОГО СУСТАВА НА ФОНЕ ВВЕДЕНИЯ ДЕКСАМЕТАЗОНА

А. С. Иванов[1,2] ✉, Т. П. Тананакина[1], С. А. Кащенко[1], И. А. Погорелова[1]

[1] ФГБОУ ВО ЛГМУ имени Свтятителя Луки, Россия
[2] Негосударственное частное учреждение Научно-диагностический центр «Поликлиника на Смоленской»

МикроРНК не поддаются действию РНКаз и высокоспецифичны для различных патологических состояний, в частности воспаления, что позволило рассматривать их как биомаркеры данного патологического процесса. Обнаружить их удалось во всех жидкостях организма, в патогенезе воспаления ключевую роль играют микроРНК miR146a. Целью работы было определить уровень экспресии miR146a у крыс с гонартрозом, сочетанным ожирением и коррекцией дексаметазоном с целью разработки дальнейших патогенетических механизмов лечения остеоартроза. Для исследования отобрали 180 самцов белых крыс линии Вистар в возрасте 8–10 недель массой 200–250 г. Животные были разделены на пять групп по 36 в каждой: в первой группе вводили физиологический раствор хлорида натрия внутримышечно, остальным экспериментально смоделировано ожирение и артроз коленного сустава. Особям второй группы вводили 1,0 мл раствора хлорида натрия внутримышечно, третьей, четвертой и пятой — дексаметазон в дозе 1 нг/мл, 10 нг/мл и 100 нг/мл соответственно. Забор крови для проведения исследования проводили на 3, 5, 10 сутки. Полученные показатели исследовали при уровне статистической значимости ($p < 0,05$). Установлено повышение уровня miR146a у животных второй группы в сравнении с остальными, за счет развития воспаления на фоне ожирения и сопутствующего гонартроза. В третьей группе уровень экспрессии незначительно снижался, но оставался высоким. В четвертой группе на фоне применения 10 нг/мл дексаметазона уровень экспрессии miR-146a снижался максимально на 3 и 5 сутки. В пятой группе изменения практически отсутствовали, показатель снижался незначительно. Наибольшую эффективность в процессе эксперимента выявлена при дозе дексаметазона 10 нг/мл — она обладала набольшей противовоспалительной активностью по отношению к остальным.

Ключевые слова: гонартроз, дексаметазон, микроРНК, воспаление, ожирение, экспрессия, miR146a

Вклад авторов: А. С. Иванов — дизайн исследования, проведение экспериментальной части работы; Т. П. Тананакина — дизайн исследования, проведение экспериментальной части, научное сопровождение; С. А. Кащенко — редактирование, научное сопровождение, участие в подготовке эксперимента; И. А. Погорелова — техническое редактирование, участие в подготовке эксперимента.

Соблюдение этических стандартов: исследование одобрено на заседании этического комитета ФГБОУ ВО «ЛГМУ им. Свт. Луки» МЗ РФ (протокол № 1 от 23 сентября 2025 г.), проведено в соответствии с нормами приказа Минздрава России № 199н «Об утверждении Правил надлежащей лабораторной практики», принципами Европейской конвенции о защите позвоночных животных, используемых для экспериментов или в иных научных целях, а также директивой Европейского парламента и совета Европейского союза по охране животных, используемых в научных экспериментах.

✉ **Для корреспонденции:** Алексей Сергеевич Иванов
ул. А. Дикого, д. 16А, кв. 73, 111396, г. Москва, Россия; sashatravmatolog1985@mail.ru

Статья получена: 04.10.2025 **Статья принята к печати:** 30.10.2025 **Опубликована онлайн:** 11.11.2025

DOI: 10.24075/vrgmu.2025.056

Авторские права: © 2025 принадлежат авторам. **Лицензиат:** РНИМУ им. Н. И. Пирогова. Статья размещена в открытом доступе и распространяется на условиях лицензии Creative Commons Attribution (CC BY) (https://creativecommons.org/licenses/by/4.0/).

In 2008, Tewari et al. experimentally discovered the presence of some forms of microRNA in blood plasma in a stable form that excludes the influence of RNases, which served as the beginning of their study as biomarkers of the inflammatory process [1–5]. Stability is ensured by dysregulation of cellular expression of microRNA, which can be observed during infection; the cell is also capable of releasing some forms into the extracellular space. Further studies showed the presence of biomarkers not only in blood plasma, but also in saliva, urine, bile, breast milk and other body fluids [6]. Currently, there is data on specific changes in the microRNA expression profile in various pathological conditions, for example, in oncology, cardiovascular diseases, inflammation, aging, etc. [7–8]. Advances in understanding the relationships between various genes, their products, and environmental factors have highlighted the role of epigenetic variation, which involves changes in gene expression that do not affect DNA structure but can be transmitted across generations. There are three levels of epigenetic regulation: genomic (DNA methylation), proteomic (responsible for histone modification), and transcriptomic (RNA regulation). MicroRNA is a large class of small, non-coding RNA molecules, 18–25 nucleotides in length, that regulate gene expression through complementary interactions with the 3'-untranslated regions of mRNA, leading to RNA degradation or inhibition of translation processes [9].

Today, a large number of microRNAs are known that are specific to each pathological condition and enable early diagnosis for timely treatment. Recent data have shown that miR21 and miR146a microRNAs are involved in the pathogenesis of inflammatory diseases [10]. The role of miR146a in the regulation of the cell cycle, apoptosis, proliferation, and cell differentiation, as well as in the pathogenesis of infectious diseases, has been elucidated [11–13].

Over the past 10 years, microRNA markers have been discovered as specific factors in osteoarthritis and rheumatic diseases [14–18]. Detection of miR146a in synovial fluid and plasma in osteoarthritis is a potential diagnostic and prognostic marker [19]. Increased miR146a levels in blood plasma indicate the development and progression of gonarthrosis, which in the vast majority of cases is associated with excess body weight [20]. MiR146a is considered a marker of obesity and can influence its development and progression when elevated in blood plasma. Physical activity promotes weight loss, which reduces miR146a expression [21].

The use of nonsteroidal and steroidal anti-inflammatory drugs (e.g., celecoxib, ibuprofen, dexamethasone, methotrexate, etc.) in the treatment of gonarthrosis helps suppress the synthesis of proinflammatory cytokines and miR146a by increasing the expression of miR149-5p and miR-let-7c-5p [22, 23]. Among glucocorticosteroids for the treatment of inflammatory joint diseases, including osteoarthritis, one of the most frequently used drugs is dexamethasone [24]. A 2018 meta-analysis found that miR146a expression levels are higher in patients with rheumatoid arthritis and osteoarthritis than in healthy controls, as it serves as a regulator of the primary immune response and is involved in the pathogenesis of osteoarthritis [22]. The question of miR146a expression levels in obesity associated with osteoarthritis treated with glucocorticosteroids remains open.

Investigating miR146a expression levels in rats with obesity and osteoarthritis provides insight into the pathogenetic mechanisms of disease development and the development of optimal treatment regimens. The aim of this study was to develop a pathogenetic treatment regimen for osteoarthritis associated with obesity using dexamethasone, taking into account the level of miR146a expression, and to evaluate the effect of different doses of dexamethasone (1 ng/ml, 10 ng/ml, and 100 ng/ml) on the level of miR146a expression in rats with an experimental model of obesity and gonarthrosis.

METHODS

The experiment was conducted at the Ask-Health Research Center, Bulgaria, and the Leningrad State Medical University named after St. Luki" of the Ministry of Health of the Russian Federation.

For the experiment, 180 male Wistar albino laboratory rats, 8–10 weeks old, weighing 200–250 g, were selected. The animals were maintained in a vivarium at a temperature of 22 ± 2 °C and a 12-hour day/night cycle and nights with free access to water and food. The animals were randomly divided into 5 groups (n = 36). The first served as a control and received 1.0 ml of saline solution; the second (obese + gonarthrosis) received 1.0 ml of saline solution; the third, fourth, and fifth (obese + gonarthrosis) received 1.0 ng/ml, 10 ng/ml, and 100 ng/ml of dexamethasone solution, respectively.

Dexamethasone doses were selected based on the following: 1 ng/ml is a low dose, reflecting the minimum effective concentration to simulate a minimal anti-inflammatory effect without significant immunosuppression; 10 ng/ml is a therapeutic dose used to suppress cytokine-induced inflammation in rats; 100 ng/ml — a high dose was used to simulate a possible “paradoxical” effect with glucocorticoid overexposure. The dose range was selected to evaluate the dose-dependent responses of miR146a from minimal to supertherapeutic. Saline and dexamethasone were administered intramuscularly once daily for 10 days. On days 3, 5, and 10, blood was collected from the tail vein and centrifuged to obtain serum to determine the dynamics of miR146a expression. This scheme is fully consistent with previously published studies on modeling the anti-inflammatory effect of dexamethasone in laboratory rats [24]. Adverse effects of dexamethasone were assessed based on behavioral activity (open field test), body weight, the Lee index, coat and skin condition, and blood glucose levels (no significant dose-dependent adverse effects were observed with 1 and 10 ng/ml; signs of hyperglycemia and decreased activity were observed at 100 ng/ml, consistent with the known adverse effects of high doses of glucocorticosteroids).

Obesity in animals was modeled using a high-calorie diet supplemented with increased amounts of fat (45%), plant-based carbohydrates (35%), and animal-based carbohydrates (35%) for 8 weeks. The Li index was used to evaluate the result (Li = 1000 — (body weight (g)) / (length from the tip of the nose to the anus (cm)). The presence of obesity was indicated by an index of more than 310 and an increase in body weight by 25–40% compared to the initial value, which indicates a moderate degree of obesity [25]. Gonarthrosis was modeled according to the author's method by repeated damage to the articular cartilage using a minimally invasive method, followed by immobilization for 2–4 weeks using the author's device until reliable radiographic signs of arthrosis were achieved using a high-frequency portable dental X-ray machine Posdion Rextar X, 70 kV, Posdion, South Korea.

Determination of microRNA (miR146a) was performed by quantitative reverse transcription followed by polymerase chain reaction in real time. Serum was obtained by centrifugation of 1.0 ml of venous blood of rats obtained from the tail vein at 12,000 rpm for 15 minutes at 4 °C. The resulting samples were immediately frozen at –80 °C until analysis.

Total RNA was isolated using the miRNeasy Serum/Plasma Kit (Qiagen, Germany; No. 217184) according to the

Table 1. Dynamics of serum miR146a expression in rats in groups 1, 2, and 3 on days 3, 5, and 10

Indicator	miR146a			*p*		
Day	3	5	10	3	5	10
group 1, *n* = 36	0.97	0.97	1.03	0.07	0.03	0.07
group 2, *n* = 36	1.83	1.79	1.77	0.08	0.08	0.02
group 3, *n* = 36	1.47	1.52	1.51	0.05	0.05	0.05

Note: *p* — the root mean square error at a value level of 0,05.

manufacturer's protocol. Extraction efficiency was monitored by adding an external synthetic controller (cel-miR-39, Qiagen, Germany). RNA was purified on silica gel columns and eluted with 14 µl of RNase-free water. For cDNA synthesis, TaqMan™ MicroRNA Reverse Transcription Kit reagents (Applied Biosystems, Thermo Fisher Scientific, USA; No. 4366596) were used together with strain-specific TaqMan™ MicroRNA Assays primers (USA) for miR146a (#000468).

Quantitative PCR was performed in 96-well plates on a QuantStudio™ 5 Real-Time PCR System (Applied Biosystems, USA) using TaqMan™ Universal PCR Master Mix reagents, No. AmpErase UNG, USA, #4324018. U6 snRNA, whose expression level remained stable across all study groups, was used as reference RNA.

Three technical replicates were used for each reaction, and the Livak method (2^-ΔΔCt) was used to estimate relative miRNA expression.

Statistical Analysis of Results

After digital data collection, the mean and standard deviation were calculated. Statistical analysis was performed using one-way analysis of variance (ANOVA) in SPSS (v.16.0 for Windows, 2007; SPSS, Inc., Chicago, IL). Significant differences are indicated as $p < 0.05$; when calculating percentages, the data from the first group were taken as 100%. Box-and-whisker plots were used to check the unidimensionality of the distribution of results [26]. Statistical processing and the construction of diagrams and graphs were performed using the Statistica10 program.

RESULTS

This study revealed a correlation between miR146a microRNA expression and obesity, gonarthrosis, and dexamethasone use. In the body, miR146a is involved in the regulation of the immune response and inflammation by suppressing the latter. MiR146a leads to a decrease in the production of proinflammatory cytokines (IL-6, IL-8, and TNFα) and is actively involved in the regulation of T-cell differentiation and neuroinflammatory processes.

The study found an increase in miR146a in group II, suggesting the development of inflammation in the body caused by cytokines produced by adipocytes and as a result of the inflammation that triggers gonarthrosis. The use of dexamethasone in the experiment resulted in decreased plasma miR146a levels in all study groups, despite its long-term use as an anti-inflammatory agent for the treatment of gonarthrosis associated with excess body weight (Table 1).

The study found an increase in the miR146a index on day 3 in group 2 by 188.6% ($p < 0.05$), on day 5 by 184.5% ($p < 0.05$), on day 10 by 146.6% ($p < 0.05$), compared to group 1, which may represent the body's response to inflammation caused by obesity combined with gonarthrosis. In group 3, a decrease in the miR146a index was observed compared to group 2, but the index remained high. On day 3, miR146a increased by 151.1% ($p < 0.05$), while on day 5 the index increased by 156.7% ($p < 0.05$), after 10 days of the experiment, an increase of 146.6% ($p < 0.05$) was observed compared to group 1. When comparing the parameters of groups 1 and 3, an increase in miR146a levels by 151.5% ($p < 0.05$) was observed on day 3, on day 5 by 156.7% ($p < 0.05$), and on day 10 by 146.6% ($p < 0.05$).

Dynamic analysis of miR146a expression in group I revealed no increase on day 5, while on day 10 there was an increase of 106.1% ($p < 0.05$). In group 2, a decrease in miR146a by 2.2% ($p < 0.05$) was observed on day 5, and on day 10 the indicator decreased by 3.3% ($p < 0.05$) compared to day 3, and by 1.2% ($p < 0.05$) compared to day 5 of the experiment. In group 3, there was a 103.4% increase ($p < 0.05$) on Day 5 compared to Day 3, a 102.7% increase ($p < 0.05$) on Day 10 compared to Day 3, and a 0.7% decrease ($p < 0.05$) compared to Day 5.

Administration of 10 ng/ml dexamethasone had a more pronounced anti-inflammatory effect in group 3 compared to the others. The miR146a microRNA level was significantly higher than in group 1, but decreased relative to group 2 (Table 2).

Experimentally, an increase in the miR146a expression level was found on day 3 of the experiment by 112.3% ($p < 0.05$), on day 5 by 108.2% ($p < 0.05$), and on day 10 by 113.5% ($p < 0.05$) compared to group 1, which was statistically less than in group 2. When comparing the miR146a expression level in group IV with group 2, a decrease of 40.5% ($p < 0.05$) was found on day 3, 41.4% ($p < 0.05$) on day 5, and 39.9% ($p < 0.05$) on day 10.

Dynamic analysis of the indicator within group 4 reveals a clear trend toward a decrease in miR146a expression on Day 5 by 3.7% ($p < 0.05$) compared to Day 3. On Day 10, the level increased by 107.3% ($p < 0.05$) compared to Day 3, and by 111.4% ($p < 0.05$) compared to Day 5.

A different result was observed when the dexamethasone dose was increased to 100 ng/ml. The miR146a microRNA

Table 2. Dynamics of miR146a expression in rat serum in groups 1, 2, and 4 on Days 3, 5, and 10

Indicator	miR146a			*p*		
Day	3	5	10	3	5	10
group 1, *n* = 36	0.97	0.97	1.03	0.07	0.03	0.07
group 2, *n* = 36	1.83	1.79	1.77	0.08	0.08	0.02
group 3, *n* = 36	1.09	1.05	1.17	0.04	0.07	0.04

Note: *p* — the root mean square error at a value level of 0,05.

Table 3. Dynamics of miR146a expression indicators in rat serum in groups 1, 2, and 5 on Days 3, 5, and 10

Indicator	miR146a			*p*		
Day	3	5	10	3	5	10
group 1, *n* = 36	0.97	0.97	1.03	0.07	0.03	0.07
group 2, *n* = 36	1.83	1.79	1.77	0.08	0.08	0.02
group 3, *n* = 36	1.71	1.73	1.67	0.03	0.04	0.03

Note: *p* — the root mean square error at a value level of 0,05.

level was significantly higher than in group 1. Compared to group 2, the indicators differed slightly but were significantly lower (Table 3).

A significant increase in miR146a was observed in group 5 on day 3 by 176.2% ($p < 0.05$) compared to group 1. When studying microRNA in the blood plasma of group 5 on day 5, the indicator increased by 178.3% ($p < 0.05$) compared to group 1. On day 10 of the experiment, a significant increase in the miR146a concentration in group 5 by 159.2% ($p < 0.05$) was observed compared to group 1. When comparing the indicators of group 5 with group 3, a decrease in concentration was established against the background of dexamethasone administration: on day 3 by 6.6% ($p < 0.05$), on day 5 by 3.4% ($p < 0.05$), on day 10 by 5.7% ($p < 0.05$).

The dynamics of the parameter within group 5 showed a change in miR146a expression levels following dexamethasone administration. On Day 5, the parameter increased by 101.1% ($p < 0.05$) compared to Day 3, on Day 10, it decreased by 2.4% ($p < 0.05$) compared to Day 3, and by 3.5% ($p < 0.05$) compared to Day 5.

A visual representation of the dynamics of miR146a changes in blood plasma in all study groups can be presented using a graphical representation (Fig. 1).

DISCUSSION

The study revealed an increase in the miR146a microRNA concentration in the blood plasma of rats in all groups exposed to dexamethasone, compared to the control group. The highest level was observed in animals in group 2, indicating an inflammatory process caused by a group of cytokines secreted by adipocytes and the development and progression of gonarthrosis [27]. This is confirmed by an increase in miR146a expression in animals in group 3. Following administration of dexamethasone at a dose of 1 ng/ml, a decrease in miR146a expression was observed in animals in group 3 compared to group 2, indicating the anti-inflammatory properties of dexamethasone even at a low dose. The miR146a expression level in group 3 remained high compared to group 1, suggesting a low efficacy of 1 ng/ml dexamethasone on the studied parameter throughout the entire study period compared to a dose of 10 ng/ml [28].

In group 4, a more pronounced decrease in miR146a expression was observed with dexamethasone administration, which can also be explained by cytokine inhibition and suppression of inflammation caused by obesity and excess body weight [24]. The maximum result in this group was observed on day 5 of the experiment, which may indicate a cumulative effect of the drug due to its daily use or blockade of cellular receptors sensitive to cytokines [29]. On day 10, while the anti-inflammatory effect was maintained, miR146a expression levels increased slightly, which may be associated with decreased receptor sensitivity to the drug or its increased metabolism.

In group 5, no significant changes in miR146a levels were observed with dexamethasone administration compared to group 2, which supports the low efficacy of the 100 ng/ml dexamethasone dose throughout the entire experimental

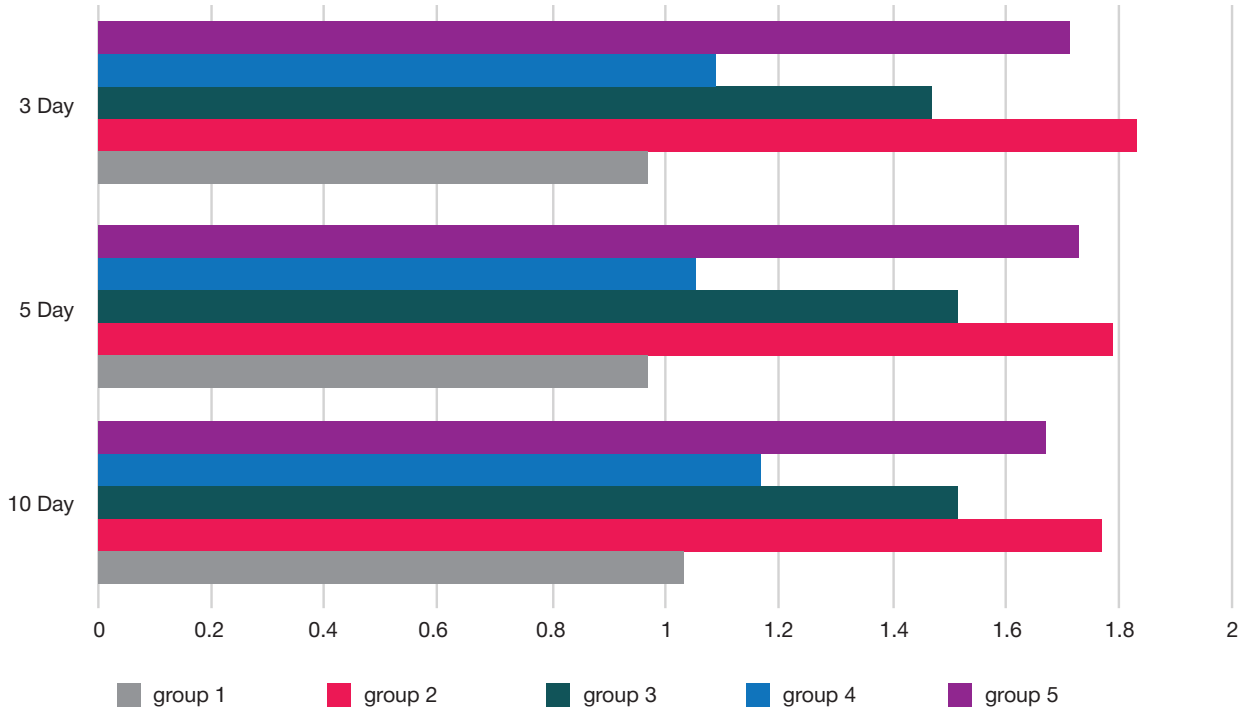


Fig. Dynamics of changes in the miR146a parameter in blood plasma of rats in groups 1, 2, 3, 4, and 5 on Days 3, 5 and 10

period. This may indicate the loss of dexamethasone receptors due to its high concentration or resistance to it at high doses, despite the drug's anti-inflammatory properties [30].

CONCLUSIONS

The study found that the maximum positive effect was achieved in group 4, as evidenced by a persistent and maximal reduction in miR146a expression. This circumstance allows us to recommend a dose of 10 ng/ml as a pathogenetically justified treatment for gonarthrosis associated with obesity over a long period of time. A minor positive effect from dexamethasone administration was observed in group III, as dexamethasone led to a decrease in miR146a expression; however, the level remained high compared to group 1. Dexamethasone at a dose of 1 ng/ml can be recommended as a pathogenetic therapy for pain syndrome or minor inflammation, as well as for the treatment of gonarthrosis not associated with obesity. It was found that a dose of 100 ng/ml dexamethasone was ineffective throughout the entire treatment period and did not significantly reduce miR146a expression in group V, which remained high, with minor fluctuations throughout the entire experimental period. Therefore, a dose-dependent effect of 100 mg dexamethasone on miR146a cannot be concluded and requires further clinical study. Potential for further research includes examining other plasma microRNA variants in patients with gonarthrosis associated with obesity, as well as blood glucose levels during dexamethasone treatment, dexamethasone receptor function, proinflammatory cytokine concentrations, and adrenal cortex function. Further study and titration of dexamethasone dose based on miR146a expression levels in clinical practice are of interest.

References

1. Mitchell PS, Parkin RK, Kroh EM, Fritz BR, Wyman SK, Pogosova Agadjanyan EL, et al. Circulating microRNAs as stable blood-based markers for cancer detection. Proc Natl Acad Sci USA. 2008; 105 (30): 10513–8. DOI: 10.1073/pnas.0804549105.
2. Shirshova AN, Shamovskaja DA, Bojarskih UA, Apalko SV, Leskov LS, Sokolov AV, et al. Ocenka znachimosti opredelenija kolichestva miR-146a v plazme krovi cheloveka dlja diagnostiki kolorektal'nogo raka. Vestnik Rossijskogo gosudarstvennogo medicinskogo universiteta. 2017; 4: 31–36. Russian.
3. Gareev IF, Bejlerli OA. Cirkulirujushhie mikroRNK kak biomarkery: kakie perspektivy? Profilakticheskaja medicina. 2018; 21 (6): 142–50. Russian.
4. Vasilev SV, Akselrod AS, Zhelankin AV, Shhekochihin DYu, Generozov JeV, Sharova EI, et al. Cirkulirujushhie mikroRNK-21-5r, mikroRNK146a-5r, mikroRNK320a3r u pacientov s fibrilljaciej predserdij v sochetanii s gipertonicheskoj bolezn'ju i ishemicheskoj bolezn'ju serdca. Kardiovaskuljarnaja terapija i profilaktika. 2022; 21 (1): 2814. Russian.
5. Li Y, Tan W, Ye F, et al. Identification of microRNAs and genes as biomarkers of atrial fibrillation using a bioinformatics approach. J Intern Med Res. 2019; 47 (8): 3580–9. DOI:10.1177/0300060519852235.
6. Duan X, Wang L, Sun G, Yan W, Yang Y. Understanding the cross-talk between host and virus in poultry from the perspectives of microRNA. Poult Sci. 2020; 99 (4): 1838–46. DOI: 10.1016/j.psj.2019.11.053.
7. Shang R, Lee S. Senavirathne G, Lai EC. MicroRNAs in action: Biogenesis, function and regulation. Na. Rev Genet. 2023; 24: 816–33. Available from: https://doi.org/10.1038/s41576-023-00611-y.
8. Nemeth K, Bayraktar R, Ferracin M, Calin GA. Non-coding RNAs in disease: From mechanisms to therapeutics. Nat Rev Genet. 2024; 25: 211–32. Available from: https://doi.org/10.1038/s41576-023-00662-1.
9. Djachenko NA, Ulitina AS, Lukina OV, Pchelina SN, Trofimov VI, Mironova ZhA. Jekspressija mikroRNK miR-21 i miR-146a u pacientov muzhskogo pola s perekrestnym fenotipom bronhial'noj astmy i hronicheskoj obstruktivnoj bolezni legkih. Pul'monologija. 2020; 30 (3): 263–69. Russian.
10. Gareev IF, Bejlerli OA, Pavlov VN i dr. Potencial'naja rol' mikrornk v patogeneze gemorragicheskoj lihoradki s pochechnym sindromom. Urologija. 2021: 112–19. Russian. Available from: https://dx.doi.org/10.18565/urology.2021.1.112-119.
11. Zhou Y, Chen L, Du J, Hu X, Xie Y, Wu J, et al. MicroRNA-7 Inhibits Rotavirus Replication by Targeting Viral NSP5 In Vivo and In Vitro. Viruses. 2020; 12 (2). pii: E209. DOI: 10.3390/v12020209.
12. Chen L, Ming X, Li W, Bi M, Yan B, Wang X, Yang P, Yang B. The microRNA-155 mediates hepatitis B virus replication by reinforcing SOCS1 signalling-induced autophagy. Cell Biochem Funct. 2020. DOI: 10.1002/cbf.3488.
13. Fioravanti A, Cheleschi S, Cavalier E, Reginster J-Y, Alokail M, Ladang A, et al. Can Circulating MicroRNAs, Cytokines, and Adipokines Help to Differentiate Psoriatic Arthritis from Erosive Osteoarthritis of the Hand? A Case–Control Study. International Journal of Molecular Sciences. 2025; 26 (10): 4621. Available from: https://doi.org/10.3390/ijms26104621.
14. Ali SA, Peffers MJ, Ormseth MJ, Jurisica I, Kapoor M. The non-coding RNA interactome in joint health and disease. Nat. Rev. Rheumatol. 2021; 17: 692–705. Available from: https://doi.org/10.1038/s41584-021-00687-y.
15. Shaikh FS, Siegel RJ, Srivastava A, Fox DA, Ahmed S. Challenges and promise of targeting miRNA in rheumatic diseases: A computational approach to identify miRNA association with cell types, cytokines, and disease mechanisms. Front Immunol. 2023; 14: 1322806. Available from: https://doi.org/10.3389/fimmu.2023.1322806.
16. Wade SM, McGarry T, Wade SC, Fearon U, Veale DJ. Serum MicroRNA Signature as a diagnostic and therapeutic marker in patients with Psoriatic Arthritis. J Rheumatol. 2020; 47: 1760–7. Available from: https://doi.org/10.3899/jrheum.190602.
17. Motta F, Pederzani A, Carena MC, Ceribelli A, Wordsworth PB, De Santis M, et al. MicroRNAs in Axial Spondylarthritis: An overview of the recent progresses in the field with a focus on Ankylosing Spondylitis and Psoriatic Arthritis. Curr Rheumatol Rep. 2021; 23: 59. Available from: https://doi.org/10.1007/s11926-021-01027-5.
18. Bonek K, Kuca Warnawin E, Kornatka A, Plebanczyk M, Burakowski T, Maslinski W, et al. Circulating miRNA Correlates with lipid profile and disease activity in psoriatic arthritis, rheumatoid arthritis, and ankylosing spondylitis patients. Biomedicines. 2022; 10: 893. Available from: https://doi.org/10.3390/biomedicines10040893.
19. Haschka J, Simon D, Bayat S, Messner Z, Kampylafka E, Fagni F, et al. Identification of circulating microRNA patterns in patients in psoriasis and psoriatic arthritis. Rheumatology. 2023; 62: 3448–58. Available from: https://doi.org/10.1093/rheumatology/kead059.
20. Baloun J, Pekacova A, Svec X, Kropackova T, Horvathova V, Hulejova H, et al. Circulating miRNAs in hand osteoarthritis. Osteoarthr Cartil. 2023; 31: 228–37. DOI: 10.1016/j.joca.2022.10.021.
21. Cheleschi S, Tenti S, Bedogni G, Fioravanti A. Circulating Mir-140 and leptin improve the accuracy of the differential diagnosis between psoriatic arthritis and rheumatoid arthritis: A case-control study. Transl Res. 2022; 239: 18–34. DOI: 10.1016/j.trsl.2021.08.001.
22. Mustafin RN. Identichnost' patogeneza, geneticheskikh i epigeneticheskikh mekhanizmov razvitiya osteoartrita i revmatoidnogo artrita. Kazanskii meditsinskii zhurnal. 2024; 105(5): 797–812. Russian. Available from: https://doi.org/10.17816/KMJ627530.
23. Law YY, Lee WF, Hsu CJ, Lin YY, Tsai CH, Huang CC, et al. miR-let-7c-5p and miR-149-5p inhibit proinflammatory cytokine production in osteoarthritis and rheumatoid arthritis synovial fibroblasts. Aging (Albany NY). 2021; 13 (13): 17227–36. DOI: 10.18632/aging.203201.
24. Madamsetty Vijay Sagar Mohammadinejad, Reza Uzieliene, Ilona Nabavi, et al. Dexamethasone: insights into pharmacological aspects, therapeutic mechanisms, and delivery systems. ACS

biomaterials science & engineering. 2022; 8 (5): 1763–90. Available from: https://doi.org/10.1021/acsbiomaterials.2c00026.
25. Bairasheva VK, Pchelin BYu, Egorova AE, Vasilkova ON, Kornyushin OV. Eksperimental'nye modeli alimentarnogo ozhireniya u krys. Juvenis scientia. 2019; 9–10: 8–13. DOI: 10.32415/jscientia.2019.09-10.02. Russian.
26. Russo A, Bartolini D, at al. Physical Activity Modulates the Overexpression of the Inflammatory miR-146a-5p in Obese Patients. IUBMB Life. 2018; 70 (10): 1012–22. DOI: 10.1002/iub.1926.
27. Vorotnikov AV, Stafeev YuS, Menshikov MYu, Shestakova MV, Parfenova EV. Latentnoe vospalenie i narushenie obnovleniya zhirovykh depo kak mekhanizm razvitiya rezistentnosti k insulinu pri ozhirenii. Biokhimiya. 2019; 84 (11): 1649–67. DOI: 10.1134/S0320972519110095.Russian.
28. Chae BS. Effect of low-dose corticosterone pretreatment on the production of inflammatory mediators in super-low-dose LPS-primed immune cells. Toxicol Res. 2021; 37: 47–57. Available from: https://doi.org/10.1007/s43188-020-00051-4.
29. Rajen Dey, Biswadev Bishayi. Dexamethasone exhibits its anti-inflammatory effects in S. aureus induced microglial inflammation via modulating TLR-2 and glucocorticoid receptor expression. International Immunopharmacology. 2019; 75: 105806. Available from: https://doi.org/10.1016/j.intimp.2019.105806.
30. Voloshin NI, Pugach VA, Salukhov VV, Tyunin MA, Ilinskii NS, Levchuk EV, et al. Eksperimental'noe issledovanie effektivnosti deksametazona na modeli lipopolisakharid-indutsirovannogo ostrogo povrezhdeniya legkikh u krys. Byulleten' sibirskoi meditsiny. 2023; 22 (4): 22–30. DOI: 10.20538/1682-0363-2023-4-22-30. Russian.

Литература

1. Mitchell PS, Parkin RK, Kroh EM, Fritz BR, Wyman SK, Pogosova Agadjanyan EL, et al. Circulating microRNAs as stable blood-based markers for cancer detection. Proc Natl Acad Sci USA. 2008; 105 (30): 10513–8. DOI: 10.1073/pnas.0804549105.
2. Ширшова А. Н., Шамовская Д. А., Боярских У. А., Апалько С. В., Лесков Л. С., Соколов А. В., и др. Оценка значимости определения количества miR-146a в плазме крови человека для диагностики колоректального рака. Вестник Российского государственного медицинского университета. 2017; 4: 31–36.
3. Гареев И. Ф., Бейлерли О. А. Циркулирующие микроРНК как биомаркеры: какие перспективы? Профилактическая медицина. 2018; 21 (6): 142–50. DOI: 10.17116/ profmed201821061142.
4. Васильев С. В., Аксельрод А. С., Желанкин А. В., Щекочихин Д. Ю., Генерозов Э. В., Шарова Е. И., и др. Циркулирующие микроРНК-21-5р, микроРНК146а-5р, микроРНК320а3р у пациентов с фибрилляцией предсердий в сочетании с гипертонической болезнью и ишемической болезнью сердца. Кардиоваскулярная терапия и профилактика. 2022; 21(1): 2814. DOI: 10.15829/1728-8800-2022-2814.
5. Li Y, Tan W, Ye F, et al. Identification of microRNAs and genes as biomarkers of atrial fibrillation using a bioinformatics approach. J Intern Med Res. 2019; 47 (8): 3580–9. DOI:10.1177/0300060519852235.
6. Duan X, Wang L, Sun G, Yan W, Yang Y. Understanding the cross-talk between host and virus in poultry from the perspectives of microRNA. Poult Sci. 2020; 99 (4): 1838–46. DOI: 10.1016/j.psj.2019.11.053.
7. Shang R, Lee S. Senavirathne G, Lai EC. MicroRNAs in action: Biogenesis, function and regulation. Na. Rev Genet. 2023; 24: 816–33. Available from: https://doi.org/10.1038/s41576-023-00611-y.
8. Nemeth K, Bayraktar R, Ferracin M, Calin GA. Non-coding RNAs in disease: From mechanisms to therapeutics. Nat Rev Genet. 2024; 25: 211–32. Available from: https://doi.org/10.1038/s41576-023-00662-1.
9. Дьяченко Н. А., Улитина А. С., Лукина О. В., Пчелина С. Н., Трофимов В. И., Миронова Ж. А. Экспрессия микроРНК miR-21 и miR-146a у пациентов мужского пола с перекрестным фенотипом бронхиальной астмы и хронической обструктивной болезни легких. Пульмонология. 2020; 30 (3): 263–69. DOI: 10.18093/0869-0189-2020-30-3-263-269.
10. Гареев И. Ф., Бейлерли О. А., Павлов В. Н. и др. Потенциальная роль микроРНК в патогенезе геморрагической лихорадки с почечным синдромом. Урология. 2021: 112–19. Доступно по ссылке: https://dx.doi.org/10.18565/urology.2021.1.112-119.
11. Zhou Y, Chen L, Du J, Hu X, Xie Y, Wu J, et al. MicroRNA-7 Inhibits Rotavirus Replication by Targeting Viral NSP5 In Vivo and In Vitro. Viruses. 2020; 12 (2). pii: E209. DOI: 10.3390/v12020209.
12. Chen L, Ming X, Li W, Bi M, Yan B, Wang X, Yang P, Yang B. The microRNA-155 mediates hepatitis B virus replication by reinforcing SOCS1 signalling-induced autophagy. Cell Biochem Funct. 2020. DOI: 10.1002/cbf.3488.
13. Fioravanti A, Cheleschi S, Cavalier E, Reginster J-Y, Alokail M, Ladang A, et al. Can Circulating MicroRNAs, Cytokines, and Adipokines Help to Differentiate Psoriatic Arthritis from Erosive Osteoarthritis of the Hand? A Case–Control Study. International Journal of Molecular Sciences. 2025; 26 (10): 4621. Available from: https://doi.org/10.3390/ijms26104621.
14. Ali SA, Peffers MJ, Ormseth MJ, Jurisica I, Kapoor M. The non-coding RNA interactome in joint health and disease. Nat. Rev. Rheumatol. 2021; 17: 692–705. Available from: https://doi.org/10.1038/s41584-021-00687-y.
15. Shaikh FS, Siegel RJ, Srivastava A, Fox DA, Ahmed S. Challenges and promise of targeting miRNA in rheumatic diseases: A computational approach to identify miRNA association with cell types, cytokines, and disease mechanisms. Front Immunol. 2023; 14: 1322806. Available from: https://doi.org/10.3389/fimmu.2023.1322806.
16. Wade SM, McGarry T, Wade SC, Fearon U, Veale DJ. Serum MicroRNA Signature as a diagnostic and therapeutic marker in patients with Psoriatic Arthritis. J Rheumatol. 2020; 47: 1760–7. Available from: https://doi.org/10.3899/jrheum.190602.
17. Motta F, Pederzani A, Carena MC, Ceribelli A, Wordsworth PB, De Santis M, et al. MicroRNAs in Axial Spondylarthritis: An overview of the recent progresses in the field with a focus on Ankylosing Spondylitis and Psoriatic Arthritis. Curr Rheumatol Rep. 2021; 23: 59. Available from: https://doi.org/10.1007/s11926-021-01027-5.
18. Bonek K, Kuca Warnawin E, Kornatka A, Plebanczyk M, Burakowski T, Maslinski W, et al. Circulating miRNA Correlates with lipid profile and disease activity in psoriatic arthritis, rheumatoid arthritis, and ankylosing spondylitis patients. Biomedicines. 2022; 10: 893. Available from: https://doi.org/10.3390/biomedicines10040893.
19. Haschka J, Simon D, Bayat S, Messner Z, Kampylafka E, Fagni F, et al. Identification of circulating microRNA patterns in patients in psoriasis and psoriatic arthritis. Rheumatology. 2023; 62: 3448–58. Available from: https://doi.org/10.1093/rheumatology/kead059.
20. Baloun J, Pekacova A, Svec X, Kropackova T, Horvathova V, Hulejova H, et al. Circulating miRNAs in hand osteoarthritis. Osteoarthr Cartil. 2023; 31: 228–37. DOI: 10.1016/j.joca.2022.10.021.
21. Cheleschi S, Tenti S, Bedogni G, Fioravanti A. Circulating Mir-140 and leptin improve the accuracy of the differential diagnosis between psoriatic arthritis and rheumatoid arthritis: A case-control study. Transl Res. 2022; 239: 18–34. DOI: 10.1016/j.trsl.2021.08.001.
22. Мустафин Р. Н. Идентичность патогенеза, генетических и эпигенетических механизмов развития остеоартрита и ревматоидного артрита. Казанский медицинский журнал. 2024; 105 (5): 797–812. Доступно по ссылке: https://doi.org/10.17816/KMJ627530.
23. Law YY, Lee WF, Hsu CJ, Lin YY, Tsai CH, Huang CC, et al. miR-let-7c-5p and miR-149-5p inhibit proinflammatory cytokine production in osteoarthritis and rheumatoid arthritis synovial fibroblasts. Aging (Albany NY). 2021; 13 (13): 17227–36. DOI: 10.18632/aging.203201.
24. Madamsetty Vijay Sagar Mohammadinejad, Reza Uzieliene, Ilona Nabavi, et al. Dexamethasone: insights into pharmacological aspects, therapeutic mechanisms, and delivery systems. ACS biomaterials science & engineering. 2022; 8 (5): 1763–90. Available from: https://doi.org/10.1021/acsbiomaterials.2c00026.
25. Байрашева В. К., Пчелин В.Ю., Егорова А.Э., Василькова О.Н., Корнюшин О.В. Экспериментальные модели алиментарного ожирения у крыс. Juvenis scientia. 2019; 9–10: 8–13. DOI: 10.32415/jscientia.2019.09-10.02.
26. Russo A, Bartolini D, at al. Physical Activity Modulates the

Overexpression of the Inflammatory miR-146a-5p in Obese Patients. IUBMB Life. 2018; 70 (10): 1012–22. DOI: 10.1002/iub.1926.
27. Воротников А. В., Стафеев Ю. С., Меньшиков М. Ю., Шестакова М. В., Парфенова Е. В. Латентное воспаление и нарушение обновления жировых депо как механизм развития резистентности к инсулину при ожирении. Биохимия. 2019; 84 (11): 1649–67. DOI: 10.1134/S0320972519110095.
28. Chae BS. Effect of low-dose corticosterone pretreatment on the production of inflammatory mediators in super-low-dose LPS-primed immune cells. Toxicol Res. 2021; 37: 47–57. Available from: https://doi.org/10.1007/s43188-020-00051-4.
29. Rajen Dey, Biswadev Bishayi. Dexamethasone exhibits its anti-inflammatory effects in S. aureus induced microglial inflammation via modulating TLR-2 and glucocorticoid receptor expression. International Immunopharmacology. 2019; 75: 105806. Available from: https://doi.org/10.1016/j.intimp.2019.105806.
30. Волошин Н. И., Пугач В. А., Салухов В. В., Тюнин М. А. Ильинский Н. С., Левчук Е. В., Минаков А. А. Экспериментальное исследование эффективности дексаметазона на модели липополисахарид-индуцированного острого повреждения легких у крыс. Бюллетень сибирской медицины. 2023; 22 (4): 22–30. DOI: 10.20538/1682-0363-2023-4-22-30.

SEVERE ACUTE α-PVP POISONING COMPLICATED BY SYSTEMIC RHABDOMYOLYSIS SYNDROME: CASE REPORT

Makarovskaya NP[1,2], Lodyagin AN[1,2,3] ✉, Batocyrenov ChB[4], Razamasova SYu[3], Antonova AM[1], Narzikulov RA[1], Sokolova ES[1]

[1] Dzhanelidze Research Institute of Emergency Care, Saint Petersburg, Russia
[2] Pavlov First Saint Petersburg State Medical University, Saint Petersburg, Russia
[3] Mechnikov North-Western State Medical University, Saint Petersburg, Russia
[4] Golikov Research Center of Toxicology, Saint Petersburg, Russia

Today, acute poisoning with modern psychoactive substances and narcotic drugs is among the major causes of emergency admissions to toxicology units. There is a clear upward trend in the number of life-threatening complications of poisoning with psychoactive substances, one of which is rhabdomyolysis. Here we report a clinical case of severe acute α-PVP poisoning complicated by systemic rhabdomyolysis, describe the features of the clinical course and intensive care for this disorder. The early diagnosis, timely and effective treatment by conducting aggressive detoxification infusion therapy made it possible to prevent progression to the anuric phase of acute kidney injury, as well as to avoid invasive procedures of extracorporeal detoxification methods and probably avoid the adverse outcome of the acute α-PVP poisoning complicated by systemic rhabdomyolysis.

Keywords: cathinones, alpha-PVP, α-PVP, α-pyrrolidinovalerophenone, acute poisoning signs and symptoms, diagnosis, treatment, rhabdomyolysis

Author contribution: Makarovskaya NP — study concept and design, manuscript writing, data acquisition and processing; Batocyrenov ChB, Razamasova SYu, Narzikulov RA, Sokolova ES — data acquisition and processing; Lodyagin AN — editing; Antonova AM — X-ray data description.

Compliance with ethical standards: the study was approved by the Ethics Committee of the Pavlov First Saint Petersburg State Medical University (protocol No. 277 dated 23 October 2023).

✉ **Correspondence should be addressed:** Alexej N. Lodyagin
Budapeshtskaya, 3, Saint Petersburg, 192242, Russia; alodyagin@mail.ru

Received: 02.10.2025 **Accepted:** 12.11.2025 **Published online:** 19.11.2025

DOI: 10.24075/brsmu.2025.058

Copyright: © 2025 by the authors. **Licensee:** Pirogov University. This article is an open access article distributed under the terms and conditions of the Creative Commons Attribution (CC BY) license (https://creativecommons.org/licenses/by/4.0/).

КЛИНИЧЕСКИЙ СЛУЧАЙ ОСТРОГО ТЯЖЕЛОГО ОТРАВЛЕНИЯ α-PVP, ОСЛОЖНЕННЫЙ РАЗВИТИЕМ СИНДРОМА СИСТЕМНОГО РАБДОМИОЛИЗА

Н. П. Макаровская[1,2], А. Н. Лодягин[1,2,3] ✉, Ч. Б. Батоцыренов[4], С. Ю. Разамасова[3], А. М. Антонова[1], Р. А. Нарзикулов[1], Е. С. Соколова[1]

[1] Санкт-Петербургский научно-исследовательский институт скорой помощи имени И. И. Джанелидзе, Санкт-Петербург, Россия
[2] Первый Санкт-Петербургский государственный медицинский университет имени И. П. Павлова, Санкт-Петербург, Россия
[3] Северо-Западный государственный медицинский университет имени И. И. Мечникова, Санкт-Петербург, Россия
[4] Научно-клинический центр токсикологии имени С. Н. Голикова, Санкт-Петербург, Россия

В настоящее время острые отравления современными психоактивными веществами и наркотическими веществами входят в число основных причин экстренной госпитализации лиц в отделения токсикологии. Имеется четкая тенденция к росту числа жизнеугрожающих осложнений при отравлениях психоактивными веществами, одним из которых является рабдомиолиз. Представлен клинический случай острого тяжелого отравления альфа-PVP, осложненного развитием системного рабдомиолиза, описаны особенности клинического течения и интенсивной терапии при данной патологии. Ранняя диагностика, своевременное и эффективное лечение путем проведения агрессивной инфузионно-детоксикационной терапии позволили избежать развития анурической стадии острого повреждения почек, а также отказаться от проведения инвазивных процедур экстракорпоральных методов детоксикации и, вероятно, избежать неблагоприятного исхода острого отравления α-PVP, осложненного развитием системного рабдомиолиза.

Ключевые слова: катиноны, альфа-PVP, α-PVP, α-пирролидиновалерофенон, клиника острого отравления, диагностика, лечение, рабдомиолиз

Вклад авторов: Н. П. Макаровская — концепция и дизайн исследования, написание текста, сбор и обработка материала; Ч. Б. Батоцыренов, С. Ю. Разамасова, Р. А. Нарзикулов, Е. С. Соколова — сбор и обработка материала; А. Н. Лодягин — редактирование; А. М. Антонова — описание рентгеновских данных.

Соблюдение этических стандартов: исследование одобрено этическим комитетом ФГБОУ ВО «Первый Санкт-Петербургский государственный медицинский университет имени академика И. П. Павлова» (протокол № 277 от 23 октября 2023 г.).

✉ **Для корреспонденции:** Алексей Николаевич Лодягин
ул. Будапештская, д. 3, г. Санкт-Петербург, 192242, Россия; alodyagin@mail.ru

Статья получена: 02.10.2025 **Статья принята к печати:** 12.11.2025 **Опубликована онлайн:** 19.11.2025

DOI: 10.24075/vrgmu.2025.058

Авторские права: © 2025 принадлежат авторам. **Лицензиат:** РНИМУ им. Н. И. Пирогова. Статья размещена в открытом доступе и распространяется на условиях лицензии Creative Commons Attribution (CC BY) (https://creativecommons.org/licenses/by/4.0/).

Today, acute poisoning with narcotic drugs occupy leading positions in the structure of the patients' admission to toxicology units; there is no trend towards the decrease in the number of such patients, which determines high relevance of the issue.

Among the most numerous are cases of acute poisoning with synthetic cathinones ("designer drugs" in slang) showing strong psycho-stimulating activity and the high rate of life-threatening conditions affecting the CNS, respiratory and cardiovascular system [1]. Thus, based on the epidemiological situation in Saint Petersburg, a total of 2596 patients poisoned with the synthetic cathinone α-pyrrolidinovalerophenone (α-PVP) were delivered to the Acute Poisoning Center of the Dzhanelidze Research Institute of Emergency Care in 2024, which far exceeded the number of cases of acute poisoning

with other drugs, such as methadone (a total of 1422 patients were admitted in 2024), cocaine (a total of 68 patients were delivered within the same period). All the above emphasizes predominance of acute α-PVP poisoning in the structure of acute poisoning at the moment.

The α-PVP properties were first reported in 1963 by researchers of the Boehringer Ingelheim pharma company (Germany) [2]. However, later successful therapeutic use of α-PVP was not confirmed. Since early 2010s, the α-PVP chemical compound appeared on the illegal drug market in European countries, where it was distributed under the guise of "bath salts" (that is why it is referred to as "salt"), then it was noted to be distributed in Moscow, Saint Petersburg, and Russia [3]. Considering social dangerousness of this toxicant, the α-PVP turnover is currently controlled in 16 countries of the European Union and prohibited in the Russian Federation [4].

The recreation effects of synthetic cathinones, including α-PVP, are associated with the strong stimulating effect on the CNS and cardiovascular system. In individuals with the extremely severe poisoning, along with the toxic damage to the nervous and cardiovascular systems, the condition severity is aggravated by the early development of severe metabolic disorders in the form of decompensated metabolic acidosis, coagulopathy [5, 6]. Systemic rhabdomyolysis that is usually accompanied by acute kidney injury represents one of the most severe complications of severe acute α-PVP poisoning.

Rhabdomyolysis is a syndrome characterized by muscle necrosis and the release of the muscle intracellular components into bloodstream [1]. The development of systemic rhabdomyolysis being one of the most severe complications of acute poisoning, including poisoning with narcotic drugs, is currently poorly understood [3]. The study aimed to present a clinical case of acute α-PVP poisoning complicated by systemic rhabdomyolysis with identification of early diagnostic criteria and the efficacy of the conservative therapy applied.

Clinical case

Patient M., male, 23 years old, was admitted to the Acute Poisoning Center of the Dzhanelidze Research Institute of Emergency Care with the following referral diagnosis: "Moderate acute poisoning with the unknown neurotropic substance". The patient examination revealed mental confusion, psychomotor agitation, disorientation in space, time and own personality. Conciousness scored +3 on the RASS scale. To jugulate psychomotor agitation, the patient was intramuscularly administered Elzepam 2.0 mg. Hemodynamics were stable, heart rate (HR) was 125 bpm, the rhythm was sinus tachycardia, blood pressure was 150 and 80 mmHg.

The clinical laboratory testing revealed leucocytosis up to 26.58×10^{12}/L with the neutrophil right shift in complete blood counts, along with the increase in creatinine levels to 227 μmol/L and urea levels to 19.7 mmol/L in the blood biochemistry panel. Urinalysis revealed proteinuria (with the increase in protein levels to 0.75 g/L), hematuria (with the increase in red blood cell counts to 2.5×10^2/μL). Chemical toxicology testing by gas chromatography–mass spectrometry (GC–MS) detected α-PVP in the urine.

Within 12 h after admission the patient was transferred to the intensive care unit (ICU) No. 11 due to deterioration in his condition. The patient's overall condition was assessed as severe at admission to the ICU. Pupil size D = S, mydriasis. Lively papillary light response. Normal muscle tone. Normal reflexes. No abnormal reflexes. Respiratory rate 16 breaths per minute. Oxygen saturation 98%. Stable nemodynamics, HR was 89 bpm, blood pressure was 120 and 70 mmHg, central venous pressure was (+2) cm H_2O. A total of 100 mL of urine were collected by bladder catheterization. The urine color was brown. The following diagnosis was established: "Severe acute α-PVP poisoning. Toxic encephalopathy. Complication: Systemic rhabdomyolysis. Acute kidney injury".

On day 2 after admission the decrease in leucocyte counts to 14.9×10^{12}/L was reported; as for blood biochemistry parameters, worsening in the form of the increase in creatinine levels to 235 μmol/L and urea levels to 25.1 mmol/L was noted, along with the increase in cytolytic enzyme levels (ALT to 462.6 U/L, AST to 1782 U/L), creatine kinase levels to 88,980 U/L and hyperkalemia to 5.4 mmol/L. Along with negative values of blood biochemistry parameters, the urine output decrease to 100 mL/day was reported, which corresponded to stage 2 acute kidney injury according to the KDIGO classification [5].

Furthermore, when assessing the patient's mixed venous blood gas and acid-base state, we observed the development of subcompensated metabolic acidosis with the electrolyte balance disturbances: pH — 7.285, HCO_3^- — 16 mmol/L, BEb — (–9.3) mmol/L, BEect — (–10.6) mmol/L, Na^+ — 133 mmol/L, K^+ — 4.49 mmol/L, Ca^{2+} — 1.018 mmol/L, blood osmolality — 266 mOsm/L.

Improvement of a number of parameters was reported within 6 h after the beginning of the intensive metabolic acidosis correction: pH — 7.523, HCO_3^- — 27.9 mmol/L, BEb — 5.1 mmol/L, BEect — 5.1 mmol/L, K^+ — 2.87 mmol/L.

The infusion therapy prescribed included the use of infusion solutions to adjust metabolic acidosis (Sol. Natrii hydrocarbonatis 4% — 200.0 No. 3). Sodium hydrocarbonate was quantified using the Mellengaard-Astrup formula: the required amount of sodium hydrocarbonate (in mmol) is equal to the product of body weight in kilograms by 0.3 by BE (base excess) [7]. According to calculations, the required hydrocarbonate quantity was 297 mmol, which was 623.9 when recalculated for the 4% sodium hydrocarbonate solution. Hyperkalemia was adjusted using the glucose-insulin solution (Sol. Glucosae 10% — 500.0 + Sol. Magnii sulf. 25% — 10.0 + Insulini 2 ED No. 3/day). Lactic acidosis was adjusted via infusion of Sol. Reamberini 500.0 No. 2/day. Sol. Natrii chloridi 0.9% — 500.0 No. 2/day was prescribed to adjust the volemic status. The infusion therapy volume was calculated based on the urine output, which was 1 mL/kg/h (the daily volume reached 2160 mL), perspiration losses calculated as 0.5 mL/kg/h and hyperthermia over 38 °C (0.5 mL/kg/h — 1580.0). After the first 24 h of hospital stay the daily urine output was 2900 mL/day. Furthermore, the urine color changed from black to straw-yellow. In response to the infusion therapy applied, the daily urine output became 3900 mL with the central venous pressure of (+4) cm H_2O on day 2 after the beginning of treatment.

On day 4 of intensive care, improvement was noted in the form of the decrease in creatine kinase levels to 35,000 U/L, cytolytic enzyme levels (ALT to 372.7 U/L, AST to 760 U/L). The complete blood count test revealed the decrease in leucocyte counts to 6.4×10^{12} L. The daily urine output was 5200 mL with the central venous pressure of (+8) cm H_2O.

On day 5 of treatment, the blood biochemistry test showed improvement in the form of the decrease in creatinine levels to 183 μmol/L, urea levels to 10.9 mmol/L, creatine kinase levels to 14,220 U/L, K^+ levels of 3.35 mmol/L. The daily urine output was 6200 mL, and the central venous pressure was (+8) cm H_2O.

On day 8, the patient was transferred to the toxicology unit and discharged home in a satisfactory condition.

Thus, the early diagnosis and timely, effective intensive care made it possible to avoid progression to the anuric phase of acute kidney injury and probably avoid the adverse outcome of the acute α-PVP poisoning complicated by systemic rhabdomyolysis.

Clinical case discussion

This case report demonstrates the development of systemic rhabdomyolysis in acute α-PVP poisoning, resulting from the combination of the direct and indirect factors causing the early development of this life-threatening condition. Myoglobin is the main endotoxin associated with systemic rhabdomyolysis [8–10]. Normally, myoglobin is filtered freely in the renal glomeruli, but under conditions of metabolic acidosis and hypovolemia it precipitates to form insoluble compartments that obturate the tubule lumen, thereby causing myoglobinuric acute kidney injury (AKI), as observed in the patient (urine color change to brown, oliguria, increase in creatinine and urea levels). The increase in creatine kinase levels is a diagnostic marker of damage to the skeletal muscles. In this case, these increased to 98,780 U/L, which was a diagnostic criterion of systemic rhabdomyolysis.

Given the above, in this clinical case, treatment was based on the aggressive detoxification infusion therapy aimed to ensure the rapid and effective metabolic acidosis adjustment by using sodium hydrocarbonate and then Reamberin, the infusion medication with the base reserve, massive infusion therapy with strict monitoring of the central venous pressure and urine output. The total infusion volume was calculated considering the volume deficit, perspiratory losses, and the need to maintain sufficient urine output (> 1 mL/kg/h) [11]. This made it possible to "cleanse" the renal tubules and prevent obstruction with the myoglobin cylinders. The urine output preservation and urine color change from brown to straw-yellow represent a clinical criterion of the applied therapy efficacy. Rapid hyperkalemia adjustment by using the glucose-insulin mixture was used to eliminate hyperkalemia resulting from massive cellular decay. Furthermore, vitamin therapy, gastroprotective therapy, anticoagulant therapy represented the important comprehensive treatment components [12–14].

CONCLUSION

Thus, this case report shows that acute α-PVP poisoning can lead to the early development of severe systemic rhabdomyolysis with the high risk of acute kidney injury, metabolic acidosis and toxic CNS damage. The key factors of the beneficial outcome are the early systemic rhabdomyolysis disgnosis and the rapid, effective intensive infusion therapy aimed at the early effective adjustment of metabolic disorders and maintenance of adequate renal blood flow for prevention of the irreversible kidney damage.

References

1. Sinenchenko AG, Lodyagin AN, SHilov VV, Batocyrenov BV, Balabanova OL, SHikalova IA. Analiz struktury ostryh otravlenij sovremennymi psihoaktivnymi veshchestvami. Gigiena i sanitariya, 2020; (6): 569–74. Russian.
2. Wander A. α-Pyrrolidinovalerophenones; British Patent 403 GB927475; Bern, Switzerland; 1963.
3. European Monitoring Centre for Drugs and Drug Addiction. EMCDDA-Europol. Risk Assessment Report on 1-Phenyl-2-(pyrrolidin-1-yl)pentan-1-one (α-Pyrrolidinovalerophenone, α-PVP); 2016. Available from: http://www.emcdda.europa.eu/system/files/publications/2934/TDAK16001ENN.pdf [Data obrashcheniya: 10 iyulya 2024].
4. Zawilska JB, Wojcieszak J. α-Pyrrolidinophenones: a new wave of designer cathinones. Forensic Toxicology. 2017; 35: 201–16.
5. Kidney Disease: Improving Global Outcomes (KDIGO) Acute Kidney Injury Work Group. KDIGO Clinical Practice Guideline for Acute Kidney Injury. Kidney Int Suppl. 2012; 2 (1): 1–138.
6. Makarovskaya NP, Lodyagin AN, Batocyrenov BV, Balabanova OL, Evdokimova EA. Ostrye otravleniya katinonami: epidemiologiya, patogenez, klinicheskaya kartina, diagnostika i principy lecheniya (obzor literatury). Toksikologicheskij vestnik. 2025; 1: 39–49. DOI: 10.47470/0869-7922-2025-33-1-39-49. Russian.
7. Amanollahi A, Babeveynezhad T, Sedighi M, et al. Incidence of rhabdomyolysis occurrence in psychoactive substances intoxication: a systematic review and meta-analysis. Scientific Reports. 2023; 13: 17693. DOI: 10.1038/s41598-023-45031-4.
8. Torres PA, Helmstetter JA, Kaye AM, Kaye AD. Rhabdomyolysis: pathogenesis, diagnosis, and treatment. Ochsner Journal. 2015; 15: 58–69.
9. Cervellin G, Comelli I, Lippi G. Rhabdomyolysis: historical background, clinical, diagnostic and therapeutic features. Clinical Chemistry and Laboratory Medicine. 2010; 48: 749–56.
10. Talaie H, Shahrokhian S, Malekpour F, Azizi F, Ghanei M. Rhabdomyolysis among acute human poisoning cases. Human & Experimental Toxicology. 2007; 26: 557–61.
11. Richards JR, Bretz SW, Johnson EB, Turnipseed SD, Brofeldt BT, Derlet RW. Methamphetamine abuse and emergency department utilization. Western Journal of Medicine. 1999; 170: 198–202.
12. Lodyagin AN, Batocyrenov BV, Narzikulov RA, i dr. Ostroe tyazhyoloe otravlenie opioidnym narkoticheskim veshchestvom metadonom, oslozhnyonnoe razvitiem sindroma dlitel'nogo sdavleniya (klinicheskij sluchaj). Zhurnal neotlozhnoj hirurgii imeni I. I. Dzhanelidze. 2024; 1 (14): 119–25. Russian.
13. Tepaev RF, Lastovka VA, Pytal AV, i dr. Metabolicheskij acidoz: diagnostika i lechenie. Pediatricheskaya farmakologiya. 2016; 13 (4): 384–89. Russian.
14. Livanov GA, Lodyagin AN, Razina AA, Glushkov SI, Ivanova AA, Volchkova EV, Batocyrenov BV. Blagopriyatnyj iskhod ostrogo tyazhelogo otravleniya metadonom (klinicheskoe nablyudenie). Obshchaya reanimatologiya. 2018; 14 (5): 25–31. Russian.

Литература

1. Синенченко А. Г., Лодягин А. Н., Шилов В. В., Батоцыренов Б. В., Балабанова О. Л., Шикалова И. А. Анализ структуры острых отравлений современными психоактивными веществами. Гигиена и санитария. 2020; (6): 569–74.
2. Wander A. α-Pyrrolidinovalerophenones; British Patent 403 GB927475; Bern, Switzerland; 1963.
3. European Monitoring Centre for Drugs and Drug Addiction. EMCDDA-Europol. Risk Assessment Report on 1-Phenyl-2-(pyrrolidin-1-yl)pentan-1-one (α-Pyrrolidinovalerophenone, α-PVP); 2016. Доступно по ссылке: http://www.emcdda.europa.eu/system/files/publications/2934/TDAK16001ENN.pdf [Дата обращения: 10 июля 2024].
4. Zawilska JB, Wojcieszak J. α-Pyrrolidinophenones: a new wave of designer cathinones. Forensic Toxicology. 2017; 35: 201–16.
5. Kidney Disease: Improving Global Outcomes (KDIGO) Acute Kidney Injury Work Group. KDIGO Clinical Practice Guideline for

Acute Kidney Injury. Kidney Int Suppl. 2012; 2 (1): 1–138.
6. Макаровская Н. П., Лодягин А. Н., Батоцыренов Б. В., Балабанова О. Л., Евдокимова Е.А. Острые отравления катинонами: эпидемиология, патогенез, клиническая картина, диагностика и принципы лечения (обзор литературы). Токсикологический вестник. 2025; 1: 39–49. DOI: 10.47470/0869-7922-2025-33-1-39-49.
7. Amanollahi A, Babeveynezhad T, Sedighi M, et al. Incidence of rhabdomyolysis occurrence in psychoactive substances intoxication: a systematic review and meta-analysis. Scientific Reports. 2023; 13: 17693. DOI: 10.1038/s41598-023-45031-4.
8. Torres PA, Helmstetter JA, Kaye AM, Kaye AD. Rhabdomyolysis: pathogenesis, diagnosis, and treatment. Ochsner Journal. 2015; 15: 58–69.
9. Cervellin G, Comelli I, Lippi G. Rhabdomyolysis: historical background, clinical, diagnostic and therapeutic features. Clinical Chemistry and Laboratory Medicine. 2010; 48: 749–56.
10. Talaie H, Shahrokhian S, Malekpour F, Azizi F, Ghanei M. Rhabdomyolysis among acute human poisoning cases. Human & Experimental Toxicology. 2007; 26: 557–61.
11. Richards JR, Bretz SW, Johnson EB, Turnipseed SD, Brofeldt BT, Derlet RW. Methamphetamine abuse and emergency department utilization. Western Journal of Medicine. 1999; 170: 198–202.
12. Лодягин А. Н., Батоцыренов Б. В., Нарзикулов Р. А., и др. Острое тяжелое отравление опиоидным наркотическим веществом метадоном, осложненное развитием синдрома длительного сдавления (клинический случай). Журнал неотложной хирургии имени И. И. Джанелидзе. 2024; 1 (14): 119–25.
13. Тепаев Р. Ф., Ластовка В. А., Пыталь А. В., и др. Метаболический ацидоз: диагностика и лечение. Педиатрическая фармакология. 2016; 13 (4): 384–89.
14. Ливанов Г. А., Лодягин А. Н., Разина А. А., Глушков С. И., Иванова А. А., Волчкова Е. В., Батоцыренов Б. В. Благоприятный исход острого тяжелого отравления метадоном (клиническое наблюдение). Общая реаниматология. 2018; 14 (5): 25–31.

EARTHWORMS AS A SOURCE OF NEW APPROACHES IN BIOMEDICAL RESEARCH

Khokhlova AN[1,2], Vavilov MV[1,2], Chepurnykh TV[1], Rodionova NS[3], Petushkov VN[3], Yampolsky IV[1,4], Dubinnyi MA[1] ✉

[1] Shemyakin-Ovchinnikov Institute of Bioorganic Chemistry, Russian Academy of Sciences, Moscow, Russia

[2] HSE University, Moscow, Russia

[3] Institute of Biophysics, Krasnoyarsk Research Center, Siberian Branch, Russian Academy of Sciences

[4] Pirogov Russian National Research Medical University, Moscow, Russia

Traditional medicine has been using earthworms to treat a wide range of pathological conditions for many centuries. Current research focuses primarily on the isolation and characterization of biologically active compounds, including notable examples such as glycoprotein G90, which exhibits thrombolytic and antitumor properties; the enzyme complex lumbrokinase; and the extracellular oxygen transport protein erythrocruorin, regarded as a potential basis for blood substitute development. Model organisms such as *Caenorhabditis elegans*, which are used to study the mechanisms of aging, neurodegenerative diseases, and evaluate the effectiveness of medicines, also play an important role. Bioluminescent systems of annelids are of particular interest because they exhibit a variety of chemical mechanisms of luminescence and unique cofactors that hold promise for applications in biomedicine. The combination of these properties and abilities underscores the importance of worms as a source of enzymes, proteins, and metabolites, as well as model systems for finding solutions to both fundamental and applied biomedical problems.

Keywords: bioluminescence, biomedical research, earthworms, *Henlea*, C-mannosyl tryptophan

Funding: the work was supported by the Russian Science Foundation grant No. 24-14-00421, https://rscf.ru/project/24-14-00421/.

Acknowledgements: the authors would like to thank Z.M. Osipova from Shemyakin-Ovchinnikov Institute of Bioorganic Chemistry and Yu.A. Ovchinnikov for their valuable critical comments on the manuscript.

Author contribution: Khokhlova AN, Vavilov MV, Chepurnykh TV — literature analysis, manuscript authoring; Rodionova NS, Petushkov VN — literature analysis; Yampolsky IV — financing and project management; Dubinnyi MA — financing and project management, manuscript editing.

✉ **Correspondence should be addressed:** Maxim A. Dubinnyi
Miklukho-Maklaya, 16/10, Moscow, 117997, Russia; dumkas@yandex.ru

Received: 21.10.2025 **Accepted:** 29.11.2025 **Published online:** 10.12.2025

DOI: 10.24075/brsmu.2025.067

Copyright: © 2025 by the authors. **Licensee:** Pirogov University. This article is an open access article distributed under the terms and conditions of the Creative Commons Attribution (CC BY) license (https://creativecommons.org/licenses/by/4.0/).

ПОЧВЕННЫЕ ЧЕРВИ КАК ИСТОЧНИК НОВЫХ ПОДХОДОВ В БИОМЕДИЦИНСКИХ ИССЛЕДОВАНИЯХ

А. Н. Хохлова[1,2], М. В. Вавилов[1,2], Т. В. Чепурных[1], Н. С. Родионова[3], В. Н. Петушков[3], И. В. Ямпольский[1,4], М. А. Дубинный[1] ✉

[1] Институт биоорганической химии имени М. М. Шемякина и Ю. А. Овчинникова Российской академии наук, Москва, Россия

[2] Национальный исследовательский университет «Высшая школа экономики», Москва, Россия

[3] Институт биофизики Федерального исследовательского центра “Красноярский научный центр Сибирского отделения Российской Академии наук”, Красноярск

[4] Российский национальный исследовательский медицинский университет имени Н. И. Пирогова, Москва, Россия

Применение почвенных червей в традиционной медицине имеет многовековую историю и охватывает широкий спектр патологических состояний. Современные исследования сосредоточены в основном на выделении и изучении биологически активных соединений. Среди значимых примеров можно выделить гликопротеин G90 с тромболитическими и противоопухолевыми свойствами, комплекс ферментов люмброкиназу, а также внеклеточный кислородтранспортный белок эритрокруорин, рассматриваемый как основа для разработки заменителей крови. Важную роль играют и модельные организмы, такие как *Caenorhabditis elegans*, используемые для изучения механизмов старения, нейродегенеративных заболеваний и оценки эффективности лекарственных средств. Особый интерес представляют биолюминесцентные системы кольчатых червей, продемонстрировавшие разнообразие химических механизмов свечения и наличие уникальных кофакторов, перспективные для развития практических приложений биомедицины. Совокупность этих направлений подчеркивает значимость червей как источника ферментов, белков, метаболитов и модельных систем, способных решать как фундаментальные, так и прикладные задачи в биомедицине.

Ключевые слова: биолюминесценция, биомедицинские исследования, почвенные черви, *Henlea*, С-маннозил триптофан

Финансирование: исследование выполнено за счет гранта Российского научного фонда № 24-14-00421, https://rscf.ru/project/24-14-00421/.

Благодарности: авторы благодарят З. М. Осипову из Института биоорганической химии имени М. М. Шемякина и Ю. А. Овчинникова за ценные критические замечания к рукописи.

Вклад авторов: А. Н. Хохлова, М. В. Вавилов, Т. В. Чепурных — анализ литературы, написание рукописи; Н. С. Родионова, В. Н. Петушков — анализ литературы; И. В. Ямпольский — финансирование и руководство проектом; М. А. Дубинный — финансирование и руководство проектом, редактирование рукописи.

✉ **Для корреспонденции:** Максим Анатольевич Дубинный
ул. Миклухо-Маклая, 16/10, г. Москва, 117997, Россия; dumkas@yandex.ru

Статья получена: 21.10.2025 **Статья принята к печати:** 29.11.2025 **Опубликована онлайн:** 10.12.2025

DOI: 10.24075/vrgmu.2025.067

Авторские права: © 2025 принадлежат авторам. **Лицензиат:** РНИМУ им. Н. И. Пирогова. Статья размещена в открытом доступе и распространяется на условиях лицензии Creative Commons Attribution (CC BY) (https://creativecommons.org/licenses/by/4.0/).

Earthworms have long been used in traditional medicine for the treatment of various diseases. Extracts from various worm species were prescribed for allergic and asthmatic conditions, to lower blood pressure and detoxify the body, and more generally in cases requiring antithrombotic, antipyretic, diuretic, or antispasmodic treatment [1]. The development of biochemical and pharmacological analysis methods allowed to translate these empirical observations into systematic research and to purposefully isolate biologically active compounds of animal origin. For example, in 1992, glycoprotein G90, which has

thrombolytic and antitumor properties, was isolated from the homogenate of earthworm tissues. Lumbrokinase, a complex of fibrinolytic enzymes also sourced from earthworms, is used as a dietary supplement supporting cardiovascular system — it can improve blood circulation and dissolve blood clots [1]. In addition to enzyme complexes, there is erythrocruorin, an extracellular molecular complex that is a functional analog of hemoglobin; isolated from annelids, it is a promising base for the development of blood substitutes [2]. Erythrocruorin is considered as a potential next-generation oxygen carrier for the following reasons: it is an extracellular protein with high stability and low susceptibility to oxidative processes, it maintains stability across a wide temperature range, and it can bind and transfer nitrogen monoxide, reducing the risk of vasoconstriction [3]

Currently, worms are considered not only as a source of biologically active compounds and protein complexes but also as model organisms. One of the species fit for this purpose is a soil nematode *Caenorhabditis elegans*. Short life cycle, transparent body, fully sequenced genome, low cultivation requirements, and ability to produce numerous offspring in a short time through self-fertilization make this model a popular choice for studies on aging processes, the pathogenesis of neurodegenerative diseases such as Alzheimer's disease, and the testing of antitumor and antimicrobial drugs [4].

Current biotechnology progress allowed to exploit another unique biological phenomenon characteristic of annelids — bioluminescence, the emission of light by living organisms — which is used in biomedical research. Most of the two dozen luminous annelids live in tropical regions, but some are found in Siberia, where their glow can be observed at night with the naked eye. Practical significance of studying bioluminescent systems lies in the creation of new analytical tools and the improvement of molecular imaging methods. Bioluminescent bioimaging offers several advantages over fluorescent methods: it does not require an external excitation source, thereby preventing autofluorescence, produces a low background signal, provides high sensitivity and allows detection of emission at the level of individual cells [5]. Currently, only a few insect and marine luciferins are used, including D-luciferin, coelenterazine, and its synthetic analog furimazine [6]. However, the expansion of the set of luciferin-luciferase pairs for multicolor imaging, which allows simultaneous monitoring of various molecular processes, is an actively discussed subject [7].

For a long time, it was believed that there is only *Diplocardia longa* peroxide-dependent mechanism (λ_{max} = 490 nm) that is responsible for the bioluminescence of all earthworms (Fig. 1A) [8]. With *D. longa*, the luminescence is the result of oxidation of a low-molecular-weight luciferin substrate, N-isovaleryl-3-aminopropanal, in the presence of the luciferase enzyme. However, the discovery of three new species in Siberia — *Fridericia heliota*, *Henlea petushkovi*, and *Henlea rodionovae* — has shown that annelids have at least two other distinct luminescence systems [9]. *F. heliota's* luciferin (λ_{max} = 478 nm) is a tetrapeptide oxidized by oxygen in the presence of ATP, Mg^{2+}, and luciferase (Fig. 1B). In *Henlea sp*. (λ_{max} = 464 nm), luciferin has tryptophan residue and is oxidized by oxygen in the presence of Ca^{2+} and a luciferase [8] (Fig. 1B). The additional luminescence enhancer in this system is a cofactor F0 (ActH), a structural analog of riboflavin, which receives energy from excited oxyluciferin and re-emits it, the bioluminescence is amplified 33-fold and shifts from 410 to 464 nm, using the Förster Resonance Energy Transfer (FRET) mechanism [10, 11]. Due to the high stability of luciferin and the presence of an enhancer cofactor, it is the *Henlea sp*. bioluminescent system that is of particular interest as a base for the development of new platforms for bioluminescent bioimaging and multicolor monitoring of intracellular events.

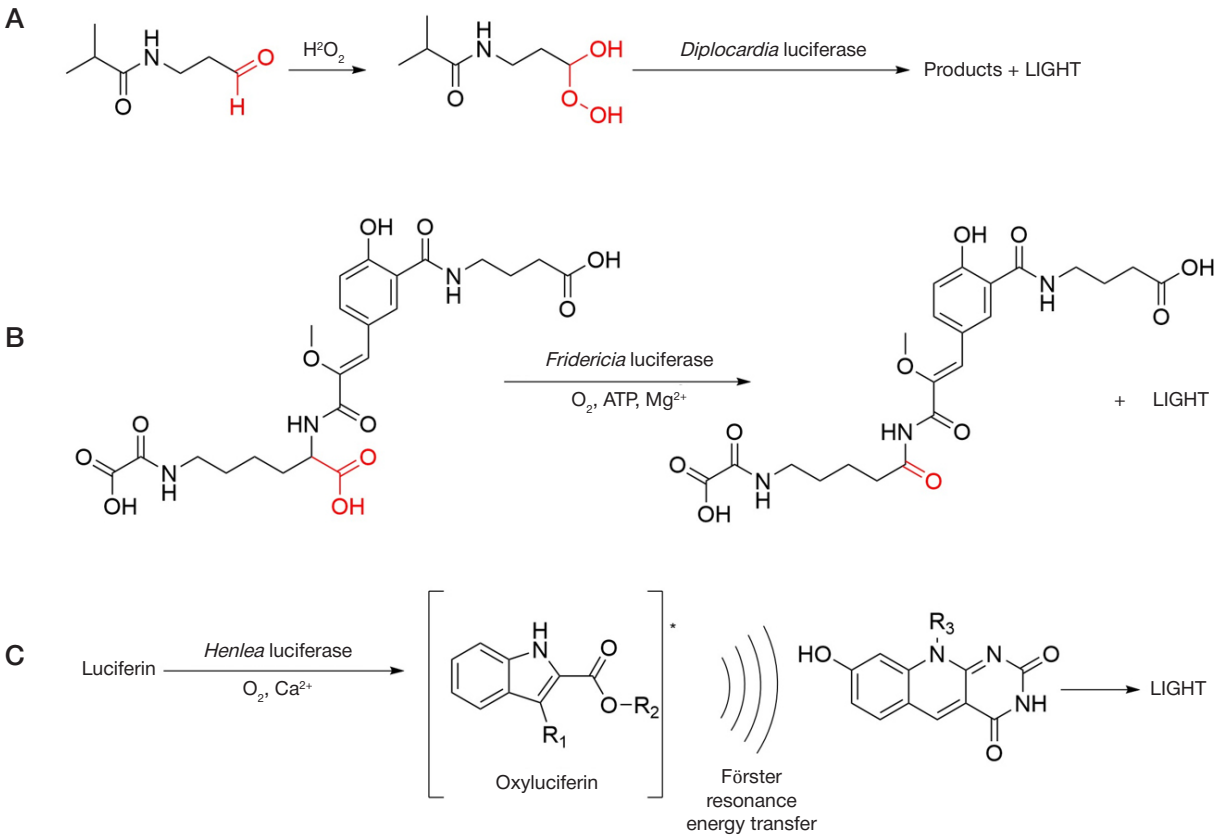


Fig. 1. Bioluminescent reactions of *D. longa* (**A**), *F. heliota* (**B**), *Henlea sp.* (**C**)

Additionally, analysis of *Henlea sp*. metabolites revealed a significant amount of α-C-Mannosyltryptophan (ManTrp), a new compound to bioluminescent systems. The absorption and fluorescence spectra of ManTrp coincided with those of *Henlea's* luciferin, therefore ManTrp was considered as its probable metabolic precursor. In nature mannosyltryptophan occurs either as a free ManTrp monomer or as part of a protein's polypeptide chain, resulting from an unusual C-glycosylation at the C2 position of the indole ring. The mechanism of C-glycosylation in a polypeptide chain was discovered in 1994 using human RNase. Monomeric ManTrp was found in blood and urine of humans and other mammals, including mice and rats, as well as some sea sponges [12]. The concentration of ManTrp in blood plasma increases in a number of pathologic conditions, including myelofibrosis, type 2 diabetes mellitus, chronic kidney disease, ovarian cancer, and platelet growth dysregulation. Thus, ManTrp can be considered as a promising biomarker for the diagnosis of oncological diseases.

One of possible options of practical application of the *Henlea sp.* luciferin-luciferase system is using it in a bioluminescent test system for the diagnosis of ovarian cancer based on specific recognition of ManTrp. The change in the BRET index associated with ManTrp binding can be exploited as a highly sensitive diagnostic signal with ActH/F0 cofactor acting as luminescence enhancer. Similar strategies found practical implementation in "luciferase-nanoparticle" systems in BRET-activated photodynamic therapy [13]. Moreover, stable hybrid constructs combining gold-based nanoparticles, the luciferase enzyme (including *Phrixotrix hirtus*) and a photosensitizer were created. These bioconjugates exhibit a stable bioluminescent signal and retain their functional activity in cellular conditions [14]. The results demonstrate that luciferase systems can be integrated into nanoplatforms and enable both visualization and activation of therapeutic processes [15]. This opens up the possibility of creating molecular theranostics systems that use ManTrp as a diagnostic marker and an activating trigger for the bioluminescent system in future.

Thus, sensors based on the *Henlea s*p. bioluminescent system and ManTrp specific recognition can serve as a basis of new platforms for early diagnosis and monitoring of ovarian cancer and other metabolic disorders.

CONCLUSION

The use of earthworms in medicine has evolved beyond traditional practices: once material for folk remedies, they are currently screened for biologically active compounds using modern scientific methods. Today, earthworms and nematodes are considered as sources of enzymes and protein complexes, as well as model systems for finding solutions to both fundamental and applied biomedical problems.

Bioluminescent systems of annelids are of particular interest: they exhibit a variety of chemical mechanisms of luminescence and have unique cofactors. Studying them not only deepens the understanding of the evolution and biochemistry of luminescence, but also opens the way to the creation of new molecular imaging tools [16]. In particular, the combination of luciferin-luciferase systems with energy transfer mechanisms (e.g., FRET) makes them potentially applicable in photodynamic therapy (PDT), especially in cases when it is necessary to generate light directly inside body cells. The study of bioluminescent worm systems remains a vital and promising field in modern biology, integrating evolutionary and biochemical perspectives with innovative applications in diagnostics, therapy, targeted drug delivery, and bioluminescent imaging.

References

1. Zhu Z, Deng X, Xie W, Li H, Li Y, Deng Z. Pharmacological effects of bioactive agents in earthworm extract: A comprehensive review. Anim Models Exp Med. 2024; 7: 653–72. Available from: https://doi.org/10.1002/ame2.12465.
2. Elmer J, Palmer AF. Biophysical Properties of Lumbricus terrestris Erythrocruorin and Its Potential Use as a Red Blood Cell Substitute. J Funct Biomater. 2012; 3: 49–60. Available from: https://doi.org/10.3390/jfb3010049.
3. Zimmerman D, Dilusto M, Dienes J, Abdulmalik O, Elmer JJ. Direct comparison of oligochaete erythrocruorins as potential blood substitutes. Bioeng Transl Med. 2017; 2: 212–21. Available from: https://doi.org/10.1002/btm2.10067.
4. Meneely PM, Dahlberg CL, Rose JK. Working with Worms: Caenorhabditis elegans as a Model Organism. Curr Protoc Essent Lab Tech. 2019; 19: e35. Available from: https://doi.org/10.1002/cpet.35.
5. Yeh H-W, Ai H-W. Development and Applications of Bioluminescent and Chemiluminescent Reporters and Biosensors. Annu Rev Anal Chem Palo Alto Calif. 2019; 12: 129–50. Available from: https://doi.org/10.1146/annurev-anchem-061318-115027.
6. Close DM, Patterson SS, Ripp S, Baek SJ, Sanseverino J, Sayler GS. Autonomous bioluminescent expression of the bacterial luciferase gene cassette (lux) in a mammalian cell line. PloS One. 2010; 5: e12441. Available from: https://doi.org/10.1371/journal.pone.0012441.
7. Navarro MX, Brennan CK, Love AC, Prescher JA. Caged luciferins enable rapid multicomponent bioluminescence imaging. Photochem Photobiol. 2023; 100: 67–74. Available from: https://doi.org/10.1111/php.13814.
8. Rodionova NS, Rota E, Tsarkova AS, Petushkov VN. Progress in the Study of Bioluminescent Earthworms. Photochem Photobiol. 2017; 93: 416–28. Available from: https://doi.org/10.1111/php.12709.
9. Kaskova ZM, Tsarkova AS, Yampolsky IV. 1001 lights: luciferins, luciferases, their mechanisms of action and applications in chemical analysis, biology and medicine. Chem Soc Rev. 2016; 45: 6048–77. Available from: https://doi.org/10.1039/C6CS00296J.
10. Petushkov VN, Vavilov MV, Khokhlova AN, Zagitova RI, Belozerova OA, Shcheglov AS, et al. Henlea earthworm bioluminescence comprises violet-blue BRET from tryptophan 2-carboxylate to deazaflavin cofactor. Biochem Biophys Res Commun. 2024; 708: 149787. Available from: https://doi.org/10.1016/j.bbrc.2024.149787.
11. Dubinnyi MA, Ivanov IA, Rodionova NS, Kovalchuk SI, Kaskova ZM, Petushkov VN. α-C-Mannosyltryptophan is a Structural Analog of the Luciferin from Bioluminescent Siberian Earthworm Henlea sp. Chemistry Select. 2020; 5: 13155–9. Available from: https://doi.org/10.1002/slct.202003075.
12. Minakata S, Inai Y, Manabe S, Nishitsuji K, Ito Y, Ihara Y. Monomeric C-mannosyl tryptophan is a degradation product of autophagy in cultured cells. Glycoconj J. 2020; 37: 635–45. Available from: https://doi.org/10.1007/s10719-020-09938-8.
13. Blum NT, Zhang Y, Qu J, Lin J, Huang P. Recent Advances in Self-Exciting Photodynamic Therapy. Front Bioeng Biotechnol. 2020; 8: 594491. Available from: https://doi.org/10.3389/fbioe.2020.594491.
14. Belleti E, Bevilaqua VR, Brito AMM, Modesto DA, Lanfredi AJC, Viviani VR, et al. Synthesis of bioluminescent gold nanoparticle-luciferase hybrid systems for technological applications. Photochem Photobiol Sci Off J Eur Photochem Assoc Eur Soc Photobiol. 2021; 20: 1439–53. Available from: https://doi.org/10.1007/s43630-021-00111-0.
15. Kim Y-P, Daniel WL, Xia Z, Xie H, Mirkin CA, Rao J. Bioluminescent nanosensors for protease detection based upon gold nanoparticle-luciferase conjugates. Chem Commun Camb Engl. 2010; 46: 76–8. Available from: https://doi.org/10.1039/b915612g.

16. Dunuweera AN, Dunuweera SP, Ranganathan K. A Comprehensive Exploration of Bioluminescence Systems, Mechanisms, and Advanced Assays for Versatile Applications. Biochem Res Int. 2024; 2024: 8273237. Available from: https://doi.org/10.1155/2024/8273237.

Литература

1. Zhu Z, Deng X, Xie W, Li H, Li Y, Deng Z. Pharmacological effects of bioactive agents in earthworm extract: A comprehensive review. Anim Models Exp Med. 2024; 7: 653–72. Available from: https://doi.org/10.1002/ame2.12465.
2. Elmer J, Palmer AF. Biophysical Properties of Lumbricus terrestris Erythrocruorin and Its Potential Use as a Red Blood Cell Substitute. J Funct Biomater. 2012; 3: 49–60. Available from: https://doi.org/10.3390/jfb3010049.
3. Zimmerman D, Dilusto M, Dienes J, Abdulmalik O, Elmer JJ. Direct comparison of oligochaete erythrocruorins as potential blood substitutes. Bioeng Transl Med. 2017; 2: 212–21. Available from: https://doi.org/10.1002/btm2.10067.
4. Meneely PM, Dahlberg CL, Rose JK. Working with Worms: Caenorhabditis elegans as a Model Organism. Curr Protoc Essent Lab Tech. 2019; 19: e35. Available from: https://doi.org/10.1002/cpet.35.
5. Yeh H-W, Ai H-W. Development and Applications of Bioluminescent and Chemiluminescent Reporters and Biosensors. Annu Rev Anal Chem Palo Alto Calif. 2019; 12: 129–50. Available from: https://doi.org/10.1146/annurev-anchem-061318-115027.
6. Close DM, Patterson SS, Ripp S, Baek SJ, Sanseverino J, Sayler GS. Autonomous bioluminescent expression of the bacterial luciferase gene cassette (lux) in a mammalian cell line. PloS One. 2010; 5: e12441. Available from: https://doi.org/10.1371/journal.pone.0012441.
7. Navarro MX, Brennan CK, Love AC, Prescher JA. Caged luciferins enable rapid multicomponent bioluminescence imaging. Photochem Photobiol. 2023; 100: 67–74. Available from: https://doi.org/10.1111/php.13814.
8. Rodionova NS, Rota E, Tsarkova AS, Petushkov VN. Progress in the Study of Bioluminescent Earthworms. Photochem Photobiol. 2017; 93: 416–28. Available from: https://doi.org/10.1111/php.12709.
9. Kaskova ZM, Tsarkova AS, Yampolsky IV. 1001 lights: luciferins, luciferases, their mechanisms of action and applications in chemical analysis, biology and medicine. Chem Soc Rev. 2016; 45: 6048–77. Available from: https://doi.org/10.1039/C6CS00296J.
10. Petushkov VN, Vavilov MV, Khokhlova AN, Zagitova RI, Belozerova OA, Shcheglov AS, et al. Henlea earthworm bioluminescence comprises violet-blue BRET from tryptophan 2-carboxylate to deazaflavin cofactor. Biochem Biophys Res Commun. 2024; 708: 149787. Available from: https://doi.org/10.1016/j.bbrc.2024.149787.
11. Dubinnyi MA, Ivanov IA, Rodionova NS, Kovalchuk SI, Kaskova ZM, Petushkov VN. α-C-Mannosyltryptophan is a Structural Analog of the Luciferin from Bioluminescent Siberian Earthworm Henlea sp. Chemistry Select. 2020; 5: 13155–9. Available from: https://doi.org/10.1002/slct.202003075.
12. Minakata S, Inai Y, Manabe S, Nishitsuji K, Ito Y, Ihara Y. Monomeric C-mannosyl tryptophan is a degradation product of autophagy in cultured cells. Glycoconj J. 2020; 37: 635–45. Available from: https://doi.org/10.1007/s10719-020-09938-8.
13. Blum NT, Zhang Y, Qu J, Lin J, Huang P. Recent Advances in Self-Exciting Photodynamic Therapy. Front Bioeng Biotechnol. 2020; 8: 594491. Available from: https://doi.org/10.3389/fbioe.2020.594491.
14. Belleti E, Bevilaqua VR, Brito AMM, Modesto DA, Lanfredi AJC, Viviani VR, et al. Synthesis of bioluminescent gold nanoparticle-luciferase hybrid systems for technological applications. Photochem Photobiol Sci Off J Eur Photochem Assoc Eur Soc Photobiol. 2021; 20: 1439–53. Available from: https://doi.org/10.1007/s43630-021-00111-0.
15. Kim Y-P, Daniel WL, Xia Z, Xie H, Mirkin CA, Rao J. Bioluminescent nanosensors for protease detection based upon gold nanoparticle-luciferase conjugates. Chem Commun Camb Engl. 2010; 46: 76–8. Available from: https://doi.org/10.1039/b915612g.
16. Dunuweera AN, Dunuweera SP, Ranganathan K. A Comprehensive Exploration of Bioluminescence Systems, Mechanisms, and Advanced Assays for Versatile Applications. Biochem Res Int. 2024; 2024: 8273237. Available from: https://doi.org/10.1155/2024/8273237.